IntechOpen

Polypropylene

Edited by Fatih Doğan

POLYPROPYLENE

Edited by **Fatih Doğan**

Polypropylene
http://dx.doi.org/10.5772/2229
Edited by Fatih Dogan

Contributors

Alireza Zakariya Aslani, Salih Taner Yildirim, Somaye Allahvaisi, Maciej Jaroszewski, Janina Pospieszna, Jan Ziaja, Mariusz Ozimek, Soraia Borges, Luydmila Sergeevna Shibryaeva, Igor Novak, Anton Popelka, Ivan Chodák, Marián Lehocký, Alenka Vesel, Marian Valentín, Ewa Markiewicz, Dominik Paukszta, Sławomir Borysiak, Wanda Wadas, Karim Shelesh-Nezhad, Jan Broda, Asya Viraneva, Temenuzhka Yovcheva, Georgi Mekishev, Yosuke Nishitani, Chiharu Ishii, Takeshi Kitano, Fatih Dogan, Leonora Mansur Mattos, Celso Moretti, Marcos Ferreira, Diene Ndiaye, Abdou Karim Farota, Bouya Diop, Adams Tidjani, Coumba Thiandoum, Papa Alioune Fall, Yan Wu, Dingguo Zhou, Siqun Wang, Yang Zhang, Zhi Hui Wu, Azza Mazrouaa, Zulkifli Mohamad Ariff, Nor Azura Abdul Rahim, Azlan Ariffin, Suzi Salwah Jikan, Jia Ma, Ton Peijs, Luis Castejon, Hugo Malon, Maciej Szanser, Fukuzo Yoshida, Valerio Brucato, Vincenzo La Carrubba, Konrad Schneider

Notice

First published in Croatia, 2012 by INTECH d.o.o.
eBook (PDF) Published by IN TECH d.o.o.
Place and year of publication of eBook (PDF): Rijeka, 2019.
IntechOpen is the global imprint of IN TECH d.o.o.
Printed in Croatia

Legal deposit, Croatia: National and University Library in Zagreb

Additional hard and PDF copies can be obtained from orders@intechopen.com

Polypropylene
Edited by Fatih Dogan

p. cm.

ISBN 978-953-51-0636-4

eBook (PDF) ISBN 978-953-51-6214-8

Meet the editor

Fatih Doğan is an associate professor of Chemistry department at Çanakkale Onsekiz Mart University, Turkey. He received his B.Sc. degree from Selcuk University in 1996, and received his Ph.D. degree in Polymer Science from the Ege University–İzmir in 2006. In 2008 he joined the faculty of the Department of Science and letters at the Çanakkale Onsekiz Mart as Assistant Professor. He has published about 40 original research papers in different peer-reviewed international journals. Dr Doğan has supervised several M.Sc. students. He serves as member of the editorial board of many international journals. His research interests involve synthesis of macromolecular structures and high performance materials. Specific areas of current research also are properties of phenol-based polymer solid state decomposition kinetic of different materials and polymer architecture for optoelectronic applications.

Contents

Preface

Number of the equipments used in everyday life remarkably increased after the invention of synthetic polymers, especially of styrene-butadiene rubber in 1930 and of PVC in 1936, and thanks to fast-developing polymer technologies. Polymers are light, cheap and ductile inert materials, which have good mechanical and thermal properties, suitable to use for various purposes and are highly resistant to corrosion. Thanks to such properties, they play an essential and ubiquitous role in many industrial fields. For instance, a modern car contains 150 kg of polymers (not including the weight of tyres, plastic fibres, upholstery and paint). Polypropylene is a thermoplastic polymer, which is used in a wide variety of applications and becoming more and more important because of its lightness, high rigidity, durability and heat resistance, mouldability, recyclability and low cost. Also, it is widely used to produce high volume plastic materials. It becomes stiffer at lower density and more resistant to higher temperatures when not subjected to mechanical stress. It can continue to be resistant to UV radiations for up to 20 years when reinforced with some fillers (a 2% carbon black addition). Moreover, polypropylene offers good fatigue resistance, good environmental stress-cracking resistance, good detergent resistance, good hardness and contact transparency. Besides, polypropylene can be processed using typical thermoplastic processing techniques, such as injection moulding and extrusion. It is opaque and white in colour, but can be dyed different colours.

"Montecatini" was the first to produce polypropylene on an industrial scale, in 1957, in order to manufacture a durable textile material. Then in 1962, USA began the mass-production of polypropylene. It came to be widely used in auto upholstery fabric. Till 1968, efforts were made to diversify its applications and reduce the cost of production and processing. From then onwards, its production and application fields rapidly increased.

Recently, nanotechnology has increasingly made its effect felt not only in every field of industry but also in composite science and technology. Nanocomposites, the newest composites, are produced by adding nanoparticles to polymers. It is known that nanocomposites possess superior properties when compared to traditional composites and ordinary polymers. Major advantages of polymer nanocomposites are their hardness, high resistance and increased dimensional stability, liquid and gas

permeability, and low cost. Polymer nanocomposites are produced by reinforcing polymer matrix with certain fillers. Polymer nanocomposite materials are produced by combining the properties of different materials to manufacture multi-purpose materials. By adding nanoparticles to polypropylenes, their mechanical and thermal stability and impact-resistance are increased while their oxygen and water vapour transmission rates are reduced in comparison to traditional materials. Nanocomposite materials produced following this process have attracted remarkable attention, and as a result extensive research has been carried out on polypropylene.

On the other side, whereas polypropylene is used as a raw material to manufacture a great number of durable and elastic materials, it is also added, in various forms and amounts, into other materials. It offers a wide range of application possibilities for construction engineering when used in the form of polypropylene or with ordinary engineering materials. As shortly and partly mentioned above, despite its wide variety of applications, number of the studies over polypropylenes is continually growing and some properties are being improved further thanks to the emergence of new technologies and ever-increasing and -expanding application areas in everyday life. Therefore, it has become inevitable to compile such studies and make them accessible for young and senior researchers.

The present work contains the most recent works of the researchers, all polypropylene experts, across the world. This book, titled “Polypropylene”, includes texts on Sciences, Engineering and Technology and the latest polypropylene technologies. It aims to partially fill the vacuum in the field and present young and senior researchers with papers on the abovementioned subjects.

The work consists of two parts. A special effort was made to place the relevant texts one after the other. Relevance was one of the key points to increase the readability and comprehension. Texts on pure polypropylene are presented in the first part, while one can find the ones on modified polypropylenes in the second. In forming the chapters, everyday life applications of polypropylene are given the priority, whereas texts on new technologies and applications are provided at the end.

In addition, papers produced by 25 researchers were included in the work. Any information was provided to enable an effortless contact with the authors and an easy access to the referred works.

Figures, charts and chemical structures were so neatly and meticulously designed that both young and senior researchers could easily see and read them. Every paper was required to have an introduction, a body, a conclusion and a references section.

I would love to thank InTech company and especially Jana Sertic for their invaluable support in the making of this compilation.

I wish that the present work, which was produced by the support of InTech company, will prove beneficial for the researchers from the industrial and academic milieus.

May 2012

Dr. Fatih Doğan
Professor of Chemistry Department,
Çanakkale Onsekiz Mart University,
Turkey

Section 1

Polypropylene in the Industry

1

Polypropylene in the Industry of Food Packaging

Somaye Allahvaisi
Department of Entomology and Toxicology,
Faculty of Agriculture, Islamic Azad University of Tehran,
Branch of Sciences & Researches,
Iran

1. Introduction

Various pests expose agriculture and food products to attack from storage until consumption by consumers. Insects and fungi are the most serious pests that can contaminate food products in warehouses. Despite modern food and other agricultural products storage and distribution systems, most packaged food products, with the exception of canned and frozen goods, are subject to attack and penetration by insects (Mullen & Highland, 1988). When a packaging containing one of insect life stages enters into storages (infested packaging), it could cause the prevalence of infestation. In addition to reducing food quantity, insects annihilate quality, too. By nourishing into the foods, they prepare the conditions for the attack by pathogen microorganisms, such as fungi and as such, the consumption of these foodstuffs could be followed by dangerous present day diseases e.g. cancer types as contaminated foods to pathogens like fungi are one of the most important problems in the industry of storage foods and they are susceptible to mycotoxins (Jakic-Dimic et al., 2009). There are few categories of mycotoxins regarding their chemical structure, sensitivity of certain organs and origin of fungi that produce them. Aflatoxin is a secondary metabolite produced by *Aspergillus flavus* (Lopez-Diaz &Flannigan, 1997). Aflatoxin is potential to cause liver damage, cirrhosis, and liver cancer and aflatoxin B1 is the most dangerous toxin for animal and human health (Syarief et al., 2003). So, huge losses have been observed in agriculture produce and different ways are designed for controlling stored-product pests. Storing foodstuffs in bulk or sacks is a usual method for controlling pests without application of chemical methods. These sacks are made of different materials such as sheeted polymers used for packaging agricultural products to prevent the entrance of pests and contaminations (Allahvaisi, 2009). Wastage varies from 5-35% depending on nature of crops. Majority of wastage takes place in each of the steps viz. storage, transportation and at retail market due to improper packaging. Bulk Packaging made of polymers provides a solution for commodities weighing 10-50 kg during handling, storage and transportation, while smaller packaging for food products range from 50 ml to 5kg. Polymeric packaging fulfils the diverse role from protecting products, preventing spoilage, contamination, extending shelf life, ensuring safe storage thereby helping to make them readily available to consumers in our day to day life. This chapter will be a very helpful to

all its readers, entrepreneurs, scientists, existing industries, technical institution, etc in the field of packaging (Anonymous, 2011).

2. Why plastics for packing?

Today, several polymer types are currently used for foodstuff packaging. Plastics have emerged as the most preferred choice of packaging materials for various products- from food, beverages, chemicals, electronic items and so on. They offer unique advantages over conventional materials (Anonymous, 2011):

- Safety: Plastics are safer materials for packaging of food products specially polyolefins which do not react with food. Pilferage and contamination is difficult.
- Shelf Life: Plastics packaging material offer better shelf life
- Cost: Plastics are the most cost effective medium of packaging when compared with any other material, the cost of transportation is reduced considerable on account of lower weight and less damage
- Convenience: Plastics can be converted in any form with various processing techniques, thus can pack any type of substances like liquids, powders, flakes, granules, solids.
- Waste: Packaging in plastics reduces the wastage of various food products, typical example is potatoes or onions packed in leno.
- Aesthetics: A right choice of plastics packaging increased the aesthetic value of products and helps in brand identity
- Handling and Storage: Products packed in plastics are easiest to handle and store as well as transport.
- Plastic products are easy to recycle.

Every day there are new products packed in plastics replacing conventional products and when a thought is given to pack a new product the first choice appears in the mind is Plastic packaging material.

3. Flexible plastic films

In general, flexible plastic films have relatively low cost and good barrier properties against moisture and gases; they are heat sealable to prevent leakage of contents; they add little weight to the product and they fit closely to the shape of the food, thereby wasting little space during storage and distribution; they have wet and dry strength, and they are easy to handle and convenient for the manufacturer, retailer and consumer. The main disadvantages are that (except cellulose) they are produced from non-renewable oil reserves and are not biodegradable. Concern over the environmental effects of non-biodegradable oil-based plastic packaging materials has increased research into the development of 'bioplastics' that are derived from renewable sources, and are biodegradable (Stewart, 1995). However, these materials are not yet available commercially in developing countries. There is a very wide choice of plastic films made from different types of plastic polymer. Each can have ranges of mechanical, optical, thermal and moisture/gas barrier properties. These are produced by variations in film thickness and the amount and type of additives that are used in their production. Some films (e.g. polyester, polyethylene, polypropylene) can be 'oriented' by stretching the

material to align the molecules in either one direction (uniaxial orientation) or two (biaxial orientation) to increase their strength, clarity, flexibility and moisture/gas barrier properties. There are thus a very large number of plastic films and small-scale processors should obtain professional advice when selecting a material to ensure that it is suitable for the intended product and shelf life. Typically, the information required includes: type of plastic polymer(s) required; thickness/strength; moisture and gas permeability; heat seal temperature; printability on one or both sides; and suitability for use on the intended filling machinery (Ramsland, 1989; Robertson, 1993). Some may offer virtually no resistance against insects while others may be extremely resistant (Highland, 1981). Plastics based on Polypropylene (PP), polyethylene (PE), Polyvinylchloride (PVC) and Cellophane is mainly used for packaging applications (Table 1) (Odian, 2004).

Properties	Polyethylene	Polypropylene	Polyvinyl chloride	Cellophane
Max. heat tolerance (°C)	82-93	132-149	66-93	90-140
Min. heat tolerance (°C)	-57	-18	-46 to -29	-77
Sun light resistance	Moderate to good	moderate	good	good
Gas transmission ($mm/100\ cm^2$ in 24 h and 25°C)	O_2 500	160	8-160	122-480
	N_2 180	20	1-70	33-90
	CO_2 2700	540	20-1900	2220
H_2O Absorption %	<0.01	<0.05	0	<0.03
H_2O Vapor transmission ($g/100\ cm^2$ in 24h & 37.8°C & R.H. 90%)	1-1.5	0.25	4-10	0.2-1

Table 1. Some properties of used different polymers for packaging foodstuffs

A summary of the main different types of flexible plastic films is as follows (Anonymous, 2008):

3.1 Cellulose

Plain cellulose is a glossy transparent film that is odourless, tasteless and biodegradable (within approximately 100 days). It is tough and puncture resistant, although it tears easily. It has dead-folding properties that make it suitable for twist-wrapping (e.g. sugar confectionery). However, it is not heat sealable and the dimensions and permeability of the film vary with changes in humidity. It is used for foods that do not require a complete moisture or gas barrier, including fresh bread and some types of sugar confectionery. Cellulose acetate is a clear, glossy transparent, sparkling film that is permeable to water vapour, odours and gases and is mainly used as a window material for paperboard cartons (Chiellini, 2008).

3.2 Polyethylene (or polythene)

Low-density polyethylene (LDPE) is heat sealable, inert, odour free and shrinks when heated. It is a good moisture barrier but is relatively permeable to oxygen and is a poor

odour barrier. It is less expensive than most films and is therefore widely used for bags, for coating papers or boards and as a component in laminates. LDPE is also used for shrink- or stretch-wrapping (see Technical Brief: Filling and Sealing Packaged Foods). Stretch-wrapping uses thinner LDPE (25 - 38 μm) than shrink-wrapping (45-75 μm), or alternatively, linear low-density polyethylene is used at thicknesses of 17 - 24 μm. The cling properties of both films are adjusted to increase adhesion between layers of the film and to reduce adhesion between adjacent packages (Fellows & Axtell, 2003). High-density polyethylene (HDPE) is stronger, thicker, less flexible and more brittle than LDPE and a better barrier to gases and moisture. Sacks made from HDPE have high tear and puncture resistance and have good seal strength. They are waterproof and chemically resistant and are increasingly used instead of paper or sisal sacks.

3.3 Polypropylene

Polypropylene is a clear glossy film with a high strength and puncture resistance. It has a moderate barrier to moisture, gases and odours, which is not affected by changes in humidity. It stretches, although less than polyethylene. It is used in similar applications to LDPE. Oriented polypropylene is a clear glossy film with good optical properties and a high tensile strength and puncture resistance (Bowditch, 1997). It has moderate permeability to gases and odours and a higher barrier to water vapour, which is not affected by changes in humidity. It is widely used to pack biscuits, snackfoods and dried foods (Hirsch, 1991).

3.4 Other films

Polyvinylidene chloride is very strong and is therefore used in thin films. It has a high barrier to gas and water vapour and is heat shrinkable and heat sealable. However, it has a brown tint which limits its use in some applications. Polyamides (or Nylons) are clear, strong films over a wide temperature range (from – 60 to 200°C) that have low permeability to gases and are greaseproof. However, the films are expensive to produce, require high temperatures to heat seal, and the permeability changes at different storage moistures. They are used with other polymers to make them heat sealable at lower temperatures and to improve the barrier properties, and are used to pack meats and cheeses (Paine & Paine, 1992).

3.5 Coated films

Films are coated with other polymers or aluminium to improve their barrier properties or to impart heat sealability. For example a nitrocellulose coating on both sides of cellulose film improves the barrier to oxygen, moisture and odours, and enables the film to be heat sealed when broad seals are used. Packs made from cellulose that has a coating of vinyl acetate are tough, stretchable and permeable to air, smoke and moisture. They are used for packaging meats before smoking and cooking. A thin coating of aluminium (termed 'metallisation') produces a very good barrier to oils, gases, moisture, odours and light (Lamberti and Escher, 2007). This metallised film is less expensive and more flexible than plastic/aluminium foil laminates (Lamberti & Escher, 2007).

3.6 Laminated films

Lamination (bonding together) of two or more films improves the appearance, barrier properties or mechanical strength of a package (Ramsland, 1989).

3.7 Coextruded films

Coextrusion is the simultaneous extrusion of two or more layers of different polymers to make a film. Coextruded films have three main advantages over other types of film: they have very high barrier properties, similar to laminates but produced at a lower cost; they are thinner than laminates and are therefore easier to use on filling equipment; and the layers do not separate. There are three main groups of polymers that are coextruded:

- Low-density and high-density polyethylene, and polypropylene.
- Polystyrene and acrylonitrile-butadiene-styrene.
- Polyvinyl chloride.

Typically,a three-layer coextrusion has an outside layer that has a high gloss and printability, a middle bulk layer which provides stiffness and strength, and an inner layer which is suitable for heat sealing. They are used, for example, for confectionery, snack-foods, cereals and dried foods. Thicker coextrusions (75 - 3000 μm) are formed into pots, tubs or trays.

4. Polymer films for packaging foodstuffs

Polymeric films have the most application in industry and are used in many packaging applications specially greenhouse and agricultural. In agricultural products that is the important subject in packaging, there are specific products include cereal, spices, edible oils, drinking water, chocolate and confectionery, fruits and vegetables, marine products and many more. So, there are various food items those are effectively and economically packed in various types of plastic packaging materials.

4.1 Physical properties of polymers

Physical properties of polymers include the degree of polymerization, molar mass distribution, crystallinity, as well as the thermal phase transitions:

- Tg, glass transition temperature
- Tm, melting point (for thermoplastics).

A plastic film suitable for use in fabricating a trash bag must exhibit strong physical properties in order to resist internal and external stresses on the bag. Such a bag could also be suitable for use as a container for shipping goods. In addition to resisting stresses, it is highly advantageous if the plastic film is easily heat sealable in order to simplify the manufacturing operations for producing the bags. The heat sealed seams must be strong and be capable of resisting stresses tending to break the seams (Liu et al., 2004).

4.1.1 Packaging polymers for preventing penetration of pest insects

Although finished products can be shipped from production facilities uninfested, stored product insects can enter packaged goods during transportation, storage in the

warehouse, or in retail stores. As from storage to consumption by consumers, the agriculture products are exposed to attack by pest insects. Insects are the most serious pests that can contaminate the food by penetration of products in warehouses. The packaging of products is the last line of defense for processors against insect infestation of their finished products. There are two types of insects that attack packaged products: ''penetrators'', which are insects that can bore holes through packaging materials; and ''invaders'', which are insects that enter packages through existing holes, such as folds and seams and air vents (Highland, 1984; Newton, 1988). The most insects use their sense of olfaction to find food. The foodstuffs packages are made of different materials such as sheeted polymers which are used for packaging the agricultural products in order to prevention of entrance of pests. Consumer-size food packages vary considerably in their resistance to insects. Sometimes the contamination was created by entrance of one infested package. When neglected, such an infestation will serve as a source of infestation for other commodities in the storage area. So, the packaging polymers should not only be resistance to insects, but also should be permeable to gases used for disinfecting in stores. Thus, the polymer thickness and manner of placing packages in storage should be corrected to prevent serious damage in the products (Cline, 1978). Although, the polymer`s kind is more important than thickness. In a study determined that the difference between thicknesses of 16.5 and 29 µm is significant (Fig. 1). This figure shows that the ability of species to penetrate materials may vary between life stages (Allahvaisi, 2010).

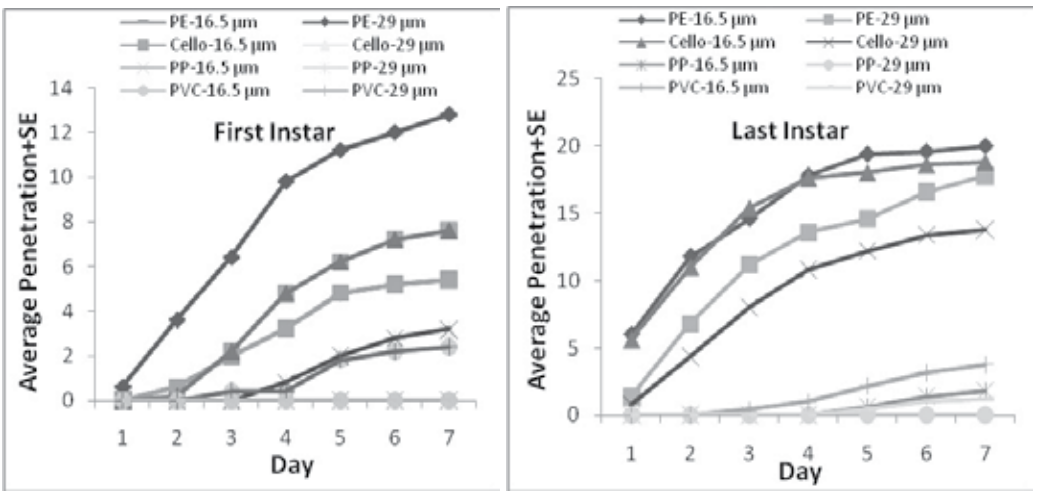

(PE=polyethylene, PP=polypropylene, PVC=polyvinylchloride and Cello=cellophane)

Fig. 1. Number of first and last instar larvae of *S. cerealella* that penetrated tested polymeric pouches with two thick in lack of food conditions during 7-d period

As, remaining constant and subsequently decreasing the slope of the curves at insects' penetration last days (after maximum penetration) prove that insects always attempt to penetrate new food packages and their high activity is for availability to more food sources. In bottom table you see the permeability percentage of four current polymers for packaging foodstuffs in two thicknesses to some stored-pest insects starved.

Pest insecs`s penetration in polymeric packagings (Average±SE)									
Polymer		Polyethylene		Cellophane		Polyvinyl chloride		Polypropylene	
Thickness (µm)		16.5	29	16.5	29	16.5	29	16.5	29
T. castaneum	A	12±0.45	4.2±0.36	13.8±0.5	6.4±0.76	3.6±0.4	0.0±0.0	0.0±0.0	0.0±0.0
	[1]	a	b	a	c	c	d	d	d
	F	0.0±0.0	0.0±0.0	0.0±0.0	0.0±0.0	0.0±0.0	0.0±0.0	0.0±0.0	0.0±0.0
	L	11.45±0.0	3.8±0.36	10.6±0.4	3.4±0.4	0.0±0.0	0.0±0.0	0.0±0.0	0.0±0.0
	[2]								
O. surinamensis	A	4±0.54	0.0±0.0	0.0±0.0	0.0±0.0	0.0±0.0	0.0±0.0	0.0±0.0	0.0±0.0
	[4]								
C. maculates	A	9±0.31	2.4±0.22	6.2±0.36	5.4±0.22	0.0±0.0	0.0±0.0	0.0±0.0	0.0±0.0
	[3]								
T. granarium	A	0.0±0.0	0.0±0.0	0.0±0.0	0.0±0.0	0.0±0.0	0.0±0.0	0.0±0.0	0.0±0.0
	F	15.6±0.5	9.2±0.5	12.2±0.5	3.6±0.22	2.4±0.24	0.0±0.0	0.0±0.0	0.0±0.0
	[1]	a	c	b	d	e	f	f	f
	L	20±0.5	19.2±0.4	20±0.002	18.2±0.4	10±0.45	2.4±0.7	3.6±0.93	0.0±0.0
	[1]	a	a	a	a	b	c	c	d
B. amydraula	F	8.8±0.36	3.6±0.22	5.8±0.36	5.8±0.36	1.8±0.2	0.0±0.0	0.0±0.0	0.0±0.0
	[1]	b	d	a	d	c	e	d	f
	L	20±0.002	18.02±0.32	19.4±0.22	18.6±0.4	7.6±0.22	5.4±0.22	10.4±0.22	3.4±0.22
	[1]	a	a	a	a	b	d	c	e

([1]: Being Bilateral Effect and Duncan's Test Grouping , [2]: Disbilateral Effect of Polymer and Thickness , A: Adult, F: First Instar Larvae , L: Last Instar Larvae , [3]: Being Bilateral Effect , [4]: T-value)

Table 2. Average permeability percentage of different polymers to major stored-product insects in state of without food

Packaging polymers with repellents for preventing penetration of pest insects

In addition to improving the packaging material and design, insect repellents are used to prevent insects from entering packages by modifying the behavior of insects (Highland, 1984; Mullen, 1994; Watson and Barson, 1996; Mullen and Mowery, 2000). Pyrethrins synergized with piperonyl butoxide were approved for use as a treatment for insect-resistant packaging on the outer layer of packages or with adhesive in the USA (Highland, 1991). The repellency of pyrethrins was the primary mode of action against insect penetration and invasion (Laudani & Davis, 1955). Methyl salicylate, an insect repellent, has been registered to be used in food packaging to control stored-product insects in the USA (Radwan & Allin, 1997). DEET, neem, and protein-enriched pea flour are repellent to manystored-product insects when tested by exposure on filter paper or in preference chambers (Khan & Wohlgemuth, 1980; Xie et al., 1995; Fields et al., 2001). Included in the construction of the multiple-wall bags was a barrier layer that prevented the migration of repellents into the foodstuffs. So, a resistant polymer to insect`s penetration with a repellent of pests is the most suitable cover for packaging because it can prevent insect penetration and can be as a safe method for IPM programs which could in further reduce the application of the synthetic chemical pesticides and prevent the infestation of the stored-product pests. In some researches polypropylene polymer films are introduced as a suitable polymer with repellent for controlling the pest insects of stored-products. Research performed by Hou and colleagues (2004) showed that the repellents such as DEET reduce the number of insects entering the envelopes (Table 3).

Insect	Number of insects		χ^2	*P*
	Treated	Untreated		
Sitophilus oryzae	270.3	18973	735.82	<0.0001
Tribolium castaneum	1773	10178	197.88	<0.0001
Cryptolestes ferrugineus	470.7	117728	354.1	<0.0001
Oryzaephilus surinamensis	1173	10078	246.77	<0.0001
All insects	3475	507731	1481.56	<0.0001

Table 3. Number of insects (±SEM) in envelopes treated with DEET at 50 ml/envelope, 1 week after insects were released (n = 4)

4.2 Chemical properties of polymers

The attractive forces between polymer chains play a large part in determining a polymer's properties. Because polymer chains are so long, these interchain forces are amplified far beyond the attractions between conventional molecules. Also, longer chains are more amorphous (randomly oriented). Polymers can be visualised as tangled spaghetti chains - pulling any one spaghetti strand out is a lot harder the more tangled the chains are. These stronger forces typically result in high tensile strength and melting points. The intermolecular forces in polymers are determined by dipoles in the monomer units. Polymers containing amide groups can form hydrogen bonds between adjacent chains; the positive hydrogen atoms in N-H groups of one chain are strongly attracted to the oxygen atoms in C=O groups on another. These strong hydrogen bonds result in, for example, the high tensile strength and melting point of Kevlar (Anonymous, 2011).

4.2.1 Polymers and permeability to fumigants for controlling pests through packages

In spite of the advances recorded in many aspects of stored product pest control, fumigation being a no residual chemical treatment has remained the mainstay for control of stored product pests. Therefore, it is accepted that fumigation is the most universal and the less hazardous method for maintaining of agricultural products under storage conditions (Keita et al., 2001).

Frequently products are packed in jute bags or plastic bags. Since penetration of the fumigant into the bags is a critical factor it is evident that fumigations under tarps or plastic sheeting should take into account the properties of the packaging materials. For controlling the insect pests by fumigants, the gas must penetrate from the air-space beneath the tarps into the bags containing the stored products. The passage of gas through these polymers to lower layers for eradicating the contamination into packaged foodstuffs is one of the other goals of storage in long-times. Polymers with various thicknesses have different permeability to fumigants (Stout, 1983; Appert, 1987; ACIAR, 1989; Iqbal et al., 1993; Valentini, 1997; Hall, 1970; Marouf & Momen, 2004) (Table 4). So, determining the best thickness of polymer is important in packaging for controlling pests. By incomplete fumigation; specially quarantine pests into packagings can easily enter countries within packaged products. In certain cases such as dried fruit, which are packed in plastic bags, entrance of fumigant into the bags is critical in controlling stored-product insect pests that

originate in the field. Some studies are evident that polypropylene liners of less than 100μm thickness are suitable as inner liners of jute bags to allow the fumigant to enter the bags (because of their high permeability) (Fleural – Lessard & Serrano, 1990; Sedlacek, 2001).

CO2 gas insecs`s penetration in polymeric packagings (Average±SE)								
Polymer	Polyethylene		Cellophane		Polyvinyl chloride		Polypropylene	
Thickness (μm)	16.5	29	16.5	29	16.5	29	16.5	29
	1.3±0.013	0.44±0.004	1.28±0.01	0.443±0.005	0.4±0.012	0.23±0.004	0.73±0.004	0.32±0.007
	a	b	a	c	d	f	c	e

Table 4. The tested polymers to mean permeability the polymers to CO2 gas

4.2.2 Antimicrobial polymers

The subject is covalently bonding anti-microbial agents to the surface of a selected polymer and its method of use as an anti-microbial agent to reduce surface bacterial, fungus, and/or virus count of the material it contacts (Jo et al., 2009). This can be applied to a variety of applications such as film and container packaging of foodstuffs, cosmetics, medical equipment and devices, environmental, hygienic and sanitary applications, as well as other consumer and commercial use (Kenaway et al., 2007). So, the applied polymers for packaging should be have the ability of coating to materials like nano metals such as silver nanoparticles to gain antimicrobial properties because in usual conditions, there is much growth of microbe agents on packaging polymers (Fig. 2).

Edible coatings have long been known to protect perishable food products from deterioration by retarding dehydration, suppressing respiration, improving textural quality, helping retain volatile flavor compounds and reducing microbial growth (Debeaufort et al., 1998). Specially formulated edible coatings may provide additional protection against contamination of microorganism while serving the similar effect as modified atmosphere storage in modifying internal gas composition (Park, 1999). Among noble-metal nanomaterials, silver nanoparticles have received considerable attentions due to their attractive physicochemical properties. It is well known that silver in various chemical forms has strong toxicity to a wide range of microorganisms (Liau et al., 1997). The larger surface area of silver nanoparticles can improve their antibacterial effectiveness against 150 types of microbes. Although the coating has been extensively studied to increase the shelf life of many agricultural products, little information is available regarding the application of silver nanoparticles-polymers coating for these products.

On the other hand, antimicrobial Polymers, known as polymeric biocides, are a class of polymers with antimicrobial activity, or the ability to inhibit the growth of microorganisms such as bacteria, fungi or protozoans (Fig. 3). In this figure, normal bacterial membranes (panel a) are stabilized by Ca+2 ions binding anionic charged phospholipids. NIMBUS™ quat-polymer rapidly displaces Ca+2 (panel b) leading to loss of fluidity (panel c) and eventual phase separation of different lipids. Domains in the membrane then undergo a transition to smaller micelles. These polymers have been engineered to mimic antimicrobial peptides which are used by the immune systems of living things to kill bacteria. Typically, antimicrobial polymers are produced by attaching or inserting an active antimicrobial agent onto a polymer

backbone via an alkyl or acetyl linker. Antimicrobial polymers may enhance the efficiency and selectivity of currently used antimicrobial agents, while decreasing associated environmental hazards because antimicrobial polymers are generally nonvolatile and chemically stable. This makes this material a prime candidate for use in areas of medicine as a means to fight infection, in the food industry to prevent bacterial contamination, and in water sanitation to inhibit the growth of microorganisms in drinking water (Pyatenko et al., 2004).

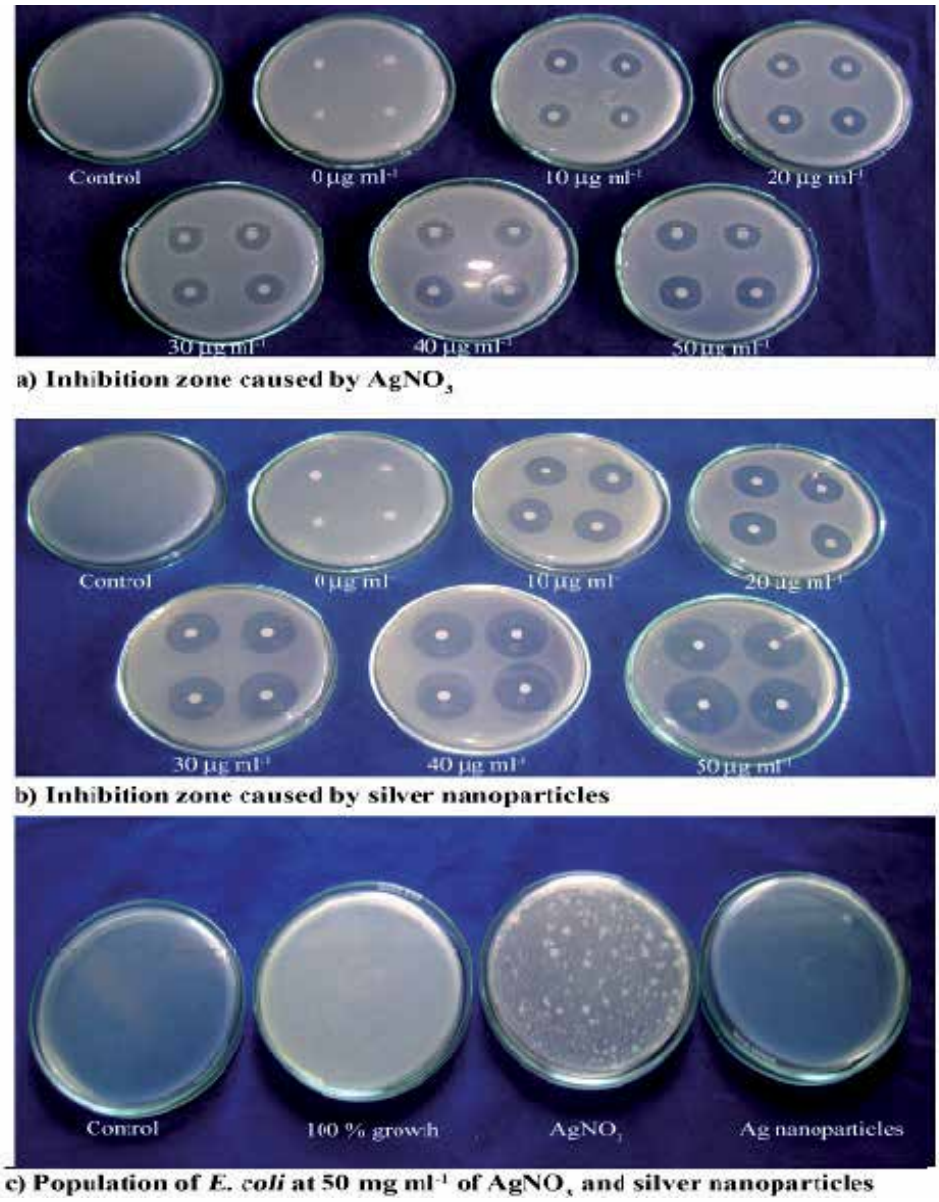

Fig. 2. Comparison of E.coli growth inhibition by AgNO3 and silver nanoparticles (Parameswari et al., 2010)

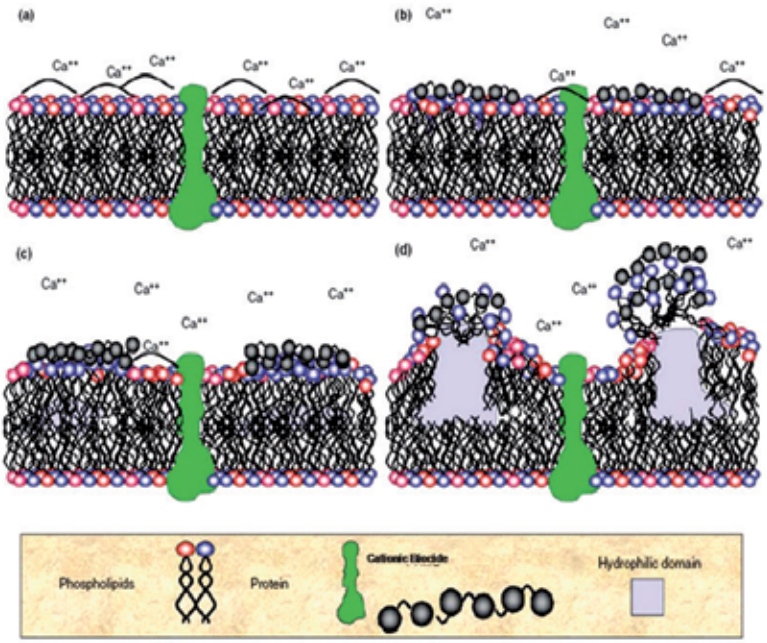

Fig. 3. Action of polymeric cationic biocidal agent (Gilbert and Moore, 2005)

4.2.3 Edible films and coatings

An edible film or coating is simply defined as thin continuous layer of edible material formed on, placed on or between foods or food components (Torres, 1994). Edible packaging refers to the use of edible films, coatings, pouches, bags and other containers as a means of ensuring the safe delivery of food product to the consumer in a sound condition (McHugh & Krochta, 1994). These films can also act as carrier of antioxidant, flavour and bacteriostats and can improve mechanical integrity of food products (Pathania, 2000). Since, package is an integral part of the whole food product, therefore, the composition of the edible packaging must meet with the following specific functional requirements:

- Neutral organoleptic properties (clear, transparent, odourless, tasteless etc.)
- Water vapour tightness to prevent desiccation.
- Good barrier against microbial invasion to reduce spoilage and decay.
- Predetermined permeability to water vapour, O_2 and CO_2 to have complete control over the water and gas exchanges between the product and surrounding atmosphere.
- Good mechanical characteristics (like tensile and yield strength, Spencer impact elongation, etc.) to impart abuse resistence.
- Enchance the surface appearance (e.g. brilliance) and tactile characteristics (e.g. reduced stickiness) of foods (Kaushik, 1999).

4.2.4 Nanotechnology applications in foodstuffs packaging polymers

The development of nanodevices and nanomaterials could open up novel applications in agriculture (Scrinis & Lyons, 2007). Nanophasic and nanostructured materials are attracting

a great deal of attention because of their potential for achieving specific processes and selectivity, especially in biological and pharmaceutical applications (Pal et al., 2007). Nanotechnology derived food packaging materials are the largest category of current nanotechnology applications for the food sector. The main applications for food contact materials (FCMs) including:

1. FCMs incorporating nanomaterials to improve packaging properties (flexibility, gas barrier properties, temperature/moisture stability).
2. ''Active'' FCMs that incorporate nanoparticles with antimicrobial or oxygen scavenging properties.
3. ''Intelligent''food packaging incorporating nanosensors to monitor and report the condition of the food.
4. Biodegradable polymer–nanomaterial composites (Chaudhry et al., 2008).

Polymer composites are mixtures of polymers with inorganic or organic fillers with certain geometries (fibers, flakes, spheres, particulates). The use of fillers which have at least one dimension in the nanometric range (nanoparticles) produces polymer nanocomposites. Three types of fillers can be distinguished, depending on how many dimensions are in the nanometric range. Isodimensional nanoparticles, such as spherical silica nanoparticles or semiconductor nanoclusters, have three nanometric dimensions. Nanotubes or whiskers are elongated structures in which two dimensions are in the nanometer scale and the third is larger. When only one dimension is in the nanometer range, the composites are known as polymer-layered crystal nanocomposites, almost exclusively obtained by the intercalation of the polymer (or a monomer subsequently polymerized) inside the galleries of layered host crystals (Azeredo, 2009). There are three common methods used to process nanocomposites: solution method, *in situ* or interlamellar polymerization technique, and melt processing. The solution method can be used to formboth intercalated and exfoliated nanocomposite materials. In the solution method, the nanocomposite clay is first swollen in a solvent. Next, it is added to a polymer solution, and polymer molecules are allowed to extend between the layers of filler. The solvent is then allowed to evaporate. The *in situ* or interlamellar method swells the fillers by absorption of a liquid monomer. After the monomer has penetrated in between the layers of silicates, polymerization is initiated by heat, radiation, or incorporation of an initiator. The melt method is the most commonly used method due to the lack of solvents. In melt processing, the nanocomposite filler is incorporated into a molten polymer and then formed into the final material (Brody et al., 2008). The results of tests performed by An and colleagues (2008) shown in Fig. 4 revealed the evidence for the formation of silver nanoparticles in the coating solutions prepared under the experimental condition. The solutions with PVP formed a thin coating on the surface of asparagus when water evaporated, leaving the nanoparticles evenly distributed in the coating matrix (Jianshen et al., 2008).

Nanocomposite packages are predicted to make up a significant portion of the food packaging market in the near future. Silver is well known for its strong toxicity to a wide range of microorganisms (Liau et al., 1997), besides some processing advantages such as high temperature stability and low volatility (Kumar & Münstedt, 2005). Silver nanoparticles have been shown to be effective antimicrobials (Aymonier et al., 2002; Sondi & Salopek-Sondi, 2004; Son et al., 2006; Yu et al., 2007; Tankhiwale & Bajpai, 2009), even more effective than larger silver particles, thanks to their larger surface area available for

interaction with microbial cells (An et al., 2008; Kvítek et al., 2008). In fact, the most common nanocomposites used as antimicrobial films for food packaging are based on silver nanoparticles, whose antimicrobial activity has been ascribed to different mechanisms, namely: (a) adhesion to the cell surface, degradation of lipopolysaccharides and formation of ''pits'' in the membranes, largely increasing permeability (Sondi & Salopek-Sondi, 2004); (b) penetration inside bacterial cell, damaging DNA (Li et al., 2008); and (c) releasing antimicrobial Ag+ ions by dissolution of silver nanoparticles (Morones et al., 2005). The latter mechanism is consistent with findings by Kumar & Münstedt (2005), who have concluded that the antimicrobial activity of silverbased systems depends on releasing of Ag+, which binds to electron donor groups in biological molecules containing sulphur, oxygen or nitrogen. Besides the antimicrobial activity, silver nanoparticles have been reported to absorb and decompose ethylene, which may contribute to their effects on extending shelf life of fruits and vegetables (Li et al., 2009).

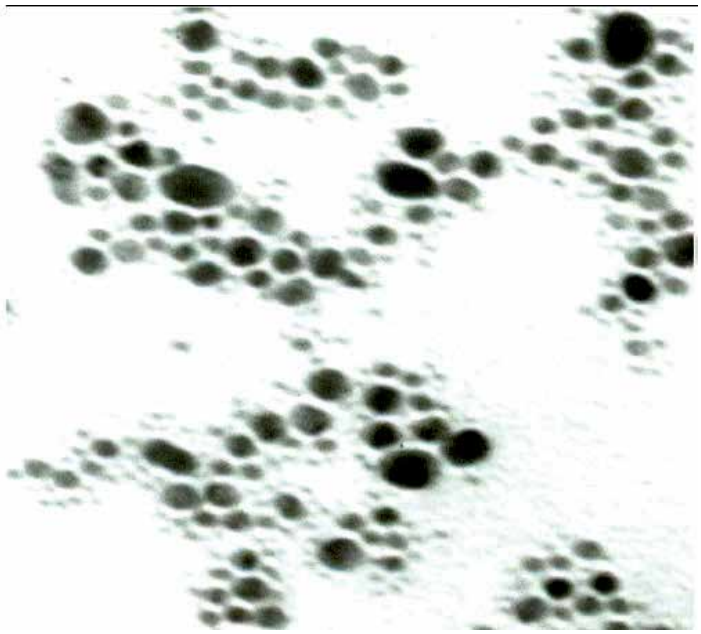

Fig. 4. Transmission electron microscopy (TEM) of silver nanoparticles (×100,000) (An et al, 2008)

5. Suitable polymer for stored-product packaging

Plastics based on Polypropylene, Polyethylene, Polyvinyl Chloride and Cellophane, hugely used for packagings, has some of these properties but this is different at them. For example, these polymers rank generally from the easiest to the most difficult to penetration against insect pests; Cellophane, polyethylene, Polyvinylchloride and Polypropylene. The least penetration is carried out in PP and PVC polymers. Foodstuffs packaged by polymer films of PP and PVC could provide the conditions and so, by suitable packaging the stored pest insects do not access to food and without food they become extinct. But in the comparison between polypropylene and polyvinylchloride, PVC isn't a safe polymer for packaging

foodstuffs in order to release HCl gas and the only importance of PVC in storage industry is often to be used as a gas-tight cover on agricultural products to keep a suitable concentration of gas and it is important for controlling quarantine pests. Furthermore, other two polymers, Polyethylene and Cellophane have a high permeability to gases but a very low resistance to pests as the product packaged into them becomes more contamination than ones into PVC and PP. The polymer films of Polyethylene and Cellophane; specially Cellophane, is greatly used for packaging the products be consumed daily. Moreover, Cellophane is 100% biodegradable. Some studies show that polypropylene had a good degradability in environment in comparative to polyethylene and polyvinylchloride. Also, new studies show that polypropylene has a suitable property for coating with nano metals and repellents for decreasing the losses of stored-products in effect of pest infestation. Hence, according to the investigations of researchers (in above) polypropylene usually is used as a suitable cover for packaging foodstuffs in stores and has perfect physical and chemical properties for the packaging works which should be performed in stores of maintaining foodstuffs.

6. Polypropylene as packaging polymer

PP known as polypropene, is one of those most versatile polymers available with applications, both as a plastic and as a fibre, in virtually all of the plastics end-use markets. Professor Giulio Natta produced the first polypropylene resin in Spain in 1954. Natta utilised catalysts developed for the polyethylene industry and applied the technology to propylene gas. Commercial production began in 1957 and polypropylene usage has displayed strong growth from this date. PP is a linear hydrocarbon polymer, expressed as

Polypropylene	
IUPAC name poly(propene)	
Other names Polypropylene; Polypropene; Polipropene 25 [USAN];Propene polymers; Propylene polymers; 1-Propene	
Identifiers	
CAS number	9003-07-0
Properties	
Molecular formula	$(C3H6)_n$
Density	0.855 g/cm3, amorphous 0.946 g/cm3, crystalline
Melting point	130–171°C
(what is this?) (verify) Except where noted otherwise, data are given for materials in their standard state (at 25°C, 100 kPa)	

C_nH_{2n}. PP, like polyethylene (see HDPE, L/LLDPE) and polybutene (PB), is a polyolefin or saturated polymer. (Semi-rigid, translucent, good chemical resistance, tough, good fatigue resistance, integral hinge property, good heat resistance). PP does not present stress-cracking problems and offers excellent electrical and chemical resistance at higher temperatures. While the properties of PP are similar to those of Polyethylene, there are specific differences. These include a lower density, higher softening point (PP doesn't melt below 160^{o}C, Polyethylene, a more common plastic, will anneal at around 100^{o}C) and higher rigidity and hardness (Cacciari, 1993). Additives are applied to all commercially produced polypropylene resins to protect the polymer during processing and to enhance end-use performance. PP is a thermoplastic which is commonly used for plastic moldings, stationary folders, packaging materials, plastic tubs, non-absorbable sutures, diapers etc. PP can be degraded when it is exposed to ultraviolet radiation from sunlight. Furthermore, at high temperatures, PP is oxidized. The possibility of degrading PP with microorganisms has been investigated.

Three main types of PP polymer types are used in household packaging:

1. Homopolymer PP: this is a translucent polymer, with high Heat Distortion Temperature (HDT), with a lower impact strength (particularly at low temperatures) and is used for applications such as closures and soup pots;
2. Block copolymer PP: this polymer has a lower transparency and generally a lower HDT, with a higher impact strength (particularly at low temperatures) and is used for applications such as ice cream containers and for chilled foods;
3. Random copolymer PP: this polymer has a high transparency and the lowest HDT. It is a product with the greatest flexibility and possesses reasonable impact strength. Typical applications requiring high transparency are bottles and salad bowls; Homopolymer and copolymer (random and block) PP polymer types may be used with either of the two main types of moulding process (extrusion/thermoforming or extrusion blow moulding) and therefore can be made with different melt flow characteristics as follows:
4. Thermoforming and blow moulding: used for meat trays and bottles, with a low MFR (Melt Flow Rate) (1 to 4);
5. Injection moulding: used for thin walled packaging, such as soup pots, with a high MFR (33 and higher).

Thus, Polypropylene is a thermoplastic polymer used in a wide variety of applications including packaging, textiles (e.g. ropes, thermal underwear and carpets), stationery, plastic parts and reusable containers of various types, laboratory equipment, loudspeakers, automotive components, and polymer banknotes. An addition polymer made from the monomer propylene, it is rugged and unusually resistant to many chemical solvents, bases and acids. The versatility of the polymer (the ability to adapt to a wide range of fabrication methods and applications) has sustained growth rates enabling PP to challenge the market share of a host of alternative materials in plethora of applications. In 2007, the global market for polypropylene had a volume of 45.1 million tons, which led to a turnover of about 65 billion US-dollars (47.4 billion Euro) (Kenaway et al., 2007). PP films are used in household paper packing, stationery packaging, portfolios and food packaging. In stationer industry, they are used for photo albums and page protectors. PP films are used as a lamination layer, both as sealant and as heat resistant layer and in the pressure sensitive industry for adhesive coating and diaper closures. Various packaging of products could be made of this film.

7. Conclusion

According to the results of performed works in the field of packaging, it is proved that a polymeric cover usually made of polypropylene with thickness <100 µm is the most suitable one for foodstuffs packaging. In the less thickness, some polymers have less resistant to the infestation of pest insects although polypropylene shows resistance well ever in lower thicknesses. Such cover would undoubtedly reduce the danger of crossinfestation and on the one hand, propylene is permeable to stored gases such as phosphine for ruining the contaminations into stored products and has the ability of coating to nano metals in the thickness and thus could obtain the antimicrobial properties. Also, propylene has a good degradability among polyolefines. A consultation exercise with the PP packaging supply chain explored the levels of interest of using a food grade PP in packaging applications. Little recycled PP is currently used in packaging because little is currently available. There is certainly interest from all levels of the supply chain – retailers, brand owners, food manufacturers and packaging manufacturers – in using recycled PP, if a recycling system existed that could meet regulatory standards and company food performance standards (Anonymous, 2010). Such a change would undoubtedly reduce the too using of chemical pesticides and increase the storages food maintaining and therefore reduce economic losses associated with infestation and minimize injury to company image as a manufacture of high quality foodstuffs.

8. Acknowledgment

I would like to thank Ms. H. Salimizand, Dr. A.A. Pourmirza and Dr. M.H. Safaralizade for considerable assistance. I also acknowledge younger researchers club of Sanandaj for some facilities.

9. References

[1] Aciar, A. (1989). Suggested recommendations for the fumigation of grain in the ASEAN region, Part 1. *Principles and General Practice. 131 pp, ISSN 1832-1879.*

[2] Appert, J. (1987). The storage of food grains and seeds. *Macmillan. London, 146 pp, ISBN 13: 9780333448274.*

[3] Allahvaisi, S.; Pourmirza, A.A. & Safaralizade, M.H. (2009). Packaging of Agricultural Products for Preventing Tobacco Beetles Contaminations. *Notul. B. Horti Agrobo. Cluj-N. 37(2): 218-222, ISSN 0255-965X.*

[4] Allahvaisi, S.; Pourmirza, A.A. & Safaralizade, M.H. (2010). The study on polymers permeability for foodstuffs packaging by some serious species of stored pest insects and phosphine gas. *J. Agri. Tech. 6 (4): 747-759, ISSN 1680-7073.*

[5] An, J.; Zhang, M.; Wang, S. & Tang, J. (2008). Physical, chemical and microbiological changes in stored green asparagus spears as affected by coating of silver nanoparticles-PVP. *LWT – Food Science and Technology. 41(6): 1100– 1107, ISSN 0023-6438.*

[6] Anonymous. (2008). Packaging materials for food. *Technical Brief, Practical Action.*

[7] Anonymous. (2010). Scoping study into food grade polypropylene recycling. *Available in:* www.wrap.org.uk/foodgradepp,

[8] Anonymous. (2011). Plastics in food packaging in India.

[9] Anonymous. (2011). Physical and chemical properties of polymers. *Available in: Plastics.indiabizclub.com.*

[10] Aymonier, C.; Schlotterbeck, U.; Antonietti, L.; Zacharias, P.; Thomann, R. & Tiller, J.C. (2002). Hybrids of silver nanoparticles with amphiphilic hyperbranched macromolecules exhibiting antimicrobial properties. *Chemi. Commun. 24: 3018–3019, ISSN 1364-548X.*

[11] Azeredo, H.M.C. (2009). Nanocomposites for food packaging applications. *Food Res. Intern. 42(9): 1240-1253, ISSN 0963-9969, ISSN 0963-9969.*

[12] Bowditch, T.G. (1997). Penetration of Polyvinyl Choloride and Polypropylene Packaging Films by *Ephestia cautella* (*Lepidoptera: Pyralidae*) and *Plodia interpunctella* (*Lepidoptera: Pyralidae*) Larvae, and *Tribolium confusom* (*Coleoptera: Tenebrionida*e). *J. Eco. Entomol. 90(4):1028-101, ISSN 0022-0493.*

[13] Brody, A.; Bugusu, B.; Han, J.H.; Sand, C.K. & Machugh, T.H. (2008). Inovative food packaging solutions. *J. Food Sci. 73(8): 107 - 116, ISSN 1750-3841.*

[14] Cacciari, I.; Quatrini, P.; Zirletta, G.; Mincione, E.; Vinciguerra, V.; Lupatelli & P.; Sermanni, G.G. (1993). Isotactic polypropylene biodegradation by a microbial community: Physico-chemical characterization of metabolites produced. *Appl. Environ. Microbiol. 59: 3695-3700, ISSN 0099-2240.*

[15] Chaudhry, Q. (2008). "Applications and Implications of Nanotechnologies for the Food Sector." *Food Addi. and Contami. 25(3): 241–258, ISSN 1464–5122.*

[16] Chiellini, E. (2008). Environmentally-compatible Food Packaging. *Woodhead Publishing, Cambridge, ISSN 1811-5209.*

[17] Cline, L.D. (1978). Penetration of seven common packaging materials by larvae and adults of eleven species of stored-product insects. *J. Eco. Entomol. 71:726-729, ISSN 0022-0493.*

[18] Debeaufort, F.; Quezada-Gallo, J.A. & Voilley, A. (1998). Edible films and coatings: Tomorrow's packaging: A review. *Critical revi. In Food Sci. 38:299–313, ISSN 1750-3841.*

[19] Fellows, P.J. & Axtell, B.L. (2003). Appropriate Food Packaging: Materials and methods for small businesses. *2nd Edn. Practical Action Publishing, ISSN 0254-6019.*

[20] Fields, P.G; Y.S., Xie & Hou, X. (2001). Repellent effect of pea (Pisum sativum) fractions against stored-product insects. *J. Stored Pro. Res. 37: 359–370, ISSN 0022-474X.*

[21] Fleural – Lessard, F. & Serrano, B. (1990). Resistance to insect perforation of plastic films for stored – product packing, "methodological study on tests with rice weevil and layer grain borer. *Sci. Aliments. 10(3): 521-532, ISSN 0240-8813.*

[22] Gilbert, P. and L. E., Moore. 2005. Cationic Antiseptics: diversity of action under a common epithet, *J. Appl. Microbiol. 99(4):703-15, ISSN 1365-2672.*

[23] Hall, D.W. (1970). Handling and storage of food grains in tropical and subtropical areas. *FAO, Rome, 350 pp, ISSN 1045-7127.*

[24] Highland, H.A. (1975). Insect-resistant textile bags: new construction and treatment techniques. *USDA Technical Bulletin, pp.1511, ISSN 0082-9811.*

[25] Highland, H.A. (1981). Resistant barriers for stored- product insects. In: CRC Handbook of transportation and marketing in agriculture. *Vol. 1: Food commodities, 41-45, ISSN 0817-8038.*

[26] Highland, H.A. (1984). Insect infestation of packages, 311-320 pp. In: F. J. Baur (Eds.). Insect Management for Food Processing. *American Association of Cereal Chemists, St. Paul, MN, ISSN 0714-6221.*

[27] Highland, H.A.; Kamel, A.H.; Sayed, M.M.EL.; Fam, E.Z.; Simonaitis, R. & Cline, L.D. (1984). Evaluation of permethrin as an insect-resistant treatment on paper bags and of tricalcium phosphate as a suppressant of storedproduct insects. *J. Eco. Entomol. 77: 240–245, ISSN 1938-291X.*

[28] Highland, H.A. (1991). Protecting packages against insects. In: Gorham, J.R. (Ed.), Ecologyand Management of Food-Industry Pests. *Association of Official Analytical Chemists, Arlington, VA, pp. 345–350, ISSN 1516-8913.*

[29] Hirsch, A. (1991). Flexible Food Packaging. *Van Nostrand Reinhold, New York, ISSN 1092-3659.*

[30] Hou, X.; Fields, P. & Taylor, W. (2004). The effect of repellents on penetration into packaging by stored-product insects. *J. Stored Prod. Res. 40: 47–54, ISSN 0022-474X.*

[31] Iqbal, J.; Irshad, & Khalil, S.K. (1993) Sack fumigation of wheat under polythene sheets. *Sarhad J. Agri. IX (5): 399-402, ISSN 1016-4383.*

[32] Jakic-Dimic, D.; Nesic, K. & Petrovic, M. (2009): Contamination of cereals with aflatoxins, metabolites of fungi *Aspergillus flavus*. Biotech. *In Animal Husba. 25: 1203–1208, ISSN 0378-4320.*

[33] Jianshen A.; Min, Zh.; Shaojin, W. & Juming, T. (2008). Physical, chemical and microbiological changes in stored green asparagus spears as affected by coating of silver nanoparticles-PVP. *J. scin. dir. 41:1100–1107, ISSN.*

[34] Jo, Y.; Kim, B. & Jung, G. (2009). Antifungal activity of silver ions and nanoparticles on phytopathogenic fungi. *Plant Disease. 93:1037-1043, ISSN 0191-2917.*

[35] Khan, M.A. & Wohlgemuth, R. (1980). Diethyltoluamide as a repellent against stored-products pests. *Anzeiger fur Schadlingskunde Pflanzenschutz Umweltschutz 53, 126–127, ISSN 1439-0280.*

[36] Keita, S.M.; Vincent, C.; Schmit, J.; Arnason, J.T. & Belanger, A. (2001). Efficacy of essential oil of *Ocimum basilicum* L. and *O. gratissimum* L. applied as an insecticidal fumigant and powder to control *Callosobruchus maculatus* (Fab.) (Coleoptera: Bruchidae). *J. Stored Prod. Res. 37: 339-349, ISSN 0022-474X.*

[37] Kenaway, El-Refaie; Worley, S.D. & Roy, B. (2007). "The Chemistry and Applications of Antimicrobial Polymers: A State of the Art Review". BioMacromolecules (American Chemi. Soc.). 8 (5): 1359–1384, ISSN 0002-7863.

[38] Kumar, R. & Munstedt, H. (2005). *Silver ion release from antimicrobial polyamide/silver composites. Biomaterials. 26: 2081– 2088, ISSN 0142-9612.*

[39] Kvitek, L.; Panac_ek, A.; Soukupova, J.; Kolarˇ, M.; Vec_erˇova, R. & Prucek, R. (2008). Effect of surfactants and polymers on stability and antibacterial activity of silver nanoparticles (NPs). *J. Physi. Chemi. C. 112(15): 5825–5834, ISSN 1932-7455.*

[40] Lamberti, M. & Escher, F. (2007). Aluminium foil as a food packaging material in comparison with other materials. *Food Rev. Intern. 23 (4): 407-433, ISSN 8755-9129.*

[41] Laudani, H. & Davis, D.F. (1955). The status of federal research on the development of insect-resistant packaging. *TAPPI. 38: 322–326, ISSN 0734-1415.*

[42] Li, H.; Li, F.; Wang, L.; Sheng, J.; Xin, Z.; Zhao, L.; Xiao, H.; Zheng, Y. & Hu, Q. (2009). Effect of nano-packing on preservation quality of Chinese jujube (*Ziziphus jujuba* Mill. var. inermis (Bunge) Rehd). *Food Chemistry, Vol. 114, No. 2, 547-552, ISSN 0308-8146.*

[43] Li, Q.; Mahendra, S.; Lyon, D. Y.; Brunet, L.; Liga, M.V.; Li, D. & Alvarez, P.J.J. (2008). Antimicrobial nanomaterials for water disinfection and microbial control: potential applications and implications. *Water Research, 42(18): 4591– 4602, ISSN 0043-1354.*

[44] Liau, S.Y.; Read, D.C.; Pugh, W.J.; Furr, J.R. & Russell, A.D. (1997). Interaction of silver nitrate with readily identifiable groups: relationship to the antibacterial action of silver ions. *Letters in Applied Microbiology, 25: 279– 283, ISSN 1472-765X.*

[45] Liu, Ch.; Tellez-Garay, A.M. & Castell-Perez, M.E. (2004). Physical and mechanical properties of peanut protein films. J. Food Sci.and Techn. 37(7)*: 731-738, ISSN 1750-3841.*

[46] Marouf, A. & Momen, R.F. (2004). An evaluation of the permeability to phosphine through different polymers used for the bag storage of grain. *Int. Conf. Controlled Atmosphere and Fumigation in Stored Prod. Gold-Coast Australia, 8-13 August, FTIC Ltd. Publishing, Israel, ISSN 1021-9730.*

[47] McHugh, T.Habig; Avena-Bustillos, R.D. & Krochta, J.M. (1993). Hydrophilic edible films-modified procedure for water vapor permeability and explanation of thickness effects. *J. Food Sci. 58: 899–903, ISSN 1750-3841.*

[48] Morones, J.R.; Elechiguerra, J.L.; Camacho, A.; Holt, K.; Kouri, J.B. & Ramirez, J.T. (2005). The bactericidal effect of silver nanoparticles. *Nanotechnology. 16(10): 2346–2353, ISSN 1361-6528.*

[49] Mullen, M.A. & Highland, H.A. (1988). Package Defects and Their Effect on Insect Infectation of Infestation of Instant Non-fat Dry Milk. *J. Packag. Tech. 2:226-269, ISSN 1099-1522.*

[50] Mullen, M.A. & Mowery, S.V. (2000). Insect-resistant packaging. *Intern. Food Hyg. J. 11: 13–14, ISSN 0015-6426.*

[51] Newton, J. (1988). Insects and packaging—a review. Intern. Biodet. *J. 24: 175–187, ISSN 0964-8305.*

[52] Odian, G. (2004). Principles of polymerization. *USA. 4 edition, 832 pp.*

[53] Paine, F.A. & Paine, H.Y. (1992). A Handbook of Food Packaging, 2nd Edition, *Blackie Academic and Professional, London, ISSN 1532-1738.*

[54] Pal, S., Tak, Y.K. & Song, J. M. (2007). Does the antibacterial activity of silver nanoparticles depend on the shape of the nanoparticle? A study of the gram-negative bacterium *Escherichia coli. Appl. Environl. Microbiol. 73: 1712-1720, ISSN 0099-2240.*

[55] Parameswari, E.; Udayasoorian, C.; Paul Sebastian, S. & Jayabalakrishnan, R.M. 2010. The bactericidal potential of silver nanoparticles. *Intern. Res. J.Biotech. 1(3): 044-049, ISSN 2141-5153.*

[56] Park, E.-S. & Lee, H.-J. (2001). "Synthesis and biocidal activities of polymer. III. Bactericical activity of homopolymer of AcDP and copolymer of acdp with St". *J. Appl. Polym. Sci. 80 (7): 728–736, ISSN 1097-4628.*Proctor, D.L. & Ashman, F. (1972). The control of insects in exported Zambian groundnuts using phosphine and polyethylene lined sacks. *J. Stored Pro. Res. 8: 137-137, ISSN 0022-474X.*

[58] Pyatenko, A.; Shimokowa, K. & Yameguchi, M. (2004). Synthesis of silver nanoparticles by laser ablation in pure water. *J. Appl. Phys. A: Mater. Sci. Proces. A79: 803-806, ISSN 1392–1320.*

[59] Radwan, M.N. & Allin, G.P. (1997). Controlled-release insect repellent device. *US Patent 5,688,509, ISSN 0168-3659.*

[60] Ramsland, T. (J. Selin, Ed.). (1989). Handbook on procurement of packaging. *PRODEC, Toolonkatu 11A, 00100 Helsinki, Finland, ISSN 1456-4491.*

[61] Robertson, G.L. (1993). Food Packaging- principles and practice. *Marcel Dekker, New York, ISSN 0065-2415.*

[62] Scrinis, G. & Lyons, K. (2007). The emerging nano-corporate paradigm: nanotechnology and the transformation of nature, food and agri-food systems. Int. *J. Sociol. Food Agric. 15: pp. 22–44, ISSN 0798-1759.*

[63] Sedlacek, J.D.; Komaravalli, S.R.; Hanley, A.M.; Price, B.D. & Davis P.M. (2001). Life history attributes of indian meal moth (Lepidoptera: Pyralidae) and angoumois grain moth (Lepidoptera: Gelechidae) reared on transgenic corn kernels. *J. Eco. Ento. 94(2): 586-592 ISSN 0022-0493.*

[64] Son, W.K.; Youk, J.H. & Park, W.H. (2006). Antimicrobial cellulose acetate nanofibers containing silver nanoparticles. *Carbohydrate Polymers, 65, 430– 434, ISSN 0144-8617.*

[65] Sondi, I., & Salopek-Sondi, B. (2004). Silver nanoparticles as antimicrobial agent: a case study on *E. coli* as a model for Gram-negative bacteria. *J. Colloid Interf. Sci. 275: 177–182, ISSN 0021-9797.*

[66] Stewart, B. (1995). Packaging as an Effective Marketing Tool. PIRA International, Leatherhead, Surrey, UK, ISSN 1471-5694.

[67] Stout, O.O. (1983). International plant quarantine treatment manual. *Plant Production and Protection Paper, FAO, Rome, 220pp, ISSN 0259-2517.*

[68] Tankhiwale, R., & Bajpai, S.K. (2009). Graft co-polymerization onto cellulose-based filter paper and its further development as silver nanoparticles-loaded antibacterial food packaging material. *Colloid Interf. Sci. 69(2): 164-168, ISSN 0927-7765.*

[69] Taylor, R.W.D. & Harris, A.H. (1994). The fumigation of bag- stacks with phosphine under gas-proof sheets using techniques to avoid development of insect resistance. In: Proceeding of the 6th International Working Conference on Stored- Product Protection, (Edited by: Highley E., Wright E.J., Banks H.J. & Champ B.R.). *CAB International, Wallingford, UK. Vol. 1: 210-214, ISSN 1043-4526.*

[70] Torres, J. A. (1994). Edible films and coatings from proteins. Pages 467- 507 in: Protein Functionality in Food Systems. N. S. Hettiarachchy and G. R. Ziegler, eds. *Marcel Dekker: New York, ISSN 0065-2415.*

[71] Valentini, S.R.T. (1997). Eficiencia de lonas PVC e polietileno para fumigacao de graos comfosfina. *Rev.Bras. de Armaz. Vicosa, 22(1): 3-8, ISSN 1807-1929.*

[72] Watson, E. & Barson, G. (1996). A laboratoryassessment of the behavioural response of *Oryzaephilus surinamensis* (L.) (Coleoptera: Silvanidae) to three insecticides and the insect repellent N, N-diethyl-m-toluamide. *J. Stored Pro. Res. 32: 59–67, ISSN 0022-474X.*

[73] Xie, Y.S.; Fields, P.G. & Isman, M.B. (1995). Repellencyand toxicityof azadirachtin and neem concentrates to three stored-product beetles. *J. Eco. Ento. 88: 1024–1031, ISSN 0022-0493.*

[74] Yu, H.; Xu, X.; Chen, X.; Lu, T.; Zhang, P. & Jing, X. (2007). Preparation and antibacterial effects of PVA–PVP hydrogels containing silver nanoparticles. *J. Appl. Polymer Sci., 103: 125– 133, ISSN 0021-8995.*

[75] Zhang, Y., Chen, F. & Zhuang, J. (2002). Synthesis of silver nanoparticles via electrochemical reduction on Chem. *Commun. (Camb.) 7: 2814-2815, ISSN 1359-7345.*

2

Shelf Life of Jams in Polypropylene Packaging

Soraia Vilela Borges
Universidade Federal de Lavras,
Departamento de Ciência dos Alimentos,
Brazil

1. Introduction

The shelf life of a product represents the period in which the product remains in good sensory and microbiological for consumption, without harming the taste or health. These conditions are dependent on physical, chemical and microbiological that occur during storage, which depend on the nature of the product, packaging and storage conditions (temperature, relative humidity, storage time) (Man & Jones , 2000).

Jams are generally preserved by applying a combination of obstacles such as lowering the pH, the reduction of water activity by addition of solutes, heat treatment and the use of preservatives and has an expressive consumption in Brazil, given the wide variety existing fruit rich in nutrients, and versatility in the use of these products. From microbiological point of view, these products, according to the packaging and processing conditions and storage, has a shelf life that can vary from 6 months to 1 year (Tfouni & Toledo, 2002), which can be extended by adding sorbic acid and its salts that has good performance in the pH range from 4.0 to 6.0 (Jay 1996).

Among various options for these products packagings stands out the use of polypropylene due to their low water absorption and light (70% at 800nm) compared to cellophane (cheaper), support at high temperatures and low temperatures during the filling and cooling cycle without suffering deformation and be more economical compared to metal packaging (Alves et al., 2007).

Based on the above this chapter aims to report the physical, chemical, physical-chemical, microbiological and sensory occurred in different jams of tropical fruits, stored in jars of polypropylene at different temperature conditions (25-40°C).

2. Materials and methods

2.1 Processing of the jam

The fruits were sanitized with100-ppm chlorine solution, blanched and pulped in a pulper. The jams was processed according to the methodology described by Policarpo *et al*. (2003). The flowchart in Figure 1 contains the elaboration stages of the preserves. Pulp, sugars,

calcium carbonate and other ingredients were placed in a stainless steel pan and concentrated to different concentrations according to fruit (72–78°Brix) by heating with constant stirring, according to the formulation. Pectin and acid were added at the end of the cooking period. The preserve was packaged in fixed amounts (100 g) while still hot, using round polypropylene pots (6.7-cm diameter and 7.1-cm height), in cellophane, and molded in these pots, with the same dimensions.

2.2 Experimental design to determine the shelf life

A factorial experimental design: formulations x packaging materials x storage temperature x evaluation times, with two repetitions were used. The physical, chemical, physicochemical and sensorial alterations were evaluated and their means compared by Tukey's test at the 5% level of probability or by statistical models (Cochram & Cox, 1992).

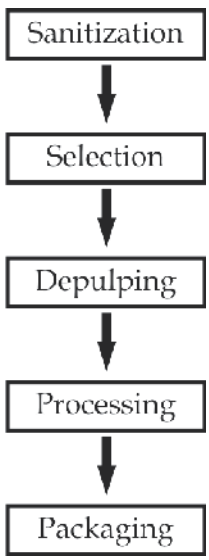

Fig. 1. Flowchart of fruit processing production

2.3 Analytical methods

Chemical and physicochemical analyses were carried out in triplicate according to the following methodologies as described by the Association of Official Analytical Chemists (AOAC 1995): total titratable acidity by titration with NaOH in the presence of phenolphthalein, total and reducing sugars by titration with the Fehling reagent, pH using a potentiometer and total soluble solids by refractometry. Soluble pectin was determined using the methodology described by Bitter and Muir (1962), based on the reaction of the pectin hydrolyzed with carbazol.

Yeasts and molds were determined according to Speak (1976), making serial dilutions with peptone water and plating on potato dextrose agar with or without 18% glucose to detect osmophilic and other species of yeast. Plates were incubated at 25–30 C, and the results were analyzed after 48 and 72 h of incubation and expressed in colony-forming units per gram. Water activity (*A*w) was measured at 33 °C in an AquaLab device (model Cx-2, Decagon Device, Pullman, WA).

Color parameters (*L**, *a**, *b** and hue angle) were determined in a Minolta colorimeter (model CM-3600d, Konica Minolta,Ramsey, NJ), using the standard D65/10° illuminant, without including the shine factor.

Texture profile analysis (TPA) was determined using the TA.TX2i texturometer (Stable Micro Systems, Surrey, UK), operated with the Texture Expert software, using a pretest velocity of 2 mm/s, test velocity of 1 mm/s and posttest velocity of 2 mm/s, with a distance of 5 mm and time of 5 s, the test body being acrylic (P25/L) with a diameter of 25 mm. The product was placed in an aluminium capsule with a diameter of 50 mm and height of 25 mm for standardization. A graph of force x time was constructed, each characteristic peak corresponding to one of the TPA characteristics.

The sensory evaluation of the jams was carried out by 60 potential consumers and the attributes appraised (appearance, aroma, texture, color, flavor and global impression) judged using a structured 9 point hedonic scale (1= disliked extremely to 9= liked extremely). The experiment was applied to a balanced complete block design according to Stone and Sidel (2004), and 20 g of each treatment presented in plastic cups codified with three digit numbers. The tests were carried out in individual booths in the food sensory analysis laboratory. The results were submitted to an analysis of variance (ANOVA) and the differences between the averages compared by the test of Tukey at 5% of probability (Cochram & Cox, 1992).

3. Results

In several studies on the shelf life to tropical fruit jams (banana, guava, umbu, shell passion fruit juice) packaged in polypropylene, physical, physicochemical, chemical and sensory characteristics were recorded during storage, while microbiological characteristics these products were stable for 4-6 months of storage at temperatures of 25-40 ° C (Policarpo et al. 2007; Nascimento, 2002, Menezes et al. 2011; Martins et al, 2010; Martins et al, 2011). This is due to the fact they were manufactured using good manufacturing practices, the products are low pH and high concentration of sugar, and good sealing of packaging, conditions that minimize or prevent microbial growth of fungi and yeasts, this typical range of water activity.

Regarding the physicochemical properties, there was a slight drop in pH and concomitant increase in titrable acidity (Martins, 2009, Martins et al. 2010, Nascimento et al., 2002) and in some products the pH remained unchanged (Policarpo et al.,2007, Menezes et al. 2011). Soluble solids tend to increase due to syneresis or water evaporation during storage at high temperatures as observed in the work of Policarpo et al. 2007; Menezes et al. 2011; Martins et al., 2010; Martins et al. 2011. The syneresis due to conditions of low pH of the gel formed

and inability to retain moisture in the product and considering that polypropylene has a certain permeability is possible the migration of water into the environment during storage, especially the high temperatures (Fizman & Duran, 1992). The total sugars tend to increase for the same reason the total solids (effect of concentration) and sucrose hydrolysis occurs in glucose due to the increased acidity (Policarpo et al., 2007, Menezes, et al. 2011, Martins et al., 2010). These sugars are hygroscopic and reduce the water activity during storage (Martins et al., 2011). Pectins, when added to preserves or jelly to stabilize the gel network formed and increase the firmness, are also hydrolyzed by the increase in acidity during storage, especially at higher temperatures (Policarpo et al., 2007).

Color parameters (L *, a *, b *) and texture profile, depending on the chemical changes that occur are also altered. Was noticed a decrease in the value of L * in all the above products, indicating darkening, which is due to several reactions accelerated by high temperatures, and exposure to light, such as oxidation of vitamins and pigments in fruits and others reactions. In parallel b parameters relating to color tone characteristic of the fruit, by factors similar to the luminosity are reduced (Policarpo et al. 2007; Martins et al, 2010) or increased (Menezes, et al.,2011; Martins et al., 2011), according to the processed fruit. In the texture profile in all work we observed an increase in firmness with increasing soluble solids, and in some cases increasing of gumminess, due to syneresis. Other parameters of texture profile analysis showed no significant changes.

Regarding the sensory evaluation tests for affective attributes of color, texture, flavor and overall impression, using a hedonic scale of 9 points and untrained judges (Stone & Sidel, 2004) showed that there is reduction in all attributes during the storage. For jelly albedo of passion fruit / passion fruit juice the result of global acceptance at 90 days/25° C were averaging close to 7, corresponding to liked moderately (Nascimento et al., 2002). For guava preserve showed an average between 7-6 (like slightly-like moderately) for different attributes to 150 days of storage at 20 ° C, and detected the appearance of crystals after 90 days, enhanced by the use of potassium sorbate as a preservative (Menezes, 2008). For banana cv prata preserve, kept at 20 -30 ^{o} C for 75 days had a good overall acceptance (in the scores in the range 6-7).

4. Conclusions

The packaging of polypropylene due to low gas permeability and light is appropriate and economical for a short time to market for packaging fruit jams (up to 150 days), maintaining acceptable products in terms of sensory and microbiological changes.

5. Acknowledgements

At FAPERJ (Rio de Janeiro) and FAPEMIG (Minas Gerais) for financial support to these projects, CNPq and CAPES for the scholarships awarded to students of post graduate and undergraduate; to EMBRAPA (CPATSA-Petrolina, CTAA, Rio de Janeiro-RJ) SENAI (CETIQT-Rio de Janeiro, CETEC-Vassouras) for collaborating in different analysis of these projects, students, teachers, researchers and contributors of UFRRJ, UFLA, EMBRAPA and ITAL.

6. References

Alves, R.M.; Dender, A.G.F. Van; Jaime, S.B.M.; Moreno, I. & Pereira, B.C. (2007).Effect of light and packages on stability of spreadable processed cheese. *International of Dairy Journal*, Vol. 17, No. 4, pp. 365-373, ISSN 09586946

Association of Official Analytical Chemists (AOAC) (1995) *Official Methods of Analysis of the Association of Analytical Chemistry*. AOAC, ISBN 0935584544, Arlington.

Bitter, T. & Muir, H.M. (1962). A modified uronic acid carbazole reaction. Anal. Biochem. V.*4*, No. 4, pp. 30–334. ISSN 003-2697

Cochram G. & COX, G.M. (1992) *Experimental Design*, J. Willey, ISBN 0477545678, New York.

Fizman, S.M. & Duran, L. (1992). Effect of fruit pulps and sucrose on the compression response of different polysaccharides gel systems. *Carbohydrate Polymers*, Vol.17, No.1, pp.11-17, ISSN :01448617

Jay, J.M. (1996). *Modern Food Microbiology*, Chapmam & Hall, ISBN 0442244452, New York.

Man, C.M.D. & Jones, A.A. (2000). *Shelf life Evaluation of Foods*. IBlackie Academic and Professional, ISBN 0834217821, Glasgow.

Martins, M.L.A.; Borges, S.V.; Cunha, A.C.; Oliveira, F.P.; Augusta, I.M. & Amorim, E. (2010). Alterações físico-quimicas e microbiológicas durante o armazenamento de doces de umbu (Spondias tuberosa Arr. Câmara) verde e maduro. *Ciência e Tecnologia de Alimentos*, Vol.30, No.1., pp. 6-7, ISSN 0101-2061

Martins, G.S.M.; Ferrua, F.Q.; Mesquita, K.S.; Borges, S.V.; Carneiro, J.D.S. (2011). Estabilidade de doces em massa de banana prata. *Revista do Instituto Adolfo Lutz*, Vol. 70, No. 1, pp. 1-20, ISSN 0073-9855.

Menezes, C.C.; Borges, S. V.; Ferrua, F.Q., Vilela, C.P.; Carneiro, J.D.S. (2011). Influence of packaging and potassium sorbate on the physical, physicochemical and microbiological alterations of guava preserves. *Ciência e Tecnologia de Alimentos*, Vol.31, No.3., pp. 674-680, ISSN 0101-2061.

Menezes, C.C. (2008) *Otimização do processo de elaboração e avaliação da presença de sorbato e embalagens sobre o doce de goiaba durante armazenamento*. UFLA, Lavras.

Nascimento, M.R.F.; Oliveira, L.F. & Borges, S.B. Estudo da conservação de doce de corte de casca do maracujá à temperatura ambiente. *Proceeding of the 13th Congresso Brasileiro de Ciência e Tecnologia de Alimentos*. August, pp. 4-7, 2002, Porto Alegre, Brazil (cd rom)

Policarpo, V.M.N.; Borges, S.V.; Endo, E.; Castro, F.T.; Anjos, V.D. & Cavalcanti, N.B. (2007). Green umbu (Spondias Tuberosa Arr. Cam.) preserve: physical, chemical and microbiological changes during storage. *Journal of Food Processing and Pres*ervation, Vol. 31, No. 2, pp. 201-210, ISSN 01458892

Tfouni, S.A.V. & Toledo, M.C.F. (2002). Determination of benzoic and sorbic acids in Brasilian food. *Food Control*, Vol.13, No.2, pp. 117-123, ISSN 09567135

Speak, M.L. (1976) *Compendium of Methods for the Microbiological Examinations of Foods*. ISBN 0875530818, American Public Health Association, Washington.

Stone, H. & Sidel, J. (2004). *Sensory evaluation practices*. ISBN 0126726906, Academic Press, New York.

3

Rheological Behaviour of Polypropylene Through Extrusion and Capillary Rheometry

Zulkifli Mohamad Ariff[1], Azlan Ariffin[1],
Suzi Salwah Jikan[2] and Nor Azura Abdul Rahim[3]
[1]*Universiti Sains Malaysia,*
[2]*Universiti Tun Hussein Onn Malaysia,*
[3]*Universiti Malaysia Perlis,*
Malaysia

1. Introduction

For the past decade, polypropylene (PP) has become one of the most widely use polyolefin especially for intensive activities in research, product development and commercialization. The factor is strongly contributed by the high demands and usage predominantly in food packaging, automotive industries, fabrication of electric and electronic components and currently its utilization in building structural component for civil needs. Despite their variety in terms of its applications, PP has to be brought into melted stage first before it can be transformed into desired shapes. PP possesses relatively high melting point, low density, high tensile modulus and it is relatively low-priced compared to other thermoplastics. In addition, commercial PP consists of generally linear molecular structure thus it can provide low melt strength and exhibits no strain hardening behaviour in the melted stage. This suggests that PP is suitable for injection moulding, blow moulding and extrusion processing techniques (Rahim[a] et al., 2011).

During the melt processing, polymeric materials are subjected to various rigorous conditions such as high shear deformation and relatively high temperature that could trigger chemical transformation which subsequently leads to molecular degradation and structural development as well as flows through narrow and complex geometries (Ariff, 2003). These factors will definitely influence the rheological behaviour or to be specific the melt viscosity of PP. If the viscosity of molten PP is not suitable within the processing conditions, short shot or flashing may occur in injection moulding. These problems are essentially crucial to be addressed since the modification on thermoplastic viscosity will also modify the end properties of the produced product. Upon the conversion, there are discrete or usually combinations of chemical and physical changes taking place such as chemical reaction, flow or a permanent change which will directly affect the product end properties. With regards to its flow behaviour, a better understanding of PP rheological characteristic can overcome the existing difficulties and literally secure a successful processing.

Moreover, because of the special characteristic (i.e. viscoelastic behaviour) that PP owns, the processing operations are usually more complex than mechanical of chemical engineering

unit operations. In PP melt, both viscous and elastic component will deform and this would bring about scenarios that are associated with elastic respond of the polymeric materials which are commonly known as melt fracture or flow instabilities. These phenomena can be easily demonstrated by extruding PP melts through capillary or extrusion die above and below the critical wall shear stress. Another common elastic effect occurring in polymer processing besides flow instability is extrudate swell. It is the most common defect found during extrusion process where the diameter of the extrudate appears to be larger than that of the die (Ariffin et al., 2006). Nevertheless, the knowledge of PP rheological behaviour will equip manufacturers with better quantitative processing responses to cater the actual processing complexity.

2. The importance of polymer rheology

Before PP is turned into product, it will undergo fabrication processes that involve deformation and flow which can be said to be the essence of rheology. Polymer rheological data is used in determining whether or not a type of polymer can be extruded, moulded or shaped into a practical and useable product. Having knowledge of polymer rheology would probably help in determining the optimal design of processing equipment such as extrusion die design, screw geometries of an extruder, various mould cavities for injection moulding and mixing devices. This indicates that in polymer processing operations, an understanding of polymer rheology is the key to efficient design, material and process selection, efficient fabrication and satisfactory service performance. Fig 1 further shows numbers of area where a better understanding of polymer rheology can lead to successful polymer processing operation. (Han, 1976)

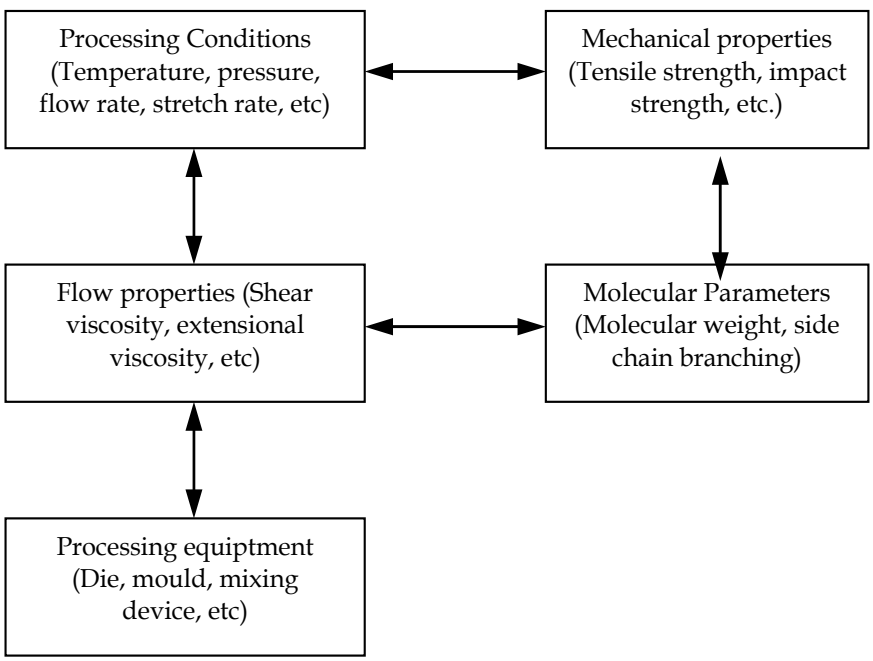

Fig. 1. Schematic of the interrelationship that exists between the processing variables and flow properties, and between the molecular parameters and flow properties (Han, 1976)

Currently there are numbers of methods and instruments available to measure the rheological data of polymers. Since PP is a pseudoplastic thermoplastic fluid that requires relatively high processing temperatures to achieve suitable melt viscosity, it demands a rheological measurement instrument that is able to operate at such temperature under wide of shear rate range. In view of this, capillary rheometer is the simplest and most popular rheological instrument used to measure PP rheological properties (Rahim, 2011; Ariffin et al., 2008; Liang and Ness, 1998; Muksing et al., 2008). This is due to the fact that it has number of advantages over other types of rheometers. First, it is relatively easy to fill which is crucial when dealing with high viscous melt at high processing temperature. Second, the shear rate and flow geometry are similar to the actual condition found in processes such as extrusion and injection moulding (Gupta, 2000). Basically, there are two types of capillary rheometers to measure the viscosity of molten PP namely the pressure-driven type (constant shear stress) and the piston driven type (constant shear rate), yet the approach of their measurement procedure is quite similar where it depends on the applied force (Fig. 2).

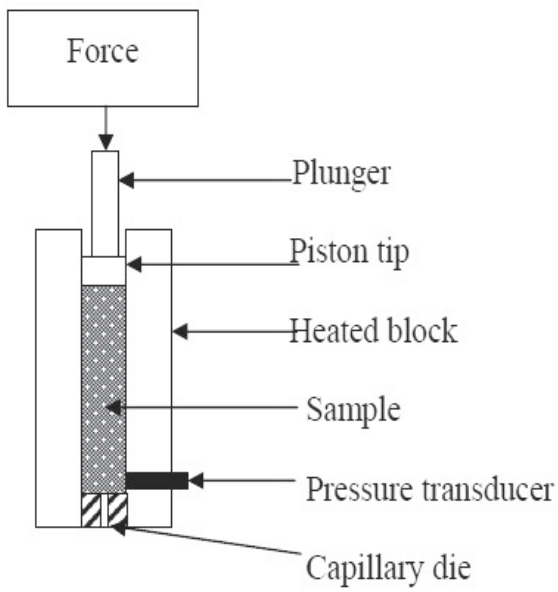

Fig. 2. Schematic diagram for capillary rheometer

The deformation and flow from shear mechanism introduced during polymer processing will results in molecular orientation which creates a dramatic effect on the physical and the mechanical properties of the moulded parts, profile extrudates, film, etc. The kind and degree of molecular orientation are largely determined by rheological behaviour of the polymer and the nature of flow in the fabrication process. Furthermore, PP is a semicrystalline material which always be affected by the application of shear stress under the action of shear flow during processing. Simultaneously upon solidification, the generated shear flow will bring a profound effect on the nucleation and crystallization of polypropylene. Crystallization process involves the transportation of molecules from disordered liquid to ordered solid stage. It is a unique phenomenon which occurs due to chain orientation of PP molecular structure. In recent years, many experimental results have

confirmed that the orientations of the polypropylene molecules are strongly affected by the flow field acting on the molten PP (Jikan[a] et al., 2010; Jikan, 2010; Rahim[b] et al., 2011).

Other than experimental or practical assistance, rheology can also be a great help to polymer processing in carrying out theoretical analysis of the mechanics of flow of rheologically complex of polymer in various kind of processing equipments. Theoretical model requires rheological models which describe reasonably well the flow behaviour of polymeric materials under consideration. Hence given a flow field of specifically PP, the development of an acceptable rheological model is very important to the success of theoretical study of flow problems. Such a theoretical study should be useful for designing better processing equipment and determining optimal processing conditions. Reviewing the mentioned importance, one should note that behind the complexity of rheology measurement there is significant importance that makes rheological studies unavoidable to polymer scientists and polymer design engineers (Ariff, 2003).

3. Factors affecting the rheological behaviour of polypropylene

Previously, many have reported (Gonzalez et al., 1998; Liang, 2008; Brydson, 1970) on factors affecting the rheological behaviour of PP. Basically, reports usually regulate around four fields of studies. The first field of study involves molecular structure influence on rheological behaviour of PP such as the type of backbone chain, chain branching and chain branching configuration. The second area which is the most likely favoured by researchers is the study on how composition of polymer system or heterogeneity affects rheological behaviour such as those found when PP are blended with other polymers, addition of fillers and other additives are also of interest. The third part involves the study on the dependence of PP rheological behaviour towards fabrication process parameters like pressure, temperature and equipment's geometrical factor. Lastly, the fourth covers the PP theoretical analyses using various rheological models of PP and their implementation in simulation software which regulates around all three fields of studies previously discussed. The extent of these factors will be forwarded in the following sections.

3.1 Molecular structure of polypropylene

PP can be made from the propylene monomer by a process known as Ziegler-Natta catalyzed polymerization or by metallocene catalysis polymerization. PP is a linear hydrocarbon polymer that contains little or no unsaturation in its chain structure. Structurally, it is a vinyl polymer with every other carbon (C) atom in the backbone chain is attached to a methyl (CH_3) group. Compared to polyethylene, PP has some similarities in their characteristics such as swell in solution. The characteristics of PP vary according to the molecular weight and grade. The Ziegler-Natta catalysts have several active sites and accordingly the obtained PP exhibits broad tacticity and molecular weight distributions. It is discovered that by using different types of catalysts and polymerization methods, the molecular configuration can be arranged to produce three types of PP (Jikan, 2010; Karger-Kocsis, 1995).

Mechanical properties, solubility and melt level can be ascertained with knowledge on polymer tacticity. (Andres et al., 2007). The presence of methyl group in PP backbone chain can provide various differing characteristics for PP, depending on the arrangement of methyl group in PP carbon atom, whether in isotactic, syndiotactic or atactic configuration

(as shown in Fig. 3). This tacticity will dictate the viscosity of PP that directly contributes to different end properties. Most (90-95%) of commercial PP are isotactic PP produced by Ziegler-Natta catalyst with head-to-tail incorporation of propylene monomer. Isotactic configuration is the most stable structure since the methyl group is arranged at only one side in the PP chain structure. This structure prevents PP from crystallizing in a zig-zag planar shape, but rather in helical crystal structure. With those conditions, the degree of crystallization of isotactic PP can normally reach up to 50% that causes an increase in PP softening temperature which means an increase in the melt viscosity throughout the processing procedure. However, the presence of methyl group attach on the PP backbone are easily oxidized when high processing temperature is utilized and these sites are prone to be chemically attacked by certain chemical agents.

a)

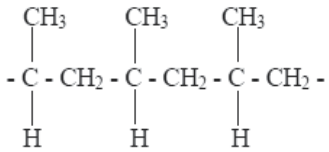

b)

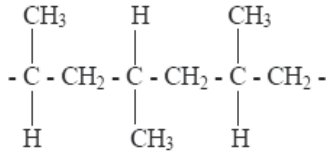

c)

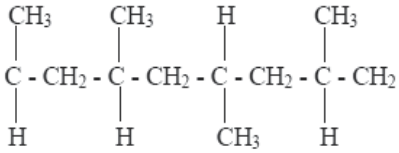

Fig. 3. The three basic structures for polypropylene (a) isotactic, (b) syndiotactic and (c) atactic.

However, PP chain configuration is directly related to density which can be classified in many forms such as homopolymer, copolymer with ethylene, or homo- or copolymer blended (which will be discussed later) with ethylene propylene diene monomer (EPDM) rubber or known as thermoplastic polyolefins (TPE-O or TPO, when elastomeric properties appear at higher levels of EPDM). All these components that exist in either PP site chain or partially associate within the PP matrix will definitely influence the molecular weight (MW) and molecular weight distributions (MWD) of the produced PP. It has been revealed in Fig. 4 that the viscosity of PP copolymer (with ethylene monomer) is much lower than that of homopolymer PP obtained using twin screw extruder. The developed viscosity curve has shown to be strongly dependent on the molecular architecture of PP backbone which is well associated with polyethylene group link to its backbone. Higher amount of side group i.e. the methyl side group has fairly raised the disentanglement to the PP polymer chain and caused

reduction to the chain mobility. This indicates that the viscosity of PP is virtually dependent on the irrespective molecular chain characteristic (Gonzalez et al., 1996; Andres et al., 2007).

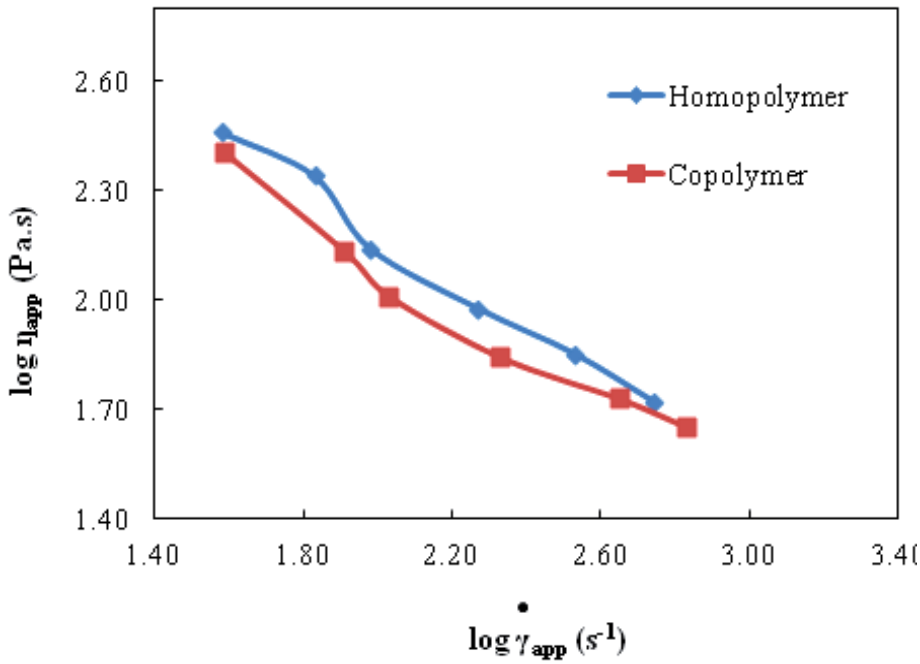

Fig. 4. Viscosity flow curves of PP copolymer (with ethylene monomer) and PP homopolymer obtained using a twin screw extruder

Moreover, the types of manufactured PP differ resulted from their large range of MW. Higher MW usually indicates the existence of longer molecular chains that provide more points of contact or even entanglement between chains. Short branches normally do not affect the viscosity on the molten PP significantly compared to long branching system. Such branching reduces the viscosity of the polymers yet unlike LDPE, PP branch is greater that they can take part in formation of entanglement (Bydson, 1970; Samsudin et al., 2006; Ariff, 2003). Depending on the degree of chain entanglement, it is more likely that a secondary crosslink or known as physical crosslink would form and cause reduction in the mobility of PP molecules. Due to that matter, high shear forces are required to move these PP melts. Gotsis and co-workers has systematically approved that branches existing in polypropylene has increased the zero shear viscosity and increase the polypropylene melt elasticity and improve the melt strength (Gotsis et al., 2004). Hingmann and Marczinki have suggested that the PP shear viscosity increased with chain branching using the Lodge Model (Hingmann and Marczinki, 1994). Meanwhile, Ogawa has finalised that the higher the PP molecular weight, the higher the PP mechanical properties will be (Ogawa, 1994).

In recent years, many researchers (Azizi et al., 2008; Samsudin et al., 2006) are aware and have made considerable interests in dedicating their work in modifying the chain configuration of PP to alter the melt flowability of the material. The most preferred method is by additions of degradation substance such as peroxides. These peroxides are introduced to control the rheological behaviour of PP by lowering the viscosity of the viscous PP melts

during processing. Previously, Azizi and colleague has soundly concluded that the addition of high amount dicumyl peroxide has significantly reduced the melt viscosities of PP using either MFI or twin screw extruder. They also found that the addition of peroxide has subsequently lowered the MW and MWD of PP by chain scission reactions which has shortened the PP chain length consequently leads to decreasing values of PP viscosities. The statement is in good agreement with Berzin et al. who also claimed that PP molecular weight distribution are narrowed and high molecular weight species has decreased when the amount of peroxide was increased which enable it to form free radical during thermal decomposition (Berzin et al., 2001).

Another common way to configure the chain achitecture of PP is by thermal, mechanical, oxidative or combinations of these mechanisms. Initially, the identification of these mechanisms would equip manufacturers with good information in selecting PP processing conditions either to promote or to prevent it. It was demonstrated by Gonzalez et. al that during multiple extrusion of PP, MW and viscosity can be reduced with increasing number of extrusion cycles. The chain scission is thought to be provoked by thermomechanical reactions rather than degradations (Gonzalez et al., 1998). On the contrary, PP which contains tertiary hydrogen atoms are most susceptile to oxidation reactions. Other than chain scission, PP also has the tendency to form a crosslinking. The reaction is highly contributed by radical-radical combinations where it literally increase the MW and MWD. Traditionally, intrinsic viscosity measurement were implemented as an indicator of the MW of a PP. However, intrinsic viscosity test have been largely replaced by gel permeation chromatography (GPC) which enables a direct assesment of MW. The occurence of PP crosslinking are commonly found during multiple extrusions with the contributions by various enviromental factors and radiation (Scheirs, 2000).

3.2 Composition or heterogeneity effect of polypropylene

The composition or heterogeneity effects are classified as external factors since all of them are included during the mixing process. One of the factors involving the composition of polymer system includes addition of one or more system which known as blends. Consequently, PP blends have been extensively studied and developed by many researches for the past 20 years either with thermoplastic or elastomeric materials such as ethylene-propylene copolymer (EPR) and ethylene propylene diene monomer (EPDM). Blending is a common useful method to improve PP properties but it is not as simple as adding other polymers into an extruder and mechanically mixing them in the molten state. Typically, morphology and compatibility issue as well as processing difficulties which closely related to flow ability of the blends will rise. The viscosity may increase and decrease depending on the structure of the added block of polymer into the molten PP. Normally the increase in viscosities are caused by the addition of immiscible block like styrene or by the change of bulk properties or the addition of blend component that enhanced the degradation effect in PP blends (Keawwattana, 2002).

The second types of blends that can be produced are miscible blends where the blend may have a higher viscosity than PP and appears to be remarkably elastic. The chemical structure of the miscible block appears to be more important in governing the observed viscosity of the system where it has increased the viscosity of the system. For instance, Song et. al has shown that the rheological behaviour of blend PP and POE (polyethylene-1-octene) is highly

depended on the blend ratio of the system. Higher dynamic complex viscosity and loss modulus were observed for the blends with portions of 10 wt% and 20 wt% PEO where miscibility was achieved. Later on, incorporations of higher content of PEO have subsequently reduced the dynamic complex viscosity and loss modulus which attributed to the immiscibility between the two matrices (Song et al., 2008). Besides miscibility, the increase in viscosity of PP blends can also correspond to the effect of crosslinking of the other blend materials. Previously, the rheological behaviour of PP-natural rubber blends was investigated by Thitithammawong and co-workers. They have found that the shear stress and the viscosities of the blends have increased as a result of crosslinking of rubber molecules (Thitithammawong et al., 2007).

On the other hand, filler and reinforcement have always played an important role in modifying PP properties. Fillers incorporated inside PP matrix is purposely to reduce overall cost, improving and controlling process characteristic, density control, dimensional stability and etc. The inclusion of fillers into PP can affect almost all of its properties which also include surface, colour, expansion coefficient, conductivity, permeability, mechanical and rheological properties. Many factors influence the behaviour of fillers in PP melts. The type, compounding method and loading of filler dictate its effectiveness. Fillers can be categorized into two groups, i.e. inert fillers which act as cheapeners and reinforcing fillers that are sometimes used in engineering applications. Among these types of fillers are mineral fillers such as calcium carbonate, talc and kaolin which are most commonly used in PP (Ariffin et al., 2008). The addition of these fillers in PP however, would bring a significant change in the rheological properties such as the viscosity of the base resin. From Fig. 5, it can be seen that the viscosities of PP-kaolin composites have risen as the addition of higher kaolin content measured using a Melt Flow Indexer (MFI) at 210°C. This fact is attributed to the substitution of PP matrix which consists of flexible molecules with more rigid kaolin particles. The ease of melt flow is highly dependent upon the mobility of the molecular chains and force or entanglement holding the molecules together. As the kaolin loading increases, the PP chain mobility are significantly affected by the overloading of kaolin particles in the system which perturb the normal flow and hinder the mobility of chain segments in melt flow, consequently increasing the value of the apparent viscosity (Rahim[a] et al., 2011; Jikan et al., 2009, Rahim, 2010)

Particle shape is another crucial factor in the incorporation of filler in polymer since this affects the polymer characteristics and processing method. Shapes of particles can be categorized as cubic, needle-like (acicular), block, plate or fibre. Spherical particles that flow and disperse well throughout the molten polymer cause the least problem related to stress concentration (Jikan, 2010; Pukanszky, 1995). Needle-like (acicular), fibrous and platy shape fillers can be more difficult to disperse and they can act as stress concentrators, which reduces impact strength (Rothon, 2002). Depending on the filler shape, the addition of fillers at low concentration is able to increase the flow resistance and reduce the built up pressure within the processing equipment. Maiti et al, has mentioned that the apparent viscosity of iPP/$CaSiO_3$ system exhibited lower shear stress compared to pure PP. The reason was claimed to be interrelated with $CaSiO_3$ flake-shape. Same scenario was discovered for PP-kaolin composites where kaolin has similar flaky geometry. The flake-like shape of these filler particles make them able to slide within the PP system during the application of shear forces causing a flow-favouring orientation which subsequently lowered the viscosity of PP matrix (Rahim[a] et al., 2011; Maiti et al., 2002)

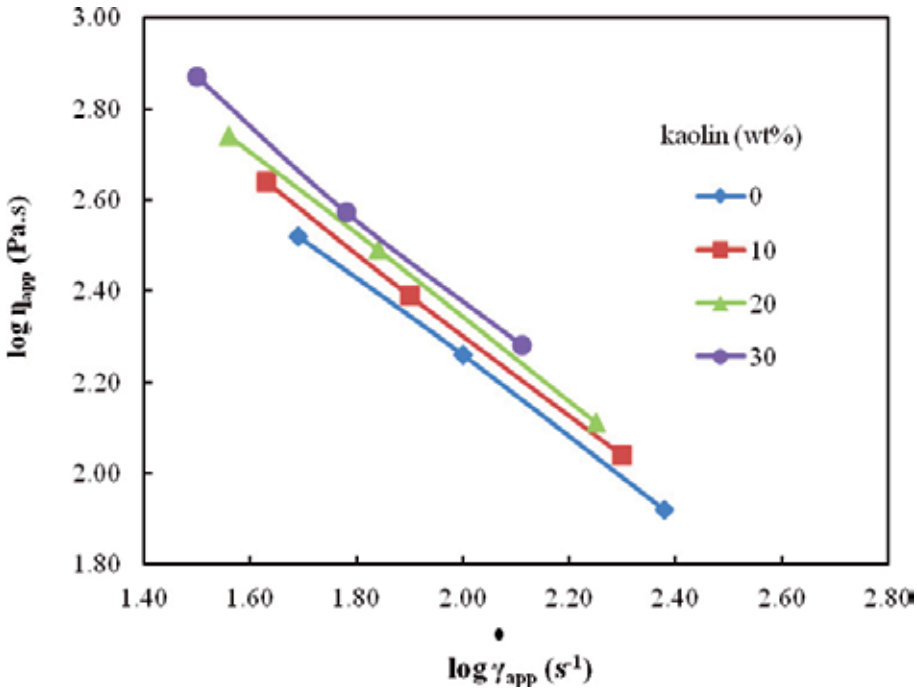

Fig. 5. Viscosity curve of PP-kaolin composites using a Melt Flow Indexer (MFI) at 210°C

Since PP macromolecules do not have polar groups, the homogeneous dispersion of hydrophilic particles in PP is difficult. Therefore, it is necessary to modify the system so that the filler and PP have proper interaction and distribution. To encounter the issue, compatibilizer or coupling agent is usually added to act as a wetting agent between the filler and PP. Among the highly used compatibilizer in PP is maleic anhydride-graft-polypropylene (PPgMA). In the investigation of Liaw et al. the incorporation of PPgMA has reduced the composites viscosity depending on the amount used for PP/clay nanocomposites. To reconfirm the statement, we made an attempt to analyze it with a wide range of shear rate using a capillary rheometer for 20 wt % kaolin loading with the addition of 5 wt% PPgMA and without the addition of PPgMA at 210ºC. The claim and our finding is in good approximation where PPgMA has played a role as a flow promoter in PP matrix. The softening effect brought by the maleic anhydride group (MA) content has lowered the system melting temperature. Hence, the decreasing value of the composites viscosities throughout the shear rate range is attributed by the plasticizing effect by the PPgMA in the composites (Liaw et al., 2008).

Other composition factor that affects the processing of PP melt is the inclusion of necessary additives such as plasticizer, lubricant or flow enhancer, environmental stabilising agents and pigment or colorant. The last two usually do not bring significant effect on the flow behaviour of PP melt since they are added in small quantities unless they are able to carry multiple functions which includes plasticizing (similar to PPgMA) and lubricating the compounding system. Nevertheless, the first two additives, i.e. plasticizer and lubricant proved to have a bound effect on the PP melt flow. Due to their ability to dissolve in PP

matrix, they are able to space out the PP molecules thus increasing their mobility and consequently reduce the viscosity of the system. Apart from reducing the viscosity, they also tend to reduce the glass transition (T_g) temperature of PP and elastic modulus of the melt (Liaw et al., 2008; Ariffin et al., 2008; Maiti et al., 2002).

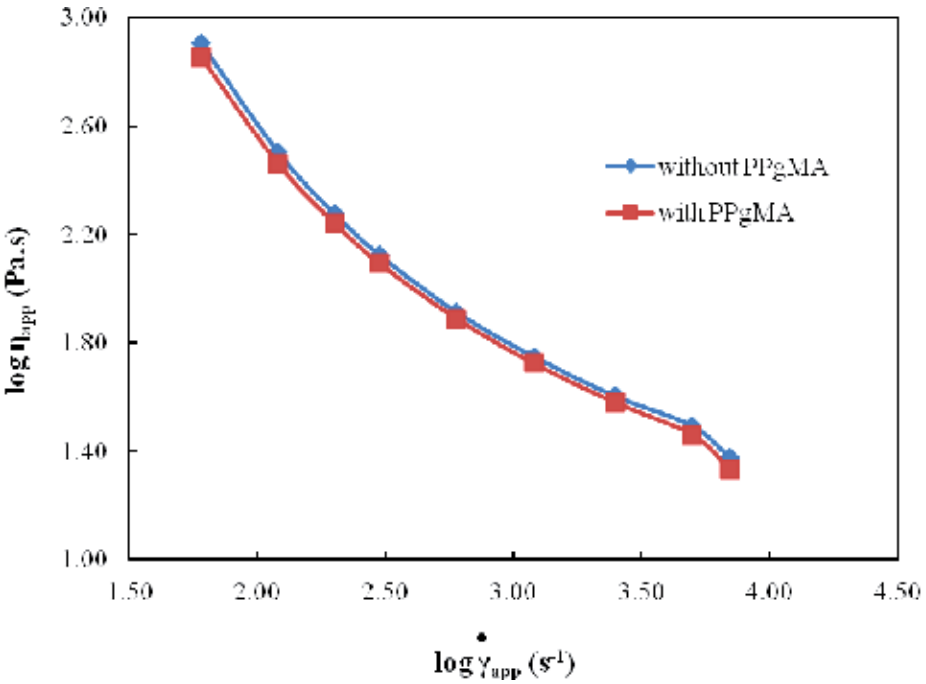

Fig. 6. Viscosity curves of 20 wt % kaolin loading with and without PPgMA for PP-kaolin composites obtained using capillary rheometer at 210°C

3.3 Fabrication process parameters of polypropylene

For the ease of flow, polymer molecules must have enough thermal energy to make it mobile which also associates with having enough space surrounding the molecule which allows it to past other molecules. Thereby, the melting of PP is strongly dependent upon the mobility of its polymer chains. Below T_g, the latter condition is not met, and PP is still in solid state. Above T_g, the magnitude of shear viscosity is totally dependent on the availability of free volume. Whereas at temperature far above the glass transition temperature or the melting point of PP, there is ample free volume available and the temperature dependence of the zero-shear viscosity is determined by energy barriers to motion. A number of researches have come into agreement that the viscosity of PP follows the Arrhenius equation to a good approximation where it is common to observe a decreasing function of viscosity and shear rate that varies considerably (Gupta, 2000).

For isotactic PP, it is expected that the overall viscosity for the high processing temperature is respectively lower than that of at low processing temperature (Fig. 7). From the molecular level, the flow occurs when PP molecules slide past each other. Whereby, the ease of melt flow depends upon the mobility of PP molecular chains and forces of entanglements

holding the molecules together. As the free volume increases with temperature, PP molecules occupy more space due to an increase in the distance between them making it easier to slide among each other and together with the introduction of high shear rate will eventually reduce the PP matrix viscosity significantly (Scheirs, 2000). Similar trend was observed for PP composites system by Rahim[b] et al. and blend system of LDPE/PP blends by Liang and Ness where the viscosities of the compounds are lowered at high processing temperature (Rahim[b] et al., 2011; Liang and Ness, 1998).

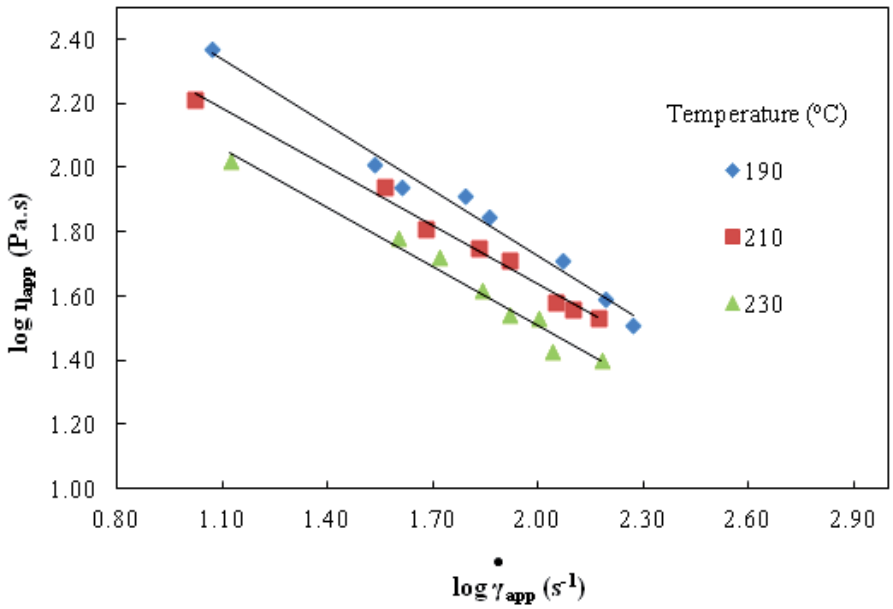

Fig. 7. Viscosity curves of isotactic PP obtained using single screw extruder at various processing temperatures.

In contrast to the effects of temperature and pressure play significant roles in altering the viscosity of polypropylene melt. During polymer processing operations such as extrusion and injection moulding, the applied pressure can reach up to thousands of atmospheres. Large hydrostatic pressure will results in a decrease in the free volume in the melt and accordingly, it should display an increase in viscosity near to polymer T_g. In addition, the reduction of free volume will result in the mobility of polypropylene molecules in the melt to become more restricted. Since viscosity is very dependent towards the distance between each molecule, it is expected that an increasing pressure would increase the viscosity by the way of that a low molecular weight liquids decreases its distance between particle and molecules. Thus, the influence of pressure can be considered quantitatively equivalent to that of temperature but acts the opposite way (Brydson, 1970).

Besides temperature and pressure, in various polymer operations, molten polymer is forced to flow into a wide variety of geometrical configurations; indeed the rheological properties of the polypropylene melt are influenced by the flow geometry (Micheali, 1992; Liang, 2001). Extrusion process have the most critical dependence on flow geometry, where the final product properties as well as appearance is directly related to the geometry or die through

where the molten PP is extruded out which will be further discussed in detail in the extrudate swell sections. Experimentally, a non-overlapping rheological experimental data of viscosity curve of different length to diameter (*L/D*) die ratios can be observed. The results are more obvious for low ratio of *L/D*. Theoretically, it should form a single curve despite of the different die geometries since the measurements are implemented on the same material. The cause of this problem is highly due to the existence of large error in pressure drop measurement within the measuring instrument. To address the erroneous pressure measurement, Bagley correction procedure was applied and has proven to be successful not just for PP but also for other thermoplastic materials (Rahim, 2010).

4. Viscoelasticity of polypropylene

Viscoelastic properties, as their name implies, display responses towards an applied stress which is a combination of elastic and viscous deformations. The two most commonly used models are those attributed to Maxwell and Kelvin. Kelvin model describes very well the concept of 'creep' (the change in strain at constant stress), whilst the Maxwell model quite reasonably describes 'stress relaxation' (the change in stress at constant strain). In combination, the elements of Maxwell-Kelvin model display both elastic and viscous (namely viscoelastic) characters at deformation rates in between the two extremes (i.e. low and high rates) in varying proportions. A number of different effects may be noted depending upon the degree of elastic character possessed by a viscoelastic polymer melt (Prentice, 1997). Generally, the relative proportions of each property are highly dependent on the rate of deformation.

It is well known that PP possesses viscoelastic behaviour during polymer processing. Both viscous and elastic component will deform and this would bring about the occurrences of phenomena that are associated with elastic response for PP. During the flowing process, the melt will travelled from a large reservoir (i.e. barrel) to very small die geometry under the application of shear forces. Under normal circumstances, entanglement between molecules prevents the molecules from sliding past each other. When shear forces are introduced, the chain will uncoil and the melt will start to move. On release of the applied shear stress, the chain will recoil and in conjunction they can be pulled back by the restraining forces (i.e. molecular orientation). This theoretically explains the most common effect observed during extrusion process involving extrudate swell and flow instabilities which are going to be deliberated in the next couple of sections.

4.1 Extrudate swell

Extrudate swell is strongly related to elastic recovery of PP at the inlet of a die. Newtonian liquids can also display swelling occurrence, but can only be observed at a very high flow rates. Whereas for PP (which is a non-Newtonian liquid), the swelling will increase with increasing flow rate. When a polymer melt is deformed, either by stretching, shearing or often by a combination of both, the molecules chain are stretched and untangled. In time, the molecules will try to recover their initial shape, by then getting used to their new state of deformation. If the deformation is maintained for a short period of time, the molecules may return to their initial configuration and the shape of the melt is fully restored to its initial shape. It can be said that the molecules remembered their initial configuration. However, if

the shearing or stretching goes on for an extended period of time, the molecules cannot recover to their initial arrangement, in essence forgetting their initial positions (Osswald, 1998). Thus, when elastic liquid (such as in PP melt) is extruded from a die or flowed from the exit of a tube, it usually swells to a much greater diameter than that of the die hole. Besides shear rate, the swelling behaviour is highly affected by a number of factors such as temperatures, *L/D* of the die, shape of the die, filler loading and etc. (Ariffin et al., 2008).

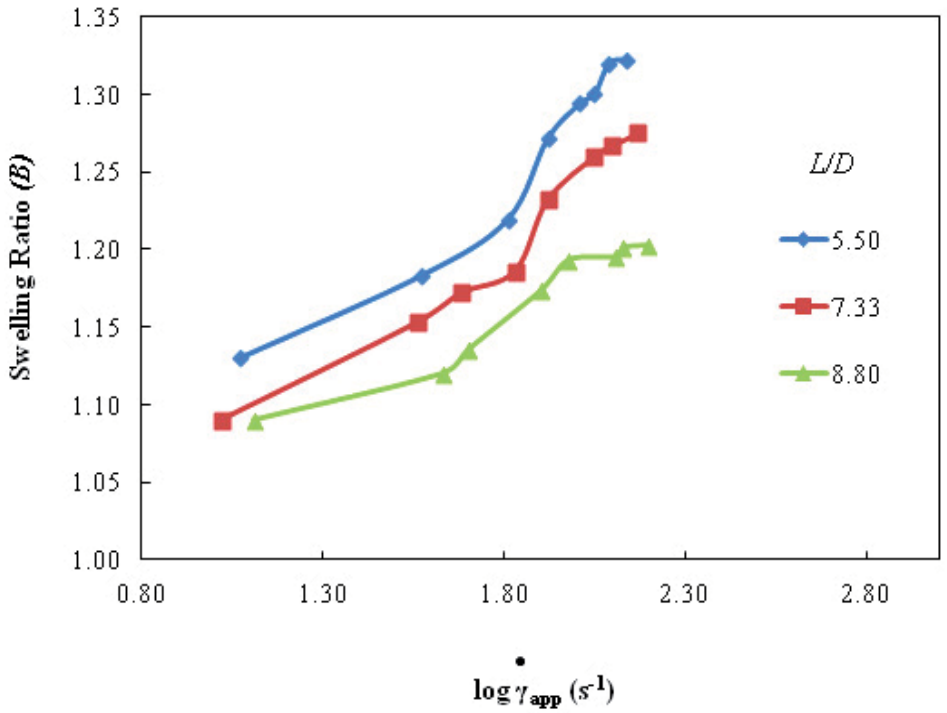

Fig. 8. Swelling ratio of isotactic PP recorded from extrusion process using single screw extruder at various processing temperatures.

One of the affecting parameters for extrudate swell is the influence of die design which is easily illustrated through the die *L/D* ratio. The extrudate swell phenomenon is indicated by the swelling ratio (*B*) obtained by dividing of extrudate diameter with the die diameter. For a given rate of flow or shear, the extrudate swell decreases as the *L/D* ratio of the capillary increases and ultimately attains an equilibrium value as shown in Fig. 8 for pure PP. The root for this condition is the extensional flow at the capillary entrance that imparts greater molecular orientation compared to shear flow within the capillary. Thus, in a long capillary die, some of the molecular orientation imparted to the polymer in the entrance region can relax out in the capillary itself. Also at a constant shear rate, extrudate swell tends to decrease fairly as the temperature is increased since the molecular orientation relaxes faster at higher temperatures (Gupta, 2000). In addition, as the temperature rise, the contributions of viscous component will become more pronounce than that of the elastic component. Furthermore, until it solidifies, the extrudate will sag under the influence of gravity and its diameter will then be reduced. The simplest practice to reduce the extrudate swell is by

using a capillary die with a large *L/D* ratio that will eliminate the effect of the entrance flow on the swelling extrudate.

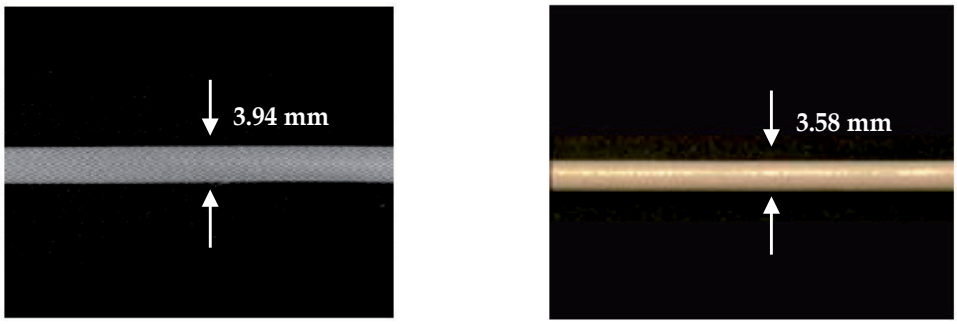

Pure PP 30 wt% kaolin

Fig. 9. Swelled extrudates of pure PP and PP-kaolin composites with 30 wt% filler loading for obtained from extrusion process using capillary rheometer at 200°C

It can be observed from Fig. 9 that PP with 30% kaolin loading had predominantly experienced a reduction of extrudate swell ratio. This behaviour can be due to the fact that the PP chain remains unchanged because of the present of filler particles thus providing more oriented and aligned structures. It is obvious that filled compounds offer greater deformation resistance, due to a reduction in mobility of the polymer chains. This concurs with Muksing et al. (2008) who stated in his research that the layer of fillers create molecular chain barrier in vertical plane towards extrusion direction when leaving the capillary die which limits elastic recovery thus causes reduction in extrudate swell (Liang, 2002). Whereas different scenario can be observed in unfilled PP, an increase in deformation rates in this system is generated by greater molecular realignment and reorientation which reduced relaxation of molecules, which leads to enhanced chain rigidity and shattered melt strength. The addition of rigid particulate filler such as kaolin clearly has similar qualitatively effect on the melt strength of thermoplastics, as noted by Tanaka and White (1980).

4.2 Flow Instabilities

Besides extrudate swell, another common elastic effect occurring in polymer processing is flow instabilities such as melt fracture. Distortion of extrudate is a result of polymer molecules reaching their elastic limit of storing energy, thus causing melt fracture as a way of relieving stress either at the die wall or at the die entrance. Another opinion forwarded by White (1973), is that the extrudate distortion is caused by differential flow-induced molecular orientation between the extrudate skin, holding highly oriented molecules, and the core which has no significant molecular orientation. It is of course, possible that the melt fracture occurs due to a combination of the stress relief theory and the differential flow induced molecular orientation (Shenoy, 1999). In conjunction, PP body consists of long chain molecules and when high pressure is applied; the system would simplify the movement of PP molecules to slide past each other. A rapid and random movement of molecules might cause disordered configuration to the chain that allowed deformations to take place. More likely when stress is removed as the extrudate emerge from the die, the elastic behaviour of

the melt flow will struggle to recover predominantly from the elastic memories attained by the large deformation. This elastic property could be seen when extrudate flowing out of the die and it manifest itself in many ways such as the extrudate exhibiting flow instabilities after experiencing extrusion process (Liang and Ness, 1998).

Shear Stress	Pure PP	30 wt% kaolin
122 MPa		
245 MPa	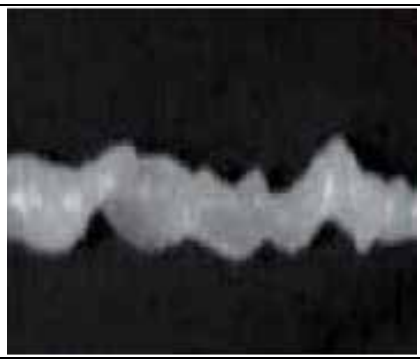	

Fig. 10. Flow instabilities of pure PP and PP-kaolin composites with 30 wt% filler loading obtained from extrusion process using capillary rheometer at 165oC for L/D = 4

Since the flow instability is more available for shorter die and at lower die tempereture, an experiment was conducted using a capillary rheometer at 122 MPa and 245 MPa of shear stress for a capillary die with L/D = 4 and at the temperature of 165^{o}C to verify the scene. Based on Fig. 10 for pure PP and 30 wt% kaolin loading for PP-kaolin composites, it has plainly shown that the incorporation of fillers in the composite systems is able to reduce melt flow instability from appearing. This was caused by the presence of a large amount of filler that reduced chain recovery memory by preventing the polymer molecules from returning to their original configuration after stress was withdrawn from the system. Fillers are able to restrict the mobility and deformability of the matrix by introducing mechanical restraint. Whereas, unfilled PP did not have any additional structures that can hold and restrain PP molecules from returning to their original configuration. Furthermore, fillers have the ability to delay melt fracture given that filler particles tend to travel to the surface (skin) of the sample melt thus improving sticking effect between melt and die wall (Gupta, 2000) thus the stick-slip scenario will then be reduced. It clearly elucidates that filler loading highly influences this phenomenon.

Accumulated from the effect of filler loading, preliminary testing has evidenced that low shear stress applied to the sample melt (at low processing temperature of 165°C) was unable to extrude the sample out of the die due to the fact that the system is still in a semisolid state. Nevertheless, different scenario could be seen when the samples were processed using higher shear stress (≥122 MPa). It is believed that the ability of extrudate to emerge from die even at semisolid state is brought about by pressure that surpasses the critical shear stress. When exceeding that value, pressure This led to fluctuation in flow propagation which contributed slip or stick phenomenon (Shore et al., 1997). Extrudate with shear stress of 245 MPa shows further distortion compared to extrudate with shear stress of 122 MPa. This means that flow instability increased when shear stress was increased. The flow instability experienced in this research is commonly identified as melt fracture. Normally, melt fracture is caused by nonlaminar or turbulence flow due to the *L/D*, type of polymer and processing parameter (Cogswell, 1981). During the extrusion process, the flow direction of PP melt in the barrel was in a form of laminar flow. Nevertheless, it started to experience disturbance when entering the die area. This is due to the fact that the melt in the middle of the die entry started to fracture when high shear stress was applied to the system. This led to fluctuation in flow propagation which contributed towards the flow instability experienced by the extrudate surface.

The effect of temperature plays a vital role in reducing the flow instability of PP system. At a temperature well above melting point, molecules start to enhance their movements. The swift activities of these molecules rise the collisions between them and lead to a molecule's repulsion scenario. Simultaneously, these molecules take up more volume given that the space between them has been increased. At this phase, the molecules are in a tranquil state and some of the elastic memory of the system has faded away due to the relaxation condition. Therefore, when shear is applied to the system (at temperature above melting point) molecular chains could effortlessly align themselves according to the flow path without causing any collisions. In this situation, elastic recovery is relatively low or even absent, consequently decreases the deformation rate which is closely related to the flow instability mechanism. On the contrary, most of the extrudate surfaces exhibit relatively different degree of distortion at low processing temperature. At low temperature, the surface is not as smooth as in the case of samples processed at high temperature. These extrudates in fact have rough, irregular surfaces, loss of glossiness and non-uniform diameter. This is due to the melt fracture that occurs in the elastically deformed polymer, in which the shear stress exceeds the strength of the melt. The extensive slipping and sticking of the polymer layer at the wall of the capillary is also one of the factors that contribute towards extrudate deformation (Georgiou, 2004; Rahim[b] et al, 2011).

Apart from causing extrudate distortion, flow instability for PP may also manifest in other ways such as blisters are formed on the surface of the extrudates and void in the cross section of the extrudates as shown in Fig. 11 obtained at the temperature of 210ºC for PP-kaolin composites using a single-screw extruder. The first reason is that as more kaolin was incorporated inside the matrix, the activation energy barrier was reduced due to the particle–molecule interface which led to increasing number of nucleation sites and was able to increase the nucleation rate. Consequently, less force was required to overcome the activation energy barrier, resulting in the formation of more bubbles on the extrudate surface. Whereas for the second reason is due to the melt suddenly goes from high pressure to atmospheric pressure during the emergence of extrudate of the die exit and then undergo a sudden quench in cool water that provided a large temperature gradient (Rahim[a] et al., 2011; Rahim, 2010).

Void in PP-kaolin composites extrudates cross section

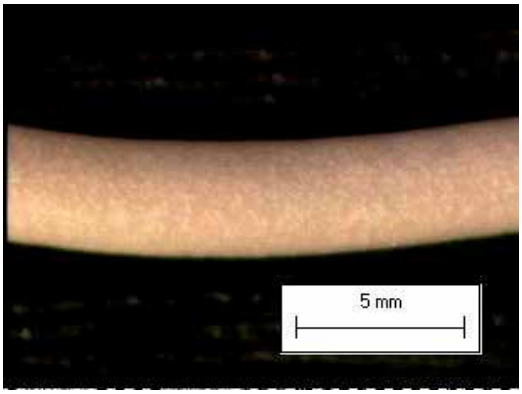

Bubble formations on PP-kaolin composites surface

Fig. 11. Flow instabilities for PP-kaolin composites using single screw extruder at 210°C

The extensional flow along the melt will cause an orientation to the polymer chains. Solidification through this type of process condition is favorable for residual stress formation which is one of the factors that can cause shrinkage in many polymer products and in this case, the extrudates. The polymer will freeze the surface in this orientation direction and in the meantime, the meantime, the flow between the solid layer is affected by the temperature gradient resulting in unbalanced cooling where the inner layer cools slowly with respect to the skin layer. As mentioned previously, after exiting the die, the composites will swell first then followed by cooling. Thereby after quenching, the surface layer of the extrudates will solidify first while the inner layer is still in a molten stage. Soon after, as the inner melted layer cools down, it will be attracted to the cooled skin of the extrudate layer. Thus, a void is created in the composites extrudate since the total composites volume reduces with time as the temperature gradient drops (Rahim[a] et al, 2011; Rahim[b] et al., 2011).

5. Conclusion

Overall, the rheological properties of PP are highly dictated by its molecular structure. The chain configuration of the methyl group placement will create different tacticity for PP and subsequently leads to different rheological characteristics. Another contributing factor is the presence of ethylene group such found in some PP copolymers which may increase the flowability of the resin during processing as forwarded in the preceding sections. Besides these internal factors, externally, the rheological behaviour of PP is highly influenced by additives, which are either added to modify the properties of the base compound or for the ease of processability. Incorporation of fillers normally creates higher viscosity of PP melts compared to the pure PP matrix. Whereas, the incorporation of plasticizers, compatibilizers, degradation promoters and incompatible components in the PP blends can correspondingly caused a decreasing trend of viscosity.

Capillary rheometry and extrusion have shown significant importance in measuring rheological behaviour of polymers. As for PP, the above forwarded discussion has proven that its rheological behaviour can be evaluated successfully with both instruments. Our

study also proved that both instruments are able to reveal viscoelastic responses of PP melt such as extrudate swell and several types of flow instabilities which cannot be investigated with other types of rheological instrument. The extrudate swell behaviour is caused by a number of factors such as temperature, *L/D* ratio of the die, flow geometry, filler loading which are eventually connected to the memory effect of the PP melt. Various types of flow instabilities can be observed through capillary rheometry and extrusion process; from periodic extrudate distortion to severe melt fracture. Flow instabilities may also be revealed as loss of glossiness, formation of blistered extrudate surface and even formation of void within the extrudate cross section. These flow instabilities are triggered whenever processing conditions are not optimized and/or exceeded the elastic limit of the PP melt which can be controlled via several approaches such as incorporation of fillers, increasing the die *L/D* ratio and incorporation of suitable flow promoter.

6. References

Andres, J. A., Pena, B., Benavente, R., Perez, E., Perez, E., Carrada, M. L. (2007). Influence of isotacticity and molecular weight on the properties of metallocenic isotactic polypropylene. *Eur. Polym. J., 43, 2357-2370*

Ariff, Z. M. (2003). Melt rheology and injection moulding of acrylonitrile-butadiene-styrene (ABS) using a capillary rheometer. *Phd Thesis*, Universiti Sains Malaysia

Ariffin, A., Mansor, A.S., Ariff, Z. M., Jikan, S.S., Ishak, Z.A.M. (2008). Effect of filler treatments on rheological behaviour of calcium carbonate and talc-filled polypropylene hybrid composites *J. Appl. Polym. Sci*, *108, 3901-3916*

Ariffin, A., Jikan, S. S., Samsudin, M. S. F., Ariff, Z. M., Ishak, Z. A. M. (2006). Melt elasticity phenomenon of multicomponent (talc and calcium carbonate) filled polypropylene. *J. Reinf. Plas. Compos., 25, 913-923*

Ariffin, A., Ariff, Z. M., Jikan, S. S. (2011). Evaluation on extrudate swell and melt fracture of polypropylene/kaolin composites at high shear stress. *J. Reinf. Plas. Compos., 30, 609-619*

Azizi, H., Ghasemi, I., Karrabi, M. (2008). Controled-peroxide degradation of polypropylene: rheological properties and prediction of MWD from rheological data. *Polym.Test., 27, 548-554*

Berzin, F., Vergnes, B., Delamare, L. (2001). Rheological behavior of controlled-rheology polypropyles obtained by peroxide-promoted degradation during extrusion: Comparison between homopolymer and copolymer. *J. Appl. Polym. Sci*, *80, 1243-1252*

Brydson J.A. (1970). *Flow Properties of Polymer Melts*. London; Iliffe Books.

Cogswell, N. (1981) *Polymer melt rheology: A guide for industrial practice*. Woodhead Publishing Limited.

Georgiou, G. (2004) Stick-Slip Instability. Polymer Processing Instabilities: Control and Understanding. Marcel Dekker, New York.

Gonzales, V. A., Velazquez, G. N., Sanchez, J. L. A. (1998). Polypropylene chain scissions and molecular weight changes in multiple extrusions. *Polym. Degrad. Stab., 60, 33-42*

Gotsis, A. D., Zeevenhoven, B. L. F., Tsenoglou, C. (2004). Effect of long branches on the rheological behaviour of polypropylene. *J. Rheo. 48, 895-914*

Gupta, R.K. (2000). *Polymer and Composite Rheology*. Marcel Dekker Inc. New York

Han C. D. (1976). *Rheology in Polymer Processing*. Academic Press. New York

Hingmann, R., Marczinke, B. L. (1994). Shear and elongational flow properties of polypropylene melts. *J. Rheo. 39, 573-588*

Jikan, S. S., Samsudin, M. S. F., Ariff, Z. M., Ishak, Z. A. M., Ariffin, A. (2009). Relationship of rheological study with morphological characteristics of multicomponent (talc and calcium carbonate) filled polypropylene hybrid composites. *J. Reinf. Plast. Compos. 28, 2577-2587*

Jikan S. S. (2010). Evaluation on flow behaviour of polypropylene/kaolin composites at high shear stress. *Phd Thesis*, Universiti Sains Malaysia.

Jikan, S. S[a]., Ariff, Z. M., Ariffin, A. (2010). Influence of filler content and processing parameter on the crystallization behaviour of PP/kaolin composites. *J. Therm. Anal.Calorm., 102, 1011-1017*

Karger-Kocsis J. (1995) *Polypropylene: structure and morphology*. Chapman and Hall, Cambridge.

Keawwattana, W. (2002). Phase behaviour, crystallization and morphological development in blends of polypropylene (PP) isomers and poly(ethylene-octane) copolymer. *Phd Thesis*. University of Akron.

Liang, J. Z. (2001). Pressure effect of viscosity for polymer fluids in die flow. *Polym., 42, 3709-3712*

Liang J. Z., Ness J. N. (1998). The melt die-swell behaviour during capillary extrusion of LDPE/PP blends. *Polym. Test.*, 17, 179-189

Liang, J. Z. (2008) Effects of extrusion conditions on die-swell behavior of polypropylene/diatomite composite melts. *Polym. Test., 27, 936-940.*

Liang, J. Z. (2002) The Melt Elastic Behaviour of Polypropylene/Glass Bead Composites in Capillary Flow. *Polym. Test, 21, 927-931.*

Liaw, W. C., Huang, P. C., Chen, C. S., Lo, L. C., Chang J. L. (2008). PPgMA/APTS compound coupling compatibilizer in PP/Clay hybrid nanocomposites. J. Appl. Polym. Sci.,*109, 1871-1880*

Maiti, S. N., Singth, G., Ibrahim, M. N. (2003). Rheological properties of calcium silicate-filled isotactic polypropylene. *J. Apply. Polym. Sci., 8, 1511-1218*

Muksing, N., Nithitanakul, M., Grady, B. P., Magaraphan, R. (2008). Melt rheology and extrudate swell of organobentonite-filled polypropylene nanocomposites. *Polym. Test., 27, 470-479*

Micheali, W. (1992). *Extrusion dies for plastic and rubber: design and engineering*. Munich. Hanser Publishers.

Ogawa, T. 1992. Effect of molecular weight on mechanical properties of polypropylene. *J. Appl. Polym. Sci, 31, 1151-1154*

Osswald, T.A. (1998) *Polymer processing fundamentals.* Munich. Carls Hanser Verlag.

Prentice, P. (1997). *Rheology and its role in plastics processing, Vol 7*, Rapra Technology Limited, United Kingdom.

Rahim N. A. A. (2010). Flow behaviour and viscoelastic properties of polypropylene-kaolin composites. *MSc Thesis*, Universiti Sains Malaysia.

Rahim,[a] N. A. A., Ariff, Z. M., Ariffin, A. and Jikan, S. S. (2011). A study on the effect of filler loading on flow and viscoelastic behavior of polypropylene/kaolin composites. *J. Appl. Polym. Sci., 119, 73-83*

Rahim[b], N. A. A., Ariff, Z. M., Ariffin, A. (2011). Flow behaviour and viscoelasticity of polypropylene-kaolin extruded composites at different temperatures. *Pertanika J. Sci. & Technol. 19, 383-388*

Rothon, R.N. (2003) *Particulate-filled polymer composites*. Rapra Technology Limited, United Kingdom.

Samsudin, M. S. F., Ishak, Z. A. M., Jikan, S. S., Ariff, Z. M., Ariffin, A. (2006). Effect of filler treatment on rheological behaviour of calcium carbonate and talc-filled polypropylene hybrid composites. *J. Appl. Polym. Sci*, *102, 5421-5426*.

Scheirs, J. (2000). *Compositional and Failure Analysis of Polymers.* England: John Wiley & Sons, Ltd.

Song, N., Zhu, L., Yan, X., Xu, Y., Xu, X. (2008). Effect of blend composition on the rheology property of polypropylene/poly (ethylene-1-octene) blends. *J. Mater. Sci., 43, 3218-3222.*

Shenoy, A.V., Saini, D.R. (1996) *Thermoplastic melt rheology and processing*. Marcel Dekker, Inc., New York.

Tanaka, H., White, J. L. (1980) Experimental investigations of shear and elongational flow properties of polystyrene melts reinforced with calcium carbonate,titanium dioxide and carbon black. *Polym Eng. Sci, 20, 946-956.*

Thitithammawong, A., Nakason, C., Sahakaro, K., Noordermer., J. (2007). Effect of different type of peroxide on rheological, mechanical, and morphological properties of thermoplastic based vulcanizates based on natural rubber/ polypropylene blends. *Polym. Test., 26, 537-546*

Wen, S. H., Liu, T. J., Tsou, J. D. (1994). Three-dimensional finite element analysis of polymeric fluid flow in an extrusion die. Part I: Entrance effect. *Polym. Eng. Sci., 14, 212-222*

White, J. L. (1973). Critique on flow patterns in polymer fluids at the entrance of a die and instabilities leading to extrudate distortion. *Appl. Polym. Symp, 20, 155-174.*

Yu, Y. W., Wu, P. V., Liu, T. J. (1997). Validity of one-dimensional equation governing extrusion die flow. *AlChe Journal, 43, 3117-3120*

4

Mechanical Behavior Variation of an Isotactic Polypropylene Copolymer Subjected to Artificial Aging

Hugo Malon, Jesus Martin and Luis Castejon
University of Zaragoza
Spain

1. Introduction

Most of the injuries suffered by motorcyclists and cyclists on Spanish highways are due to collision with guardrails, particularly with the posts that support these protective devices.

In order to lessen the effect of such accidents, the research group "New Technologies applied on Vehicles and Road Safety" (VEHIVIAL) of the University of Zaragoza is carrying out a series of studies, in collaboration with the company Taexpa S. A.

These studies are developing an innovative a system that will protect motorcyclists and cyclists from crashes against guardrails.

The material chosen for the development of this absorption system is commercial isotactic polypropylene copolymer, due to its great capacity to transform the kinetic energy of the shock into strain energy.

The developed system can be installed on the posts of the highways guardrails, where the polypropylene is affected by the environment, modifying the material mechanical properties.

The isotactic polypropylene is found in almost all of the polypropylene market. It is a crystalline thermoplastic material, so mechanical properties mainly depend on their molecular structure, their crystal structure and the macro-structure induced by the transformation process (Monasse & Haudin, 1995; Rodriguez et al, 2004; Varga, 1992; Fujiyama et al, 2002).

The chapter shows the analysis of the mechanical properties variation of an isotactic polypropylene copolymer, when this material is subjected to artificial aging according to the standard UNE 4892.

The selected material is polypropylene because it is the polymer that has a better impact resistance-price ratio.

2. Materials and experimental techniques

In order to obtain the variation of the mechanical behaviour of polypropylene copolymer under study, experimental and virtual testing techniques have been used.

In the first phase of the developed process a series of samples was subjected to artificial aging in a climatic chamber. The mechanical properties of the original material used and the aged polypropylene were obtained by tensile tests.

Once the mechanical properties of both materials were obtained, a series of numerical calculations by means of the Finite Elements Method (FEM) were made. The results of the numerical tests allow for obtaining the variation of the mechanical behaviour of the material subjected to artificial aging with respect to the original polypropylene.

2.1 Materials

The material used in the study is an isotactic polypropylene copolymer, because it is the polymer that has a better impact resistance-price ratio. To carry out the experimental tests 10 dumbbell-shaped samples of type 1B were mechanized from a square sheet of side 1000 mm and a thickness of 3 mm of this material .These samples were manufactured according to the standard UNE-EN-ISO 527-2.

2.2 Artificial aging of isotactic polypropylene copolymer

The aim of this test is to reproduce the effects that occur when materials are exposed to the environment.

Artificial aging tests of materials were carried out in laboratory under more controlled conditions than in the natural processes of aging. These tests were designed to accelerate the degradation of the polymer and the material failures.

For this, 5 samples were subjected to cyclical periods of UV exposure, followed by periods without radiation. During these cycles, changes in temperature and humidity were carried out according to the standard UNE 4892. This standard is the one governing the artificial aging tests and it was used as a guide in the investigation developed.

The artificial aging cycle applied consists in two hours of UV exposure at a temperature of 30ºC and a relative humidity of 62%, followed by one hour of condensation without radiation at a temperature of 40°C and a relative humidity of 90%. The duration of artificial aging process developed had been 78 hours, which corresponds to 26 cycles.

The equipment used in carrying out the artificial aging process is a climatic chamber Ineltec CC-150, which is located in the premises of the Department of Science and Technology of Materials and Fluids of the University of Zaragoza. The climatic chamber capacity is 125l and the maximum and minimum working temperatures of the machine are 150ºC and 10°C respectively.

Figure 1 shows the inside of the climatic chamber with the samples subjected to artificial aging. Figure 2 shows the position of the samples in the climatic chamber, which were positioned in the irradiation zone of the lamp. This lamp is represented in the figure 2 by an X.

2.3 Tensile test of mechanized samples

Once the samples of isotactic polypropylene copolymer were subjected to the artificial aging process, the next phase in the development process was to obtain and compare the mechanical properties of the aged material and the mechanical properties of the original material.

Fig. 1. Inside the climate chamber with 5 samples

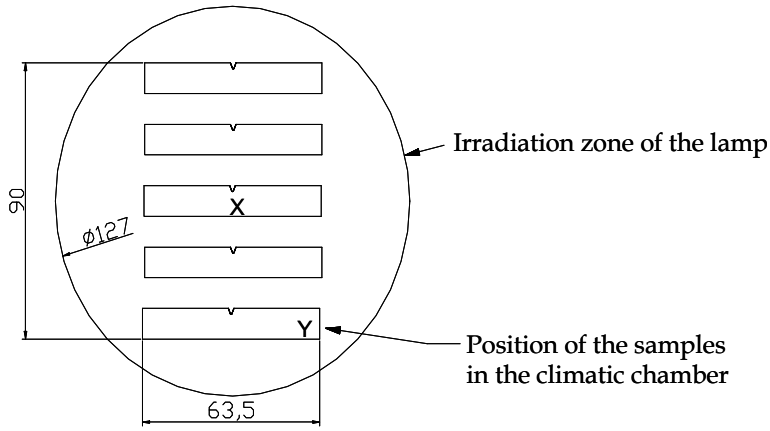

Fig. 2. Position of the samples in the climate chamber

The tensile test is the testing to obtain information of the mechanical properties of materials. The aim of this test is to obtain the elastic modulus, stress-strain curve, yield strength, tensile strength and elongation of a material.

In order to obtain these values, 5 samples with artificial aging (A1-5) and 5 samples without aging process (N1-5) had been tested according to the standard UNE-EN ISO 527 - 1996.

Tensile tests were carried out in an Instron 8032 testing machine at the Department of Mechanical Engineering at the University of Zaragoza. This testing machine has a load capacity of 100kN.

2.4 Numerical analysis by means of the Finite Elements Method (FEM)

The last phase of the study was to obtain the variation of the mechanical behaviour of the material subjected to artificial aging with respect to the original polypropylene in an impact.

The impact analysis in polymers has a number of difficulties (Kalthoff, 1993; Richardson & Wisheart, 1996; Moyre et al, 2000; Read et al, 2001; Tarim et al, 2001; Dean & Wright; 2003; Trudel-Boucher et al, 2003; Jimenez et al, 2004; Aretxabaleta et al, 2004; Aretxabaleta et al, 2004; Aretxabaleta et al, 2005; Davies et al, 2005; Alcock, 2006; Martinez et al, 2008; Aurrekoetxea et al, 2011), which complicate the analysis of such situations. The causes of this complexity have been summarized in the following points:

- The dynamic nature of the problem, including the phenomena of wave propagation Justify, single space (Aita et al, 1992; Bigi,1998)
- The three-dimensionality of the problem, often asymmetric and two-dimensional simplifications being insufficient (Wierzbicki, 1989)
- The behaviour of materials at extreme loads caused by an impacts is almost always non-linear (Krieg & Key, 1976)
- The simulation of material behaviour must be representative of the entire range of strains rates that develop in the impact (Hull, 1985)

The numerical analysis by means of the FEM is a tool to provide solutions to the problems described. This numerical technique has been used and validated in previous studies (Martin et al, 2007). In these previous studies, reliable results were obtained in polypropylene impact.

2.4.1 Application of the FEM

The test to reproduce numerically, by means of the FEM, is the freefall impact of a steel semisphere of diameter 25mm against a square sheet of side 110mm and a thickness of 3mm of polypropylene. This model was validated in previous studies to analyze impact polypropylene sheets. The sheet has been discretized with shell elements of 4 nodes (S4R) and the semi-sphere has been discretized with volumetric elements of 6 or 8 nodes (C3D6 o C3D8R). Figure 3 shows the sheet in green and the semisphere in red. The model consists of 5352 elements and 5568 nodes.

The mechanical properties used in the definition of polypropylene were the averages of the results obtained in tensile tests carried out on the samples subjected to artificial aging and the initial polypropylene samples. The material of the semi-sphere was defined as a linear steel with a Young modulus E = 210GPa, density γ = 7850 kg/m^3 and Poison ratio υ = 0.3.

The methodology applied in the virtual test development has been based on the application of numerical techniques by means of the Finite Element Method (FEM) with the explicit integration of a dynamic equilibrium equation.

Changes in Kinetic energy and strain energy, as well as the displacements in the sheet, are obtained from the simulations for the material with and without artificial aging.

These results provide important information in the optimization process of the developed protection system, because they indicate how the material behaviour changes with the environment, and how it affects the functionality of the energy absorption system developed.

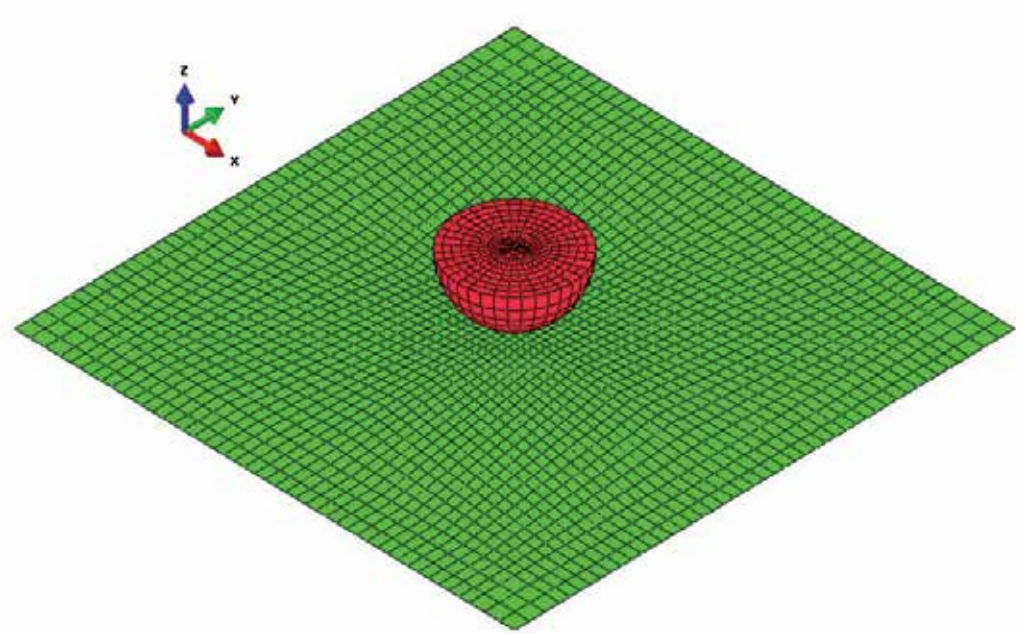

Fig. 3. Finite elements model

2.4.2 Load cases and boundary conditions

The load cases analyzed corresponds to the freefall impact of a steel semi -sphere of 25 mm diameter against a polypropylene sheet of a thickness of 3mm.

In order to obtain greater reliability in the results, three load cases have been analyzed. The difference in load cases is the difference of the height at which the semi-sphere drops.

In order to reduce the computational cost (computation time) of the simulations, the simulation was not carried out on the total trajectory of the semi sphere. Instead, the speed of the semi sphere in the instant previous to the impact was calculated. With this speed and in that position of the semi sphere, the numerical simulation test was initiated. This technique allows for saving the computation time in which the semi-sphere covers the distance from the initial height of the test to the instant previous to the impact with the sheet.

The speed at the instant previous to the impact was obtained by an energy balance, in which at the initial instant of the test, the kinetic energy of the semi sphere is zero ($v_1 = 0$) and at the instant previous to the impact, the potential energy of the semi sphere is zero ($h_2 = 0$). Therefore the potential energy of the sphere at the initial instant of the test is transformed into kinetic energy of the semi sphere in the instant previous to the impact. The following equations show the process developed in order to obtain the speed of the semi sphere at the instant previous to the impact against to the polypropylene sheet.

$$EC_1 + EP_1 = EC_2 + EP_2 \tag{1}$$

$$\frac{1}{2} * m_1 * v_1^2 + m_1 * g * h_1 = \frac{1}{2} * m_2 * v_2^2 + m_2 * g * h_2 \quad (2)$$

$$\frac{1}{2} * m_1 * 0 + m_1 * g * h_1 = \frac{1}{2} * m_2 * v_2^2 + m_2 * g * 0 \quad (3)$$

$$m_1 * g * h_1 = \frac{1}{2} * m_2 * v_2^2 \quad (4)$$

$$v_2 = \sqrt{2 * g * h_1} \quad (5)$$

Figure 4 shows a diagram of the starting position and the instant previous to the impact

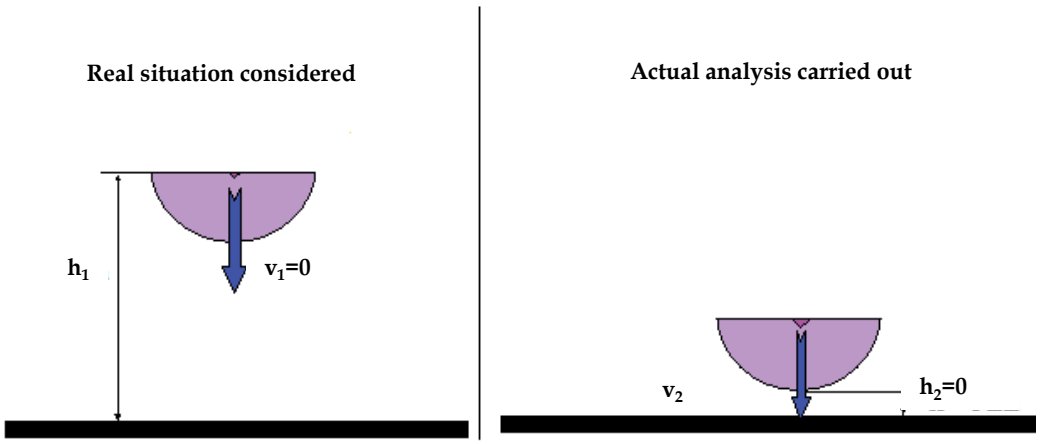

Fig. 4. Diagram of the starting position and the instant previous to the impact

The load cases analyzed are shown in Table 1. The table shows the initial height in the test and the velocity of the semi sphere at the previous instant of the impact.

Load case	Initial height (mm)	Impact velocity (m/s)
1	1,575	5.56
2	790	3.94
3	527	3.21

Table 1. Initial height and impact velocity of the load cases

The imposed boundary conditions reproduce those of a freefall impact test, in which the contour of the sheet is fastened. In virtual testing, rotations and displacements were constrained in nodes located less than 10mm from the edge of the sheet, which are shown in red in Figure 5.

3. Results

Tensile tests carried out on samples of original polypropylene and polypropylene subjected to artificial aging had provided force-displacement curves of the materials, which are shown in figures 6 and 7.

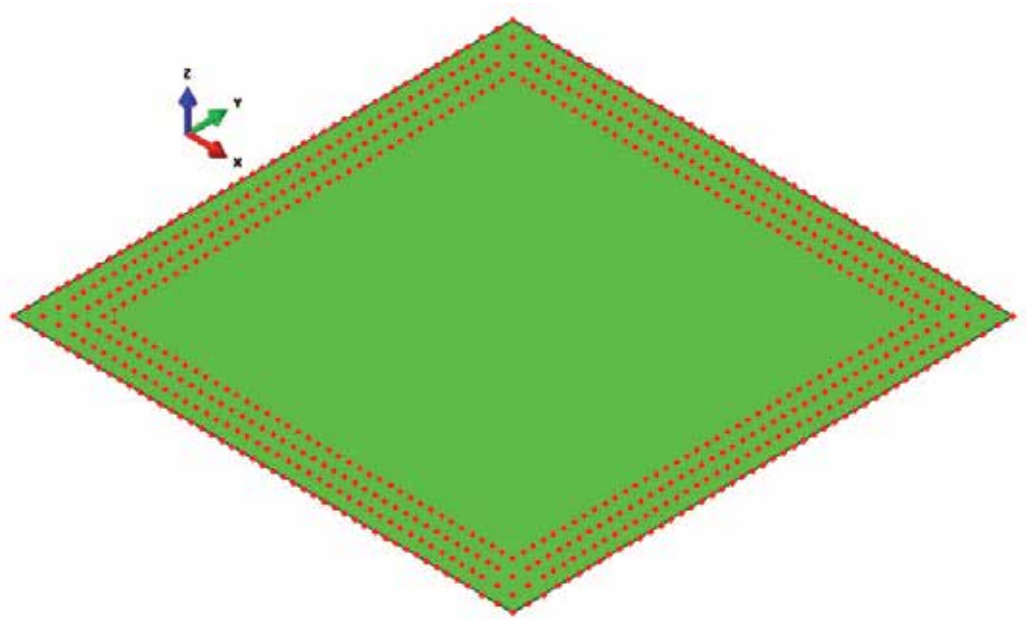

Fig. 5. Nodes with displacements and rotation constrained by the boundary conditions

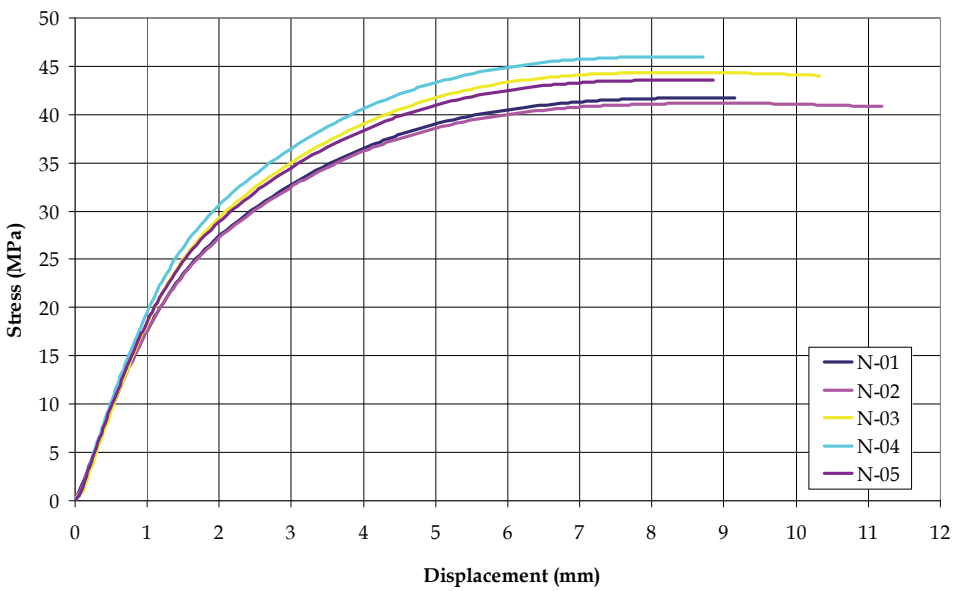

Fig. 6. Stress-displacements curves of the original polypropylene samples

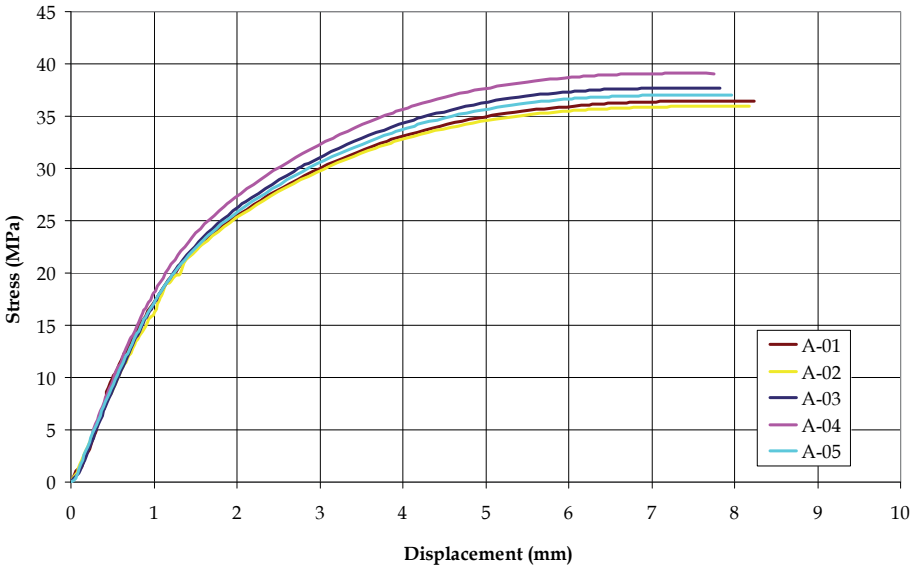

Fig. 7. Stress-displacements curves of the polypropylene subjected to artificial aging samples

The results of tensile tests recorded allow for obtaining the mechanical properties of the materials studied. The Young's modulus of both materials was calculated from σ_1 (stress at a strain of 0.0005) and σ_2 (stress at a strain of 0.0025) according to the standard UNE-EN ISO 527-1. Tables 2 and 3 shown the Young's modulus and the tensile strength obtained of the tensile tests. The other mechanical properties used were density γ = 7850 kg/m^3 and Poison ratio υ = 0.3.

Non-aged samples	E_t [MPa]	R_m [MPa]
N1	671,160	41,732
N2	718,130	41,177
N3	841,690	44,369
N4	744,030	46,011
N5	746,610	43,563
Mean	744,324	43,370
Standard deviation	55,72	1,77

Table 2. Mechanical properties of non-aged polypropylene

Aged samples	E_t [MPa]	R_m [MPa]
A1	717,650	38,338
A2	724,760	36,001
A3	652,320	36,472
A4	688,720	37,025
A5	805,950	37,714
Mean	717,880	37,110
Standard deviation	50,89	0,839

Table 3. Mechanical properties of aged polypropylene

Once the virtual tests through the MEF had been run, the analysis of the mechanical behaviour variation of the polypropylene subjected to artificial aging with respect to the original material began. First, the maximum vertical displacements in the sheet were compared for each of the three load cases analyzed. In all cases the maximum vertical displacement and permanent deformation were higher in samples subjected to artificial aging. The difference of vertical displacement and permanent deformation between sheets of material subjected to artificial aging and sheets of original material was greater on increasing initial height of the test. These results are shown in figure 8.

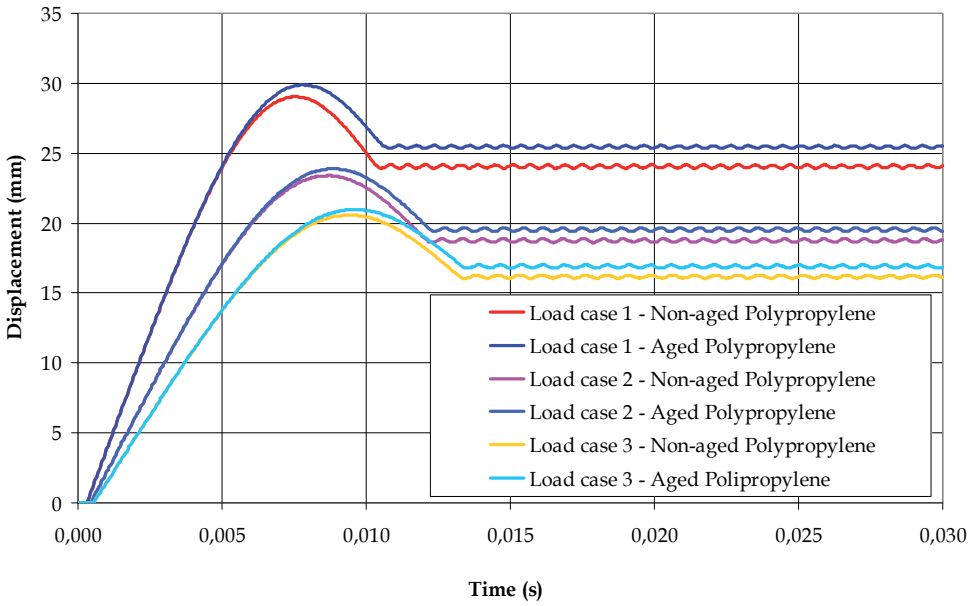

Fig. 8. Maximum vertical displacement on the sheet

The second parameter analyzed is the kinetic energy of the semi sphere, figure 9. The results obtained show that the kinetic energy of the semi sphere after the impact against the sheets of polypropylene subjected to artificial aging is lower than in the impact against the original material sheets for the three load cases analyzed. This greater reduction of the kinetic energy implies a lower speed of the semi sphere in the simulations with polypropylene subjected to artificial aging with respect to the simulation with original material.

The third parameter analyzed is the strain energy, figure 10. This parameter represents the energy used in the deformation of the Polypropylene sheet on the impact. The results obtained show that the energy used in the deformation of the polypropylene sheet subjected to artificial aging is higher than in the original material for the three load cases analyzed.

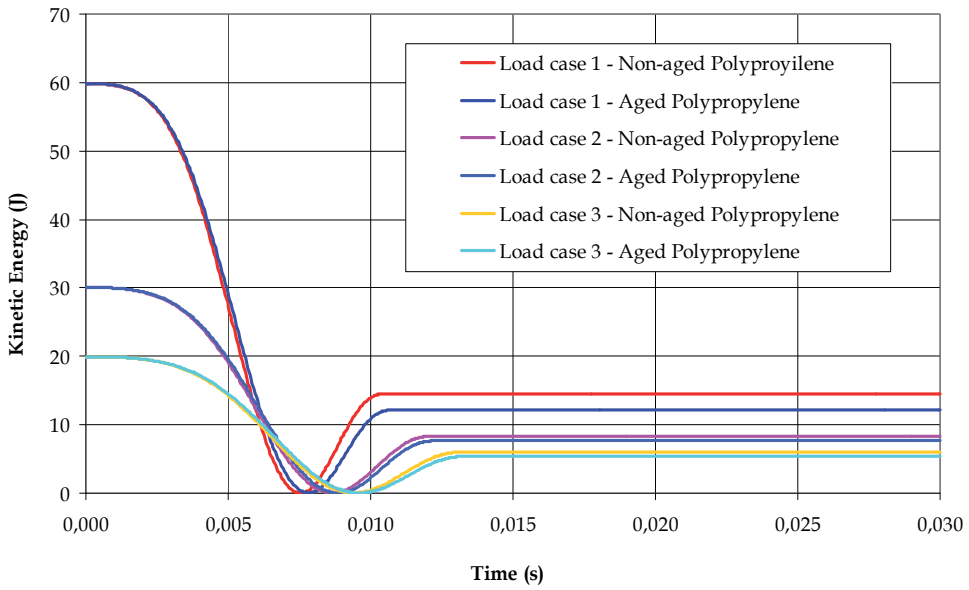

Fig. 9. Kinetic energy of the semi-sphere

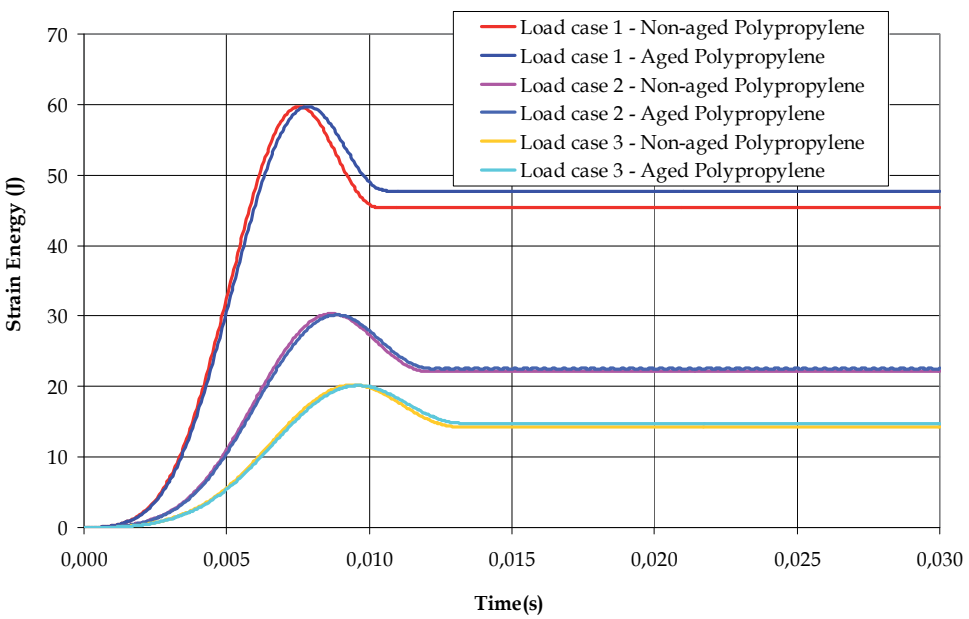

Fig. 10. Strain energy in the sheet

Table 4 summarizes the results of maximum displacements and strain energy in the sheet and the kinetic energy of the semi sphere obtained of the virtual simulations by means of the MEF.

Load case		Non-aged Polypropylene	Aged Polypropylene
1	Initial Kinetic Energy (J)	59,85	59,85
	Final Kinetic Energy(J)	14,44	12,12
	Reduction of Kinetic energy (%)	75,87	79,75
	Reduction of Kinetic energy (J)	45,41	47,73
	Final Strain Energy (J)	45,34	47,72
2	Initial Kinetic Energy (J)	30,05	30,05
	Final Kinetic Energy(J)	8,32	7,63
	Reduction of Kinetic energy (%)	72,31	74,61
	Reduction of Kinetic energy (J)	21,73	22,42
	Final Strain Energy (J)	21,21	22,35
3	Initial Kinetic Energy (J)	19,95	19,95
	Final Kinetic Energy(J)	6,02	5,39
	Reduction of Kinetic energy (%)	69,82	72,98
	Reduction of Kinetic energy (J)	13,93	14,56
	Final Strain Energy (J)	13,86	14,25

Table 4. Results obtained of the virtual simulations by means of the FEM

4. Conclusions

The research process developed allows for obtaining the mechanical properties variation of isotactic polypropylene copolymer subjected to artificial aging.

For this, 10 samples were machined from a sheet of polypropylene copolymer. Five samples were subjected to artificial aging in a climatic chamber.

Subsequently, 10 samples (5 of material subjected to artificial aging and 5 samples of original polypropylene) were subjected to tensile tests in order to obtain the mechanical properties of the original polypropylene and the material subjected to artificial aging.

After obtaining the mechanical properties, numerical analysis by Means of the Finite Element Method (FEM) with explicit integration of dynamic equilibrium equation was carried out. These numerical techniques allow for obtaining reliable results of impacts against polypropylene sheets. Virtual simulations allow for obtaining the maximum displacements in the sheets, the kinetic energy reduction of the semisphere and the energy absorbed by the sheet in the load cases analyzed.

The results show a mechanical behaviour similar to the material subjected to artificial aging with respect to original polypropylene in all the load cases analyzed. Moreover, in all the load cases analyzed the sheets of the material subjected to artificial aging reduce the kinetic energy by a greater amount with respect to the sheets of the original polypropylene. Thus, artificial aging improves the behaviour of the material for use in energy absorption systems.

The minimal variations obtained of the mechanical properties of polypropylene subjected to artificial aging with respect to the original material show that the polypropylene is a suitable material for the design of systems to protect motorists and cyclists. These protection systems are continually exposed to environmental effects, and therefore a continuous aging process.

5. References

Aita, S., El-Khaldi, F., Fontaine ,L., Tamada, T, & Tamura, E., (1992) Numerical Simulation of Stretch Drawn Autobody. Part 1:Assessment of Simulation Methodology and Modelling of Stamping Components,1992 *Proceedings of SAE International Congress 1992*, Detroit,USA

Alcock B. (2006) Low velocity impact performance of recyclable all-polypropylene composites. *Compos. Sci. Technol.*, 66(11–12), pp. 1724–1737.

Aretxabaleta, L., Aurrekoetxea, J., Urrutibeascoa, I. & Sánchez Soto. M. (2004) Caracterización de materiales termoplásticos sometidos a impactos de baja velocidad, *2º Congreso nacional de jóvenes investigadores en polímeros*, Zarauz (Guipúzcoa), 6-10 junio

Aretxabaleta, L., Aurrekoetxea, J., Urrutibeascoa, I. & Sánchez Soto M. (2004) Caracterización a impacto de plásticos: modelos con criterio de fallo, *Anales de mecánica de la fractura*, Vol. 21, pp.310-314

Aretxabaleta L., Aurrekoetxea J., Urrutibeascoa I.& Sánchez-Soto M. (2005) Characterisation of the impact behaviour of polymer thermoplastics. *Polymer Testing*, Vol.24, pp.145–151.

Aurrekoetxea J.; Sarrionandia M.; Mateos M & Aretxabaleta L. (2011) Repeated low energy impact behaviour of self-reinforced polypropylene composites. *Polymer testing*. Vol.30, Issue. 2, pp. 216-221.

Bigi, D., (1988) Simulazione numerica dei problemi di crash veicolistico. *ATA Ingegneria automotoristica*, Vol.41, nb.5, pp386-392.

Davies G.A.O., Zhang X., Zhou G. & Watson S. (2005) Numerical modelling of impact damage. *100th Anniversary Conference and Exhibition of the Centre-for-Composite-*

Materials, *Imperial College of Science Technology and Medicine*. *Composites* Vol. 25 Issue.5, pp. 342-350

Dean, G. & Wright, L., (2003) An evaluation of the use of finite element analysis for predicting the deformation of plastics under impact loading, *Polymer Testing*, VOl.22, pp.625-631

Fujiyama, M., Kitajima, Y. & Inata, H. (2002) Structure and properties of injection-molded polypropylenes with different molecular weight distribution and tacticity characteristics. Journal of applied polymer Science. Vol.84 (12), pp.2142-2156

Hull,D., (1985) Impac Response of Structural Composites, *Composite Materals*, pp.35-38

Jiménez, O., Sánchez-Soto, M., Santana, O. O., Maspoch, M. Ll., Gordillo, A.,. Velasco. J. I & Martínez. A. B., (2004), Identación por impacto de baja energía: modelo completo, *Boletín de la Sociedad Española de Cerámica y Vidrio*, Vol.43, pp. 324-326

Kalthoff J.F. (1993) On the validity of impact energies measured with polymeric specimens in instrumented impact tests. *Impact Dynamic Fract Polym Compos ESIS*, Vol. 19.

Krieg, R.D. & Key, S.W. (1976) Implementation of a time dependent plasticity into structural computer programs. Constitutive equations in Viscoplasticity: Computational and Engineering aspects, Vol.20

Martin, J., Malon, H. & Castejón, L. (2008) Validation of the Finite Element Method Applied to Isotactic Polypropylene Homopolymers. *Polymers & Polymer Composites*, Vol.16(0), pp.457-463.

Martínez A.B., Velasco J.I., Gordillo A., & Jiménez, O. (2008) Impacto de baja energía en polímeros y composites. *IX Simposio Latinoamericano de Polímeros/VII Congreso Iberoamericano de polímeros.* Valencia (Spain).

Monasse, B., & Haudin, J.M. (1995). *Popypropylene: Structure, Blends and Composites, Vol I, Structure and Morfology*, Ed.Chapman .Hall, London, pp.3-30.

Morye S.S., Hine P.J., Duckett R.A., Carr D.J. &. Ward I.M (2000), Modelling of the energy absorption of polymer composites upon ballistic impact. *Compos Sci Technol*, Vol. 60, pp.2631–2642

Read B.E., Dean G.D, & Wright L. (2001) Modelling non-linear stress-strain behaviour of rubber-toughened plastics. *Plastics, Rubber and Composites*, Vol. 30, pp. 328.

Richardson M.O.W. & Wisheart M.J. (1996) Review of low-velocity impact properties of composite materials. *Composites: Part A*, 27A, pp. 1123–1131

Rodríguez, S., Perea, J. M., & Vargas, L. (2004) Modelización de propiedades mecánicas del polipropileno: Parte I, grados de síntesis. *Revista de plásticos modernos: Ciencia y Tecnología de polímeros,* nº. 573, pp. 257-262, *ISSN 0034-8708*.

Tarim N., Findik F. & Uzun H. (2001) Ballistic impact performance of composite structures. *Compos Struct*, Vol. 56, pp. 13–20.

Trudel-Boucher D., Bureau M.N., Denault J, & Fisa B. (2003) Low-velocity impacts in continuous glass fiber/polypropylene composites. *Polymer Composites* 24(4), pp.499–511.

Varga, J.(1992) Review: Supermolecular structure of isotactic polipropylene, *Journal of Materials Science* Vol.27, pp. 2557-2579

Wierzbicki, T., (1989) *Geometrical Modeling for Crash*, Post Symposium Short Course of the 2nd International Symposium of Plasticity, Nogoya Agosto1989

5

Thermal Oxidation of Polypropylene and Modified Polypropylene – Structure Effects

Lyudmila Shibryaeva
N.M. Emanuel Institute of Biochemical Physics,
Russian Academy of Sciences,
Russia

1. Introduction

Ageing and stabilization polymers is a major part of materials science. Aging of polymers defined as a set of chemical and physical transformations, leads to the loss of their set the desired properties. The main role in these transformations belong to chemical processes of degradation and crosslinking of macromolecules. Processes decomposition and structuring polymer conjugates include radical - chain, ionic and molecular reactions. Traditionally, the distinction is made between thermal, thermal-, photo-and radiation-chemical aging. Thermal oxidation and thermal-oxidative destruction are the most common and important processes in which polymer materials participate. It accompanies the posed for chemists-experimenters and producers engaged in polymer materials creation is the problem of maintenance of high quality of output, prolongation of its service life at conditions of thermal oxidation influence and thermal-oxidative destruction. Thermal oxidation of polymers leads to a modification and functionalization of the polymer chains. At the same time thermal oxidation is accompanied by the destruction of bonds in the macromolecules and influence the destructive processes. Thermal oxidation of polymers - a radical chain process with degenerate branching of kinetic chains of oxidation. The structure of polymer significantly influences on chain oxidation and destructive processes. Heterogeneity of polymers structures, the presence of regions differing in amplitudes of molecular motions, decrease of segment mobility, reduction of oxygen diffusion coefficient underlie this effect. These factors change kinetics and mechanism of process. As new methods and polymeric materials, researchers returned to the discussion of the induction period of oxidation of polymers. However, often in the literature there is confusion in the very concept and definition of the period induction. For example, when studying the thermal oxidative degradation of PP with different tacticity by thermogravimetric analysis (Chan J.H., Balke S.T., 1997; Nakatani H. and al., 2005) determine the induction period as a time corresponding to the onset of weight loss. I.e in fact, the period induction regarded not as the beginning of oxidation in infancy kinetic chain, and the time corresponding to the branching of kinetic chains in the collapse of hydroperoxide. This is a fundamental difference, so it is important this issue be considered. Often thermal-oxidative degradation is identified with the thermal oxidation. However, in depending on the nature of the polymer,

thermal oxidation process can take place without destruction chains, and with functionalization. As in the case of isotactic polypropylene. The author of the chapters of the book sets the task of separating the concepts related to the kinetics and mechanism.

2. The particularities of oxidation of polypropylene

2.1 The kinetics and mechanism of autooxidation of solid polymers

Three types reactions can be in the polymers in the presence of oxygen. 1) Separately occurring molecule reactions. 2) The radical - chain mechanism 3) The products of thermal decomposition and oxidation of polymers catalyze further decomposition of the polymer. The thermal oxidation of polyolefynes has been extensively investigated in various works. The investigation of the kinetics and mechanism of oxidation of solid polymers have shown convincingly that this process is a radical - chain with degenerate branching of kinetic chains. In the thermal degradation, thermooxidation and thermal oxidative degradation of polymers play a major role alkyd (R*), alkoxide (RO*) and peroxide (RO_2*) macroradicals and low molecular weight radicals (r*). The high reactivity of the past towards macromolecules strongly influences on aging processes. The chain reaction of the oxidation of a polymer includes alternate steps of the chain propagation proceeding either inside the same macromolecule or between two molecules. The investigation of kinetics of oxidation of the polymers, containing aliphatic groups (≡ C-H, -CH_2- or –CH_3), showed that this process was described by scheme, corresponding to the mechanism of chain oxidation of liquid phase (Denisov E.T. and all., 1975).

2.1.1 Initiation of kinetic chain of oxidation

For the oxidation of the polymer to the formation of macroradicals R *.

$$RH \longrightarrow R^* + H^* \quad (1)$$

Where RH - the monomer units of polymer. Reaction can be triggered by physical factors such as ultraviolet and ionizing radiation, heat, ultrasound, or mechanical treatment chemical factors, such as catalysis, a direct reaction with molecular, singlet or atomic oxygen and ozone. However, initiation by direct interaction of molecular oxygen with the polymer, leads to detachment of a hydrogen atom, was unlikely, because it is endothermic reaction, enthalpy is 126-189 kJ/mol (Chan J.H., Balke S.T., 1997). Often, the birth of the chain portrayed as the bimolecular interaction of oxygen with the monomer units of polymer

$$RH + O_2 \longrightarrow [RHO_2] \longrightarrow R^* + HO_2^* \quad (2)$$

HO_2* radicals, which formed, can enter on reaction with neighboring RH or on reaction of recombination with the primary radical R *

$$RH + O_2 \xrightarrow{k_o} [R^* + HO_2^*; RH] \longrightarrow \sigma R^* \quad (3)$$

Therefore, the radical yield (f) is: $0 < \sigma < 2$. RH- may be neighboring monomer units of one macromolecule or belong to different macromolecules. At the origin of the chain oxidation may participate impurities of transition metals, residues of catalysts or initiators, etc. These impurities get into the polymer as a result of receiving or processing the polymer. Table. 1

shows the rate of nucleation of chains, obtained by different authors inhibitor method, calculated from the rate of inhibitor consumption in polyethylene, polypropylene and some liquid hydrocarbons. The values of W_o are small, so usually, when considering the kinetics of the autoxidation of polyolefins, nucleation rate of the chain is neglected compared with the rate of branching.

Substance	T,K	po_2, millimeters of mercury	Wo_2, mol/l• s	E, kJ/mol
PEHD	404	750	$1.3\ 10^{-6}$	117.0
PELD	377	750	$3.4\ 10^{-7}$	146.5
PE	391	750	$1.5\ 10^{-7}$	-
PE melt	473	300	$8.0\ 10^{-7}$	-
PP	405	750	$2.1\ 10^{-6}$	92.0
	403	750	$2.4\ 10^{-6}$	-
Atactic PP	403	300	$<1.2\ 10^{-8}$	-
	423	300	$<6.0\ 10^{-8}$	-
Isotactic PP	453	300	$< 7.0\ 10^{-8}$	-
	463	300	$< 2.7\ 10^{-6}$	-
2-Methylbutane	473	300	$< 5.6.10^{-6}$	-
	410	4725	$2.2\ 10^{-9}$	159.0
n-Heptane	406	4100	$1.4\ 10^{-9}$	181.0

Table 1. The kinetic parameters of nucleation reaction chain (RH +O2) in polyethylene, 7 polypropylene and liquid hydrocarbons

2.1.2 Growth of the chain

The development of the kinetic chain by alternation of two reactions: the formation of peroxide radicals (RO_2 *) and hydroperoxide (ROOH). Macroradicals R*, appeared in the initiation can easily react with oxygen molecules to give peroxide radicals RO_2 * Peroxide radical can pull hydrogen from another polymer molecules to form polymeric hydroperoxides:

$$R^* + O_2 \xrightarrow{k_1} RO_2^* \quad (4)$$

$$RO_2^* + RH \xrightarrow{k_2} \alpha ROOH + R^* \quad (5)$$

where k_2 - the constant of continuation of kinetic chain rate.α - the yield of hydroperoxide per mole of absorbed oxygen. In the solid polymer free radical R * and hydroperoxide group, formed in reaction (5) can not be away from each other. Part of ROOH is destroyed immediately after the formation of the reaction:

$$ROOH + R^* \longrightarrow RO^* + ROH \quad (6)$$

The reaction of (6) leads to a decrease in the yield of hydroperoxides during the oxidation of polymers in comparison with the oxidation of liquid hydrocarbon model. Their output ROOH is close to 100%. In the presence of oxygen even at low concentrations of the radicals

R* are converted into RO_2* continue to ROOH. The concentration of the radicals R* is negligible compared to RO_2*, so oxidation rate (Wo_2) is determined (limited) reaction rate (5). In this case: $Wo_2 = k_1 [R^*] [O_2] = k_2 [RO_2^*] [RH]$.

2.1.3 The stage of branching of kinetic chain

Branching of the kinetic chain of oxidation occurs in the decay of polymer hydroperoxides. Generally, consider a few basic mechanisms of decomposition of hydroperoxide

$$ROOH \xrightarrow{k'_d} RO^* + OH^* \quad (7)$$

$$ROOH + RH \xrightarrow{k_d} RO^* + R^* + H_2O \quad (8)$$

$$2\,ROOH \xrightarrow{k''_d} RO^* + H_2O + RO_2^* \quad (9)$$

where k_d, k'_d, k''_d - the constants of ROOH decomposition rate.

Monomolecular decay (7) comes with a large activation energy (140-160 kJ / mol). It occurs only in the oxidation of hydrocarbon fluids in the case of low concentrations of ROOH in solvents not containing weakly bound hydrogen atoms. Are more favorable reaction (8) and (9). Heat of reaction (9) is ~ 36 kJ / mol, and for reaction (8) varies widely depending on the binding energy of the R-H. Reaction (9) dominates at high concentrations of hydroperoxide, the reaction (8) - in small quantities. In polymers containing weakly bound hydrogen atoms are predominant mechanism (8). As usual [ROOH] <<[RH], ROOH decay is described by a kinetic equation of first order.

2.1.4 Chain transfer

The particularity of harden phase oxidation of polyolefyne is reaction of chain transfer – interaction of alkyl (R*) or alkoxy radical (RO*) with polymer competitive to its reaction with oxygen:

$$R^* + R'H \xrightarrow{k''_2} R'^* + RH \quad (10)$$

$$[R'^*, R''^*, RO^*, OH^* + RH \longrightarrow R^* + R'H, R''H, ROH, H_2O]$$

2.1.5 Chain termination

Break radical chain due to the interaction of free radicals with each other to form inactive products. There is quadratic termination of peroxide radicals at high pressure of oxygen:

$$RO_2^* + RO_2^* \xrightarrow{k_t} O_2 + \text{molecular products} \quad (11)$$

Chain termination at low pressure of oxygen is quadratic termination of alkyl radicals

$$R^* + R^* \xrightarrow{k_4} R - R \quad (12)$$

and alkyl with peroxide radicals:

$$RO_2^* + R^* \xrightarrow{k_5} ROOR \quad (13)$$

Where k_t, k_4, k_5 – the constants of chain termination rate.

2.2 The kinetics and mechanism of autooxidation PP

Oxidation PP occurs in the amorphous regions of the polymer. Localization process in the amorphous regions was confirmed by small-angle X-ray scattering, by direct measurements of oxygen solubility in the samples with varying degrees of crystallinity, by the spin-paramagnetic resonance and other methods. The soluble oxygen, impurities, that contribute to the initiation of oxidation (traces of polymerization catalysts, traces of carbonyl groups, hydroperoxide and unsaturated groups) are localized in the amorphous regions polymer. This leads to a higher initiation rate in the amorphous areas compared to the total weight of the polymer. In the crystalline phase of PP on steric reasons, prohibited further kinetic chain reaction of oxidation. Even with the presence of peroxide radicals in the crystalline phase are not involved in the development of kinetic chains of oxidation of the crystallites. These radicals can formed by the action of γ- radiation on the polymer. RO_2^* slowly dying in the crystallites by the decay of education low-molecular radicals, which may go into an amorphous phase, initiating there oxidation.

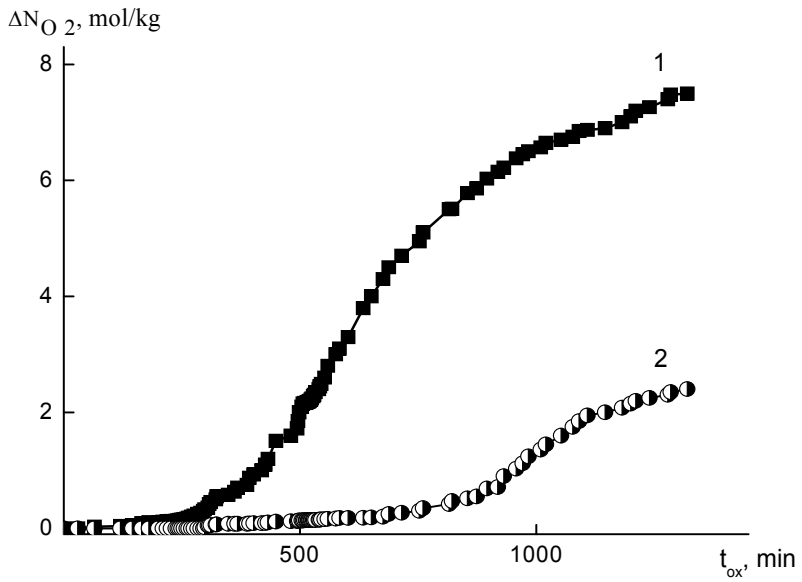

Fig. 1. The kinetic curve of oxygen absorption PP (1), and PE (2) T_{ox} =110°C, p_{o2} = 600 mm Hg

Oxidation of polypropylene describes the kinetic curve of oxygen absorption, which has an S-shape (fig.1). This curve is characterized by an induction period of self-acceleration and deceleration of oxidation in a deep stage of the process. A typical kinetic curve of oxygen uptake for isotactic PP is shown in Figure 1. For comparison, the kinetic curve for polyethylene (PEHD). The kinetic equation represents the dependence of the amount of

absorbed oxygen from the oxidation time was determined applied to the polypropylene in (Emanuel N.M., Buchachenko A.L., 1982). With this purpose it was used a special mathematical model for handling the above proposed scheme of oxidation of solid polymers. It was suggested the following approach: the origin of kinetic chain occurs at hydroperoxide decomposition (equation (8).The rate of this reaction (which is reaction of degenerate branching of kinetic chains) in the early stages process considerably exceeds the rate of primary initiation (1).This allows to neglect the primary initiation reaction (1) and assume that the nucleation rate kinetic chain is the speed of degenerate branching. In this case, the initiation rate is determined from the equation:

$$w_i = 2\delta k_d[RH][ROOH]$$

where δ- probability going out of the radicals on one hydroperoxide group which is broken, i.e. probability of degenerate branching, 2δ - number of kinetic chains, born of every molecule of hydroperoxide decomposed. Type of reaction, limiting the development of kinetic chains (4) or (5), depends on the oxygen concentration $[O_2]$, consequently on the concentration of radicals R * and RO_2 *. Concentration ratio $[R^*]/[RO_2^*]$ from the condition

$$k_1[O_2][R^*] = k_2[RH][RO_2^*]$$

whence $[R^*] / [RO_2^*] = k_2[RH]/ k_1[O_2] \cong 10^{-2} \div 10^{-4}$. Thus, the kinetic chain termination occurs only with peroxide radicals. The termination of kinetic chain occurs by a quadratic law:

$$2RO_2^* \xrightarrow{k_t} ROOR + O_2$$

Kinetic equations for determining the rate of oxygen absorption can be obtained from the kinetic equations for the intermediate concentrations of particulate matter:

$$d[R^*]/dt = 2\delta k_d[RH][ROOH]+ k_2[RH][RO_2^*]- k_1[O_2][R^*] \quad (14)$$

$$d[RO_2^*]/dt = k_1[O_2][R^*] – k_2[RH][RO_2^*]- k_t[RO_2^*]^2 \quad (15)$$

$$d[ROOH]/dt = k_2[RH][RO_2^*]- k_d[RH][ROOH] \quad (16)$$

Since the slow processes of oxidation can be applied to the quasi-steady concentration of radicals, i.e. $d[R^*]/dt= d[RO_2^*]/dt = 0$.From the equation (14) and (15) follows the expression

$$[RO_2^*] = (2\delta k_d[RH][ROOH]/k_t)^{1/2} \quad (17)$$

Where the rate of oxygen uptake

$$d\Delta[O_2])/dt = k_1[O_2][R^*] = 2\delta k_d[RH][ROOH]+ k_2[RH][RO_2^*] =$$

$$= 2\delta k_d[RH][ROOH]+ k_2(2\delta k_d/k_t)^{1/2}[RH]^{3/2}[ROOH]^{1/2} \quad (18)$$

$\Delta[O_2]$ - means the amount of oxygen, which absorbed at a given moment of time.

From equations (14) and (16)

$$d(\Delta[O_2])/dt = d[ROOH]/dt + (1+2\delta)k_d[RH][ROOH] \quad (19)$$

From equation (19) that since the maximum concentration of hydroperoxide (d[ROOH]/ dt = 0), the rate of oxidation is proportional to the speed of its disintegration. The proportionality factor ((1+2δ) can vary from 1 to 3 (as 0 ≤δ≤ 1). Substitute equation (17) in the equation (16) gives:

$$d[ROOH]/dt = k_2(2\delta k_d/k_t)^{1/2}[RH]^{3/2}[ROOH]^{1/2} - k_2[RH][ROOH] \quad (20)$$

Integration (20) at [RH] = const, gives the equation:

$$[ROOH] = [ROOH]_{max}\{1-[1-([ROOH]_o/[ROOH]_{max})^{1/2}]\exp(-k_d[RH]\, t/\, 2)\}^2 \quad (21)$$

Where $[ROOH]_{max} = (2\delta k^2_2/\, k_d\, k_t)\, [RH]\, t$; $[ROOH]_{max}$, $[ROOH]_o$ -maximum and the initial concentration of hydroperoxide, respectively. So far as $[ROOH]_o << [ROOH]_{max}$,value ratio $[ROOH]_o/[ROOH]_{max}$ - infinitely small quantity, which can be neglected. In this case the expression (21) takes the form:

$$[ROOH] = [ROOH]_{max}[1-\exp((-k_d[RH]/2)t)]^2 \quad (22)$$

Substituting equation (19) in (15) and integrating gives the expression

$$\Delta[O_2]/[ROOH]_{max} = k_d(1+2\delta)[RH]t +2(1+4\delta)[\exp(-k_d[RH]t/2)-1]-$$

$$-2\delta[\exp(-k_d[RH]t)-1] \quad (23)$$

Equation (23) represents the integral form of the dependence of the amount of absorbed oxygen from the oxidation time. This dependence is valid for shallow oxidation, we can neglect the flow of the polymer and assume [RH] = const. Expanding the exponential terms in the series for small t, and only the first three terms, gives the expression:

$$\Delta[O_2] = (k^2_2\delta k_d[RH]^3/\, 2k_t)t^2 = \Phi^2t^2 = 1\, /\, 2\, [ROOH]_{max}k^2_d[RH]^2\, t^2 \quad (24)$$

So. oxygen uptake at the beginning of oxidation should be proportional to t^2; Φ - self-acceleration factor of the reaction.

$$\Phi= (1\, /.2^{1/2})\, (k_2/k^{1/2}_t)\, (\delta k_d)^{1/2}[RH]^{3/2} \text{ or } \quad \Phi= (1\, /.2^{1/2})[ROOH]^{1/2}_{max}\, k_d[RH] \quad (25)$$

Substituting this expression in (20) and assuming that the oxidized monomer units of the polymer in the subsequent oxidation do not participate, gives:

$$d[ROOH]/dt = k_2(2\delta k_d\, /\, k_t\,)^{1/2}([RH]_o-\Delta[O_2])^{3/2}[ROOH]^{1/2}- k_d([RH]_o-\Delta[O_2])[ROOH \quad (26)$$

$$d(\Delta[O_2])/dt = k_2(2\delta k_d/k_t\,)^{1/2}([RH]_o-\Delta[O_2])^{3/2}[ROOH]^{1/2}- 2\delta k_d([RH]_o-\Delta[O_2])[ROOH] \quad (27)$$

From some point set a quasi-stationary concentration of hydroperoxide,

i.e d[ROOH]/ dt = 0. Under this condition, equation (26) can be simplified

$$[ROOH] = k_2^2\delta\, /\, k_d\, k_t = ([RH]_o - \Delta[O_2]) \quad (28)$$

i.e quasistationary concentration of hydroperoxide is proportional to the concentration of unoxidized polymer. When substituting this relation into equation (27) can be obtained

$$d(\Delta[O_2])/dt = 2(1+2\delta)\,\delta k_2^2/k_t\,([RH]_o - \Delta[O_2]) \quad (29)$$

After integrating the initial condition $\Delta[O_2] = (\Delta[O_2])_1$ and $t = t_1$, is obtained

$$1/([RH]_o - \Delta[O_2]) = 2(1+2\delta)(\delta k_2^2/k_t)t_1 + \alpha \quad (30)$$

whence

$$\alpha = 1/([RH]_o - \Delta[O_2]) - 2(1+2\delta)(\delta k_2^2/k_t)t_1, \quad (31)$$

where t_1 means the time from which the concentration of hydroperoxide can be considered quasi-stationary. , it is still time to reach maximum concentration of hydroperoxide. Another model, describing the kinetics oxidation of PP, based the same pattern as discussed in (Shlyapnikov Yu. and al., 1986). This work identified two stages of the oxidation process. The initial stage of reaction and phase deep oxidation. At the initial stage of the reaction rate of hydroperoxide significantly higher than the rate of its thermal decomposition. The latter can be neglected. The equation of balance of free radicals and hydroperoxide in amorphous material in the absence of a linear chain termination is as follows:

$$d[RO_2^*]/dt = Wo + \alpha k_d[RH][ROOH] - 2k_t[RO_2^*] \quad (32)$$

$$d[ROOH]/dt = \alpha k_2[RH][RO_2^*] \quad (33)$$

System of equations (32) and (33) is solved in a quasistationary approximation $d[RO_2^*]/dt = o$; $d[ROOH]/dt \neq 0$ The solution of equation (31) has the form:

$$[RO_2^*] = \{W_o + \sigma k_d[RH][ROOH]/2k_t\}^{1/2}, \quad (34)$$

where $W_o = f\,k_o\,[RH]\,[O_2]$ - rate of nucleation of chain , which negligible compared with that of chain branching in the early stages process. Substituting the values of $[RO_2^*]$ (34) and (33) and integration of this expression gives the variation of the expression ROOH concentration in time:

$$[ROOH] = \alpha No_2 = \alpha \cdot 2\sigma\, k_2^2 k_d[RH]^3 t^2/8k_t = At^2 \quad (35)$$

So manner of equation (35) shows that in the initial stage reaction oxidation of the amount of oxygen absorbed during oxidation, and concentration hydroperoxide proportional to the square of oxidation time. This is consistent with the conclusion drawn in previous work (Emanuel N.M., Buchachenko A.L.,1982). Comparison (36) and (37) provided in the form of dependence changes in the concentration oxygen from the oxidation time:

$$\Delta[O_2] = (k_2^2\delta k_d[RH]^3/2k_t)\,t^2 = \Phi^2 t^2 \quad (36)$$

$$No_2 = (\sigma\, k_2^2 k_d[RH]^3/4k_t)\,t^2 = At^2 \quad (37)$$

show that the process oxygen uptake in the initial phase described by a parabolic law. For PP parabolic law is obeyed up to $\Delta[O_2] = 1$ mole/kg. At a more profound stage of a deviation from this law. Deviations from parabolic law is also observed at short times of oxidation, when still not satisfied quasistationarity the concentration of hydroperoxide (in the induction period).

2.3 Oxidation polymer on the deep stage

At deep stages of oxidation the rate of decomposition of hydroperoxide increases with its concentration. The rate of quadratic chain termination is proportional to the square concentration of radicals. At this point plays an important role expenditure monomer units of the polymer. Nucleation rate of the chain compared with the rate of branching can be neglected. The reaction is carried out at a high concentration of oxygen and the contribution reaction $R^*+RO_2^*$ is negligible, $[R^*]<<[RO_2^*]$. For these conditions, the balance equation of free radicals and hydroperoxide is:

$$d[R^*]/dt = k_2[RH][RO_2^*] - k_1[O_2][R^*] + \sigma k_d[RH][ROOH] \quad (38)$$

$$d[RO_2^*]/dt = k_1[O_2][R^*] - k_2[RH][RO_2^*] - 2k_t[RO_2^*]^2 \quad (39)$$

$$d[ROOH]/dt = \alpha k_2[RH][RO_2^*] - k_d[RH][ROOH] \quad (40)$$

Using the method of quasistationary concentrations for $[RO_2^*]$ can be obtained:

$$[RO_2^*] = (\sigma k_d[RH]/2k_t)^{1/2}[ROOH]^{1/2} \quad (41)$$

$$d[ROOH]/dt = \alpha\sigma^{1/2}\{k_2k_d^{1/2}[RH]^{3/2}/\sqrt{2}k_t^{1/2}\}[ROOH] - k_d[RH][ROOH] \quad (42)$$

The solution of equation (40) $[ROOH]o = 0$ has the form:

$$[ROOH] = [ROOH]_{max}[1 - \exp((-k_d[RH])/2)\ t)]^2 \quad (43)$$

$$[ROOH]_{max} = \alpha^2\sigma k_2^2[RH]/2k_dk_t \quad (44)$$

$[ROOH]_{max}$ –limit sought by the concentration of hydroperoxide in the case of [RH] = const.

In the same conditions, the rate of oxygen consumption varies as

$$Wo_2 = dNo_2/dt = \alpha\sigma\ k_2^2[RH]^2/\ k_dk_t\ [1 - \exp((-k_d[RH])/2)\ t)] \quad (45)$$

Equations (23), (24) describe the dependence of the amount of absorbed oxygen from the oxidation time and the equation takes into account the flow of the polymer during the reaction (31) allow us to establish the oxidation characteristics of polypropylene and the factors influencing this process. The above equation (35) does not take into account the flow of the polymer during the reaction. Because the rate of consumption of the polymer is the rate of absorption of oxygen:

$$d[RH]/dt = d(\Delta[O_2])/dt, \quad (46)$$

$$[RH] = [RH]_o - \Delta[O_2], \quad (47)$$

Where $[RH]_o$, [RH] - the concentration of polymer in the beginning of the reaction and at time t; $\Delta[O_2]$ – the amount of oxygen, absorbed by this time.

2.4 The reaction to continue the kinetic chain of oxidation $RO_2^* + RH \longrightarrow ROOH + R^*$

A key step in the radical chain oxidation of polypropylene is the reaction to continue the kinetic chain of oxidation (5). It determines the overall speed of the process leads to spatial

displacement of the free valence, it is the product of hydroperoxide, which is the degenerate branching of kinetic oxidation chains. In polyolefins, the reaction can take place both inside and intermolecularly. The oxidate polymer chain fragment may be a part of one macromolecule to which the RO_2* radical belongs or a part of the neighbouring macromolecule. The consequences of the intra- and intermolecular chain propagation are different for . various polyolefins. So, in polyethylene, the main mode of reaction is intermolecular (Emanuel N.M., Buchachenko A.L., 1982). In contrast to PE, in polypropylene, this reaction is carried out intramolecularly (Shlyapnikov Yu. A. and al., 1986; Rapoport N.Ya. and al, 1986). The reason for the differences between the PP and PE is the conformational structure of the polymer chain. With the continuation of the intramolecular kinetic chain the probability of activated complex optimal structure should depend on the local conformation of the site of a macromolecule carrying a peroxide macroradical. Conformation of the reaction complex is given below:

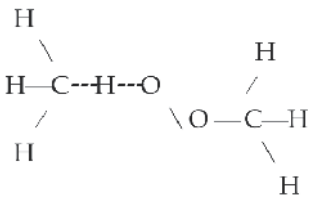

In this complex bond angles ∠H-C-H) = 109°, ∠C-H-O) = 180°, ∠HOO = 100-105°, the distance between the atoms O···H = 1,4 Å , C·H =1,2 Å. Reaction does not occur, if the distance O···H more than 1,8 Å (Rapoport N.Ya., Mostovaya E.M., and all 1986). With the help of analysis of molecular models of Stuart-Briegleb, it was show that the probability of formation of activated complex of optimal structure depends on the set of conformations of the macromolecule. For example in PE, the linear activated complex is not formed in a macromolecule, having a straightened conformation of trans - zigzag, consisting of a sequence of trans-conformers (~ TT ~). For the occurrence of an intramolecular reaction of the chain oxidation of PE required sequence of two folded gosh-conformers type GG or G-G- . Where are the angles of internal rotation around C-C bonds for G and G-conformers are equal to 120°, the angles of internal rotation for T-conformers are equal 0°. However, the equilibrium fraction of dyads GG in PE low, at room temperature it is approximately 9%. On the other hand, in PE not bulky lateral substituents create steric hindrance to intermolecular continuation of the kinetic chain of oxidation. Due to these factors, education linear activated complex with PE in intermolecular reaction is realized inorder are more likely than in intramolecular (Popov A.A. and al. 1987). The presence of side substituents in the macromolecule of polypropylene leads to the formation of helical conformation, which consists of a series of trans and gauche-conformers ~ TGTGTG ~. This sequence forms an extremely straightened conformation of the chain, which is "hard", and corresponds to the minimum energy on potential curve of interaction of valence-not bonded atoms. Folded conformation is formed by alternating joints left-and right dextro-rotatory sites spirals type ~TGTGTGG*TGT~. Where G* - gauche conformer with the angle of internal rotation, deviating from 120°, relevant ± 60°. The relative position of atoms H adjacent tertiary C-H bonds in PP is determined by the type of dyad conformer: TT, TG and GG. Dyad TT in PP is not implemented due to the overlap of methyl groups in dyad TG peroxide radical is shielded from neighboring tertiary connection CH. Education of the reaction complex is most likely if the conformation of the reaction center meets the dyad GG *. This dyad is a

prelaunch conformers for the intramolecular reaction. This explains why in contrast to PE in polypropylene the reaction of RO_2 * + RH proceeds mainly intramolecularly. In (Rapoport N.Ya. and al, 1986), this reaction was considered from the perspective of a reaction "pair" the radical RO_2 * - GG *-conformer:

$$RO_2^* + GG^* \underset{k_{-r}}{\overset{k_r}{\Leftrightarrow}} [RO^*_2\ (GG^*)] \xrightarrow{k_x} ROOH$$

For the case $k_r \simeq k_{-r}$ speed of reaction in the quasistationary approximation is:

$$W_2 = (k_x k_r / k_x + k_r)[RO^*_2][GG^*] = k_{эф}[RO^*_2][GG^*]$$

If the limiting stage will be meeting with conformer GG *- radical, $k_{ef} = k_r$, if the reaction is limited by a pair of $k_{ef} = k_x$; in the intermediate case k_r and k_x are added by law to the kinetic resistances. Thus, in theory, developed in (Rapoport N.Ya. and all, 1986; Popov A.A. and all., 1987) the rate of intramolecular reactions continue oxidation chains, occurring in isotactic PP is proportional to the concentration of GG *- conformers in the macromolecule. Number of gauche-conformers at the site of a macromolecule depends on the contour length, the distance between the ends of the site. In the PP amorphous phase always there is a distribution on lengths of chains in the intercrystalline regions, hence, on the contour length and concentrations of GG *- conformers. This leads to the presence distribution on values of the constants k_2. Determined from the gross - value of the kinetics of k_2 are effective for the average values distribution. The smallest value of k_2 in the crystalline phase of PP, which have macrochain conformation of the helix. In (Roginsky V.A., 1977; 1982) studied the reaction of the chain oxidation crystal PP-phase at 200-300°C. Estimate of the effective values gave the value of $k_2 = 2.10^{-5}$ s^{-1}, it is 3 orders of magnitude lower than in the amorphous phase k_{2ef} PP. Hence, PP different grades with different molecular weight distribution have different width of the distribution on values of k_2 and values constants k_{2eff}.

2.5 The reactions of accumulation and disintegration of hydroperoxide PP

As has been shown, PP oxidation occurs predominantly intramolecularly, the kinetic chain moves along the macromolecule. Macroradical RO_2*, formed by the oxidation of polypropylene, reacts with a hydrogen atom from the tertiary C atom located in the β-position relative to the peroxide radical of their molecules. As a result, intramolecular transfer of a macromolecule oxidized PP formed "blocks" of several adjacent OH-groups.

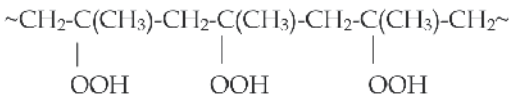

However, the low-temperature oxidation of solid polypropylene (70-110°C) proceeds with alternating intramolecular and intermolecular chain transfer. Intramolecular kinetic of extension chains is limited to small parts of the macromolecule with a favorable set of conformations. As a result, blocks of hydroperoxide can be short. In the solid polypropylene has found about 60% of paired units and about 20% of triads, the share of units with a higher number of hydroperoxide groups is small. It should be noted that in other carbon-chain polymers increases the probability of intramolecular reaction at the high rate of conformational motions. For example, in the polymers with a saturated C-C bond (such as

PE), the kinetic chain are transmitted preferably via a carbon atom (in γ-position), in other polymers (with unsaturated bonds, heteroatoms, phenyl rings, etc.) the transfer of kinetic chains are statistically.In oxidizing polypropylene along with the main hydroperoxide:

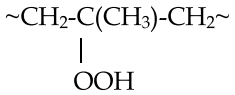

hydroperoxides can be formed type:

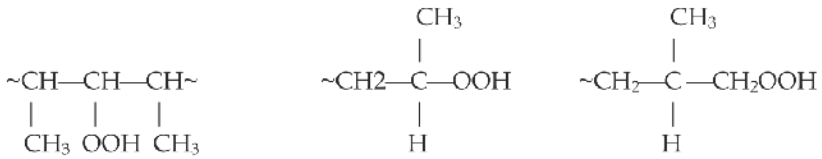

These hydroperoxides are formed as a result of intermolecular transfer of kinetic chains of oxidation. In the PP also form low molecular weight hydroperoxides such as methyl, ethyl, etc. The hydroperoxide, obtained by thermal oxidation of polypropylene, is not an individual compound, but is a combination of –OOH and other oxygen-containing groups, and the concentrations and location of these groups in the polymer are not unambiguous functions of the hydroperoxide concentration.

2.6 The yield of hydroperoxide per mole of absorbed oxygen

Relationship between the concentration of hydroperoxide and absorption rate of oxygen stored in various pressures of oxygen and described by the following empirical equation:

$$Wo_2=a[ROOH]^{1/2} + b[ROOH], \quad (48)$$

where $a=k_2(\delta k_d/k_t)^{1/2}$, $b=\sigma k_d[RH]$; k_d – the constant of ROOH decomposition rate; δ - the probability of degenerated branching of kinetic chains;$\delta = \alpha\sigma$, σ-the yield of radicals from cell; α - the yield of hydroperoxide per mole of absorbed oxygen. The rate of polymers oxidation depends on concentration and constant of ROOH destruction. In its turn concentration of ROOH depends on yield per mole of absorbed oxygen. To determine the hydroperoxide yield may be used balance of hydroperoxide in the oxidation of solid polypropylene. For this the obvious fact may be used that at the maximal hydroperoxide concentration the rates of its formation and decomposition are the same.

$$d[ROOH]/dt = \alpha Wo_2 - k_d[ROOH]^n, \quad (49)$$

where n - the order of decomposition reaction of hydroperoxide. Substituting the experimental values for apparent rate constant of hydroperoxide decomposition k_p, and its maximal concentration at which d [ROOH]/dt becomes zero. Assuming that the initial stage of polyolefin hydroperoxide decomposition obeys the first-order law, we get:

$$\alpha = k_d[ROOH]_{max} / (Wo_2)_{max} \quad (50)$$

In liquid-phase oxidation of hydrocarbons the rate of oxygen uptake equals the rate of accumulation of hydroperoxide. The yield ROOH per mole of absorbed oxygen α=1. In the autoxidation of solid polymer α much less than unity. For isotactic polypropylene,

polyethylene, poly-4-methylpentene from (Emanuel N.M., Buchachenko A.L., 1982) a ≈ 0,2-0,5. This means that only 20-50% of the absorbed oxygen passes into the hydroperoxide, the remaining 80-50% goes into the reaction products, bypassing the stage education hydroperoxide. According to (Shlyapnikov Yu.A. and al, 1986) for PP α = 0,05-0,3. There are several reasons for the drop out hydroperoxide per mole of absorbed oxygen. As a result of intramolecular chain transfer to ROOH appears next to the free valence and forms β-hydroperoxyalkyl radical.The interaction of the free valence with a freshly formed hydroperoxide group can occur in three ways, according to reactions (1′), (2′) and (3′).

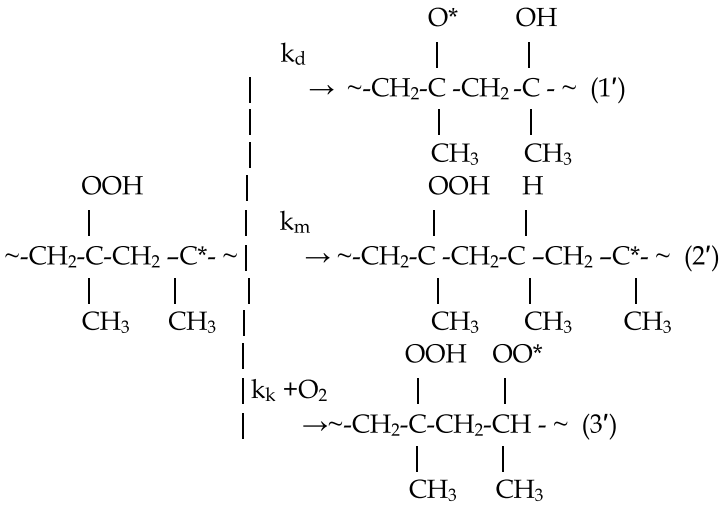

The first way to becoming peroksialkil radical would lead to the death of hydroperoxide group (1′), the second and third - the removal of the reaction center and stabilize the group. The yield of the stabilized hydroperoxide is equal to the sum of relative rates of reactions (2′) and (3′) to the sum of the rates of all three reactions, i.e. the expression for the yield of hydroperoxide (α) in PP is:

$$\alpha = k_k[O_2] + k_m$$

$$k_k[O_2]+k_m+k_d \text{ or}$$

$$1/\alpha = 1+\{k_d/k_k ([O_2] + k_m/k_k)\} \quad (51)$$

In the works (Kiryushkin S.G., Shlyapnikov Y.A., 1975; 1986), reaction (1′) is considered as ″ induced″ decay of hydroperoxide. The kinetic chain is moved along macromolecules formed alkyl macroradical who takes a step "backwards", reacts with the preceding neighboring hydroperoxide group to form alcohol and alkoksiradikal.

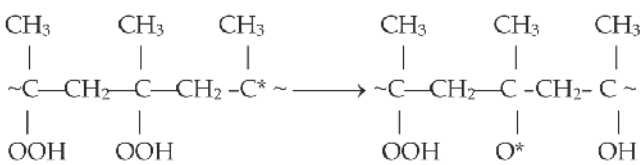

It should be noted that "return motion" of the kinetic chain R* + ROOH ⟶RO* + ROH , which leads to the induced decomposition of hydroperoxide not necessarily occurs intramolecularly, it can also occur when the intermolecular kinetic extension chains. Only the probability of the latter case will be considerably less than intramolecular reaction, when the local concentration of ROOH and R * is high and partners reactions can not break up the diffusion way. Intramolecular continuation of the kinetic chain of oxidation is not the sole reason for the low yield of hydroperoxide per mole of absorbed oxygen. If the kinetic chain oxidation of long, almost all oxygen passes into the hydroperoxide, with short chains, much of it remains products in the termination of kinetic chains, so α depends on the length kinetic chain. The oxidation of polypropylene in the induction period (long kinetic chain) α = 0.85, almost all the oxygen passes into the hydroperoxide. For short chains of about 30% absorbed oxygen is consumed in the initiation of intracellular processes and termination of kinetic chains, with what shorter kinetic chain, the lower yield of hydroperoxide. On the same reason, the value of α particularly low in crystalline polymers, where kinetic chains are short. Thus low the value of α is not a strict criterion of intramolecular oxidation. It may also be a sign of short kinetic chains. Kinetic chain length (ν) - the number of molecules absorbed oxygen or hydroperoxide at a kinetic chain is

$$\nu = W_{ROOH}/W_i = k_2[RH]k_t^{-1/2} W_i^{-1/2} \quad (52)$$

(Emanuel N.M., Buchachenko A.L., 1982). Another reason low yield of hydroperoxide is the decay of the peroxide macroradical before it turns into a hydroperoxide. In this case, kinetic chain extension occurs without the formation of hydroperoxide. However, the decay of peroxide radicals PP is small compared with the probability of becoming it hydroperoxide. The collapse of the radical RO_2* can occur at temperatures above 200-300°C. According to eq.(49) the hydroperoxide yield in the polymer oxidation must depend on the oxygen pressure over the polymer (on its concentration in the polymer). At the same time, oxygen concentration, affecting the ratio of the reaction rates, must affect the hydroperoxide structure, i.e. the distribution of hydroperoxide and other oxygen – containing groups along macromolecules and in polymer bulk. This distribution must affect the hydroperoxide properties. Experiments have proved this conclusion: the rate constant of hydroperoxide decomposition varies depending on the oxygen pressure at which the hydroperoxide has been prepared.

2.7 The probability of degenerate branching

The effectiveness of the emergence of new kinetic chains in the decay of the hydroperoxide has two features. First, the radical yield on one broken hydroperoxide group is small and amounts to several percent. Second, the probability of extinction branching depends on the oxygen pressure. The yield of low molecular weight hydrocarbons (methane, propylene) - the decay products of alkoxide and terminal alkyl macroradicals with an increase in oxygen pressure is not reduced to zero, and reaches a limiting finite value, independent of pressure oxygen. This means that oxygen is not only reduces the concentration of alkyl radicals, converting them into peroxide, but also participates in the reactions of their formation, by increasing output radicals from the cage. Calculated from data on collapse GP isotactic polypropylene dependence of d on the oxygen pressure in 100°Cmeet view $d = (7.10^{-3} + 1.10^{-4}) \cdot p_{O_2}$, where p_{O_2} in mm Hg. Probability degenerate branching of the oxygen pressure for isotactic PP and PE are found from the kinetics of autoxidation is presented in the table.2.

$po_{2,mmHg}$	0	50	100	200	400
σpp	0.017	0.12	0.25	0.40	0.65
σpe	-	-	0.26	-	0.32

Table 2. Probability degenerate branching for isotactic PP and PE

To explain the dependence of δ on oxygen pressure offered two hypotheses. Firstly, the probability of degenerate branching, δ is the initiating ability of ROOH depends on its structure and hence on the oxygen pressure at which the obtained hydroperoxide. Initiation efficiency block hydroperoxides, an order of magnitude higher than the efficiency of initiation isolated groups. However, this hypothesis is realized at low pressures oxygen (less than 150-200 mm Hg). Second, it increases the oxygen probability of degenerate branching root in the primary radical pair converts it into the secondary:

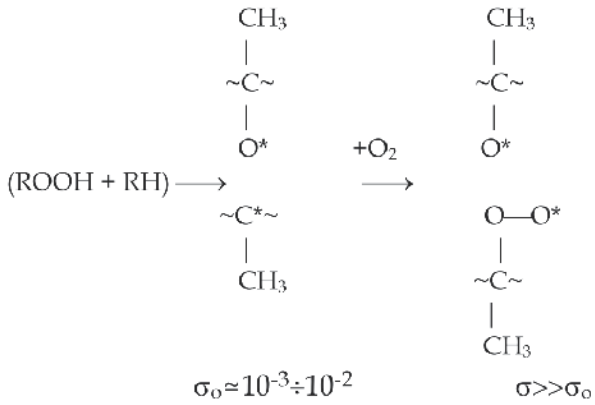

The radical yield of primary pair (σ_o) very low, and from the secondary - much higher, order of unity. The higher the oxygen pressure, the greater the concentration in the polymer, the greater the contribution secondary pairs, and, consequently, the higher the probability of degenerate branching.

2.8 Autoxidation induction period of the PP

The changes, occurring at oxidation of the polymer are laid in the induction period, so it is important establish the nature of this stage of the oxidation process. The parabolic law of oxidation of isotactic PP is established not immediately but after some time. This time was proposed to call the true induction period of uninhibited oxidation (Rapoport N.Ya and all 1986; Popov A.A. and al., 1987). For example, in PP at 403K the true induction period is equal ~ 80% of the experimental period, which correspond to time of absorbed oxygen [No_2] ~ 0,1 mol/kg. Probably mechanisms of oxidation of the polymer in the period induction and on the stage of more extensive oxidation are different. In the literature discusses the possible reasons for the differences of the kinetics of oxidation PP in the induction period, and after leaving it. The following explanation of the features mechanism of oxidation in the induction period are offered in the literature. First, the initial stage oxidation corresponds to the accumulation of hydroperoxide. However, the quasi-steady on hydroperoxide do not run in the induction period. The low yield of hydroperoxide per mole of absorbed oxygen, and low initiating ability of hydroperoxide, which formed at the initial stage, leads to slow

down the rate of process of branching of kinetic chains (Popov A.A. and al, 1987). Secondly, the induction period may be associate with the low rate constant of radical decay. The rate constant of radical decay is changed during oxidation. Low - molecular radicals formed at the beginning of oxidation is exchanged for macromolecular radicals in reactions with hydroperoxide (Roginsky V.A. and al., 1976; 1982; Emanuel N.M. and al, 1982). Third, the existence of the period induction may be explained of the localization of the oxidation in the zones (Shlyapnikov. Yu.A. and al 1986; Richters P., 1970; Graeme A.and all., 1997; Livanova, Zaikov G.E., 1997). Localization of oxidation in the zones of polymer is the consequence of the structural and physical microinhomogeneity, nonequivalence of the structural elements , that differ frequencies and amplitudes of molecular motions. This creates spatial heterogeneity in distribution of the reactants in a polymer. Their local concentration may differ significantly from the average. This leads to distribution of reactivity, rate constants and energies activation, as a result, to polychromatic kinetics. This creates spatial heterogeneity in distribution of the reactants in a polymer. This means that oxidative processes is localized to the centers, "Microreactors", which are amorphous interlayers and interfibrillar areas. Polyethylene and polypropylene are not homogeneous. They have amorphous and crystalline regions. In the PE crystalline regions are impermeable and inaccessible for oxygen. The solubility of oxygen in the crystalline regions of PP on order of magnitude smaller than in the amorphous regions. The oxidation rate, calculated on the unit volume, and the limiting amount of absorbed oxygen are decreased proportionally with increasing crystallinity in both polymers (Bogayevskya TA, and al., 1978). Ther are several models of local oxidation of polymers proposed in the literature. In the framework of the local oxidation, polypropylene is considered as a set of kinetically nonequivalent “zones”. This zones are differ of molecular dynamics, values of the radical yield of cells, which initiated the kinetic chains, and of termination rate constants k_t. (Makedonov Yu. V. and al, 1986; George A.G.and al., 1997). High molecular mobility, the velocities of the initiation and radical decay in zones leading to rapid establishment of steady-state concentration of radicals in these zones. In the more hard regions, where the rate constants k_t are low and the rate of initiation are small due to cellular effects the process of establishing steady-state concentration of radicals slows down. Therefore, initiating of the radical process in PP by irradiation with light leads to high rates of population of the soft zones of polymer by radicals with high rates of destruction. At longer initiating of the radicals they inhabit the rigid zones, resulting in the experimentally observed rate constant destruction of free radicals decreases. Thus, induction period of oxidation of PP is explained with in terms of non-homogeneous oxidation. By the end of the true induction period is set steady-state distribution of radicals in the zones, the parameters of oxidation are characterize the process of development and not change during further oxidation. Next "zone`s model" of oxidation of the polymer has been proposed (Shlyapnikov and al,1986; 1989). If in the previous model are considered as zones of amorphous regions as a whole, in the second model - it's part amorphous layers in violation of the short-range order. So, the amorphous interlayers of PP include through-passage chains in the folded conformation. In these areas, are concentrated oxygen and other low molecular weight substances. These areas are possess a high segmental mobility and high activity with respect to oxygen. These zones are considered as microreactors, which are surrounded by a more orderly and, therefore, less reactive substance. The model, which offers Shlyapnikov, has different mechanism of oxidation. From the perspective of this model, free valence, formed in the zone of violation of the order, begins a chain reaction, which has no stage of chain termination.The average

concentration of RO_2* in the zone will be equal to one particle per volume area (particles / cm ^{3} or cm^{-3}.) $[RO_2*]_z = 1/V_z$. Accepted that V_z = const and we can neglect differences in the individual properties of zones. The expenditure of reactionary capable RH - groups in the some areas (RH_z) are proceedung of the law:

$$d[RH]_z / dt = k_2[RH]_z / V_z . \quad (53)$$

It concentration of groups in the area of RH, which does not coincide with average concentration of monomeric in the polymer. During $t_z = 5k_2^{-1}V$ reactive substance in violation of the order of the area consumed almost completely. Then there are two possibilities. First, if the average time of free valence in a separate zone t_z much less than θ, then the kinetics of reactions in polymer is not significantly different from the kinetics of the same reaction in low molecular weight liquid only in the reaction will not participate the entire polymer and part of it is equal to $[RH]_e = [Z] V_z [RH]_z$, where Z-density zones. Second, if the stay of free valence in the area of more than θ, then reaction rate is determined by the amount of matter in a separate area and speed displacement of the free valence from zone to zone:

$$W = V_z [RH]_z \theta^{-1} [RO_2*] \quad (54)$$

where $[RO_2*]$ - average concentration of peroxide radicals, calculated on the entire polymer. At the same time the observed rate constant of chain transfer is

$$k_{2e} = V_z [RH]_z [RH]^{-1}\theta^{-1} \quad (55)$$

and, consequently, will not coincide with the true constant reaction rate RO_2* + RH, where this constant attribute. The rate of chain termination is determined by the frequency hit two free valences in the same area, i.e. will be:

$$W=2 [Z]^{-1}\theta^{-1} (1-\varepsilon) [RO_2*]^2, \quad (56)$$

where ε – chance what a pair of free valences, which has appeared in the same area, come out of it without recombination. Assuming, ε we can write $k_{t\,ef} = 2 [Z]^{-1}\theta^{-1}$ kinetic parameter of oxidation k_{2ef2}/k_{tef} can be:

$$k^2_{2ef}/k_{t\,ef} = V_z^2 [RH]_z^2 N_{av} 10^{-6} / 2 [RH]^2 \theta \quad (57)$$

$$\text{where } \theta = V_z [RH]_z [RO_2*] N_{av} 10^{-3}/W_{o2} \quad (58)$$

Substituting (56) into (55) we find:

$$k^2_{2ef}/k_{t\,ef} = V_z [RH]_z W_{o2} N_{av} 10^{-6} Z / 2[RH]^2 [RO_2*] \quad (59)$$

substitution (57) into (35) gives:

$$N_{o2} = \delta k_d [RH] V_z [RH]_z W_{o2} N_{av} 10^{-6} Z t^2/16 [RO_2*] \quad (60)$$

Under provision, "the zone model" $[RO_2*] = 1/V_z$, then one can assume that

$V_z [RO_2*]$ = const. Whence

$$N_{o2} = B Z W_{o2} t^2 \quad (61)$$

$$\text{where } B = \delta k_d [RH] V_z N_{av} 10^{-3}/16 [RO_2*] \quad (62)$$

On the initial stage of oxidation $W_{o2} = N_{o2}/t_{ind}$. Substituting this expression (60) we obtain

$$W_{o2} = B\, N_{o2}\, Z\, t^2/t_{ind} \quad (63)$$

Simplifying (55), we obtain the desired dependence:

$$t = (t_{ind}/Z)^{1/2}\,(1/B)^{1/2} \quad (64)$$

Within the "zone`s model" of the induction period is correlated with the autoxidation of PP time location of the free valence in the area, the low yield of hydroperoxide a can be explained by high local concentrations UN Teams and the radicals R* in the zone, which is why the probability of their interaction is significant. Low yield of free radicals in decay. In within the "zone`s model" of the induction period is correlated with the autoxidation of PP time finding free valence in the area, low yield hydroperoxide can be explained by a high local concentrations of the ROOH and the radicals R * in the zone, which is why the probability their interaction is significant. Low yield of free radicals the decay of the polymer hydroperoxides due to the fact that, unlike low molecular weight Fluid pair of free radicals, emerged from the primary cell is a long time in a small volume of zone violations of the order, where the probability of recombination radicals is high. The low molecular weight scavengers of free radicals dissolved in the polymer are in the same zones violations of the order in which reaction occurs, and may react with the radicals issued from the primary cells, but do not go out of the volume of the zone, are able to initiate the reaction of oxidation. Polymer hydroperoxides due to the fact that in contrast to low molecular weight Fluid pair of free radicals, emerged from the primary cell is a long time in a small volume of zone violations of the order, where the probability of recombination radicals is high. The low molecular weight scavengers of free radicals dissolved in the polymer. Zone`s model allows us to understand the dependence of the oxidation rate related polymers on the content of foreign links. Expression for the effective rate constants of the chain contains as one of the factors value of V_z - volume of the zone violations of short-range order rate constant of quadratic chain termination depends only onthe total concentration of these zones. Introduction to the polymer chain side substituents leads to loosening of the polymer structure and hence, increases the volume of the zone V_z and the rate of oxidation of the polymer. For the same reason, reduces the probability of radical recombination in the area and increases. The transition from PE to PP leads to an increase in the rate of oxidation and reduction induction period (Shlyapnikov Yu. A., 1989). The rate of primary initiation, therefore induction period of oxidation of PP determined not only by the amount and concentration of reactive zones, but also nature of the substances, which are localized in these zones. In the papers convincingly (Livanova, Zaikov G.E., 1997) shown that the polymer (PP) of preexisting primary foci of initiation rate of radicals in which is significantly higher than those in microreactors, which can occur under the influence of stress and other influences on the RH bond PP. The main reason initiation of the primary foci are microscopic debris size (residual polymerization catalysts - transition metal valence and their products conversion).

2.9 Thermooxidative degradation of polypropylene

Hydroperoxide is not only branching agent, but also a precursor of low-molecular products and breaks the molecular chains, resulting in to a change in molecular weight and molecular weight distribution (Shlyapnikov Yu. A., and al. 1986; 1989). Basic mechanisms of decomposition of hydroperoxide in the polypropylene - the bimolecular reaction involving communication C-H at the tertiary carbon atom of the macromolecule eq (8). Among decay

products detected ROOH PP: water, acetone, acetaldehyde, formaldehyde, methane, ethane, propane, propylene, ethylene, etc. The rate of formation of these products proportional to the concentration hydroperoxide. Comparative analysis of oxidation products and degradation products hydroperoxide. in an inert atmosphere, showed the same qualitative and quantitative composition. So products oxidation of PP is mainly formed by the decay of hydroperoxides. The total rate of formation of volatile products (of which the main product water-based) half the rate of decomposition of hydroperoxide. Ie 50% of productsoxidation remains in the solid phase in the form of alcohol, peroxide and ketone groups of macromolecules. The main source of low-molecular products are alkoxide macroradicals:

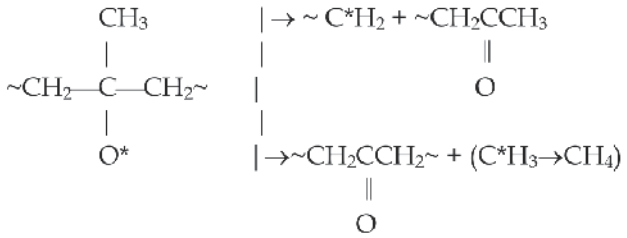

Low molecular weight hydrocarbons obtained from the terminal alkyl macroradicals:

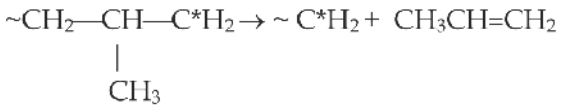

Isomerization

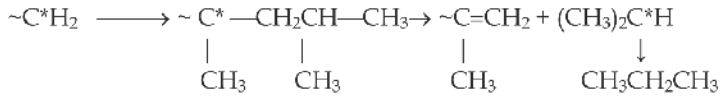

Acetone and aldehydes are obtained of hydroperoxide groups and alkoxide radicals, respectively, located near the ends of macromolecules:

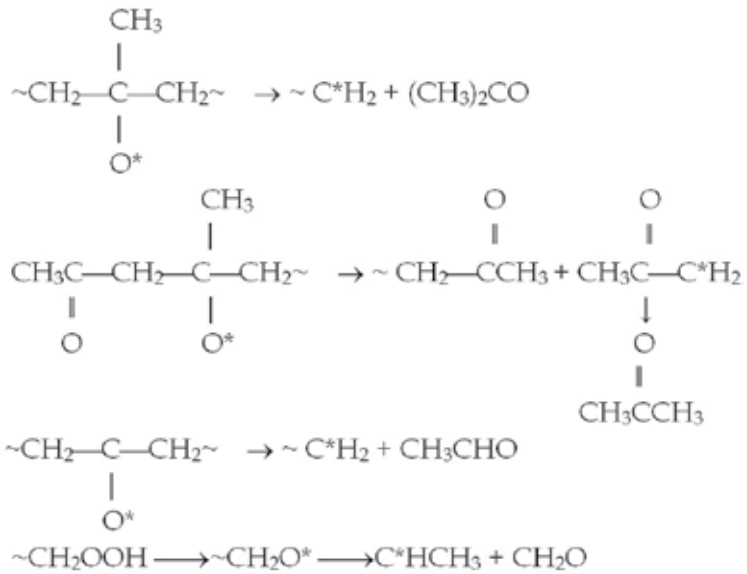

In polyethylene formation of the products described in the following scheme (Ranby B., Rabek J.F., 1978)

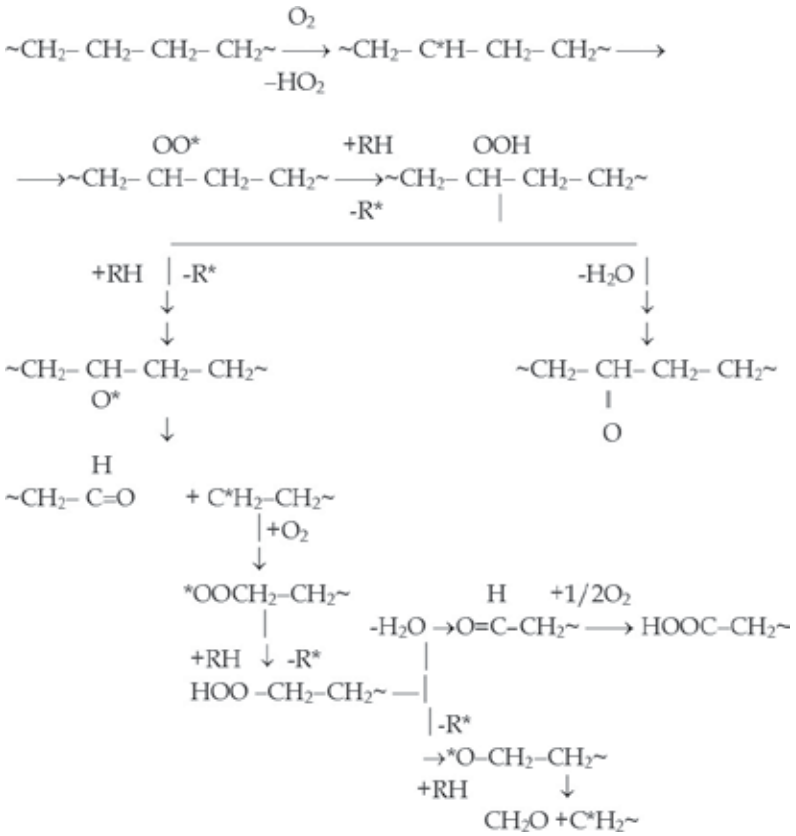

Polymer oxidation is accompanied by polymer chain destruction. When measuring the molecular weight of polymer, one can see only large remnants of the polymer chain, and if a short segment of the polymer chain takes place a few breaksthey will be treated as one scission .Denoting the probability of the scission of a macromolecule as a result of one step of chain reaction propagation ρ_1, the probability that there is no scission is $(1-\rho_1)$, and the probability of at least one scission resulting from ν_b reaction steps proceeding in the same region (block) of the macromolecule is (Shlyapnikov Yu. A., 1989):

$$\rho_b = 1-(1-\rho_1)^{\nu_b} \tag{65}$$

The rate of formation of such oxidatized regions (or blocks) of polymer chains is the sum of rates of chain initiation and of chain transition from one molecule to another. Supposing the latter to be directly proportional to the overall concentration of free radicals in the system, gets this:

$$W_b = W_o + k_{tr} [\, RO_2^*], \tag{66}$$

where W_o is the chain initiation rate. It is assumed that the oxygen concentration is high enough and we can neglect reactions of R* radicals. The rate of recorded scission formation is proportional to W_b, and if ρ_b=1 it is virtually equal to W_b. If the oxidation chains are long

enough, or k_{tr} is small, the rate of polymer destruction, i.e. the rate of recorded scission formation, will be equal to W_o , i.e. to the rate of chain initiation. The rate of chain initiation plus the rate of chain branching are always equal to the rate of chain termination; thus the rate of chain scission is proportional to that of chain termination, and at ρ_b =1 is approximately equal to it (Shlyapnikov Yu. A. 1986; 1989).

3. The effects of structure on thermooxidation kinetics of polypropylene

The direct correlation between initial structure of polymer and kinetics of oxygen absorption is consequent from our scheme (Shibryaeva L.S.and al.,2003; 2006; 2010.)

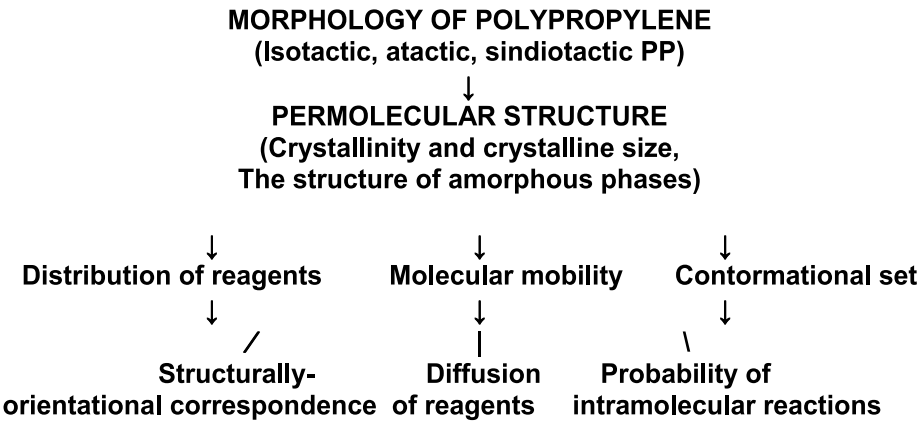

The thermal oxidation is complex process including chain oxidation of hydrocarbon radicals, destruction of macro-chains and structure formation (cross-linking, crystallization). Thermal oxidation is accompanied by structural-physical processes leading to structure change (structural reconstruction) under the action of high temperature. The mechanism of these processes will depend on polymer's morphology and in its turn will influence on oxidation kinetics. The effect of polymer crystallites in vacuum and on air: the effect of high temperature may lead to perfection of crystallites structure, rise of temperature and melting heat, at the same time at long high temperature effect the destruction of chains occurs and crystallites and decomposed. There are the data demonstrating the influence of annealing temperature on relaxation parameters in polymer which allow concluding that there is significant change of structure of amorphous regions. At that the amorphous regions to a greater extent determine the particularities of oxidation radical reactions kinetics developing in them. With the aim of revealing of the role of structure (conformational set) of polymer macro-chains we also studied structure reconstructions, accompanying oxidation of oriented samples of PP with various extract degree. Structure parameters of PP: crystallites and amorphous regions, make it polymer heterophase system. These parameters of systems will determine localization of oxidation in zones having high segment mobility. In these Section is proposed a model for heterogeneous thermal oxidation of PP. Morphological irregularity of polymer results from the presence of crystalline and amorphous regions in the same polymer. This type of irregularity affects the regularities and rates of polymer oxidation. Crystallites are characterized by long-range order in the arrangement of macromolecules and of their monomeric units. Oxygen solubility in the crystallites is very low or zero, and

the R* radicals present in crystalline zones of the polymer cannot transform into peroxide ones. On the other hand, these radicals can move inside the crystals by subsequent reactions R* + RH. The capture of free radicals R* by crystallites is equivalent to the kinetic chain termination if these radicals remain in the crystallites or recombine in them. It was shown (Shlyapnikov Yu.A., 1986) that if these radicals are only kept inside the crystallites for a certain time, this is equivalent to chain termination if the reaction is self – accelerated.

4. Isotactic pp, modified by oil

The given section is devoted to regularities of thermal oxidation and to structural reconstructions in the course of oxidation of model heterogeneous systems (Shibryaeva L.S., 2010). The change of destruction rate of PP chains in the presence of modifier may be explained by the change of mechanism of polymer oxidation. Increase of segment mobility of chain leads to increase of contribution of intermolecular transfer of kinetic chains of oxidation. As a result of this kinetic chains of oxidation become shorter and the number of breakages in macromolecules is increased. But in the case of destruction process acceleration at the stage of kinetic chains continuation at the expense of prevailing of intermolecular transfer in composition of hydroxyl containing products the single OH-groups will prevail. However analysis of products composition did not reveal prevailing of single OH-groups over block ones. Increase of chains mobility is observed not only in the case of PP with compatible additives, but also for uncompatible, nevertheless the rate of PP oxidation in its presence is reduced. The most probable reason of oxidation process acceleration in samples of PP with compatible additives, of the rise of PP chain destruction rate is joint oxidation (co-oxidation) of polymer and additives. There are two fundamental hypotheses concerning the mechanism of these reactions which can be derived from the present experimental knowledge of structure and reactivity of macroradicals. (1) Hypothesis of physical migration by which the reactions of reactants are controlled either by mobility of the chains or their parts (segments) with fixed free valence or by diffusion of the low-molecular products of macroradical decomposition, e.i. the so-called radical fragments. (2) Hypothesis of chemical migration by which the reactions of reactants are controlled by various reactions of macroradicals of low-molecular fragments.

5. Experimental part

The samples of Isotactic PP non-inhibited powder of polymerizate was purified by standard technique.

5.1 The methods of investigation

5.1.1 Kinetics of oxidation

The kinetics of oxidation of isotactic polypropylene was investigated in circulating apparatus with freeze-volatile products of oxidation at the temperature of liquid nitrogen. When the film thickness is less than 60 microns maximum rate of oxidation of the sample is proportional to its thickness. Consequently, at a thickness of less than 60 microns ($l<60$ mcm) kinetic regime is realized, i.e. diffusion of oxygen is a rapid process and does not affect the rate of oxidation. On the contrary, for $l > 200$ microns oxidation occurs in the diffusion regime and the maximum speed calculated for 1 cm^2 the surface is practically independent of the thickness.

5.1.2 The research methods

Differential scanning calorimetry, X-ray analysis, IR-spectroscopy, Electronic microscopy, ESR-study.

6. List of abbreviations

PE - polyetylene
PP - polypropylene
PEHD - polyethylene of high density
PELD - polyethylene of low density

7. References

Bogayevskya TA, Monakhova TV, & Shlyapnikov YA (1978) "On the connection between the crystallinity of polypropylene and the kinetics of the oxidation" *Vysocomolek. Soedin*. V.20 B. № 6.PP.465-468.

Chan J.H., & Balke S.T. "The thermal degradation kinetics of polypropylene. *Polymer Degradation and Stability* (1997). V. 57.№ 2. Part. I. Molecular weight distribution. PP 113-125. Part II. Time-temperature superposition. PP.127-134. Part III. Thermogravimetric analyses. PP.135-149.

Denisov E.T., Miscavige N.I., & Agabekov V.E..(1975). *The mechanism of liquid-phase oxidation of oxygen-containing compounds*. Minsk: Science and Technology. P. 200.(In Russian)

Emanuel N.M., Buchachenko A.L.. (1982). *Chemical Physics of aging and stabilization of polymers*. Moscow: Nauka. P. 360. (In Russian)

George A.G., Celina M., & Lerf C. at al. (1997) "A Spreading Model for the Oxidation of Polypropylene" *Makromol. Chem., Macromol. Symp.*V 115. № 1. PP.69-92.

Livanova N.M., & Zaikov G.E. (1997) "The Initiation of Polypropylene Oxidation"*Intern. J. Polymeric. Mater.* V.36. №1. PP.23-31.

Makedonov Yu.V., Margolin A.L., & Rapoport N.Ya. and al. (1986)." On the causes of changes in the effective rate constants continue and chain termination in the induction period of oxidation of isotropic and oriented isotactic polypropylene". *Vysocomolek. Soedin*. V.28 A. № 7. PP.1380-1385. (In Russian)

Nakatani H., Suzuki S., & Tanaka T. and al. "New kinetic aspects on the mechanism of thermal oxidative degradation of polypropylenes with various tacticities". (2005). *Polymer*. V.46. № 11.PP.12366-12371.

Popov A.A, Rapoport N.Ya, & Zaikov G.E.. (1987). *Oxidation-oriented and stressed polymers*. Moscow: Khimiya. P. 168. (In Russian)

Ranby B.,& Rabek J.F (1978). *Photodegradation, Photo-oxidation and Photostabilization of Polymers*. Moscow: Mir. (In Russian).

Rapoport N.Ya., Mostovaya E.M., & Zaikov G.E. (1986)."Simulation of Polychromatic Kinetics of the Propagation step of the Chain Oxidation Reaction in Strained Polypropylene Basing on the Rotational Isomers Model " *Vysokomolek. Soedin*. 28 A. № 8. PP.1620 -1628. (In Russian)

Roginsky, VA, Shanina EL,& Miller, VB (1976) "The cellular effect of the decay of the initiators in solid polypropylene" *Dokladii of the Academy of Sciences of USSR* V. 227.

№ 5. PP.1167-1170.; (1982) "The loss of peroxide macroradicals in the crystalline phase of isotactic polypropylene". *Vysokomolek. Soedin*.V. 24. № 6. PP.1241-1246.

Shibryaeva L.S., Shatalova O.V., & Krivandin A.V. and al. (2003) "Structure Effects in the Oxidation of Isotactic Polypropylene" *Vysokomolek. Soedin*. 45 A. № 3.PP.421-435.

Shibryaeva L.S.,Popov A.A., & Zaikov G.E. (2006). *Thermal Oxidation of Polymer Blends*. Ch.2"Structure effects in thermal oxidation of polyolefines".Leiden, Boston: VSP P.35-55. ISBN -13: 978-90-6764-451-8; ISBN-10:90-6764-451-X.

Shibryaeva L.S., Shatalova O.V., & Solovova J.V. and al. (2010). "Features of thermal oxidation of polypropylene modified with paraffin oil." *Theoretical osnovy himicheskoy technologii*. V.44. № 4. P. 454-466.

Shlyapnikov, Yu.A., Kiryushkin S.G & Marin. A.P.1986. *Antioxidantive stabilization of polymers*. Moscow. Chemistry.P. 254. (In Russian).

Shlyapnikov Yu.A. (1989) "Specific features of polymer oxidation" *Makromol. Chem., Macromol. Symp.* V.27. № 1. PP. 121-138.

6

Decomposition of Artificial Litter Made of Polypropylene

M. Szanser
Polish Academy of Sciences,
Centre for Ecological Research, Łomianki,
Poland

1. Introduction

Environmental pollution with plastic, especially polyolefins increased during the last decades. Due to recalcitrance of these substrates the studies on procedures speeding up the degradation and biological decomposition of polyolefins are carried intensively. The data concerning polypropylene (PP) disappearance rate are scarce comparing to the decomposition of polyethylene (PE) products (Ammala et al., 2011, Arutchelvi et al., 2008, Eubeler et al., 2010). It has been shown that pretreated PP disappear more quickly than poly(propylene-co-ethylene) (CPP) and PE polymers (Arutchelvi et al., 2008, Meligi et al., 1995, Sivan, 2011). However slower degradability of PP comparing to other plastics has been reported (Yang et al., 2005). It is known that UV radiation and weathering processes can speed up biodegradation processes of plastics in later stages of disappearance. Some studies of the PP and PE biodegradation showed that microorganisms, both bacteria and fungi, colonised the pre-treated or composted plastic substrata to greater extent comparing to control treatments (Ammala et al., 2011, Arutchelvi et al., 2008, Eubeler et al., 2010, Grunz et al., 1999, Meligi et al., 1995). There is a little information about the biodegradability of PP in the natural environment and impact of fresh organic matter input on PP decomposition. It seems that the natural input of nitrogen-rich organic matter both of plant and invertebrate origin might accelerate microbial activity and in consequence speed up the decomposition processes of recalcitrant materials (Crow et al., 2009, Dekker et al., 2005, Griffiths, 1994 Prévost-Bouré et al., 2010, Szanser, 2000).

The aim of the study was to compare the decomposition rate of the PP and natural plant litter (NPL). The hypothesis was that the decomposition of artificial litter made of PP will proceed effectively as in the case of natural litters due to additive effects of the input of plant and invertebrate remains into the litter.

2. Materials and methods

2.1 Study site and experimental design

The study was carried out in a permanent meadow of the type Arrhenatheretalia situated in the buffer zone of Kampinos National Park (52°15'30" N and 20°17' E, east-central Poland).

An experiment was conducted to compare the decomposition pattern of natural plant litters (NPL) and of artificial litter composed of natural not dyed PP agricultural string. The experimental meadow of an area of 190 x 10 m had 182 microplots (0.5 x 0.5m area and 0.15 m depth). Five natural and one artificial litter treatments in 32 and 22 plot replicates respectively according to RCB design were applied (Pearce, 1983). Eight litter containers per plot were placed. Natural litter was obtained from meadow plants, both grasses and weeds cut in August 2001 which had to simulate the input of decaying plants to soil. The same amount of PP and NPL (9 g dry wt.) irrespective of the number of plant species was exposed in modified litter containers. Experimental plots were filled with sand mixed with loam to the depth of 15 cm. Such type of simplified and uniform substrate, among them, enabled assessing the input of organic matter morphous particles in exposed litter and in underlying substrate.

Litter samples were mounted under stainless steel wires stuck into the substrate. In that way a more compact structure of exposed material which adhered to the substratum was obtained, providing fauna with better access to the litter without covering containers by a net on the top. NPL were either monospecific (I: *Dactylis glomerata*; II: *Festuca rubra* and III: *Trifolium pratense*) or were species mixtures (IV: mixture of three species I, II and III; V: mixture of twelve species, IV and nine other meadow plants). In the latter case, the following species were used: grasses: brome grass (*Bromus inermis*), meadow foxtail (*Alopecurus pratensis*), perennial ryegrass (*Lolium perenne*), oat grass (*Arrhenatherum elatius*), cocksfoot (*Dactylis glomerata*), and red fescue (*Festuca rubra*); and herbs: small plantain (*Plantago lanceolata*), common chicory (*Cichorium intybus*), red clover (*Trifolium pratense*), milfoil (*Achillea millefolium*), carrot (*Daucus carota*), and common silverweed (*Potentilla anserina*).

2.2 Sample collecting and processing

The experiment started on 24-25 March 2002. Samples were taken on 27 September 2002, 11 May 2004, 9 September 2004, i.e., 6, 26, and 30 months after litter exposure.

Litter and soil samples were taken per 5-11 in every sampling occasion. Soil samples for assessments of plant and invertebrate organic matter input were taken to the depth of 1 cm with a soil corer 100 cm^2 in area.

2.3 Plant and invertebrate materials

2.3.1 Litter mass loss

Litter mass loss was determined using the gravimetric method by drying at 65^oC.

2.3.2 Input of wind-borne plant matter and invertebrate remnants into litter and underlying substrate

The input of the remnants of invertebrate origin (exuviae, cocoons, other remants) was assessed in the litter and soil layer 0-1 cm underneath the litter by hand-sorting and using the stereoscope microscopy.

2.4 Statistical analysis

Statistical analyses of results (one-way *ANOVA* and regression) were performed using Statistica 8.0. software (StatSoft, Inc. (2007). Natural litter and remnants' data had no normal

distribution. Only total data for PP litter and remnants had normal distribution. Differences in mass of litter and remnants between treatments were assessed using non-parametric Wilcoxon Sum-of-Ranks (Mann-Whitney) test for comparing two unmatched samples. The regression between masses of remaining litter and remnants were assessed using the Kendall tau Rank Correlation test and linear regression analysis for natural and polypropylene treatments, respectively.

3. Results

3.1 Litter decomposition

The highest values of the NPL mass loss were recorded in the initial period, while the loss of PP litter was the slowest (Table 1). In the first 6 months following exposure, the loss of dry weight mass of litter reached 59.8 and 28.1% respectively for NPL and PP treatments (Table 1). Later, further losses of litter, during over two years period, were observed being 70.53 and 72.45% for NPL and PP treatments respectively. In the final period, i.e., between the 26th and 30th months of the experiment, the increases of both types litter mass were larger than its losses. This could be explained by the organic matter (of plant and animal origin) input and colonisation of the litter by invertebrates and microorganisms during long period of the exposure (2.5 years).

Months since beginning of the experiment		Litter type		Significance of differences between treatments
		NPL	PP	
6	g dry weight m^{-2}	362.28 (7.22)	646.78 (24.69)	n = 55, W = 502.5, p<=0.00000
	%	40.25	71.86	
26	g dry weight m^{-2}	265.26 (9.98)	337.98 (28.61)	n = 35, W = 106.5, p<=0.4229
	%	29.47	37.55	
30	g dry weight m^{-2}	293.78 (14.23)	360.88 (58.91)	n = 35, W = 111.5, p<=0.1573
	%	32.64	40.1	

Table 1. Mass (g dry weight m^{-2}) of remaining and percent (%) of initial mass of exposed natural plant (NPL) and polypropylene (PP) litter during the course of the experiment. Significance of differences between treatments are assessed by non-parametric Wilcoxon Sum-of-Ranks (Mann-Whitney) test. All data from five natural litter treatments (I: *Dactylis glomerata*; II: *Festuca rubra* and III: *Trifolium pratense*), IV: mixture of three species I, II and III; V: mixture of twelve species, IV and nine other meadow plants) were analyzed with the exception of 26th month where only data of treatments I and III were used. Standard errors in parentheses.

Differences between NPL(data taken together) and PP treatments in the litter decomposition rate resulted from litter origin. Remaining mass of artificial litter (PP) was higher in every sampling time by 43.9%, 27.4% and 22.8% comparing to natural (NPL) ones respectively after 6, 26 and 30 months of the experiment but the differences were significant only for the first sampling occasion (Table 1). Interestingly slight increase of litter mass occurred in PP treatment similarly as in natural litter at the end of the experiment.

3.2 Input of plant and invertebrate remnants

There was considerably large input of wind-borne plant material into exposed litter. It was still low after 6 months of the experiment and was particularly high by the 26th month. There was further slight increase of plant remnants input between 26th and 30th month of the experiment. PP litter had significantly higher input of wind-borne plant matter comparing to NPL only after 6 months of the experiment (Table 2). Later the differences between treatments were not significant. The values of wind-borne plant materials were 43.4 and 39.6 g dry wt. m^{-2} for NPL and PP treatments respectively at the end of the experiment. This input constituted 4.82 and 4.4 % of the initial mass of natural and artificial litter, respectively. Much smaller was the mass of invertebrate origin (exuviae, cocoons, other remnants) found in both treatments but the differences between treatments were not significant (Table 3). The mass of invertebrate remnants amounted to 2.0 and 1.2 g dry wt. m^{-2} for NPL and PP treatments respectively at the end of the experiment.

Months since beginning of the experiment	Litter type		Significance of differences between treatments
	NPL	PP	
6	3.71 (0.37)	9.31 (1.99)	n = 60, W = 305, p <= 0.9921
26	36.77 (9.26)	14.14 (2.67)	n = 24, W = 69, p <=0.7139
30	43.40 (5.72)	39.60 (15.52)	n = 51, W = 138, p <= 0.6089

Table 2. Mass of wind-borne plant remnants (g dry weight m^{-2}) in natural plant (NPL) and polypropylene (PP) litter during the course of the experiment. Differences between treatments are assessed by non-parametric Wilcoxon Sum-of-Ranks (Mann-Whitney) test. All data from five natural litter treatments (I: *Dactylis glomerata*; II: *Festuca rubra* and III: *Trifolium pratense*), IV: mixture of three species I, II and III; V: mixture of twelve species, IV and nine other meadow plants) were analyzed with the exception of 26th month where only data of treatments I and III were used. Standard errors in parentheses.

Months since beginning of the experiment	Litter type		Significance of differences between treatments
	NPL	PP	
6	1.48 (0.23)	2.49 (0.50)	n = 60, W = 305, p <= 0.9921
26	0.85 (0.33)	0.58 (0.33)	n = 24, W = 75, p <= 0.9734
30	2.00 (0.36)	1.17 (0.33)	n = 51, , W = 156, p <= 0.9883

Table 3. Mass of invertebrate remnants (g dry weight m^{-2}) in NPL and PP litter during the course of the experiment. Differences between treatments are assessed by non-parametric Wilcoxon Sum-of-Ranks (Mann-Whitney) test. All data from five natural litter treatments (I: *Dactylis glomerata*; II: *Festuca rubra* and III: *Trifolium pratense*), IV: mixture of three species I, II and III; V: mixture of twelve species, IV and nine other meadow plants) were analyzed with the exception of 26th month where only data of treatments I and III were used. Standard errors in parentheses.

Summarized data of both plant and invertebrate material revealed that significantly higher was the mass of new organic material in PP comparing to natural treatments after 6 months of the experiment (Table 4). Later the differences between treatments were not significant. The values of total organic matter input were 45.4 and 40.8 g dry wt. m^{-2} for natural and PP treatments respectively at the end of the experiment.

The negative correlations between mass of remaining litter and input of both types of remnants were found for NPL ($r = -0.456$, $Z = -7.230$, $P < 0.00000$, $n = 115$) and PP ($r = -0.415$, $r^2 = 0.172$, $F = 3.743$, $P < 0.0689$, $n = 20$) treatments taking the entire study period data.

Months since beginning of the experiment	Litter type		Significance of differences between treatments
	NPL	PP	
6	5.19 (0.42)	11.8 (2.08)	n = 60, W = 305, p <= 0.9921
26	37.62 (9.32)	14.73 (2.66)	n = 24, W = 69, p <=0.7139
30	45.40 (5.73)	40.78 (15.66)	n = 51, W = 138, p <= 0.6089

Table 4. Sum of plant and invertebrate remnants (g dry weight m^{-2}) in NPL and PP litter during the course of the experiment. Differences between treatments are assessed by non-parametric Wilcoxon Sum-of-Ranks (Mann-Whitney) test. All data from five natural litter treatments (I: *Dactylis glomerata*; II: *Festuca rubra* and III: *Trifolium pratense*), IV: mixture of three species I, II and III; V: mixture of twelve species, IV and nine other meadow plants) were analyzed with the exception of 26th month where only data of treatments I and III were used. Standard errors in parentheses.

4. Discussion

The meteorological data indicated that climatic conditions in the study period were unfavourable for soil organisms (Szanser et al., 2011). Artificial litter (PP) was drier comparing to natural litters (NPL) and retained a maximum of 5% moisture even during rainfall, while its underlying substrate was similarly wet as that under natural litters (Szanser et al., 2011). Lower mass loss of PP comparing to NPL was coincided with significantly lower numbers of fungi and bacteria in the PP litter and its respiration by 3.4, 44.8 and 61.4 times respectively comparing to natural treatments (Górska unpubl., Szanser et al., 2011). Interestingly number of fungi was the parameter the least differentiating between PP and other treatments. It may signify that the decomposition of PP was of fungal nature. Nevertheless it was found that almost 60 and 70% of the exposed PP and natural litters degraded by 26th month of the experiment. It seems that degradation of PP was quite effective as far as there were no significant differences between applied treatments at the end of the experiment. Thirty months after litter exposure, the input of wind-borne plant material was similar in both treatments. Considerably smaller was the mass of invertebrate origin (exuviae, cocoons, other remnants in both treatments. Similar input of invertebrate organic matter found in later stages of the experiment is corroborated by the lack of significant differences between PP and natural litters in invertebrate macrofauna penetration (Kajak, Szanser, unpubl.). Similar values of the input of plant and invertebrate remnants into natural litter and underlying substrate were found in other agricultural and meadow environments (Szanser,

2003, Szanser, unpubl.). It seems that input of organic matter into PP had some effect on its biodegradation. It should be pointed out that the absorption of different ions (Na^+, $N\text{-}NH_4^+$, K^+, Mg^{2+}, Cl^-, $N\text{-}NO_3^-$, $S\text{-}SO_4^{2-}$) by exposed PP from aerosol-gaseous input, although not measured in this study, can have additional impact on speeding up PP biodegradation. It was found that absorption of elements by polymers used as "artificial leaves" can be quite high and increase with surface area of the exposed plastic (Kram, 2005, Stachurski & Zimka 2000). It seems that the aerosol-gaseous input of elements together with input of new organic matter and further development of microorganisms in fibrous PP resulted in efficient decomposition of the PP. Observed slight increase of polymer mass towards the end of the experiment simultaneously as in natural litter can be explained by the organic matter input and development of microbial communities. The mechanisms involved in PP biodegradation are corroborated by data obtained from experimental underlying substrates. There were no significant differences in microbial activity (soil respiration, microbial biomass and numbers of bacteria and fungi) between PP and NPL treatments in underlying substrate during the third year of the experiment (Górska, Szanser, unpubl.). On the opposite algal biomass and production were by 36% and 39.7% respectively higher under PP comparing to NPL treatments for entire study time (Sieminiak, unpubl.). The increase of carbon content under the PP was higher by 47% than in natural treatments at the end of the experiment (Kusińska & Szanser unpubl.). It should be pointed out that the paper presents results obtained from long-time field experiment while most of the research on degrading the polymers are short time studies.

5. Conclusions

In general, the results suggest that (1) the long term decomposition of artificial litter (PP) proceeded efficiently but was still quite low comparing to natural treatments; (2) the input of plant and invertebrate remains into the PP can be considerably large and may have an additive effect on its decomposition; (3) it seems that longtime decomposition of natural PP may be quite effective comparing to plant litters and (4) the presence of PP did not inhibit severely soil biota activity and organic matter accumulation in soil during the experiment.

6. Acknowledgments

This research was supported by a grant from the Polish State Committee for Scientific Research, project P04 F 03820.

7. References

Ammala, A., Bateman, S., Dean, K., Petinakis, E., Sangwan, P., Wong, S., Yuan, Q., Yu, L., Patrick, C., and Leong, K. H. (2011). An overview of degradable and biodegradable polyolefins. *Progress in Polymer Science* Vol. 36, No. 8, (August 2011), pp. 1015-1049, ISSN: 0079-6700.

Arutchelvi, J., Sudhakar, M., Arkatkar, A., Doble, M., Bhaduri, S., and Uppara, P. V. (2008). Biodegradation of polyethylene and polypropylene. *Indian Journal of Biotechnology*, Vol. 7, No. 1, (January 2008), pp. 9-22, ISSN: 0972-5849.

Chemidlin Prévost-Bouré, N., Soudani, K., Damesin, C., Berveiller, D., Lata, J.-C., and Dufrêne, E. (2010). Increase in aboveground fresh litter quantity over-stimulates soil respiration in a temperate deciduous forest. *Applied Soil Ecology*, Vol. 46, No. 1, (September 2010), pp. 26-34, ISSN: 0929-1393.

Crow, S. E., Lajtha, K., Bowden, R. D., Yano, Y., Brant, J. B., Caldwell, B. A., and Sulzman, E. W. (2009). Increased coniferous needle inputs accelerate decomposition of soil carbon in an old-growth forest. *Forest Ecology and Management*, Vol. 258, No 10, (October 2009), pp. 2224-2232 ISSN: 0378-1127.

Dekker, S. C., Scheu, S., Schröter D., Setälä, H., Szanser, M. and Traas, T. P. (2005). Towards a new generation of dynamical soil decomposer food web models. Pages 590 *in* P. C. De Ruiter, V. Wolters, and J. C. Moore, editors. *Dynamic Food Webs -multispecies assemblages, ecosystem development and environmental change*, (No information 2006) pp. 258-269 Elsevier, Amsterdam, ISBN: 978-0-12-088458-2.

Eubeler, J. P., Bernhard, M., and Knepper, T. P. (2010). Environmental biodegradation of synthetic polymers II. Biodegradation of different polymer groups. *TrAC Trends in Analytical Chemistry* , Vol. 29,No 1, (January 2010), pp. 84-100, ISSN: 0165-9936.

Griffiths B. S. 1994 - Microbial-feeding nematodes and protozoa in soil: Their effects on microbial activity and nitrogen mineralization in decomposition hotspots and the rhizosphere - *Plant and Soil*, Vol. 164, No 1, (January 1994), pp. 25-33, ISSN: 0032-079X.

Kram K.J. (2005). Bulk precipitation and aerosol-gaseous input of elements in the forested area of coastal region (Pomerania, north Poland). *Polish Journal of Ecology*, Vol. 53, No. 2, pp. 261–268, (June 2005), ISSN 1505-2249.

Meligi, G., Yoshii, F., Sasaki. T., Makuuchi, K., Rabie, A. M. and Nishimoto, S-I., 1995. Comparison of the degradability of irradiated polypropylene and poly(propylene-co-ethylene) in the natural environment, *Polymer Degradation and Stability*, Vol. 49, No. 2, (No information 1995), pp 323-327, ISSN: 0141-3910.

Grunz, A., Dayss, E., and Leps, G. (1999). Biomass covering of plastics substrates depending on plasma treatment. *Surface and Coatings Technology* Vol. 116-119, (September 1999), pp. 831-835, ISSN: 0257-8972.

Pearce, S.C. (1983). *The Agricultural Field Experiment: a Statistical Examination of Theory and Practice*. New York: John Wiley & Sons, (No information 1983), pp. 335, ISBN-10: 0471105112.

Sivan, A. (2011). New perspectives in plastic biodegradation. *Current Opinion in Biotechnology* , Vol. 22, No. 3, (June 2011), pp. 422-426, ISSN: 0958-1669.

Stachurski, A., and Zimka, J. R. (2000). Atmospheric input of elements to forest ecosystems: a method of estimation using artificial foliage placed above rain collectors. *Environmental Pollution*, Vol. 110, No. 2, (November 2000), pp. 345-356, ISSN: 0269-7491.

STATISTICA (data analysis software system), version 8.0. www.statsoft.com).

Szanser M. 2000 - Effect of macroarthropods patrolling soil surface on decomposition rate of grass litter (*Dactylis glomerata*) in a field experiment – Polish Journal of Ecology Vol. 48, No. 4, (October 2000), pp. 283-297, ISSN 1505-2249.

Szanser, M. 2003 - The effect of shelterbelts on litter decomposition and fauna of adjacent fields: In situ experiment - Polish Journal of Ecology, Vol.51, No.3, (September 2003), pp.309-321, ISSN 1505-2249.

Szanser, M., Ilieva-Makulec, K., Kajak, A., Kusińska, A., Kisiel, M., Olejniczak, I., Russel, S., Sieminiak, D., Wojewoda, D. (2011). Impact of litter species diversity on decomposition processes and communities of soil organisms - *Soil Biology and Biochemistry*, Vol. 43, No. 1, (January 2011), pp. 9-19, ISSN: 0038-0717.

Yang, H.-S., Yoon, J.-S., and Kim, M.-N. (2005). Dependence of biodegradability of plastics in compost on the shape of specimens. Polymer Degradation and Stability, Vol. 87, No. 1, (December 2004), pp. 131-135 ISSN: 0141-3910.

7

Modified Atmosphere Packaging for Perishable Plant Products

Leonora M. Mattos[1], Celso L. Moretti[1] and Marcos D. Ferreira[2]
[1]*Embrapa Vegetables,*
[2]*Embrapa Instrumentation*
Brazil

1. Introduction

Packaging perishable plant products is one of the more important steps in the long and complicated journey from grower to consumer. Millions of different types of packages are used for produce around the world and the number continues to increase as the industry introduces new packaging materials and concepts. Packing and packaging materials contribute a significant cost to the produce industry; therefore it is important that packers, shippers, buyers, and consumers have a clear understanding of the wide range of packaging options available (Boyette et al., 1996). This fact chapter describes some of the many types of packaging materials, including their functions, uses, and limitations. Within packaging plastics for plant products, if commodity and film permeability characteristics are properly matched, an appropriate atmosphere can evolve passively through consumption of O_2 and production of CO_2 during respiration (Mir & Beaudry, 2002). Gas exchange and respiration rate through the package material are the processes involved in creating a modified atmosphere inside a package that will extend shelf life of fresh fruits and vegetables. The major methods for measuring respiration rates, along with their advantages and limitations are discussed. Modified atmosphere technologies have great potential in a wide range of applications in plant products. The usual methods of respiration rate determination can be the static system, the flowing system and the permeable system (Fonseca et al., 2002). The respiration rate of fresh produce can be expressed as O_2 consumption rate and/or CO_2 production rate. Factors affecting the respiration rate and respiratory quotient are outlined, stressing the importance of temperature, O_2 and CO_2 concentrations, and storage time (Kader et al., 1989). Modified atmosphere packaging should always be considered as a supplement to proper temperature and relative humidity management. The differences between beneficial and harmful concentrations of oxygen and carbon dioxide for each kind of produce are relatively small, so great care must be taken when using these technologies. Temperature has been identified as the most important external factor influencing respiration (Tano et al., 2007). The internal factors affecting respiration are the type and maturity stage of the commodity. Vegetables include a great diversity of plant organs such as fruits, roots, tubers, seeds, bulbs, sprouts, leaves and stems that have different metabolic activities and consequently different respiration rates. Different varieties of the same product exhibit specific respiration rates. The success of modified atmosphere packaging greatly depends on the accuracy of the predictive respiration rate (Kader, 2002). The main objective of this chapter is to present different packaging materials using modified atmosphere for perishable plant products, focusing

particularly on aspects of the respiration process, usual methods of measuring respiration rates and factors can be affect the respiration rate.

2. Modified atmosphere packaging

Modified atmosphere packaging (MAP) of fresh fruits and vegetables is based on modifying the levels of O_2 and CO_2 in the atmosphere produced inside a package sealed with some type of polymer film. It is desirable that the natural interaction that occurs between the respiration of the product and the packaging generates an atmosphere with low levels of O_2 and / or a high concentration of CO_2. The growth of organisms that cause decay is thereby reduced and the life of the product is thus extended. Additionally, the desired atmosphere can reduce the respiration rate, and ethylene production, physiological changes. For example, it can inhibit chemical, enzymatic and microbiological mechanisms associated with the decay of fresh products, thus avoiding the use of other chemical or thermal process such as freezing, dehydration, and sterilization (Kader et al. 1989; Gorris & Tauscher, 1999; Saltveit, 1997; Fonseca et al., 2002).

The use of modified and controlled atmospheres has grown over the past 50 years, contributing significantly to extend the postharvest life and maintain the quality of various fruits and vegetables. So that changing the atmosphere occurs must have a combination of factors that influence the permeability of the product packaging and respiration in order to achieve an atmosphere of great balance for the conservation of the product. This balance is achieved when the respiration of the product consumes the same amount of O_2 entering the packaging and the production of CO_2 by respiration is equal to the amount that leaves the packaging (Day, 1993).

The first studies on modified atmospheres used reduced levels of O_2 in apple packaging in order to slow the ripening of fruits. The first challenge was to control the levels of O_2 in the package. Since then, an enormous variety of polymers with different properties have been developed to offer a wide range of options in features such as gas permeability, tensile strength and flexibility, among others. Presently, diverse systems of modified atmosphere packaging have been developed and used with a wide range of fruits and vegetables in order to provide optimal storage conditions and product longevity. Table 1 summarizes the optimal conditions of temperature and gas composition of O_2 and CO_2 for the transport and / or storage of some fruits and vegetables.

2.1 Passive

Modified atmospheres can be obtained passively between plant material and sealed package or intentionally using determined concentrations of gases. Modified atmosphere is formed as a result of vegetable respiration, which consumes CO_2 and releases O_2 in sealed package. In passive modification, the respiring product is placed in a polymeric package and sealed hermetically. Only the respiration of the product and the gas permeability of the film influence the change in gaseous composition of the environment surrounding the product. If the product's respiration characteristics are properly matched to the film permeability values, then a beneficial modified atmosphere can be passively created within a package. The polymer itself variably restricts gas exchange between the internal and external environments due to its selective permeability to O_2 and CO_2. After a period of time, the

system reaches an equilibrium atmosphere containing of lower concentrations of O_2 and higher concentrations of CO_2 than in atmospheric air.

Product	Temperature range (^{0}C)	Atmosphere	
		%O_2	%CO_2
Apples	0-5	1-2	0-3
Banana	12-16	2-5	2-5
Blackberry	0-5	5-10	15-20
Blueberry	0-5	2-5	12-20
Cherry, sweet	0-5	3-10	10-15
Cranberry	2-5	1-2	0-5
Grape	0-5	2-5	1-3
Kiwifruit	0-5	1-2	3-5
Lemon	10-15	5-10	0-10
Lychee (Lichti)	5-12	3-5	3-5
Mango	10-15	3-7	5-8
Nuts and dried fruits	0-10	0-1	0-100
Orange	5-10	5-10	0-5
Papaya	10-15	2-5	5-8
Persimmon	0-15	3-5	5-8
Pineapple	8-13	2-5	5-10
Plum	0-5	1-2	0-5
Raspberry	0-5	5-10	15-20
Strawberry	0-5	5-10	15-20
Artichoke	0-5	2-3	2-3
Asparagus	1-5	Air	10-14
Beans	5-10	2-3	4-7
Broccoli	0-5	1-2	5-10
Brussels sprouts	0-5	1-2	5-7
Cabbage	0-5	2-3	3-6
Cantaloupes	2-7	3-5	10-20
Cauliflower	0-5	2-3	3-4
Celery	0-5	1-4	3-5
Cucumbers	8-12	1-4	0
Herbs*	0-5	5-10	4-6
Lettuce	0-5	1-3	0
Onions	0-5	1-2	0-10
Parsley	0-5	8-10	8-10
Pepper	5-12	2-5	2-5
Radish	0-5	1-2	2-3
Spinach	0-5	7-10	5-10
Tomatoes	12-20	3-5	2-3

*Herbs: chervil, chives, coriander, dill, sorrel and watercress, Adapted from Kader (2002)

Table 1. Summary of optimal conditions for modified atmosphere and temperature during transport and / or storage of fruits and vegetables

2.2 Active

The concept of active packaging has been developed to adjust the deficiencies in passive packaging such as when a film is a good barrier to moisture, but not to oxygen, the film can still be used along with an oxygen scavenger to exclude oxygen from the pack. An intentionally or actively obtained modified atmosphere occurs when the desired gas mixture is introduced into the container before sealing. In this way, atmospheric balance inside the package is reached faster or almost immediately. Sometimes, certain additives are incorporated into the polymeric packaging film or within packaging containers to modify the headspace atmosphere and to extend shelf-life. Another process is the acceleration of atmospheric balance under partial vacuum packaging is the process of removing the air before sealing, reducing the free space. Although the active modification of the atmosphere within the package incurrs additional costs, the advantage is that the desired atmosphere is securely achieved in considerably less time.

2.3 O_2 and CO_2 limits

Safe levels of O_2 and CO_2 are important for package design. A lower O_2 limit has been associated with onset of fermentation and accumulation of ethanol and acetaldehyde (Beaudry et al., 1993). Fermentation is linked to the development of off-flavors and/or tissue damage. Effect of temperature on lower O_2 limit has been measured for a number of commodities including whole apple, apple slices, blueberry, and raspberry. In each case, lower O_2 limit increased with temperature. Lower O_2 limits vary from 0.15% to 5% and are influenced by temperature, commodity and cultivar (Beaudry and Gran, 1993).

It is necessary to know the main effects of gases on fresh fruits and vegetables and the interactions between gas and produce on the one hand and between gas and packaging material on the other hand to achieve the goal. It is important to recognize that while atmosphere modification can improve the storability of some fruits and vegetables, it also has the potential to induce undesirable effects. Fermentation and off-flavors may develop if decreased O_2 levels cannot sustain aerobic respiration (Kays, 1997). Similarly, injury will occur if CO_2 exceeds tolerable levels. Ranges of non-damaging O_2 and CO_2 levels have been published for a numbers of fruits and vegetables (Kader, 1997; Kupferman, 1997; Richardson and Kupferman, 1997; Saltveit, 1997; Beaudry 1999, 2000), minimally processed products (Gorny, 1997), and flowers and ornamentals (Reid, 1997). Horticultural crops differ in their tolerance for O_2 (Table 2) and CO_2 (Table 3).

3. Types of plastic films used in MAP

In a modified atmosphere packaging, changes start to take place immediately after packing the fresh produce as a result of the respiration of the packaged produce. The gases of the contained atmosphere and the external ambient atmosphere try to equilibrate by permeation through the package walls at a rate dependant upon the differential pressures between the gases of the headspace and those of the ambient atmosphere. It is in this context that the barrier to gases and water vapor provided by the packaging material must be considered. Thus, the success of the modified atmosphere packaging depends upon the barrier material used. MAP for fresh produce must also allow entry of oxygen to maintain the aerobic

O_2 (%)	Commodity
2	Lettuce (crisphead), pear
3	Artichoke, tomato
5	Apple (most cultivars), apricot, cauliflower, cucumber, grape, nashi, olive, orange, peach (clingstone), potato, pepper (bell)
7	Banana, bean (green snap), kiwi fruit
8	Papaya
10	Asparagus, brussels sprouts, cabbage, celery, lemon, mango, nectarine, peach, persimmon, pineapple, sweet corn
15	Avocado, broccoli, lychee, plum, pomegranate, sweetsop
20	Cantaloupe (muskmelon), durian, mushroom, rambutan
25	Blackberry, blueberry, fig, raspberry, strawberry

*Data are from Beaudry (2000), Gorny (1997), Kader (1997), Kupferman (1997), Richardson and Kupferman (1997), and Saltveit (1997)

Table 2. O_2 limits below which injury can occur for selected horticultural crops held at typical storage temperatures

CO_2 (kPa)	Commodity
< 0.5	Chopped greenleaf, Romaine and iceberg lettuce, spinach, sliced pear, broccoli
1.0	Broccoli florets, chopped butterhead lettuce, sliced apple, brussels sprouts, cantaloupe, cucumber, crisphead lettuce, onion, apricot, avocado, banana, cherimoya, sweet cherry, cranberry, grape, kiwifruit, litchi, peach, plum
2.0	Shredded and cut carrots, artichoke, cabbage, cauliflower, celery, bell and chili pepper, sweet corn, tomato, blackberry, fig, mango, olive, papaya, pineapple, pomegranate, raspberry, strawberry
2.5	Shredded cabbage, blueberry
3.0	Cubed or sliced cantaloupe, low permeability apples and pears, persimmon
4.0	Sliced mushrooms
5.0	Green snap beans, lemon, lime, orange
10.0	Asparagus
14.0	Orange sections

* Adapted from Herner (1987), Kader (1997), and Saltveit (1997)

Table 3. CO_2 partial pressures above which injury will occur for selected horticultural crops

metabolism of the product. In addition, some carbon dioxide must exit from the package to avoid build up of injurious levels of the gas. These packages are made of plastic films with relatively high gas permeability.

Packaging films that provide a wide range of physical properties, many of these individual films are combined through processes like lamination and co-extrusion. There are several groupings in MAP films such as in the plural, Vinyl Polymers, Styrene Polymers,

Polyamides, Polyesters and other polymers. Polypropylene is part of the Polyolefin group and used largely in MAP, in both forms: continuous and perforated. Sanz et al. (1999) studied the quality of strawberries packaged with polypropylene film, with proper perforations, during commercial postharvest practices. They concluded that perforated-mediated MA packaging helped to preserve fruit ripeness degree better, maintaining its nutritional value, measured as ascorbic acid content.

Many type of plastic films for packaging are available, but relatively few have been used to pack fresh fruits and vegetables, and even fewer have a gas permeability that makes them suitable for modified atmosphere packaging. The permeability of CO_2 should be 3 to 5 times the permeability of O_2. Many polymers used to formulate packaging films are within this criterion (Table 4).

Film type	Permeabilities (cc/m²/mil/dia a 1 atm)		
	CO_2	O_2	CO_2:O_2 ratio
Polyester	180-390	52-130	3.0-3.5
Polyethylene, low density	7,700-77,000	3,900-13,000	2.0-5.9
Polypropylene	7,700-21,000	1,300-6,400	3.3-5.9
Polystrene	10,000-26,000	2,600-7,700	3.4-3.8
Polyvinyl chloride	4,263-8,138	620-2,248	3.6-6.9

*Adapted from Kader (2002)

Table 4. Permeability for packaging fresh fruits and vegetables

4. Package parameters

Modified atmosphere (MA) packaging systems designed to produce optimum O_2 and CO_2 concentrations at suitable temperatures have been mathematically modeled (Chinnan, 1989; Lee et al., 1991; Exama et al., 1993; Talasila et al., 1995; Cameron et al., 1995).

The composition of the atmosphere inside the packaging results from the interaction of several factors including the permeability characteristics of the packaging material, the respiratory behavior of the plant material and the environment. Packaging films are selected so that the package has specific permeability characteristics and so that changes to these characteristics (temperature and humidity) over time, following the laws of physics. The concentration of gases within the packaging can be controlled to provide specific conditions. In contrast to these known and controllable factors are the often unknown and uncontrollable responses of the plant material. The plant species, the cultivar, cultural practices, the development stage, harvest management, the tissue type and post harvest handling all contribute and influence the response of the material to the atmosphere generated.

The scope of plant responses can be modified by the initial flow of gas before sealing the packaging as well as by the inclusion of chemical treatments to slow undesirable processes or decrease contamination. Each component of the packaging process needs to be examined separately to improve the understanding of what it contributes to potential packaging strategies.

Mathematical models can integrate the film permeability to O_2, CO_2 and H_2O, and the respiratory response of the commodity to O_2, in some cases, CO_2, along with its lower O_2 limit and upper CO_2 limit (Beaudry et al., 1992; Cameron et al., 1994; Lakakul et al., 1999; Fishman et al., 1996; Hertog et al., 1998). These models permit the identification of limiting features of the film, package design, and product and environment conditions.

The major factors to be taken into account while selecting the packaging materials are the type of package, the barrier properties needed (permeabilities of individual gases and gas ratios when more than one gas is used), physical properties of machinability and strength, integrity of closure (heat sealing), fogging of the film as a result of product respiration, printability and others.

4.1 Respiration rate

Respiration is a process in which chemical reactions oxidize lipids and carbohydrates to carbon dioxide and water to produce energy, while the organelle responsible for aerobic respiration known as mitochondria. Part of the released energy is stored as chemical energy adenosine triphosphate (ATP) and part is lost as heat. This complex process can be influenced by several intrinsic factors such as product size, variety, maturity, type of tissue and extrinsic factors such as temperature, concentration of O_2 and CO_2 and mechanical damage (Day, 1993).

Knowledge of the minimum required for O_2 aerobic respiration is very important to avoid that the anaerobic pathway is the predominant route of respiration, which causes the accelerated loss of product quality. In order to maintain food safety, it is important to know the potential hazards of each product, the permeability of the films and the rate of respiration of fruits and vegetables (Watada et al., 1996).

Since both the rate of respiration and the permeability of the film are sensitive to temperature variations, and respond to these changes differently, it is expected that the package under modified atmosphere remains determined only within an atmosphere given temperature range (Zagory, 2000).

The maximal rate of respiration for most fruit and vegetable products undergoes a 4- to 6-fold increase from 0 to 15 °C (Beaudry et al., 1992; Cameron et al., 1994, 1995; Lakakul et al., 1999). This means that product respiration increases at two or three times the rate of LDPE permeability, and thirty times the rate of perforation permeability with increasing temperature. When respiratory demand for O_2 increases faster than O_2 permeation as temperature increases, O_2 levels decline and may pose a risk to product quality. This limits the usefulness of MAP in some situations.

Variation in the respiration rate of the product and the variation in film or permeability can influence package design. Variation in product respiration and package permeability has been measured for broccoli and the effect on package O_2 modeled (Cameron et al., 1993). Cameron et al. (1993) concluded that there is an estimable risk of the package O_2 falling sufficiently low to promote fermentation in any product. Packages should be designed to generate O_2 levels well above the lower limit to ensure aerobic conditions. Products such as broccoli, mushrooms, leeks and others have very high rates of respiration, and most continuous films do not have the capacity to provide enough O_2 to avoid fermentation.

Accordingly, there is commercial interest to develop films with high gas transmission rates. Films that have improved rates of gas transmission by virtue of their polymeric nature are often blends of two or three different polymers, where each polymer performs a specific function such as strength, transparency and improved gas transmission. Similarly, films can be laminated to achieve needed properties.

4.2 Temperature

Temperature is one of the most important factors in extending the shelf-life of perishable products. Optimum storage temperature must be established for every product. Permeability of polymeric packaging films is also a function of temperature and it generally increases with the increase in temperature.

The effects of temperature on chemical reactions, including respiratory rate, traditionally quantified by Q_{10}, which is a coefficient by which it is possible to calculate how many times increases the rate of a reaction for each increase in temperature of 10 °C. The effect of temperature can also be quantified by the Arrhenius model, where the effect of temperature increase is given by the activation energy (Ea) (Cameron et al., 1995). The temperature quotient is useful because it allows us to calculate the respiration rates at one temperature from a known rate at another temperature. However, the respiration rate does not follow ideal behavior, and the Q_{10} can vary considerably with temperature. At higher temperatures, the Q_{10} is usually smaller than at lower temperatures.

The storage temperature is very important for the evolution of microbial and visual quality of fresh fruits and vegetables. Knowledge of weather conditions and temperature in the cold chain for fresh produce is needed to determine the influence of the cold chain in real loss of quality and shelf life of these products (Cortez et al., 2002).

The temperature of the produce in the package is managed by circulating cool air around the outside of the package. The film and the headspace atmosphere are barriers to heat movement, prevent rapid cooling, and reduce the effectiveness of refrigeration. A 'safe radius' for the distance from the center of the package to the circulated air can be calculated based on the heat of respiration and the rate at which heat can be removed by the cooler air (Sharp et al., 1993). For instance, the center of a package of broccoli must have a radius of less than 14 cm to keep it within 1 °C of the refrigerated air.

Temperature control, when combined with correct use of packaging and modified atmosphere technology, is effective in controlling metabolic processes described above. However, the ideal temperature handling, storage and marketing of fresh fruits and vegetable is generally not respected. Some examples of the ranges of temperature and relative humidity are to be respected in Table 1.

If it is necessary to choose between mild temperatures that cause symptoms of chilling injury and temperatures accelerate senescence and microbial growth, the first must be chosen (Watada and Qi, 1999).

4.3 Permeability

The permeability of the packaging material determines the atmospheric conditions in the headspace and ultimately the shelf-life of the product. If an atmosphere higher in carbon

dioxide and / or lower in oxygen is required, the material should be impermeable to the gases. Vegetables and fruits require a certain amount of oxygen in the headspace for maintenance of quality, therefore, packaging material for these products should be quite permeable to the oxygen, to allow atmospheric oxygen to replenish the gas in the package.

Transparency of packaging material to light is also important.

The choice of packaging material is an extremely important part of the MAP operation. The materials must be cost effective, have low water vapor transmission rate, high gas barrier, mechanical strength to withstand machine handling and subsequent storage and distribution of the finished pack as well as have the capability of giving high integrity seals to ensure retention of gas within the pack until opened by consumer. Also, once a gas atmosphere is applied, the level and proportion of headspace gas/gases is controlled only by judicious selection of packaging material with specified permeability characteristics. . Thickness is also a factor controlling permeability.

There are two ways to create barriers using film. The first strategy employs continuous films that control the movement of gases in and out of the box. The second strategy uses film with small openings or microperforations.

With continuous films, the movement of O_2 and CO_2 is directly proportional to the differences in gas concentration across the film. Constant levels of gases in the package are achieved when the product's consumption of O_2 and production of CO_2 are equal. This situation exists only when the respiration rate is constant (Fishman et al., 1996).

In perforated films, the rate of movement of gas through the perforated film is the sum of gas diffusion and atmospheric air infiltration through the polymer film. Generally, total gas flow through the perforations is much greater than gas movement through the film. The rate of gas exchange through microperforations is much greater than through continuous films. Perforated packaging is more suitable for vegetables that have a high demand for O_2 (Gonzalez et al., 2008).

5. Respiration rate measurement

The respiration rate of fresh fruits and vegetables can be expressed as the rate of O_2 consumption and CO_2 production rate. The usual methods for determining the concentration of respiration are static or closed system, continuous flow system, and permeable system. The respiration rate is measured in permeable system, in other words, the product is within the dimensions and permeability of packaging film known (Beaudry, 1993; Joles et al., 1994; Lakakul, Beaudry, & Hernandez, 1999; Lee, Song, & Yam, 1996; Piergiovanni, Fava, & Ceriani, 1999; Smyth et al., 1998). The concentrations of O_2 and CO_2 are determined and stable mass balance is done on the system in order to estimate respiration rates.

The concentrations of gases in the system depend on the permeability characteristics of permeability, package size and weight of the product that were discussed previously. The time to reach equilibrium can be seen as a limitation of this method to measure the respiration rate. Definition of the steady-state concentration values is another difficulty of the permeable method.

For all methods have limitations, but this involves a greater number of variables, since the size of the packet are involved other parameters such as free volume, surface area and thickness of the gas exchange and the permeability characteristics. None of methods is clearly preferable over the others. When choosing the respiration rate determination method for a specific study, the benefits and limitations of each method should be taken into consideration. Fonseca et al. (1992) studied three different methods (closed, flow through and permeable systems) to measure respiration rate and observed their advantages and limitations. The main characteristics of these methods are summarized in Table 5.

Characteristics	System		
	Closed	Flow through	Permeable
Non-destructive	✓	✓	✓
Complexity of experimental set-up	✓	✓	✓
Ability to test different combinations of gases	Simple	Complex	Complex
Concentration is kept constant during the experiment	x	✓	✓
Suitable for low respiring products	✓	x	
Suitable for high respiring products	x	✓	✓
Accuracy is very sensitive to determination of	Free volume	Flow-rate	Permeability package dimensions, steady-state concentrations

*Adapted from Fonseca et al. (1992)

Table 5. Main characteristics of the three methods of respiration rate measurement

5.1 Factors affecting respiration rate

The factors affecting respiration are type and maturity stage of the commodity. Vegetables include a great diversity of plant organs such as roots, tubers, seeds, bulbs, fruits, sprouts, stems and leaves that have different metabolic activities and consequently different respiration rates. Even different varieties of the same product can exhibit different respiration rates (Fidler & North, 1967; Gran & Beaudry, 1992; Song et al., 1992). In general, non-climacteric commodities have higher respiration rates in the early stages of development that steadily decline during maturation (Lopez-Galvez, El-Bassuoni, Nie, & Cantwell, 2004). Respiration can also be affected by a wide range of environmental factors that include light, chemical stress, radiation stress, water stress, growth regulators, and pathogen attack. The most important postharvest factors are temperature, atmospheric composition, and physical stress.

One method to improve these problems would be to choose a film with permeability changes for O_2 similar to that of the respiration of the product, so if temperature increases, respiration and permeability of the film increase an equivalent amount.

5.2 Influence of temperature

Indeed the most important factor affecting postharvest life is temperature. This is because temperature has a profound effect on the rates of biological reactions, specifically metabolism and respiration. Over the physiological range of most crops, 0 to 30 °C increased temperatures cause an exponential rise in respiration.

Temperature of the product affects storability more than any other factor. Pre-cooling and temperature maintenance during handling and shipping are critical in preserving quality. Temperature also significantly affects film permeability and thereby the O_2 and CO_2 content of the package.

The elevated rate of respiration at high temperature could be used to rapidly establish the desired package atmosphere, but this would only be useful in the few situations in which it would be more important to rapidly establish the atmosphere than to slow physiological processes, eg., to reduce cut-surface browning.

Another solution to the MAP temperature problem is to develop a package system that senses either the environment or the physiological status of the enclosed product and responds by increasing the permeability to O_2 (Cameron et al., 1993). Such 'sense-and-respond' packaging is technically difficult to develop, and progress has only been conceptual at this time (Smyth et al., 1999). A third approach is to design packages to function at the highest temperatures typically encountered in the distribution and retail cool chain and, as far as possible, maintain control over the temperature of the packaged product, thereby adapting to the limitations imposed by the film. Most companies using MAP have adopted this simple solution. Generally, the lowest temperature feasible is maintained, since temperature has a much more significant influence on preserving quality than the application of low O_2 (Kays, 1997).

Reações metabólicas, entre elas a respiração, são reduzidas em 2 a 3 vezes para cada decréscimo de 10 °C na temperatura, o que permite retardar a maturação e a senescência do produto (Brecht, 1995).

5.3 Influence of gas composition

In MAP, the pack is flushed with a gas or a combination of gases. The common gases used are oxygen, nitrogen and carbon dioxide. Traces of carbon monoxide, nitrous oxide, ozone, argon, ethanol vapour and sulphur dioxide are also used. Minimum oxygen levels are used to pack plant under MA because oxygen can react with the fruits and vegetables resulting in the oxidative breakdown of them into their constitutive parts. Nitrogen is an inert gas. Carbon dioxide is responsible for the bacteriostatic and fungistatic effect in MA packaged fruits and vegetables. It retards the growth of moulds and aerobic bacteria. The inhibitory effect of carbon dioxide to micro-organisms is increased as the temperature is lowered.

The tolerance of any plant tissue at low O_2 tension is smaller as the storage temperature increases, since the requirements for aerobic respiration of the tissue increases with increasing temperature. Depending on the product damage associated with CO_2 can both increase and decrease with rise in temperature. CO_2 production increases with temperature, but its solubility decreases. Thus, the CO_2 concentration in the tissue may decrease or increase with increasing temperature. In addition, the physiological effect of CO_2 could be temperature dependent.

The activation energy is a parameter that has been used to characterize plastic packaging. Knowledge of the activation energy of the breath of product and packaging serves as an important tool to predict the effects of temperature fluctuations on the concentration of gases inside the package (Cameron et al., 1995).

6. Plant responses of MAP

Some of the most important factors that affect shelf life of fresh horticultural products are ripening and/or senescence, decay, and cut surface browning. The effect of modified atmosphere on these factors has been studied for different crops. The application of MA to affect these limiting factors can be restricted for some crops by adverse and/or non-beneficial physiological responses. Additionally, the good temperature management should be associated to by atmosphere modification.

Low O_2 and elevated CO_2 concentrations can significantly reduce the rates of ripening and senescence primarily by reducing the synthesis and perception of ethylene (Burg and Burg, 1967; Abeles et al., 1992). Changes in respiration and starch, sugars, chlorophyll, and cell wall constituents during this period can be reduced, and in some cases nearly arrested, by eliminating ethylene action through the use of low O_2/high CO_2 atmospheres.

Chlorophyll loss, a desirable trait for many climacteric fruits, results in quality loss for many vegetables. Chlorophyll degradation during the senescence of green vegetables can be reduced by low O_2 and elevated CO_2 (Ku and Wills, 1999).

Modified atmospheres are most effective at reducing ripening prior to the onset of ripening, rather than at a later stage. At the same time, packaged fruits and vegetables are usually intended for immediate consumption by the consumer and an unripe product is not immediately edible or is of reduced quality relative to the ripe product. Thus, the advantage of extend shelf-life by retarding ripening runs counter to the needs of the consumer when retail MAP systems are used. Nevertheless, MAP can reduce the rate of ripening of some commodities such as tomato even during its later stages (Yang and Chinnan, 1988).

Decay control is a particularly important problem for many crops. Levels of above 10% CO_2 effectively slow or stop the growth of numerous decay organisms (Brown, 1922). Low O_2 has a very limited effect on decay organism activity or survival at levels above the fermentation threshold of most commodities. Strawberry, blueberry, blackberry, raspberry and cherry, they are examples that can be stored at CO_2 atmosphere between 10 and 20%.

A negative plant responses to modified atmosphere packaging is when the respiration is reduced as O_2 becomes limiting. Although there is a limit to which O_2 can be reduced. The lower O_2 limit is frequently considered to be the level of O_2 that induces fermentation. However there are lower O_2 levels that may confer benefits that outweigh the loss in flavor or other quality parameters. Ethanol, acetaldehyde, ethyl acetate and lactate are products of fermentation that can contribute to the development of off-flavors (Kays, 1997; Mattheis and Fellman, 2000).

Synthesis of aroma compounds are generally suppressed by high CO_2 and low O_2 levels, in part by their action on ethylene sensitivity, but also via action of O_2 on oxidative processes, including respiration required for substrate production. But low O_2 MAP may suppress aroma production so consumers perceive reduced quality upon opening the container.

7. Conclusions

The benefits of MAP technology to the manufacturer, retailer as well as consumer far outweigh the drawbacks. Nevertheless some critical points should be considered in this technology. The following list some advantages and disadvantages of MAP.

- Advantages
  - Increased shelf-life allowing lesser frequency of loading of retail display shelves.
- Improved presentation of the product
  - Hygienic stackable pack sealed and free from product drip and odor
  - Shelf-life can be increase by 50 to 400%.
  - Reduction in production and storage costs due to better utilization of space and equipment.
- Disadvantages
  - Capital cost of gas packaging machinery
  - Increased pack volume increases transport costs and retail display space
  - Cost of gases and packaging materials
  - Temperature control is of critical importance and, by itself, has a greater impact than atmosphere modification for most products
  - Potential growth of food borne pathogens due to non-maintenance of required storage temperature by retailers and consumers.

8. References

Abeles, F. B., Morgan, P. W., & Saltveit, M. E. *Ethylene in plant biology*. 2nd ed. San Diego: Academic Press, 1992. 414 p.

Beaudry, R.M., & Gran, C. D. (1993). Using a modified-atmosphere packaging approach to answer some postharvest questions: Factors affecting the lower oxygen limit. *Acta Hort*., Vol. 362, pp. 203-212.

Beaudry, R. M. (2000). Responses of horticultural commodities to low oxygen: limits to the expanded use of modified atmosphere packaging. *HortTechnology*, Vol. 10, pp. 491-500.

Beaudry, R. M. (1999). Effect of O_2 and CO_2 partial pressure on selected phenomena affecting fruit and vegetable quality. *Postharvest Biol. Technol.*, Vol 14, pp. 293-303.

Beaudry, R. M., Cameron, A. C., Shirazi, A, & Dostal-Lange, D. L. (1992). Modified-atmosphere packaging of blueberry fruit: Effect of temperature on package O_2 and CO_2. *Amer. Soc. Hort.* Vol. 117, pp. 436-441.

Beaudry, R. M., & Gran, C. D. (1993). Using a modified-atmosphere packaging approach to answer some postharvest questions: Factors affecting the lower oxygen limit. *Acta Hort.* Vol. 362, pp. 203-212.

Boyette, M.D., Sanders, D.C., & Rutledge, G.A. (1996). Package requirements for fresh fruits and vegetables. The North Carolina Agricultural Extension Service. North Carolina State University, Ralley, NC. USA. Publication no 9/96-3m-TWK-260373-AG-414-8.

Brecht, J. K. (1995). Physiology of lightly processed fruits and vegetables. *HortScience,* Vol. 30, No. 1, pp. 18-21.

Brown, W. (1922). On the germination and growth of fungi at various temperatures and in various concentrations of oxygen and carbon dioxide. *Ann. Bot.* Vol. 36, pp. 257-283.

Burg, S. P., & Burg, E. A. (1967). Molecular requirements for the biological activity of ethylene. *Plant Physiol,* Vol.42, pp. 114-152.

Cameron, A. C., Beaudry, R. M., Banks, N. H., & Yelanich, M. V. (1994). Modified atmosphere packaging of blueberry fruit: modeling respiration and package oxygen partial pressures as a function of temperature. *Journal of the American Society for Horticultural Science.* Vol. 119, no. 3, pp. 534-539.

Cameron, A. C., Patterson, B. D., Talasila, P. C., & Joles, D. W. (1993). Modeling the risk in modified atmosphere packaging: A case for sense-and-respond packaging. In: Proc. 6th Intl. Controlled Atmosphere Res. Conf., Ithaca, NY, pp. 95-112.

Cameron, A. C., Talasila, P. C., & Joles, D.J. (1995). Predicting the film permeability needs for modified atmosphere packaging of lightly processed fruits and vegetables. *HortScience* Vol. 30, pp. 25-34.

Cantwell, M. (2004).*Fresh-cut vegetables*. USA: University of California, Davis. p. 78-85. (Postharvest Horticulture Series n. 10.)

Chinnan, M. S. (1989). Modeling gaseous environment and physio-chemical changes in fresh fruits and vegetables in modified atmospheric storage. (In) "Quality factors of fruits and vegetables - Chemistry and Technology". J. J. Jen (ed.). ACS Symposium Series No. 405, p. 189-202. Washington, D.C.

Day, B. P. F. (1996). High oxygen modified atmosphere packaging for fresh prepared produce. *Postharvest News and Information*, Wallingford, v. 7, n. 3, p. 1N-34N.

Fidler, J. C., & North, C. J. (1967). The effect of conditions of storage on the respiration of apples. I. The effects of temperature and concentrations of carbon dioxide and oxygen on the production of carbon dioxide and uptake of oxygen. Journal of Horticultural Science, 42, 189–206.

Fishman, S., Rodov, V., & Ben-Yehoshua, S. (1996). Mathematical Model for Perforation Effect on Oxygen and Water Vapor Dynamics in Modified-Atmosphere Packages. *Journal of Food Science*, Vol. 61, No. 5, pp. 956–961.

Fonseca, S. C., Oliveira, F. A. R., & Brecht, J. K. (2002). Modelling respiration rate of fresh fruits and vegetables for modified atmosphere packages: a review. *Journal of Food Engineering*, v. 52, p. 99–119.

Fonseca, S.C., Oliveira, F.A.R., & Brecht, J.K. (2002). Modelling respiration rate of fresh fruits and vegetables for modified atmosphere packages: a review. *Journal of Food Engineering*, Vol. 52, pp. 99–119.

González, J., Ferrer, A., Oria, R., & Salvador, M. L. (2008). Determination of O_2 and CO_2 transmission rates through microperforated films for modified atmosphere packaging of fresh fruits and vegetables. *Journal of Food Engineering*, Vol. 86, No. 2, pp. 194-201.

Gorny, J. R. (1997). A summary of CA and MA requirements and recommendations for fresh-cut (minimally-processed) fruits and vegetables. In: J. Gorny (ed) Fresh-cut fruits and vegetables and MAP. Postharvest Hort. Series No. 19, Univ. Calif., Davis CA, CA'97 Proc. 5:30-66.

Gorris, L., & Tauscher, B. (1999). Quality and safety aspects of novel minimal processing technology. *Processing of foods: Quality optimization and process assessment.* CRC Press, USA, pp. 325-339.

Herner, R.C. (1987). High CO_2 effects on plant organs. In: J. Weichman (ed) Postharvest Physiology of Vegetables, Marcel Dekker, NY, pp. 239-253.

Hertog, M.L.A.T.M., Peppelenbos, H. W., Evelo, R.G., & Tijskens, L.M.M. (1998). A dynamic and generic model of gas exchange of respiring produce: the effects of oxygen, carbon dioxide and temperature. *Postharvest Biol. Technol*. Vol. 14, PP. 335-349.

Joles, D. W., Cameron, A. C., Shirazi, A., Petracek, P. D., & Beaudry, R. M. (1994). Modified atmosphere packaging oh 'Heritage' red raspberry fruit: respiratory response to reduce oxygen, enhanced carbon dioxide and temperature. *Journal of the American Society for horticultural Science.* Vol. 119, No. 3, pp. 540-545.

Kader, A.A. (2002). *Post-harvest technology of horticultural crops.* Oakland: University of California, Division of Agriculture and Natural Resources Publication 3311, 535 pp.

Kader, A.A. (1997). A summary of CA requirements and recommendations for fruits other than apples and pears. In: A. Kader (ed) Fruits other than apples and pears. Postharvest *Hort. Series* No. 17, Univ. Calif., Davis CA, CA'97 Proc. 2:1-36.

Kader, A. A., Zagory, D., & Kerbel, E. L. (1989).Modified atmosphere packaging of fruits and vegetables. *Rev. Food Science and Nutrition*, Vol. 28, No. 1, pp. 1-30.

Kays, S. J. (1997). Postharvest physiology of perishable plant products. Van Nostrand Reinhold, NY.

Ku, V. V. V., & Wills, R. B. H. (1999). Effect of 1-methylcyclopropene on the storage life of broccoli. *Postharvest Biol. Technol*, Vol. 17, pp. 127-132.

Kupferman, E. (1997). Controlled atmosphere storage of apples. In: E.J. Mitcham (ed) Apples and Pears. *Postharvest Hort. Series* No. 16, Univ. Calif., Davis CA, CA'97 Proc. 3:1-30.

Lakakul, R., Beaudry, R. M., & Hernandez, R. J. (1999). Modeling respiration of apple slices in modified-atmosphere packages. *Journal of Food Science.* Vol. 64, No. 1, pp. 105-110.

Lee, D. S., Haggar, P. E., Lee, J., & Yam, K. L. (1991). Model for fresh produce respiration in modified atmospheres based on principles of enzyme kinetics. *Journal of food Science*, Vol. 56, No. 6, pp. 1580-1585.

Mattheis, J.P., Fellman, & J.P. (2000). Impact of modified atmosphere packaging and controlled atmosphere on aroma, flavor and quality of horticultural produce. *HortTechnology,* Vol. 10, pp. 507-510.

Mir, N., & Beaudry, R. M. (1986). Modified Atmosphere Packaging. USDA Handbook 66. Washington, D.C. GPO. 7/11/2011, Available from: <http://www.ba.ars.usda.gov/hb66/015map.pdf>.

Reid, M.S. (1997). A summary of CA and MA requirements and recommendations for ornamentals and cut flowers. In: M.E. Saltveit (ed) Vegetables and ornamentals. *Postharvest Hort. Series* No. 18, Univ. Calif., Davis CA, CA'97 Proc. 4:129-136.

Richardson, D. G., & Kupferman, E. (1997). Controlled atmosphere storage of pears. In: E.J. Mitcham (ed) Apples and pears. *Postharvest Hort. Series* No. 16, Univ. Calif., Davis CA, CA'97 Proc. 2:31-35.

Saltveit, M. E. (1997). A summary of CA and MA recommendations for harvested vegetables. In: M.E. Saltveit (ed) Vegetables and ornamentals. *Postharvest Hort. Series* No. 18, Univ. Calif., Davis CA, CA'97 Proc. 4:98-117.

Sanz, C., Pérez, A.G., Olías, R., & Olías, J.M. (1999). Quality of Strawberries Packed with Perforated Polypropylene. *Journal of Food Science*, Vol. 64, No. 4, pp. 748-752.

Sharp, A. K., Irving, A.R., & Morris, S.C. (1993). Does temperature variation limit the use of MA packaging during shipment in freight containers? In: G. Blanpied, J. Bartsch and J. Hicks (eds) Proc. 6th Intl Contr. Atmos. Res. Conf., Cornell Univ., Ithaca NY, pp. 238-251.

Shirazi, A., & Cameron, A.C. (1992). Controlling relative humidity in modified-atmosphere packages of tomato fruit. *HortScience*, Vol. 27, pp. 336-339.

Smyth, A. B., Song, J., & Cameron, A. C. (1998). Modified atmosphere packaged cut iceberg lettuce: effect of temperature and O_2 partial pressure on respiration and quality. *Journal of Agricultural and Food Chemistry*, Vol. 46, pp. 4556-4562

Smyth, A. B., Talasila, P. C., & Cameron, A. C. (1999). An ethanol biosensor can detect low-oxygen injury in modified atmosphere packages of fresh-cut produce. *Postharvest Biol. Technol,* Vol. 15, pp.127-134.

Talasila, P. C., Chau, K. V., & Brecht, J. K. (1995). Modified atmosphere packaging under varying surrounding temperature. *Trans. ASAE*,Vol. 38, pp. 869–876.

Tano, K., Oulé, M. K., Doyon, G., Lencki, R. W., & Arul, J. (2007). *Postharvest Biology and Technology*, Vol. 46, pp. 212–221.

Yang, C. C., & Chinnan, M.S. (1988). Modeling the effect of O_2 and CO_2 on respiration and quality of stored tomatoes. *Trans. ASAE,* Vol. 31, pp. 920-925.

8

Use of Nonwoven Polypropylene Covers in Early Crop Potato Culture

Wanda Wadas
Siedlce University of Natural Sciences and Humanities
Poland

1. Introduction

In view of the high prices obtained for new potatoes, their production is more profitable than other ways of potato usage. Early potato production is associated with considerable risk producers have to take due to high yield variability over years and rapid price decrease as a result of increased supply. The success of potato production for an early crop is dependent to the higher extent on the weather conditions in the initial period of plants vegetation, especially temperature (Nishibe et al., 1989; Sale, 1979). Too low soil temperature retards the emergence and inhibits the initial plant growth. High income obtained from early potato production is possible under conditions assuring early tuber setting and rapid gain of tuber yield, and its marketing when the price is highest. In case of early potato production, its location in regions where vegetation begin early is of high importance. In the regions with delayed vegetation, the crop of new potatoes can be forced by applying perforated polyethylene film or nonwoven polypropylene covers directly on the planted field. The favourable microclimate under the cover faciliates the emergence and futher plant growth and development in the period with less favourable weather conditions for early potatoes (Hamouz et al., 2006; Jenkins & Gillison, 1995; Michaud et al., 1990; Wadas & Kosterna, 2007a). The earlier plant emergence resulted in a more extensive ground cover during early growth and the higher leaf area index (LAI). The growth duration and leaf area determine the amount of solar radiation intercepted by the canopy and influences on the extent of photosynthesis, evaporation, transpiration and final dry matter yield (Gordon et al., 1997; Nelson & Jenkins, 1990). In Europe the covers that were most frequently used in the early crop potato culture were those of perforated polyethylene film (Friessleben, 1984; Hamouz & Rybáček, 1988; Jenkins & Gillison, 1995; Lang, 1984). Widespread availability on the market of nonwoven polypropylene and extensive promotion of these covers have resulted in a frequently reduced perforated polyethylene film with nonwoven polypropylene in the field cultivation of earlies. Polypropylene covers were introduced into agriculture on a large scale in the 1990s. Globally, they are commonly known under the name of nonwoven fabrics (Cholakov & Nacheva, 2009). This material is light, water permeable, transparent and airy. The weight of 1 m^2 of nonwoven polypropylene fabric is about 2.5 times lower than the weight of perforated polyethylene film, therefore, the covering does not cause any hinder for plant developing.

2. Field microclimate under the polypropylene cover

The environmental factor which restricts early potato planting to the highest extent is soil temperature (Nishibe et al., 1989; Sale, 1979). Presprouting seed-potatoes can be planted when soil temperature at the depth of 5-10 cm is maintained at the level of 5-6°C for several subsequent days. Earlier planting into insufficiently heated soil is risky, since even short but excessive over-cooling of young plants strongly weakens their further growth and delays obtaining marketable yield.The unfavourable effect of low temperatures in the early period of potato growth can be reduced by applying nonwoven polypropylene cover. The study carried out in the Czech Republic, Germany and Poland showed that soil temperature at a depth of 5 cm under nonwoven polypropylene was higher by 1-2°C, and at the depth of 10 cm by 2-3°C than the temperature of uncovered soil, while the air temperature at the ground was higher by 2.0°C (Demmler 1998; Hamouz et al., 2006; Lutomirska & Szutkowska, 1999; Prośba-Białczyk & Mydlarski, 1998; Wadas & Kosterna, 2007a). Soil temperature under nonwoven polypropylene was on average 1-2°C lower than under perforated polyethylene film. The difference in temperatures in afternoon hours reached even 5°C (Figure 1). In Bulgaria, soil temperature at the depth of 5 cm under nonwoven polypropylene at 8.00 a.m. was higher by 0.4-2.4°C, and at 2 p.m. on sunny days, even by 4.6°C (Cholakov & Nacheva, 2009). Higher soil temperature, as well as isolation by means of the nonwoven polypropylene cover from a relative drop in air temperature at night creates a more favourable microclimate for plant growth. According to Bizer (1997) and Dvořák et al. (2004), nonwoven polypropylene cover creates a favourable microclimate for potato emergence and growth, even when the temperature at the ground drops to -7°C. Soil temperature at the depth of 10 cm was by then almost 3°C higher (and above 0°C) in comparison to the uncovered field.

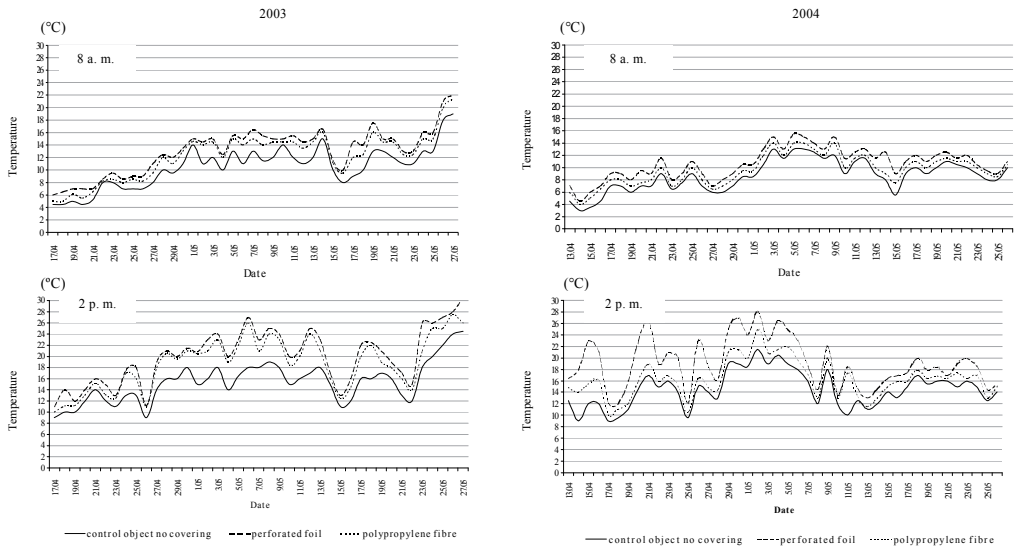

Fig. 1. Soil temperature at depth of 10 cm [°C] depending on the kind of cover at 8^{00} a.m. and 2^{00} p.m. in 2003 – 2004 (Wadas & Kosterna, 2007a)

3. Growth and development of plants

Profitable yield of new potatoes after 60 days from planting can already be obtained when the period between planting and plant emergence lasts 15-21 days, from plant emergence to the end of tuber seeting – 19-24 days, and the period of yield accumulation lasts a minimum 20 days (Kubiak & Gaziński, 1996). The period from planting to plant emergence is reduced along with an increase in soil temperature (Bizer, 1994). The application of nonwoven polypropylene cover enables earlier potato planting, forcing plant emergence and in the case of unfavourable thermal conditions, protects emerging plants against ground frosts. Presprouting seed-potatoes can be planted in the field when the soil warms up to 5-6°C. With the use of nonwoven polypropylene cover, planting can be started when soil temperature at the depth of 10 cm is about 3-4°C (Bizer, 1994; Lutomirska, 2006). Studies carried out in the Czech Republic, Poland, Bulgaria and Croatia showed that an increase in soil temperature as a result of applying nonwoven polypropylene cover in early crop potato culture shortened the period between planting to plant emergence by 2-8 days and forcing growth and development of plants in the later period (Table 1). Yearly variation of those differences are explained by environmental factors. The application of covering results in higher forcing of individual plant development phases in years with less favourable meteorological conditions during the initial period of potato growth. A higher increase of soil temperature under perforated polyethylene film, on average by 1-2°C as compared to nonwoven polypropylene, resulted in earlier occurrence of successive plant development phases by only 1-2 days (Ban et al. 2011; Cholakov & Nacheva, 2009; Hamouz et al., 2006; Lutomirska, 1995; Prośba-Białczyk & Mydlarski, 1998; Wadas & Kosterna, 2007a). Plants growing under nonwoven polypropylene were more uniform in size, higher, and developed a larger mass of aboveground parts as compared to cultivation without covering (Cholakov & Nacheva, 2009; Rekowska & Orłowski., 2000; Wadas & Kosterna 2007b; Wadas et al., 2009). Earlier plant development as a result of covering allow for the higher solar radiation interception and rapid enlargement of assimilation leaf area. A higher value of the leaf area index (LAI) has a favourable effect on the growth of tubers during the vegetation period, as well as on the final yield (Firman & Allen, 1989; Zrůst & Cepl, 1991; Zrůst et al. 1999). Forcing plant emergence as a result of applying covers results in more extensive ground cover by leaves only during early potato growth. Later, there were smaller differences as leaf senescence began under the cover sooner (Nelson & Jenkins, 1990). In the agro-meteorological conditions of east-central Poland, at the time of cover removal, the plants covered for two weeks after emergence were on average 9.4 cm higher, and after a 3-week

Country	Number of days	Reported by
Czech Republic	4-8	Hamouz et al., 2006
Poland	4-5	Lutomirska, 1995
	3-6	Prośba-Białczyk & Mydlarski, 1998; Wadas & Kosterna, 2007a
Bulgaria	2-7	Cholakov & Nacheva, 2009
Croatia	6	Ban et al., 2011

Table 1. Forcing of potato plant emergence as a result of nonwoven polypropylene covering

period of plant covering by 11.7 cm higher in comparison to plants cultivated without any covering, while the assimilation leaf area was 2 and 1.6 times higher, respectively. With the application of perforated polyethylene film, the plants were higher by 4.5 cm, on average, after 2 weeks from emergence, and by 7 cm after 3 weeks from emergence, in comparison to plants covered by nonwoven polypropylene fabric (Table 2). The type of cover applied had a smaller effect on the size of assimilation leaf area (Wadas & Kosterna 2007b; Wadas et al., 2009). The effect of covering on the assimilation leaf area depends to a high degree on meteorological conditions. In years with more favourable thermal conditions for early crop potato culture, leaving the covering (especially perforated film) for too long over plants after emergence can hinder the development of the assimilation leaf area, while in the lower temperature the effect is more favourable (Lutomirska & Szutkowska, 1999). When nonwoven polypropylene is removed too long after plant emergence, the transmision of photoactive radiation through this cover varied from 85 to 65%, depending on dust accumulation on the cover and water vapour condensation on the inner surface of the cover (Gimenez et al., 2002). A change of conditions in the initial period of plant growth as a result of applying nonwoven polypropylene cover could advance new potato harvest by up to 2-3 weeks, as compared to cultivation without plant covering (Bizer, 1994; Hamouz et al., 2005, as cited in Jaša, 1994; Sawicka & Pszczółkowski, 2002).

Specification		No covering	Nonwoven polypropylene	Perforated polyethylene film
Height of plants (cm)	2 weeks after plant emergence	17.7	27.1	31.6
	3 weeks after plant emergence	22.0	33.7	40.7
Weight of leaves per plant (g)	2 weeks after plant emergence	31	57	62
	3 weeks after plant emergence	52	77	90
Weight of stems per plant (g)	2 weeks after plant emergence	20	47	62
	3 weeks after plant emergence	33	71	109
Assimilatiom leaf area (cm^2)	2 weeks after plant emergence	918	1867	1916
	3 weeks after plant emergence	1632	2665	2896
Leaf area index	2 weeks after plant emergence	0.49	0.99	1.02
	3 weeks after plant emergence	0.87	1.42	1.48

Table 2. Effect of nonwoven polypropylene and perforated polyethylene film covering on growth of early potato cultivars (Wadas & Kosterna, 2007b; Wadas et al., 2009)

4. Tuber yield

The use of nonwoven polypropylene cover makes possible to start harvesting early, to increase the yield of new potatoes and to reduce yield variability in successive years, in comparison to cultivation without plant covering. The production effect of applying cover reflected in an increase in the tuber yield depends, to a high degree, on soil and climatic conditions and on the potato harvesting date (Table 3).

Country	Increase in tuber yield (t ha^{-1})	Reported by
Czech Republic	1.01-15.66	Hamouz et al., 2006, 2007
Poland	4.0-5.40	Prośba-Białczyk & Mydlarski, 1998
	2.87-9.97	Pszczółkowski & Sawicka, 1999
	6.36-10.04	Rekowska et al., 1999
	1.19-11.80	Wadas et al., 2001, 2008
Bulgaria	1.91-14.31	Cholakov & Nacheva, 2009
Croatia	1.85	Ban et al., 2011

Table 3. Effect of nonwoven polypropylene covering on marketable tuber yield of early potato

In conditions of east-central Poland (the Siedlce Region), covering the crop with nonwoven polypropylene resulted in an increase in marketable tuber yield after 60 days from planting very early cultivars of potato on average by 4.63 t ha^{-1} (33%), while after 75 days from planting, the average yield increase was 3.72 t ha^{-1} (13%) (Wadas et al., 2001). A similar increase in the early tuber yield of potato was obtained in the central part of Poland (Lutomirska, 1995). In later study carried out in east-central Poland, after 60 days from planting, the marketable tuber yield of early potato cultivars in cultivation with the use of nonwoven polypropylene was higher on average by 5.82 t ha^{-1} (81%) (Wadas et al., 2008). In the Lublin Region, the average tuber yield increase as a result of nonwoven polypropylene covering amounted to 7.34 t ha^{-1} (71.7%) after 60 days from planting, and 5.51 t ha^{-1} (22.5%) at harvest date two weeks later (Pszczółkowski & Sawicka, 1999). In conditions of north-western Poland (the Szczecin Region), plant covering with nonwoven polypropylene resulted in increased marketable tuber yield after 55 days from planting on average by 9.84 t ha^{-1} (52%), and after 65 days from planting - by 7.52 t ha^{-1} (27%) (Rekowska et al., 1999). On the other hand, in south-western Poland (the Wrocław Region), where thermal conditions in spring are more favourable for production of early potatoes, plant covering with nonwoven polypropylene increased marketable tuber yield after about 60 days from planting very early potato cultivars on average by 4.5 t ha^{-1} (74%), and when the harvest was carried out two weeks later, the difference in tuber yield amounted to 4.7 t ha^{-1} (30%) (Prośba-Białczyk & Mydlarski, 1998). In the central part of the Czech Republic, plant covering with nonwoven polypropylene brought about an increase of marketable tuber yield on average by 6.28 t ha^{-1} (50%) after 60 days from planting, and by 5.38 t ha^{-1} (22%) when the harvest was carried out one week later (Hamouz et al., 2006, 2007), while in Croatia, the increase in tuber yield was 1.85 t ha^{-1} (12%) (Ban et al., 2011). In Bulgaria, where the practice of growing cultures using nonwoven polypropylene covers is almost unknown, the increase in early potato yield as a result of using the cover amounted, on average, to 8.98 t ha^{-1} (32%) after 60 days from plant emergence, and 6.21 t ha^{-1} (16%) after 75 days from

plant emergence (Cholakov & Nacheva, 2009). The study carried out in Poland, Germany and in eastern Canada (Quebéc) showed a higher favourable effect of covering with nonwoven polypropylene as compared to perforated polyethylene film in early crop potato culture. The application of nonwoven polypropylene made it possible to obtain a similar or even higher marketable tuber yield after 60 days from planting (Bizer, 1994; Demmler, 1998; Lutomirska, 1995; Michaud et al., 1990; Pszczółkowski & Sawicka, 2003; Rekowska & Orłowski 2000). Only in a year with a very cold spring, when the application of perforated polyethylene film obtained, in east-central Poland, a higher marketable tuber yield of early cultivars after 60 days from planting, on average by 4.18 t ha^{-1} (32%), while in years with warmer springs and at later harvesting date, yields obtained with application of perforated polyethylene film or nonwoven polypropylene were similar (Wadas et al. 2007). According to Bizer (1994), in years with dry springs, nonwoven polypropylene proves to be better covering, particularly on light soils, since a water shortage is likely to occur under perforated film. Cover use has the greatest effect on the potato tuber yield at very early harvest date, but when harvest is delayed, the effect of covering, reflecting in an increase in the new potato tuber yield in comparison to the cultivation without covering, is reduced. The study carried out in the central part of Czech Republic showed an increase in tuber yield as a result of applying covers in the period before the end of June, while along with the delay of the harvest date, the difference in the tuber yield in cultivation with and without covering was reduced, to reach an insignificant level by the end of June (Hamouz et al., 2004, 2005). The effect of applying nonwoven polypropylene cover in early crop potato culture depends to a high degree on meteorological conditions during the period of plant vegetation (Hamouz et al., 2004, 2006; Jabłońska-Ceglarek & Wadas, 2005; Lutomirska, 1995, 2006; Wadas et al., 2001, 2008). A higher increase of tuber yield as a result of applying the cover is obtained in years with less favourable thermal conditions in the initial period of potato growth. In east-central Poland in years with very cold springs, covering the crops with nonwoven polypropylene made it possible to obtain, after 60 days from planting, up to four times higher marketable tuber yield than in cultivation without covering (Jabłońska-Ceglarek & Wadas, 2005; Wadas et al., 2008). In the Czech Republic, potato cultivation under nonwoven polypropylene in the year with an exceptionally cold spring resulted in even six times higher marketable tuber yield after 60 days from planting (Dvořák et al., 2004; Hamouz et al., 2004, 2005). The application of covers assures to a high yield of potato tubers at an early harvest date, provided that the covers are removed at the proper time (Dvořák et al., 2007; Lutomirska & Szutkowska, 1999; Reust, 1980). Leaving the cover over the plants for too long after emergence can hinder development of assimilation leaf area and reduce the number of setting tubers. In conditions of east-central Poland, the length of plant covering period (two or three weeks after emergence) did not have any significant effect on the tuber yield after 60 days from planting, while for the harvest date delayed by two weeks, the yield was higher when the covers were removed two weeks after plant emergence (Wadas et al., 2008). The date of removing perforated polyethylene film had a greater effect on tuber yield than the date of removing nonwoven polypropylene, especially in years with warmer springs. The application of nonwoven polypropylene cover in the early crop potato culture assures not only a higher tuber yield, but also contributes to improvement of its structure by increasing the productivity of marketable tuber fractions, and simultaneously increasing share of large tubers in the yield, with diameters above 50 mm (Ban et al., 2011; Prośba-Białczyk & Mydlarski, 1998; Pszczółkowski & Sawicka, 2003; Rekowska et al., 1999; Wadas et al., 2001, 2008).

5. Tuber quality

A change in conditions for the initial growth and development of potato plants by applying nonwoven polypropylene or perforated polyethylene film cover affects not only the volume of the tuber yield, but also the chemical composition of tubers. Forcing of plant growth as a result of using covers results in an increase in dry matter and starch content in tubers. While applying nonwoven polypropylene, the dry matter content in tubers was higher by 0.69-2.17%, and starch by 0.45-1.46% than in cultivation without plant covering (Dvořák et al., 2006, 2008; Hamouz et al., 2006; Jabłońska-Ceglarek & Wadas, 2005; Wadas et al., 2003, 2004, 2006). A greater beneficial effect of applying covers in the form of an increase of dry matter content in tubers is found for early harvest date and in years with high air temperatures and abundant sunshine. According to other authors, the application of nonwoven polypropylene or perforated polyethylene film covers created less favourable conditions for accumulation of dry matter in tubers of very early potato cultivars (Prośba-Białczyk & Mydlarski, 1998; Sawicka & Pszczółkowski, 2005). Changed conditions for initial growth and development of potato plants as a result of applying the covers resulted in an increase in content of total sugars, reducing sugars and saccharose in tubers (Sawicka & Pszczółkowski, 2005). The study did not show any effect of applying nonwoven polypropylene in early crop potato culture on protein accumulation in tubers. On the other hand, a tendency was observed towards an increase in the ascorbic acid (vitamin C) concentration and a decrease in the concentration of carotenoids and polyphenols (Dvořák et al., 2006, 2008; Jabłońska-Ceglarek & Wadas, 2005; Lachman et al., 2003; Wadas et al., 2003, 2004, 2006). This method of potato cultivation resulted in a lower content of ascorbic acid in tubers as compared to cultivation without plant covering (Prośba-Białczyk & Mydlarski, 1998). Plant growth forcing as a result of nonwoven polypropylene covering contributes to an improvement of the tuber quality by reducing the concentration of nitrates, aspecially for the early harvesting date. In this method of potato cultivation, the content of nitrates was lower by 29-239 mg $N0_3$ in 1 kg of fresh weight of tubers (Dvořák et al., 2006; Lachman et al., 2003; Wadas et al., 2005). Covering the plants with nonwoven polypropylene also created very favourable conditions for accumulation of phosphorus and potassium in tubers (Wadas et al., 2007, 2008). The application of covers in early crop potato culture should be also considered in the aspect of plant health. Higher soil moisture under the cover can contribute to an increased occurrence of tubers infected with *Streptomyces scabies* and *Rhizoctonia solani* and to a faster rate of *Phytophthora infestans* spreading (Pszczółkowski & Sawicka, 1998).

6. Cost effectiveness of the production

The application of nonwoven polypropylene cover in potato production requires higher inputs incurred related not only to the purchase of nonwoven polypropylene, but also to labour input for its spreading and removing, as well as for harvesting the crops (Prośba-Białczyk et al., 1997; Pszczółkowski et al., 2000/2001; Wadas, 2003; Wadas et al., 2003, 2006; Wadas & Sawicki, 2009). Increasing production inputs is effective when the value of the tuber yield increase obtained as a result of plant covering is higher than the costs incurred. German studies showed that for the cost of purchasing nonwoven polypropylene

amounting to 2000 DM per 1 ha, when the cover is used 2-2.5 times, yearly costs ranged from 800 and 1000 DM per 1 ha, while for the cost of purchasing perforated polyethylene film amounting to 1400 DM per 1 ha, and using the cover 1.5-2 times, yearly costs ranged from 700 to 1050 DM. Therefore, yearly costs of using both covers were similar (Demmler, 1998). The amount of actually incurred costs depends, first of all, on how many times the nonwoven polypropylene cover is reused. The reuse rate of nonwoven polypropylene depends on its mechanical damage, sun radiation and degree of contamination. In the Czech Republic, at the cost of purchasing nonwoven polypropylene amounting to 1000-1200 EURO per 1 ha, its two-time application proved cost-effective for farmers (Hamouz & Dvořák 2004). In Poland, the cost of purchasing nonwoven polypropylene calculated for three seasons of its use amounted to PLN 5200-6300 per 1 ha (Prośba-Białczyk et al., 1997; Wadas, 2003). In south-western Poland, the production cost of early potatoes under nonwoven polypropylene was higher, depending on the year, between 85-92% as compared to cultivation without the cover, and the cost of nonwoven polypropylene accounted for 37-41% of incurred costs (Prośba-Białczyk et al., 1997). Such method of producing early potatoes in east-central Poland required incurring costs which were higher by 47-89%, and the cost of purchasing the nonwoven polypropylene accounted for 24-40% of direct costs. Due to a higher price, the direct costs of producing early potatoes under nonwoven polypropylene were higher by 18-25% than under perforated polyethylene film (Wadas, 2003; Wadas et al., 2003, 2006; Wadas & Sawicki, 2005, 2009). While assessing the cost-effectiveness of early potato production under nonwoven polypropylene cover, it is not only the sum of incurred costs which is important, but also unit costs, which provide information about the level of selling price which will balance the costs incurred. In south-western Poland, the costs of producing 1 kg of tubers under nonwoven polypropylene were 1.3-1.5 times higher, and in a year with very favourable conditions for early crop potato culture, it was almost the same as in the cultivation without covering. In the agro-meteorological conditions of east-central Poland, covering the crop with nonwoven polypropylene increased unit costs of production by 1.2 to 2.1 times. Unit costs of production were lower than in cultivation without covering only in the year with unfavourable thermal conditions for early crop potato culture, due to high yields obtained in cultivation under nonwoven polypropylene. Unit costs of production under nonwoven polypropylene were 1.3 to 1.6 times higher compared with perforated polyethylene film. Only in one year which was very favourable for early crop potato culture were they almost the same to that of applying perforated polyethylene film. It is more efficient to increase imputs for early potato production by applying nonwoven polypropylene in less favourable thermal conditions during the initial period of potato growth. In such a case, a significant yield increase in cultivation under covers balances the costs incurred and makes it possible to obtain a higher direct surplus from production than without covering (Table 4).

The cost-effectiveness of early potatoes production under nonwoven polypropylene cover depends on the income-to-costs ratio. Applying the nonwoven polypropylene in the early crop potato culture ensures high cost-effectiveness of production in years with cold springs. In conditions favouring rapid growth of potatoes, production costs of 1 kg tubers under cover are higher, which makes production less profitable in comparison to cultivation without plant covering.

Specification	Nonwoven polypropylene			Perforated polyethylene film		
	Years with warm spring		Year with cold spring	Years with warm spring		Year with cold spring
	2002	2003	2004	2002	2003	2004
Increase in production costs (PLN ha^{-1})	4067.5	4032.2	4330.0	2229.1	2340.8	2665.3
Increase in tuber yield (t ha^{-1})	6.09	1.79	9.59	2.79	2.39	13.78
Value of additional tuber yield (PLN ha^{-1})	10953.0	3585.0	16311.5	5022.0	4780.0	23413.2
Marginal effectiveness	2.67	0.89	3.76	2.22	2.03	8.77

Table 4. Cost effectiveness of nonwoven polypropylene and perforated polyethylene film covers use in early potato production (Wadas & Sawicki, 2009)

7. Conclusions

Success in early crop potato culture depends to a high degrre on the soil and air temperature in the initial period of plant growth. Obtaining early yields from field production is possible in soil and climatic conditions which enable early planting and rapid plant growth. The unfavourable effect of low temperatures in the initial period of potato growth can be reduced by the application of nonwoven polypropylene cover directly on the planted field. With the use of covers, potato planting can be started when the soil temperature at the depth of 10 cm is about 3-4°C. The application of covers enables earlier potato planting, forcing plant emergence and the growth and development of plants in the later period, and consequently, results in earlier setting of tubers, rapid yield gain and reduction of the yield variability in any years. A change in conditions during the initial period of plant growth as a result of applying covers could advance new potato harvest by up to 2-3 weeks. Such a method of production requires higher input incurred, while the effect of applying covers, reflected in an increase in the tuber yield, to a high degree depends on soil and climatic conditions. An increase in production inputs by the application of nonwoven polypropylene cover is more effective in less favourable thermal conditions in the initial period of potato growth. A considerable tuber yield increase in cultivation under cover results in such a case in decrease of unit costs and consequently, the cost-effectiveness of production is higher than without covering. In conditions favouring rapid potato growth, the application of covers increases unit costs, which makes production less profitable as compared to cultivation without covering. The application of nonwoven polypropylene cover facilitates a significant increase in income from potato production at a very early harvest date. Along with a delay in harvesting, the effect of applying the cover, reflected in an increase in the tuber yield, decreases in comparison to cultivation without covering.

8. Acknowledgment

Krystyna Struk, Director of Agricultural Experimental Station in Zawady, is acknowledged for her valuable technical assistance during the field experiments and during harvest operations. The author would like to acknowledge the Reviewers and Editors for their valuable comments and suggestions for this paper.

9. References

Ban, D.; Vrtačić, M.; Goreta Ban, S.; Dumičić G.; Oplanić, M.; Horvat, J. & Žnidarčić. D. (2011). Effect of variety, direct covering and date of harvest on the early potato growth and yield. *Proceedings of 46th Croatian and 6th International Symposium on Agriculture*, pp. 496-500, ISBN 978-953-6135-71-3, Opatija, Croatia, February 14-18, 2011

Bizer, E. (1994). Frühkartoffelanbau unter Vlies und Folie. *Kartoffelbau*, Vol. 45, No. 2, pp. 462-466

Bizer, E. (1997). Ernteverfruhung durch Vliesabdeckung. *Kartoffelbau*, Vol. 48, No. 1/2, pp. 60-61

Cholakov, T.L. & Nacheva, E.K. (2009). Results from using polypropylene cover in production of early potatoes. *Acta Horticulturae*, Vol. 839, pp. 603-608, ISSN 0567-7572, ISBN 978-90-66050157-7

Demmler, D. (1998). Vergleich von Folie und Vlies zur Ernteverfrühung in Frühkartoffeln. *Kartoffelbau*, Vol. 49, No. 12, pp. 429-430, ISSN 0022-9156

Dvořák, P.; Hamouz, K.; Bicanova, E. & Prasilova, M. (2007). Effect of the date of polypropylene textile removal and site on yield-forming components of early potatoes. *Scentia Agriculturae Bohemica*, Vol. 38, No. 4, pp. 162-167, ISSN 1211-3174

Dvořák, P.; Hamouz. K.; Ćepl, J. & Pivec, J. (2004). The non-woven fleece as an implement for acceleration of early potatoes harvest. *Scientia Agriculturae Bohemica*, Vol. 35, No. 4, pp. 127-130, ISSN 1211-3174

Dvořák, P.; Hamouz, K.; Jůzl, M. & Erhartowa, D. (2006). Influence of row covering with non-woven textile on tubers quality in early potatoes. *Zeszyty Problemowe Postępów Nauk Rolniczych*, No. 511, pp. 225-231, ISSN 0084-5477

Dvořák, P.; Hamouz, K. & Lachman, J. (2008). Effect the polypropylene textile cover on tubers quality of early potatoes. *Proceedings of 43rd Croatian and 3ed International Symposium on Agriculture*, pp. 628-631, ISBN 978-953-6135-68-4, Opatija, Croatia, February 18-21, 2008

Firman, D. M. & Allen, E. J. (1989). Relationship between light interception, ground cover and leaf area index in potatoes. *The Journal of Agricultural Science*, Vol. 113, pp. 355-359, ISSN 0021-8596, EISSN 1469-5146

Friessleben, R. (1984). Untersuchungen zum Anbau von Speisefrühkartoffeln inter perforierter Polyäthylenfolie. *Archiv für Acker- und Pflanzenbau und Bodenkunde*, Vol. 28, pp. 133-142, ISSN 0365-0340

Gimenez, C.; Otto, R.F. & Castilla, N. (2002). Productivity of leaf and root vegetable crop under direct cover. *Scientia Horticulturae*, Vol. 94, No. 1/2, pp. 1-11, ISSN 0304-4238

Gordon, R.; Brown, D.M. & Dixon, M.A. (1997). Estimating potato leaf area index for specific cultivars. *Potato Research*, Vol. 40, pp. 251-266, ISSN 0014-3065

Hamouz, K. & Dvořák, P. (2004). Influence of white fleece on the yield formation of early potatoes. *Proceedings of 39th Croatian Symposium on Agriculture*, pp. 395-396, Croatia, February 17-20,2004

Hamouz, K.; Dvořák, P.; Ćepl, J. & Pivec, J. (2005). The effect of polypropylene fleece covering on the yield of early potatoes. *Horticultural Science (Prague)*, Vol. 32, No. 2, pp. 56-59, ISSN 0862-867X

Hamouz, K.; Dvořák, P. & Erhartova, D. (2007). Effect of polypropylene covering on the yield formation dynamics of early potatoes. *Acta Phytotechnica et Zootechnica*, Vol. 3, pp. 57-60, ISSN 1336-9245

Hamouz, K.; Dvořák, P. & Šařec, O. (2004). Efficiency of white fleece during the cultivation of early potatoes. *Zeszyty Problemowe Postępów Nauk Rolniczych*, Vol. 500, pp. 271-276, ISSN 0084-5477

Hamouz, K.; Lachman, J.; Dvořák, P. & Trnková, E. (2006). Influence of non-woven fleece on the yield formation of early potatoes. *Plant Soil and Environment*, Vol. 52, No. 7, pp. 289-294, ISSN 1214-1178

Hamouz, K. & Rybáček V. (1988). Porous foil mulching of the stands of very early potatoes. *Rostlinná Výroba*, Vol. 34, pp. 1095-1102, ISSN 0035-8371

Jabłońska-Ceglarek, R. & Wadas, W. (2005). Effect of nonwoven polypropylene covers on early tuber yield of potato crops. *Plant Soil and Environment*, Vol. 51, No. 5, pp. 226-231, ISSN 1214-1178

Jenkins, P.D. & Gillison, T.C. (1995). Effects of plastic film covers on dry-matter production and early tuber yield in potato crop. *Annals of Applied Biology*, Vol. 127, pp. 201-213, ISSN 0003-4746

Kubiak, K. & Gaziński, B. (1996). The early potato marked in Poland. *Postępy Nauk Rolniczych*, No. 5, pp. 43-51, PL ISSN 0032-5547

Lachman, J.; Hamouz, K.; Hejtmánková, A.; Dudjak, J.; Orsák, M. & Pivec, V. (2003). Effect of white fleece on the selected quality parameters of early potato (*Solanum tuberosum*, L.) tubers. *Plant Soild and Environment*, Vol. 49, No. 8, pp. 370-377, ISSN 1214-1178

Lang, H. (1984). Folieneinsatz im Frühkartoffelbau für Sicherheit, Ertrag und Qualität. *Kartoffelbau*, Vol. 35, pp. 65-69, ISSN 0022-9156

Lutomirska, B. (1995). Usage of agrotextile to forceing the yielding of potatoes. *Ziemniak Polski*, No. 3, pp. 13-19, ISSN 1425-4263

Lutomirska, B. (1995). Acceleration of the accumulation of the commercial yield in early cultivars throught the use of covers. *Proceedings of 28th Scientific Conference Potato cultivation technology and selected problems from storage,* pp. 49-54, Research Institute of Potato, Bonin, March 9-10, 1995

Lutomirska, B. (2006). Forcing of very early potatoes harvest. *Ziemniak Polski,* No. 1, pp. 12-15, ISSN 1425-4263

Lutomirska, B. & Szutkowska, M. (1999). Assimilation area and early yield under the cover application in the potato cultivation. *Proceedings of Conference Potato for consumption and for food processing – agricultural and storage factors ensuring quality,* pp. 169-171, Plant Breeding and Acclimatization Institute, Radzików, February 23-25, 1999

Michaud, M. H.; Dubé, P. A. & Bégin, S. (1990). Influence of floating row covers on microclimate for production of early potatoes (*Solanum tuberosum* L.). *American Potato Journal*, Vol. 67, pp. 565-566, ISSN 0003-0589

Nelson, D. G. & Jenkins, P. D. (1990). Effects of physiological age and floating plastic film on tuber dry-matter percentage of potatoes, cv. Record. *Potato Research*, Vol. 33, pp. 159-169, ISSN 0014-3065

Nishibe, S.; Satoh, M.; Mori, M.; Isoda, A. & Nakaseko, K. (1989). Effect of climatic conditions on intercepted radiation and some growth parameters in potato. *Japanese Journal of Crop Science*, Vol. 52, No. 2, pp. 171-179, ISSN 0011-1848

Prośba-Białczyk, U. & Mydlarski, M. (1998). Growth potato on early harvest under cover with polypropylene sheets. *Fragmenta Agronomica*, No. 1 (57), pp. 74-84, PL ISSN 0860-4088

Prośba-Białczyk, U.; Paluch, F. & Mydlarski, M. (1997). Economic effectiveness of early potato production under woven polypropylene sheets. *Bibliotheka Fragmenta Agronomica*, No. 3, pp. 181-188, ISSN 0860-4088

Pszczółkowski, P.; Harasim, A. & Sawicka, B. (2000/2001). Economic performance of the production technologies for early consumption potatoes harvested on different dates. *Roczniki Nauk Rolniczych*, Ser. G, Vol. 89, No. 1, pp. 89-99, ISSN 0080-3715

Pszczółkowski, P. & Sawicka, B. (1998). Application of shields and various techniques in cultivation of early potato varieties in a bearing of plant health. *Roczniki AR Poznań*, CCCVII, Rolnictwo, No. 52, pp. 191-196, ISSN 0137-1754

Pszczółkowski, P. & Sawicka, B. (1999). Tuber yield of very early potato cultivars cultivated under polypropylene fibre cover. *Proceedings of Science Conference Cultivation of horticultural plants at the threshold of 21st century,* pp. 31-34, AR Lublin, February 4-5, 1999

Pszczółkowski, P. & Sawicka, B. (2003). Productivity of early potato cultivars cultivated under coverage. Part. I. Yield and its structure. *Acta Scientiarum Polonorum*, *Agricultura*, Vol. 2, No. 2, pp. 61-72, ISSN 1644-0625

Rekowska, E. & Orłowski, M. (2000). Effect of cultivation methods on the quantity and quality of the yield of early potato. *Annales UMCS*, Sectio EEE, vol. VIII, Suppl.: pp. 129-135, ISSN 1233-2127

Rekowska, E.; Orłowski, M. & Słodkowski, P. (1999). Yielding of early potato as affected by covering application and the terms of harvest. *Zeszyty Problemowe Postępów Nauk Rolniczych,* Vol. 466, pp. 181-189, ISSN 0084-5477

Reust, W. (1980). Culture de pommes de terre primeur sous film en matière plastique. *Revue Suisse Agriculture.*, Vol. 12, No. 2, pp. 61-64 , ISSN 0375-1325

Sale, P.J.M. (1979). Growth of potatoes (*Solanum tuberosum* L.) to small tuber stage as related to soil temperature. *Australian Journal of Agricultural Research*, Vol. 30, No. 4, pp. 667-675, ISSN 0004-9409

Sawicka, B. & Pszczółkowski, P. (2002). Progress in under cover technology of early potato cultivars production. *Pamiętnik Puławski*, Vol. 130, No. 2, pp. 673-683, ISSN 0552-9778

Sawicka, B. & Pszczółkowski, P. (2005). Dry matter and carbohydrates content in the tubers of very early potato varieties cultivated under coverage. *Acta Scientiarum Polonorum*, *Hortorum Cultus*, Vol. 4, No. 2, pp. 111-122, ISSN 1644-0692

Wadas, W. (2003). The economic effectiveness of early potato production under agrotextile covers. *Pamiętnik Puławski*, Vol. 133, pp. 207-214, ISSN 0552-9778

Wadas, W.; Jabłońska-Ceglarek, R. & Kosterna, E. (2003). The effect of nonwoven polypropylene covering in cultivation of very early potato cultivars on the content of some nutrient components in immature tubers. *Żywność (Nauka, Technologia, Jakość)*, No. 3 (36), pp. 110-118, ISSN 1425-6959

Wadas, W.; Jabłońska-Ceglarek, R. & Kosterna E. (2004). Effect of plastic covering and nitrogen fertilization on yield and quality of early potatoes. *Folia Horticulturae*, Vol. 16, No. 2, pp. 41-48, PL ISSN 0867-1761

Wadas, W.; Jabłońska-Ceglarek, R. & Kosterna E. (2005). The nitrates content in early potato tubers depending on growing conditions. *Electronic Journal of Polish Agricultural Universities*, Horticulture, Vol. 8, Issue 1, ISSN 1505-0297, Available online: http://www.ejpau.media.pl/volume8/issue1/art-26.html

Wadas, W.; Jabłońska-Ceglarek, R.; Kosterna, E. & Łęczycka, T. (2007). The potassium content in early potato tubers depending on cultivation method. *Roczniki Akademii Rolniczej w Poznaniu, Ogrodnictwo*, Vol. 41, pp. 643-647, PL ISSN 0137-1738

Wadas, W.; Jabłońska-Ceglarek, R. & Kurowska, A. (2008). Effect of using covers in early crop potato culture on the content of phosphorus and magnesium in tubers. *Journal of Elementology*, Vol. 13, No. 2, pp. 275-280, ISSN 1664-2296

Wadas, W.; Jabłońska-Ceglarek, R. & Rosa, R. (2001). A posssibility of increasing the yield of young potato tubers by using a polypropylene fibre covers. *Electronic Journal of Polish Agricultural Universities*, Horticulture, Vol. 4, Issue 2, ISSN 1505-0297, Available online: http://www.ejpau.media.pl/series/volume4/issue2/horticulture/art-06.html

Wadas, W. & Kosterna, E. (2007a). Effect of perforated foil and polypropylene fibre covers on development of early potato cultivars. *Plant, Soil and Environment*,Vol. 53, No. 3, pp. 136-141, ISSN 1214-1178

Wadas, W. & Kosterna, E. (2007b). Effect of perforated foil and polypropylene fibre covers on assimilation leaf area of early potato cultivars. *Plant, Soil and Environment*,Vol. 53, No. 7, pp. 299-305, ISSN 1214-1178

Wadas, W.; Kosterna, E. & Kurowska, A. (2009). Effect of perforated foil and polypropylene fibre covers on growth of early potato cultivars. *Plant, Soil and Environment*,Vol. 55, No. 1, pp. 33-41, ISSN 1214-1178

Wadas, W.; Kosterna, E. & Sawicki, M. (2007). Productivity of early potato cultivar in the cultivation under perforated foil and polypropylene fibre covers. *Fragmenta Agronomica*, No. 2, pp. 364-372, PL ISSN 0860-4088

Wadas, W.; Kosterna, E. & Sawicki, M. (2008). Effect of perforated film and polypropylene nonwoven covering on the marketable value of early potato yield. *Vegetable Crops Research Bulletin*, Vol. 69, pp.51-61, PL ISSN 1506-9427

Wadas, W.; Kosterna, E. & Żebrowska, T. (2006). The effect of using covers in cultivation of early potato cultivars on the content of some nutrients in tubers. *Zeszyty Problemowe Postępów Nauk Rolniczych*, No. 511, pp. 233-243, ISSN 0084-5477

Wadas, W. & Sawicki, M. (2005). Estimation of early potato production profitability in mid-eastern Poland conditions. *Pamiętnik Puławski*, Vol. 139, pp. 289-297, ISSN 0552-9778

Wadas, W. & Sawicki, M. (2009). The economic effectiveness of early potato production depending on the kind of cover. *Polish Journal of Agronomy*, Vol. 1, pp. 56-61, ISSN 2081-2787

Wadas, W.; Sawicki, M. & Kosterna, E. (2006). Production costs of the potatoes for early harvest under perforated foil and polypropylene fibre covers. *Zeszyty Problemowe Postępów Nauk Rolniczych*, Vol. 511, pp. 417-427, ISSN 0084-5477

Zrůst, J. & Cepl, J. (1991). Dependence of early potato yield on some growth characteristics. *Rostlinná Výroba*, Vol. 37, No. 11, pp. 925-933, ISSN 0035-8371

Zrůst, J.; Hlušek, J.; Jůzl, M. & Přichystalowá, V. (1999). Relationship between some chosen growth characteristics and yield of very early potato varieties. *Rostlinná Výroba*, Vol. 45, No, 11, pp. 503-509, ISSN 0035-8371

9

Study of Adhesion and Surface Properties of Modified Polypropylene

Igor Novák[1], Anton Popelka[1], Ivan Chodák[1] and Ján Sedliačik[2]
[1]*Polymer Institute, Slovak Academy of Science,*
[2]*Technical University in Zvolen,*
Slovakia

1. Introduction

Isotactic polypropylene (iPP) is one of the most frequently applied polymers. Unfortunately, it has a disadvantage of being non-polar which makes the adhesive joints formed with other, more polar polymers, rather week (Brewis & Mathieson, 2002; Chodák & Novák, 1999; Pocius, 1997; Kinloch, 1987; Schultz & Nardin, 1994; Kolluri, 1994; Denes & Manolache, 2004). From the point of view of application of iPP it is desirable that their adhesive properties are improved (Yalizis et al.,2000; Ohare et al., 2002; Shenton et al., 2001; Kim et al., 2002; Moosheimer & Bichler, 1999). This demand can be met by a modification of iPP, while polymer can be modified either at the surface directly, e.g. by plasma of electric discharge (Denes & Manolache, 2004), or in bulk, by addition of a suitable polar low- or high-molecular compound to the polymeric matrix (Novák & Florián, 1994; Novák et al., 2004; Novák & Florián, 2001; Novák, 1996). The presented contribution aims at offering the efficient methods of surface modification of iPP, from the point of view of improving its adhesion properties. Recent achievements will be discussed to evaluate physical and chemical changes taking place as a result of modification.

The analysis of the low adhesive properties of iPP leads to the two different approaches of explanation (Brewis & Mathieson, 2002; Chodák & Novák, 1999, Kinloch, 1987). By the first explanation the low adhesion of iPP consists in a formation of thin layer of low-molecular substances on the interfacial boundary. The primary function of modification is then a removal of the thin low-molecular substance layer from the polymer surface, while the chemical modification itself is of a secondary importance. The second explanation attributes the low adhesive properties of iPP to its non-polar character and low surface energy, stressing the dependence of the adhesive properties of iPP on their super molecular structure. The chemical changes resulted in the increase of the polarity and surface energy are considering for the most important in the modification of iPP.

Low-molecular substances present in iPP (Brewis & Mathieson, 20021; Kinloch, 1987) such as antioxidants, lubricants, impurities introduced into polymer during polymerization process, the ends of polymer chains originating from the initiator, as well as impurities introduced into polymer during granulation and foil processing reduce the strength of adhesive joints due to their low cohesion. After removing the low- molecular substances by precipitation, the resulting polymer dispatched the higher adhesive properties. For iPP with

wide distribution of molecular masses polymer-homologues with lower molar mass and higher mobility penetrate to the region of interfacial boundary by diffusion, reducing thus the interfacial tension. As a result of the thermal and Brown's motions, the interfacial boundary is enriched by oligomers and the value of the surface energy is reduced. In the region of iPP surface after cross linking in inert atmosphere by UV irradiation short polymer chains became cross linked removing thus the thin adhesion reducing layer of low-molecular substances on the interfacial boundary and as a result of this modification an increase of adhesive properties was observed.

IPP as a non-polar polymer has a very low (near zero) value of the polar component (PC) of the surface energy (Brewis & Mathieson, 2002; Chodák & Novák, 1999). When the polarity of iPP is increased also the value of the surface energy and its PC are increased as well. The growth of iPP polarity can be reached by utilization of some of existing methods of modification (Kinloch 1987), e.g. by flame modification. In the course of modification of iPP suitable polar functional groups are introduced. This process results into an increase of the compatibility of iPP with the polar polymers and the growth of its adhesion. Increasing the polarity of iPP can also be obtained by the addition of polar low-molecular substances or polymer to the matrix of iPP. In the case of this modification the increase of adhesion is to a large extent caused by an increasing mobility of polymer chains, e.g. by addition of fatty acids and their salts or oxidized and/or maleic anhydride grafted paraffin wax to iPP. From the point of view of the diffusion theory of adhesion (Schultz & Nardin, 1994) it is the kinetic effect taking part in this increase.

The iPP has in comparison with low-density polyethylene a higher degree of crystallinity (Brewis & Mathieson, 2002; Kinloch, 1987). During crystallization of iPP a smectic or a crystalline monoclinic form is formed depending on the thermal history of the sample. The smectic form is relatively stable up to temperature 50 ^{o}C; at higher temperature it is transformed into the monoclinic crystalline form. It was experimentally proved that the adhesive properties of monoclinic crystalline form are higher than those of smectic form, while the value of the surface energy of iPP grows with the degree of changes from smectic form to monoclinic crystalline form.

The presence of low-molecular substances in iPP results in a formation of thin layer on the interfacial boundary decreasing the value of the surface energy. This effect prevails over the effect of increasing surface energy during the change of smectic form to crystalline monoclinic form and thus the adhesion of iPP is decreased after conditioning of adhesive joints at the temperature of 50 - 90 ^{o}C. The increased adhesion of iPP can be reached by heating the polymer above the temperature of 170 ^{o}C (or above the melting point of iPP) and subsequent fast cooling. Utilization of this procedure inhibits formation of the thin interfacial layer of low-molecular substances and iPP crystallized in the smectic form.

During the surface modification of iPP the structure of its surface changes and becomes rough. The changes of the surface structure during the modification of iPP depend on the applied modification method and on the thermal history of the polymer sample. It was found that there is a linear relationship between the roughness of the polymeric surface and the value of the mechanical work of adhesion. An increase of the mechanical properties of iPP is in this case related to mechanical fixation of adhesive in pores, or to micro defects of the polymeric surface. The change of the physical character of the surface takes place also in modification of iPP in mass by addition of suitable additives increasing iPP adhesion accompanied by simultaneous changes of super molecular structure of polymer.

IPP relatively easily undergoes the oxidation (Chodák & Novák, 1999). This is observed under the effect of light, heat, UV irradiation, plasma of electric discharge and oxidation agents while functional groups are formed which are capable of participating in the further chemical reactions (Brewis & Mathieson, 2002; Kinloch, 1987; Kolluri, 1994). In the course of oxidation of iPP hydroperoxide, carbonyl, carboxyl and hydroxyl groups are formed. In previous studies a formation of ozonides and peroxides during oxidation has been observed. In the case of halogenization methods of iPP modification halogens are attached to the polymer chain, and are often combined with the oxygen.

2. Experimental

2.1 Used polymers

For corona discharge modification experiments these sorts of iPP have been used:

- biaxially oriented foils of iPP Mosten 59 4928 (Chemopetrol, Czech Republic): thickness = 0.02 mm, density (23 ^{o}C) = 0. 956 g.cm^{-3}, T_{melt} = 170 ^{o}C, ΔH_{melt} = 94.4 J.g^{-1}. Extruded iPP of 0.02 mm thickness (Chemopetrol, Czech Republic): density (23 ^{o}C) = 0.905 g.cm^{-3}, T_{melt} = 165 ^{o}C, ΔH_{melt} = 49.4 J.g^{-1}. iPP backing fabric produced from Mosten 58 512 (Chemopetrol, Czech Republic) containing 0,2 wt.% of 2,6 - di (tertbutyl) -1,4 - dimethyl phenol: density (23 ^{o}C) = 0.920 g.cm^{-3}, T_{melt} = 162 ^{o}C, ΔH_{melt} = 89.7 J.g^{-1}. Aqueous dispersion of butyl acrylate-vinyl acetate copolymer Duvilax KA-31 (Duslo, Slovakia) containing 53.1 wt.% of dry content, pH = 4 - 6, content of free monomer 0.9 wt.%, viscosity 10 - 70 mPa.s^{-1}, was used as a polymer deposit on iPP backing fabric.

For grafting experiments were used these polymers as following:

- stabilised iPP Mosten 58 512 (Chemopetrol, Czech Republic) containing 0,2 wt.% of 2,6-ditertbutyl-1,4-dimethylphenol: density (23 ^{o}C) = 0.920 g.cm^{-3}, T_{melt} = 162 ^{o}C, ΔH_{melt} = 89.7 J.g^{-1}, polyamide Silamid 30 SW13 (PCHZ, Slovakia), polyvinyl acetate (Polysciences, USA) and cellulose acetate (Czech Republic), aluminum (Slovakia).

For modification by chromyl chloride and chromo sulfuric acid a stabilized polymer iPP Tatren TF- 411, M_v = 2.16.10^5 (Slovnaft-Mol, Slovakia) was used.

The halogenization experiments were performed using a commercial iPP:

- iPP Tatren FD 420 containing 0.2 wt.% of UV stabilizer (Slovnaft-Mol, Slovak Republic), MFI = 3.2 g/10min, density (23 ^{o}C) = 0.905 g.cm^{-3}, polyvinyl acetate, M_w = 1.6 x 10^5 g.mol^{-1} (Polysciences, USA).

2.2 Measurements methods

2.2.1 Contact angles and surface energy

The values of contact angles were determined by direct goniometric measurement using a Contact Angle Meter Amplival Pol (Zeiss, Germany). The drops of testing liquid (V = 3 μl) were introduced onto the polymeric surface. Each measurement was carried out with a set of the testing liquids: glycerol, formamide (Serva, Germany), thio diglycol, ethylene glycol, α-bromo naphthalene (Aldrich, USA), methylene iodide (Fluka, Switzerland), benzyl alcohol, diethylester of anthranil acid (Merck, Germany), twice distilled water. Each

measurement was repeated 5 times at 25 °C and the dependencies θ = f (t) were extrapolated to t = 0. The dispersive and PC of the surface energy of polymer were calculated according to the relation (47-50):

$$\frac{(1+\cos\theta)\cdot(\gamma_{LV}^{d}+\gamma_{LV}^{p})}{2}=(\gamma_{LV}^{d}\cdot\gamma_{s}^{d})^{1/2}+(\gamma_{LV}^{p}\cdot\gamma_{s}^{p})^{1/2} \quad (1)$$

where θ is the contact angle (deg), γ_{LV}^{d}, γ_{LV}^{p} is the polar and dispersive component of the surface energy of testing liquid (mJ.m^{-2}), while

$$\gamma_{s}^{total}=\gamma_{s}^{p}+\gamma_{s}^{d} \quad (2)$$

where γ_{s}^{total} is the total surface energy and γ_{s}^{p}, γ_{s}^{d} is the polar and dispersive component of the surface energy of polymer (mJ.m^{-2}).

2.2.2 Interfacial equilibrium work of adhesion and interfacial tension

Interfacial equilibrium work of adhesion was calculated using the values of polar and dispersive components of the surface energy according to the relation:

$$W_{a1,2}=\frac{4\cdot(\gamma_{1}^{d}+\gamma_{2}^{d})}{\gamma_{1}^{d}+\gamma_{2}^{d}}+\frac{4\cdot(\gamma_{1}^{p}+\gamma_{2}^{p})}{\gamma_{1}^{p}+\gamma_{2}^{p}}=W_{a1,2}^{d}+W_{a1,2}^{p} \quad (3)$$

$$\gamma_{1,2}=\gamma_{1}+\gamma_{2}-W_{a1,2} \quad (4)$$

where $W_{a1,2}^{d}$ and $W_{a1,2}^{p}$ are the dispersive and polar component (PC) of interfacial equilibrium work of adhesion, (mJ.m^{-2}), γ_{1}^{d}, γ_{2}^{d} are the dispersive components of the surface energy of the polymer 1 and 2 respectively (mJ.m^{-2}), γ_{1}^{p}, γ_{2}^{p} are the PC of the surface energy of the polymer 1 and 2 respectively (mJ.m^{-2}), $\gamma_{1,2}$ is the interfacial tension between polymer 1 and polymer 2 (mJ.m^{-2}).

2.2.3 Mechanical work of adhesion by peeling

The mechanical work of adhesion was measured by peeling of adhesive joints using an 5 kN universal testing machine Instron 4301 with a peeling wheel with adjustable angle of peeling 90° at speed 10 mm.min^{-1}. The adhesive joints have been prepared by the application of polyvinyl acetate from ethyl acetate solution onto the technical cotton fabric "Molino" using a coating pad Dioptra (Czech Republic). The iPP foil and impregnated cotton fabric have been fixed together and the adhesive joints have been dried at 60 °C to a constant weight, then they were cut to strips with dimensions 25 x 200 mm. The peeling length of an adhesive joint was 100 mm. The values of mechanical work of adhesion A_m (J.m^{-2}) were calculated by equation:

$$A_m=F_s/b \quad (5)$$

where F_s is the medium peeling force (N) and b is the width of the adhesive joint (m).

Measurements were carried out using a software developed for universal testing device Instron, Series IX.

2.2.4 Strength of adhesive joint by shear

The strength of adhesive joint was determined by testing of single overlapped adhesive joints in shear using a dynamometer Instron 4301 with aluminum slabs having dimensions 10 x 60 mm, the thickness was 2 mm, the length of overlapping area was 15 mm and the thickness of deposited adhesive was 0.1 mm.

2.2.5 Molecular weight

The molecular weight of iPP was determined on a high-temperature viscometer heated with silicone oil. The viscosity of iPP was measured in α-chloro naphthalene at 145 °C. The molecular weight was calculated from the following equation:

$$[\eta]=4.9\cdot10^{-3}\cdot M_v^{0.80} \tag{6}$$

where $[\eta]$ is limiting viscosity number ($dl.g^{-1}$) and M_v is molecular weight of polymer obtained viscometrically.

2.2.6 ESR analysis

IPP modified by chromyl chloride was subjected to electromagnetic spin resonance measurements using a spectrophotometer E4. The following parameters were applied: frequency 100 kHz, microwave power 200 mW, resolution 100 mG, sensitivity 5 x 10^{10} $spin.G^{-1}$. The relative concentration of Cr^{IV} was calculated according to the equation:

$$C_{rel}=\frac{I\cdot\Delta H^2}{m\cdot s} \tag{7}$$

where I, H, m and s are intensity of spectrum, width of band, amount of weighed sample and sensitivity of device respectively.

2.2.7 Hydroperoxides determination

Hydroperoxides content was determined spectrophotochemically. A sample of modified iPP was kept for 12 hours in vacuum for removing the physically adsorbed oxygen. Acetic acid and n-heptane were distilled and nitrogen was allowed to bubble through solutions. Then 3 ml of saturated solution of potassium iodide in isopropyl alcohol, 1 ml of glacial acetic acid and 1 ml of n-heptane were placed into a 10 ml Erlemayer flask.

The samples of foils of the modified iPP (2 x 2 cm) were put into the solution and left for 24 hours in inert atmosphere of carbon dioxide (dry ice). The absorbance at λ = 365 nm was measured with respect to blank experiment by using a UV spectrometer. The concentration of hydroperoxides was calculated from the expression:

$$A=\varepsilon\cdot c\cdot dA \tag{8}$$

where A, ε, c and d are the absorbance, molar extinction coefficient (ε = 25 x 10^3 $kg.mol^{-1}.cm^{-1}$), concentration of hydroperoxides (mol $O_2.kg^{-1}$ polymer) and thickness of absorption cell (cm) respectively.

2.2.8 Carbonyl groups determination

The method of determination of carbonyl groups in oxidized iPP was based on UV spectrophotometric determination of 2,4-dinitrophenylhydrazones by means of the absorption band at λ = 365 nm. Hydrazones originated in the reaction of oxidized iPP with 2,4-dinitrophenylhydrazine.

The reagent solution included 1 g of 2,4-dinitrophenylhydrazine, 100 ml of ethanol, 5 ml of hydrochloric acid and 5 ml of distilled water. Before each measurement a fresh solution of 2,4-dinitrophenylhydrazine was prepared. The formation of hydrazones proceeded at 70 °C in the course of 20 minutes. Then iPP was repeatedly washed with hot ethanol and perfectly dried. The disappearance of the infrared absorption bands corresponding to carbonyl groups supports the assumption that these groups were quantitatively consumed in the reaction with 2,4-dinitrophenylhydrazine.

The reaction with 2,4-dinitrophenylhydrazine finished the modified iPP was used for molding the foils that were liable to UV spectrophotometric measurements. Di (heptadecyl) ketone was used as model substance. It was added in the amount of 1wt.% to iPP, exposed to the reaction with 2,4-dinitrophenylhydrazine and thus a sample of standard was formed. According to the Beer´s law it is valid:

$$\varepsilon = \frac{A_1}{c_1 \cdot d} \tag{9}$$

where ε, A_1, c_1 are stand for extinction coefficient, absorbance, the known concentration of carbonyl groups in sample of standard and width of foil, respectively.
The value of extinction coefficient calculated from equation (9) was used for calculation of the concentrations of carbonyl groups:

$$c_x = \frac{A_x}{\varepsilon \cdot d} \tag{10}$$

where A_x, c_x and d are absorbance of the investigated sample, the determined concentration of carbonyl groups and the width of the foil, respectively.

2.3 Modification methods

2.3.1 Modification by corona discharge

The modification of polypropylene foils by corona discharge was performed in a pilot plant (Softal 2005, Germany) in the medium of air oxygen at atmospheric pressure and temperature of 295 K. The used cylindrical electrodes were of 98 mm. The electrode voltage was equal to 9000 V and current density varied in the range among 0.3 and 0.8 mA.

2.3.2 Grafting by itaconic acid (IA)

Grafting of onto iPP was performed in an extruder in the polymeric melt at 220 °C during 180 sec. Itaconic acid (IA) concentration was up to 5 wt.%. Benzoyl peroxide (Aldrich, England) was added as an initiator and its concentration varied between 0.1 and 1 wt.%. Unreacted IA was then removed by Soxhlet extraction in boiling n-heptane. Pellets of IA

modified iPP have been obtained. The pellets were compression molded at 210 °C to films 0.05 mm thick suitable for goniometric measurements of contact angles.

2.3.3 Oxidation by chromyl chloride and chromo sulfuric acid

The modifications of iPP by chromyl chloride was accomplished in chromyl chloride vapor. The samples of iPP were individually prepared in Petri dishes and processed at individual temperatures by using particular reaction times. The reactions of oxidized iPP with 2,4-dinitrophenylhydrazine took place in a solution containing 1 gram of 2,4-dinitrophenylhydrazine as well as hydrochloric acid, ethanol and water in volume ratio 5 : 100 : 5.

Powdered iPP was modified by chromo sulfuric acid comprising sulfuric acid 96 %, potassium dichromate and water in weight ratio 100 : 5 : 8. Different reaction times and different temperatures were used for this method of modification.

2.3.4 Halogenization by UV/ phosphoryl chloride

The LDPE foils were placed in the glass vessel in the atmosphere of saturated vapors of phosphoryl chloride. The sorption of the UV sensitizer onto the surface of the PO foils took 24 hours. The foils were then irradiated by UV radiation in an open quartz tube having a diameter of 50 mm. The UV light with a wavelength λ = 366 nm was emitted by a 400 W mercury discharge lamp. The distance (d) of the UV tube from the surface of polymer varied between 50 and 200 mm. The relative intensity of UV radiation is inversely proportional to the square ratio of the UV source distances according to the relation:

$$I_r = \frac{I}{I_0} = (d_0/d)^2 \tag{11}$$

where I_r is the relative intensity of UV radiation, I_0 (W.s/m^2) is the intensity of UV radiation at the reference distance d_0 = 50 mm and I (W.s/m^2) is the intensity of UV radiation at the distance d (mm).

3. Results and discussion

3.1 Modification by corona discharge

During the modification of iPP by electric discharge plasma the surface of polymer interacts with the particles of plasma (Yalizis et al., 2000; OHare et al., 2002; Shenton et al., 2001; Kim et al., 2002; Novák et al., 2004; Noeske et al., 2004; Guimond et al., 2002; Mikula et al., 2003; Strobel et al., 2003; Poncin-Epaillard, 2002; Štefečka et al., 2003; Ráhel et al., 2003; Lehocký et al., 2003; Drnovská et al., 2003; Kuzuya et al., 2003). The active particles of plasma can originate either from the electric discharge at the atmospheric pressure (corona discharge) in air or from high (radio) frequency (RF) discharge at lower pressure in an inert atmosphere, or other atmosphere. The active particles of discharge plasma transferring the energy during the modification are ionic and neutral particles, electrons and UV radiation. Energy captured from the particles by the surface initiates chemical reactions leading to changed polarity and adhesion properties of iPP. The effect of plasma on the polymer surface includes the act of photons of UV irradiation having important role during the formation of

radicals. Electrons and ions do not participate in the surface modification directly but are crucial for the formation of excited atoms and molecules in the volume of the discharge and these particles in contacts with the surface induce a formation of free radicals and chemical reactions. In the interaction of polymer surface with discharge plasma of inert gas, O, N, or the air the following reactions are effective (Kinloch, 1987; Kolluri, 1994):

a) direct reactions of active particles of plasma (surface oxidation by oxygen atoms in oxygen plasma or in the air), b) creating of free radicals and their consequent reactions (polymer degradation, grafting copolymerisation, incorporation of oxygen). The oxidation effect of corona discharge on the surface of the polymer can be schematically represented by following equations:

$$RH + 2O^{\bullet} \rightarrow R^{\bullet} + H^{\bullet} + O_2 \tag{12}$$

$$RH \xrightarrow[UV]{hv} R^{\bullet} + H^{\bullet} \tag{13}$$

Equation (12) represents a dissociation enabled by the absorption of dissociation energy of oxygen and equation (13) of dissociation by absorption of UV energy.

During the modification of iPP by the discharge plasma following reactions take place:

$$R^{\bullet} + O_2 \rightarrow ROO^{\bullet} \tag{14}$$

$$ROO^{\bullet} + RH \rightarrow ROOH + R^{\bullet} \tag{15}$$

$$ROOH \rightarrow RO^{\bullet} + OH^{\bullet} \tag{16}$$

Equations (14) and (15) represent the formation of hydroperoxides during the modification, equation (16) on the other hand represents the decomposition of hydroperoxides and the formation of carbonyl groups. For the modification of iPP the modification by corona discharge at atmospheric pressure as well as a high-frequency discharge with frequency 13.56 MHz at low pressures (RF discharge) is used most often. The following scheme to represent the effect of corona discharge on iPP has been proposed:

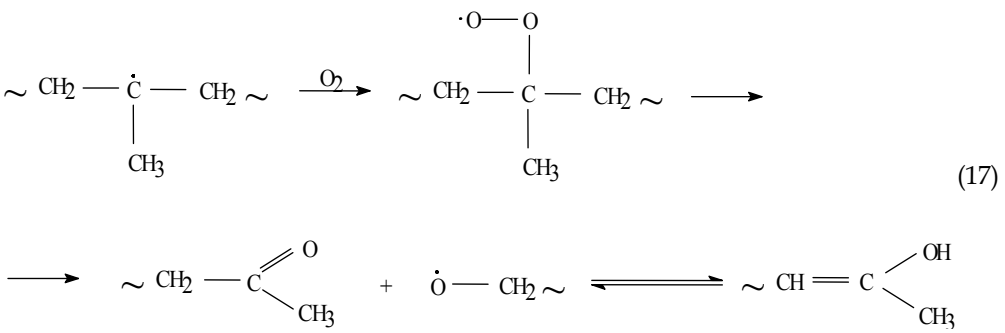

(17)

whereupon between enolic hydrogen of enolyzed ketogroup and other ketogroup in the macromolecule hydrogen bonds are formed.

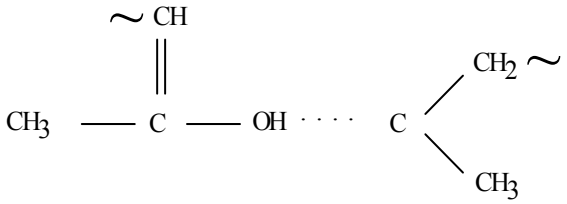

(18)

In the case of humid environment during the corona treatment of iPP the reaction of radical with oxygen is competing with a reaction of radical with water according to the scheme:

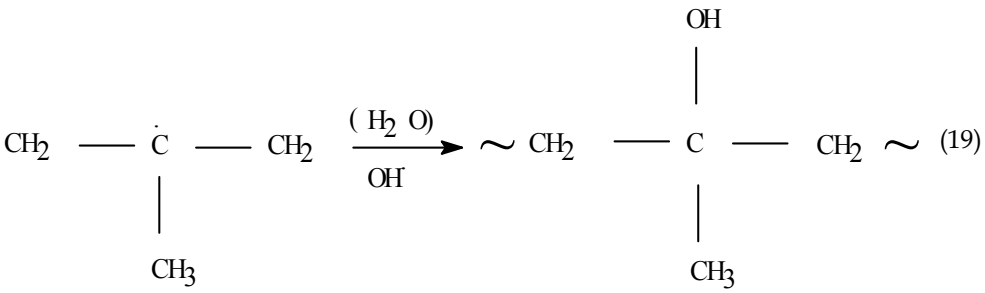

(19)

at which compounds are formed which do not contribute to the adhesive joint. A stronger decay was observed for the iPP polymerized in the discharge plasma than for that prepared by a conventional method.

The adhesion properties of iPP modified by high-frequency electric discharge in the air, oxygen and in nitrogen have been studied (Strobel et al., 2003). It was observed that after 30 seconds of exposure of the polymer in oxygen plasma the concentration of hydroperoxides reached 1.6 x 10^{-5} mol O_2/kg^{-1} iPP and the contact angle of redistilled water decreased from 94° to 40°. By further treatment by plasma the changes in contact angles periodically oscillated around the value 52°, while by the aging of treated samples the contact angle was increasing.

An important group of electric discharge methods is the modification by corona discharge (Yalizis et al., 2000). The treatment of iPP by corona discharge is strongly affected by humidity. By identification of chemical changes in iPP modified in dry air via ATR spectroscopy the presence of following functional groups was shown: C=O, OH, C=C, and COOH, and observed >C=O group to reach the highest concentration. The PC of the surface energy of iPP modified by corona discharge increased non-linearly with the degree of modification while the dispersion component is practically not changed. A decrease of temperature during the modification leads to a decrease of PC of the surface energy.

The adhesive properties of iPP modified by corona discharge are decreasing if a polymer surface makes contact with a compound forming the hydrogen bonds (most often a liquid). The formation of adhesive forces on the modified surface of iPP is related to the hydrogen bond of enolic group on one polymer surface and a similar polar group (e.g. carbonyl) on the other polymer surface and by heating up the surface or by the effect of heat formed by friction one can cancel the effect of modification and original good adhesive properties decrease.

The correlation between the adhesion of corona discharge modified iPP and the formation of hydroperoxides has also been studied (Novák & Florián, 2001; Novák & Florián, 2004). A linear increase of concentration of hydroperoxides and the PC of the surface energy with the current density of corona discharge has been found. At the same time it was shown that the efficiency of the surface treatment was strongly influenced by the super molecular structure of iPP: for extruded iPP foil a higher adhesion was found than for a biaxially oriented one. Furthermore by the study of a time elapsed from the modification they found that the adhesion of extruded polymer decreases with the time while the adhesion of biaxially oriented iPP does not vary with the time. The detail analysis of chemical changes of iPP modified by corona discharge is given also by other authors whose point to the fact that the reactive groups formed at the surface modification can participate in the further reactions.

A significant increase of adhesion of iPP was obtained by grafting a suitable monomer such as acryl amide (Novák & Florián, 1995) on the surface of iPP modified by discharge plasma. A very effective is the grafting mechanism with free radicals of the polymer in the case when the free radicals are formed relatively slowly. For the surface energy of biaxially oriented iPP modified by corona discharge and grafted by acryl amide a linear dependence on the current density was found (Lei et al., 2000). At the same time, after the grafting a decrease of concentration of hydroperoxides exhibited the result of linking of acryl amide on the active centers of modified iPP. In the case of modification of PO a time factor negatively affects the adhesion properties. The efficiency of modification decreases with the time elapsed from modification. For the given reasons a condition for the formation of strong adhesive bonds is an immediate processing of iPP after the modification.

3.1.1 Modification of iPP by corona discharge

One of the most effective methods of modification of iPP is its surface modification using electric discharge plasma at the atmospheric pressure (corona discharge) (Sun et al., 1999; Strobel et al., 2003). This method of modification allows preservation of the original mechanical properties of the iPP provided the optimum parameters of electric discharge have been set while the surface energy and polarity increase. In our experiments (Novák & Chodák, 1998), summarized in Figs. 1 – 8, the surface properties of iPP modified by corona discharge at varying parameters, e.g. current density, exposition time, aging, have been studied and the influence of polymer crystallinity on the surface properties has been investigated, too.

The dependence of the surface energy of the iPP modified by corona discharge on current density is represented in Fig. 1. After an initial induction period (up to 0.4 mA) a more rapid increase in surface energy was observed. As seen in Fig. 1, the increase in surface energy is by 3 - 5 $mJ.m^{-2}$ higher for the extruded iPP compared to the biaxially oriented polymer. According to Fig. 1, an increase of the surface energy was observed for biaxially oriented iPP (curve b) from 30 to 39 $mJ.m^{-2}$, while for extruded iPP (curve a) surface energy value was found to be 49 $mJ.m^{-2}$. At higher current densities ($I > 0.6$ mA) the difference between the surface energy values of modified extruded and biaxially oriented iPP was enhanced from 3 to 10 $mJ.m^{-2}$. Retardation was observed for biaxially oriented iPP above the current density of 0.6 mA. On the other hand, no retardation occurred for the extruded iPP with lower crystallinity. The observed phenomena can be explained by some kind of saturation of the surface of biaxially oriented iPP by degradation products formed during modification.

The difference in the values of the surface energy between two corona discharge modified iPP results from the different degree of crystallinity. A higher degree of crystallinity of biaxially oriented iPP prevents surface oxidation. The oxidation takes place in amorphous phase and at defect spots, which are expected to be more frequent on the surface of extruded foil when compared with the surface of the biaxially oriented iPP foil.

The dependence of the total surface energy of biaxially oriented iPP as well as its dispersive component on current density is shown in Fig. 2. The surface energy of non-modified biaxially oriented iPP is very low and consists mainly of the dispersive component. These results reflect poor adhesive properties of non-modified iPP. A substantial rise of the surface energy was observed after an initial induction period (Fig. 2, curves a, b). A more intensive retardation was observed for dispersive component of the surface energy (plot b) at the current density above 0.6 mA. On the other hand, lower retardation occurred for the total surface energy (plot a). The explanation of observed dependences in Fig. 2 is similar to that for dependences in previous Fig. 1, i.e. the saturation of polymer surface by degradation products formed during the modification. The values of dispersive part of the surface energy are stabilized.

The dependence of PC of the surface energy on the current density is shown in Fig. 3 for biaxially oriented iPP modified by corona discharge. The PC of the surface energy for unmodified biaxially oriented iPP is low (0.4 $mJ.m^{-2}$). Modification by corona discharge results in a significant increase of the PC of the surface energy. The increase in current density leads to a linear rise of the PC of the surface energy. The value 5 $mJ.m^{-2}$ was reached at I = 0.8 A representing 12.8 % of the value of the surface energy.

The dependence of the surface energy of iPP modified by corona discharge on exposure time defined by a speed of the foil drive is represented in Fig. 4. The increase in surface energy of both iPP is much less pronounced at higher speed of foil drive, which is inversely proportional to the exposure time of corona discharge modification. According to the Fig. 4, extruded iPP is more sensitive to the changes of speed of foil drive than biaxially oriented foil since the increase in the speed of foil drive from 4.8 to 90 $m.min^{-1}$ leads to a decrease of the surface energy for extruded iPP from 49 to 25 $mJ.m^{-2}$ while for biaxially oriented iPP the values change from 39 to 32.5 $mJ.m^{-2}$.

The concentration of hydroperoxides in the biaxially oriented iPP modified by corona discharge increased linearly with current density (Fig. 5). If the current density rises by 0.5 mA, the concentration of hydroperoxides increased by a factor 2.9. A determination of hydroperoxides groups amount as a function of corona discharge current density allows estimating the iPP hydrophilicity according to the concentration of polar groups. The dependence in Fig. 5 is in agreement with the dependence of PC of the surface energy shown in Fig. 3. From the comparison of these two dependences a linear dependence of PC of the surface energy with hydroperoxide concentration can be expected.

If the time of exposure to corona discharge of the sample of biaxially oriented iPP is shortened, the concentration of hydroperoxides decreases (Fig. 6). The effect of the increase in the speed of the foil movement at continuous modification of PP by a corona treatment is similar to the decrease of current density. The dependences in Fig. 6 are nonlinear and demonstrate the reciprocal relation between the effect of speed of foil movement, i.e. the time of corona treatment, and current density. According to Fig. 6 the hydroperoxide concentration was the same if the speed was 90 $m.min^{-1}$ and I = 0.8 mA or if the foil moved

4.8 m.min^{-1} at I = 0.3 mA. If the speed of foil drive rises from 40 m.min^{-1} up to 80 m.min^{-1}, the concentration of hydroperoxide is only about 6 % of the value for lower speed.

The most serious problem preventing wide application of corona discharge modification of polymers is the durability of the effect, i.e. a rapid decrease of wettability during hydrophobic recovery. One explanation of the deterioration in surface properties of modified iPP has been considered to be migration of the created polar moieties into the polymer bulk. Another explanation is based on a decomposition of polar groups formed during aging. Because of hydrophobic recovery the surface energy of extruded iPP rapidly decreases during the first 24 hours (Fig. 7, plot a), then the decrease slows down and after 240 hours it levels off. Different behaviour was observed for the biaxially oriented iPP (Fig. 7, plot b). The surface energy in this case did not change significantly during storing. The value of the surface energy of biaxially oriented iPP is almost identical with the corresponding value for the foil of extruded iPP stored for a long time.

The modified layer on iPP surface consisting from macromolecules with many oxidizing groups contributes to the self-adhesive properties of iPP. The weak cohesion of this, only several micrometers thick layer, causes the adhesive joints to be less mechanically resistant. The stability of hydroperoxides at the surface was investigated by measuring the strength of auto adhesive joints (Fig. 8). At the contact of two surfaces of modified iPP foils new bonding may arise between these surfaces because of hydroperoxide decomposition. The data in Fig. 8 indicate that the work of auto adhesion increases with temperature of the formation of auto adhesive joints. This fact corresponds well with the decrease of the concentration of hydroperoxides determined after destruction of auto-adhesive joints. The concentration of hydroperoxides is almost zero at 423 K.

The practical aspect of the iPP surface modification by the corona discharge can be demonstrated on the adhesive properties of modified and unmodified iPP carpet fabrics treated by rubbing pastes based on butyl acrylate-vinyl acetate copolymer. The results are summarized in Table 1. According to Table 1 the value of mechanical work of adhesion towards PP is rising with the increase of the rubbing paste mass.

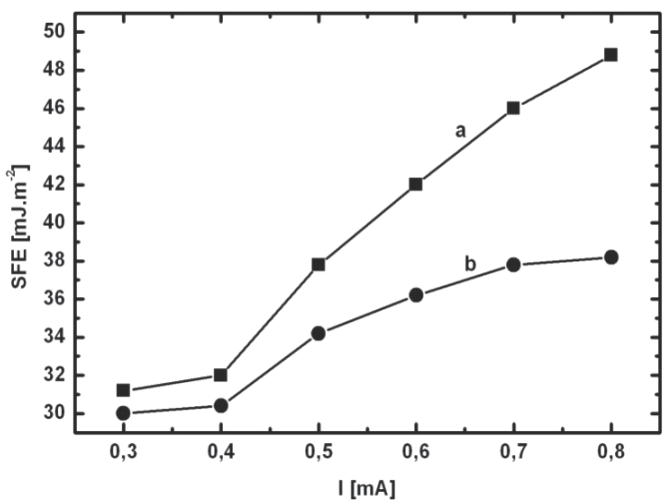

Fig. 1. Surface energy of iPP modified by corona discharge (v = 4.8 m.min^{-1}) as a function of current density: a - extruded iPP, b - biaxially oriented iPP

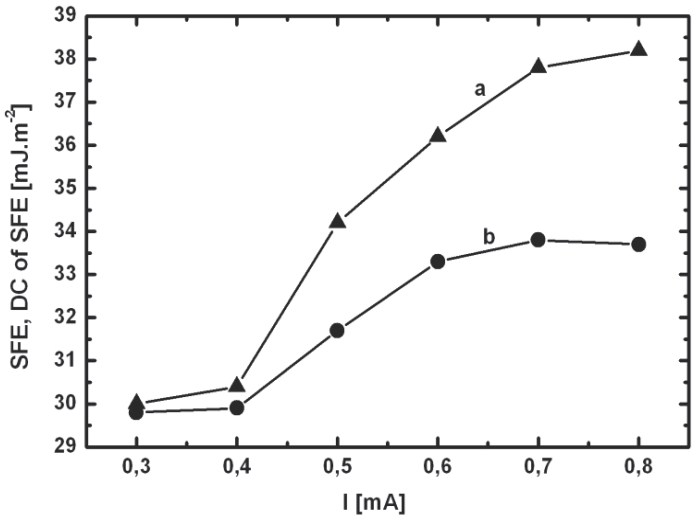

Fig. 2. Surface energy and its dispersive component as a function of current density for the biaxially oriented iPP modified (v = 4.8 m.min $^{-1}$) by corona discharge: a - surface energy, b - dispersive component of the surface energy

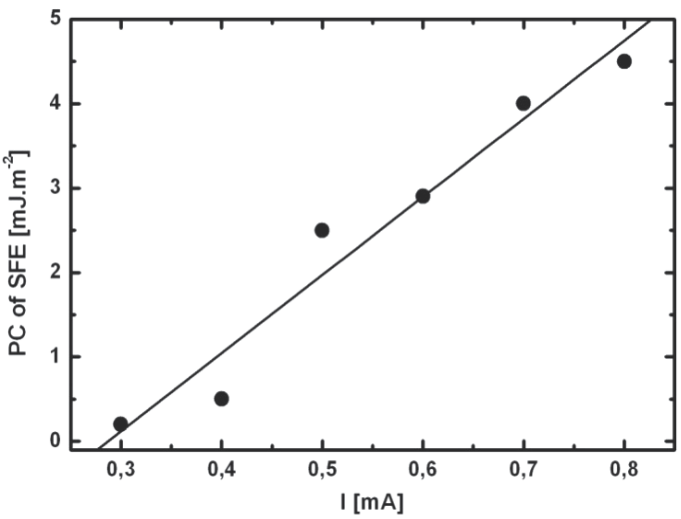

Fig. 3. PC of the surface energy as a function of current density for the biaxially oriented iPP modified (v = 4.8 m.min^{-1}) by corona discharge

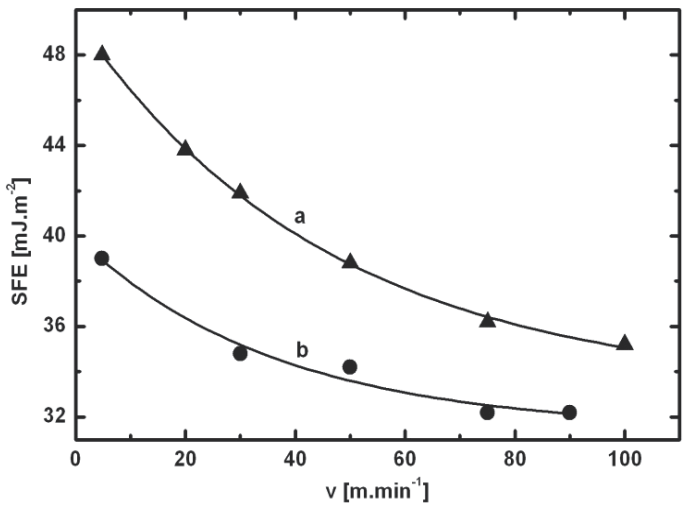

Fig. 4. Surface energy of iPP modified by corona discharge as a function of foil drive (I = 0.8 mA): a - extruded iPP, b - biaxially oriented iPP.

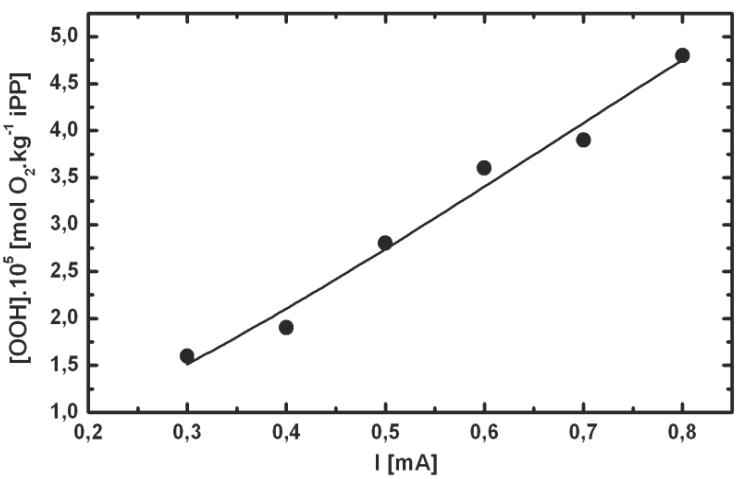

Fig. 5. Concentration of hydroperoxides in the biaxially oriented iPP modifiedby corona discharge as a function of current density (v = 4.8 m.min^{-1})

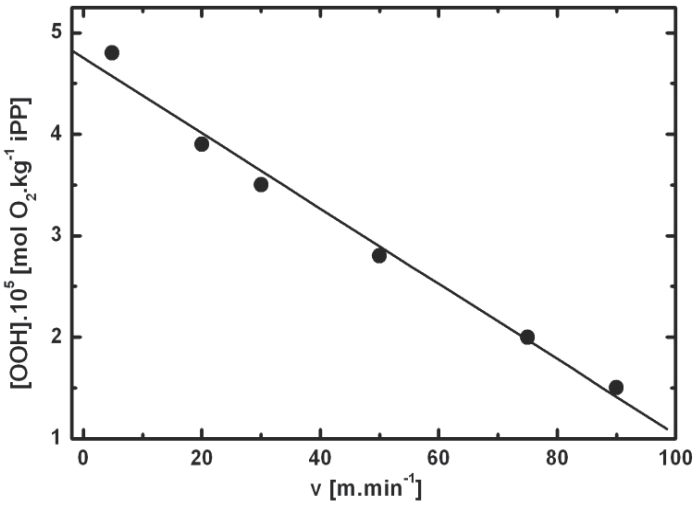

Fig. 6. Concentration of hydroperoxides in the biaxially oriented iPP modified by corona discharge as a function of foil drive speed (I = 0.8 mA)

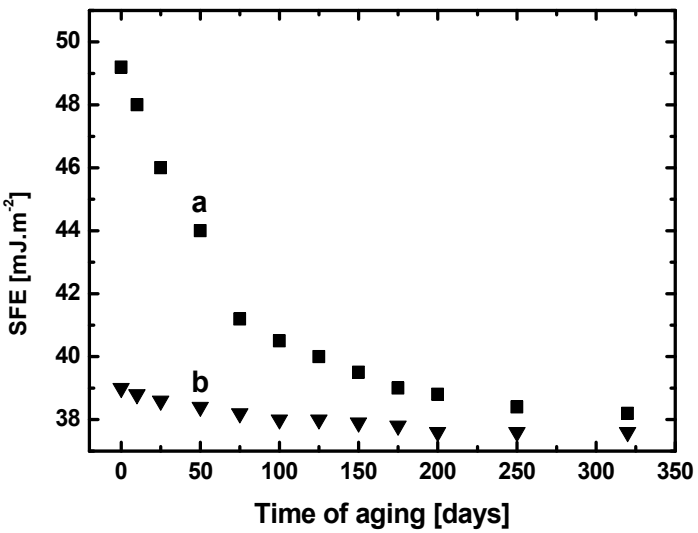

Fig. 7. Variation of the surface energy of iPP modified by corona discharge with time of aging: a – extruded PP, b – biaxially oriented PP

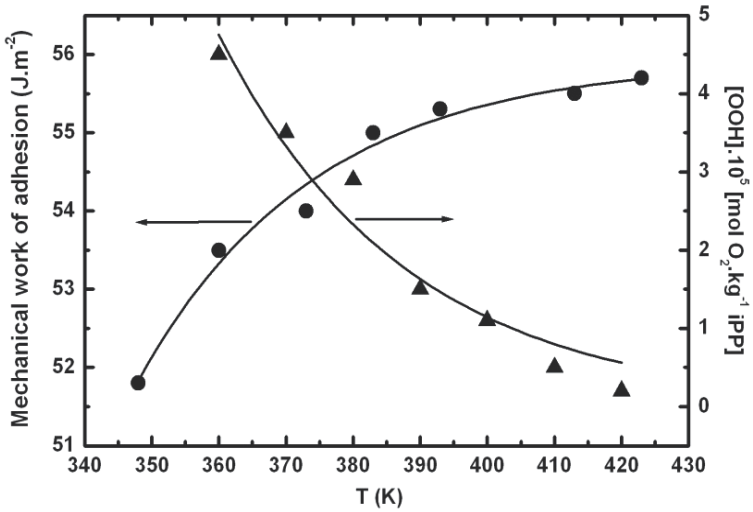

Fig. 8. Variation of auto-adhesion work and hydroperoxide concentration of iPP modified by corona discharge with the time of auto-adhesive joint formation

	Deposit of butyl acrylate-vinyl acetate copolymer (g.m-2)			
	50	100	130	150
	Am (J.m-2)			
Unmodified tissue	42	50	59	69
Modified tissue	78	84	94	102

Table 1. Mechanical work of adhesion in the adhesive joint iPP backing fabric-butyl acrylate-vinyl acetate copolymer deposit

Modification is the most important factor, since with 50 g.cm-2 of the rubbing paste on iPP fabric the mechanical work of adhesion was higher than that for unmodified PP fabric with 150 g.cm-2 layer of the rubbing paste. The adhesive properties given as the values of the work of adhesion improved, on average, by 65 % when compared the backing fabric based on modified PP fabrics non-modified material.

The higher efficiency of the modification for extruded iPP when compared to biaxially oriented iPP was explained by different susceptibility to oxidation due to different crystallinity. Linear dependence of either PC of the surface energy or hydroperoxide concentration of modified iPP on current density was observed. A decrease in the exposition time of iPP foil resulted in lower modification effect. The sensitivity on exposition time was more pronounced for extruded iPP. Aging of modified PP foil leads to a significant drop in surface energy during first 24 hours for extruded iPP, while for biaxially oriented iPP the decrease was small. An increase of the mechanical work of adhesion was observed if temperature of auto-adhesive joints rised. The observed decrease of hydroperoxide concentration after a destruction of the auto-adhesive joints is in accordance with the previous data.

The insufficient stability of the polarity of such a polymer surface after modification by the corona discharge brings some difficulties, i.e. due to the fact that some instable oxygenic functional groups such as peroxide or hydroperoxide groups are formed and subsequently decompose to give the more stable ketone and aldehyde groups. Because of thermodynamic preference, the surface energy of the polymer decreases due to the transfer of polar functional groups from the surface of polymer into the bulk. Owing to hydrophobic recovery following modification of iPP its polarity decreases and the original modification effect grows weak. The process of hydrophobic recovery takes place on the surface of polymer after modification and is dependent on the current density used as well as on the polymer crystallinity. The decrease in polarity of the modified polymer manifests itself by a decrease in wettability of the polymer surface with polar liquids, e. g. water, glycerol, liquid polar inks etc. It is therefore important to scrutinize the process of hydrophobic recovery of iPP modified by corona discharge plasma and to take into account this fact before further processing of the stored modified iPP films.

Variation of the surface energy and its PC with time after modification is represented in Fig. 9 for biaxially oriented iPP modified by corona discharge. During aging the hydrophilicity of the modified biaxially oriented iPP films initially dropped. The decrease in hydrophilicity (Fig. 9) manifested itself by a non-linear fall in surface energy (plot a) as well as PC of the surface energy (plot b) while the greatest fall in surface energy and its PC was found after 30 days following modification when the value of the surface energy had fallen from 39.2 to 37.0 mJm^{-2}. A greater relative decrease was observed for PC of the surface energy, which fell from 9.2 to 6.8 $mJ.m^{-2}$ during 30 days after modification. In the course of further aging the process of iPP hydrophobization proceeds rather slow and after 360 days the surface energy and its PC reached 35.7 $mJ.m^{-2}$ and 5.5 $mJ.m^{-2}$, respectively. From these values, one year after modification of the biaxially oriented iPP by the electric discharge the total surface energy decreased only a little - 9%, while the PC of the surface energy fell up to 40% when compared with that of a fresh modified sample. The measurements of the surface energy and its PC biaxially oriented iPP modified by the corona discharge show an increase of investigated surface parameters while the dispersive component of the surface energy remained practically unchanged.

Dependencies of the surface energy and its PC against long-term aging are represented in Fig.10 for extruded iPP modified by corona discharge (Novák & Florián, 2001; Novák & Florián, 2004). In comparison with biaxially oriented iPP the hydrophobic recovery of extruded iPP films subjected to modification by the electric discharge was much more obvious and the total surface energy (plot a) and its PC (plot b) fell especially in the course of the first 30 days after modification in the same manner as observed for biaxially oriented iPP. According to Fig. 10 the decrease in the hydrophilicity of extruded iPP manifested itself by a non-linear decrease in the surface energy and the PC of the surface energy. While the value of the total surface energy dropped significantly from 46 to 35 $mJ.m^{-2}$, the PC of the surface energy declined still more in this interval, i.e. from 15.8 to 4.6 $mJ.m^{-2}$. In the course of further aging of the extruded iPP the process of hydrophobic recovery of modified surface became slower and after 360 days the values of the surface energy and its PC attained 33.4 $mJ.m^{-2}$ and 3 $mJ.m^{-2}$, respectively. On this basis we can state that the total surface energy of the modified extruded iPP decreased by 24% after 30 days and 27% after 360 days following modification. On the other hand, the PC of the surface energy decreased by 71% after 30 days, and by 81% after 360 days when compared with original modified sample. If we compare the values of the surface energy and its PC obtained for the biaxially oriented iPP and the extruded iPP

modified by the corona discharge, we can conclude that the extruded iPP exhibits essentially higher dynamics for the hydrophobic recovery process than biaxially oriented iPP does (compare Fig. 9 a and Fig. 10). This difference is to be attributed to the different crystallinity of extruded and biaxially oriented iPP. The modification of iPP due to linking polar functional groups to the polymer chain takes place in the amorphous phase of the polymer. This is more significant in the case of extruded iPP, which has lower crystallinity when compared with biaxially oriented iPP. Owing to this lower crystallinity of modified extruded iPP a higher polymer polarity and thus a higher value of its surface energy results. Fig. 11 depicts the polar fraction for biaxially oriented iPP (plot a) and for extruded iPP (plot b) after modification by the electric discharge in the process of long-term hydrophobic recovery.

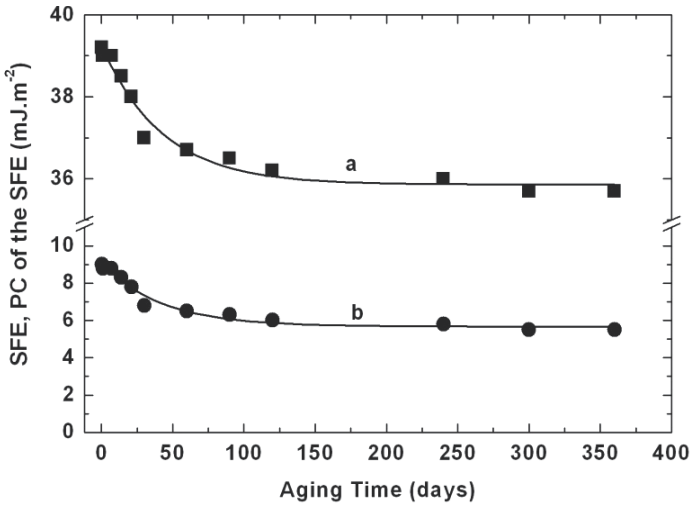

Fig. 9. Surface energy and its PC of biaxially oriented iPP modified by corona discharge during long-term hydrophobic recovery: a – surface energy, b – PC of the SFE

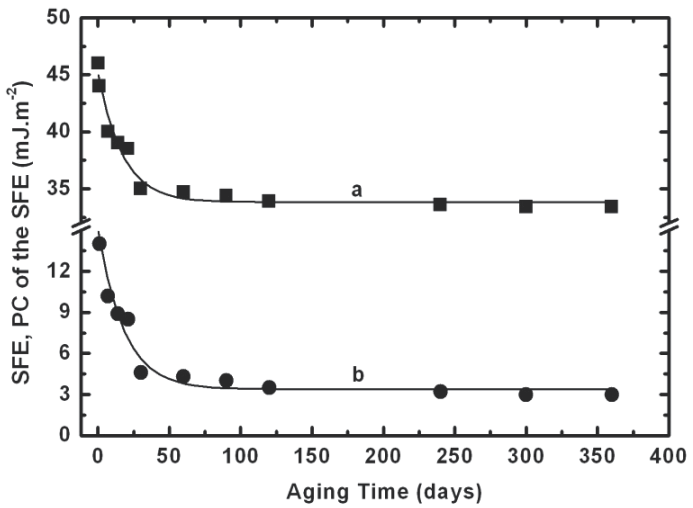

Fig. 10. Surface energy and its PC of extruded iPP modified by corona discharge during long-term hydrophobic recovery: a – surface energy, b – PC of the SFE

According to Fig.11 both relationships exhibit non-linear character and the marked decrease in the case of extruded iPP amounted to 62 % after 30 days and after 360 days following modification it was 74%. A slight decrease in hydrophilicity was observed after modification of biaxially oriented polymer, i.e. the polar fraction was reduced by 22% after 30 days and 35% after 360 days following treatment. The greatest decrease in the polar fraction of iPP modified by electric discharge was observed over 30 days after modification and during further aging the decrease was rather less for both extruded and biaxially oriented iPP. If we compare plot a with plot b in Fig.11, we can state that the decrease in the polar fraction for extruded iPP modified by the electric discharge and exposed to long-term aging was twofold when compared with that of biaxially oriented iPP.

Fig.12 presents the dependence of the mechanical work of adhesion of iPP modified by the electric discharge for an adhesive joint with polyvinyl acetate on aging the modified biaxially oriented iPP (plot a) and extruded iPP (plot b). In the course of aging of the iPP films the mechanical work of adhesion to polyvinyl acetate fell in a non-linear manner. After 360 days of aging the mechanical work of adhesion fell 26 % for modified biaxially oriented iPP when compared with original value of the mechanical work of adhesion and by 52 % for modified extruded iPP. As for the polar fraction the greatest decrease in mechanical work of adhesion to polyvinyl acetate produced by hydrophobic recovery of the surface of modified iPP was observed after 30 days following modification. During further aging a significant decrease in mechanical work of adhesion was also observed.

Because of the apparent correlation between mechanical work of adhesion and the polar fraction found for iPP modified by the electric discharge we have constructed the relationship between mechanical work of adhesion and polar fraction given in Fig. 13. The polar fraction faithfully expresses the change in polarity of the modified iPP during long-term aging. Thus Fig. 13 gives the change in mechanical work of adhesion in the course of long-term hydrophobic recovery of the surface of the modified iPP. The discussed relationship exhibits linear character and can be described by the equation:

$$A_m=65.9+3.9\cdot10^2\cdot x_s^p,\ r^2=0.99 \tag{20}$$

Because of the value of correlation coefficient found we can state that the linearity of the relationship given in Fig. 13 has been confirmed for the long-term aging of iPP after modification.

The relative decrease in the strength of adhesive joints of the modified iPP to polyvinyl acetate arising during the process of hydrophobic recovery is represented in Fig. 14 for biaxially oriented iPP (plot a) and extruded iPP (plot b) modified by the electric discharge. According to Fig. 14 the decrease in adhesive properties is significantly smaller for biaxially oriented iPP when compared with that of the extruded iPP in contradiction with assumptions based on the values found of the PC of the SFE. The decrease in values of the PC of the surface energy, the polar fraction and the mechanical work of adhesion for iPP modified by electric discharge may attributed to the successive destruction of unstable oxygenic functional groups (peroxides and hydroperoxides) arising in the initial stage of modification which give rise to the formation of more stable products. The process of hydrophobic recovery after iPP modification results from the tendency of the polymer to reduce the surface energy because of the thermodynamic preferences present and thus to

rearrange the polar functional groups in the direction of polymer bulk. Because of this, the degree of surface modification of iPP by the corona discharge is, to certain extent, dependent on the crystallinity of the polymer and on time elapsed after polymer modification.

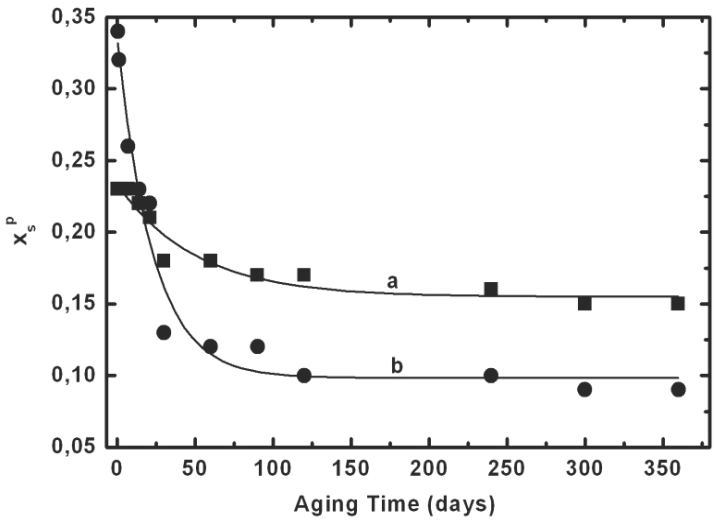

Fig. 11. Polar fraction of the iPP surface modified by corona discharge during long-term hydrophobic recovery: a – biaxially oriented iPP, b – extruded iPP

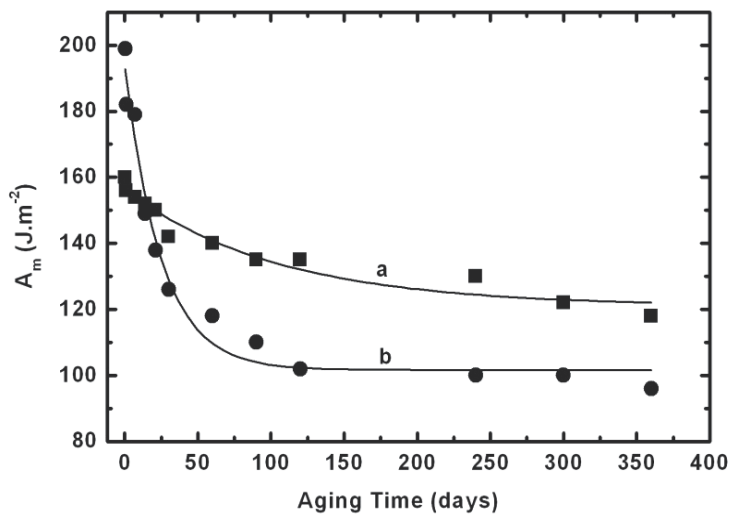

Fig. 12. Mechanical work of adhesion to polyvinyl acetate for iPP modified by corona discharge during long-term aging: a – biaxially oriented iPP, b – extruded iPP

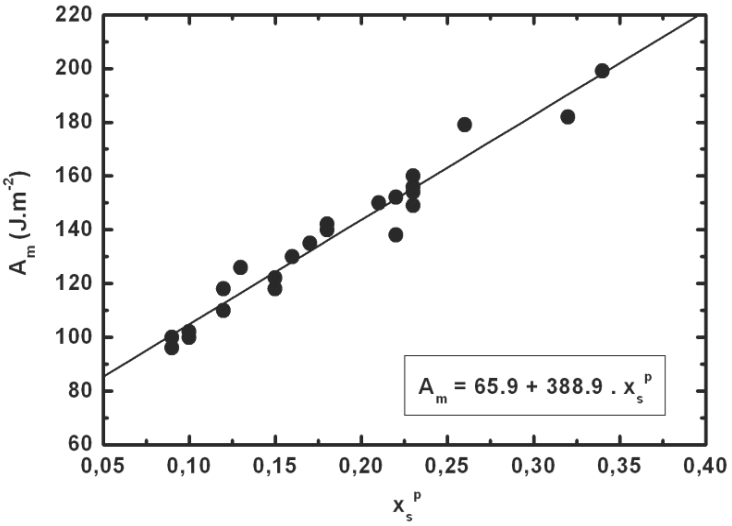

Fig. 13. Dependence of the mechanical work of adhesion to polyvinyl acetate for iPP modified by corona discharge plasma vs. polar fraction

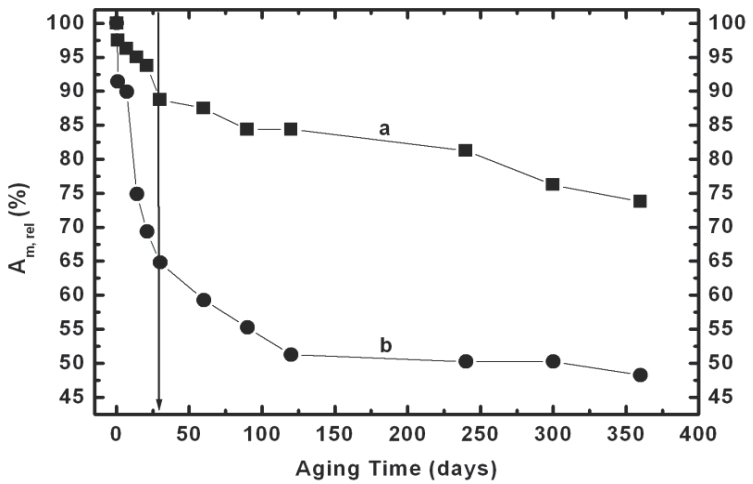

Fig. 14. Variation of the relative change in the strength of the adhesive joint modified iPP – polyvinyl acetate during long-term hydrophobic recovery: a – biaxially oriented, b – extruded iPP.

3.2 Modification by grafting

Grafting of some polar polymers (Rätzsch et al., 2002; Castell et al., 2004; Kuhn et al., 2000; Scarlatti et al., 2004; Shi et al., 2001; Pesetskii et al., 2001; Kato et al., 2003; Sulek et al., 2001; Tao et al., 2001; Flores-Gallardo et al., 2001; Yamada et al., 2003), such as acryl amide, maleic anhydride, methyl methacrylate, itaconic acid (IA) onto iPP chain, is a possibility for the increase of both the surface polarity and hydrophilicity of iPP. The free-radical

polymerization methods are most widely used and inexpensive procedures for the synthesis of graft copolymers of iPP because they are relatively simple. This is a common method of increasing of iPP adhesive properties. The main chain and the branch chains in grafted iPP are usually thermodynamically incompatible. Grafting improves adhesion, dyeing, tensile strength, compatibility, thermal stability and abrasion resistance of the copolymer.

The results of surface characteristics of iPP grafted by IA (Novák & Florián, 1995; Novák & Chodák, 1995) are shown in Fig. 15. As seen in Fig. 15, plot a, the surface energy of iPP grows with the increase of concentration of grafted IA. The grafting of 5 wt. % of IA onto iPP macromolecule increased the surface energy by 19.5 % in comparison with unmodified iPP. This increase should be attributed mainly to the growth of PC of the surface energy (Fig. 15, plot b). The PC of the surface energy increased after grafting of iPP by 5 wt.% from the value 0.4 $mJ.m^{-2}$ (non-modified polymer) to 9.5 $mJ.m^{-2}$ obtained for iPP containing 5 wt.% of grafted IA.

The results in Fig. 16 show that the adhesion of iPP to more polar polymers as well as to metals (Fig. 17) is low. The difference between a polarity of iPP and other more polar polymer as a consequence of iPP grafting by IA was diminished. The adhesion parameters in the system iPP grafted by IA - more polar polymer increases with an increase of the IA grafted content. Grafting of iPP by 5 wt.% of IA leads to a growth of mechanical work of adhesion of iPP 6.9 times, 7.2 times and 18.1 times when considering the adhesion of iPP to cellulose acetate, polyamide and aluminum, respectively.

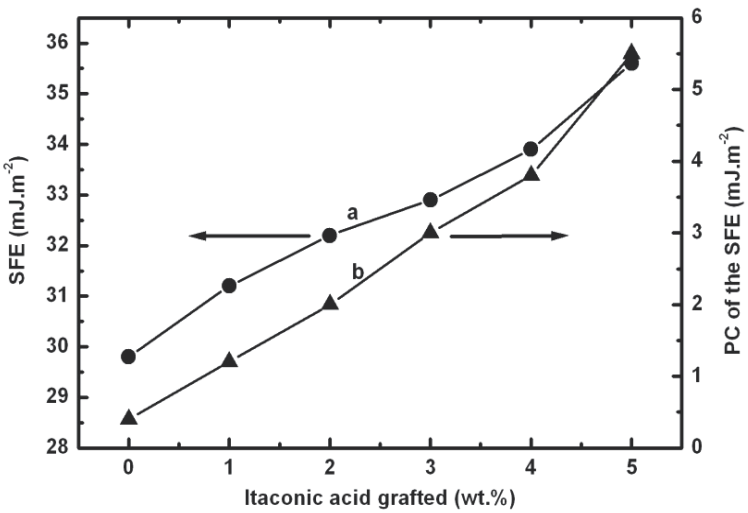

Fig. 15. Surface energy and its PC of iPP grafted by itaconic acid against itaconic acid grafted content

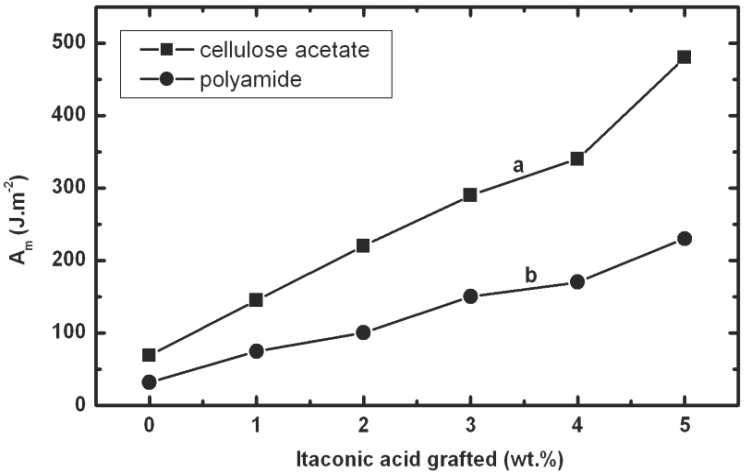

Fig. 16. Mechanical work of adhesion of iPP grafted by itaconic acid to cellulose acetate (a) and polyamide (b) against itaconic acid grafted concentration

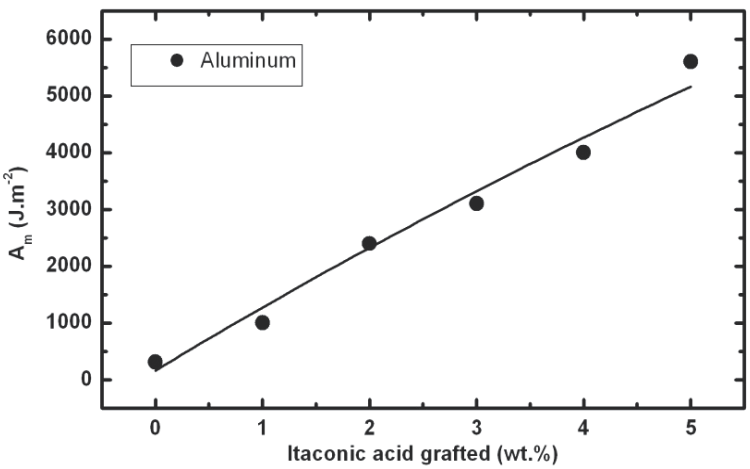

Fig. 17. Mechanical work of adhesion of iPP grafted by itaconic acid to aluminum against itaconic acid grafted concentration

3.3 Modification by oxidation

The significant groups of adhesive properties of iPP increasing present oxidation methods (Brewis & Mathieson, 2002; Chodák & Novák, 1999; Ashana et al., 1997; Novák, 1996; Yang et al., 2003; Nie et al., 2000; Novák & Pollák, 1994; Novák, 1996; Dibyendu et al.,1998; Vasconcellos et al.,1997; Novák & Chodák, 2001). As a result of formation of carbonyl groups in the course of iPP modification the adhesive properties of polymers are increased. Using a strong oxidation agent and higher temperatures of modification a partial decomposition of the polymer can occur when the bulk unmodified zones of polymer reach the surface. On spherollitic surfaces of iPP chromic acid preferentially etches the less

ordered (amorphous) regions between the arms of spherullites, producing ca 10 μm deep cavities. On lamellar surfaces, chromo sulfuric acid preferentially attacks interlamelar regions, producing deep cavities. The deeply etched spherullitic and lamellar surfaces have numerous mechanical anchoring sites for metal to adhere strongly. For the increase of adhesion of iPP functional groups =C=O and -SO_3H are responsible, which are formed during the modification and are present in the near-surface layer. In iPP modified by chromo sulfuric acid there is also a high concentration of carboxyl groups. After the modification of iPP by chromo sulfuric acid a very rough surface is formed and that the roughness itself can cause a good adhesion of treated iPP. A different opinion on the better adhesion properties after modification by chromo sulfuric mixture considers a main reason for the better adhesion properties to be the higher polarity of pre-treated iPP, while the higher roughness to be a secondary importance contributing the higher adhesion only. For the modified iPP similar correlations were found between the degree of oxidation or concentration of carboxyl group and adhesion. From the results of the studies on the surface energy of iPP modified by chromo sulfuric acid it follows that after initial fast increase, during 1 - 2 minutes of modification, the value of the surface energy levels off. The most suitable temperature for modification of iPP by chromo sulfuric acid is 70 ^oC, at which the degradation of polymer is still not extensive. In the measurement of mechanical work of adhesion of iPP modified by chromo sulfuric acid in a joint with polyvinyl acetate the result was six times larger relatively to the untreated iPP. This result is similar to that for the modification by corona discharge besides the fact that the modification by chromo sulfuric acid has a lasting character.

An efficient method of modification of iPP from the point of view of enhancement of adhesion properties is a modification by vapors of chromyl chloride (Novák, 1996; Novák & Pollák, 1994). In contrast to the modification by chromo sulfuric acid a considerably longer time of modification is needed (40 - 60 min.) and the treatment is performed in the temperature range of 30 - 60 ^oC. The study shows few times higher concentration of carbonyl groups in comparison to treatment by chromo sulfuric acid, while Cr^{VI} was reduced to lower oxidation degrees up to Cr^{IV}. In the study of a dependence of PC of the surface energy on time of modification a maximum was observed and it was confirmed at the same conditions also for the similar dependence of concentration Cr^{IV} by ESR method. In the course of modification of iPP by chromyl chloride at higher degrees of oxidation a degradation of iPP (linear decrease of molar mass with the time of modification) was observed. The modification mechanism of chemical etching by oxidizing agents consists in the abstraction of the hydrogen atoms from the polymer backbone and their replacement with polar groups. These polar groups introduced on the iPP surface by pretreatment should increase the surface energy and enhance the wetting. The surface pretreatment by some oxidizers has also another aim - to remove all weak boundary layers on the polymer surface e.g. stabilizers and other additives, which are responding for the weak adhesive bonds. The oxidizing chemical methods of iPP modification are efficient and in addition to this fact they give a more durable result than modification by corona discharge.

The results of the investigation of surface properties of iPP pretreated by chromyl chloride and/or chromo sulfuric acid are presented in Figs. 18 – 26.

Variation of the surface energy of iPP modified by chromyl chloride with modification time is represented in Fig. 18. It follows that the surface energy non-linearly increases with modification time. However, it becomes stable after a certain period of time. The lower the temperature of modification, the later the stable state appears. For instance, the stable state of the relationship described in Fig. 18 appeared after 30 minutes if the modification was performed at 333 K and after 60 minutes if the modification was performed at 303 K. The stabilization of the values of the surface energy and the shift towards longer time due to the decrease in the temperature of oxidation (Fig. 18) can be explained by stepwise saturation of the polymer surface with polar (mainly carbonyl) groups, which originate from modification of iPP by chromyl chloride. The increase in surface energy of iPP modified by chromyl chloride (Fig. 18, plots a, b, c) was 36 % for the temperature of 333 K, 28 % for 313 K and 13 % for 303 K with respect to non-modified polymer.

The dependence of the surface energy and its PC against time of oxidation is represented in Fig. 19 for iPP modified by chromyl chloride. According to Fig. 19, the PC of the surface energy of modified iPP increases during the first 30 - 40 min. of modification, after this period the value of PC decreases. The reaching the maximum of PC of the surface energy may be probably ascribed to degradation processes occuring at the modified polymeric surface, which could decrease the polarity of the surface. After a certain period of time the degradation products accumulate at the surface of iPP reducing the polarity, which brings a decrease in surface energy of polymer.

In iPP modified by chromyl chloride the concentration of carbonyl groups was determined (Fig. 20). The concentration of the carbonyl groups increased with the time of oxidation and reaches a constant value after 30 - 60 min., depending on the temperature of modification. Plots a, b, c in Fig. 20 correspond to the temperatures 333 K, 313 K and 303 K, respectively, exhibit analogous course like the plots of the surface energy in Fig. 24. Change the temperature of modification from 303 to 333 K, the concentration of the surface carbonyl groups increases by the factor 4.4. Saturation of the surface with carbonyl groups is probably the reason for the stabilization of the carbonyl groups concentration after a given time.

Determination of the reaction rate constant of iPP oxidation by chromyl chloride showed a strong dependence of the reaction rate on the temperature (Fig. 21). The growth of the temperature from 303 K to 333 K caused an increase of the reaction rate by the factor 1.9.

The results of the CrVI to CrIV reduction in iPP modified by chromyl chloride obtained using electron spin resonance are represented in Fig. 22. It can be seen that the maximum Cr^{IV} concentration at 333 K is reached after 40 min. of oxidation. As it can be seen, the maximum concentration of Cr^{IV} was reached after 40 minutes of iPP oxidation at the temperature of 333 K and the curves in Fig. 22 and Fig. 20 are in good correlation.

The dependence of the surface energy and its PC vs. concentration of C=O groups is shown in Fig. 23. The PC of the surface energy reaches a maximum at the C=O groups concentration equal to 1.6×10^{-2} mol $O^2.kg^{-1}$ iPP. The following decrease in the C=O groups concentration is probably caused by an increased amount of the degradation products thus resulting in the decrease of the value of the surface energy.

The degree of the iPP degradation during the modification by chromyl chloride was estimated from the determination of its molecular weights. Like it can be seen from Fig. 24,

the molecular weight of iPP decreases linearly with the time of modification, the slope of the curves is increasing with increased temperature. After 60 min. of modification the molecular weight decrease of iPP is about 10 % for T = 303 K, 26 % for T = 313 K and 42 % for T = 333 K, in comparison with the unmodified iPP.

The decrease of the surface energy with time after iPP modification is described in Fig. 25. As it follows from this figure, the iPP surface after modification by chromyl chloride has a relatively good stability. The decrease of the surface energy value 120 hours after finishing modification is close to 7%, while this decrease reaches 30 – 40 % in 24 hours after modification of iPP by corona discharge.

The mechanical work of adhesion of iPP modified by chromyl chloride and chromo sulfuric acid vs. time of modification is illustrated in Fig. 26. It was found that the mechanical work of adhesion is 36 % higher in the case of chromyl chloride compared to the modification with chromo sulfuric acid. The value of mechanical work of adhesion increased rapidly, in a short time (2 min.) reached the maximum value and soon afterwards assumes a constant value.

It has been found that the surface energy of iPP pretreated by chromyl chloride versus modification time rapidly increases and assumes a constant value. Equal character was observed for the relationship between free surface energy and carbonyl group concentration of modified polymer. After a certain time interval subsequent to modification the decrease in surface energy of treated iPP is negligible. A maximum of the relationship between PC of the surface energy and modification time was revealed.

A quite often used method of modification of iPP is the modification by UV light. In analogy to the treatment by the electric discharge the effect of UV light is exhibited in the air by the formation of hydroperoxides which are consequently transformed by photolysis to ketones. It is known that by the decomposition of hydroperoxides, OOH radicals are formed which can lead to formation of ester, carboxyl and lacton groups and thus enhance the adhesion of iPP. A grafting of polar monomers such as N-vynilpyrrolidon or methacrylic acid to iPP modified by UV light can be used. Enhancement of adhesion was observed and could be effectively expressed by a decrease of contact angle of redistilled water on the surface of polymer from 94 deg to 35 – 60 deg. For modification of iPP is very important to know the effect of the intensity and the distance of the UV source from the treated polymeric surface. A very efficient method of adhesion enhancement of iPP is the modification by phosphorus trichloride with participation of the UV light. By the decomposition of phosphorus trichloride active chlorine is formed which reacts with iPP. This is also accompanied at the same time by the oxidation by ozone formed from oxygen in the air. A significant enhancement of adhesion was observed without a considerable decrease of the film transparency.

The inferior adhesive properties of polyolefins result in many serious problems especially if gluing or printing on these materials is considered. The effective surface modification of polyolefin should lead to a formation of a very thin surface layer with the thickness of several micrometers without affecting the bulk properties of the material. The fine layer of modified polymer on the surface of polyolefin should contain sufficient concentration of the polar moieties leading to an increase of the surface energy of polymer.

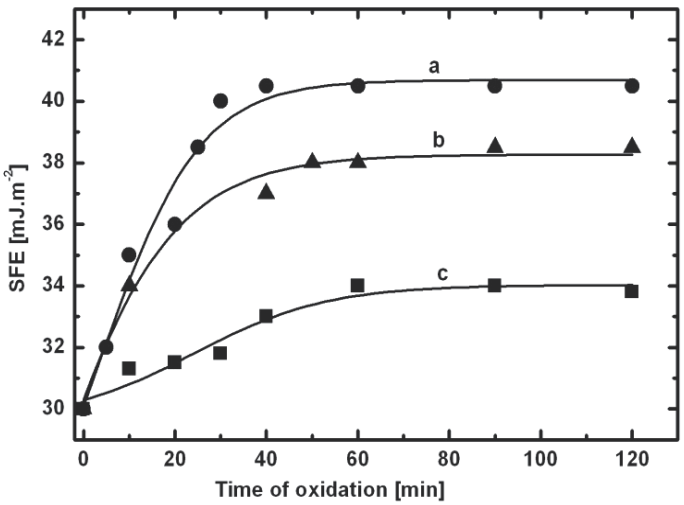

Fig. 18. Surface energy of iPP modified by chromyl chloride against modification time: a - T = 333 K, b - T = 313 K, c - T = 303 K

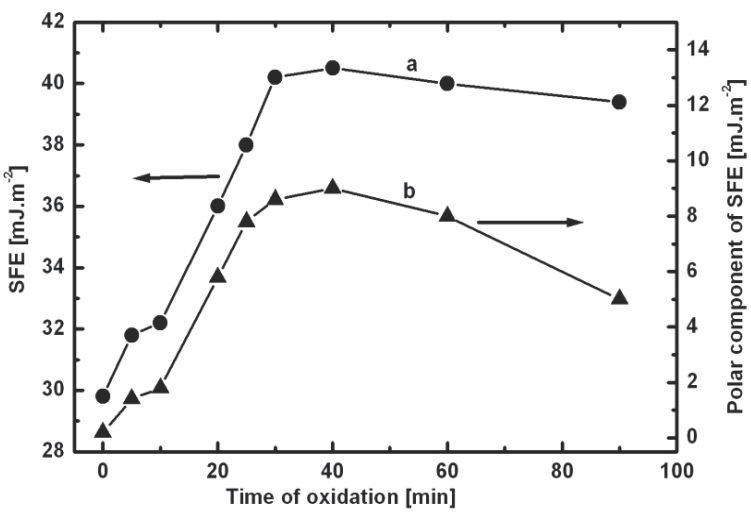

Fig. 19. Surface energy and its PC against time of modification for iPP modified by chromyl chloride: a - surface energy, b - PC of the surface energy.

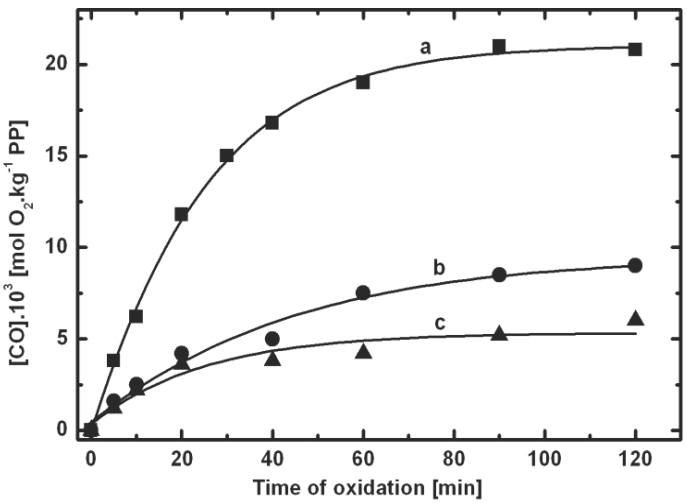

Fig. 20. Concentration of carbonyl groups of iPP modified by chromyl chloride against time of modification: a - T = 333 K, b - T = 313 K, c - T = 303 K

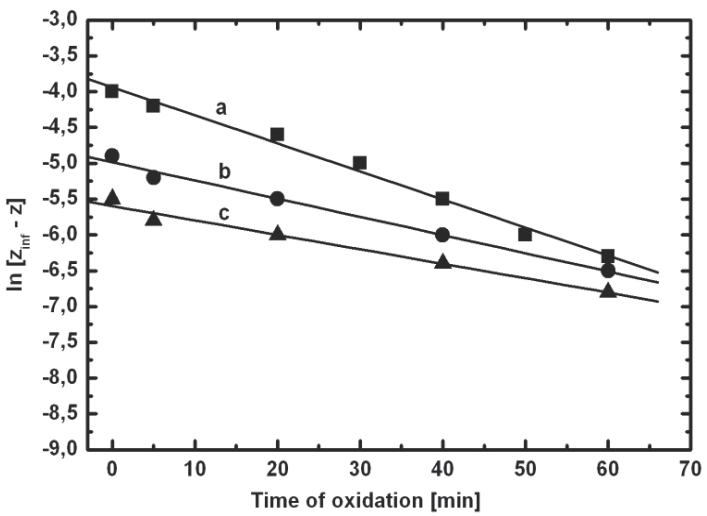

Fig. 21. Determination of the reaction rate constant of iPP modified by chromyl chloride at different temperatures: a – 333 K, b - 313 K, c - 303 K

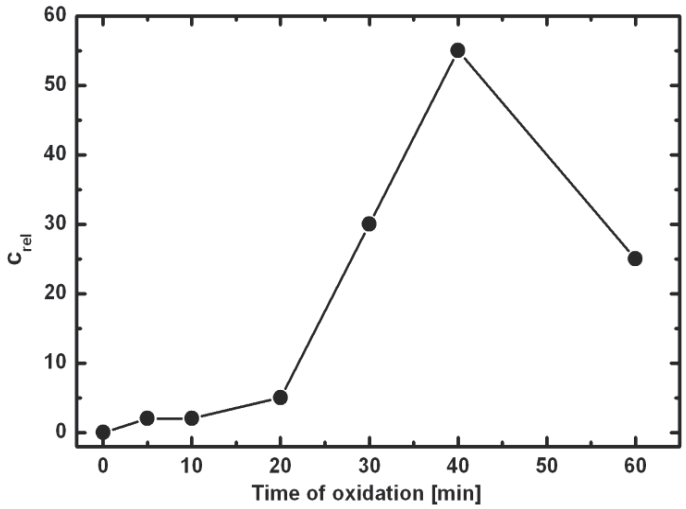

Fig. 22. ESR measurements of Cr^{IV} concentration of iPP modified by chromyl chloride against time of modification (T = 333 K)

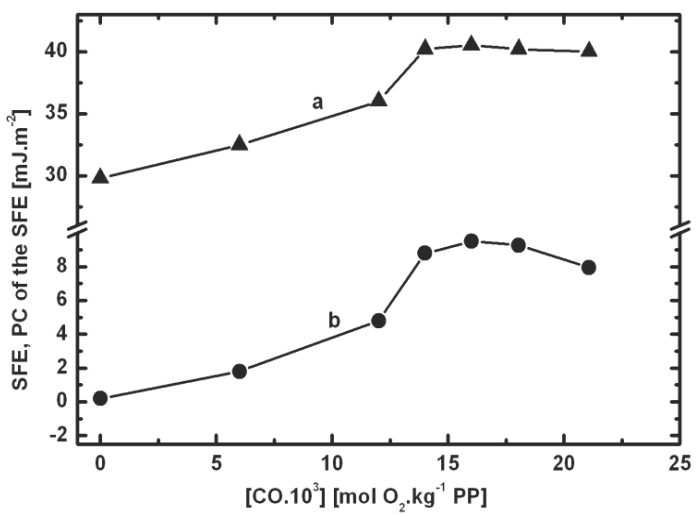

Fig. 23. Surface energy and its PC of iPP modified by chromyl chloride against carbonyl groups concentration: a – surface energy, b – PC of the surface energy

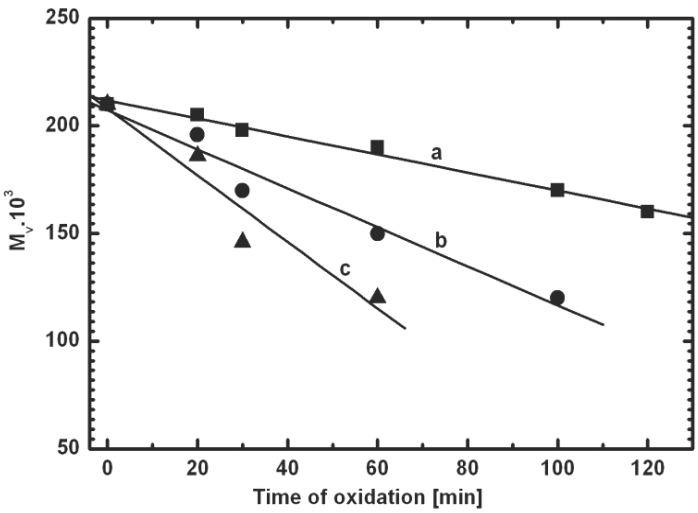

Fig. 24. Figure 24 Molar weight of iPP modified by chromyl chloride vs. time of modification: a – T = 303 K, b – T = 313 K, c - T = 333 K

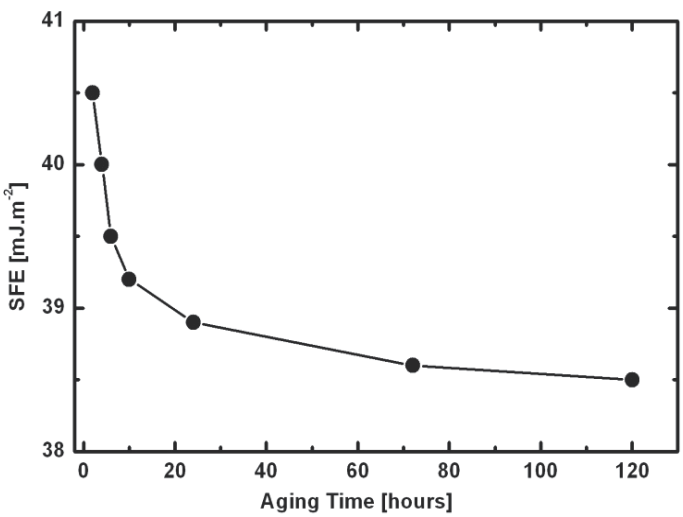

Fig. 25. Surface energy of iPP modified by chromyl chloride vs. time elapsed from modification

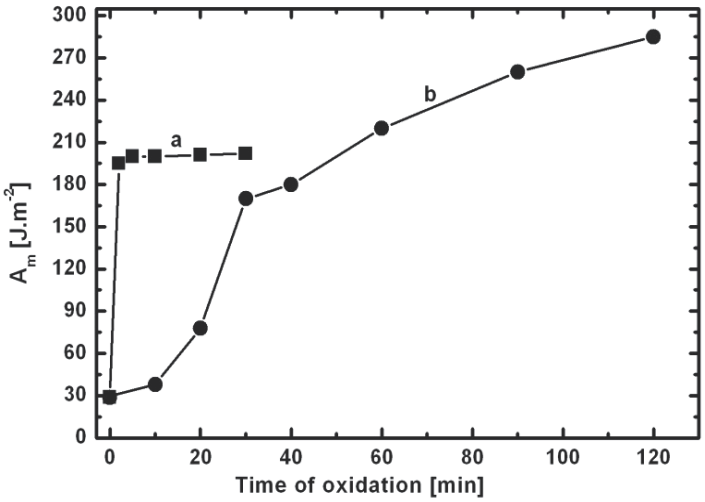

Fig. 26. Mechanical work of adhesion of iPP modified by chromyl chloride to polyvinyl acetate against time of modification: a – chromo sulfuric acid, b – chromyl chloride

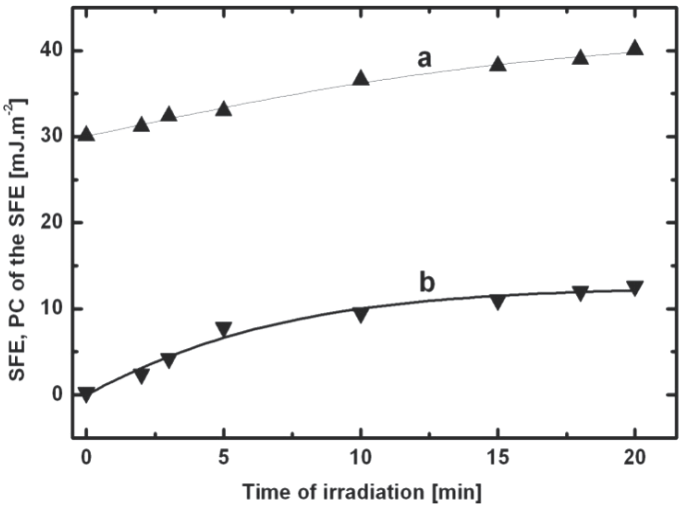

Fig. 27. Variation of the surface energy and its PC of iPP pre-treated by UV/$POCl_3$ with the time of UV exposure (d_{UV} = 50 mm): a – surface energy, b - PC of the surface energy

3.4 Modification by halogenization

Surface modification of iPP in vapours of halogen compounds (Novák & Chodák, 2001; Novák & Chodák, 2001; Kharitonov, 2000; Novák& Chodák, 2001; Hruska & Lepot, 2000; Carstens et al., 2000) under UV irradiation represents an efficient method for the increase of the adhesive properties. The presented method is based on the influence of the UV radiation and vapours of phosphoryl chloride on the iPP surface. UV-irradiation results in a faster decomposition of the halogen compound and leads to the UV-oxidation of the surface of polymer. Surface modification of iPP vapours of phosphoryl chloride under UV irradiation

(UV/$POCl_3$) (Novák & Chodák, 2001; Novák & Chodák, 1999) is a suitable method for the increase of adhesive properties. Phosphoryl chloride behaves as a sensitizer, which decomposes under the effect of UV irradiation. Its decomposition is followed by a formation of active chlorine, which takes part in the free radical reactions with PO macromolecules leading to a formation of -$POCl_2$ groups attached to the polymer chains. At the same time the reaction with oxygen initiated by UV irradiation takes place resulting in a generation of polar oxygen-containing sites.

The surface and adhesive properties of iPP modified by UV radiation in the presence of $POCl_3$ have been studied. Modification of iPP by UV/$POCl_3$ results in an increase in surface energy of polymer as well as in an improvement of the mechanical work of adhesion of modified iPP to more polar polymers.

Fig. 27 illustrates a non-linear increase of the surface energy (curve a) and its PC (curve b) for iPP modified by UV/$POCl_3$ in the dependence on the time of modification at the UV source distance of 50 mm. The surface energy for non-modified polymer was 30.1 $mJ.m^{-2}$. The surface energy and its PC of iPP pre-treated by UV/$POCl_3$ increased non-linearly with time up to the value 40.1 $mJ.m^{-2}$ after 20 minutes. The PC of the surface energy of modified iPP increased after 20 min. of modification from 0.25 $mJ.m^{-2}$ up to 12.6 $mJ.m^{-2}$. The time-dependence of the PC of the surface energy (Fig. 27, curve b) leveled off after an initial increase enduring about 10 min. As expected, the strength of adhesive joints of modified iPP increases in accordance with the degree of hydrophilicity of modified polymer. Thus, adhesive properties of polymer are strongly related to the values of the PC of the surface energy.

The surface energy of iPP modified by UV/$POCl_3$ was essentially higher in comparison with non-modified polymer. A non-linear increase of the surface energy and its PC against time of UV exposure was observed. The pre-treatment of iPP by UV/$POCl_3$ method leads to a considerable growth in the surface and adhesive properties of the polymer and it depends on the intensity of the UV radiation as well as on the time of UV exposure. The values of the strength of adhesive joint to polyvinyl acetate of UV/$POCl_3$ modified iPP correspond with the measured values of the PC of the surface energy. The efficiency of iPP modification by UV/$POCl_3$ substantially increased by diminishing the distance of UV radiation source from the surface of polymer or by increasing the intensity of UV source.

4. Conclusion

The selection and application of modification procedure for the enhancement of adhesion properties of iPP depends mostly on the specific demands required on the adhesive joints in practice. When deciding about suitability of the modification method a detailed knowledge about physical and chemical changes undergoing on the surface, experimental demands and also aggressiveness of the reagents employed is needed. Based on this point of view the most practical surface treatments are the flame and electric discharge treatments which enables a continual modification during the processing, for instance in printing. This modification meets also the demand on a fast processing of the treated surface. On the other hand some very effective modification methods such as the modification by chromyl chloride vapours or phosphorus trichloride with UV light application are less popular because of implausibility of the modification reagents, in spite of the lasting effect of the modification. The surface modification of iPP is observed in a very narrow layer not

exceeding thickness of 10 μm and is easily destroyed by heat or friction by which the effect of modification disappears. For practical purposes according to this reason, there is also suitable method of modification based on the modification of polymer in bulk consisting of the addition of polar low-molecular compound or a polymer respectively. As a matter of fact, the most efficient method of modification is grafting, e.g. by maleic anhydride, acrylic or itaconic acid, as well as the modification by block copolymers of the A-B-C type where A is a polar monomer and B is non-polar one. This modification is now intensively studied because it enables us to obtain good properties of iPP without significant deterioration of its physico-mechanical properties.

5. Acknowledgement

The authors are grateful to Slovak Grant Agency VEGA (grants No. 2/0185/10 and 1/0581/12), Slovak Research and Development Agency (grants APVV 51-010405 and APVV-0742-11).

6. References

Ashana, H.; Erickson, B. L. & Drzal, L. T. (1997). Sulfonation of polymer surfaces. 2. Chemical changes on polypropylene and polystyrene surfaces after gas phase sulfonation. *J. Adhes. Sci. Technol.*, Vol. 11, pp. 1269-1288, ISSN 0169-4243.

Brewis, D. & Mathieson, I. (2002). M. Adhesion and bonding to polyolefins, *Rapra Review Reports: Shrewsburry,* pp. 10-14, ISBN 1-85957-323-1.

Castell, P.; Wouters, M.; De With, G.; Fischer, H. & Huijs, F. (2004). Surface modification of polypropylene by photoinitiators: Improvement of adhesion and wettability. *J. Appl. Polym. Sci.*, Vol. 92, pp. 2341-2350, ISSN 1096-4628.

Carstens, P. A. B.; Marais, S. A. & Thompson. C. J. (2000). Improved and novel surface fluorinated products. *J. Fluor. Chem.*, Vol. 104, pp. 97-107, ISSN 0022-1139.

Chodák, I. & Novák, I. (1999). Surface modification of polypropylene by additives. An A-Z Reference. *Karger-Kocsis, J.; ed.; Kluwer Acad. Publ.: Dordrecht*, pp. 790-793, ISSN 2080-8259.

Denes, F. S. & Manolache, S. (2004). Macromolecular plasma-chemistry: an emerging field of polymer science, *Progr. Polym. Sci.* Vol. 29, pp. 815 – 885, ISSN 0079-6700.

Dibyendu, S. B.; Ghosh, S. N. & Maiti, S. (1998). Surafce modification and evaluation of polyehylene film. *Eur. Polym. J.*, Vol. 34, pp. 855-861, ISSN 0014-3057.

Flores-Gallardo, S. G.; Sanchez-Valdez, S. & De Valle L. F. R. (2001). Polypropylene/polypropylene–grafted acrylic acid blends for multilayer films: preparation and characterization. *J. Appl. Polym. Sci.*, Vol. 79, pp. 1497-1505, ISSN 1096-4628.

Guimond, S.; Radu, I.; Cyeremusykin, G.; Carlsson, D. J. & Wertheimer, M. R. (2002). Biaxially oriented polypropylene [BOPP] surface modification by nitrogen atmospheric pressure glow discharge [APDD] and by air corona. *Plasmas Polymers,* Vol. 7, pp. 71-88, ISSN 1084-0184.

Hruska, Z. & Lepot, X. (2000). Ageing of oxyfluorinated polypropylene surface: Evolution of the acid-base surface characterisitics with time. *J. Fluor. Chem.*, Vol. 105, pp. 87-93, ISSN 0022-1139.

Kinloch, A.J. (1987). Surface pretreatments. In: *Adhesion and Adhesives,* pp. 101-170,Chapman & Hall: London, ISBN 0-412-27440-X.

Kolluri, O. S. (1994). Application of plasma technology for improved adhesion of materials. In: *Handbook of adhesive technology,* pp. 35-46, Pizzi, A.; Mittal, K. L; eds.; Marcel Dekker,: New York, ISBN 0-8247-8974-1.

Kim, K. S.; Yun, Y. I.; Kim, D. H.; Ryu, C. M. & Park, C.E. (2002). Inhibition of aging in plasma-Treated high-density polyethylene. *J. Adhes. Sci. Technol.*, Vol. 16, pp. 1155-1169, ISSN 0169-4243.

Kim, B. K.; Kim, K. S. & Park, C. E. (2002). Improvement of wettabilitty and reduction of aging effect by plasma treatment of low-density polyethylene with argon and oxygen mixtures. *J. Adhes. Sci. Technol.*, Vol. 16, pp. 509-521, ISSN 0169-4243.

Kuhn, G.; Ghode, A.; Weidner, S.; Retzko, I.; Unger, W. E. S. & Friedrich, J. F. (2000). Chemically well-defined surface functionalization of polyethylene and polypropylene by pulsed plasma modification followed by grafting of molecules. In: *Polymer surface modification: Relevance to adhesion*, Vol. 2, pp. 45-64, Mittal, K. L. Ed., VSP: Utrecht, ISBN-10 9067643270.

Kato, K.; Uchida, E., Kang, E. T.; Uyama, Y. & Ikada, Y. (2003). Polymer surface with graft chains. *Progr. Polym. Sci.*, Vol. 28, pp. 209-259, ISSN 0079-6700.

Kharitonov, A. P. (2000). Practical applications of the direct fluorination of polymers. *J. Fluor. Chem.,* Vol. 103, pp. 123-127, ISSN 0022-1139,

Lei, J. X.; Li, Q. M.; He, G. J. & Lin, X. H. (2000). Surface graft copolymerization of acryl amide onto BOPP film through corona discharge. *Acta Chim. Sinica*, Vol. 58, pp. 598-600, ISSN 0567-7351.

Mikula, M.; Jakubíková, Z. & Záhoranová, A. (2003). Surface and adhesion changes of atmospheric barrier discharge treated polypropylene in air and nitrogen. *J. Adhes. Sci. Technol.,* Vol. 17, pp. 2097-2110 ISSN 0169-4243.

Moosheimer, U. & Bichler, C. (1999). Plasma pretreatment of polymer films as a key issue for high food packaging. *Surf. Coat. Technol.*, Vol. 116-119, pp. 812-819, ISSN 0257-8972.

Nie, H. Y.; Walzak, M. J. & McIntyre, N. S. (2000). Atomic force study of UV/ozone treated polypropylene film. In: *Polymer surface modification: Relevance to adhesion*, Vol. 2, pp. 377-392, Mittal, K. L. Ed., VSP: Utrecht, ISBN-10 9067643270.

Noeske, M.; Degenhardt, J.; Strudthoff, S. & Lommatzsch, U. (2004) Plasma jet treatment of five polymers at atmospheric pressure: surface modifications and the relevance for adhesion. *Intern. J. Adhes. Adhesives.*, Vol. 24, pp. 171-177, ISSN 0169-4243.

Novák, I.; Krupa, I. & Luyt, A. S. (2004) Modification of the polarity of isotactic polypropylene through blending with oxidized paraffin wax. *J. Appl. Polym. Sci.,* Vol. 94, pp. 529-533, ISSN 1096-4628.

Novák, I. & Florián, S. (2001). Influence of aging on adhesive properties polypropylene modified by discharge plasma. *Polym. Intern.*, Vol. 50, pp. 49-52, ISSN 0959-8103.

Novák, I. & Florián, S. (2004). Investigation of long-term hydrophobic recovery of plasma modified polypropylene. *J. Mater. Sci.*, Vol. 39, pp. 2033-2036, ISSN 0022-2461.

Novák, I. & Chodák, I. (1998). Adhesion of polypropylene modified by corona discharge. *Angew. Makromol. Chem.*, Vol. 260, pp. 47-51, ISSN 0003-3146.

Novák, I. & Florián, S. (1995). Adhesive properties of polypropylene modified by electric discharge. *J. Mater. Sci. Lett.*, Vol. 14, pp. 1021-1022, ISSN 0261-8028.

Novák, I. & Chodák, I. (1995). Effect of grafting on polypropylene adhesive characteristics. *J. Mater. Sci. Let.*, Vol. 14, pp. 1298-1299, ISSN 0261-8028.

Novák, I. (1996). Effect of surface pretreatment on wettability of polypropylene. *J. Mater. Sci. Lett.*, Vol. 15, pp. 1137-1138, ISSN 0261-8028.

Novák, I. & Pollák, V. (1994). Surface modification of polypropylene by chromylchloride. *Angew. Makromol. Chem.*, Vol. 220, pp. 189-197, ISSN 0003-3146.

Novák, I. (1996). Surface properties of polypropylene modified by chromo suphuric acid. *J. Mater. Sci. Let.* 1996, Vol. 15, pp. 693-694, ISSN 0261-8028.

Novák, I. (1995). Increasing of the adhesive properties of polypropylene by surface modification. *Angew. Makromol. Chem.*, Vol. 231, pp. 69-77, ISSN 0003-3146.

Novák, I. & Chodák, I. (2001). Adhesive behavior of UV sensitizer modified low-density polyethylene. *J. Macromol. Sci. - Pure Appl. Chem.*, Vol. 38, pp. 11-18, ISSN 1060-1325.

Novák, I. & Chodák, I. (2001). Adhesive behavior of UV pre-treated polyolefins. In: *Thermoplastics-based blends and composites*, pp. 341-348, Macromol. Symp. Chodák, I.; Lacik, I.; eds., ISSN 1022-1360.

Novák, I. & Chodák, I. (2001). Effect of polypropylene UV modification on adhesion to polar polymers. *Petrol. Coal.*, Vol. 43, 27-28, ISSN 1337-7027.

OHare, L.A.; Leadley, S. & Parbhoo, B. (2002). Surface physicochemistry of corona-discharge treated polypropylene film. *Surf. Interface Anal.*, Vol. 333, pp. 335-342, ISSN 0142-2421.

Pocius, A. V. (1997). The surface preparation of adherends for adhesive bonding. In: Adhesion and adhesives technology. In: *An introduction,* pp. 148-182, Hanser Publ.: Munich, ISBN 3-446-21731-2.

Poncin-Epaillard, F. (2002). Characterization of CO2 plasma and interactions with polypropylene film. *Plasmas Polymers*, Vol. 7, pp. 1-17, ISSN 1084-0184.

Pesetskii, S.S.; Jurkowski, B.; Krivoguz, Y. M. & Kelar, K. (2001). Free-radical grafting of itaconic acid onto LDPE by reactive extrusion: I. Efect of initiator solubility. *Polymer*, Vol. 42, pp. 469-475, ISSN 0032-3861.

Ráhel, J.; Šimor, M.; Černák, M.; Štefečka, M.; Imahori, Y. & Kando, M. (2003). Hydrophilization of polypropylene nonwoven fabric using surface barrier discharge. *Surf. Coat. Technol.*, Vol. 169, pp. 604-608, ISSN 0257-8972.

Rätzsch, M.; Arnold, M.; Borsig, E.; Bucka, H. & Reichelt, N. (2002). Radical reactions on polypropylene in the solid state. *Progr. Polym. Sci.*, Vol. 27, pp. 1195-1282, ISSN 0079-6700.

Scarlatti, V.; Oehr, C.; Diegelmann, C. & Lobman, P. (2004). Influence of plasma functionalization of polypropylene with acrylic acid on the nucleation of $CaCO_3$. *Plasma Processes Polym.*, Vol. 1, pp. 51-56, ISSN 1612-8850.

Shenton, M. J.; Lovell-Hoare, M. C. & Stevens, G. C. (2001) Adhesion enhancement of polymer surfaces by atmospheric plasma treatment, *J. Phys. D:*, Vol. 34, pp. 2754-2760, ISSN 0022-3727.

Shi, D.; Yang, J. ; Yao, Z., Wang, Y., Huang, H.; Jing, W.; Yin, J. & Costa, G. (2001). Functionalization of isotactic polypropylene with maleic anhydride by reactive extrusion: mechanism of melt grafting. *Polymer*, Vol. 42, pp. 5549-5557, ISSN 0032-3861.

Strobel, M.; Jones, V.; Lyons, C.S.; Ulsh, M., Kushner, M. J.; Dorai, R. & Branch, M. C. (2003) A comparison of corona-treated and flame-treated polypropylene films. *Plasmas Polymers*, Vol. 8, pp. 61-95, ISSN 1084-0184.

Strobel, M.; Jones, V.; Lyons, C. S.; Ulsh, M.; Kushner, M. J.; Dorai, R. & Branch, M. C. (2003). A comparison of corona-treated and flame-treated polypropylene films. *Plasmas Polymers*, Vol. 8, pp. 61-95, ISSN 1084-0184.

Schultz, J. & Nardin, M. (1994). Theories and mechanism of adhesion. In*: Handbook of adhesive technology,* pp. 19-34, Pizzi, A.; Mittal, K. L; eds.; Marcel Dekker, New York, ISBN 10 0824789741.

Sun, C.; Zhang, D. & Wadsworth, L. C. (1999). Corona treatment of polyolefin films – A rewiev. *Adv. Polym. Technol.*, Vol. 18, pp. 171-180, ISSN 1098-2329.

Sulek, P.; Knaus, S. & Liska, R. (2001). Grafting of functional maleimides onto oligo- and polyolefins. *Macromol. Symp.*, Vol. 176, pp. 155-165, ISSN 1521-3900.

Štefečka, M.; Kando, M.; Matsuo, H.; Nakashima, Y.; Koyanagi, M.; Kamiya, T. & Černák, M. (2004). Electromagnetic shielding efficiency of plasma treated and electroless metal plated polypropylene nonwoven fabrics. *J. Mater. Sci.*, Vol. 39, pp. 2215-2217, ISSN 0022-2461.

Štefečka, M.; Kando, M.; Černák, M.; Korzec, D.; Finantu-Dinu, E. G.; Dinu, G. L. & Engemann, J. (2003). Spatial distribution of surface treatment efficiency in coplanar barrier discharge operated with oxygen-nitrogen gas mixtures. *Surf. Coat. Technol.*, Vol. 174, pp. 553-558, ISSN 0257-8972.

Tao, G.; Gong, A.; Lu, J.; Sue, H. J. & Bergbreiter, D. E. (2001). Surface functionalized polypropylene: synthesis, characterization and adhesion properties. *Macromolecules*, Vol. 34, pp. 7672-7679, ISSN 0024-9297.

Vasconcellos, A. S.; Oliveira, J. A. P. & Baumhardt-Neto, R. (1997). Adhesion of polypropylene treated with nitric and sulfuric acid. *Eur. Polym. J.*, Vol. 33, pp. 1731-1734, ISSN: 0014-3057.

Yalizis, A.; Pirzada, S. A. & Decker, W. (2000). A novel atmospheric plasma system for polymer surface tretment. In: *Polymer surface modification: Relevance to adhesion*, pp. 65-76, Mittal, K. L. Ed., VSP: Utrecht, ISBN-10: 9067643270.

Yamada, K.; Takeda, S. & Hirata, M. (2003). Auto-hesion of polyethylene plates by the photo induced grafting of methacryl amide. *A.C.S. Symp. Ser.*, Vol. 847, pp. 511-521, ISSN: 0097-6156.

Yang, P.; Deng, J. Y. & Yang, W. T. (2003). Confined photo-catalytic oxidation: a fast surface hydrophilic modification method for polymeric materials. *Polymer*, Vol. 44, pp. 7157-7164, ISSN: 0032-3861.

10

Influence of Low Pressure on the Stability of Polypropylene Electrets Films

Asya Viraneva, Temenuzhka Yovcheva and Georgi Mekishev
University of Plovdiv, Department of Experimental Physics
Bulgaria

1. Introduction

Electret is an important cross-scientific subject of dielectric physics, material science, sensor engineering, medical and bio-engineering (Sessler G., Sessler et al., Nalwa H., Goel M.). Over the years, considerable interest has been shown in the surface potential decay of corona-charged polymeric materials. Besides the electrets material and conditions of producing electrets the surface potential decay depends on number of factors under which the electrets have been stored or used, for example temperature, humidity, pressure etc. (Zhongfu et al., Gang-Jin et al., Ribeiro et al.).

The pressure effect has been investigated in number of papers. But there are only a few papers dealing with the influence of pressure lower than atmospheric on the electrets behaviour (Shepard et al., Wild et al., Gubkin et al., Draughn et al., Palaia et al., Mekishev et al., 2003, Mekishev et al., 2005). Moreover, the conclusions which have been made are contradictory. Some of the authors assume that charge decay is a result of sparking breakdown in the air according to Paschen's low and the others assume ions desorption from electret surface. Sheppard and Stranathan (Shepard et al.) investigated the effect of ambient pressure on the electret charge of thermoelectrets and showed that in the region of a few torr to 200 torr the charge of electrets increases proportionally to pressure. The linear dependence of the surface charge on pressure is in keeping with Henry's law of adsorption (Adamson et al.). Analogous linear dependence of electret surface potential on pressure in the range of 20 torr to 200 torr is observed in (Mekishev et al., 2003).

Wild and Stranathan (Wild et al.) studied the influence of external treatments on carnauba wax electret behaviour including the pressure effect in a wide range of pressures ranging from 10^{-5} torr to 3000 torr. Except for the plateaus at both low and high pressures, the curve obtained is similar to the curve of the sparking potential of air versus the logarithm of air pressure. Draughn and Catlin (Draughn et al.) investigated the effect of low pressure on surface charge of polystyrene and mylar electrets. All samples were stored with their surfaces exposed to the environment, i.e. unshielded. Authors conclude that the decrease in effective surface charge observed when electrets are exposed to low pressure is not the result of a spark breakdown between the electret surface and nearby conductors. The data indicate that the charge drops are due to ion desorption. After a discussion by B. Gross (Gross B.), Palaia and Catlin (Palaia et al.) investigated again the behaviour of oriented

polystyrene film and mylar electrets at low pressure. The results were found to be as predicted by the spark breakdown theory. It should be noted that in the papers referred above the method of dissectible capacitor was used to measure the effective surface charge. In (Mekishev et al., 2003, Mekishev et al., 2005) the electrets surface potential was measured by the vibrating-electrode method with compensation. The measurement system was located in a chamber connected to a vacuum pump and a vacuum gauge to measure the pressure in the chamber. After charging, the samples were placed in the measurement system and the initial electrets surface potential was measured. Then the pump produced low pressure, and the electrets surface potential vs storage time relationship at various pressure (20, 50, 100, 200 and 300 Torr) was measured for 1 h. It was shown (Mekishev et al., 2003) that the dependence of the surface potential on pressure is described by an equation which is analogous to the Langmuir law of adsorption. Furthermore, it was found in (Mekishev et al., 2005) that the time dependence of the electret surface potential at various pressures is described well by the differential equation for desorption. The authors proposed that ions desorption from the electret surface is most likely to occur. Polypropylene (PP) is one of the polymers, which has been widely used for preparing electrets, because of its excellent dielectric properties (Ono et al., Mohmeyer et al.).

The present paper reports the results of investigations on the low pressure effect on the behaviour of corona charged PP electrets. The PP films are charged in a positive or a negative corona at different charging temperatures: T=20^{o}C and T=90^{o}C. In the vacuum chamber some electrets were stored between two plate shorted electrodes with various air gaps and the other ones were put only onto a metal electrode. The time and temperature dependences of the surface potential of electrets were also studied.

2. Experimental

2.1 Used material and sample preparation

In the present paper isotactic PP films with thickness of 20μm produced by "Assenova Krepost" LTD – Bulgaria were investigated. Initially, the PP films were cleaned in an ultrasonic bath with alcohol for 4 minutes then washed in distilled water and dried on filter paper under room conditions. Samples of 30mm diameter were cut from the films. All the samples were put onto the same diameter metal pads.

2.2 Corona charging and surface potential measurement of the samples

The charging of the samples in a corona discharge was carried out by means of a conventional corona triode system (Jeda et al.) consisting of a corona electrode (needle), a grounded plate electrode and a grid placed between them – Fig. 1. The distance between the corona electrode and the grid was 10mm and the grid to grounded plate electrode distance was 3mm.

The samples 1 together with their metal pads were placed on the grounded plate electrode 4 and were charged for 1 minute at different charging temperatures (T=20^{o}C and T=90^{o}C). Positive or negative 5kV voltage was applied to the corona electrode 2. Voltages of the same polarity as that of the corona electrode from a power supply NB-825 were applied to the grid 3 and their values were 350V, 500V, 650V, 800V and 950V respectively. Electrets surface

potential was measured by the method of the vibrating electrode with compensation (Reedyk et al.) by which the estimated error was better than 5%.

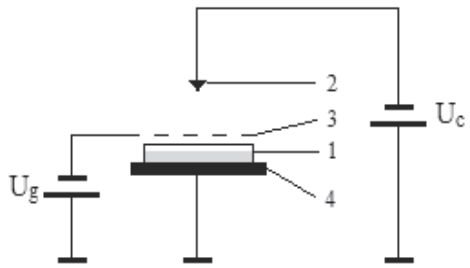

Fig. 1. Arrangement of the corona charging set-up.
1 – sample on a metal pad; 2 – corona electrode; 3 – grid; 4 – grounded plate electrode; U_g – grid voltage power supply; U_c –corona voltage power supply.

2.3 Low pressure treatment

After measuring the initial surface potential V_0, the samples, together with their metal pads, were placed for 30 minutes in a vacuum chamber under various low pressures.

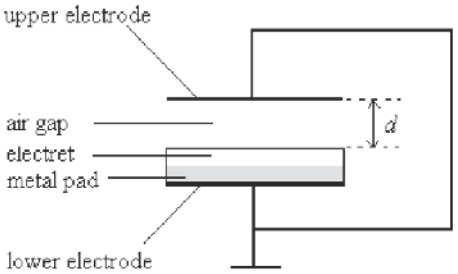

Fig. 2. Schematic diagram of the electret storage in the vacuum chamber between two short circuited plate electrodes (d is the air gap thickness).

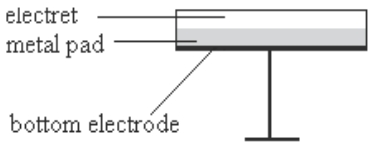

Fig. 3. Schematic diagram of the electret storage in the vacuum chamber in the absence of a second electrode.

The pressures in the vacuum chamber were 0.1mbar, 1mbar, 10mbar, 20mbar, 66mbar, 132mbar and 1000mbar. In the vacuum chamber the electrets were placed between two short circuited plate electrodes (Fig. 2) or deposited on metal pads in the absence of a second electrode (Fig. 3). After removing the electrets from the vacuum chamber, their surface potentials V were measured again and the normalized surface potentials V/V_0 were calculated.

3. Results and discussion

3.1 Results

3.1.1 Influence of the type of electrode

Two groups of experiments were carried out. The first group samples were non-metalized and placed on metal pads and the ones from the second group – metalized on one side. All samples were corona charged to the initial value of about 660V for the surface potential. The samples were then placed in a vacuum chamber at pressure of 0.1mbar for 30 minutes. The results obtained are presented in Table 1, where V_0 is the initial surface potential and V is the surface potential measured just after the samples were taken out of the vacuum chamber.

Samples	Surface potential		V / V_0
	Just after charging, V_0, V	After storage at 0.1mbar for 30 min., V, V	
Non-metalized	655±7	186±6	0.28±0.01
One-side metalized	671±7	189±7	0.28±0.01

Table 1. Surface potential for PP samples stored at pressure of 0.1mbar.

The results displayed in Table 1 show that the one-side metalized samples do not behave differently, compared with the non-metalized and placed on metal pads ones. In both cases the normalized surface potential decreases to about 0.28.

3.1.2 Charging time influence

The influence of the charging time on the surface potential of the electrets was studied. For that purpose the PP samples were corona charged using a three-electrode system (Fig. 1) at different charge time t_{ch} – 1, 5, 10, 20 and 30 minutes. The voltage U_c = -5kV was applied to the corona electrode and U_g = -650V to the grid.

Charging time, min.	V_0, V
1	657±7
5	664±6
10	660±6
20	650±5
30	648±9

Table 2. Surface potential of PP samples at different values for the charging time.

After the charging the initial surface potential V_0 of the samples was measured by the vibrating electrode method with compensation (Reedyk et al.). The measured surface potential values are presented in Table 2. The results obtained show that the charging time to 30 minutes does not influence the surface potential of the PP films.

3.1.3 Influence of the storage time under low pressure

The influence of sample storage time in the vacuum chamber on the surface potential decay was studied. For this purpose the samples were corona charged (Fig. 1) at a corona voltage of U_c = -5kV and a grid voltage of U_g = -650V. The initial surface potential V_0 was measured by the vibrating electrode method with compensation. Then the samples were placed in a vacuum chamber at a pressure of 0.1mbar at different time periods - 1, 15, 30 and 60 minutes. After the samples being taken out of the vacuum chamber their surface potential V was measured again. The results obtained are presented in Table 3.

Storage time at 0.1mbar, min.	Surface potential		V / V_0
	V_0, V	V, V	
1	642±9	187±21	0.29±0.04
15	639±9	184±18	0.29±0.03
30	648±5	172±5	0.27±0.01
60	646±4	177±20	0.27±0.03

Table 3. Surface potential of PP samples at different values of storage time, at 0.1 mbar.

It can be seen from the results in the table that the surface potential decreases within the first minute and that further storage at the reduced pressure does not bring any change. Based on the results obtained in parts 3.1.1, 3.1.2, 3.1.3 the next experiments were carried out with non-metalized samples being charged for a minute in a positive or a negative corona and being stored in the vacuum chamber for 30 minutes (for greater security).

The published papers discuss two main processes causing electret discharge at low pressure - sparking breakdown in air according to Paschen's law and ions desorption from electret surface. In order these processes to be studied two groups of experiments with different samples bonding were carried out. In the vacuum chamber the electrets were placed between two short circuited plate electrodes (Fig. 2) or deposited on metal pads in the absence of a second electrode (Fig. 3). The time and temperature dependences for the surface potential of polypropylene electrets charged in a negative corona at room temperature and temperature of 90°C were also studied.

3.1.4 Electrets obtained in a corona charging and stored at low pressures between two short-circuited plate electrodes with various air gaps between the electrodes

All the samples were divided in five groups according to the thickness of the air gap. Each group was split into five series depending on the value of the initial surface potential.

The samples prepared were corona charged at room temperature by the three-electrode system (Fig. 1). Negative 5kV voltage U_c was applied to the corona electrode and to the grid – negative voltage U_g of 350V, 500V, 650V, 800V and 950V respectively. The electrets were thereby charged to different values of the initial surface potential V_0. After the samples were corona charged their initial surface potential was measured. Then the samples together with their metal pads were placed between two short-circuited flat electrodes, at a different thickness of the air gap (d – 0.10mm, 0.28mm, 0.84mm, 1.69mm and 3.00mm). The system

obtained in that way was stored in a vacuum chamber for 30 minutes at various low pressures - 0.1mbar, 1mbar, 10mbar, 20mbar, 66mbar, 132mbar and 1000mbar. For each of these pressures, after taking the samples out of the vacuum chamber their surface potential V was measured again. Normalized surface potential V / V_0 vs normalized pressure p / p_0 for negatively charged PP samples stored at two air gaps - d =0.10mm and d =3.00mm respectively - are presented in Fig. 4 and Fig. 5.

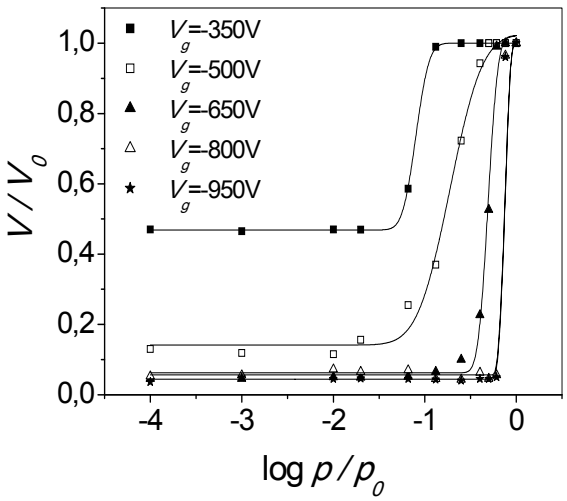

Fig. 4. Dependence of the normalized surface potential on normalized pressure for negatively charged PP samples. The air gap is d =0.10mm.

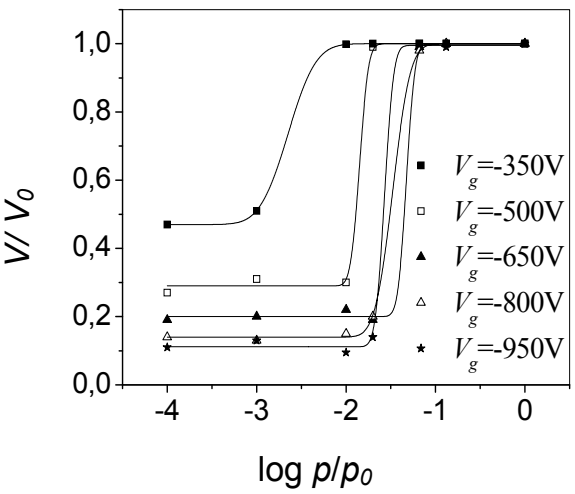

Fig. 5. Dependence of the normalized surface potential on normalized pressure for negatively charged PP samples. The air gap is d = 3.00mm.

Each figure point corresponds to an average value obtained by the measurement of 6 samples. The maximum deviation from the average values determined at confidence level

95% is 5%. The V_0 symbol stands for the initial value of the surface potential measured just after the samples charging and p_0 is the atmospheric pressure.

Analogous dependences were obtained for the other air gap values.

The results presented in Fig. 4 and Fig. 5 show the following features:

- For each curve three parts are observed. At high pressures the normalized surface potential stays constant and close to one (i.e. the surface potential at high pressures is approximately equal to the initial surface potential); at low pressures V / V_0 is also constant, however, with much lower values. For all the values of the initial surface potential, i.e. for all the series of samples there is a range of pressures within which the surface potential V_0 sharply decreases.
- The higher the initial surface potential, the higher the pressure at which the sharp decrease takes place, i.e. as the initial surface potential grows the curves are displaced to the right.
- With the increase of the air gap the decrease range is displaced to the lower pressures.

Table 4 presents the values of the normalized surface potential V / V_0 for samples stored at pressure of 0.1mbar between two short circuited plate electrodes at different thickness values d for the air gap.

U_g, V	V / V_0				
	d_1 =0.10mm	d_2 =0.28mm	d_3 =0.84mm	d_4 =1.69mm	d_5 =3.00mm
-350	0.47	0.44	0.46	0.45	0.47
-500	0.13	0.19	0.25	0.27	0.27
-650	0.05	0.07	0.11	0.14	0.19
-800	0.05	0.06	0.09	0.11	0.14
-950	0.04	0.06	0.07	0.09	0.11

Table 4. Normalized surface potential values V / V_0 (accuracy is better than 5%) for PP samples stored between two short-circuited plate electordes at the pressure of 0.1 mbar ($\log p / p_0 = -4$).

From the results presented in Table 4 the following conclusion can be made:
The final values of the surface potential at 0.1mbar decrease with the increase of the initial surface potential and grow with the increase of the air gap thickness.

3.1.5 Electrets obtained in a corona discharge and stored at low pressures in the absence of a second electrode

Two series of experiments with polypropylene samples were carried out. In the first one, the samples were charged in positive or negative coronas at room temperature, while in the second one they were charged in a positive or a negative corona at temperatures higher than the room one: 75°C and 90°C. The cleaning of the samples, their charging and the measurement of their surface potential were carried out as were described in 3.1.2. The

samples were stored in a vacuum chamber in the absence of a second electrode, i.e. in an air gap tending to infinity.

Normalized surface potential V / V_0 vs normalized p / p_0 pressure for samples charged in a positive or a negative corona respectively at room temperature are presented in Fig. 6 and Fig. 7, while the samples in Fig. 8 and Fig. 9 are charged in a positive or a negative corona respectively at temperature higher than the room one. As the electrets charged at 75°C and 90°C have the same behaviour the only presented results are the ones obtained at 90°C.

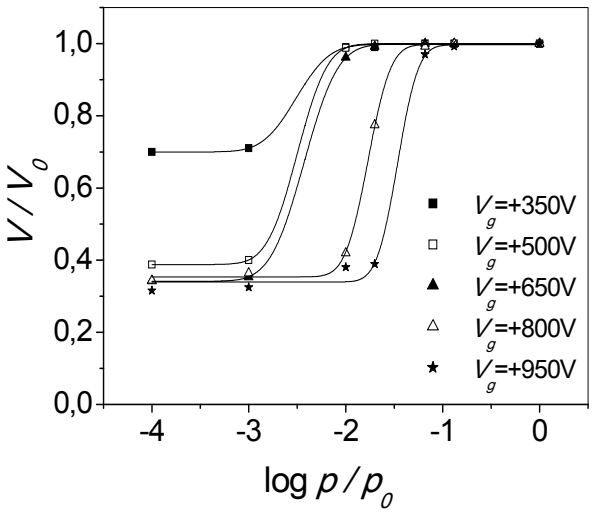

Fig. 6. Dependence of the normalized surface potential on normalized pressure for positively charged PP samples at room temperature. Infinite air gap.

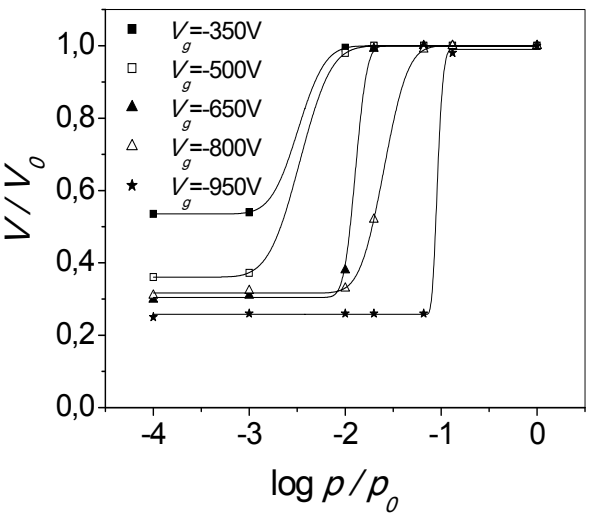

Fig. 7. Dependence of the normalized surface potential on the normalized pressure for negatively charged PP samples at room temperature. Infinite air gap.

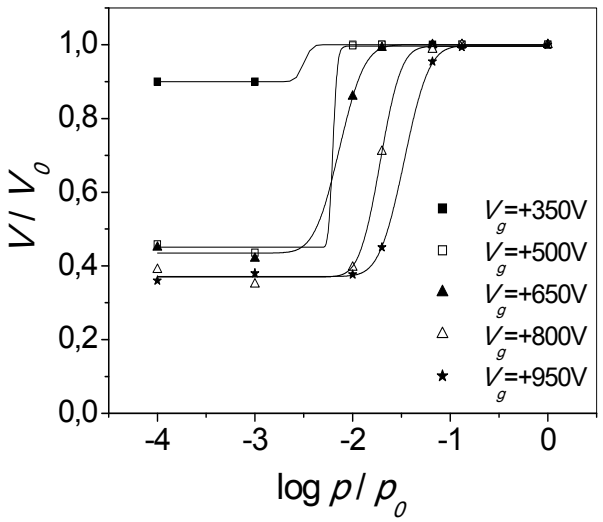

Fig. 8. Dependence of the normalized surface potential on the normalized pressure for positively charged PP samples at 90°C. Infinite air gap.

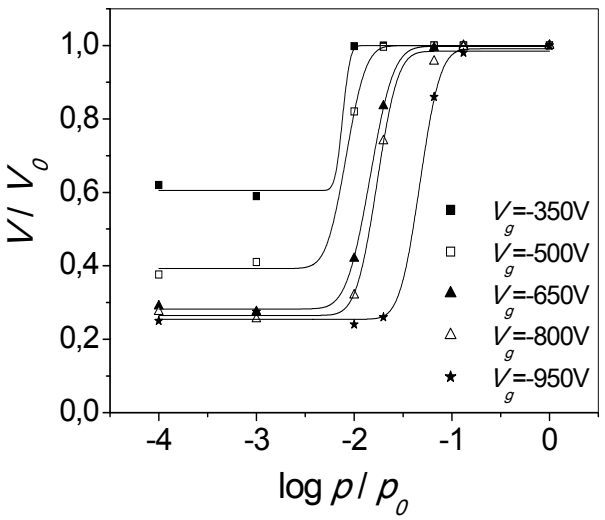

Fig. 9. Dependence of the normalized surface potential on the normalized pressure for negatively charged PP samples at 90°C. Infinite air gap.

Each point corresponds to the average value obtained by the measurement of 6 samples. The maximum deviation from the average values determined at 95% confidence level is 5%.

3.1.6 Time dependence of the surface potential of electrets obtained by corona charging and stored at low pressures in the absence of a second electrode

The storage time dependence on the decrease of the surface potential of PP electrets charged in negative corona at room temperature and at 90°C was studied. Voltage of U_c = -5kV was

applied to the corona electrode and to the grid - U_g = -800V. A part of the electrets obtained was stored at pressure of 0.1mbar for 30 minutes and after they were taken out of the vacuum chamber, their surface potential had been measured for 30 days. The surface potential of the other electrets had been measured in time just after their charging without preliminarily storage at low pressure.

The time dependence of the normalized surface potential for PP samples negatively charged at room temperature is presented in Fig. 10 and in Fig. 11 – for PP samples charged at 90°C.

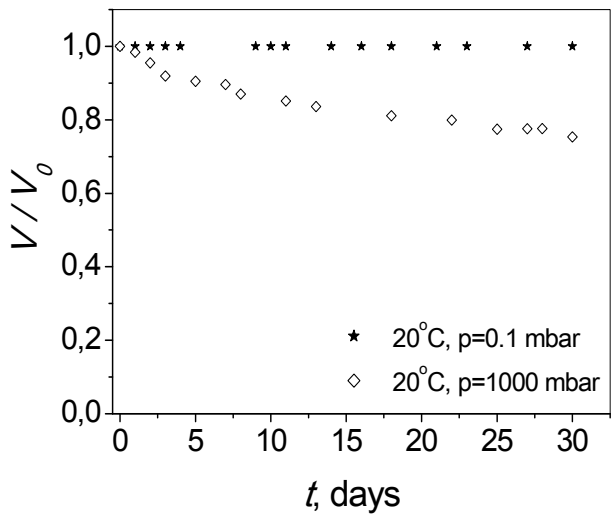

Fig. 10. Time dependence of the normalized surface potential for PP samples negatively charged at room temperature.

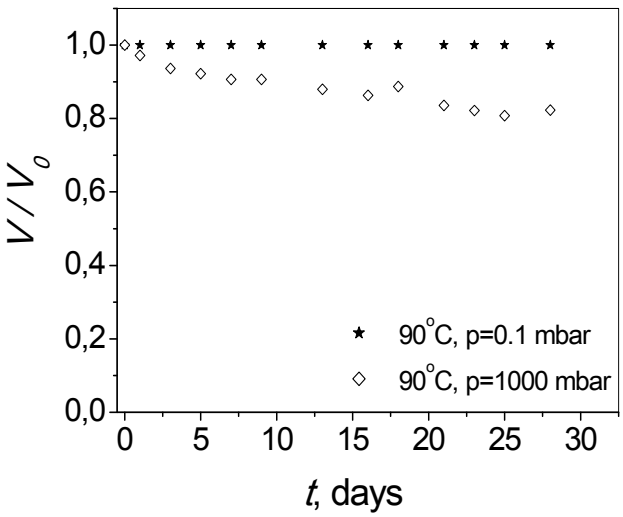

Fig. 11. Time dependence of the normalized surface potential for PP samples negatively charged at 90°C.

For each figure point the measured standard deviation does not exceed 10% of the average value at 95% confidence level.

It was found that:

- For samples preliminarily stored at pressure of 0.1mbar for 30 minutes the surface potential, independently of the charging temperature, does not change over time ;
- For samples which have not preliminarily been charged at low pressure the surface potential value decreases to a certain point over time.

Hence, the preliminarily placement of the electrets at low pressure for a certain period of time can be used as an effective method for stabilizing the electrets charge depending on their applications.

3.1.7 Temperature dependence of the surface potential of corona charged electrets

The dependences of normalized surface potential on the temperature for negatively charged PP films were investigated. Voltage of U_c = -5kV was applied to the corona electrode and to the grid - U_g = -500V. A part of the electrets was charged at room temperature and the other electrets – at temperature 90°C. The electrets obtained were preliminary stored for 30 minutes at two different pressures (0.1mbar and 1000mbar). After that the dependences of normalized surface potential on the temperature was measured.

The dependences of normalized surface potential on the temperature for negatively charged PP films are presented in Fig. 12.

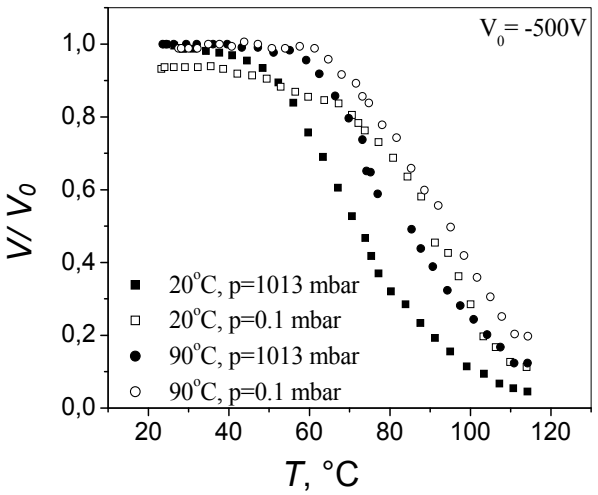

Fig. 12. Temperature surface potential decay curves after negative corona charge.

The results show that the curves of the samples which were preliminary stored at low pressure are shifted slightly to higher temperature as the shallow traps are liberated and the curves (Fig. 12) are shifted to higher temperature. When the temperature increases, the transport processes through the bulk will play a determinant role because of the increase of the injection of the carriers from the surface into the bulk and generating carriers in the bulk and the increase of their mobility.

3.2 Discussion

It is typical feature for the electret transducers that in most cases the electret is one-side metalized and is placed between two plate electrodes short-circuited by a resistor. The charged electret surface gives rise to an electric field in the air gap which is formed between the non-metalized electret surface and its adjacent electrode. This field can be found by an equation analogous to the one in (Palaia et al.):

$$E = \frac{\varepsilon V}{\varepsilon d + \varepsilon_1 L}, \tag{1}$$

where E is the air gap field, ε is the electret relative dielectric permeability, ε_1=1 and d are the relative dielectric permeability and thickness of the air gap respectively, L - the electret thickness, V is the electret surface potential.

It is assumed in most of the papers that the electrets charge decay is due to gas discharges in the electret-electrode gap which depend on the gas pressure and the thickness of the gap itself according to Paschen's law (Knoll et al., Schaffert R.).

For dry air the Paschen's curve has a minimum at pd=6.65mbar.mm corresponding to a breakdown voltage of 360V (Schaffert R.). If the air gap field creates a voltage less than the breakdown voltage for the particular gas, gas discharges will not occur in the gap. When the air gap field creates a voltage equal or higher than the breakdown voltage, a discharge will occur and the electret charge will consequently decrease. The discharge will continue until the voltage across the air gap is reduced to a value below the minimum breakdown voltage for the respective value of the product pd and will not depend on both the size and the polarity of the initial electret surface potential as well as on the air gap thickness. Therefore, the minimal voltage value in the gap at which a discharge can be begun is 360V (Schaffert R.).

The values of the fields in and the voltages across the electret-electrode gap calculated for PP samples stored between two short-circuited electrodes with air gap thickness of 0.10mm are presented in Table 5.

Surface potential V, V	400	500	650	800	950
Electric field in the air gap E, kV/cm	36.7	45.9	59.6	73.4	87.1
Voltage in the air gap U, V	367	459	596	734	871

Table 5. Electric fields and voltages in a 0.10mm air gap at different surface potential values.

Analogous calculations have been made for the other gaps used in our experiments. In all cases the voltages in the gaps do not exceed the grid surface potential. At atmospheric pressure and various thicknesses of the air gap used in our experiments the pd values change from $pd_{\min}$ (d = 0.1mm) = 100 mbar.mm to $d_{\max}$ (d = 3mm) = 300 mbar.mm, which corresponds to breakdown voltages higher than 950V. Hence, the calculations show that at atmospheric pressure at different air gap thicknesses d the voltage across the air gap is less than the breakdown voltage according to the Paschen's law (Schaffert R.) for all thicknesses d studied and for all grid voltages U_g. Therefore, there will be no discharge.

When the pressure in the vacuum chamber decreases, the breakdown voltage also decreases, while the voltage across the air gap created by the electret practically does not change. Hence, the voltage across the air gap might be found higher than the one following from the Paschen's law and it may result in a discharge.

At pressure of 0.1mbar and air gap thicknesses from 0.10mm to 3.00mm, the pd product values lay in the (0.01-0.30)mbar.mm interval. These values are much lower than the 6.65mbar.mm value where a minimum of the Paschen's curve is observed and they correspond to a higher breakdown voltage than the minimal one of 360 V. Therefore, the air gap pressure curve will cross the Paschen's curve and the surface potential is expected to decrease to the minimal value of 360V corresponding to pd =6.65mbar.mm. However, the results obtained show that the surface potential has decreased to values considerably lower than the minimal pressure value following the Paschen's law. This can be seen from the curves presented in Fig.13.

The dependence of the minimal value $V_{\min}$ to which the surface potential at pressure 0.1mbar has decreased as a function of the initial surface potential V_0 for the different air gap thicknesses is presented in Fig. 13.

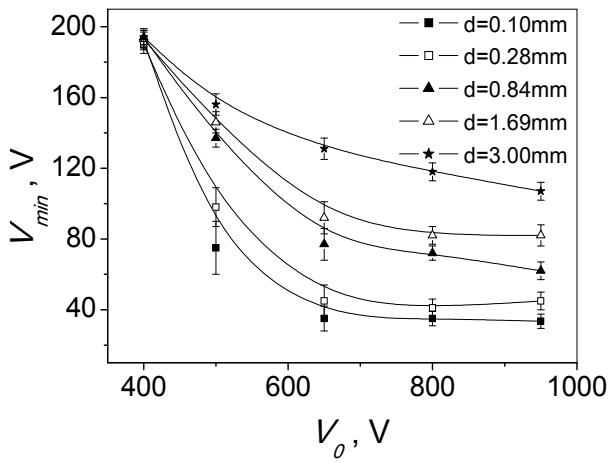

Fig. 13. Dependence of the minimum surface potential $V_{\min}$ on the initial surface potential V_0 at pressure of 0.1mbar for different air gaps.

Each figure point corresponds to an average value obtained by the measurement of 6 samples. The maximum deviation from the average values determined at 95% confidence level is 5%.

It can be seen from Fig. 13 that the surface potential decreases to a value lower than 360V for all values of the initial surface potential and all air gap thicknesses. With the air gap decrease and the initial surface potential increase the minimal value to which the electret surface potential decays is reduced. It decreases to a value of 33.5V at a gap of 0.10mm and initial surface potential 950V. This value of the surface potential corresponds to an electret-electrode gap voltage of 30.7V. This is considerably lower than the minimal value according

to the Paschen's law. On the other hand, it is supposed that as the initial surface potential decreases the minimum surface potential $V_{\min}$ tends to a value approximately equal to an initial surface potential of 300V. Some additional experiments were carried out in order to verify these values. Several series of samples were charged to an initial surface potential of 280V, 300V, 320V and 350V respectively. The electrets were stored at a pressure of 0.1mbar for 30 minutes. The gap between the electret surface and the upper electrode was 0.28mm. It was established that for samples charged to initial values of the surface potential 280V, 300V and 320V the normalized surface potential was 0.98 and for the ones charged to 350V – 0.61. Hence, if the initial surface potential value is approximately 300V, no surface potential decay takes place.

The analysis of the results obtained in different experiments shows that:

- First, discharges depend on the corona polarity and the charging temperature;
- Second, the surface potential decay process is analogous for both samples stored between two short-circuited electrodes with different air gap thicknesses and the ones with the absence of a second electrode;
- Third, the surface potential decreases to a value lower than the minimal breakdown voltage according to the Paschen's law.

If we assume that the charges obtained due to the corona discharge are located on the sample surface, we can calculate the charge surface density by the equation $\sigma = \frac{\varepsilon_0 \varepsilon}{L} U_k$.

When the electret surface potential is 950V then the surface charge density is equal to σ =9.25x10^{-8}C/cm^2. In this case the charges are found to be located at a distance thereabouts 13nm apart. When the electret surface potential is 350V this distance is thereabout 21nm. Therefore, there is a discrete charge distribution on the electret surface and it results in a nonuniform electric field having normal and tangential components, close to the surface (Neugebauer H., Pisanova et al.). At a distance three or four time larger than the distance between the charges, i.e. at a distance not greater than 80nm from the charged surface, the field is in fact homogeneous (Pisanova et al., Feynman et al.).

As it is shown in (Schaffert R.) the distribution of the electric field close to the charged surface is practically the same in both the presence and the absence of a second electrode. These results give an explanation to the similarity found in those cases when the electrets were stored in the absence of a second electrode (Mekishev et al., 2007, Viraneva et al.). It is established (Giacometti et al.) that during the corona discharge in the air, at atmospheric pressure, different types of ions are deposited on a sample while charging in a corona discharge depending on the corona polarity. In the case of a positive corona the ions are mainly $H^+(H_2O)_n$ and the ones for a negative corona - CO^{3-} (Giacometti et al.). Those ions are bound in traps of various depths and are released from them depending on the surrounding conditions. It was found in (Yovcheva et al.) by the X-ray photoelectron spectroscopy method that oxygen content in negatively charged samples is higher than that in positively charged samples. The oxygen content for non-charged samples is intermediate if compared to the values for the negatively and positively charged ones. It is assumed that the different oxygen content in the various cases is in consequence of various sorption processes on the sample surface. These results make us suppose that the main process responsible for the

surface potential decay can be associated with desorption of charged species from the electret surface under the influence of its own electric field. These might be ions deposited on the surface or groups in which the ions have given their charge away.

In the published papers one can see different models for explaining the adsorption (desorption) mechanisms. The experimental results were fitted by the Friondlih and Lengmuir equations in order to estimate how well these models describe the behavior of the surface potential of electrets stored at low pressure. The dependence of the normalized surface potential on the pressure for PP samples charged in negative corona at room temperature and stored between two plate electrodes with air gap thickness 3.00mm is presented in Fig. 14. One can see from Fig. 14 that the equations used do not describe the results obtained well enough. Analogous graphs were plotted for the other gaps (smaller than 3mm). It was established that for smaller gaps the fitting accuracy sharply decreases.

The dependences of the normalized surface potential on pressure for PP samples charged in a negative corona at room temperature and temperature 90°C to the initial surface potential value of 650V and stored in the absence of a second electrode are presented in Figs. 15, 16.

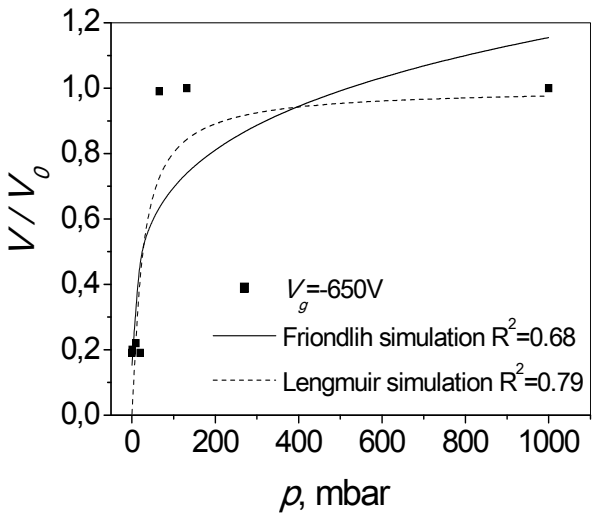

Fig. 14. Dependence of the normalized surface potential on pressure for negatively charged PP samples at temperature of 20°C, fitted by the Friondlih and Lengmuir equations. The air gap thickness is 3.00mm.

Analogous graphs were plotted for the samples charged in a positive corona.

The results presented in Fig.14-16 show that irrespective of the corona polarity and the charging temperature the Friondlih and Lengmuir equations do not describe very well the results obtained in our experiments as the determination factor is $0.36 \leq R^2 \leq 0.85$. That is why we assumed that the desorption process might run together with another process like charge movement along the surface, for example. Our assumption is based on the results reported in various papers (Protodyakonov et al., Baum et al., Karmazova et al., Atkinson et al., 1976, Atkinson et al., 1980, I, Atkinson et al., 1980, II) and some additional experiments we have carried out with electrets with an island charge distribution. It is reported in

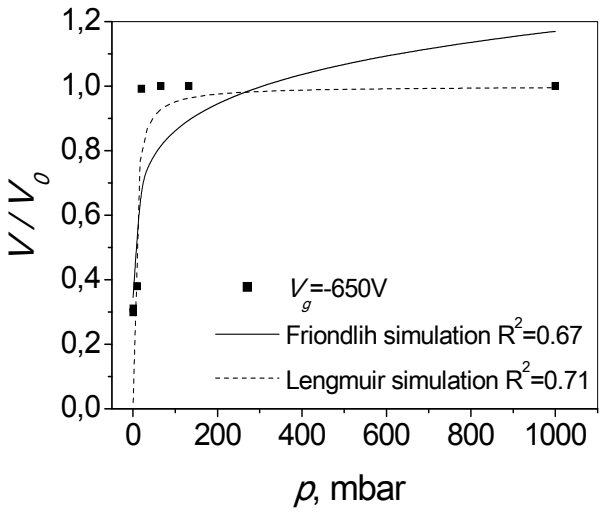

Fig. 15. Dependence of the normalized surface potential on pressure for PP samples charged in negative corona, at 20°C fitted by the Friondlih and Lengmuir equations. Infinite air gap.

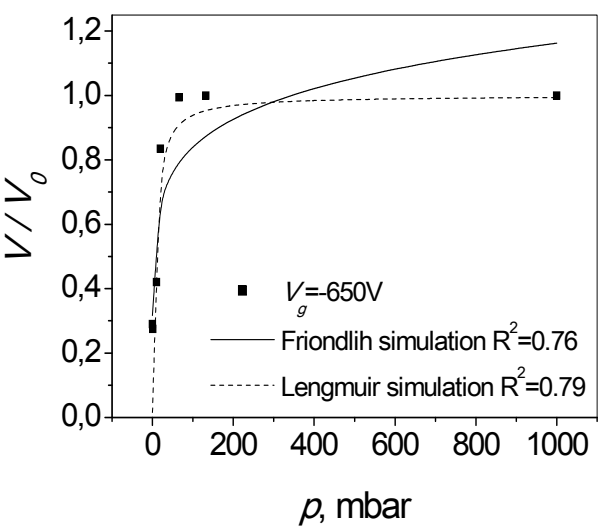

Fig. 16. Dependence of the normalized surface potential on pressure for PP samples charged in negative corona at 90°C, fitted by the Friondlih and Lengmuir equations. Infinite air gap.

(Protodyakonov et al.) that under certain conditions the adsorbate molecules located on the surface can be transferred along the surface without leaving it. The paper (Karmazova et al.) studies the influence of storage time on the surface potential decay for PP and PTFE samples with uniform and island charge distribution charged in corona discharge at room temperature and atmospheric pressure. It is shown that for samples with island charge distribution the surface potential decay is much smaller than for the ones with uniform charge distribution.

We carried out an experiment analogous to the one described in (Karmazova et al.): to charge PP samples in positive or negative corona we used a set-up for obtaining an island charge distribution described in (Karmazova et al.).

This set-up contains a grounded plate electrode, a metal mask (instead of a grid) with a numerous apertures of a definite size and distribution of the apertures and a corona electrode (a needle). The metal mask functions as a control electrode. During the charging process the polymer film was placed on the grounded plate electrode and the mask with the apertures was put on the film. The voltage U_c =±5kV was applied to the corona electrode and U_g =±650V – to the metal mask. The shape, the size and the distribution of the apertures in the mask define the shape, the size and the distribution of the charge on the electret surface (Fig.17).

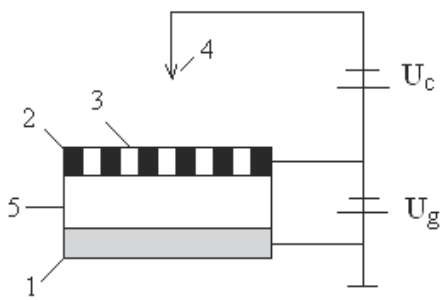

Fig. 17. Set-up for obtaining electrets with island charge distribution: 1 – grounded plate electrode; 2 – metal mask; 3 – apertures; 4 – corona electrode; 5 – electrets; U_c - corona voltage; U_g - metal mask voltage.

After obtaining the electrets the metal mask was removed from the charged film. The electret surface potential was measured by the method of vibrating electrode with compensation. Then the electrets were placed in a vacuum chamber for 30 minutes at various low pressures. After the samples were taken out of the vacuum chamber, their surface potential was measured again and the normalized surface potential V / V_0 was calculated. The dependence of the normalized surface potential V / V_0 on the normalized pressure p / p_0 for PP samples with island charge distribution is presented in Fig. 18.

Each graph point corresponds to the average value obtained by the measurement of 6 samples. The maximum deviation from the average values determined at 95% confidence level is 5%. The results for samples with island charge distribution stored at pressure of 0.1mbar are compared to the ones for samples with uniform charge distribution. These results are presented in Table 6.

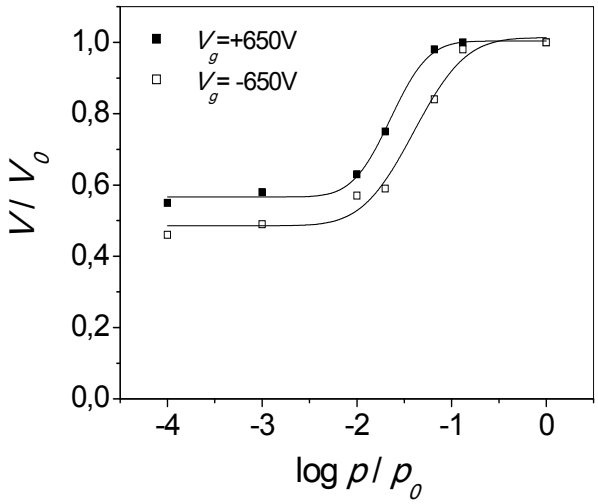

Fig. 18. Dependence of the normalized surface potential on normalized pressure for PP samples with island surface charge distribution.

Grid voltage	V / V_0	
	Uniform charge distribution	Island charge distribution
+650V	0.34	0.55
-650V	0.30	0.46

Table 6. Normalized surface potential V/V_0 values (with an error not exceeding 5%) for samples charged in positive or negative corona with uniform or island surface charge distribution. The samples were stored at pressure of 0.1mbar with the absence of a second electrode.

One can see from the table that when the samples were stored at pressure of 0.1mbar for 30 minutes the ones with an island charge distribution have higher surface potential values than the samples with uniform charge distribution, independent of the corona polarity. These results show that the assumption for the movement of the charges on surface seems completely plausible. The absorption and resorption currents in FEP teflon samples with 4.475 cm diameter are investigated in (Atkinson et al., 1976). One of the sample surfaces is completely metalized and an aluminum electrode with diameters ranging from 0.32cm to 2.54cm is evaporated in the central part of the second surface. The surface completely metalized is usually grounded and a definite voltage is applied to the upper electrode. It is established that there is a charge movement on the polymer surface between the metal electrode end and the non-metalized polymer surface. This movement is the main component of the absorption and resorption currents. The surface components of the absorption and resorption currents in vacuum for different polymers were later studied in (Atkinson et al., 1980 I). It was established for FEP teflon, polystyrene, polytetrafluorethylene and polythene that the charge movement along the polymer surface is the main component of these currents. Baum and coauthors were studied the surface

charge decay in PET films (Baum et al.). Using a corona discharge (positive or negative corona) a charged spot with a diameter of 0.5cm is created on one of the surfaces. It is established that the charges deposited by the corona source move laterally according to a diffusion law. The time dependence of the absorption currents is deduced in (Atkinson et al., 1980 II) on the assumption that these currents are entirely due to the transverse movement of charges caused by a concentration gradient of charge carriers. An equation combining linear desorption with surface diffusion is proposed for the description of some desorption processes in (Keltzev N.).

Our experimental results are well described by an equation analogous to the one in (Keltzev N.).

$$\theta = a + \frac{1}{2} b \left(1 + erf\left(\frac{x-c}{\sqrt{2}d} \right) \right), \tag{2}$$

where $\theta = V/V_0$ is the normalized surface potential, $x = p / p_0$ is the normalized pressure and a, b, c and d are constants depending on the charging conditions. Values of the parameters a, b, c and d for PP samples charged in positive or negative corona to an initial surface potential value of 800V are presented in Table 7.

Corona polarity	a	b	c	d
positive	0.3536± 0.0065	0.6439± 0.0085	-1.7702± 0.0076	0.1809± 0.0109
negative	0.3167± 0.0034	0.6835± 0.0053	-1.5964± 0.0088	0.1932± 0.0143

Table 7. Values of the parameters a, b, c and d obtained by fitting the equation 2.

The equation (2) is analyzed by using the $erf\left(\frac{x-c}{\sqrt{2}d} \right)$ values for different cases (Abramovich et al.). It should be noted that $d > 0$.

Case 1: $\left| \frac{x-c}{\sqrt{2}d} \right| >> 1$

a. $x - c > 0$

In this case $erf\left(\frac{x-c}{\sqrt{2}d} \right) = 1$ and from equation (2) it follows that: $\theta = a + b$ = const

Therefore, at high values of the ratio p / p_0, $\theta = a + b = 1$ and the surface potential practically remains equal to the initial surface potential, i.e. $V \approx V_0$. In this interval of the ratio p / p_0 no changes of the surface potential are observed.

b. $x - c < 0$

In this case $erf\left(\frac{x-c}{\sqrt{2}d} \right) = -1$ and from equation (2) it follows that:

$$\theta = a = const$$

Therefore, if $x < c$, the surface potential remains constant. Then the parameter a has the meaning of the minimum value of the normalized surface potential and b is the difference between the maximum and minimum values of the normalized surface potential.

Case 2: $\left|\frac{x-c}{\sqrt{2}d}\right| << 1$

In this case $erf\left(\frac{x-c}{\sqrt{2}d}\right)$ develops into a series and only the first linear term from the expansion can be considered:

$$erf\left(\frac{x-c}{\sqrt{2}d}\right) = \frac{2}{\sqrt{\pi}}\frac{x-c}{\sqrt{2}d}$$

and from equation (2) a linear dependence of θ on x is obtained:

$$\theta = A + Bx$$

where $A = a + \frac{b}{2} - \frac{bc}{\sqrt{2\pi}d}$ and $B = \frac{b}{\sqrt{2\pi}d}$.

If $x = c$, $erf\left(\frac{x-c}{\sqrt{2}d}\right) = 0$ and from equation (2) it follows that: $\theta = a + \frac{b}{2}$

Therefore, c is the midpoint of the range p / p_0 , within which the surface potential decay occurs.

When $x = c \pm \sqrt{2}d$, $erf\left(\frac{x-c}{\sqrt{2}d}\right) = \pm 0.843$, i.e. the decay range for the normalized surface potential is $\left(c - \sqrt{2}d, c + \sqrt{2}d\right)$.

All curves presented in Fig. 4-9 are described very well by equation (2) with a coefficient of determination $0.98 \le R^2 \le 1.00$. It was established that charging the electrets to various surface potential values leads to a curve displacement. The higher the initial surface potential the higher the pressure at which the sharp decay occurs. Therefore, there are two factors that influence the surface potential decay – the pressure at which the electrets have been stored and the initial surface potential to which they have been charged. The ratio p / V_0 is the main factor determining the surface potential decay range. Therefore, each group of experiments can be described by a generalized curve.

The dependences of the normalized surface potential V / V_0 on the normalized ratio $\left(p/V_0\right)^* = \left(p/V_0\right)\left(p_0/V_0^*\right)^{-1}$ for positively and negatively charged PP samples are presented in Fig. 19 and Fig. 20.(Mekishev et al., 2005)

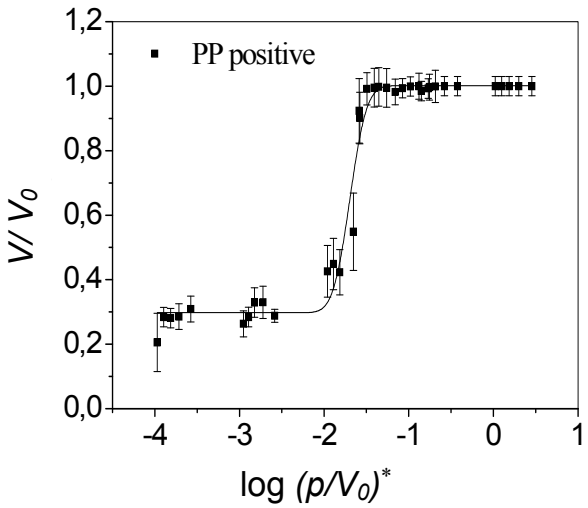

Fig. 19. Dependence of the normalized surface potential V / V_0 on the normalized ratio $(p/V_o)^*$ for positively charged PP samples.

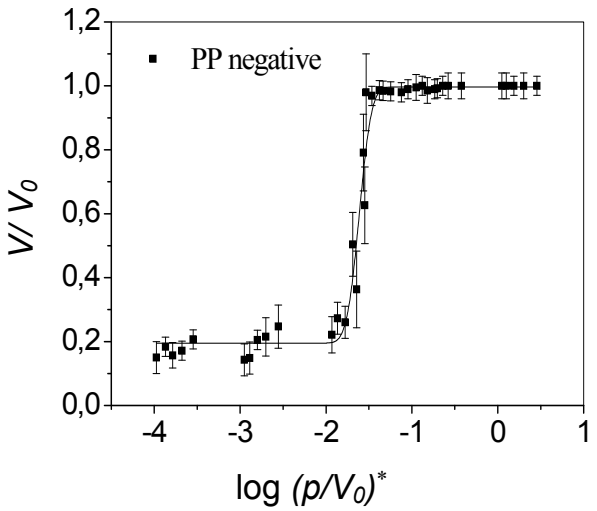

Fig. 20. Dependence of the normalized surface potential V / V_0 on the normalized ratio $(p/V_o)^*$ for negatively charged PP samples.

The symbol p_0 stands for the atmospheric pressure and $V_0^* = 1000$ V. For each graph point (Fig. 19, 20) the calculated standard deviation does not exceed 10% of the average value at 95% confidence level. It must be noted that the errors are smaller within the higher values of the normalized ratio $(p/V_o)^*$ and are higher in the range of the sharp decay.

It was found out that the results obtained can be described by an equation analogous to equation (2). The results presented so far are described very well with a coefficient of determination $0.98 \le R^2 \le 1.00$ by the following equation:

$$\theta = a^* + \frac{1}{2} b^* \left(1 + erf\left(\frac{x^* - c^*}{\sqrt{2} d^*} \right) \right), \quad (2a)$$

where $\theta = V/V_0$ is the normalized surface potential, $x^* = \log\left(p/V_0\right)^* = \log\left[\left(p/V_0\right).\left(p_0/V_0^*\right)^{-1} \right]$ and a^*, b^*, c^* and d^* are constants depending of the charging conditions. Values of this parameters for positively and negatively charged PP samples are presented in Table 8.

Corona polarity	a^*	b^*	c^*	d^*
positive	0.2977± 0.0153	0.7037± 0.0196	-1.6949± 0.0176	0.1508± 0.0214
negative	0.1950± 0.0167	0.8017± 0.0218	-1.6145± 0.0111	0.1051± 0.0159

Table 8. Values of the parameters a^*, b^*, c^* and d^* obtained by fitting the PP results by equation 2a.

It is seen from the results presented in Fig. 19, 20 and Table 8 that the minimum value of the surface potential after the sharp decrease is higher for the positively charged samples (higher values of parameter a^*). The values of the ratio p/V_0 for the midpoint of the region of the sharp surface potential decay were calculated using the values of parameter c^* from Table 8. The following values were obtained: 0.019mbar/V and 0.024mbar/V for the positively and negatively charged PP samples. Therefore, the ratio p/V_0 for the midpoint of the region, within which the sharp surface potential decay occurs, allows calculating the pressure at which the sharp electret surface potential decay will be observed if their initial surface potential is known.

4. Conclusion

The influence of low pressure on the behaviour of corona charged PP electrets was studied. The PP films were charged in a positive or a negative corona at different charging temperatures of T=20°C and T=90°C and were stored in a vacuum chamber under various low pressures. It was found that the charging time of 30 minutes does not influence the surface potential of the PP films. It was established that the surface potential decreases within the first minute and that further storage at the reduced pressure does not bring any change.

The analysis of the results obtained in different experiments shows that:

First, the surface potential decay depends on the corona polarity and the charging temperature; Second, the surface potential decay process is analogous for both samples stored between two short-circuited electrodes with different air gap thicknesses and the ones with the absence of a second electrode; Third, the surface potential decreases to a value lower than the minimal breakdown voltage according to the Paschen's law.

It is supposed that the main process responsible for the surface potential decay can be associated with desorption of charged species from the electret surface under the influence

of its own electric field accompanied by surface diffusion. An equation combining linear desorption with surface diffusion is proposed for the description of the surface potential decay. This equation described very well the results obtained with a coefficient of determination $0.98 \leq R^2 \leq 1.00$. It is proposed a generalized curve describing the dependence of normalized surface potential on the ratio p / V_0. From this curve it is possible to calculate pressure at which sharp decay will occur if the dependence of the surface potential on the pressure and the initial surface potential are known.

The preliminarily placement of the electrets at low pressure thereabout 1mbar for a certain period of time can be used as an effective method for stabilizing the electrets charge depending on their applications.

5. Acknowledgment

The authors gratefully acknowledge the financial support of National Science Fund, Bulgaria. The authors also gratefully acknowledge the financial support from the Biosupport project No 245588 (7th FWP).

6. References

Abramovich, M. & Stegun, I. (1964). (eds.) *Handbook of Mathematical Functions*, Applied Mathematics, Series 55 (National bureau of standarts)

Adamson, A. & Gast, A. (1977). *Physical chemistry of surfaces*, John Wiley @ Sons, Inc., New York-Chichester-Weinheim-Brisbane-Singapoore-Toronto

Atkinson, P. & Fleming, R. (1980). Surface component of vacuum absorption and resorption currents in polymers: I. Origin and magnitude. *Journal Phys. D: Appl. Phys.*, Vol.13, pp. 625-638

Atkinson, P. & Fleming, R. (1980). Surface component of vacuum absorption and resorption currents in polymers: II Surface charge accumulation. *Journal Phys. D: Appl. Phys.*, Vol.13, p. 639-653

Atkinson, P. & Fleming, R. (1976). Origin of absorption and resorption currents in the co-polymer poly(hexafluoropropylene-tetrafluoroethylene). *Journal Phys. D: Appl. Phys.*, Vol.9, pp. 2027-2040

Baum, E.; Lewis, T. & Toomer, R. (1978). The lateral motion of charge on thin films of polyethylene terephtalate. *Journal Phys. D: Appl. Phys.*, Vol.11, pp. 963-977

Draughn, R. & Catlin A. (1968). Effect of Low Pressure on Surface Charge of Electrets. *Journal Electrochemical Society: Solid State Science*, Vol.115, №4, pp. 391-394

Feynman, R.; Leighton, R. & Sands, M. (1964). *The Feynman lectures on physics*, Addison-Wesley Publishing Company, Inc., Reading, Massachusetts, Palo Alto, London

Gang-Jin, C.; Hui-ming, X. & Chun-feng, Z. (2004). Charge dinamic characteristics in corona-charged polytetrafluoroethylene film electrets. *Journal of Zhejiang University Science*, Vol.5, №8, pp. 923-927

Giacometti, J.; Fedosov, S. & Costa, M. (1999). Corona Charging of Polymers: Recent Advances on Constant Current Charging. *Brazilian Journal of Physics*, Vol.29, №2, pp. 269-279

Goel, M. (2003). Electret sensors, filters and MEMS devices: New challenges in materials research. *Current science*, Vol.85, №4, pp. 443-453

Gross, B. (1969). Discussion of Effect of Low Pressure on Surface Charge of Electrets. *Journal of the Electrochemical Society*, Vol.116, №6, pp. 874-874

Gubkin, A. & Skanavi, G. (1961). *Sov. Phys. – Solid state*, Vol.3, pp. 215

Jeda M., Sawa G. & Shinohara U. (1967). A decay process of surface electric charges across polyethylene film. *Japanese Journal of Applied Physics*, Vol6, №6, pp. 793-794

Karmazova, P. & Mekishev, G. (1992). Electrets with Island Surface Charge Distribution. *Europhysics Letters*, Vol.19, №6, pp. 481-484

Keltzev, N. (1984), *Bases of Adsorption Technique*, Chimie, Moskow, (in Russian)

Knoll, M.; Ollendorff, F. & Rompe, R. (1939). *Gasentladungstabelen*, Springer-Verlag, Berlin, pp. 84

Mekishev, G.; Yovcheva, T. & Viraneva, A. (2007). Investigation of PP and PTFE film electrets stored at low pressure. *Journal of Non-Crystalline Solids*, Vol.353, pp. 4453–4456

Mekishev, G.; Yovcheva, T.; Gencheva, E. & Nedev, S. (2005). Study of electrets stored at pressure lower than atmospheric. *Journal of Electrostatics*, Vol.63, pp. 1009-1015

Mekishev, G.; Yovcheva, T.; Guencheva, E. & Nedev, S. (2003). On the charge decay in PPelectrets stpred at pressures lower than atmospheric. *J.Mater.Sci.: Materials in electronics* Vol.14, pp. 779-180

Mohmeyer, N.; Behrendt, N.; Zhang, X.; Smith, P.; Altstadt, V.; Sessler, G. & Schmidt, H. (2007). Additives to improve the electret properties of isotactic polypropylene. *Polymer*, Vol.48, pp. 1612-1619

Nalwa, H. (1995). *Ferroelectric polymers*, Marcel Dekker, Inc., New York

Neugebauer, H. (1964). Electrostatic Fields in Xerography. *Applied Optics*, Vol.3, №3, pp. 385-393

Ono, R.; Nakazawa, M. & Oda T. (2004). Charge storage in Corona-Charged Polypropylene Films Analysed by LIPP and TSC Methods. *IEEE Transaction on Industry Applications*, Vol.40, №6, pp. 1482-1487

Palaia, F. & Catlin A. (1970). Electret Behavior at Low Pressure. *The Journal of chemical physics*, Vol.52, №7, pp. 3651-3654

Pisanova, E. & Mekishev, G., unpublished data

Protodyakonov, I. & Siparov S. (1985). *Mechanics of adsorption processes in system gas-solids*, Nauka, Leningrad, pp. 299

Reedyk, C. & Perlman, M. (1968). Method for measurement of surface charge on electrets. *Journal of the Electrochemical Society,* Vol 115, №1, pp. 49-51

Ribeiro, P.; Giacometti, J.; Raposo, M. & Marat Mendes, J. (1991). Effect of the air humidity on the corona polarization of β - PVDF films. *7th Int. Symp. on Electrets*, pp. 322-327

Schaffert, R. (1965). *Electrophotography*, The Focal Press, London, New York

Sessler, G. & Gerhard-Multhaupt, R. (1999). *Electrets*, third edition, Laplacian Press, Morgan Hill, California`

Sessler, G. (1980). *Electrets*, Springer - Verlag, Berlin – Heidelberg, New York

Shepard, G. & Stranathan J. (1941). Effect of Pressure on the Surface Charge of an Electret. *Physical Rev*iew, Vol.60, pp. 360-361

Viraneva, A.; Yovcheva, T.; Gencheva, E. & Mekishev, G. (2008). Study of PET corona electrets at atmospheric and lower pressures. *Journal of Optoelectronics and Advanced Materials*, Vol.10, №2, pp. 302-305

Wild, J. & Stranathan, J. (1957). Influence of External Treatments on Electret Behavior. *The Journal of Chemical Physics*, Vol.27, №5, pp. 1055-1059

Yovcheva, T.; Avramova, I.; Mekishev, G. & Marinova, T. (2007). Corona-charged polypropylene electrets analyzed by XPS. *Journal of Electrostatics*, Vol.65, pp. 667-671

Zhongfu, X.; Yuda, W.; Guamao, Y. & Ximin S. (1991). Corona Charging at Elevated Temperature and Charge Transport for Mylar PETP Foils. *7th Int. Symp. on Electrets*

11

Effects on Freeze-Thaw Durability of Fibers in Concrete

Salih Taner Yildirim[1] and Cevdet Emin Ekinci[2]
[1]*Kocaeli University, Civil Engineering Department, Kocaeli,*
[2]*Fırat University, Construction Education Department, Elazığ,*
Turkey

1. Introduction

The investigation on a construction having such properties as durability, ductility, toughness and strength has boosted interest in materials, such as concrete with fiber and high performance (Otter & Naaman, 1988; Ramakrishnan et al., 1996; P.B. Cachim et al., 2002; Singh & Kaushik, 2003). While improvement of durability of the concrete depends on these conditions, contributory improvements in both chemical and mechanical properties of the concrete are also essential. The fibers improving concrete mechanically are primarily added to minimize cracking or to increase ductility of the concrete and fracture toughness against impact or dynamic loads (Naaman & Reinhardt, 1996; Dias&Thaumaturgo, 2005).

Since short fiber types greatly increase the number of fibers used in the concrete, they are used to decrease cracking and increase durability depending on the properties of the materials used; whereas, long fibers aim more often to increase mechanical properties of the concrete. Addition of hybrid fibers created synergy in the concrete and leaded to similar significant improvements in monofiber reinforced concrete having the higher total fiber content (Qian & Stroeven, 2000).

Studies on durability have emphasized that fiber gains particular importance on increasing freeze-thaw durability. Dramatic falls have been observed in elasticity modulus reaching as many as 300 cycles in the concrete specimens kept both in a 5 % $NaSO_4$ solution and in water, whose rate of w/c was 0.26, 0.32 and 0.44. Concrete including steel fibers do fail in much higher cycles than do plain concrete. Also, the concrete specimens, including fibers with the same rate of w/c, kept in the solution have been shown to have a higher performance in comparison with concrete without fibers kept in water (Singh & Kaushik, 2003).

In some studies, external loads have been exerted upon the concrete kept in a NaCl solution under the influence of effective freeze-thaw cycles. The concrete specimens exposed to NaCl have been shown to lose twice as much weight as those exposed to water. Specimens with steel fibers lose weight maximum at the w/c ratio of 0.44 that becomes obvious after 20-25 cycles. As the rate of the tension of the burdens exerted increased, resistance of the concrete specimens to cycles decreased. Addition of steel fibers in concrete specimens has been shown to cause a delay in a decrease in the performance of the concrete in the advanced cycles in comparison with the concrete without fiber (Sun et al., 2002; Mu et al., 2002; Miao

et al., 2002). Morgan (1991) tested dry and wet hybrid shotcretes with sprayed fibers according to ASTM C 666 rapid water freeze-thaw method (A). In the case of air entraining and use of a high amount of steel and polypropylene fibers freeze-thaw durability can be achieved in wet and dry sprayed concrete. However, a rapid fall is observed in durability when there is no air entraining.

According to ASTM C 666 rapid water freeze-thaw method, 300 and 700 freeze-thaw cycles were applied. The results have shown that despite falls in durability and dynamic elasticity modulus, freeze-thaw performance of both concrete have been shown to be perfect. A study by Juska et al. (1999) on thermal effects upon concrete with glass fibers reported interesting results pertaining to durability. Gomez and Casto (1996) conducted the experiment of freeze (-17.8 °C) and thaw (4.4 °C) came in a 2 % NaCl solution upon composites with fibers. Flexural strength of the specimens and some other properties has been reported to suffer substantial loss. Moreover, Myers et al. (2001) reported flexural rigidity and strength in plaques with glass fibers to decrease more than did rigidity and strength in plaques with carbon fibers.

In this study, micro-structured polypropylene and glass fibers were both used separately and in combination with macro-structured steel fibers in the concrete. Experiments were conducted in order to determine weight-loss and durability factor based on ultrasound pulse velocity of 12 different concrete series produced according to ASTM C-666. The separate and combined effects of the fibers used in the concrete in terms of the rapid freeze-thaw period were investigated.

2. Experimental study

2.1 Materials

CEM I 42.5 R cement was used in the study (Yildirim, 2002). As the aggregate, crushed stone dust of 0-0.5 mm, natural sand of 0.5-4 mm, natural coarse aggregate of 4-16 mm and crushed stone of 16-32 mm were used. Densities of the aggregate used were 2.62, 2.65, 2.70, 2.70 gr/cm^3, respectively. The largest dimension of aggregate was 22 mm. Hooked steel fibers (SF), plain glass fiber (GF) and polypropylene fibers (PF) apart from additive materials providing superplasticizer was used. The properties of fibers have been presented in Table 1, while the properties of cement and additive providing super plasticizer have been presented in Table 2.

Properties	SF	PF	GF
Size (mm)	60	20	12
Dimension (mm)	0.75	0.05	0.014
Brittleness	80	400	857
Density (kg/mm^3)	7480	910	2680
Modulus of elasticity (MPa)	200000	3500-3900	72000
Tensile strength (MPa)	1100	320-400	1700
The number of fibers per kilogram	4600	82 Million	200 Million

Table 1. Technical properties of steel, polypropylene and glass fibers.

Concrete including fibers with different percentages were produced within the same main compounds. K represents the control concrete specimen, while S, P and G represent the concrete specimens including steel, polypropylene and glass fibers, respectively. Three series of concrete, including 0.5 (S 0.5), 0.75 (S 0.75) and 1 (S 1) % as volumetric of hooked steel fibers respectively, were produced. Another six series of concrete were produced with the use of polypropylene and glass fibers of 0.1 % (P and G). The symbols of the fiber material used in the mixture fiber specimens have been defined as SP and SG. They were both used separately and in combination with macro-structured steel fibers of 0.5 (SP 0.5 and SG 0.5), 0.75 (SP 0.75 and SG 0.75) and 1 (SP 1 and SG 1)%. Six specimens were produced from all the series so that they would be used in the experiments. Therefore, all of the twelve series of concrete were produced.

Chemical Compound	SiO_2	Al_2O_3	Fe_2O_3	CaO	MgO	SO_3	Na_2O	K_2O	Cl^-	Insoluble Remains	LOI	C	S
Cement	20.03	5.09	3.44	64.5	1.43	1.3	0.19	0.65	0.01	0.42	2.31	-	-
Superplasticizer	90	0.75	1	0.65	1.15	-	0.55	1.05	0.03	-	-	1.90	0.23

Table 2. Chemical properties of cement and superplasticizer.

As to the control concrete compound of 1 m^3, slump was constant as 130 mm. 181.0 kg of water, 281.9 kg of cement and 14.83 kg of silica fume were used, apart from superplasticizer. Water/cement rate was taken as 0.61. Fibers used as volumetric in concrete.

2.2 Experimental method

Freeze-thaw tests in the concrete series were conducted according to ASTM C 666 (Procedure B: rapid freeze-thaw under air conditions). It was applied on standard prismatic specimens at the dimensions of 80x80x360 mm. The experiment was conducted after the specimens had been cured for 28 days. Heat transfer calculations were made in order to determine how long the heat in the specimens would take to reach the optimal heat required for the experiment so that the freeze-thaw test could be made in the deep frost according to ASTM C 666. Therefore, the central heat of the specimens (20 °C) was lowered to -20 °C. The central heat of the specimens left in the water was increased to 5.4 °C. 30 cycles were made altogether, with the central heat adjusted in such a way that it would vary between -20 °C (2 hours and 40 minutes) and 5.4 °C (36 minutes).

Weight loss and ultrasound pulse velocity were measured at the beginning and the end of the cycles applied on concrete specimens. The percentage of dynamic E-modulus determined after freeze-thaw cycles through ultrasound instrument (P) was calculated by dividing the square of the pulse velocity after freeze-thaw cycles by the square of the pulse velocity before freeze-thaw cycles and then multiplying the result by 100. Afterwards, dynamic E-modulus was determined by multiplying a predetermined value (30) by the continuing number of cycles (N). The result was then divided by the final number of cycle (30) (M). After this, durability factor (DF) for the concrete specimens was determined with

DF=P.N/M formula. N and M values were equal for this study (American Society for Testing and Materials [ASTM C 666], 1999).

3. Test results and discussion

As a result of the experiment, surface damages of concrete specimens were determined after 30 freeze-thaw cycles. The specimens were seen that they have a sponge-like surface and broken edge. These damages occurred more intensively between 20 and 25 cycles (Mia et al., 2002).

As seen in Fig. 1, the plain concrete specimens had far less amounts of weight-loss than most of the concrete specimens including fiber. However, there occurred roughness over the surface. In order to obtain a more precise determination of weight-loss, the number of freeze-thaw cycles should be increased. The surface of concrete gets damaged when exposed to low freeze-thaw cycles. A much less amount of weight-loss could have been expected in fiber reinforced concrete if they had been exposed to a larger number of freeze-thaw cycles, considering the capability of fibers to keep matrixes together. Weight-loss was also determined to get affected by some of the parts falling off the corners of the specimens. In particular, the corners of the concrete with steel fibers are weaker and so may cause falling off some parts in the corners by forcing the matrix during the freeze-thaw cycles.

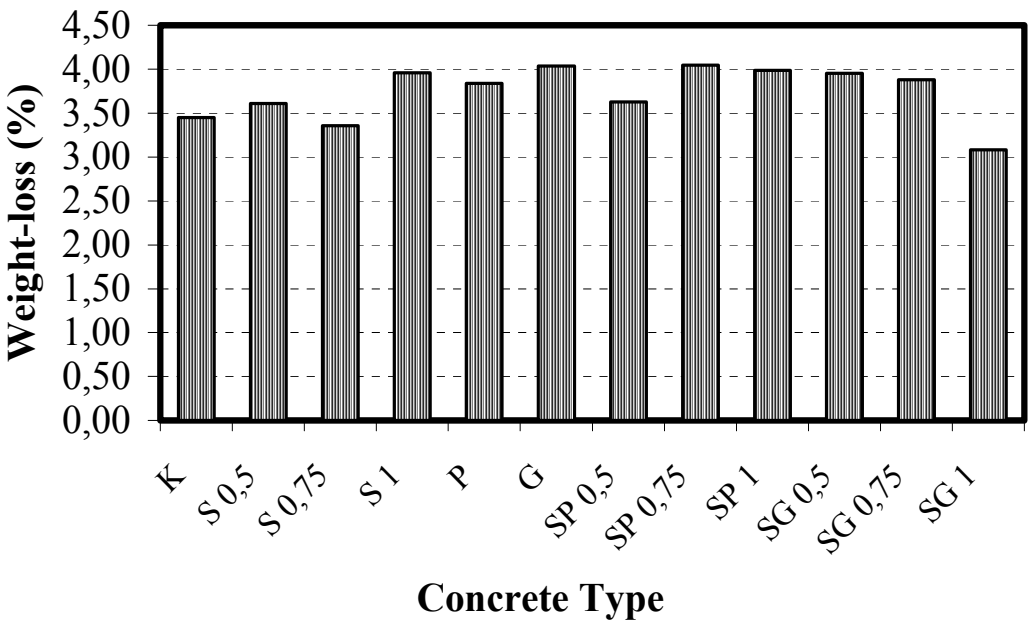

Fig. 1. Weight-loss after freeze-thaw cycles.

As seen in Fig. 2, the decrease in the pulse velocity of the specimens was obvious in contrast to their weight-loss. Polypropylene fibers demonstrated the best performance as a stand-alone and mixed with steel fibers (Morgan, 1991). A similar effect was determined for the mixture fibers. Fibers did affect the concrete specimens in agreement with their own properties. Because of the capability of polypropylene fibers to prevent cracking and to be remarkably safe from corrosion, the pulse velocity value was determined to be low.

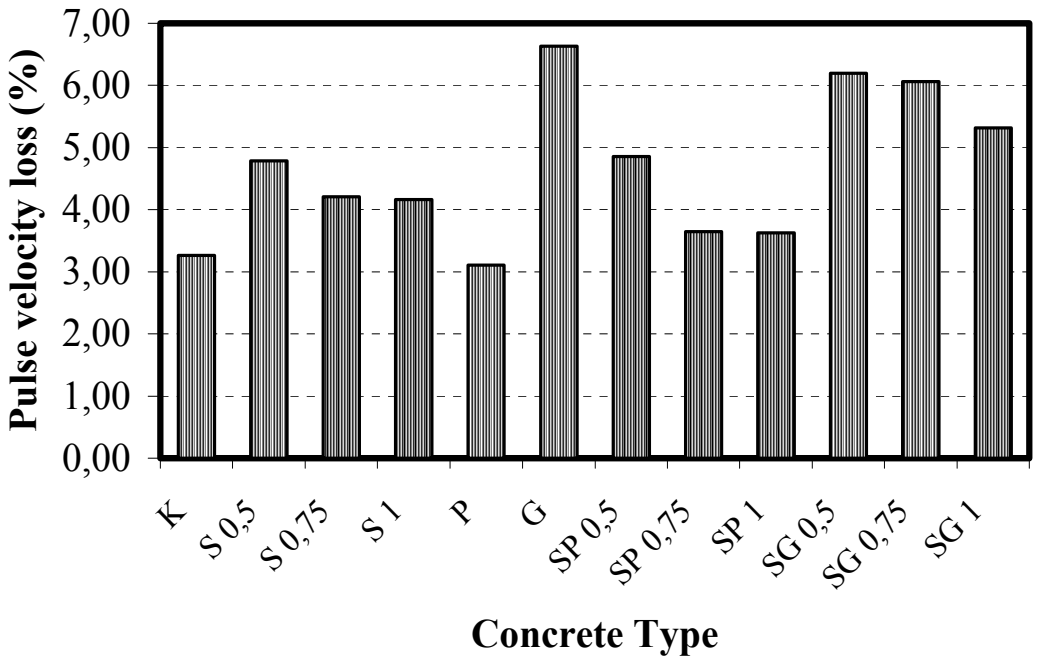

Fig. 2. Decreases in the pulse velocity following freeze-thaw cycles.

Though glass fibers have microstructures like polypropylene fibers, they showed their general weakness and the fibers were observed to have caused voids and to have affected adhesion negatively (Juska,1999). The initial decrease was in the steel fibers were attributed to the voids between the fiber-matrix interfaces. Moreover, due the fact that the ends of the fibers were curved, and that they are more resistant to dilation or contraction, the pulse velocity decreases due to the increase in the amount of fiber. However, it should be emphasized that the following cycles may change this. In other words, it is possible to say that the durability factor may be higher in following cycles (Singh & Kaushik, 2003). In order to ensure this, the number of cycles should over 30. Because the durability factors seen in Fig. 3 are inversely proportional to the decrease in the ultrasound pulse velocity, the low values are seen as high here.

Durability of the concrete series was determined to have been increased by polypropylene fibers, while glass fibers were determined to be highly unsuccessful. No concrete specimens

including steel fibers, inclusive of mixture fibers, had higher values than plain concrete specimens.

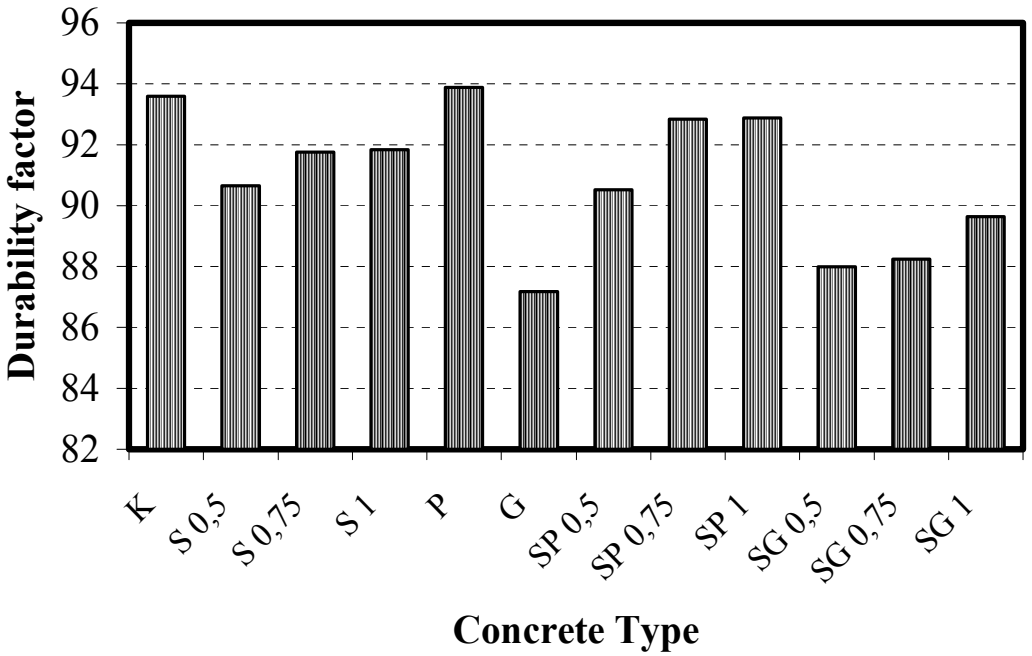

Fig. 3. Durability factors determined after freeze-thaw cycles.

4. Conclusion

20-25 of freeze-thaw cycles in concrete specimens was determined to be highly critical. Though they seem to be enough in number to form an opinion about the durability factor, 30 cycles of the freeze-thaw process seem to be insufficient to determine the precise weight loss of the concrete specimens. It was concluded that increasing the number of cycles could be advantageous to measuring weight, and that steel fibers could provide advantages for durability determination of in the following cycles. Using polypropylene fiber in all the concrete specimens to be reinforced by fibers in consideration of the effects of freeze-thaw cycles will be advantageous. Steel fibers did not cause any difference in terms of freeze-thaw cycles but did cause some negative effects for mixture concrete. Therefore, it is important that glass fibers should not be used in the places exposed to freeze-thaw cycles, or that concrete should be protected against this effect. Base on the study results, it can be suggested that steel fibers, which have different levels of brittleness, those with smaller dimensions in particular, should be investigated for the effects of freeze-thaw cycles.

5. References

ASTM C 666 (1999). Standard Test Method for Resistance of Concrete to Rapid Freezing and Thawing, Volume 04.02,

Concrete and Aggregates, *American Society for Testing and Materials*, West Conshohocken, PA.

Cachim, P.B.; Figueiras, J. A. & Pereira, P. A. A. (2002). Fatigue Behavior of Fiber-Reinforced Concrete in Compression, *Cement and Concrete Composites*, Vol. 24, pp.211–217, ISSN 0958-9465.

Otter, D.E., Naaman, A.E. (1988). Properties of Steel Fiber Reinforced Concrete Under Cyclic Loading, *ACI Materials J.*, Vol. 85, No. 4, pp. 254–261. ISSN 0889325X.

Dias, D.P., Thaumaturgo, C. (2005). Fracture toughness of geopolymeric concrete reinforced with basalt fibers, *Cement and Concrete Composites*, Vol. 27, pp. 49–54, ISSN 0958-9465.

Gomez, J.; Casto, B. (1996). Freeze-Thaw Durability of Composite Materials, *Proceedings of the 1st International Conference on Composites in Infrastructure*, *Fiber Composites in Infrastructure*, pp. 947-955.

Juska, T.; Dutta, P.; Carlson, L.; Weitsman, J.(1999). Gap Analysis for Durability of Fiber Reinforced Polymer Composites in Civil Infrastructure, *Thermal Effects*, Chapter 5, pp.40-51.

Miao, C.; Mu, R.; Tian, Q. & Sun, W. (2002). Effect of Sulphate Solution on the Frost Resistance of Concrete with and without Steel Fiber Reinforcement, *Cement and Concrete Research*, Vol. 32, No. 1, pp. 31–34, ISSN 0008-8846.

Morgan, D.R. (1991). Freeze Thaw Durability of Steel and Polypropylene Reinforced Shotcretes: a Review. Durability of Concrete. *Second International Conference*, held in Montreal, Canada; Ed. by V.M. Malhotra; American Concrete Institute, Detroit, MI, Vol. 2, pp. 901-918. (ACI SP-126).

Mu, R.; Miao, C.; Luo, X.; Sun, W. (2002). Interaction between Loading, Freeze-Thaw Cycles, and Chloride Salt Attack of Concrete with and without Steel Fiber Reinforcement, *Cement and Concrete Research*, Vol. 32, pp. 1061-1066, ISSN 0008-8846.

Myers, J.J.; Murthy, S.; Micelli, F. (2001). "Effect of Combined Environmental Cycles on the Bond of FRP Sheets to Concrete," Proceedings - Composites In Construction, *2001 International Conference*, Porto, Portugal, October 10-12.

Naaman, A. & Reinhardt, H.W., Eds (1996). High Performance Fiber Reinforced Cement Composites (HPFRCC2), *Proc., 2nd Int. RILEM Workshop*, RILEM, Proceedings 31, London, E.&FN Spon, ISBN 0419211802.

Qian, C.X. & Stroeven, P. (2000). Development of hybrid Polypropylene-Steel Fibre Reinforced Concrete, *Cement and Concrete Research*, Vol. 30, No.1, pp. 63-69, ISSN 0008-8846.

Ramakrishnan, V.; Meyer, C.; Naaman, A. ; Zhao, G. ; Fang, L. (1996).Cyclic Behavior, Fatigue Strength, Endurance Limit and Models for Fatigue Behavior of FRC, *in: A. Naaman, H.W. Reinhardt (Eds.), High performance fiber reinforced cement composites, London, E & FN Spon,* ISBN 0419211802.

Singh, S.P.& Kaushik, S.K. (2003). Fatigue Strength of Steel Fibre Reinforced Concrete in Flexure, *Cement and Concrete Composites,* Vol. 25, pp. 779-786, ISSN 0958-9465.

Sun, W.; Mu, R.; Luo, X.; Miao, C. (2002). Effect of Chloride Salt, Freeze–Thaw Cycling and Externally Applied Load on the Performance of the Concrete, Cement and Concrete Research Vol.32, pp. 1859–1864, ISSN 0008-8846.

Yildirim, S. T. (2002). The Investigation of Performance Characteristics of Fiber Reinforced Concrete, PhD Thesis, Firat University, Science Institute, Elazığ, Turkey, p.193, (in Turkish).

12

Acoustic and Dielectric Properties of Polypropylene-Lignocellulosic Materials Composites

Ewa Markiewicz[1], Dominik Paukszta[2] and Sławomir Borysiak[2]
[1]*Institute of Molecular Physics, Polish Academy of Sciences, Poznań,*
[2]*Institute of Technology and Chemical Engineering,*
Poznan University of Technology, Poznań,
Poland

1. Introduction

In recent years, one can observe the tendency to replace the thermoplastic polymers by the composite materials in several branches of industry, e.g. automotive and building engineering (Peijs, 2003), aviation and packaging industry (Bledzki & Gassan, 1999). The composite materials obtained by reinforcement of the polypropylene with lignocellulosic fillers are known to show improved mechanical and physical properties in comparison with the pure propylene (Averous & Le Digabel, 2006; Bhattacharyya et al., 2003; Mohanty et al., 2000). Composites made from polypropylene and wood fibre are characterized by significantly higher stiffness than unreinforced polypropylene (Bhattacharyya et al., 2003). The loading of the polypropylene with rice husk powder increases Young's modulus and flexural modulus of the composite, compared with those of the polypropylene (Hattotuwa et al., 2002). The studies of the fire behavior (Borysiak et al., 2006) revealed a significant decrease of such an essential parameter as the heat release rate (HRR) peak, especially low value of HRRmax in comparison with those of the polypropylene. Moreover, very important feature of the composites with lignocellulosic materials is their partial biodegradability as the filler materials come from natural resource. In this chapter we would like to point out to improved acoustic and dielectric properties of the polypropylene-lignocellulosic materials composites in comparison with the pure polypropylene based on our measurement results.

Nowadays, technical progress in manufacturing the modern equipment, generating higher sound pressure, implies the need to search for new sound absorbing materials to improve the human comfort today. The ascending requirements related to the construction materials absorbing the undesired noise occur mainly in the automotive industry and building. The commonly used and unporous materials as ceramic tile, concrete, cement, fiberboard and playwood are characterized by weak sound absorption properties with the sound absorption coefficient bellow 5% in the frequency range from 125 Hz to 8000 Hz (Tiwari et al., 2004; Yang et al., 2003). The sound absorption capacity of the environment is usually corrected by the sound absorbance systems made from glass wool, foam (metals and polyurethanes), rubber, mineral fibres and their composites. Although the sound absorption can be significantly

increased due to installation of these traditionally applied materials, they cause environmental pollution and pose danger to human health. Recent tendency towards the environmental protection stimulates the utilization of natural materials as sound absorbers, e. g. random cut rice straw (Yang et al., 2003), coconut coir (Nor et al., 2004), bamboo (Liu & Hu, 2008) and tea-leaf-fibre (Ersoy & Kucuk, 2009). We propose the use of composites made from polypropylene and lignocellulosic material derived from hemp, flax, beech wood and rapeseed straw as promising sound absorbers (Markiewicz et al., 2009).

Combination of the polymer and the lignocellulosic material results in new dielectric properties of the composite. The proper formation of the dielectric properties of the composites is very important in the field of their application, particularly when they are designed as electronic packaging. In this case, the electrical parameters of the microelectronic devices, such as signal attenuation, propagation velocity, and cross talk, are influenced by the dielectric permittivity value ε', dielectric losses ε'' and their temperature stability in a wide frequency range (Pecht et al., 1999; Chung, 1995; Subodh et al., 2007). On one hand the permittivity ε' should not be low because of the demand for the miniaturization of the device but on the other hand it cannot be too large in order to enable the high signal propagation speed. The signal delay T_d propagated through the metal embedded in the packaging material is determined by the dielectric permittivity ε' according to the formula (Tummala, 1991):

$$T_d = \sqrt{\frac{\varepsilon'}{c}} \tag{1}$$

where c is the elastic coefficient. It is evident that high dielectric permittivity ε' reduces the signal propagation speed. Similarly, in the case of application of the composite as the substrate in sensor of acoustic surface waves the signal propagation speed v is reduced due to high dielectric permittivity ε' in accordance with the relationship:

$$v = \sqrt{\frac{c + \frac{e^2}{\varepsilon'}}{\rho}} \cdot \sqrt{1 - \beta^2}\ , \tag{2}$$

where e denotes the piezoelectric coefficient, ρ stands for the density and β is the factor of decreasing the signal amplitude inside the substrate material (Soluch, 1980). In this chapter, the relationship between the dielectric permittivity ε' of the composite and the volume fraction of the lignocellulosic material is established. The effect of temperature variation from 150 to 450 K on the dielectric spectrum of polypropylene and the composites was investigated in the frequency range 100 Hz to 1MHz.

2. Methods of sample preparation

Polypropylene-lignocellulosic materials were prepared from the following materials:

- isotactic polypropylene (PP) type Malen F-401 (melt flow rate $MFR_{230/2.16}$ = 2.4 -3.2g/10 min, isotacticity 95 %), produced by Basell Orlen Polyolefins (Poland) was used as a matrix for preparation of the composites;

- lignocellulosic materials derived from hemp, flax, beech, pine, rapeseed straw were used as filling materials.

Number	Kind of material	Density [kg/m^3]
No. 1	Polypropylene (PP)	881.8
No. 2	PP+40% of crumble hemp plant	872.8
No. 3	PP+40% of long hemp fibres	927.9
No. 4	PP+40% of long flax fibres	934.6
No. 5	PP+40% of rapeseed straw Kaszub	918.8
No. 6	PP+40% of crude beech wood	803.5
No. 7	PP+20% of crude beech wood	921.0
No. 8	PP+20% of beech modified with succinic anhydride	920.7
No. 9	PP+20% of crude pine wood	850.9
No. 10	PP+20% of pine modified with succinic anhydride	974.1
No. 11	PP+30% of crude rapeseed straw Kaszub	889.6
No. 12	PP+30% of rapeseed straw Kaszub modified with acetic anhydride	904.0
No. 13	PP+30% of crude rapeseed straw Californium	924.8
No. 14	PP+30% of rapeseed straw Californium modified with acetic anhydride	969.9
No. 15	PP+25% of short hemp fibres	862.5
No. 16	PP+25% of hemp shivers	911.3
No. 17	PP+25% of short flax fibres	883.0
No. 18	PP+25% of flax shivers	943.1
No. 19	PP+30% of crude beech wood	922.1
No. 20	PP+30% of mercerized beech wood	922.0
No. 21	PP+30% of beech modified with maleic anhydride	921.9
No. 22	PP+30% of crude pine wood	861.1
No. 23	PP+30% of mercerized pine wood	895.4
No. 24	PP+30% of pine modified with maleic anhydride	901.3
No. 25	PP+30% of mercerized rapeseed straw Kaszub	902.5
No. 26	PP+30% of mercerized rapeseed straw Californium	950.7

Table 1. Specification of the samples investigated

Two different methods were used to make the composites. The first one consisted in mixing crumble lignocellulosic materials with polypropylene granulate in different proportion (20 – 40 wt. % of natural component). After that, the extrusion was carried out using a "Fairex"

(McNell Akron Repiquetn, France) single-screw extruder, L/D=25. The composite material was obtained in a granulate form (*Polish Patent* 186577, 2004). The composite granulates were melted in mould between heating plates at the temperature of 200°C under load of 3000 kG to obtain the samples required for the experiments.

The composites containing the long hemp and flax fibres were produced in a different way. A technique of hydraulic pressing at temperature 200°C under load of 3000 kG (*Polish Patent* 190405, 2005).

Finally, the samples took the shape of discs. Table 1 specifies all the samples prepared.

3. Acoustic properties of the polypropylene reinforced with lignocellulosic

3.1 Effect of reinforcement of polypropylene with lignocellulosic materials on the acoustic properties

The sound absorptive power of a given material sample is characterized by the sound absorption coefficient α defined as the ratio of the acoustic wave energy E_a absorbed by the sample to the total energy E_i incident on the sample:

$$\alpha = \frac{E_a}{E_i} . \tag{3}$$

Generally, the composites are known to exhibit better sound absorption than the homogenous materials. The fact results from the additivity of all kinds of acoustic energy losses (Epstein & Carhart, 1953; Vinogradov, 2004). The sound wave propagated through the inhomogeneous medium interacts with a great number of suspended particles, which differ by the density, compressibility and thermophysical parameters from the matrix. This leads to the additional acoustic energy losses compared to that in the matrix. The property of the additivity allows to express the sound absorption coefficient of the composite α as a sum of four components:

$$\alpha = \alpha_0 + \alpha_F + \alpha_H + \alpha_S , \tag{4}$$

where: α_0 - the coefficient of the matrix, α_F - the coefficient due to friction between filler particles and the matrix, α_H - the coefficient related to the heat exchange between the particles and the matrix and α_S - the coefficient caused by the decay of the acoustic wave in forward direction due to scattering by the particles. The results of the experimental studies by I. S. Kol'tsova et al. (Vinogradov, 2004) show that the sound absorption due to the scattering play an important role when the particle sizes are comparable or larger than the sound wave length. Thus, in the case of interaction between an acoustic waves of low frequency and the particles of micrometer/millimetre dimensions, the losses in acoustic energy due to friction and interfacial heat exchange play the main role. The different densities of the particles and the matrix are the reason for which the sound wave induced motions of both compounds can be considered as the separate ones with the friction existing between them. In real media, viscous forces arise balancing the motions of the particles and the matrix and giving rise to the sound absorption. When the heating coefficients on compression of both components are different, the effect of the variable sound pressure on the composite results in heat exchange between the components. At a macroscale, the

process of compression and expansion proceeds adiabatically. However, at a microscale, i. e. in the scale of particle sizes, the process is nonadiabatic with the degree of heat exchange dependent on the frequency. At low frequencies, the temperature difference between the particles and the matrix has time to balance and the process is microscopically isothermal. In the higher frequency range, the process follows adiabatically at a microscale because balancing does not occur. The heat transfer through the filler particle - matrix interface is the reason for acoustic energy absorption (Vinogradov, 2004). Taking into account the above considerations, it can be stated that the increased sound absorption of the composites results from friction and interfacial heat exchange. This is an isothermal process, since the filler particles are of several millimetres in length and bellow millimetre in width.

The numerical calculation related to the elastic wave propagation in anisotropic media was initiated by Biot in 1955 (Biot, 1955, 1956a, 1956b). Biot used Lagrange's equations to derive a set of differential equations that govern the separated motions of a porous solid and a compressible viscous fluid confined to it. In 1962 Biot extended the acoustic propagation theory in a wider context of the dynamics of anisotropic media (Biot,1962a, 1962b). The theory is applied to the materials where fluid and solid are of comparable densities. As follows from Table 1, the densities of the composites differ from that of the polypropylene no more than 10% and the criterion of the applicability of the Biot theory is fulfilled. The plots of frequency dependence of sound absorption were derived by Biot for different combinations of elastic constants and densities of the porous solid and that of fluid taking into account the additional apparent mass due to inertia coupling. The theoretical curves (Biot, 1956b) exhibit a maximum value of the absorption at a characteristic frequency which depends on the kinematic viscosity of the fluid and pore diameter. The maxima are very pronounced in the case of fluid - saturated porous solids characterized by the elastic properties and densities far from the "compatibility condition":

$$z_1 = \frac{V_1^2}{V_c^2} \cong 1 , \tag{5}$$

where V_1 stands for the velocity of the stress wave in a real anisotropic solid and V_c represents this velocity when the relative motion between fluid and solid is prevented in some way. The less the fraction z_1 the more enhanced are the maxima.

Acoustic standing wave method (Markiewicz et al., 2009) is the most popular way to determine the sound absorptive power of the material sample subjected to the plane acoustic wave. In this method, plane acoustic waves are generated by a loudspeaker placed at one end of a tube while the other end is terminated by the material sample. Due to the reflections from the sample, standing wave is produced in the tube as the superposition of the incident wave with the amplitude A and the reflected one with the amplitude B. The reflected wave is characterized by lower amplitude and shifted phase in comparison to the incident one. The probe microphone, moved inside the tube, receives the alternating acoustic pressure of minimum amplitude p_{min}=A-B at the distance of $\lambda/4$ (λ – wavelength) from the sample followed by the pressure of maximum value p_{max}=A+B at $\lambda/2$. As the acoustic wave energy is proportional to the square of the sound pressure, the equation (3) can be written:

$$\alpha = \frac{E_i - E_r}{E_i} = 1 - \left[\frac{B}{A}\right]^2 = 1 - \left[\frac{p_{\max} - p_{\min}}{p_{\max} + p_{\min}}\right]^2, \quad (6)$$

where E_r denotes the energy of the reflected wave. The equation (6) shows that the absorption coefficient α can be easily determined by means of the measurement of p_{min} and p_{max} amplitudes of the sound pressure inside the tube.

Figs. 1 and 2 show the results of the measurement of sound absorption coefficient α for pure polypropylene and the composites with lignocellulosic materials. The values of coefficient α were measured at the frequencies: 1000, 1800, 3000, 4000, 5000 and 6300 Hz according to the method mentioned above. As follows from the figures, the polypropylene is characterized by the relatively weak sound absorption. The values of coefficient α vary between 2 and 13% with the tendency to slightly decrease with increasing frequency. Fig. 1 shows the effect of the addition of 40 wt. % of hemp fillers on the absorption spectrum. The effect is dominant in the range of higher frequencies. Starting from the frequency of 3000Hz, the value of the coefficient α increases rapidly up to about 25% and maintains at this level up to 6300 Hz. Below the critical frequency 3000 Hz the effect of the addition of the hemp fillers is inconsiderable. One can even notice a small decrease of the coefficient α at 1800 Hz. Taking into account the fact that two different methods were used to prepare the samples No. 2 and No. 3 (extrusion and hydraulic pressing), one can conclude that the manufacturing procedure does not influence the sound absorption in the case of the composites with hemp filler. The composites containing long flax fibres, crumble rapeseed and crumble beech wood exhibit also better sound absorption in comparison with pure polypropylene but the frequency dependence of the coefficient α is quite different (Fig. 2). For these materials the maxima of α coefficient are observed at the frequencies of 3000 Hz or 4000 Hz. The differences in sound absorption by composites containing hemp and the ones based on fillers: flax, rapeseed straw, beech wood can be explained taking into account the Biot theory. The composites with hemp fillers seem to be nearest the "compatibility condition" among the investigated materials. The maxima of the absorption are not noticeable in the frequency range of the measurement, on the contrary to the remaining fillers. The composition of polypropylene and hemp results in such a combination of elastic constants and densities that the relative motion between filler and matrix is prevented. The discrepancies in sound absorption characteristics can result also from the filler morphology and its chemical composition. The width of hemp fibres (30 μm) is larger in comparison with flax fibres (20 μm). Moreover, hemp plant is known to have the dimensions of the anatomic cells larger than the remaining plants under examination. Hemp is distinguished for the highest contents of cellulose (75 wt. %) (Averous & Le Digabel, 2006). Flax contains 71 wt. % of cellulose. Beech and rapeseed are characterized by smaller contents of cellulose: beech – 42 wt. % (Nik–Azar et al., 1997) and rapeseed – from 35 to 40 wt. % (Paukszta, 2005, 2006). The contents of lignin in hemp (4 wt. %) is twice that of flax (2 wt. %) (Averous & Le Digabel, 2006). However, beech and rapeseed are known to have relatively large amount of lignin (~20 wt. %) (Paukszta, 2006). Flax is characterized by the contents of pectins (2 wt. %), fats (2 wt. %) and waxes (2 wt. %) which are twice those of hemp. It can be concluded that the higher contents of the cellulose in the hemp probably enables the sound absorption in the relatively wide frequency range.

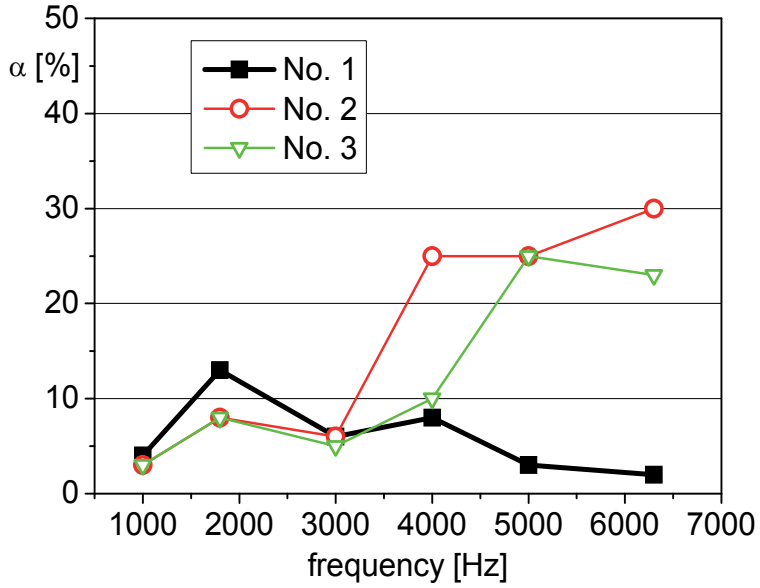

Fig. 1. Frequency dependences of sound absorption coefficient α for the samples: No. 1 - PP, No. 2 - PP + 40 wt. % of crumble hemp plant, No. 3 – PP + 40 wt. % of long hemp fibres

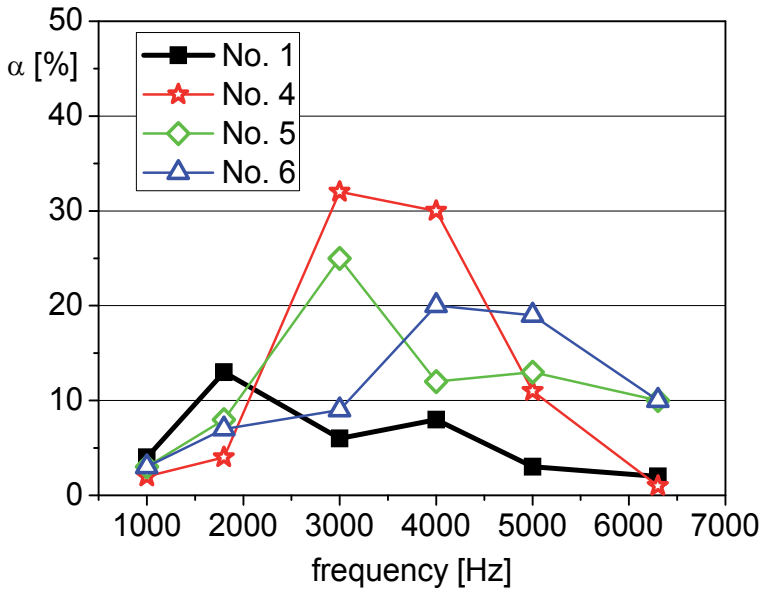

Fig. 2. Frequency dependences of sound absorption coefficient α for the samples: No. 1 – PP, No. 4 - PP + 40 wt. % of long flax fibres, No. 5 - PP + 40 wt. % of crumble rapeseed, No. 6 – PP + 40 wt. % of crumble beech wood

3.2 Effect of chemical treatment of lignocellulosic fillers on the acoustic properties of the composites

Chemical treatment of lignocellulosic filler as mercerization and modification with anhydride is often necessary to improve the mechanical properties of the composite due to better adhesion between the hydrophilic lignocellulosic filler and the hydrophobic polymer matrix (Borysiak & Garbarczyk, 2003; Borysiak & Doczekalska, 2005; Liu & Hu, 2008). Chemical treatment of the filler surface results in positive changes of the mechanical parameters of the composite as tensile strength, flexural strength and elongation at break (Bledzki et al., 2005; S.J. Kim et al., 2008; Mahlberg et al., 2001; Nachtigall et al., 2007; Yang et al., 2006). The interfacial region is the most vulnerable location to mechanical fracture. When subjected to the stress, it should show the ability to transmit the acoustic wave – induced tension from one phase to the other. Chemical treatment of the lignocellulosic filler is often necessary to get better the mechanical properties of the composite. Thus, the information about the influence of the modification on the acoustic properties is also very useful from the application point of view. In this chapter, the results of acoustic measurements for composites with crude and modified fillers are presented.

Figs. 3 – 6 show the values of sound absorption coefficient α measured for the composite samples No. 7 – 14, specified in Table 1. All composite samples, crude and modified, are compared with the pure polypropylene. The effect of the addition of the lignocellulosic filler to the polypropylene matrix is predominant in the frequency range above 3000 Hz where one can observe the improvement in the sound absorption of the order of more than ten percentage. All the investigated composite samples show the resonance characteristics of sound absorption with the maximum in the frequency range from 4000 to 6000 Hz. This behaviour can be ascribed to the combination of elastic constants and densities of both materials which makes possible the comparatively big relative motion between matrix and filler according to the Biot theory. The elastic constants and densities of the filler material result from its chemical composition. Our previous investigations, described in chapter 2.1, performed on composites with flax, hemp, rapeseed and beech fillers, showed that the increased sound absorption in a narrow frequency range can be probably related to the relatively small content of the cellulose. Now, we can confirm this presumption. The lignocellulosic materials used in this experiment are characterized by lower contents of cellulose: beech – 42 wt. % (Nik–Azar et al., 1997), pine – 41 wt. % (Gosselink et al., 2004), rapeseed Kaszub – 38 wt. % (Paukszta, 2005, 2006) and rape Californium - 37 wt. % (Paukszta, 2006) in comparison with hemp and flax which contain above 70 wt. % of cellulose (Averous & Le Digabel, 2006).

The effect of the modification of the fibre surface consists in the shift of the sound absorption maximum towards higher frequency range and is accompanied by the decrease of the sound absorption coefficient α. The reduction of the coefficient α is not large. It amounts 2.5 % in the case of composites with pine wood and rapeseed straw Californium. For the samples with beech wood filler the coefficient α remains unaffected after modification. The exception is the composite containing the rapeseed straw Kaszub as a filler that shows the decreasing in the sound absorption of 7%. The reduction of the α coefficient value at the frequency related to the maximum of the sound absorption can be associated with the increase in the density of the composite after modification (Table 1) due to better adhesion between filler particles and polypropylene matrix. The fact implies that the specific acoustic impedance of

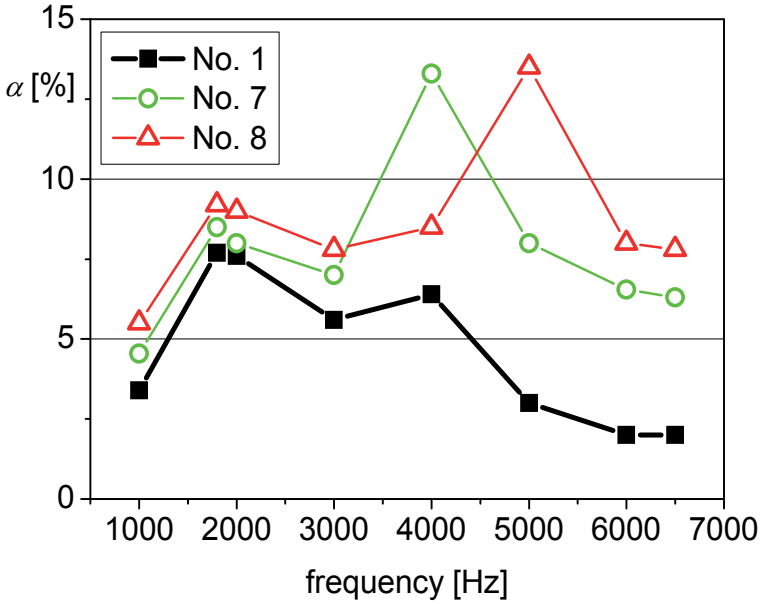

Fig. 3. Frequency dependences of sound absorption coefficient α for the samples: No. 1 – PP, No. 7 – PP + 20 wt. % of crude beech, No. 8 - PP + 20 wt. % of beech modified with succinic anhydride

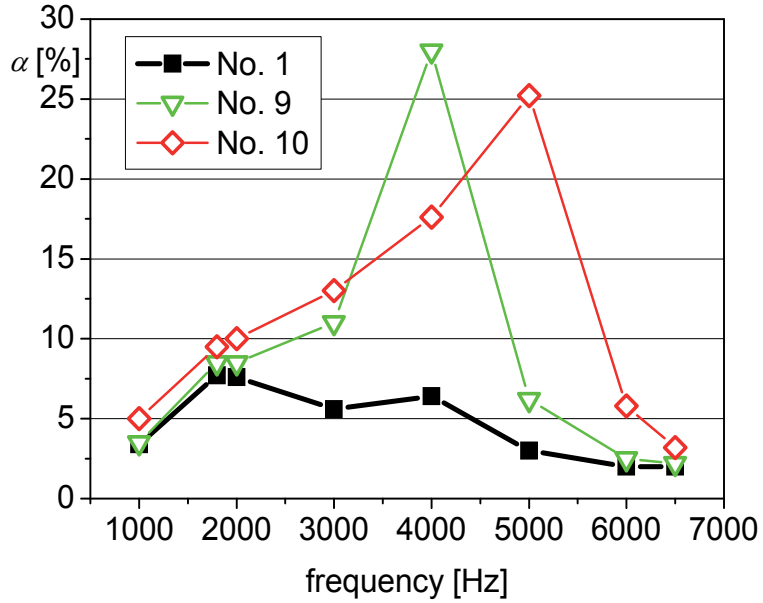

Fig. 4. Frequency dependences of sound absorption coefficient α for the samples: No. 1 – PP, No. 9 – PP + 20 wt. % of crude pine, No. 10 – PP + 20 wt. % of pine modified with succinic anhydride

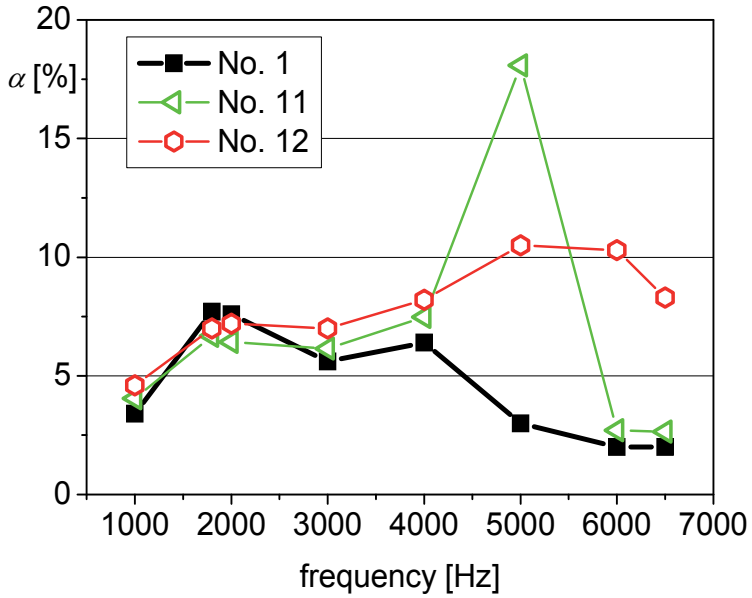

Fig. 5. Frequency dependences of sound absorption coefficient α for the samples: No. 1 – PP, No. 11 – PP + 30 wt. % of crude rapeseed straw Kaszub, No. 12 - PP + 30 wt. % of rapeseed straw Kaszub modified with acetic anhydride

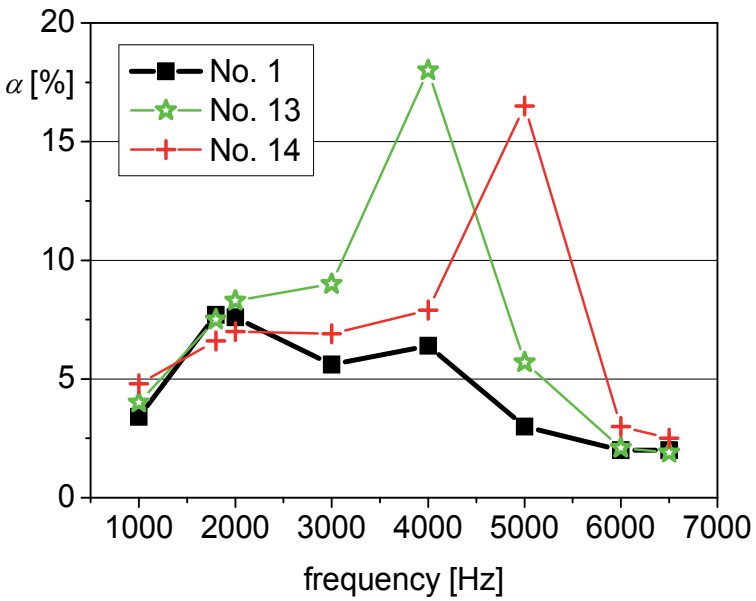

Fig. 6. Frequency dependences of sound absorption coefficient α for the samples: No. 1 – PP, No. 13 – PP + 30 wt. % of crude rapeseed straw Californium pure polypropylene (No. 1) and polypropylene composites with 30 wt. % of crude rapeseed straw Californium, No. 14 – PP + 30 wt. % of rapeseed straw Californium modified with acetic anhydride

the material, defined as the product of the density and the sound velocity (Lee & Chen, 2001), is increased. In turn, the higher the acoustic impedance the more acoustic energy is reflected from the material surface and the less of it can be absorbed. Better adhesion between polymer matrix and lignocellulosic filler leads to the better ability to transmit the acoustic wave – induced tension from one phase to the other. The process of the transmission in the composites with the modified fillers can be more rapid in comparison to that observed in non-modified composites and it can follow with higher frequency being a reason of a shift of the sound absorption band of about 1000 Hz.

4. Dielectric properties of the polypropylene reinforced with lignocellulosic materials

4.1 Effect of reinforcement of polypropylene with lignocellulosic materials on the dielectric properties

The dielectric properties of a material are determined by the polarizability of its molecules. There are three primary contributions to the electric polarization of a dielectrics: electronic, ionic and dipole reorientation – related (Uchino, 2000). The intensity with which each mechanism occurs depends on the frequency of applied electric field. The electronic polarization causes a displacement of the electrons with respect to the atomic nuclei and can follow alternating field with the frequencies up to $10^{12} – 10^{15}$ Hz. The ionic polarization relies on a displacement of the atomic nuclei relative to one another and responds up to $10^{9} – 10^{12}$ Hz. Both mentioned polarization mechanisms are related to the non-polar molecules. The third mechanism associated with the dipole reorientation is valid only in the case of polar molecules. It can follow with the frequency of alternating electric field up to $10^{6} – 10^{9}$ Hz. The dielectric permittivity ε' of a material represents the ratio of the capacitance of a plane condenser filled with the dielectric to that of the same condenser under vacuum and is to calculate from the expression:

$$\varepsilon' = \frac{C \cdot d}{\varepsilon_0 \cdot S}, \tag{7}$$

where: C is the capacitance of the condenser with the dielectric, S stands for the area of the sample covered by the electrode, d relates to the thickness of the sample and $\varepsilon_0 = 8.85 \cdot 10^{-12}$ F/m is the dielectric constant of the vacuum. The alternating current conductivity $\sigma_{a.c.}$ is described by the relationship:

$$\sigma_{a.c.} = \varepsilon_0 \cdot \omega \cdot \varepsilon' \cdot tg\delta, \tag{8}$$

where ω stands for the angular frequency.

The frequency dependencies of the dielectric constant ε' measured at room temperature for the polypropylene and its composites with various lignocellulosic materials derived from hemp and flax are presented in Figs. 7 and 8. The effect of the reinforcement of the polypropylene with a lignocellulosic material consists in the increase of the dielectric permittivity ε' over the whole measurement frequency range. The effect is predominant at lower frequencies. Pure polypropylene is a non-polar hydrophobic material which shows only instantaneous ionic and electronic polarization. Its dielectric permittivity ε' holds

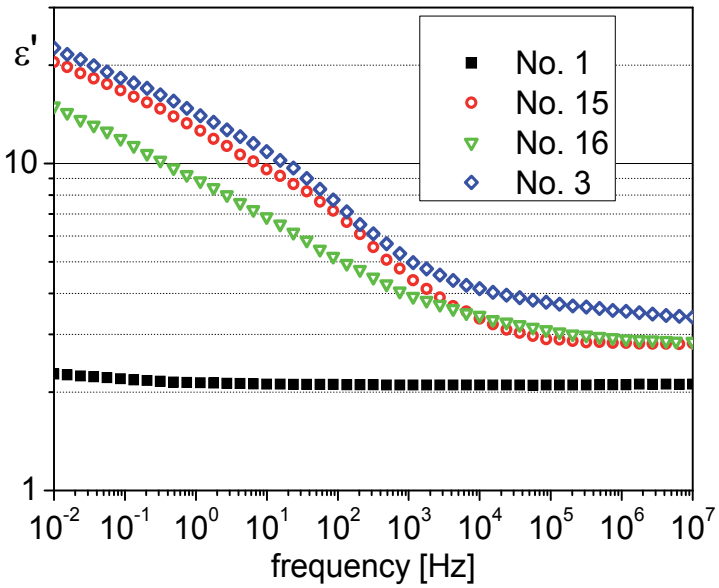

Fig. 7. Frequency dependences of dielectric permittivity ε' for the samples: No. 1 – PP, No. 15 - PP+25 wt. % of short hemp fibres, No. 16 - PP + 25 wt. % of hemp shivers, No.3 – PP + 40 wt. % of long hemp

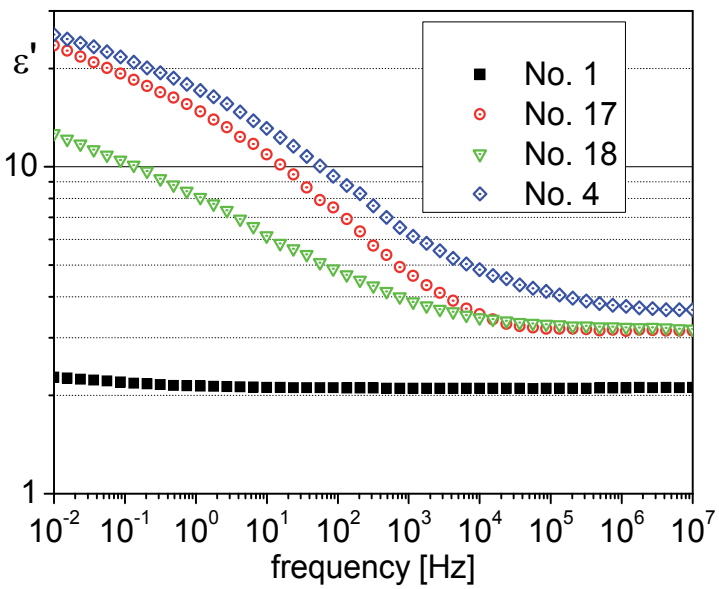

Fig. 8. Frequency dependences of dielectric permittivity ε' for the samples: No. 1 – PP, No. 17 – PP + 25 wt. % of short flax fibres, No. 18. – PP + 25 wt. % of flax shivers, No. 4 - PP + 40 wt. % of long flax fibres

nearly constant value in the whole frequency range with a slender increase bellow 10^3 Hz. The addition of a hydrophilic lignocellulosic material to the polypropylene entails the insertion of polar groups into the non-polar material giving the reason for rising the polarization related to the dipole reorientation. Moreover, the presence of the hydroxyl groups –OH in the cellulose, the hemicellulose and the lignin extends the moisture absorption due to the interaction of –OH groups and water molecules. The overall polarization of the composite, being the sum of three contributions: electronic, ionic and dipole reorientation – related ones, exhibits the maximum values at low frequencies and decreases with increasing frequency. The same behaviour shows the dielectric permittivity of the composites ε'. The value of the dielectric permittivity ε' increases with the content of the lignocellulosic material. In the higher frequency range, i.e. above 10^6 Hz, the value of the relative dielectric permittivity ε' tends to the constant value fixed by squared refractive index.

Moreover, the values for composites with the same content (25 wt.%) of different lignocellulosic materials converge. The differences in the dielectric permittivity ε' values are most significant in the low frequency range, and they are observed also for the composites comprising the same content of lignocellulosic materials derived from different parts of hemp and flax. The composites containing the shivers derived from hemp as well as from flax (25 wt.%) exhibit lower ε' than the ones comprising short fibres (also 25 wt.%). The shivers are the lignified parts of the stems, separated from the fibres and they show lower capacity of moisture absorption. This fact can indicate a smaller number of polar groups and lower polarization related to dipole reorientation.

Plots of the reciprocal of dielectric permittivity $1/\varepsilon'$ versus volume fraction of lignocellulosic material derived from hemp and flax at the frequency of 1 MHz (Fig. 9) are linear for the

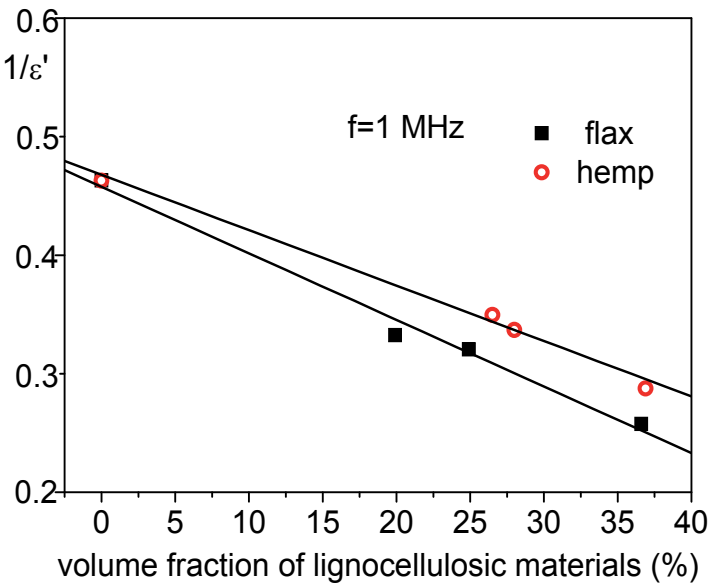

Fig. 9. Reciprocal dielectric permittivity $1/\varepsilon'$ versus volume fraction of lignocellulosic material derived from hemp and flax (Markiewicz et al., 2009)

applied contents of filler. A number of numerical relations as Lichtenecker, Maxwell Garnet, Jayasundere, Poon-Shin equations or Effective Medium Theory were developed by researchers to predict the effective dielectric constant of the composites (Subodh et al., 2007). All the mentioned models differ at higher volume fraction of the filler and they can be replaced by the linear fit at lower filler content, when the permittivity contrast between matrix and filler is low, particularly. For our investigated samples with the volume fraction less than 0.4 the dependence of the reciprocal of the dielectric permittivity on the volume fraction can be approximated by the linear fit (Sareni et al., 1997). The obtained results are in agreement with those presented by Jacob M. at al. (Jacob, 2006) for sisal-oil palm hybrid biofibre reinforced natural rubber biocomposites.

The reinforcement of the polypropylene with the lignocellulosic material results in the increase of ac conductivity (Figs. 10 and 11). The random distribution of the lignocellulosic fillers in the polypropylene matrix enables rearrangement of the fibres in a chain structure which ensures better carrier mobility in the presence of electric field. The frequency dependence of the electrical conductivity is described by the expression (Jonsher, 1997):

$$\sigma(\omega) \propto \omega^n . \tag{9}$$

The exponent n is close to 0.5 for pure polypropylene and points to diffusive carrier transport. For the composites, n changes from ~ about 0.5 at the low frequencies to ~ 1 at the high frequencies. This fact proves the existence of diffusive as well as hopping carrier transport. In the lowest frequency range the composite samples show the frequency-independent behavior pointing to the ohmic conduction. This property makes them to be better antistatic material than pure propylene.

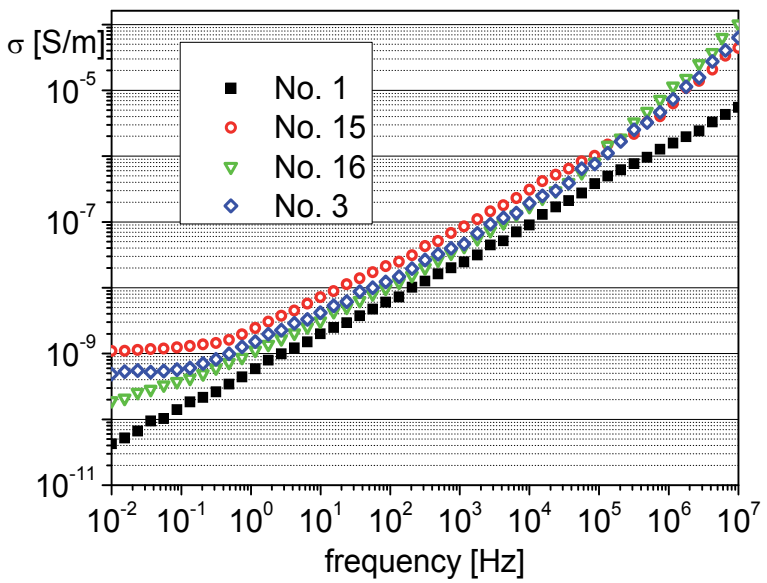

Fig. 10. Frequency dependences of ac conductivity σ' for the samples: No. 1 – PP, No. 15 – PP + 25 wt. % of short hemp fibres, No. 16 – PP + 25 wt. % of hemp shivers, No. 3 - PP+40% of long hemp fibres

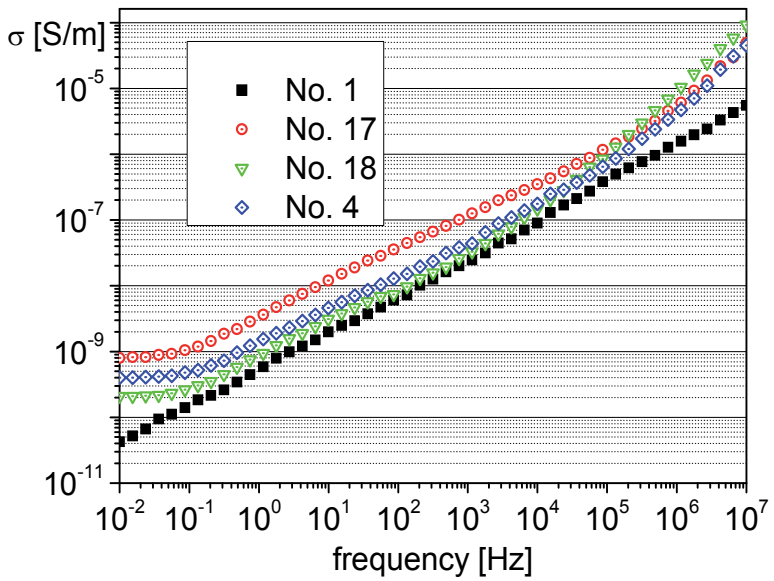

Fig. 11. Frequency dependences of ac conductivity σ' for the samples: No. 1 – PP, No. 17 – PP + 25 wt, % of short flax fibres, No. 18 - PP+25 wt. % of flax shivers, No. 4 – PP + 40 wt. % of long flax fibres

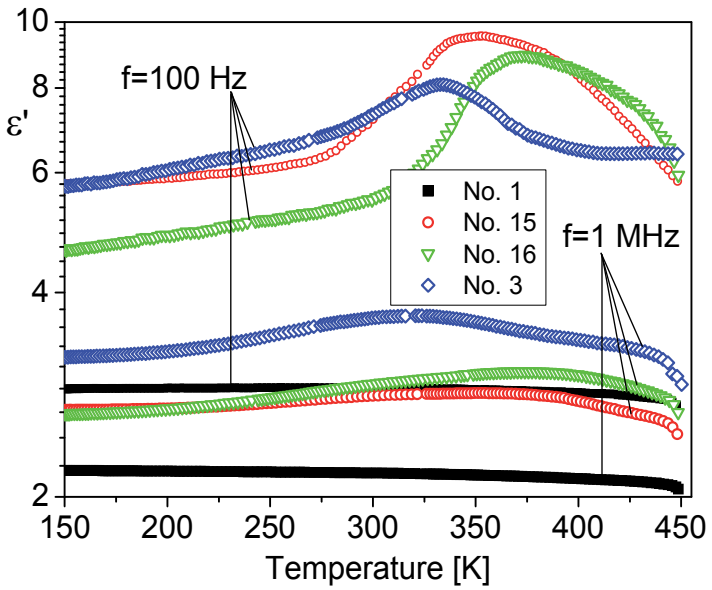

Fig. 12. Temperature dependences of dielectric permittivity ε' obtained at frequencies 100 kHz and 1 MHz for the samples: No. 1- polypropylene PP; No. 15 - PP + 25 wt.% of short hemp fibres; No. 16 – PP + 25 wt.% of hemp shivers; No. 3 – PP + 40 wt.% of long hemp fibres

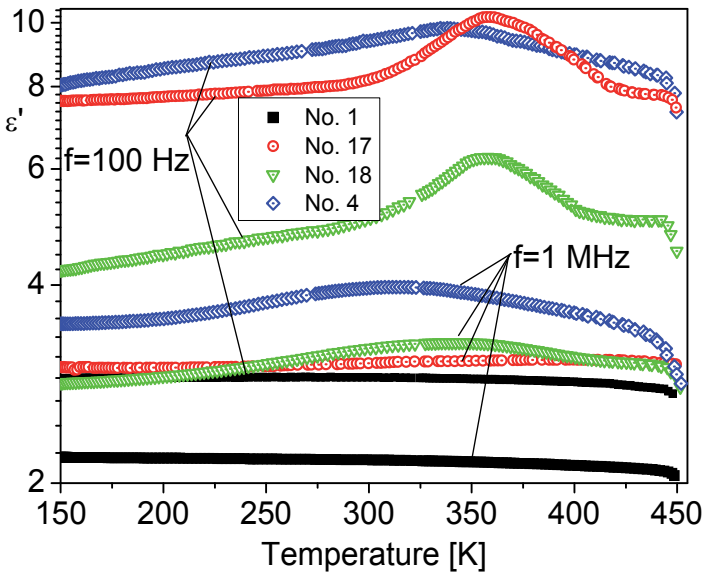

Fig. 13. Temperature dependences of dielectric permittivity ε' obtained at frequencies 100 kHz and 1 MHz for the samples: No. 1 - polypropylene PP; No. 17 - PP + 25 wt.% of short flax fibres; No. 18 – PP + 25 wt.% of flax shivers; No. 4 – PP + 40 wt.% of long flax fibres

The temperature variations of the dielectric permittivity ε' investigated for the polypropylene as well as the composite samples with hemp and flax are presented in Figs. 12 and 13. The value of ε' measured for polypropylene is nearly independent on the temperature up to the melting point at 438 K (Doh, 2005). The dielectric permittivity ε' of the composites increases with the temperature up to the maximum associated with the traces of water, and then decreases. The position of the maximum is determined by the contents of chemically bounded water which cannot be removed during the preparation. The maximum is shifted towards higher temperatures in the case of higher contents (Chand, 2005). As follows from Figs. 12 and 13, the technique of hydraulic pressing, applied for fabrication of composite samples with long fibers, implied the lowest content of water. In the vicinity of the melting point of the polypropylene, a rapid fall of the ε' value is visible. The dielectric permittivity ε' decreases with the increase of the frequency, as is seen for two frequencies: 100 Hz and 1 MHz. A weak dependency of dielectric permittivity ε' on the temperature was observed for the frequency of 1 MHz, particularly in the case of polypropylene composites with short fibres. This feature is the evidence that the composites can be recommended for application in the high frequency range because of the stable dielectric permittivity ε' value.

The dielectric loss factors ε'' of the pure polypropylene and the composites containing the lignocellulosic materials derived from hemp and flax are presented in Figs. 14 and 15 as a function of the temperature for the frequency of 1000 Hz. Pure polypropylene is known to exhibit two characteristic features (Kotek et al., 2005): a glass relaxation peak around 263 K and a high – temperature (~323 K) shoulder associated with chain relaxation in the crystalline phase. These features cannot be detected by the Dielectric Relaxation

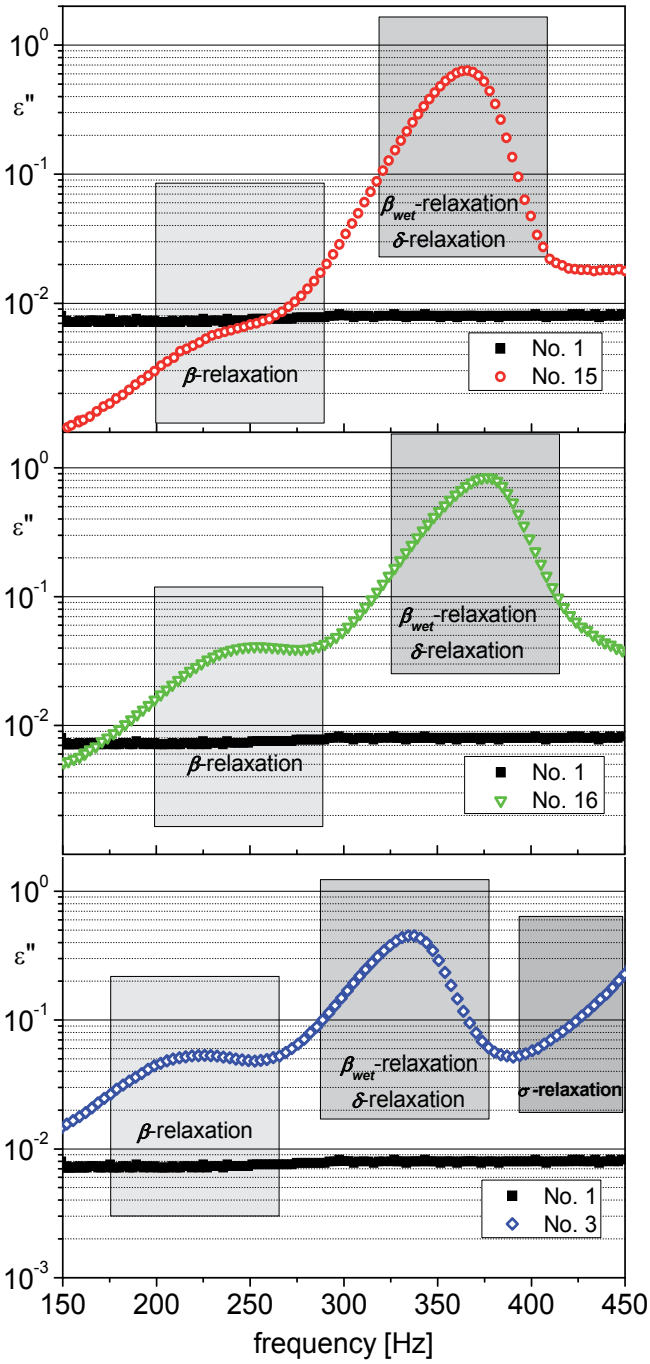

Fig. 14. Temperature dependences of dielectric losses ε'' obtained at frequency 1000 Hz for the samples: No. 1- polypropylene PP; No. 15 - PP + 25 wt.% of short hemp fibres; No. 16 – PP + 25 wt.% of hemp shivers; No. 3 – PP + 40 wt.% of long hemp fibres

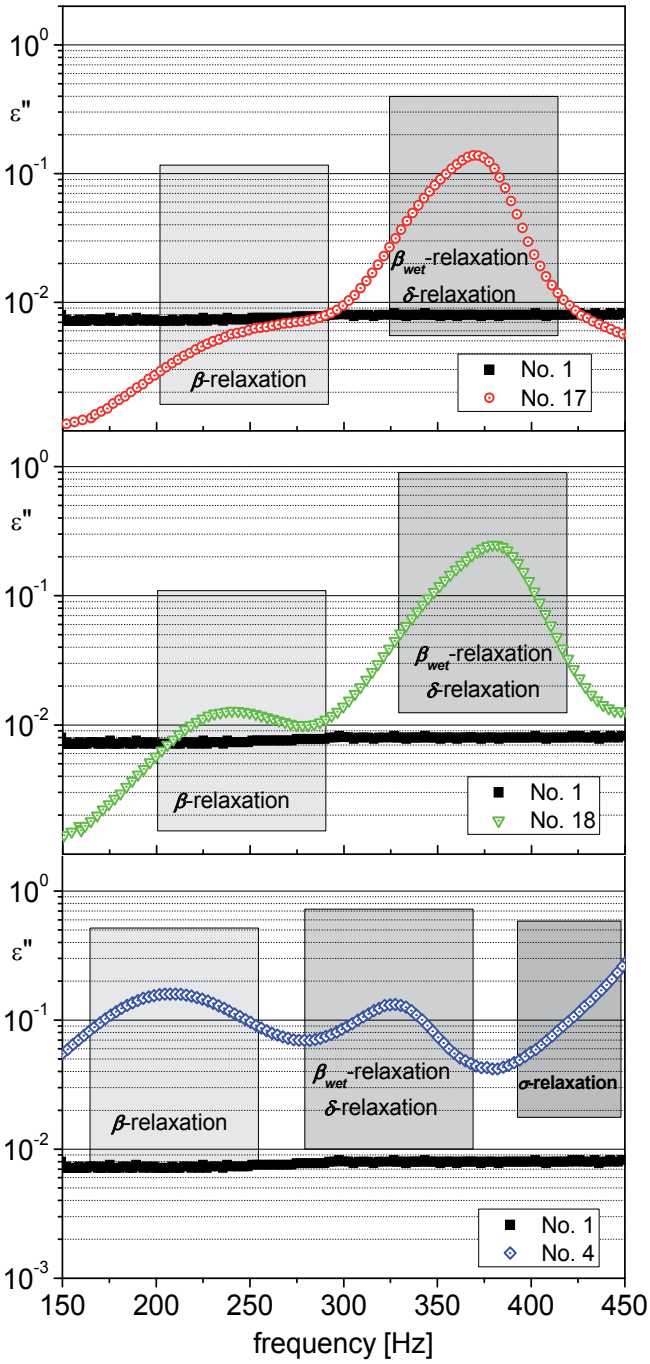

Fig. 15. Temperature dependences of dielectric losses ε'' obtained at frequency 1000 Hz for the samples: No. 1- polypropylene PP; No. 17 - PP + 25 wt.% of short flax fibres; No. 18 – PP + 25 wt.% of flax shivers; No. 3 – PP + 40 wt.% of long flax fibres

Spectroscopy (DRS) method without special modification of the polymer structure or introducing polar groups in the structure because polypropylene has no appreciable molecular dipoles and is not dielectrically active. The non-polar polypropylene does not show any anomalies in the dielectric loss spectrum. However, the temperature dependences of the dielectric loss factors ε'' measured for the composites are strongly influenced by the contribution of the lignocellulosic materials. Both kinds of the filler modify the dielectric absorption spectrum in the same way. In the low temperature range (from about 200 to 270 K) one can observe the maxima of ε'' ascribed to the β - relaxation process in the cellulose which is the main component of each lignocellulosic material. The β - relaxation is interpreted as a local motion of chain segments via the glucosidic linkages (Einfeldt et al., 2001). Above room temperature (from about 300 to 400 K) one can notice high relaxation peaks. Based on the shape of these peaks, one can deduce that two relaxation processes overlap in this temperature range: β_{wet} – the relaxation associated with the orientational motion of both cellulose and water (Baranov et al., 2003; Einfeldt et al., 2001) and δ - the relaxation ascribed to the motion of the end groups in branched polymers (Einfeldt et al, 2001) present in the lignocellulosic material (hemicellulose, pectin, lignin). Because the intensity of the δ - relaxation is significantly smaller than that of β_{wet} - relaxation (Einfeldt et al., 2001), one can state that in the polypropylene – lignocellulosic materials composites the β_{wet} - relaxation is disturbed by the δ - process. In the case of the composites with long fibres derived from flax as well as hemp, the increase in the dielectric losses was observed in the highest temperature range (above 420 K). The effect results from the electric conductivity and is called σ - relaxation (Einfeldt et al., 2001). The losses due to the electric conductivity are ascribed to charge carrier hopping between localized sites in amorphous solids. The fact that the σ - relaxation was observed only for the composites with long fibres confirms the conclusion from (Einfeldt et al., 2001) that the activation energy for the carrier hopping increases when the amount of water is reduced. The intensity of β_{wet} – relaxation is proportional to the contents of water. The low intensity of β_{wet} – relaxation in the composites with long fibers is a reason for relatively high strength of β – relaxation in comparison with that observed for other investigated samples where the β – process is suppressed by the β_{wet} – relaxation and the position of high intensive β_{wet} – relaxation peak in higher temperature range masks the σ - process.

4.2 Effect of chemical treatment of lignocellulosic fillers on the dielectric properties of the composites

The effect of chemical treatment is dominant in the low frequency range, i. e. from 10^{-2} Hz to 1 kHz. It can be opposite for various kinds of lignocellulosic fillers. Figs. 16 and 17 show the frequency dependences of dielectric permittivity ε' obtained at room temperature for the polypropylene composites containing crude, mercerized and modified lignocellulosic fillers derived from pine and beech wood as well as two kinds of rapeseed straw. The effect observed for the pine and beech wood (Fig. 16) consists in the increase of the dielectric permittivity ε' value. The modification with maleic anhydride causes greater increase than the mercerization. In the case of both kinds of rapeseed straw: Kaszub and Californium (Fig. 17), the mercerization decreases the dielectric permittivity ε' value several times and the modification with maleic anhydride reduces ε' value to that measured for composites with crude pine and crude beech. One should take into account the location of the β_{wet} - relaxation in the vicinity of room temperature to explain the opposite influence of chemical treatment

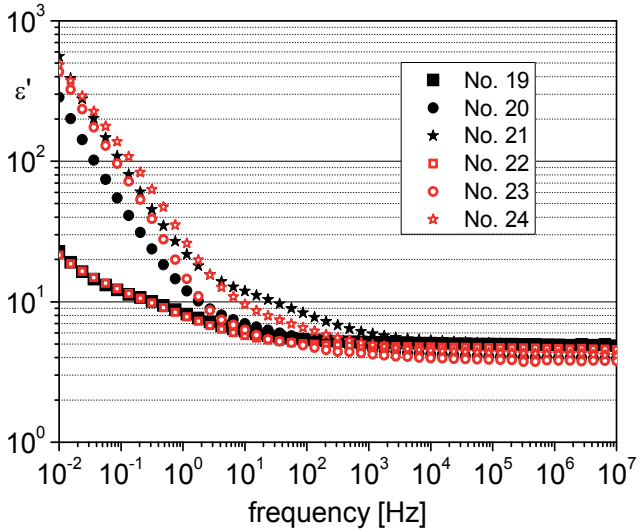

Fig. 16. Frequency dependences of dielectric permittivity ε' obtained for the samples: No. 19 – PP + 30 wt. % of crude beech; No. 20 – PP + 30 wt. % of mercerized beech; No. 21 – PP + 30 wt. % of beech modified with maleic anhydride; No. 22 – PP + 30 wt. % of crude pine; No. 23 – PP + 30 wt. % of mercerized pine; No. 24 – PP + wt. 30% of pine modified with maleic anhydride

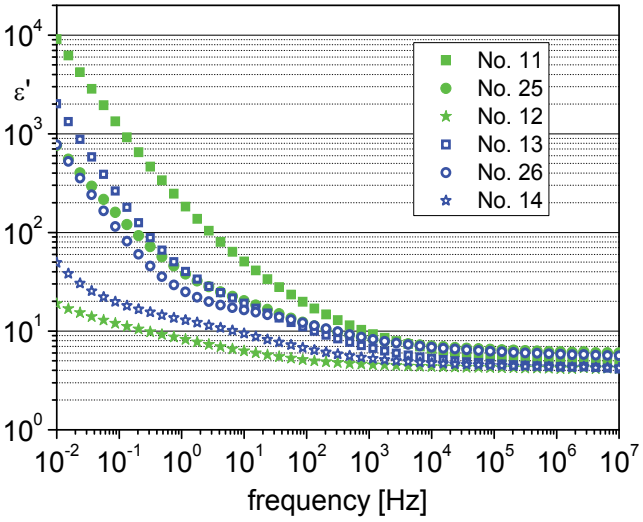

Fig. 17. Frequency dependences of dielectric permittivity ε' obtained for the samples: No. 11 – PP + 30 wt. % of crude rapeseed straw Kaszub; No. 25 – PP + 30 wt. % of mercerized rapeseed straw Kaszub; No. 12 – PP + 30 wt. % of rapeseed straw Kaszub modified with acetic anhydride; No. 13 – PP + 30 wt. % of crude rapeseed straw Californium; No. 26 – PP + 30 wt. % of mercerized rapeseed straw Californium; No. 14 – PP + 30 wt. % of rapeseed straw Californium modified with acetic anhydride

on the dielectric permittivity ε' value at low frequencies. The effect is associated with the ability of moisture absorption. The swollen structure of crude rapeseed straw facilitates the moisture absorption and the ε' value for this material is the biggest one. The mercerization and the modification with acetic anhydride make the structure more rigid and the moisture absorption is limited. However, in the case of beech and pine the crystalline structure of the cellulose confined to the fibres gets be swelled just after chemical treatment.

5. Conclusion

The investigated composite materials based on polypropylene matrix and lignocellulosic fillers can be recommended for application in building and automotive industry because of their good sound absorptive power as well as in packaging electronics due to their dielectric properties. Addition of lignocellulosic materials to the pure polypropylene increases the sound absorption coefficient by about 20% in the frequency range above 3000 Hz. The frequency dependence of the absorption coefficient can be shaped by the proper choice of the lignocellulosic filler. The shift of the sound absorption band due to chemical treatment of the lignocellulosic fibres seems to be suitable for manufacturing the composites with extended sound absorption frequency range as the effect of the adaptation of mixed filler containing the treated and untreated lignocellulosic material. The increased dielectric permittivity of the composites, in comparison with the polypropylene, is preferable in the application in the field of packaging industry. The polypropylene-lignocellulosic materials composites assure the thermal stability of the dielectric permittivity above 1 MHz and better antistatic properties than pure polypropylene.

6. Acknowledgment

The authors are grateful to Professor Józef Garbarczyk for inspiration and valuable discussion of the material presented in this manuscript. This research was supported by Grant of Poznan University of Technology 32-171/12-DS.

7. References

Averous, L. & Le Digabel, F. (2006). Properties of Biocomposites Based on Lignocellulosic Fillers. *Carbohydrate Polymers,* Vol.66, No.4, (November 2006), pp. 480-493, ISSN 0144-8617

Baranov, A.I.; Anisimova, V.N.; Khripunov, A.K. & Baklagina Y.G. (2003). Dielectric Properties and Dipole Glass Transition in Cellulose Acetobacter Xylinium. *Ferroelectrics*, Vol.286, No.1, (n. d. 2003), pp. 141-151, ISSN 0015-0193

Biot, M. A. (1955). Theory of Elasticity and Consolidation for a Porous Anisotropic Solid. *Journal of Applied Physics,* Vol.26, No.2, (February 1955), pp. 182-185, ISSN 0021-8979

Biot, M. A. (1956a). Theory of Propagation of Elastic Waves in a Fluid-Saturated Porous Solid. I. Low-Frequency Range. *Journal of the Acoustical Society of America,* Vol.28, No.2, (March 1956), pp. 168-178, ISSN 0001-4966

Biot, M. A. (1956b). Theory of Propagation of Elastic Waves in a Fluid-Saturated Porous Solid. II. Higher Frequency Range. *Journal of the Acoustical Society of America,* Vol.28, No.2, (March 1956), pp. 179-191, ISSN 0001-4966

Biot, M.A. (1962a). Mechanics of deformation and acoustic propagation in porous media. *Journal of Applied Physics,* Vol.33, No.4, (April 1962), pp. 1482-1498, ISSN 0021-8979

Biot, M.A. (1962b). Generalized theory of acoustic propagation in porous dissipative media. *Journal of the Acoustical Society of America,* Vol.34, No.9A, (September 1962), pp. 1254-1264, ISSN 0001-4966

Bledzki, A.K. & Gassan, J. (1999). Composites Reinforced with Cellulose Based Fibres. *Progress in Polymer Science,* Vol.24, No.2, (May 1999), pp. 221-274, ISSN 0079-6700

Bledzki, A.K.; Letman, M.; Viksne, A. & Rence, L. (2005). A Comparison of Compounding Processes and Wood Type for Wood Fibre—PP Composites. *Composites: Part A*, Vol.36, No.6, (June 2005), pp. 789-797, ISSN 1359-835X

Borysiak, S. & Garbarczyk, J. (2003). Crystallisation of Isotactic Polypropylene with β-Nucleating Agents under Elevated Pressure. *Fibres and Textiles in Eastern Europe,* Vol.11, No.5, (January/December 2003), pp. 50-53

Borysiak, S.; Paukszta, D. & Helwig, M. (2006). Flammability of Wood-Polypropylene Composites. *Polymer Degradation and Stability,* Vol.91, No.12, (December 2006), pp. 3339-3343, ISSN 0141-3910

Borysiak, S. & Doczekalska, B. (2005). X-Ray Diffraction Study of Pine Wood Treated with NaOH. *Fibres and Textiles in Eastern Europe,* Vol.13, No.5, (January/December 2005), pp. 87-89

Chand, N. & Jain, D. (2005). Effect of Sisal Fibre Orientation on Electrical Properties of Sisal Fibre Reinforced Epoxy Composites. *Composites: Part A*, Vol.36, No.5, (May 2005), pp. 594-602, ISSN 1359-835X

Chung , D.L. (1995). *Materials for electronic packaging,* Butterworth–Heinemann, ISBN 0-7506-9314-2, Boston, USA

Doh G.H.; Lee, S.Y.; Kang, I.A. & Kong Y.T. (2005). Thermal Behavior of Liquefied Wood Polymer Composites. *Composite Structures*, Vol.68, No.1, (April 2005), pp. 103-108, ISSN 0263-8223

Einfeldt, J.; Meissner, D. & Kwasniewski, A. (2001). Polymerdynamics of Cellulose and Other Polysaccharides in Solid State-Secondary Dielectric Relaxation Processes. *Progress in Polymer Science*, Vol.26, No.9, (November 2001), pp. 1419-1472, ISSN 0079-6700

Epstein, P.S. & Carhart, R.R. The Absorption of Sound in Suspensions and Emulsions. I. Water Fog in Air. *Journal of the Acoustical Society of America,* Vol.25, No.3, (May 1953), pp. 553-565, ISSN 0001-4966

Ersoy, S. & Kucuk, H. (2009). Investigation of industrial tea-leaf-fibre waste materialfor its sound absorption properties. *Applied Acoustics,* Vol.70, No.1, (January 2009), pp. 215-220, ISSN 0003-682X

Gosselink, R.J.A.; Krosse, A.M.A.; van der Putten, J.C.; van der Kolk, J.C.; de Klerk–Engels, B. & van Dam, J.E.G. (2004). Wood Preservation by Low-temperature Carbonisation. *Industrial Crops and Products,* Vol.19, No.1, (January 2004), pp. 3-12, ISSN 0926-6690

Hattotuwa, G.B. Premalal; Ismail, H. & Baharin, A. (2002). Comparison of the Mechanical Properties of Rice Husk Powder Filled Polypropylene Composites with Talc Filled Polypropylene Composites. *Polymer Testing,* Vol.21, No.7, (n. d. 2002), pp. 833-839, ISSN 0142-9418

Jacob, M.; Varughese, K.T. & Thomas, S., (2006). Dielectric Characteristics of Sisal–Oil Palm Hybrid Biofibre Reinforced Natural Rubber Biocomposites. *Journal of Materials Science,* Vol. 41, No. 17, (September 2006), ISSN 0022-2461

Jonsher, A.K., (1977). The "Universal" Dielectric Response. *Nature,* Vol.267, No.5613, (June 1977), pp. 673-679, ISSN 0028-0836

Kim, S.J.; Moon, J.B.; Kim, G.H. & Ha, C.S. (2008). Mechanical Properties of Polypropylene/Natural Fiber Composites: Comparison of Wood Fiber and Cotton Fiber. *Polymer Testing,* Vol.27, No. 7, (October 2008), pp. 801-806, ISSN 0142-9418

Kotek, J.; Kelnar, I.; Studenovsky, M. & Baldrian J. (2005). Chlorosulfonated polypropylene: preparation and its application as a coupling agent in polypropylene–clay nanocomposites. *Polymer,* Vol. 46, No. 16, (June 2005), pp. 4876-4881, ISSN 0032-3861

Lee, F.C. & Chen, W.H. (2001). Acoustic Transmission Analysis of Multi-Layer absorbers. *Journal of Sound and Vibration,* Vol. 248, No.4, (December 2001), pp. 621-634, ISSN 0022-460X

Liu, Y. & Hu, H. (2008). X-ray Diffraction Study of Bamboo Fibers Treated with NaOH. *Fibers and Polymers,* Vol.9, No.6, (December 2008), pp. 735-739, ISSN 1229-9197

Mahlberg, R.; Paajanen, L.; Nurmi, A.; Kivisto, A.; Koskela, K. & Rowell, R.M. (2001). Effect of Chemical Modification of Wood on the Mechanical and Adhesion Properties of Wood Fiber/Polypropylene Fiber and Polypropylene/Veneer Composites. *Holz als Roh-und Werkstoff,* Vol.59, No.5, (October 2001), pp. 319-326, ISSN 0018-3768

Markiewicz, E.; Borysiak, S. & Paukszta; D. (2009). Polypropylene-lignocellulosic material composites as promising sound absorbing materials. *Polimery,* Vol.54, No.6, (June 2009), pp. 430-435, ISSN 0032-2725

Markiewicz, E.; Paukszta D. & Borysiak S., (2009). Dielectric Properties of LignocellulosicMaterials–Polypropylene composites. *Materials Science-Poland,* Vol.27, No.2, (n. d. 2009), pp. 581-593, ISSN 0137-1339

Mohanty, A.K.; Misra, M. & Hinrichsen, G. (2000). Biofibres, Biodegradable Polymers and Biocomposites: An Overview. *Macromolecular Materials and Engineering,* Vol.276-277, No. 1, (March 2000), pp. 1 -24, ISSN 1439-2054

Nachtigall, S.M.B.; Cerveira, G.S. & Rosa, S.M.L. (2007). New Polymeric-Coupling Agent for Polypropylene/Wood-Flour Composites. *Polymer Test*ing, Vol.26, No.5, (August 2007), pp. 619-628, ISSN 0142-9418

Nik–Azar, M.; Hajaligol, M. R.; Sohrabi ,M. & Dabir, B. Mineral matter effects in rapid pyrolysis of beech wood . *Fuel Processing Technology,* Vol.51, No.1, (March 1997), pp. 7-17, ISSN 0378-3820

Nor, M.J.M.; Jamaluddin, M. & Tamiri, F.M. (2004). A Preliminary Study of Sound Absorption Using Multi-layer Coconut Coir Fibers. *Electronic Journal "Technical Acoustics*", Vol.3, (March 2004), pp. 1-8, ISSN 1819-2408, Retrieved from http://ejta.org/en/tamiri1

Paukszta, D. Investigations of Lignocellulosic Materials from Rape for the Purpose of Producing Composites with Thermoplastic Polymers. *Fibres and Textiles in Eastern Europe.* Vol.13, No.5, (January/December 2005), pp. 90-92, ISSN 1230-3666

Paukszta, D. Chemical Composition of Wooden Parts of Rape Stem. *Oilseed Crops,* Vol. XXVII, No.1, (n. d. 2006), pp. 143-150

Pecht, M.G.; Agarwal, R.; McCluskey, P.; Dishonhg, T.; Javadpour, S.& Mahajan, R. (1999). *Electronic packaging materials and their properties,* CRC Press LLC, Washington, USA
Peijs, T. (2003). Composites for Recyclability. *Materials Today*, Vol.6, No.4, (April 2003), pp. 30-35, ISSN 1369-7021

Polish Patent 186577, 2004

Polish Patent 190405, 2005

Sareni, B.; Krähenbühl, L.; Beroual, A. & Brosseau, C. (1997). Effective Dielectric Constant of Random Composite Materials. *Journal of Applied Physics,* Vol.81, No.5, (March 1997), pp. 2375 – 2383 , ISSN 0021-8979

Soluch, W. (1980). *Wstęp do piezoelektroniki*, Wydawnictwa Komunukacji i Łączności, ISBN 83-206-0041-3, Warsaw, Poland

Subodh, G.; Pavithran, C.; Mohanan, P. & Sebastian, M.T. (2007). PTFE/$Sr_2Ce_2Ti_5O_{16}$ polymer ceramic composites for electronic packaging applications. *Journal of the European Ceramic Society,* Vol.27, No.8-9, (n. d. 2007), pp. 3039-3044, ISSN 0955-2219

Tiwari, V.; Shukla, A. & Bose A. (2004). Acoustic Properties of Cenosphere Reinforced Cement and Asphalt Concrete. *Applied Acoustics,* Vol.65, No.3, (March 2004), pp. 263 -275, ISSN 0003-682X

Tummala, R.R. (1991). Ceramic and Glass-Ceramic Packaging in the 1990s. *Journal of the American Ceramic Society,* Vol.74, No.1, (May 1991), pp. 895-908, ISSN 1551-2916

Uchino, K. (2000). *Ferroelectric Devices,* Marcel Dekker, ISBN 0-8247-8133-3, New York-Basel

Vinogradov, N. (2004). Physicochemical and Acoustic Properties of Water-Based Magnetic Colloid. *Colloid Journal,* Vol.66, No.11, (January 2004), pp.29-37, ISSN 1061-933X

Yang, H.S.; Kim, D.J.; Lee, Y.K. & Kim, H.J. (2003). Rice Straw–Wood Particle Composite for Sound Absorbing Wooden Construction Materials. *Bioresource Technology,* Vol.86, No.2, (January 2003), pp. 117-121, ISSN 0960-8524

Yang, H.S.; Wolcott, M.P.; Kim, H.S.; Kim, S.& Kim, H.J. (2006). Properties of Lignocellulosic Material Filled Polypropylene Biocomposites Made with Different Manufacturing Processes. *Polymer Testing*, Vol.25, No.5, (August 2006), pp. 668-676, ISSN 0142-9418

Section 2

Polypropylene in the Science

13

Organic Materials in Nanochemistry

Alireza Aslani
[1]*Nanobiotechnology Research Center,*
Baqiyatallah University Medical of Science, Tehran,
[2]*Department of Chemistry, Faculty of Basic Science,*
Jundi Shapur University of Technology, Dizful,
Islamic Republic of Iran

1. Introduction

At the turn of twenty-first century, we entered nanoworld. These days, if our try to run a simple web search with the keyword "nano" more than thousands and thousands of references will come out: nanoparticles, nanowires, nanostructures, nanocomposite materials, nanoprobe microscopy, nanoelectronics, nanotechnology, nanochemistry, nanomaterials and so on. The list could be endless. When did this scientific nanorevolution actually happen? Perhaps, it was in the mid-1980s, when scanning tunneling microscopy (STM) was invented. Specialists in scanning electron microscopy (SEM) may strongly object to this fact by claiming decades of experience in observing features with nearly atomic resolution and later advances in electron-beam lithography. We should not omit molecular beam epitaxy, the revolutionary technology of the 1980s, which allows producing layered structures with the thickness of each layer in the nanometer range. Colloid chemists would listen to that with a wry smile, and say that in the 1960s and 1970s, they made Langmuir-Blodgett (LB) films with extremely high periodicity in nanometer scale. From this point of view, the nanorevolution was originated from the works of Irving Langmuir and Katherine Blodgett in 1930s. What is the point of such imaginary arguments? All parties were right. We cannot imagine modern nanotechnology without any of the abovementioned contributions. The fact is that we are in the nanoworld now, and the words with prefix "nano" suddenly have become everyday reality. Perhaps it is not that important how it happened. Hence nanotechnology is a very promising field for industrial applications. In fact, several products are already on the market for certain niche sectors with high added value, e.g., biomedical materials and analytic devices. The real revolution in nanomaterial applications, however, is expected to involve widely used bulk products. Polymers like polyolefins and polyvinylchloride (PVC), for example, are good candidates in this respect because of their large-scale use and versatility. Indeed, one of the first applications of nanotechnology was the production of nanofillers for the improvement of the mechanical properties of polymers. Polypropylene (PP) is particularly interesting because of its low cost and good mechanical properties. This polymer has been used in conventional composites for a long time and, in combination with nanofillers, shows better mechanical properties with even low amounts of filler. The main nanofillers used today are nanoclay (natural product) and other nanomaterials (synthetic). Synthetic carbon nanotubes are very expensive. Nanoclays (layered silicates), in contrast, are especially interesting for bulk

applications because they are relatively inexpensive and they cause an improvement in the mechanical properties of polymers. Commonly used nanoclays include montmorillonite, hectorite, and saponite, all of which belong to the same general family of 2:1 layered or phyllosilicates. As a result of the material reduction, the environmental impact of PP nanocomposite products can be expected to be lower than that of products made out of conventional material unless the production of the nanoparticles is accompanied by particularly high environmental impacts. Nanocomposites are as multiphase materials, where one of the phases has nanoscale additives. They are expected to display unusual properties emerging from the combination of each component. According to their matrix materials, nanocomposites can be classified as ceramic matrix nanocomposites (CMNC), metal matrix nanocomposites (MMNC), and polymer matrix nanocomposites (PMNC). Polymers are now the most widely used in the field of technical textiles. The widespread use of common organic polymers such as polyolefins, polyesters and polyurethanes emanates from key features such as lightweight, easy fabrication, exceptional processability, durability and relatively low cost. A major challenge in polymer science is to broaden the application window of such materials by retaining the above features while enhancing particular characteristics such as modulus, strength, fire performance and heat resistance. However, polymers have relatively poor mechanical, thermal, and electrical properties as compared to metals and ceramics. Many types of polymers such as homopolymers, co-polymers, blended polymers and modified polymers are not sufficient enough to compensate various properties, which we have demanded. Alternative approaches to improve their properties are to reinforce polymers with inclusion of fiber, whisker, platelets or particles. The choice of the polymers is usually guided mainly by their mechanical, thermal, electrical, optical and magnetic behaviors. However, other properties such as hydrophobic-hydrophilic balance, chemical stability, bio-compatibility, opto-electronic properties and chemical functionalities have to be considered in the choice of the polymers. The polymers in many cases can also allow easier shaping and better processing of the composite materials. The inorganic particles not only provide mechanical and thermal stability, but also new functionalities that depend on the chemical nature, the structure, the size, and crystallinity of the inorganic nanoparticles (silica, transition metal oxides, metallic phosphates, nanoclays, nanometals and metal chalcogenides). Indeed, the inorganic particles can implement or improve mechanical, thermal, electronic, magnetic and redox properties, density, refractive index. Organic polymer-based inorganic nanoparticle composites have attracted increasing attention because of their unique properties emerging from the combination of organic and inorganic hybrid materials. The composites have been widely used in the various fields such as military equipments, safety, protective garments, automotive, aerospace, electronics, stabilizer and optical devices. However, these application areas continuously demand additional properties and functions such as high mechanical properties, flame retardation, chemical resistance, UV resistance, electrical conductivity, environmental stability, water repellency, magnetic field resistance and radar absorption. Moreover, the effective properties of the composites are dependent upon the properties of constituents, the volume fraction of components, shape and arrangement of inclusions and interfacial interaction between matrix and inclusion. With the recent development in the nanoscience and nanotechnology fields, the correlation of material properties with filler size has become a focal point of significant interest. On the other hand Polypropylene (PP) is one of the fastest growing commercial thermoplastics due to its attractive combination of low density and

high heat distortion temperature. There are some limitations in physico-chemical properties that restrict PP applications. A typical illustration is in packaging, where PP has poor oxygen gas barrier resistance. No single polymer has shown the ideal combination of performance features. PP possesses good water vapor barrier properties, but it is easily permeated by oxygen, carbon dioxide, and hydrocarbons. The necessity of developing more effective barrier polymers has given rise to different strategies to incorporate and optimize the features from several components. Most schemes to improve PP gas barrier properties involve either addition of higher barrier plastics via a multilayer structure (co-extrusion) or by introducing filler with high aspect ratio in the polymer matrix. Co-extrusion allows tailoring of film properties through the use of different materials where each material component maintains its own set of properties, compared with blending of polymers in a mono-extrusion technique. Co-extrusion is used to generate multilayer laminate structures from separately extruded polymer films that are sandwiched together. Resulting films may comprise many layers, such as the PP-adhesive poly (ethylene-co-vinyl alcohol) (EVOH)-adhesive PP system: EVOH barrier sheet trapped between two layers of moisture resistant PP and two additional adhesive strata. However, by nature co-extrusion is a complex and expensive process. Alternatively, nano fillers with high aspect ratio can be loaded into the polymer matrix. Polymer nanocomposites are a better choice with significant property increments from some materials. Nanocomposite materials are one of the methods for improving gas barrier properties of polyolefin. Recent developments in polymer nanocomposites have attracted attention due to the possibilities offered by this technology to enhance the barrier properties of inexpensive commodity polymers. Many studies have demonstrated improvements in permeability reduction to gases, moisture and organic vapors resulting from the addition of low concentrations of layered some nanoparticles to various thermoplastic matrices. This is mainly due to their nanometer scale particle size and intraparticle distances. The desired properties are usually reached at low filler volume fraction, allowing the nanocomposites to retain macroscopic dispersion and low density of the polymer. The geometrical shape of the particle plays an important role in determining the properties of the composites. The improved nanocomposite barrier behavior illustrated by many examples has been explained by the tortuous path model, in which the presence of impermeable some platelets generates an overlapped structure that hinders penetrate diffusion and thus decreases the permeability of the material.

2. Nanotechnology

Nanotechnology is receiving a lot of attention of late across the globe. The term nano originates etymologically from the Greek, and it means "dwarf." The term indicates physical dimensions that are in the range of one-billionth (10^{-9} or $\frac{1}{10^9}$) of a meter. This scale is called colloquially nanometer scale, or also nanoscale. One nanometer is approximately the length of two hydrogen atoms. Nanotechnology relates to the design, creation, and utilization of materials whose constituent structures exist at the nanoscale; these constituent structures can, by convention, be up to 100 nm in size. Nanotechnology is a growing field that explores electrical, optical, and magnetic activity as well as structural behavior at the molecular and sub-molecular level. These questions should be answered: What is nanotechnology? What are the applications of nanotechnology? What is the market potential for nanotechnology? What are the global research activities in nanotechnology? Why would a practitioner, need to care?

Research and technology development at the atomic, molecular, or macromolecular levels, in the length scale of approximately 1 to 100 nm range called nanotechnology. Creating and using structures, devices, and systems that have novel properties and functions because of their small and/or intermediate size are application of nanomaterials. Hence, nanotechnology can be defined as the ability to work at the molecular level, atom by atom, to create large structures with fundamentally new properties and functions. Nanotechnology can be described as the precision-creation and precision-manipulation of atomic-scale matter; hence, it is also referred to as precision molecular engineering.

Nanotechnology is the application of nanoscience to control processes on the nanometer scale that is, between 1 to 100 nm or call better 2 to 50 nm. The field is also known as molecular engineering or molecular nanotechnology (MNT). MNT deals with the control of the structure of matter based on atom-by-atom and/or molecule-by-molecule engineering; also, it deals with the products and processes of molecular manufacturing. The term engineered nanoparticles describes particles that do not occur naturally; humans have been putting together different materials throughout time, and now with nanotechnology they are doing so at the nanoscale. As it might be inferred, nanotechnology is highly interdisciplinary as a field, and it requires knowledge drawn from a variety of scientific and engineering arenas: Designing at the nanoscale is working in a world where physics, chemistry, electrical engineering, mechanical engineering, and even biology become unified into an integrated field. "Building blocks" for nanomaterials include carbon-based components and organics, semiconductors, metals, and metal oxides; nanomaterials are the infrastructure, or building blocks, for nanotechnology. The term nanotechnology was introduced by Nori Taniguchi in 1974 at the Tokyo International Conference on Production Engineering. He used the word to describe ultrafine machining: the processing of a material to nanoscale precision. This work was focused on studying the mechanisms of machining hard and brittle materials such as quartz crystals, silicon, and alumina ceramics by ultrasonic machining. Years earlier, in a lecture at the annual meeting of the American Physical Society in 1959 (There's Plenty of Room at the Bottom) American Physicist and Nobel Laureate Richard Feynman argued (although he did not coin or use the word nanotechnology) that the scanning electron microscope could be improved in resolution and stability, so that one would be able to "see" atoms. Feynman proceeded to predict the ability to arrange atoms the way a researcher would want them, within the bounds of chemical stability, in order to build tiny structures that in turn would lead to molecular or atomic synthesis of materials. Based on Feynman's idea, K. E. Drexler advanced the idea of "molecular nanotechnology" in 1986 in the book Engines of Creation, where he postulated the concept of using nanoscale molecular structures to act in a machinelike manner to guide and activate the synthesis of larger molecules. Drexler proposed the use of a large number (billions) of robotic-like machines called "assemblers" (or nanobots) that would form the basis of a molecular manufacturing technology capable of building literally anything atom by atom and molecule by molecule. At this time, an engineering discipline has already grown out of the pure and applied science; however, nanoscience still remains somewhat of a maturing field. Nanotechnology can be identified precisely with the concept of "molecular manufacturing" (molecular nanotechnology) introduced above or with a broader definition that also includes laterally related sub-disciplines. The nanoscale is where physical and biological systems approach a comparable dimensional scale. A basic "difference" between systems biology and nanotechnology is the goal of the science: systems biology aims to

uncover the fundamental operation of the cell in an effort to predict the exact response to specific stimuli and genetic variations (has scientific discovery focus); nanotechnology, on the other hand, does not attempt to be so precise but is chiefly concerned with useful design.

A nanometer is about the width of four silicon atoms (with a radius of 0.13 nm) or two hydrogen atoms (radius of 0.21 nm); .For comparison purposes, the core of a single-mode fiber is 10.000 nm in diameter, and a 10 nm nanowire is 1000 times smaller than (the core of) a fiber. The nanoscale exists at a boundary between the "classical world" and the "quantum mechanical world"; therefore, realization of nanotechnology promises to afford revolutionary new capabilities.

The nanoparticles are ultrafine particles in the size of nanometer order. "Nano" is a prefix denoting the minus 9th power of ten, namely one billionth. Here it means nanometer (nm) applied for the length. One nm is extremely small length corresponding to one billionth of 1 m, one millionth of 1 mm, or one thousandth of 1 μm. The definition of nanoparticles differs depending upon the materials, fields and applications concerned. In the narrower sense, they are regarded as the particles smaller than 10 to 20 nm, where the physical properties of solid materials themselves would drastically change. On the other hand, the particles in the three digit range of nanometer from 1 nm to 1μm could be called as nanoparticles. In many cases, the particles from 1 to 100 nm are generally called as nanoparticles, but here they will be regarded as the particles smaller than those called conventionally "submicron particles", and concretely less than the wavelength of visible light (its lower limit is about 400 nm) as a measure, which need to be treated differently from the submicron particles.

3. Features of nanoparticles: "Activation of particle surface"

All the solid particles consist of the atoms or the molecules. As they are micronized, they tend to be affected by the behavior of atoms or the molecules themselves and to show different properties from those of the bulk solid of the same material. It is attributable to the change of the bonding state of the atoms or the molecules constructing the particles. The diameter of the smallest hydrogen atom is 0.074 nm, and that of the relatively large lead atom (atomic number is 82) is 0.35 nm. From these sizes, it is estimated that the particle with a size of 2 nm consists of only several tens to thousands atoms. When the particle is constructed by larger molecules, the number decreases furthermore [M. Arakawa, 2005[a] and 1983[b]]. It is indicated that the fraction of surface atoms of a 20 μm cubic particle is only 0.006%, but it increases to 0.6% for a 200 nm particle and then it is estimated almost half of the atoms are situated at the surface of a 2 nm particle. On the other hand, as the micronization of solid particles, the specific surface area increases generally in reversal proportion to the particle size. In the above-mentioned case, when the particle of 1cm is micronized to 1 μm and 10 nm, the specific surface area becomes ten thousand times and million times, respectively. As the increase in the specific surface area directly influences such properties like the solution and reaction rates of the particles, it is one of major reasons for the unique properties of the nanoparticles different from the bulk material together with the change in the surface properties of the particles itself.

4. Evaluation of size of nanoparticles

In order to elucidate the change in properties and characteristics of nanoparticles with the particle size, it is essential first of all to measure the size of the nanoparticles accurately. The

most basic method to measure the size of nanoparticles is the size analysis from the picture image using the transmission electron microscope, which could also give the particle size distribution. For this analysis, preparation of the well-dispersed particles on the sample mount is the key issue. The grain size of the particles can be obtained from peak width at half height in the X-ray diffraction analysis and it is regarded as an average primary particle size of particles. Meanwhile, the laser diffraction and scattering method, which is popular for the size analysis of micron-sized particles, would hardly measure the particle size of individual nanoparticles but that of the agglomerated particles. The photon correlation method often used for the particle analysis in the nanosized range might not give accurate results in many cases, when the particle size distribution is wide. Then the BET (Brunauer-Emmett-Teller) specific surface measurement based on the gas adsorption is often applied as a simple method to evaluate the size of nanosized primary particles. By this method, it is possible to estimate the particle size from the specific surface area under the assumption of spherical particle shape. This equivalent particle size based on the specific surface area is useful for the evaluation of nanoparticle size, though it may differ from the particle size observed by the electron microscope depending upon the surface state and the inner structure of the particles.

5. Properties of nanoparticles and size effect

As mentioned above, with the decreasing particle size, the solid particles generally tend to show different properties from the bulk material and even the physical properties like melting point and dielectric constant themselves which have been considered as specific properties may change, when the particles become in several nanometer size. These changes in the fundamental properties with the particle size are called "size effect" in a narrower sense. On the contrary, in a broader sense, it could also include the change in the various characteristics and behaviors of particles and powders with the particle size. The nanoparticles have various unique features in the morphological/structural properties, thermal properties, electromagnetic properties, optical properties, mechanical properties as described briefly in the following:

5.1 Morphological and structural properties

The ultrafine size of the nanoparticles itself is one of useful functions. For example, the finer particles are apt to be absorbed more easily through the biological membrane. It is known as the enhanced permeation and retention (EPR) effect [H. Maeda, 1992] that the particles having a particle size from about 50 to 100 nm, which would not be transferred to the normal cells through the vascular wall could be delivered selectively to a certain affected cells because of the enlarged cell gap of this part. As mentioned above, the large specific surface area of the nanoparticles is an important property to the reactivity, solubility, sintering performance etc. related with the mass and heat transfer between the particles and their surroundings from the morphological viewpoint apart from the control of the surface and inner structures of the nanoparticles. Furthermore, the crystal structure of the particles may change with the particle size in the nanosized range in some cases. Uchino et al. [K. Uchino, 1982] reported that from the X-ray diffraction analysis of the lattice constant of $BaTiO_3$ powder prepared by hydrothermal synthesis method, the c/a axis length ratio showing the tetragonal characteristics decreased to indicate the increasing symmetric

property with the decreasing particle size from about 200 nm as shown in fig 1. This is considered to be attributable to the compressive force exerted on the particles as a result of the surface tension of the particle itself. For $PbTiO_3$, it is reported that the tetragonal crystals decreased and the cubical crystal increased in the particles from the particle size of about 18 nm [H. Suzuki, 2002]. In this way, the critical particle size for the crystal structure and the size effect differ with the materials concerned.

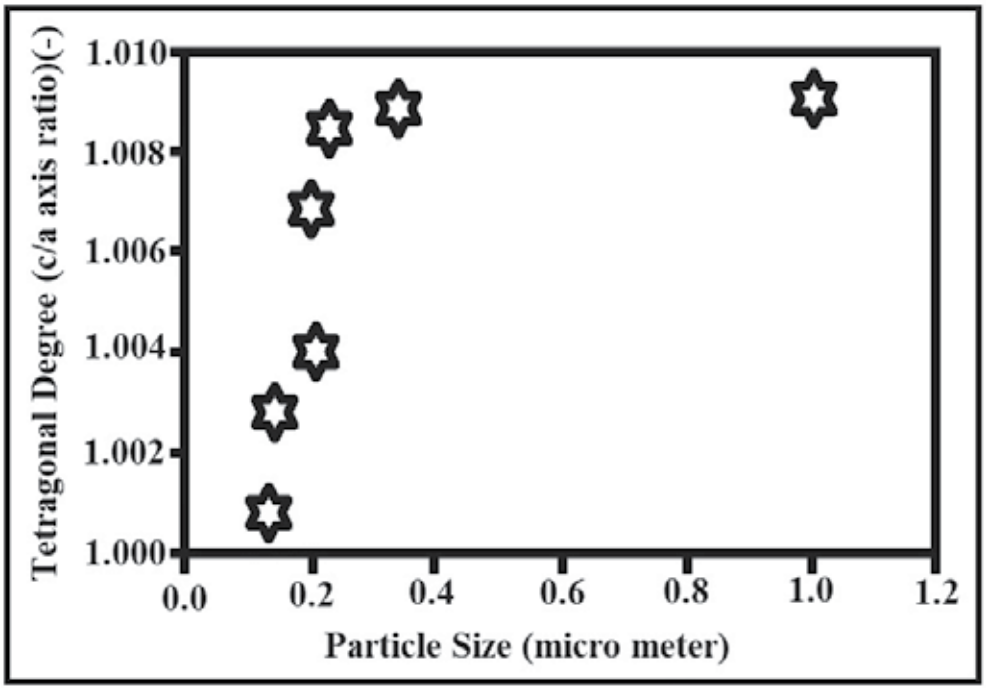

Fig. 1. Relationship between particle size and tetragonal degree (c/a axis ratio) of $BaTiO_3$ powder.

5.2 Thermal properties

As the atoms and molecules located at the particle surface become influential in the nanometer order, the melting point of the material decreases from that of the bulk material because they tend to be able to move easier at the lower temperature. For example, the melting point of gold is 1336 K as a bulk but starts to decrease remarkably below the particle size of about 20 nm and drastically below 10 nm and then becomes more than 500 degrees lower than that of the gold bulk around 2 nm. The reduction of the melting point of ultrafine particles is regarded as one of the unique features of the nanoparticles related with aggregation and grain growth of the nanoparticles or improvement of sintering performance of ceramic materials [N. Wada, 1984].

5.3 Electromagnetic properties

The nanoparticles are used as the raw material for a number of electronic devices. The electric properties and particle size of these nanoparticles play a great role for the

improvement of the product performance [I. Matsui, 2005]. As an example, there is a strong demand for the materials with a high dielectric constant to develop small and thin electronic devices. For this purpose, it has been confirmed by the X-ray diffraction analysis for instance that the dielectric constant of $PbTiO_3$ tends to increase considerably as the particles become smaller than about 20 nm. Meanwhile, it is also known that when the dielectric constant is measured with a pellet prepared by pressing these nanoparticles, it shows a peak with the raw material around 100nm and decreases with the decreasing particle size, which is attributable to the influence of the grain boundary and void in the pellet [M. Takashige, 1981].

On the other hand, the minimum particles size to keep the ferroelectric property (critical size) differs depending upon the kind and composition of the materials. Summarizing the data of various kinds of materials, it varies from 7 nm for $PbTiO_3$ to 317 nm for Ba–Pb–Ti compounds. The Curie point defined as the point changing from the ferroelectric material to the paraelectric phase of $PbTiO_3$ reduces drastically with the decreasing particle size below 20–30 nm as shown in fig 2. As for the Curie point, some equations have been proposed for its estimation [K. Ishikawa, 2001].

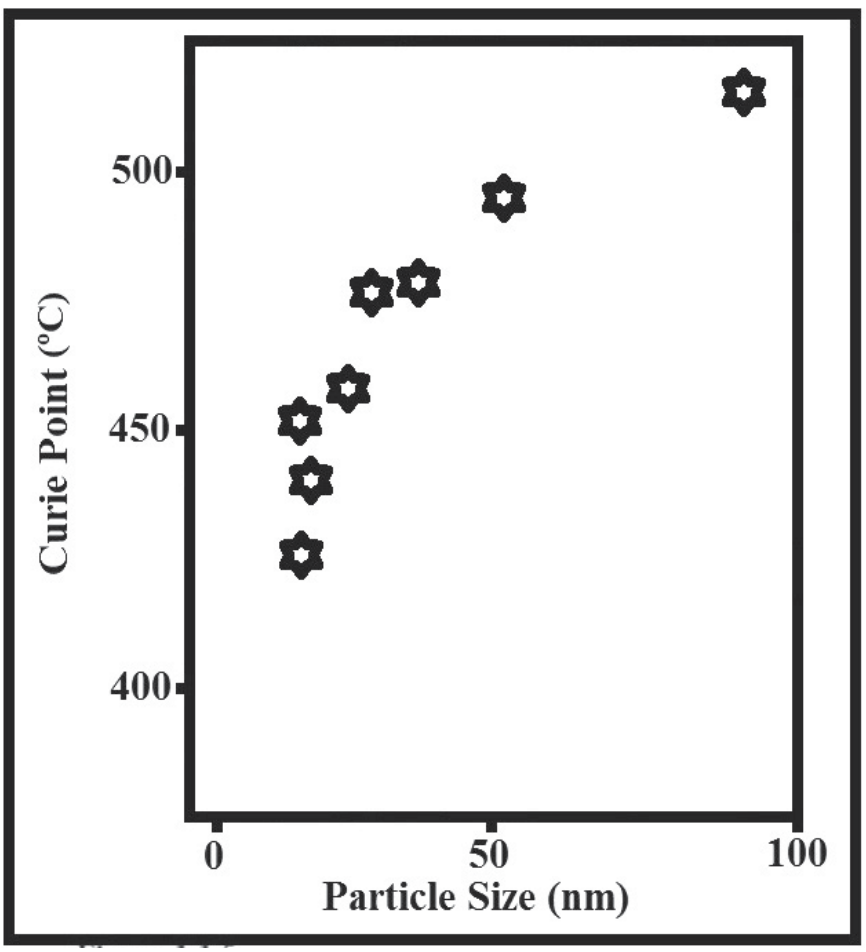

Fig. 2. Change of Curie point of $PbTiO_3$ with its particle size.

As for the magnetic property, ferromagnetic fine particles have a single magnetic domain structure as they become very small as in the order less than about 1 μm and show super-paramagnetic property, when they get further finer. In this case, although the individual particles are ferromagnetic with the single magnetic domain structure, the particles collectively behave as a paramagnetic. It is magnetized as a whole in the same direction of the external magnetic field but the magnetization disappears by the thermal fluctuation, when the external magnetic field is taken away. The time for disappearing of magnetization depends upon the particle size, namely the magnetization of the material responds promptly with the external magnetic field as a paramagnetic when the particles are small enough but it decreases gradually as the particle size becomes larger. As a result of such change in the electromagnetic properties of nanoparticles, it is known for instance that the gold which is a stable substance as a bulk shows unique catalytic characteristics as nanoparticles [K. Ishikawa, 1998 and M. Haruta, 1994].

5.4 Optical properties

As the size of particles becomes in the several nanometers range, they absorb the light with a specific wavelength as the plasmon absorption [Y. Kurokawa, 1996] caused by the plasma oscillation of the electrons and the transmitted light with different color depending upon the kind of metal and particle size is obtained [K. Kobayashi, 2004 and S. Sato, 1996].

In case of gold nanoparticles, it is reported that the maximum light absorption wavelength is 525 nm for the particles of 15nm but it is enlarged by about 50 nm for 45 nm particles. In this way, these gold and silver nanoparticles show the color phenomena with splendid tinting strength, color saturation and transparency compared with the conventional pigments for the paint in the submicron size and the tinting strength per unit volume of silver nanoparticles becomes about 100 times higher than that of organic pigments. Furthermore, since the nanoparticles are smaller than the wavelength of visible light and the light scattering by the particles becomes negligible, higher transparency can be obtained with the nanoparticles than the conventional pigment.

5.5 Mechanical properties

It is known that the hardness of the crystalline materials generally increases with the decreasing crystalline size and that the mechanical strength of the materials considerably increases by micronizing the structure of the metal and ceramic material or composing them in the nano range [K. Niihara, 1991 and T. Sekino, 2000]. Furthermore, with the ceramic material having crystalline size less than several hundred nanometers, the unique super-plastic phenomenon is seen that it is extended several to several thousand times from the original size at the elevated temperature over 50 % of the melting point [F. Wakai, 1990], which may provide the possibility of forming and processing of ceramics like metallic materials.

6. Existing conditions of particles and their properties

The nanoparticles usually exhibit collective functions. Therefore, the dispersing state and the surrounding conditions in addition to the physical properties of the particles themselves are important. In many cases, the nanoparticles exist as aggregates of the primary particles

by the adhesion and bonding during the production process because of their high adhesiveness. The existing state of the nanoparticles is greatly influenced by the surrounding conditions if they are in gas, liquid, solid or in a vacuum and what sort of interaction they have with the surrounding materials. The nanoparticles are rarely used by themselves but dispersed in other materials or combined with them. The dispersing process of the nanoparticles is a key for the nanoparticle technology as well as their preparation methods, since the performance of the final products are affected by their dispersing conditions [T. Yokoyama, 2005]. In this way, it is expected with great possibility to develop various new materials and applications by the nanoparticle technology producing and processing the nanoparticles, which have different properties from the bulk material by the size effects as mentioned above and in the following sections.

7. Wet technologies for the formation of organic nanostructures

Chemical methods of material processing were known for years, existing in parallel with physical and other methods of film deposition. Recent advances in electron microscopy and scanning nanoprobe microscopy (STM, AFM) have revealed that some of the materials produced by the chemical methods have distinctive nanocrystalline structure. Furthermore, due to the achievements of colloid chemistry in the last 20 years, a large variety of colloid nanoparticles have become available for film deposition. This has stimulated great interest in further development of chemical methods as cost-effective alternatives to such physical methods as: thermal evaporation; magnetron sputtering; chemical and physical vapor deposition (CVD, PVD); and molecular beam epitaxy (MBE).

7.1 Formation of colloid nanoparticles

The most advanced chemical method for nano-structured materials processing is the deposition of colloid inorganic particles. Recent achievements in colloid chemistry have made a large variety of colloid compounds commercially available. The list of colloid nanoparticles with uniform (low-dispersed) dimensions in the range from 3 to 50 nm includes the noble metals (e.g., Au, Ag, Pt, Pd, and Cu), semiconductors (e.g., Si, Ge, III-V and II-VI, and metal oxides), insulators (e.g., mica, silica, different ceramic materials, polymers), and magnetic materials (e.g, Fe_2O_3, Ni, Co, and Fe). The growth of colloid particles is usually stabilized during synthesis by adding surfactants to the reagents [Edelstein. A. S. 1996]. Therefore, the stable nanoparticles produced are coated with a thin shell of functionalized hydrocarbons, or some other compounds. Typical examples of the chemistry of formation of colloid nanoparticles are shown below. Gold stable colloids can be prepared by the reduction of $AuCl_4$ with sodium borohydride in the presence of alkane-thiols [Brust. M, 1994]. Other colloids, such as Ag, CdS, CdSe, and ZnS, can be prepared in a similar way. InP nanocrystals can be synthesized by the following reaction, with temperatures ranging from 150 °C to 280 °C in the presence of either primary amines, tri-*n*-octylphosphine (TOP), or tri-*n*-octylphosphine oxide (TOPO) as stabilizing agents, preventing further InP aggregation [Talapin. D. V, 2002].

$$InCl_3 + [(CH_3)_3Si]_3P \rightarrow InP + 3(CH_3)_3SiCl$$

The particles appear to be mono-dispersed, with a mean cluster size varying from 2 to 6 nm depending on the stabilizer used. The particles show strong resonance luminescence after

etching in HF. Cobalt mono-dispersed nanocrystals can be produced by rapid pyrolysis of the organic precursor $Co(CO)_8$ in an inert Ar-atmosphere, and in the presence of organic surfactants, such as oleic-acid and trioctylphosphonic acid at high temperatures [Puntes. V. F., 2001]. The particles appear to have ideal spherical, cubical, or rod-like shapes, with sizes in the range from 3 to 17 nm depending on surfactant concentration. The Co nanoparticles demonstrate superparamagnetic ferromagnetic transition. CdTe nanoparticle colloids can be prepared by the reaction of Na_2Te with CdI_2 in methanol at –78 °C.

The diameter of CdTe colloid particles is in the range from 2.2 to 2.5 nm [Schultz. D. L, 1996]. An alternative method for the formation of stabilized colloid particles is to utilize self-assembled membranes, such as micelles, microemulsions, liposomes, and vesicles. Typical dimensions are from 3 to 6 nm for reverse micelles in aqueous solutions, from 5 to 100 nm for emulsions, and from 100 to 800 nm for vesicles. Liposomes are similar to vesicles, but they have bilayer membranes made of phospholipids. Such membranes may act as the reaction cage during the formation of nanoparticles, and may prevent their further aggregation. The idea of the formation of nanoparticles inside micelles is to trap respective cations there. This can be done by sonification of the mixture of required salts and surfactants. Since the permeability of the membrane for anions is about 100 times higher than for cations, the formation of nanoparticles takes place within micelles, with a constant supply of anions from outside. A number of different colloids, such as CdSe, Ag_2O, Fe_2O_3, Al_2O_3, and cobalt ferrite, were prepared using the above methods [Bhandarkar. S, 1990, Mann. S, 1983, Mann. S. J. P, 1986, Cortan. A. R, 1990, Yaacob. I. I, 1993, and Li. S, 2001].

7.2 Self-assembly of colloid nanoparticles

The deposition of colloid nanoparticles onto solid substrates can be accomplished by different methods, such as simple casting, electrostatic deposition, Langmuir-Blodgett, or spin coating techniques. However, the simplest method of nanoparticles deposition, which gives some remarkable results, is the so-called self-assembly or chemical self-assembly method. This method, which was first introduced by Netzer and Sagiv, is based upon strong covalent bonding of the adsorbed objects (i.e., monomer or polymer molecules and nanoparticles) to the substrate via special functional groups. It is known, for example, that the compounds containing thiol (SH) or amine (NH_2) groups have strong affinity to gold. The silane group (SiH_3) with silicon is another pair having very strong affinity.

The first work on the self-assembly of gold colloid particles capped with alkanethiols was done by Brust and coworkers [Netzer, L, 1983]. This routine has been adopted by other scientists for the deposition of self-assembled monolayers of different colloid nanoparticles (e.g., Ag, CdS, CdSe, and ZnS), which were prepared using mercapto-alcohols, mercaptocarboxylic acids, and thiophenols as capping agents. Self-assembled nanoparticles usually show well-ordered lateral structures, proved by numerous observations with SEM, STM, and AFM [Collier. C, 1997, Lover. T, 1997, Rogach. A. L, 1999 and Vogel. W, 2000].

Two-dimensional ordering in self-assembled nanoparticle monolayers can be substantially improved by thermal annealing at temperatures ranging from 100 °C to 200 °C, depending on the material used. The use of bi-functional $HS-(CH_2)_{10}-COOH$ bridging molecules, which combines both the affinity of thiol groups to gold and carboxylic group to titania, can provide more flexibility in the self-assembly. Both self-assembly routes were exploited for

deposition of TiO_2 nanoparticles onto the gold surface [Rizza. R, 1997]. In the first one, unmodified TiO_2 nanoparticles were self-assembled onto the gold surface, coated with a monolayer of HS-$(CH_2)_{10}$-COOH; while in the second one, TiO_2 nanoparticles stabilized with HS-$(CH_2)_{10}$-COOH were self-assembled onto the bare gold surface. For some time, chemical self-assembly was limited to the formation of organized monolayers. The use of bi-functional bridge molecules overcomes this relative disadvantage. For example, multi-layers of Au colloid particles can be deposited using di-thiol spacing layers. A similar routine was applied for the fabrication of Au/CdS super lattices [Sarathy. K. V, 1999 and Nakanishi. T, 1998].

7.3 Morphology and crystallography of nanostructured materials prepared by chemical routes

The structural study of materials was always of a high priority, because the physical properties of materials depend very much on their structure. There are several levels of structural study, which start with the investigation of the morphology of the material surfaces, closely related to their in-plane ordering. Many nano-structured materials prepared with the help of layer-by-layer deposition techniques, such as LB or electrostatic self-assembly, have a distinctive periodicity in the direction normal to the surface, which determines their main electrical and optical properties. This is why the study of the layer-by-layer structure of such materials is of crucial importance.

The materials consisting of colloid nanoparticles have a tendency to form two dimensional structures according to the close packing order. This trend can stimulate the formation of multilayered quasi-3D structures of closely packed nanoparticles. The final stage of structural study is the crystallography of individual nanoparticles, clusters, and grains of materials. This is a very interesting and important subject, since the crystallography of nanoclusters, which consist of several hundred to several thousand atoms, is very often different from that of their respective bulk materials.

The planar order of nanostructures deposited by chemical routes has become an important issue, because of the competition with solid-state nanotechnology capable of the fabrication of fine two-dimensional structures. The main concern is with the layers of nanoparticles produced by chemical self-assembly, because methods of electrostatic self-assembly and LB is not capable of producing two-dimensional ordered arrays of nanoparticles. The features of the lateral arrangement of particles, which are buried under layers of either closely packed amphiphilic compounds or polymers, are usually smeared and difficult to observe. In the case of relatively thick (quasi-3D) films, produced by electrodeposition and sol-gel techniques, the morphology study usually reveals polycrystallites. Therefore, the quality of these materials can be assessed by the size of the crystallites and by the presence of preferential orientation, which may cause anisotropy of the electrical and optical properties of materials.

7.4 Morphology and crystallography of chemically self-assembled nanoparticles

In contrast to the previous deposition techniques (i.e., LB and electrostatic self-assembly), nanoparticles, which are chemically self-assembled onto the solid substrates, tend to form regular two-dimensional structures, especially after annealing at moderate temperatures.

The type of two-dimensional structure, which usually follows the trend of close packing arrangement, depends on the particles' shapes. For example, a simple hexagonal pattern is formed by spherical nanoparticles. A classic example of such structures is gold colloid particles chemically self-assembled onto the surface of gold via thiol groups. The observation of such structures is possible with scanning nanoprobe microscopy, such as STM and AFM, as well as with TEM and high resolution SEM [49-73][Roberts.G. G, 1983[a], 1990[b] and 1985[c], Ross. J, 1986, Lvov. Y. M, 1987[a], 1989[b] and 1994[c], 2000[d], Petty. M. C, 1990[a] and 1995[b], Ulman. A, 1991[a] and 1995[b], Wegner. G, 1993, Yarwood. J, 1993, Tredgold. R. H, 1994, Tsukruk. V. V, 1997, Bliznyuk. V. N, 1998, Bonnell. D. A, 2001, Stefanis. A, 2001, Gabriel. B. L, 1985, Keyse. R. J, 1998, Greffet. J. J, 1997, Kitaigorodski. A. L, 1961, Nabok.A. V, 1998[a] and 2003[b]].

8. Elemental and chemical composition of organic/inorganic nanostructures

8.1 Stabilization of colloidal metal particles in liquids

Before beginning a description of synthetic methods, a general and crucial aspect of colloid chemistry should be considered, and that is the means by which the metal particles are stabilized in the dispersing medium, since small metal particles are unstable with respect to agglomeration to the bulk. At short inter-particle distances, two particles would be attracted to each other by van-der-Waals forces and in the absence of repulsive forces to counteract this attraction an unprotected sol would coagulate. This counteraction can be achieved by two methods, electrostatic stabilization and steric stabilization. In classical gold sols, for example, prepared by the reduction of aqueous $[AuC1_4]^-$ by sodium citrate, the colloidal gold particles are surrounded by an electrical double layer formed by adsorbed citrate and chloride ions and cations which are attracted to them. This results in a Columbic repulsion between particles. The weak minimum in potential energy at moderate interparticle distance defines a stable arrangement of colloidal particles which is easily disrupted by medium effects and, at normal temperatures, by the thermal motion of the particles.

Thus, if the electric potential associated with the double layer is sufficiently high, electrostatic repulsion will prevent particle agglomeration, but an electrostatically stabilized sol can be coagulated if the ionic strength of the dispersing medium is increased sufficiently. If the surface charge is reduced by the displacement of adsorbed anions by a more strongly binding neutral adsorbate, the colloidal particles can now collide and agglomerate under the influence of the van-der-Waals attractive forces [J. S. Bradley, 1993]. Even in organic media, in which electrostatic effects might not normally be considered to be important, the development of charge has been demonstrated on inorganic surfaces, including metals, in contact with organic phases such as solvents and polymers. For example, the acquisition of charge by gold particles in organic liquids has been demonstrated, and the sign and magnitude of the charge has been found to vary as a function of the donor properties of the liquid [M. E. Labib, 1984]. Thus, even for colloidal metals in suspension in relatively non-polar liquids, the possibility cannot be excluded that electrostatic stabilization contributes to the stability of the sol.

A second means by which colloidal particles can be prevented from aggregating is by the adsorption of molecules such as polymers, surfactants or ligands at the surface of the particles, thus providing a protective layer. Polymers are widely used, and it is obvious that

the protectant, in order to function effectively, must not only coordinate to the particle surface, but must also be adequately solvated by the dispersing fluid - such polymers are termed amphiphilic. The choice of polymer is determined by consideration of the solubility of the metal colloid precursor. The solvent of choice and the ability of the polymer to stabilize the reduced metal particles in the colloidal state. Natural polymers such as gelatin and agar were often used before the advent of synthetic polymer chemistry, and related stabilizers such as cellulose acetate, cellulose nitrate [A. Duteil, 1993], and cyclodextrins [M. Komiyama, 1983] have been used more recently. Thiele [V. H. Thiele, 1965] proposed the Protective Value as a measure of the ability of a polymer to stabilize colloidal metal. It was defined, similarly to the older Gold Number of Zsigmondy. as the weight of the polymer which would stabilize 1 g of a standard red gold sol containing 50 mg/L gold against the coagulating effect of 1% sodium chloride solution. Several other studies have been performed on the relative ability of polymers to act as steric stabilizers [P. H. Hess, 1966, H. Hirai, 1979[a] and 1985[b]], and, despite the fact that these quite subjective studies focus on very specific (and quite different) sol systems, it seems that; of the synthetic polymers considered, vinyl polymers with polar side groups such as poly(vinylpyrro1idone) (PVP) and poly(viny1 a1cohole) are especially useful in this respect. The use of copolymers introduces another degree of variability to colloidal stabilization. As the co-monomer ratio can be varied. For example, the use of vinyl-pyrrolidone-vinyl-alcohol copolymers is reported for the preparation of platinum and silver hydrosols [K. Megure, 1988]. The silver sols were stable only in the presence of the copolymer, and the size of the silver particles decreased with an increase in vinyl-pyrrolidone content of the copolymer. Electrostatic and steric stabilization are in a sense combined in the use of long chain alkyl-ammonium cations and surfactants, either in single-phase sols or in reverse micelle synthesis of colloidal metals. A new class of metal colloids has recently been established in which the surface of the particle is covered by relatively small ligand molecules such as sulfonated triphenylphosphine or alkane-thiols.

8.2 Synthetic methods for the preparation of colloidal transition metals

The synthetic methods which have been used include modern versions of established methods of metal colloid preparation such as the mild chemical reduction of solutions of transition metal salts and complexes and newer methods such as radiolysis and photochemical reduction, metal atom extrusion from labile organometallics. And the use of metal vapor synthesis techniques. Some of these reactions have been in use for many years, and some are the results of research stimulated by the current resurgence in metal colloid chemistry. The list of preparative methods is being extended daily, and, as examples of these methods are described below, the reader will quickly be made aware that almost any organometallic reaction or physical process which results in the deposition of a metal is in fact a resource for the metal colloid chemist. The acquisition of new methods requires only the opportunism of the synthetic chemist in turning a previously negative result into a synthetic possibility.

8.3 The role of surfactants in nanomarerials synthesis

For over 2000 years, humankind has used surfactants or surface-active ingredients in various aspects of daily life, for washing, laundry, cosmetics, and housecleaning.

However, the development of more economical processes for the manufacture of surfactants has contributed to an increased consumption of synthetic detergents. However, the major surfactants common (with respect to detergent) to all regions are linear alkyl benzene sulfonates (LASs), alcohol ether sulfates (AESs), aliphatic alcohols (AEs), alcohol sulfates (ASs), and soap. In the past decades, new surfactants have proliferated mainly as nonionic or non-soap surfactants offering unique properties and features to both industrial and household markets. Non-soap surfactants are widely used in diverse applications such as detergents, paints, and in the cosmetics, stabilized and synthesis of new materials and pharmaceutical industries. Since the 1960s, biodegradability and a growing environmental awareness have been the driving forces for the introduction of new surfactants. These forces continue to grow and influence the surfactant market and production. A new class of surfactants, carbohydrate-based surfactants, has gained significant interest and increased market share. Consequently, sugar-based surfactants, such as alkyl-poly-glycoside (APG), are used as a replacement for poly-oxy-ethylene alkyl phenols (APEs) where biodegradability is a concern. They represent a new concept in compatibility and care. Nonetheless, over 40 different types of surfactants are produced and used commercially in the formulation of home care, personal care, and industrial products. Contrary to many textbooks that elaborate on surfactant physical properties or formulation guidelines. Surfactants are primarily anionic, nonionic, cationic, and amphoteric.

8.4 "Surfactant systems"– Structure

The interactions between the hydrophilic head-groups and the hydrophobic tail of the surfactants, they tend to form aggregates spontaneously when placed into water, oil, or a mixture of the two. The aggregates are thermodynamically stable and therefore long lived. This interaction can be represented by a geometric packing parameter. Because the head-groups of surfactants are either hydrated or charged, they prefer to maintain a certain distance from their nearest neighbors, which is represented by the area, a_0. Tail interactions, from energy and enthalpy differences between the solvent and the environment of hydrophobic tails, lead to another area based on the length and volume of the tail, v/lc. The packing parameter is the ratio of these two areas ($P = v/a_0l$c). For certain values of P, the surfactant packs into different preferred geometries, which are shown in fig 3. Normal phases (fig 3 a-c), where water is continuous, have packing parameters less than one, and reverse phases (fig 3d and 3e), where oil is continuous, have packing parameters greater than one. When spheres (fig 3a) are in random order, the system is called a micellar solution. If the spheres close pack into a lattice, a discrete cubic liquid crystal can be formed. As the packing parameter is increased, cylinders (fig 3b) are formed. In dilute solution when the orientation of the cylinders is random (i.e., uncorrelated), they are called rodlike micelles, but when close packed into a lattice, they form a hexagonal liquid crystal. Bilayer sheets (fig 3c) can give many structures. When P is close to one, the bilayers are parallel to each other and form the lamellar liquid crystal. If the packing parameter is less than one, these sheets can no longer remain parallel to each other and may fold back on themselves, trapping solvent in a bilayer container called a vesicle. The bilayers may also maintain a curved shape and fill space by following an infinite periodic minimal surface, IPMS. IPMS are a geometry that is periodic in three directions and has constant mean curvature. When the bilayer conforms to this geometry,

both the water and oil fractions are continuous in three directions, and because the IPMS give a cubic crystal pattern, these liquid crystals are known as bicontinuous cubic liquid crystals. The packing of bicontinuous cubics as well as all liquid crystals is thermodynamically controlled, so the structures conform to a regular array of fixed size. Once past the value $P = 1$, the geometries and ordered phase repeat in reverse order but with the oil and solvated surfactant tails becoming the continuous phase, i.e., reverse phases. Along with the ordered liquid crystal structures there are random geometries that are also thermodynamically stable. These systems are called micro-emulsions. They are related to regular emulsions in that they are dispersions of two immiscible liquids stabilized by surfactants. Unlike emulsions, micro-emulsions are thermodynamically stable and optically transparent. The basic structure of micro-emulsions is a swollen micellar solution. When water is the solvent, the systems are known as oil-in-water (O/W) micro-emulsions. Similarly, if the oil is the continuous phase and the water is within a reverse micelle, the system is water-in-oil (W/O) micro-emulsion. When the amounts of oil and water are nearly equal, a bicontinuous structure can be formed. These structures are the disordered analogues of the cubic and lamellar phases.

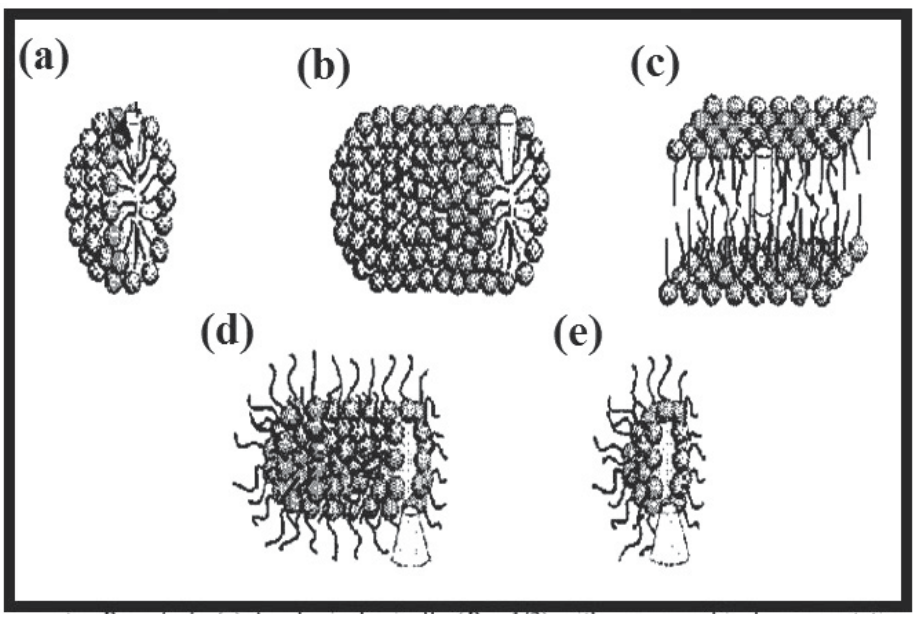

Fig. 3. Packing Parameter ($P=v/a_0l_c$). (a) Spherical Micelle ($P<1/3$) With a geographical Representation of the Three Values That Make up P. (b) A Cylindrical Micelle ($1/3<P<1/2$). (c) A Bilayer Sheet ($1/2<P<2$). (d) A Reverse Cylindrical Micelle ($2<P<3$). (e) A Reverse Spherical Micelle ($P>3$).

9. Polymers

Polymers are long chain-like giant molecules (macromolecules) made by the linkage of large numbers of small repeating molecules called monomers. Short chain lengths formed in the course of synthesis or degradation of polymers is called oligomers. The majority of

polymers, and the only ones considered here, are compounds of carbon. Polymers are very widespread and can be synthetic (e.g. nylon) or natural (e.g. rubber). They form vital components of living organisms, and the most important molecule, DNA, is a polymer of amino acids. Colloquially, polymers are often called plastics. More precisely, plastics are sometimes defined as polymers that can be easily formed at low temperatures, and sometimes as a pure polymer together with a nonpolymeric additive, which may be solid, liquid or gas. There are two main divisions of polymeric materials: thermoplastic and thermosetting. Thermoplastic materials can be formed repeatedly; that is, they can be melted and reformed a number of times. Thermosetting materials can be formed only once; they cannot be re-melted. They are usually strong, and are typified by resins. A further group of polymers merits mention, elastomers. Elastomers can be deformed a considerable amount and return to their original size rapidly when the force is removed. The properties of polymers depend both on the details of the carbon chain of the polymer molecule and on the way in which these chains fit together. The chain form can be linear, branched or cross linked, and a great variety of chemical groups can be linked to the chain backbone. The chains can be carefully packed to form crystals, or they can be tangled in amorphous regions. Amorphous polymers tend not to have a sharp melting point, but soften gradually. These materials are characterized by a glass transition temperature, Tg, and in a pure state are often transparent. Although polymers are associated with electrically insulating behavior, the increasing ability to control both the fabrication and the constitution of polymers has led to the development of polymers that show metallic conductivity superior to that of copper and to polymers that can conduct ions well enough to serve as polymer electrolytes in batteries and fuel cells.

9.1 History of conducting polymers

Historically, polymers have been considered as insulators and found application areas due to their insulating properties. Infact, so far, any electrical conduction in polymers which is generally due to loosely bound ions was mostly regarded as an undesirable fact. However, emerging as one of the most important materials in the twentieth century, the use of polymers move from primarily passive materials such as coatings and containers to active materials with useful optical, electronic, energy storage and mechanical properties. Indeed, discovery and study of conducting polymers have already started this development [Freund. M. S, 2006, Epstein. A. J, 1999 and Inzelt. G, 2008]. Electrically conducting polymers are defined as materials with an extended system of conjugated carbon-carbon double bonds (fig 4) [Advani. S. G, 2007]. They are synthesized either by reduction or oxidation reaction, which is called doping process, giving materials with electrical conductivities up to 105 S/cm. Conducting polymers are different from polymers filled with carbon black or metals, since the latter are only conductive if the individual conductive particles are mutually in contact and form a coherent phase.

Although conducting polymers are known as new materials in terms of their properties, the first work describing the synthesis of a conducting polymer was published in the ninetieth century. In 1862, Henry Letheby prepared polyaniline by anodic oxidation of aniline, which was conductive and showed electrochromic behavior. However, electronic properties of so called aniline black were not determined.

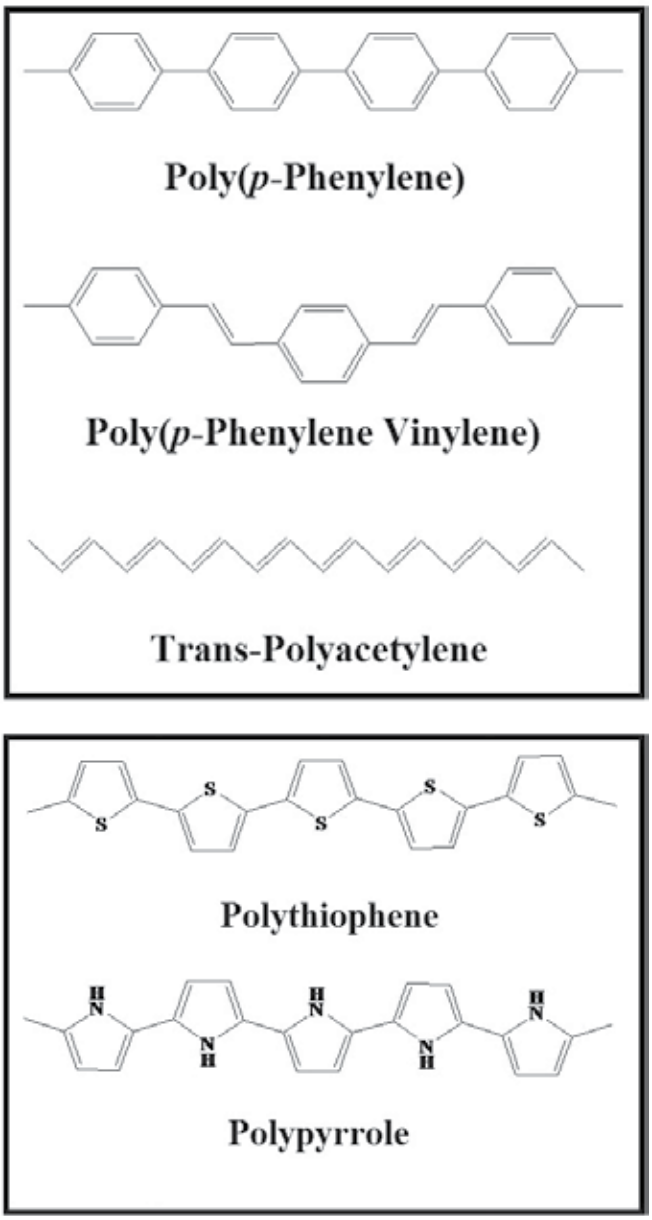

Fig. 4. Some Examples for Conducting Polymers.

In 1958, Natta et al. synthesized polyacetylene as a black powder which was found to be a semiconductor with conductivity in the range of 10-11 to 10-3 S/cm, depending on the process conditions of the polymer. In 1977, drawing attention on "conducting polymers", the first intrinsic electrically conducting organic polymer, doped polyacetylene, was reported. Intrinsically conducting polymers are a different class of materials than conducting polymers, which are a physical mixture of a non-conductive polymer with a conducting material such as metal or carbon powder. The preparation of polyacetylene by Sirakawa and coworkers and the

discovery of the large increase in its conductivity after "doping" by the group led by MacDiarmid and Heeger actually launched this new field of research.

Electronically conducting polymers possess a variety of properties related to their electrochemical behavior and are therefore active materials whose properties can be altered as a function of their electrochemical potential. The importance and potential impact of this new class of material was recognized by the world scientific community when Hideki Shirakawa, Alan J. Heeger and Alan G. MacDiarmid were awarded the Nobel Prize in Chemistry in 2000 "for the discovery and development of electronically conductive polymers".

9.2 Composites

A composite is defined as a material created by combination of two or more components namely, selected filler or reinforcing agent and a compatible matrix binder. The combination of these component results in formation of a new material with specific characteristics and properties. The synthetic assemblage of the components does not occur as a dissolvation but rather like merging into each other to act in concert. Although the components act together as a single material, both the components and the interface between them can usually be physically identified. Generally, the behavior and the properties of the composite are controlled by the interface of the components. Since the composite is a totally new material having new and specific characteristics, its properties cannot be achieved by any of its components acting alone.

The classification of composites can be done in different ways. The composites can be classified on the basis of the form of their structural components: (i) fibrous where the composite is composed of fibers in a matrix, (ii) laminar where the composite is composed of layers in a matrix, and (iii) particulate where the composite is composed of particles in a matrix [Kricheldorf. H. R, 2005, Lubin. G, 1982].

Another type of classification can be done on the basis of filler or reinforcing agent used namely polymer matrix composites (PMCs), metal matrix composites (MMCs), ceramic matrix composites (CMCs), carbon-carbon matrix composites (CCCs), intermetallic composites (IMCs), or hybrid composites [Sanjay. K, 2002].

9.3 Polymer matrix composites

Composite materials have been utilized to solve technological problems for a long time. In 1960s with the introduction of polymeric-based composites, composites start capturing the attention of industries. Since then, composite materials have become common engineering materials. They are designed and manufactured for various applications including automotive components, sporting goods, aerospace parts, consumer goods, and in the marine and oil industries. Increasing awareness of product performance and competition in the global market for lightweight components also supported the growth in composite usage. Among all materials, composite materials have the potential to replace widely used steel and aluminum, and many times with better performance. Replacing steel components with composite components can save 60 to 80% in component weight, and 20 to 50% weight by replacing aluminum parts. Today, it appears that composites are the materials of choice for many engineering applications.

The matrix material used in polymer-based composites can either be thermoset (epoxies, phenolics) or thermoplastic resins (low density polyethylene, high density polyethylene, polypropylene, nylon, acrylics). The filler or reinforcing agent can be chosen according to the desired properties. The properties of polymer matrix composites are determined by properties, orientation and concentration of fibers and properties of matrix.

The matrix has various functions such as providing rigidity, shaping the structure by transferring the load to fiber, isolating the fiber to stop or slow the propagation of crack, providing protection to reinforcing fibers against chemical attack and mechanical damage (wear), and affecting the performance characteristics such as ductility, impact strength, etc. depending on its type. The failure mode is strongly affected by the type of matrix material used in the composite as well as its compatibility with the fiber. The important functions of fibers include carrying the load, providing stiffness, strength, thermal stability, and other structural properties in the composites and providing electrical conductivity or insulation, depending on the type of fiber used [Omastova. M, 1998].

Polypropylene (PP) is one of the fastest growing commercial thermoplastics due to its attractive combination of low density and high heat distortion temperature. There are some limitations in physicochemical properties that restrict PP applications. A typical illustration is in packaging, where PP has poor oxygen gas barrier resistance. No single polymer has shown the ideal combination of performance features. PP possesses good water vapor barrier properties, but it is easily permeated by oxygen, carbon dioxide, and hydrocarbons. The necessity of developing more effective barrier polymers has given rise to different strategies to incorporate and optimize the features from several components. Most schemes to improve PP gas barrier properties involve either addition of higher barrier plastics via a multilayer structure (co-extrusion) or by introducing filler with high aspect ratio in the polymer matrix. 1. Co-extrusion allows tailoring of film properties through the use of different materials where each material component maintains its own set of properties, compared with blending of polymers in a mono-extrusion technique. Co-extrusion is used to generate multilayer laminate structures from separately extruded polymer films that are sandwiched together [109 and 110]. Resulting films may comprise many layers, such as the PP-adhesivepoly (ethylene-co-vinyl-alcohol) (EVOH)-adhesive PP system: EVOH barrier sheet trapped between two layers of moisture resistant PP and two additional adhesive strata. However, by nature co-extrusion is a complex and expensive process.

9.4 Composites of polypyrrole

Maria Omastova and Ivan Chodak prepared conductive polypropylene/polypyrrole composites using the method of chemically initiated oxidative modification of polypropylene particles in suspension by pyrrole. In order to prepare the composite, polypropylene particles were dispersed in water-methanol mixture and $FeCl_3$ was added to be used for chemical oxidation. Addition of pyrrole started formation of polypyrrole particles in polypropylene suspension. The electrical and rheological properties of the composite were compared with polypropylene/polypyrrole composite prepared by melt mixing of pure polypropylene with chemically synthesized polypyrrole and with polypropylene/carbon black composites also prepared by melt mixing. Elemental analysis verified presence of polypyrrole in polypropylene matrix. The conductivity studies show that even a very small PPy amount present in composites results in a significant increase in

conductivity. Processing conditions are observed to have a great effect on electrical conductivities of composites. The composite prepared by sintering PP particles covered with PPy shows about 7 orders of magnitude higher conductivity than the composite prepared by melt mixing of pure polypropylene with chemically synthesized polypyrrole whereas the conductivity of sintered PP/PPy composites is comparable to that of PP/Carbon black composite. The PP/CB and injection molded PP/PPy composites exhibit similar flow properties. However, for compresion molded PP/PPy composites a considerable increase of complex viscosity was observed [Pionteck. J, 1999].

10. Nanocomposites

Nanomaterials and nanocomposites have always existed in nature and have been used for centuries. However, it is only recently that characterization and control of structure at nanoscale have drawn intense interest for research and these materials start to represent new and exciting fields in material science. A nanocomposite is defined as a composite material where at least one of the dimensions of one of its constituents is on the nanometer size scale. In other words, nanocomposites can be considered as solid structures with nanometer-scale dimensional repeat distances between the different phases that constitute the structure. These materials typically consist of an inorganic (host) solid containing and an organic component or vice versa. They can consist of two or more inorganic/organic phases in some combinational form that at least one of the phases or features is in the nanosize.

In general, nanocomposite materials can exhibit different mechanical, electrical, optical, electrochemical, catalytic, and structural properties than those of each individual component. The multifunctional behavior for any specific property of the material is often more than the sum of the individual components [Mravcakova. M, 2006, Omoto. M, 1995, Ajayan. P. M, 2003 and Lee. E. S, 2004].

10.1 Polymer-based and polymer-filled nanocomposites

In recent years, the limits of optimizing composite properties of traditional micrometer-scale composite fillers have been reached due to the compromises of the obtained properties. Stiffness is traded for toughness, or toughness is obtained at the cost of optical clarity. In addition, regions of high or low volume fraction of filler often results in macroscopic defects which lead to breakdown or failure of the material. Recently, a new research area has provided the opportunity to overcome the limitations of traditional micrometer-scale polymer composites. This new investigation area is the nanoscale filled polymer composites where the filler is <100 nm in at least one dimension.

Implementation of the novel properties of nanocomposites strongly depends on processing methods that lead to controlled particle size distribution, dispersion, and interfacial interactions. Processing technologies for nanocomposites are different from those for composites with micrometer-scale fillers, and new developments in nanocomposite processing are among the reasons for their recent success.

Nanoscale fillers can be in many shapes and sizes, namely tube, plate-like or 3D particles. Fiber or tube fillers have a diameter <100 nm and an aspect ratio of at least 100. The aspect ratios can be as high as 106 (carbon nanotubes). Plate-like nanofillers are layered materials

typically with a thickness on the order of 1 nm, but with an aspect ratio in the other two dimensions of at least 25. Three dimensional (3D) nanofillers are relatively equi-axed particles <100 nm in their largest dimension. This is a convenient way to discuss polymer nanocomposites, because the processing methods used and the properties achieved depend strongly on the geometry of the fillers.

10.2 Nanocomposites of polypyrrole

Eun Seong Lee and Jae Hyung Park prepared in situ formed procesable polypyrrole nanoparticle/amphiphilic elastomer composites which could have applications in biosenors, semiconductors, artificial muscles, polymeric batteries and electrostatic dissipation due to their process ability and considerable conductivities. The polymerization process of pyrrole was achieved by chemical oxidation of the pyrrole monomer by $FeCl_3.6H_2O$ in the presence of multiblock copolymer dissolved in methanol/water mixture. The multiblock copolymer was used as a stabilizer during polypyrrole synthesis and when cast after removing the dissolved polymers, served as a flexible and elastomeric matrix. The polymerization time, concentration of multiblock copolymer and the oxidant, reaction medium composition were optimized in terms of conductivity measurements and the highest conductivity was reported as 3.0±0.2 Scm^{-1}. Mechanical properties such as tensile strength and elongation at break of the composites were found to increase with increasing amount of multiblock copolymer [Wu. T. M, 2008].

Tzong-Ming Wu and Shiang-Jie Yen have reported synthesis, characterization and properties of monodispersed magnetic coated multi-walled carbon nanotube/polypyrrole nanocomposites. Fe_3O_4 was used for coating multi-walled carbon nanotube (MWCNT). Fe_3O_4 coated c-MWCNT/PPy nanocomposites were synthesized via the in situ polymerization. The polymerization of pyrrole molecules was achieved on the surfaces of Fe_3O_4 coated c-MWCNT. The comparison of conductivities have shown that Fe_3O_4 coaed c-MWCNT/PPy nanocomposites have about 4 times higher conductivity that that of pure PPy matrix. Fe_3O_4 coated c- MWCNT/PPy nanocomposites were observed to exhibit ferromagnetic behaviour [Boukerma. K, 2006].

Kada Boukerma and Jean-Yves Piquemal prepared montmorillonite/polypyrrole nanocomposites and investigated their interfacial properties. The synthesis of MMT/PPy nanocomposites was achieved by in situ polymerization of pyrrole in the presence of MMT. Scanning electron microscopy results have shown that the surface morphology of the nanocomposites were more like the surface of untreated MMT. X-ray photoelectron spectroscopy (XPS) exhibited that the nanocomposites have MMT-rich surfaces which inicates intercalation of polypyrrole in the host galleries. The increase in interlamellar spacing was measured by transmission electron microscope. Invers gas chromatography measurements showed high surface energy of the nanocomposites [Mravcakova. M, 2006].

Miroslava Mravcakova and Kada Boukerma prepared montmorillonite/polypyrrole nanocomposites. The effects of organic modification of clay on the chemical and electrical properties were studied. The morphology investigations showed that the surface of MMT/PPy has a MMT-rich surface and relatively low conductivity (3.1×10^{-2} Scm^{-1}) indicating intercalation of PPy in the clay galleries. Whereas, the organically modified MMT/PPy nanocomposites have PPy-rich surface and higher conductivity indicating PPy

formation on the surface of MMT. The dispersive contribution of surface energy of o-MMT was measured to be significantly low compared to that of MMT due to the stearly chains from the ammonium chlorides used for organic modification [Ranaweera. A. U, 2007].

A.U. Ranaweera and H.M.N Bandara prepared electronically conducting montmorillonite-Cu_2S and montmorillonite-Cu_2S-polypyrrole nanocomposites. MMT-Cu_2S nanocomposite was prepared by cation-exchange approach and its conductivity was measured as 3.03×10^{-4} Sm^{-1}. The polymerization of pyrrole was achieved between the layers of MMT-Cu_2S to obtain MMT-Cu_2S-PPy nanocomposite. The characterization was performed by XRD, FT-IR and impedance measurements. The electronic conductivity was reported as 2.65 Sm^{-1} [Dallas. P, 2007].

Panagiotis Dallas and Dimitrios Niarchos reported interfacial polymerization of pyrrole and in situ synthesis of polypyrrole/silver nanocomposites. The oxidizing agents used were Ag(I) or Fe(III). Depending on using different surfactants (SDS or DTAB) or not using any surfactant, the average diameter of polypyrrole structures was observed to be in the range of 200-300 nm. The electron microscopy images exhibited different morphologies of polypyrrole depending on using various surfactants or not using any as well as the size and shape of the silver nanocomposites. X-ray diffractometry showed amorphous structure of polymers. Further characterization was performed by thermogravinetric analysis and FT-IR spectroscopy [Carotenuto. G, 1996].

10.3 Nanoparticle/polymer composite processing

There are three general ways of dispersing nanofillers in polymers. The first is direct mixing of the polymer and the nanoparticles either as discrete phases or in solution. The second is in-situ polymerization in the presence of the nanoparticles, and the third is both in-situ formation of the nanoparticles and in-situ polymerization. Due to intimate mixing of the two phases, the latter can result in composites called hybrid nanocomposites [Lee. E. S, 2004].

10.4 Direct mixing

Direct mixing is a well-known and established polymer processing technique. When these traditional melt-mixing or elastomeric mixing methods are feasible, they are the fastest method for introducing new products to market. Although melt mixing has been successful in many cases, for some polymers, due to rapid viscosity increase with the addition of significant volume fractions of nanofiller, this processing method has limitations. There are many examples showing melt mixing method for composite production and exhibiting some limitations for the process [Lee. E. S, 2004].

10.5 Solution mixing

In solution mixing, in order to overcome the limitations of melt mixing method, both the polymer and the nanoparticles are dissolved or dispersed in solution. This method enables modification of the particle surface without drying, which reduces particle agglomeration. After dissolvation the nanoparticle/polymer solution can be cast into a solid, or solvent evaporation or precipitation methods can be used for isolation of nanoparticle/polymer composite. Conventional techniques can be used for further processing [Lee. E. S, 2004].

10.6 In-situ polymerization

In in-situ polymerization, nanoscale particles are dispersed in the monomer or monomer solution, and the resulting mixture is polymerized by standard polymerization methods. This method provides the opportunity to graft the polymer onto the particle surface. Many different types of nanocomposites have been processed by in-situ polymerization. Some examples for in-situ polymerization are polypyrrole nanoparticle/amphiphilic elastomer composites; magnetite coated multi-walled carbon nanotube/polypyrrole nanocomposites and polypyrrole/ silver nanocomposites. The key to in-situ polymerization is appropriate dispersion of the filler in the monomer. This often requires modification of the particle surface because, although dispersion is easier in a liquid than in a viscous melt, the settling process is also more rapid.

11. Polypyrrole

Among the conjugated polymers, polypyrrole (PPy) is the most representative one for its easy polymerization and wide application in gas sensors, electrochromic devices and batteries. Polypyrrole can be produced in the form of powders, coatings, or films. It is intrinsically conductive, stable and can be quite easily produced also continuously. The preparation of polypyrrole by oxidation of pyrrole dates back to 1888 and by electrochemical polymerization to 1957. However, this organic p-system attracted general interest and was found to be electrically conductive in 1963. Polypyrrole has a high mechanical and chemical stability and can be produced continuously as flexible film (thickness 80 mm; trade name: Lutamer, BASF) by electrochemical techniques. Conductive polypyrrole films are obtained directly by anodic polymerization of pyrrole in aqueous or organic electrolytes.

Apart from electrochemical routes, polypyrrole can also be synthesized by simple chemical ways to obtain powders. Basically chemical oxidative polymerization methods can be used to synthesize bulk quantities of polypyrrole in a fast and easy way. Like other conducting polymers polypyrrole exhibit more limited environmental, thermal and chemical stability than conventional inert polymer due to the presence of dopant and its dynamic and electro active nature.

11.1 Synthesis of polypyrrole

Polypyrrole and many of its derivatives can be synthesized via simple chemical or electrochemical methods [120]. Photochemically initiated and enzyme-catalyzed polymerization routes have also been described but less developed. Different synthesis routes produce polypyrrole with different forms; chemical oxidations generally produce powders, while electrochemical synthesis leads to films deposited on the working electrode and enzymatic polymerization gives aqueous dispersions [Liu. Y. C, 2002, Tadros. T. H, 2005 and Wallace. G. G, 2003]. As mentioned above the electrochemical polymerization method is utilized extensively for production of electro active/conductive films. The film properties can be easily controlled by simply varying the electrolysis conditions such as electrode potential, current density, solvent, and electrolyte. It also enables control of thickness of the polymers. Electrochemical synthesis of polymers is a complex process and various factors such as the nature and concentration of monomer/electrolyte, cell conditions, the solvent, electrode, applied potential and temperature, pH affects the yield and the quality of the film.

Thus, optimization of all of the parameters in one experiment is difficult. In contrast, chemical polymerization does not require any special instruments; it is a rather simple and fast process. Chemical polymerization method involves oxidative polymerization of pyrrole monomer by chemical oxidants either in aqueous or non-aqueous solvents or oxidation by chemical vapor deposition in order to produce bulk polypyrrole as fine powders. Fe(III) chloride and water are found to be the best oxidant and solvent for chemical polymerization of pyrrole respectively regarding desirable conductivity characteristics.

Previous studies have shown that the optimum initial mole ratio of Fe(III)/Pyrrole for polymerization by aqueous Fe(III) chloride solution at 19 ˚C is 2.25 or 2.33. Also, several studies have revealed that factor such as solvent, reaction temperature, time, nature and concentration of oxidizing agent; affect the oxidation potential of the solution which affects the final conductivity of the product.

S.Goel and A. Gupta synthesized polypyrrole samples of different nanodimensions and morphologies by time dependent interfacial polymerization reaction. Pure chloroform was used as solvent for pyrrole and ammonium persulphate dissolved in HCl was used as the oxidizing solution. The polymerization occurred in the interface of organic and aqueous phases and polypyrrole was formed as thin layer on the interface. Morphology study of polypyrrole nanoparticles was done by scanning electron microscopy and transmission electron microscopy.

Yang Liu and Ying Chu synthesized polypyrrole nanoparticles through microemulsion polymerization. Alcohol-assisted microemulsion polymerization was performed in order to adjust the inner structure of polypyrrole nanoparticles for polymerization SDS was used as the surfactant, water was used as the solvent and aqueous solution of $NH_4S_2O_8$ was used as the oxidant. Characterization of polpyrrole was done by FT-IR and morphology study was performed by SEM and TEM. Hongxia Wang and Tong Lin synthesized polypyrrole nanoparticles by oxidation of pyrrole with ferric chloride solution during microemulsion polymerization process. Dodecyltrimethyl ammonium bromide (DTAB) was used as the surfactant. Particle characaterisation was performed by using FTIR, elemental analysis, UV-VIS spectra and SEM. Variation of particle size from about 50 to 100 and 100 to 200 nm with the change in surfactant concentration was reported. Xinyu Zhang and Sanjeev K. Manohar synthesized narrow pore-diameter polypyrrole nanotubes. The synthesis was performed by chemical oxidative polymerization of pyrrole using $FeCl_3$ oxidant and V_2O_5 nanofibers as the sacrificial template producing microns long electrically conducting polypyrrole nanotubes having 6 nm averages pore diameter. M.R. Karim and C.J. Lee synthesized polypyrrole by radiolysis polymerization method. Conducting PPy was synthesized by the in situ gamma radiation-induced chemical oxidative polymerization method. This method was reported to provide highly uniform polymer morphology. Jyongsik Jang and Joon H. Oh, synthesized polypyrrole nanoparticles via microemulsion polymerization with using various surfactants. Fe(III) chloride was used as the oxidant. The selective fabrication of amorphous polypyrrole nanoparticles as small as 2 nm in diameter using microemulsion polymerization at low temperature was reported.

12. Polypropylene

Polypropylene (PP) is a thermoplastic material that is produced by polymerization of propylene molecules into very long polymer molecule or chains (fig 5.). There are number of

different ways to link the monomers together, but its most widely used form is made with catalysts that produce crystallizable polymer chains. The resulting product is a semi crystalline solid with good physical, mechanical, and thermal properties. Another form of PP produced in much lower volumes as a byproduct of semi crystalline PP production and having very poor mechanical and thermal properties, is a soft, tacky material used in adhesives, sealants, and caulk products. The above two products are often referred to as "isotactic" (crystallizable) PP (i-PP) and "atactic" (noncrystallizable) PP (-PP), respectively.

The average length of the polymer chains and the breadth of distribution of the polymer chain lengths determine the main properties of PP. In the solid state, the main properties of the PP reflect the type and amount of crystalline and amorphous regions formed from the polymer chains. Polypropylene has excellent and desirable physical, mechanical and thermal properties when used in room temperature applications. It is relatively stiff and has a high melting point, low density and relatively good resistance to impact.

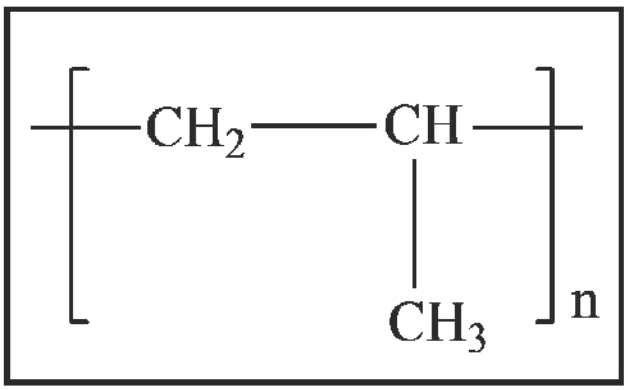

Fig. 5. Structural of Polypropylene.

Among conjugated polymers polypyrrole has attracted great interest due to its high conductivity, good thermal and environmental stability and ease of synthesis. However, it is an infusible, inprocessable Synthesis, characterization, and application of polyethylene glycol modified insulin polymer having relatively poor mechanical properties. On the other hand, polypropylene is a well-known insulating thermoplastic with outstanding mechanical properties. In this study, the synergistic assemblage of polypyrrole with polypropylene is investigated. Synthesis of polypyrrole nanoparticles via microemulsion polymerization, preparation of PP/PPy nanocomposites in order to provide some level of process ability to infusible and inprocessable PPy while inducing conductivity to insulating PP and preparation of PP/PPy nanocomposites with dispersant in order to improve the dispersion of PPy nanoparticles using identical procedures.

12.1 Preparation of PP/PPy nanocomposites

PP/PPy nanocomposites were prepared by melt mixing of pure PP with PPy using Brabender Plasti-Corder. The composition of nanocomposites varied between 1-20% PPy by weight. In order to provide a regular shape, the nanocomposites were pressed in a mould followed by fast cooling. The identical procedure is employed with addition of 2% by weight dispersant (SDS) during mixing process of pure PP with PPy.

12.2 Synthesis of polypyrrole nanoparticles

Synthesis of polypyrrole nanoparticles was achieved using micro-emulsion polymerization system by oxidation of pyrrole monomer with $FeCl_3.6H_2O$. As the oxidant was added, the color of the solution changed from colorless to deep greenish black which is an indication of oxidation of conducting polypyrrole. The reaction product polypyrrole was obtained in the form of black powder.

12.3 Scanning electron microscope analysis of polypyrrole nanoparticles

Scanning electron microscopy was performed in order to investigate the dimensions and the morphology of polypyrrole nanoparticles. The scanning electron micrographs of polypyrrole nanoparticles are presented in fig 6. The SEM micrographs of polypyrrole exhibited globular, nanometer-sized particles. The polypyrrole nanoparticles are observed

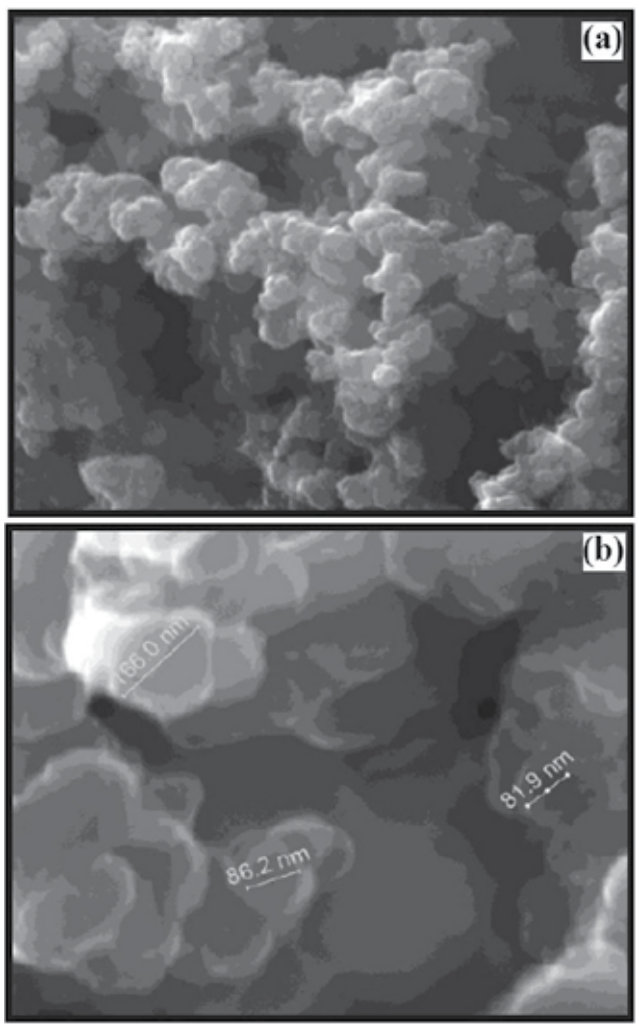

Fig. 6. SEM micrographs of PPy nanoparticles at magnifications of (a) 80000, (b) 300000.

to have a distribution of dimensions between 50 to 150 nm. The SEM results confirm that micro-emulsion polymerization system was successful in the synthesis of nano-sized polypyrrole particles. The SEM results prove that the micro-emulsion polymerization system provided similar dimensions of PPy nanoparticles with previous studies where 50 to 100 nm and 100 to 200 nm polypyrrole nanoparticles were reported.

12.4 Preparation of PP/PPy nanocomposites

The polypyrrole nanoparticles prepared by micro-emulsion polymerization system were mixed with polypropylene in order to provide some level of process ability to infusible and inprocessable polypyrrole while inducing conductivity to insulating polypropylene. In order to obtain PP/PPy nanocomposites, the polypyrrole nanoparticles were mixed with polypropylene by melt mixing technique followed by pressing to give a regular shape to nanocomposites. The nanocomposites were processed with injection molding and several black colored dog-bone shaped samples were obtained successfully. The composition of nanocomposites varied in the range of 1 to 20% by weight polypyrrole nanoparticles in polypropylene.

12.5 Characterization of PP/PPy nanocomposites

Mechanical properties of PP/PPy nanocomposites were investigated by tensile tests. The effect of loading different amounts of polypyrrole nanoparticles into thermoplastic polypropylene matrix and the changes in mechanical properties produced by incorporation of polypyrrole nanoparticles were examined. In order to understand the effect of using sodium dodecylsulphate as dispersant in PP/PPy nanocomposites, identical tests were performed also for the nanocomposites prepared with dispersant.

A stress-strain curve is known to provide information about both linear elastic properties and mechanical properties related to plastic deformation of a material. In order to specify a material as ductile or brittle, the response of the material to applied stress is investigated. The area under stress-strain curve corresponds to the energy required to break the material. As it is clearly seen in fig 7. pure PP is very ductile at a test rate of 5 cm/min and the area under the curve is very large indicating the great energy required to break the material. The Young's modulus, tensile strength and percentage strain at break values of pure polypropylene are 430 MPa, 27.8 MPa and %424 respectively.

The changes in mechanical properties that are produced by loading different amounts of polypyrrole nanoparticles can be well understood from stress-strain curves of PP/PPy nanocomposites which are illustrated in fig 8. through 3.8. As it is clearly observed in stress-strain curves of nanocomposites, addition of polypyrrole nanoparticles makes polypropylene matrix very brittle. In fact, addition of even the smallest amount of polypyrrole which is 1% causes a dramatic decrease in the energy required to break it.

The changes in mechanical properties that are produced by loading different amounts of polypyrrole nanoparticles can be well understood from stress-strain curves of PP/PPy nanocomposites which are illustrated in fig 8. through 3.8. As it is clearly observed in stress-strain curves of nanocomposites, addition of polypyrrole nanoparticles makes

polypropylene matrix very brittle. In fact, addition of even the smallest amount of polypyrrole which is 1% causes a dramatic decrease in the energy required to break it.

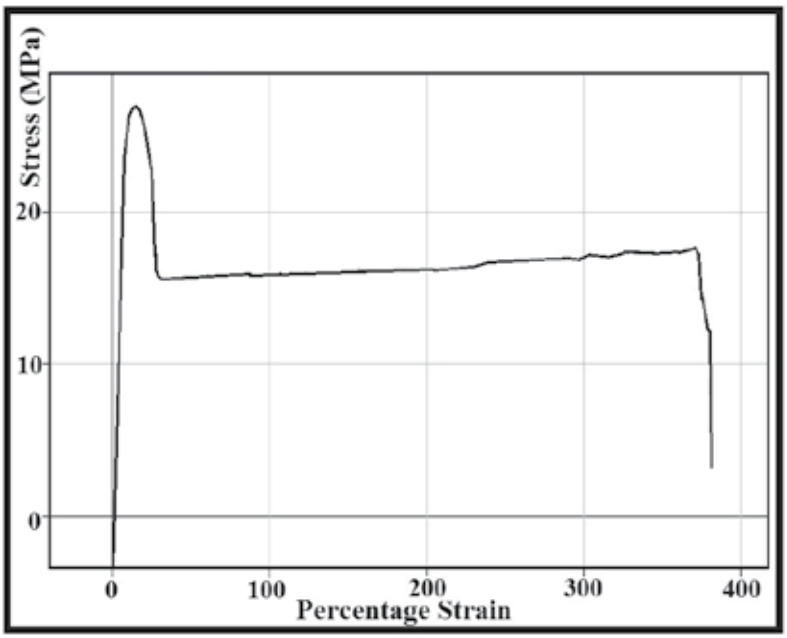

Fig. 7. Stress vs strain curve of pure PP.

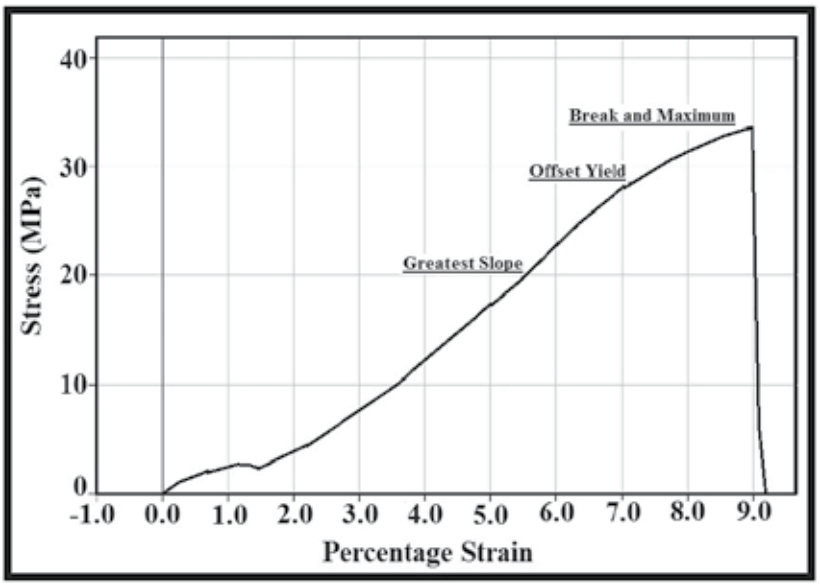

Fig. 8. Stress vs strain curve for PP/1%PPy nanocomposite without dispersant.

PPy nanoparticles in PP enhanced the strength and the stiffness of the nanocomposites. The greatest change for both properties was observed in PP/1%PPy nanocomposite. As it is seen

in fig 9. and fig 10. incorporation of 1% PPy into PP matrix increased the tensile strength and Young's modulus of pure PP considerably. Increasing amount of PPy nanoparticles in PP matrix caused gradual increase in both tensile strength and Young's modulus of nanocomposites until addition of 10% PPy nanoparticles. Further addition of PPy nanoparticles slightly changes the tensile strength and Young's modulus.

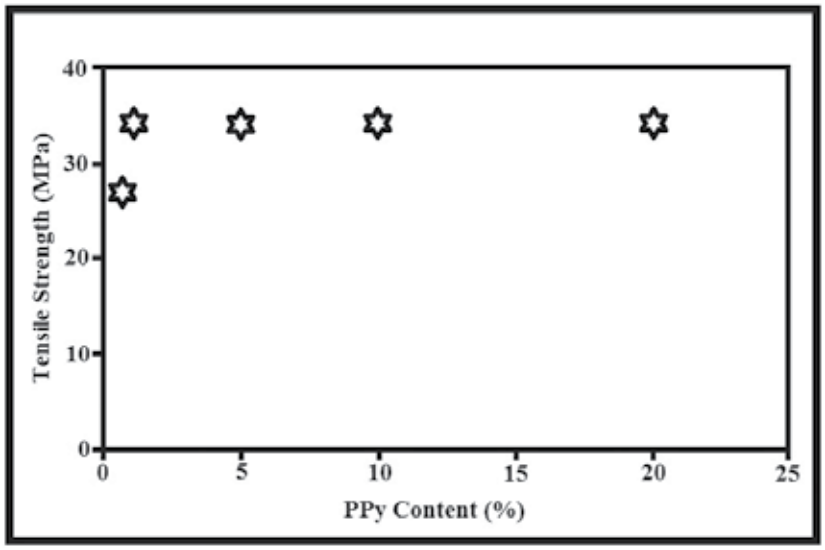

Fig. 9. Tensile strength vs PPy content for PP/PPy nanocomposites without dispersant.

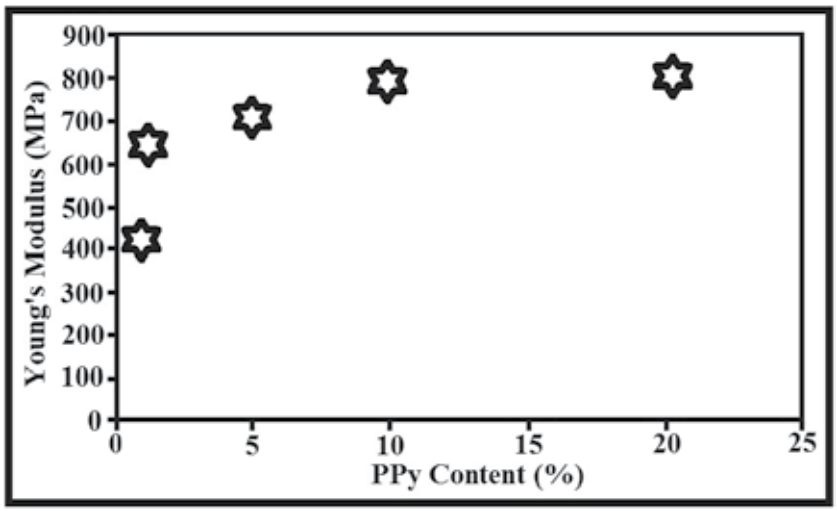

Fig. 10. Young's Modulus vs PPy Content For PP/PPy Nanocomposites Without Dispersant.

The tensile test results of PP/PPy nanocomposites show that incorporation of PPy nanoparticles in PP improves the strength and the stiffness while limiting the elongation of PP. In order to investigate the potential improvement in dispersion of PPy nanoparticles in PP, identical tensile tests were employed to nanocomposites prepared with dispersant. Due

to the effect of dispersant, the interaction between PPy nanoparticles with PP matrix is expected to be improved. The Young's modulus, tensile strength and percentage strain at break values for nanocomposites prepared with dispersant are presented in Table. 1.

PPy Content (w%)	Young's Modulus (MPa)	Tensile Strength (MPa)	Percentage Strain at Break (%)
0	430±10	27.8±0.5	424±9.0
1	583±77	30.1±0.4	14.4±0.2
5	748±53	32.8±0.6	9.3±0.9
10	786±10	32.9±0.4	8.0±0.3
20	831±31	33.2±0.6	7.1±0.2

Table 1. Young's Modulus, Tensile Strength, Percentage Strain Values For PP, PP/PPy Nanocomposites With 2% Dispersant by Weight.

The change in percentage strain at break, Young's modulus and tensile strength with increasing polypyrrole content in nanocomposites prepared with dispersant are shown in fig 11. through fig 13. The gradual decrease in percentage strain at break values for increasing amounts of PPy is clearly seen in fig 11. Addition of 1% PPy caused a significant decrease in percentage strain since it prevents extension of PP matrix.

However, the decrease in percentage strain is relatively smaller due to binding effect of dispersant used. fig 12 and fig 13 exhibit the increase in tensile strength and Young's modulus of the nanocompoites with addition of PPy.

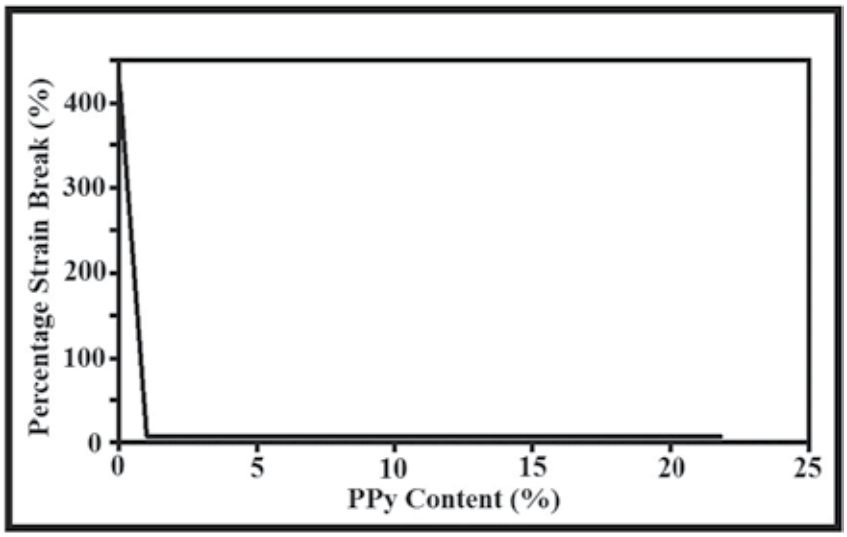

Fig. 11. Percentage strain at break vs PPy content for PP/PPy nanocomposites with dispersant.

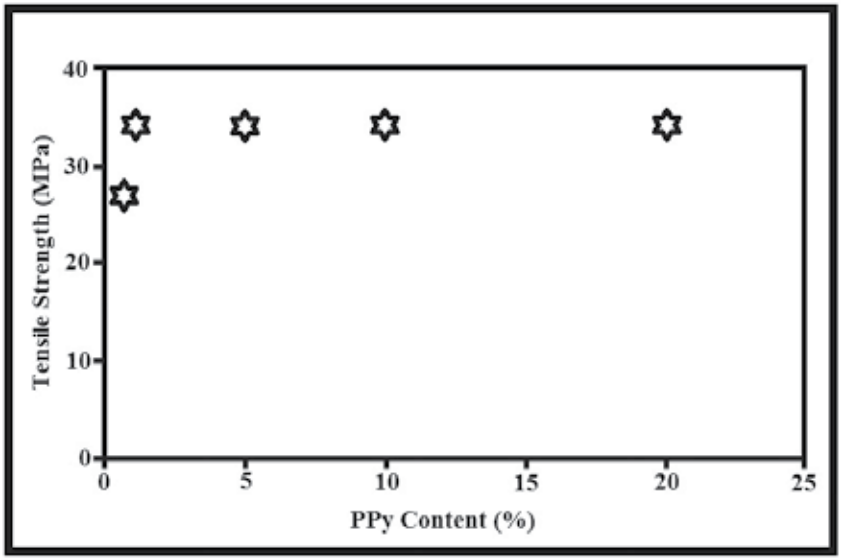

Fig. 12. Tensile strength vs PPy content for PP/PPy nanocomposites with dispersant.

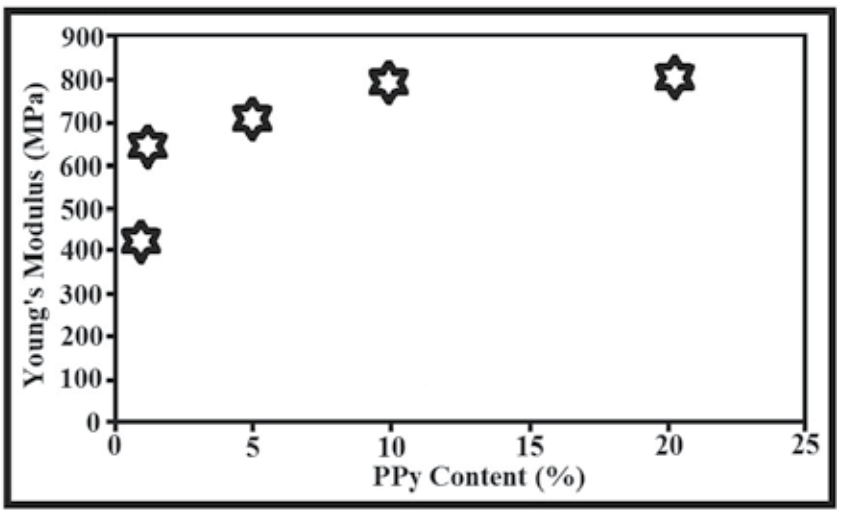

Fig. 13. Young's modulus vs PPy content for PP/PPy nanocomposites with dispersant.

The increase in both tensile strength and Young's modulus with increasing PPy content indicates the reinforcing action of PPy. In order to investigate the potential effect of dispersant in enhancement of dispersion of PPy nanoparticles, the change in tensile strength and percentage strain at break and Young's modulus for both nanocomposite sets prepared without and with dispersant are examined (Table. 1.).

The obtained results show that addition of PPy nanoparticles leads to a similar increase in tensile strength and Young's modulus of pure PP in both nanocomposite sets. Although the values are not identical, the values for nanocomposites involving dispersant did not exhibit significant difference compared to ones prepared without dispersant. However, the effect of

dispersant is perceived in percentage strain at break values. The nanocomposites prepared using dispersant exhibited a regular decrease in percentage strain at break while a sudden decrease was observed for nanocomposites prepared without dispersant. The percentage strain at break values for PP/1%PPy nanocomposite prepared with and without dispersant are found to be 15.3 and 9.5 respectively. The higher decrease in nanocomposite prepared without dispersant can be explained by considering weaker interaction of polypyrrole with polypropylene. Same case is true for also nanocomposites with 5% polypyrrole content. Although, similar behavior was observed for nanocomposites with 10% and 20% polypyrrole content, the difference in values are not as considerable as the ones for nanocomposites with 1% and 5% PPy content.

13. Application of polypropylene derivatives in synthesis of nanomaterials

13.1 Metaloxide nanoparticles

Nanoparticles of MO (NP-CuO) were prepared by a novel sonochemistry route from metal acetate and sodium hydroxide in the presence of polypropylene derivatives such as polyethylene glycol, polypropylene glycol and polyvinyl alcohol. Variations in several parameters and their effects on the structural properties of nanoparticles (particle size and morphology) were investigated. 0.05 M solution of metal acetate in the presence of polyethylene glycol gave the best results. The characterizations were carried out by X-Ray diffraction, scanning electron microscopy, IR spectroscopy, thermal gravimetric analysis and differential thermal analysis.

Ultrasonic irradiation and stabilizer (PPG, PEG and PVA) can greatly enhance the conversion rate of precursor to nanometer- sized MO particles in the presence of polyethylene glycol (PEG), polypropylene glycol (PPG) and polyvinyl alcohol (PVA). Also the role of calcinations, time, and concentration of metal acetate solution and power of ultrasound wave on the size, morphology and chemical composition of nanoparticles was investigated. For the precursor, we used metal acetate dissolved in ethanol/water/(PEG or PPG or PVA). Then MO nanoparticles were directly obtained by addition of a solution of sodium hydroxide. The influence of several parameters on the size and morphology of MO particles was reported. The powders were characterized by powder X-Ray Diffraction (XRD), Scanning Electron Microscopy (SEM), IR spectroscopy, Thermal Gravimetric Analysis and Differential Thermal Analysis (TGA/DTA).

13.2 CuO nanoparticles

Different amounts of NaOH solution with a concentration of 0.1 M were added to the 0.1, 0.05, 0.025 M solutions of Cu acetate in ethanol/water. The obtained mixtures were sonicated for 30-60 min with different ultrasound powers. To investigate the role of surfactants on the size and morphology of nanoparticles, we used 0.5g of polypropylene derivatives in the reactions with optimized conditions. Table 1 shows the conditions of reactions in detail. A multiwave ultrasonic generator (Bandlin Sonopuls Gerate-Typ: UW 3200, Germany) equipped with a converter/transducer and titanium oscillator (horn), 12.5 mm in diameter, operating at 30 kHz with a maximum power output of 780 W, was used for the ultrasonic irradiation. The ultrasonic generator automatically adjusted the power level. The wave amplitude in each experiment was adjusted as needed. The X-ray powder

diffraction (XRD) measurements were performed using a Philips diffractometer of X'pert Company with mono chromatized Cuk_{α} radiation. The crystallite sizes of the selected samples were estimated using the Scherrer method. TGA and DTA curves were recorded using a PL-STA 1500 device manufactured by Thermal Sciences. The samples were then characterized using a scanning electron microscope (SEM) (Philips XL 30) with gold coating.

Sample	$Cu(OAc)_2.2H_2O$	NaOH (0.1 M)	Aging time	Ultrasound power	Template
1	50 ml (0.1 M)	100 ml	1 hr	30W	PEG
2	50 ml (0.05 M)	100 ml	1 hr	30W	PEG
3	50 ml (0.025 M)	100 ml	1 hr	30W	PEG
4	50 ml (0.1 M)	100 ml	1 hr	45W	PEG
5	50 ml (0.05 M)	100 ml	1 hr	45W	PEG
6	50 ml (0.025 M)	100 ml	1 hr	45W	PEG
7	50 ml (0.1 M)	100 ml	30 min	30W	PEG
8	50 ml (0.05 M)	100 ml	30 min	30W	PEG
9	50 ml (0.025 M)	100 ml	30 min	30W	PEG
10	50 ml (0.1 M)	100 ml	30 min	45W	PEG
11	50 ml (0.05 M)	100 ml	30 min	45W	PEG
12	50 ml (0.025 M)	100 ml	30 min	45W	PEG
13	50 ml (0.1 M)	100 ml	1 hr	30W	PPG
14	50 ml (0.05 M)	100 ml	1 hr	30W	PPG
15	50 ml (0.025 M)	100 ml	1 hr	30W	PPG
16	50 ml (0.1 M)	100 ml	1 hr	45W	PPG
17	50 ml (0.05 M)	100 ml	1 hr	45W	PPG
18	50 ml (0.025 M)	100 ml	1 hr	45W	PPG
19	50 ml (0.1 M)	100 ml	30 min	30W	PPG
20	50 ml (0.05 M)	100 ml	30 min	30W	PPG
21	50 ml (0.025 M)	100 ml	30 min	30W	PPG
22	50 ml (0.1 M)	100 ml	30 min	45W	PPG
23	50 ml (0.05 M)	100 ml	30 min	45W	PPG
24	50 ml (0.025 M)	100 ml	30 min	45W	PPG
25	50 ml (0.1 M)	100 ml	1 hr	30W	PVA
26	50 ml (0.05 M)	100 ml	1 hr	30W	PVA
27	50 ml (0.025 M)	100 ml	1 hr	30W	PVA
28	50 ml (0.1 M)	100 ml	1 hr	45W	PVA
29	50 ml (0.05 M)	100 ml	1 hr	45W	PVA
30	50 ml (0.025 M)	100 ml	1 hr	45W	PVA
31	50 ml (0.1 M)	200 ml	30 min	30W	PVA
2	50 ml (0.05 M)	200 ml	30 min	30W	PVA
33	50 ml (0.025 M)	100 ml	30 min	30W	PVA
34	50 ml (0.1 M)	100 ml	30 min	45W	PVA
35	50 ml (0.05 M)	100 ml	30 min	45W	PVA
36	50 ml (0.025 M)	100 ml	30 min	45W	PVA

Table 2. Experimental Conditions For Preparation of CuO Nanoparticles.

Fig 14a. shows the XRD patterns of CuO nanoparticles. fig 1shows the XRD pattern of the direct sonochemicaly synthesized CuO nanoparticles and fig (14b, 14c and 14d) show the XRD patterns of this sample after calcinations for 2 hours at 500 °C. Sharp diffraction peaks shown in fig 14 indicates good crystallinity of CuO nanoparticles. No characteristic peak related to any impurity was observed. The broadening of the peaks indicates that the particles were of nanometer scale. The average size of the particles of the some samples (the best result from 36 reactions) was 80 nm, and the average size of these samples after calcinations at 500 °C for 2 hours were calculated as about 70 nm. These findings are in agreement with those observed from the SEM images.

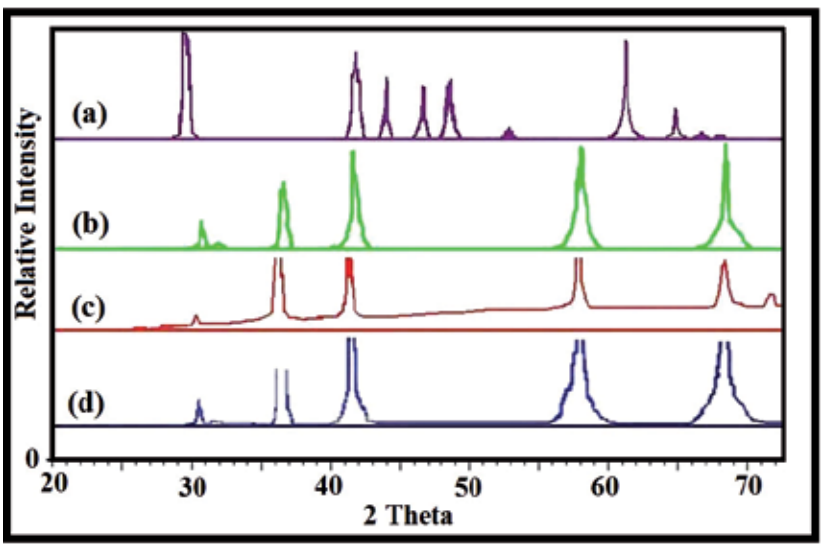

Fig. 14. X-Ray Powder Diffraction Pattern of CuO Nanoparticles (Sample No. 2) (a) Before Calcinations, (b) After Calcination (PEG Template), (c) After Calcination (PVA Template) and (d) After Calcinations (PPG Template).

The morphology, structure and size of the samples were investigated by Scanning Electron Microscopy (SEM). fig 15a indicates that the original morphology of the particles was approximately spherical with the diameter varying between 35 to 103 nm. The best morphology with smaller particles and good distribution was obtained for the sample number 2 before calcinations. fig 15b shows the SEM images of these samples after calcinations with different concentrations, it is clear from the fig 15b that the size of the particles has become small after calcinations. fig 15c shows the SEM images of the sample number 10. The role of PEG on the morphology of this sample is obvious. It has been reported that the presence of a capping molecule (such as polyvinyl alcohol, polyethylene glycol and polypropylene glycol) can alter the surface energy of crystallographic surfaces in order to promote the anisotropic growth of the nanoparticles. PEG is adsorbed on the crystal nuclei and helps the particles to grow separately. To investigate the size distribution of the nanoparticles, a particle size histogram was prepared for the sample No 2, (fig 16). Most of the particles possess sizes in the range from 30 to 103 nm. For further demonstration.

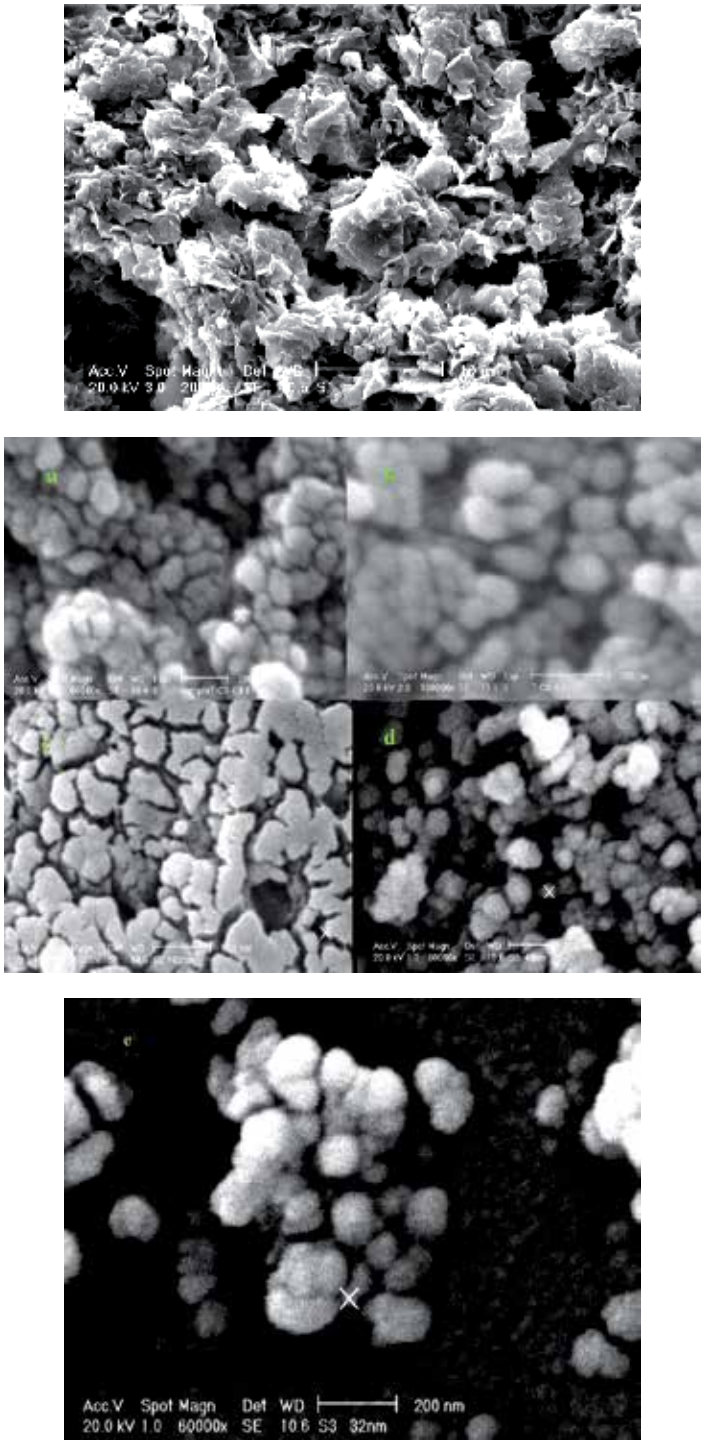

Fig. 15. The SEM images of CuO nanoparticles; (a) sample No. 2 before calcination, (b) samples No. 1(a), 3(b), 4(c), 5(d) after calcination, (c) sample No. 2 after calcinations.

Thermo-gravimetric analyses (TGA) were carried out to show that there was no difference between the curves of intermediate products and the one after calcinations. The results showed that there was no notable loss of weight in the TGA curves, proving the existence of CuO, which does not decompose at this temperature range. Further, the similarity of the TG curves of two samples shows the direct synthesis of CuO. fig 17a shows the TGA diagrams of the sample No. 2, and copper acetate and the compound before calcinations. fig 17b shows the DTA diagrams of the sample No. 2, copper acetate and the compound before calcinations.

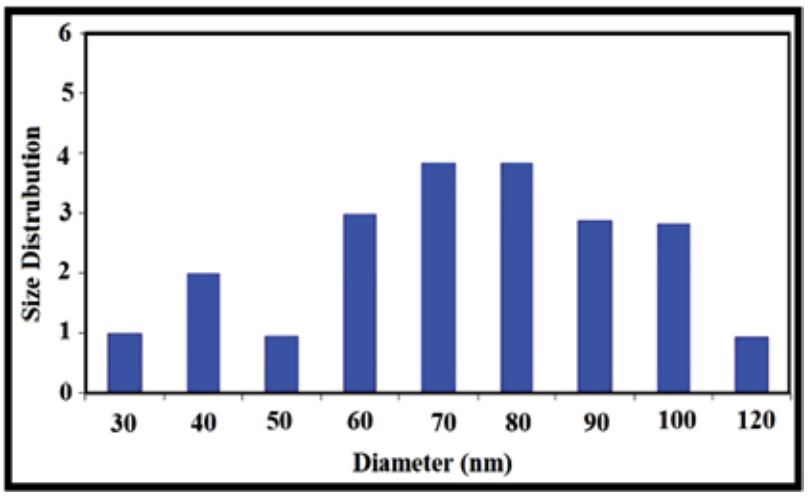

Fig. 16. Particle size histogram for the sample 2.

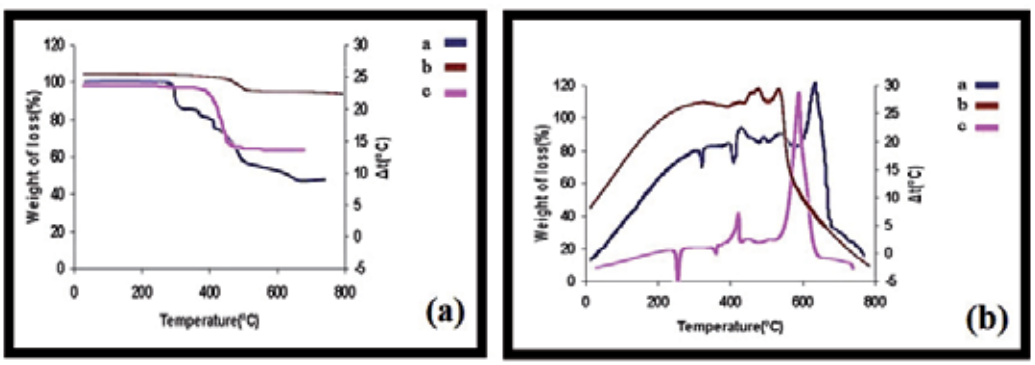

Fig. 17. The TG- DTA curves of CuO nanoparticles of the sample No. 2.

In order to investigate the role of sonication on the composition, size and morphology of the products, we carried out the reaction without sonication with the same conditions of the optimized sample. The XRD patterns of the obtained product corresponds to CuO but the SEM images show that the nanoparticles of the samples without using sonication have larger sizes as compared with the samples obtained via the sonochemical route.

It was indicated that the NP-CuO could decompose the organic pollutants by formation of exceed super oxides and/or hydroxyl radicals at the CuO interface.

13.3 Other M(II) oxide nanoparticles

Some nano-sized metal oxid (MO) such as ZnO, NiO and MnO were successfully synthesized by sonochemistry method in solutions at room temperature. The reactants used are ($M(Ac)_2.2H_2O$) and sodium hydroxide (NaOH), and H_2O/EtOH as a carrier in polyethylene glycol (PEG) template. Some of parameters such as effect concentration of NaOH solution, ultrasound power and sonicating time in growth and morphology of the nano-structures were investigated. The best morphology with smaller particles size and good distribution was obtained by using 0.025 M solution of NaOH and 45 w ultrasound powers in 1 h sonicating time. The particle size of the nano-sized metal oxid powders synthesized at room temperature is approximately between 40–80 nm. The resulting nano-sized powder was characterized by X-ray diffraction (XRD) measurements, Raman, BET, Solid state UV-vis and Scanning Electron Microscopy (SEM).

In recent years, metal oxide (MO) nanoparticles as a kind of functional material has attracted extensive interests due to its novel optical, electronic, magnetic, thermal and mechanical properties and potential application in catalyst, battery electrodes, gas sensors, electrochemical films, photo-electronic devices, and so on. In these applications, it is still needed for synthesizing high-quality and ultra-fine powders with required characteristics in terms of their size, morphology, microstructure, composition purity, crystallizability, etc. which are the most essential factors which eventually determine the microstructure and performance of the final products. Therefore, it is very important to control the powder properties during the preparation process. There are many chemical and physical methods to prepare nanometer MO, including the precipitation of metal acetate with NaOH. Recently, the interest preparation of nanometer MO has been growing. However, only few practical methods have been reported. The nanomaterials whose synthesis was reported are ZnS, Sb_2S_3, HgSe, SnS_2, CdS, CdSe, PbX (E = S, Se, Te, O), CuS, Ag_2Se and $CdCO_3$. But the sonochemical method for preparation of nanomaterials is very interesting, simple, cheap and safe. However, we have developed a simple sonochemical method to prepare NiO, MnO and ZnO nanostructures, wherein MO is synthesized by the reaction of $(CH_3CO_2)_2M.2H_2O$ and NaOH in an ultrasonic device. The MO nanoparticles have been characterized by X-ray powder diffraction (XRD), Raman spectroscopy, Solid state UV, BET and also the morphology and size of the nanostructures have been observed by scanning electron microscopy (SEM). We have performed these reactions in several conditions to find out the role of different factors such as the aging time of the reaction in the ultrasonic device and the concentration of the metal acetate on the morphology of nanostructures.

Typical procedure for preparation of MO nanoparticles: NaOH solution with a concentration of 0.1 M (100 ml) were added to the 0.05 and 0.025 M solutions of $M(CH_3COO)_2.2H_2O$ in ethanol/water. To investigate the role of surfactants on the size and morphology of nanoparticles, we used 0.5 gr of polyethylene glycol (PEG) in the reaction with optimized conditions. The mixtures were sonicated for 30-60 min, with different ultrasound powers followed by centrifuging with a centrifuge, and separation of the solid and liquid phases. The solid phase was washed for three times ethanol and water. Finally, the washed solid phase was calcinated at 500 ^oC for 30 min. Table 1 shows the conditions of reactions in detail. A multiwave ultrasonic generator (Bandlin Sonopuls Gerate-Typ: UW 3200, Germany) equipped with a converter/transducer and titanium oscillator (horn), 12.5 mm in diameter, operating at 30 kHz with a maximum power output of 780W, was used for

the ultrasonic irradiation. The ultrasonic generator automatically adjusted the power level. The wave amplitude in each experiment was adjusted as needed. X-ray powder diffraction (XRD) measurements were performed using a Philips diffractometer of X'pert Company with mono chromatized Cuk_{α} radiation. The samples were characterized with a scanning electron microscope (SEM) (Philips XL 30) with gold coating. Raman spectra were recorded on a Labram HR 800-Jobin Yvon Horbiba spectrometer. UVeVis spectra were measured with an HP 8453 diode array spectrophotometer. The specific surface area of samples was determined using the Brunauer–Emmet–Teller (BET) method in a volumetric adsorption apparatus (ASAP 2010 M, Micrometritics Instrument Corp).

Various conditions for preparation of MO nano-structures were summarized in Table. 3.

Series 1	$Mn(OAc)_2.2H_2O$	NaOH (0.1 M)	Aging time	Ultrasound power	Template
1	50 ml (0.05 M)	100 ml	1 hr	30W	PEG
2	50 ml (0.05 M)	100 ml	1 hr	45W	PEG
3	50 ml (0.025 M)	100 ml	1 hr	30W	PEG
4	50 ml (0.025 M)	100 ml	1 hr	45W	PEG
5	50 ml (0.05 M)	100 ml	30 min	30W	PEG
6	50 ml (0.05 M)	100 ml	30 min	45W	PEG
7	50 ml (0.025 M)	100 ml	30 min	30W	PEG
8	50 ml (0.025 M)	100 ml	30 min	45W	PEG
Series 2	$Ni(OAc)_2.2H_2O$	NaOH (0.1 M)	Aging time	Ultrasound power	Template
1	50 ml (0.05 M)	100 ml	1 hr	30W	PEG
2	50 ml (0.05 M)	100 ml	1 hr	45W	PEG
3	50 ml (0.025 M)	100 ml	1 hr	30W	PEG
4	50 ml (0.025 M)	100 ml	1 hr	45W	PEG
5	50 ml (0.05 M)	100 ml	30 min	30W	PEG
6	50 ml (0.05 M)	100 ml	30 min	45W	PEG
7	50 ml (0.025 M)	100 ml	30 min	30W	PEG
8	50 ml (0.025 M)	100 ml	30 min	45W	PEG
Series 3	$Zn(OAc)_2.2H_2O$	NaOH (0.1 M)	Aging time	Ultrasound power	Template
1	50 ml (0.05 M)	100 ml	1 hr	30W	PEG
2	50 ml (0.05 M)	100 ml	1 hr	45W	PEG
3	50 ml (0.025 M)	100 ml	1 hr	30W	PEG
4	50 ml (0.025 M)	100 ml	1 hr	45W	PEG
5	50 ml (0.05 M)	100 ml	30 min	30W	PEG
6	50 ml (0.05 M)	100 ml	30 min	45W	PEG
7	50 ml (0.025 M)	100 ml	30 min	30W	PEG
8	50 ml (0.025 M)	100 ml	30 min	45W	PEG

Table 3. Experimental conditions for the preparation of MO nanoparticles

The best morphology with smaller particles and good distribution was obtained for the sample number 4 in series 1, 2 and 3. fig 18(a,b and c) shows the XRD patterns of the direct sonochemicaly synthesized of the ZnO, NiO and MnO nanoparticles respectively. Sharp diffraction peaks shown in fig 18. indicate good crystallinity of MO nanoparticles. No characteristic peak related to any impurity was observed.

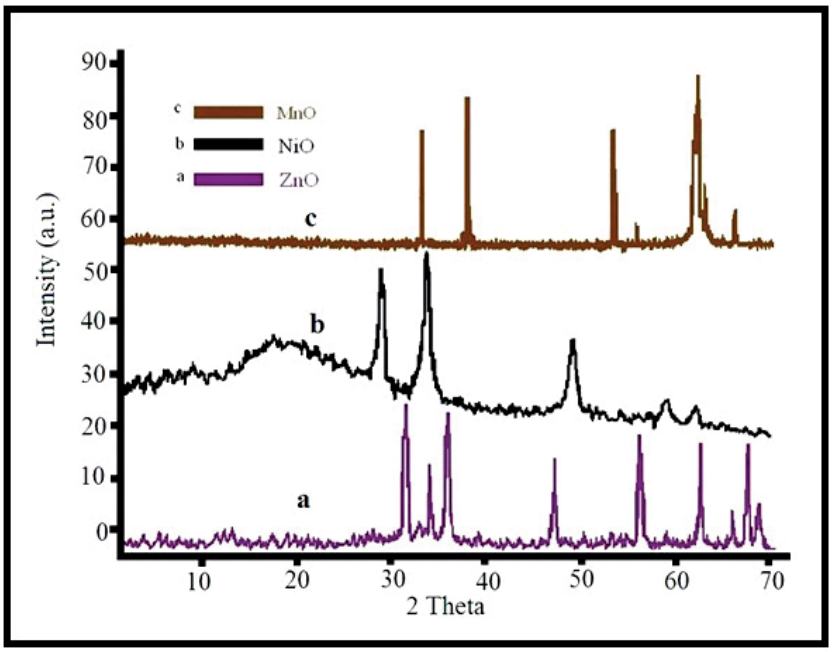

Fig. 18. X- Ray powder diffraction pattern of MO nanoparticles (a) ZnO, (b) NiO, (c) MnO.

The broadening of the peaks indicated that the particles were of nanometer scale. The morphology, structure and size of the samples are investigated by Scanning Electron Microscopy (SEM). fig 19 indicates that the original morphology of the ZnO, NiO and MnO particles are approximately spherical with the diameter varying between 40 to 80 nm. The role of PEG on the morphology of this sample is obvious. It has been reported that the presence of a capping molecule such as polyethylene glycol (PEG) can alter the surface energy of crystallographic surfaces, in order to promote the anisotropic growth of the nano particles. In this work PEG adsorbs on the crystal nuclei and it helps the particles to grow separately. To investigate the size distribution of the nano particles, a particle size histogram was prepared for MO nano particles, (fig 20).

Fig 21. demonstrates the UV-vis spectrum of the MO nanoparticles by ultrasonically dispersing in absolute ethanol. Strong absorption peak in the UV region can be observed. The absorption band gap *Eg* is usually achieved with the aid of the following equation:

$$(\alpha h\nu)^n = B(h\nu - E_g)$$

Concretely, *hν* is the photo energy; *a* is the absorption coefficient; *B* is the constant related to the material; and *n* indicates either 2 or 1/2 for direct transition and indirect transition, respectively.

The inset of fig 21 gives us the typical $(ahv)^2 \sim h\nu$ curve for the MO samples calcinated at 500 °C. By the extrapolation of *Eg.* (1), we can get the present band gaps as 4.1, 3.7 and 3.9 Ev (layout for NiO, ZnO and MnO) indicating the small blue shifts upon size reductions for MO nanoparticles.

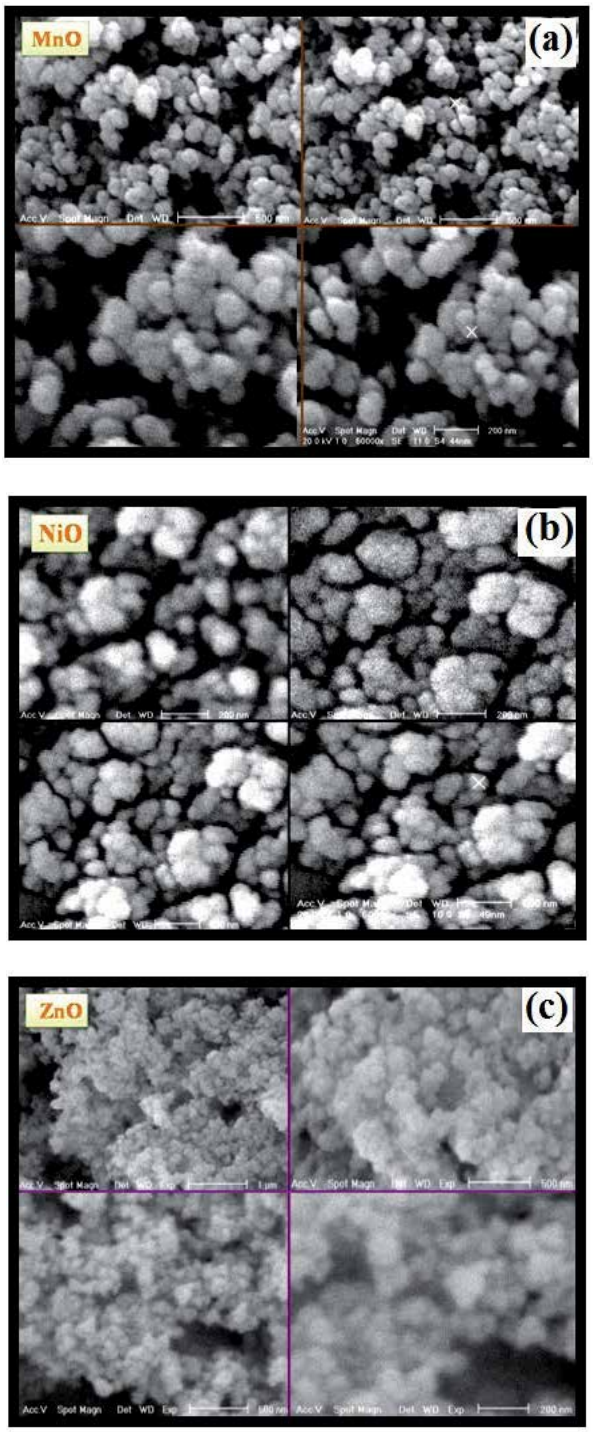

Fig. 19. Typical SEM micrographs of MO nano particles after calcinations: (a) ZnO, (b) NiO and (c) MnO.

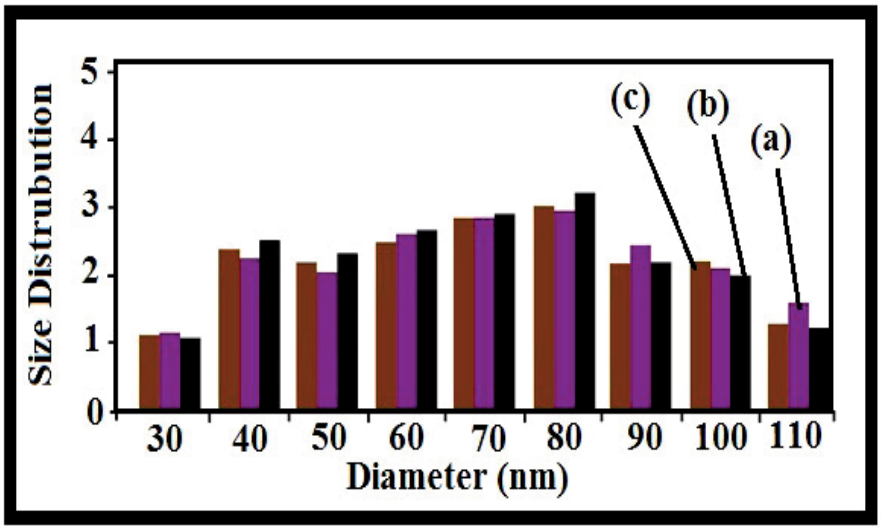

Fig. 20. Particle size Histogram of MnO, NiO and ZnO Nanopowders.

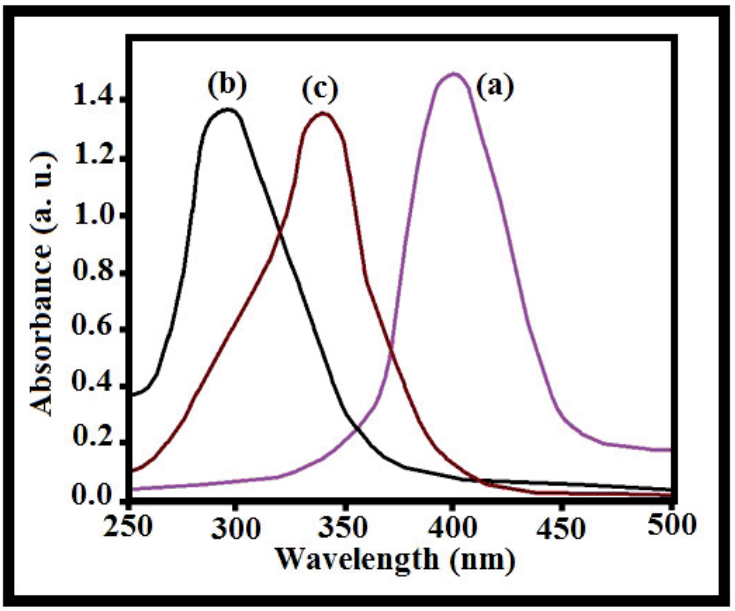

Fig. 21. Solid state UV absorption of MnO, NiO and ZnO nanoparticles

The surface area analysis was carried out on MO nanoparticles by BET method. Assuming the particles possess solid, spherical shape with smooth surface and same size, the surface area can be related to the average equivalent particle size by the equation:

$$D_{BET} = 6000/(\rho\ Sw)\ (\text{in nm})$$

Where D_{BET} is the average diameter of a spherical particle; *Sw* represents the measured surface area of the powder in m^2/g; and ρ is the theoretical density in g/cm^3. fig 22 shows

BET plots of MO nanoparticles, the specific surface area of MO nanoparticles calculated using the multi-point BET-equation are 33, 40 and 53 m^2/g (layout for NiO, ZnO and MnO), and the calculated average equivalent particle size is 36, 42 and 51 nm (layout for NiO, ZnO and MnO). We noticed that the particles size obtained from the BET and the SEM methods, agree very well with the result given by X-ray line broadening. The results of SEM observations and BET methods further confirmed and verified the relevant results obtained by XRD as mentioned above. Metal oxides are important catalyst in organic chemistry, gas sensors (such as CO_2, NO, SO_2, H_2O and CO) and battery cathode in the course of our research. The results of this investigation will be reported soon.

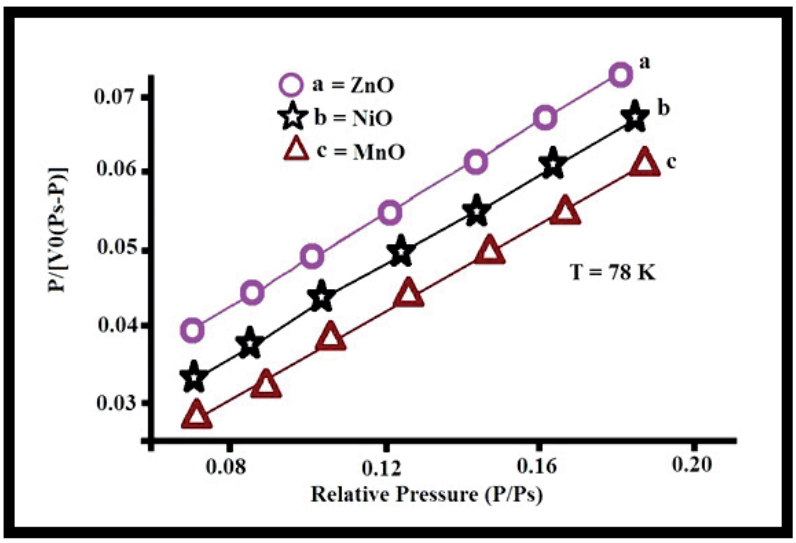

Fig. 22. BET plots of MnO, NiO and ZnO nanoparticles

Therefore Nano-sized of MnO, NiO and ZnO (MO) have been prepared by reaction between corresponding metal acetate and NaOH under ultrasound irradiation in solution at room temperature. Some of parameters such as effect concentration of NaOH solution, ultrasound power and sonicating time in growth and morphology of the nano-structures were investigated. The best morphology with smaller particles size and good distribution was obtained by using 0.025 M solution of metal acetate and 45 w ultrasound powers in 1 h sonicating time. Average particle sizes of the synthesized nano-sized MO powders were between 40-80 nm. Simple procedure, short reaction times, yields smaller particles and mild reaction conditions at room temperature are noteworthy advantages of this method. The specific surface area of MO nanoparticles calculated using the multi-point BET-equation are 33, 40 and 53 m^2/g (layout for NiO, ZnO and MnO), and the calculated average equivalent particle size is 36, 42 and 51 nm (layout for NiO, ZnO and MnO). We noticed that the particles size obtained from the BET and the SEM methods, agree very well with the result given by X-ray line broadening. The results of SEM observations and BET methods further confirmed and verified the relevant results obtained by XRD as mentioned above. The infrared absorption band of the MO nanoparticles show blue-shifts compared with that of bulk MO [Alireza Aslani, 2008[a], 2009[b], 2010[c] and 2011[d]].

14. References

A. Duteil, R. Q U. M. Chaudret, C. Roucauj,. S. Bradley, Chem. Mater. 1993. 5: 341.
Advani. S. G, Processing and Properties of Nanocomposites, World Scientific, pp. 1, 2007.
Ajayan. P. M, Schadler, L.S., Braun, P.V., Nanocomposite Science and Technology, Wiley, VCH pp 10, 77-80, 111, 112, 2003.
Alireza Aslani and A. Morsali. Inorganica Chimica Acta. 362, (2009), 5012-5016.
Alireza Aslani and V. Oroojpour. Physica B, Physics of Condensed matter. 406, (2011), 144-149.
Alireza Aslani, A. Morsali and M. Zeller. Solid State Sciences, 10, (2008), 1591-1597.
Alireza Aslani, A. Morsali, V. T. Yilmaz and C. Kazak. 929, (2009), 187-192.
Alireza Aslani, A. R. B. Shamili and K. Kaviani. Physica B, Physics of Condensed matter, 405, (2010), 3972–3976.
Alireza Aslani, A. R. B. Shamili and S. Barzegar. Physica B, Physics of Condensed matter, 405 (2010), 3585–3589.
Alireza Aslani, M. R. Arefi, A. Babapoor, A. Amiri, K. B. Shuraki. Applied Surface Science, 257, (2011), 4885-4889.
Alireza Aslani, Physica B, Physics of Condensed matter. 406, (2011), 150-154.
Alireza Aslani, V. Oroojpour, M. Fallahi, Applied Surface Science, 257, (2011), 4056-4061.
Bhandarkar, S, and A. Bose, J. Colloid Interface Sci., Vol. 135, No. 2, 1990, pp. 541–550.
Bliznyuk. V. N, A. Campbell, and C. W. Frank, ACS Symposium Series 695, New York Oxford University Press, 1998, pp. 220–232.
Bonnell. D. A, New York: Wiley-VCH, 2001.
Boukerma. K, Piquemal. J. Y, Chehimi. M. M, Mravcakova. M, Omastova. M, Beaunier. P, Polymer, 47, pp 569-576, 2006.
Brust, M, et al., J. Chem. Soc. Chem. Comm., Vol. 7, 1994, pp. 801–802.
Carotenuto. G, Her.Y. S, Matijevic. E, Ind. Eng. Chem. Res., 35,2929, 1996.
Collier, C. P, et al., Science, Vol. 277, No. 5334, 1997, pp. 1978–1981.
Cortan, A. R, et al, J. Am. Chem. Soc., Vol. 112, No. 4, 1990, pp. 1327–1332.
Dallas. P, Niarchos. D, Vrbanic. D, Boukos. N, Pejovnik. S, Trapalis. C, Petridis. D, Polymer 48, pp 2007-2013, 2007.
Edelstein, A. S, and R. C. Cammarata, Bristol, PA: IoP Publishing, 1996.
Epstein. A. J, Platics Design Library, 1, 93, 1999.
F. Wakai, Y. K, S. S. N. M, K. I and K. N, Nature, 344, 6265, 421-423 (1990).
Freund. M. S, Deore B., Self-Doped Conducting Polymers, Wiley, pp.1,2, 10-12, 2006.
Gabriel. B. L, SEM, A User's Manual for Materials Science, American Society for Metals, 1985.
Greffet. J. J, and R. Carminati, Progr. Surf. Sci., Vol. 56, No. 3, 1997, pp. 133–237.
H. Hirai, Macromol. Chem. Suppl. 1985, 14, 55.
H. Hirai, Y. Nakao, N. Toshima, J. Macromol. Sci. Chem. 1979. 13, 727.
H. Maeda, J. Control. Release, 19, 315–324 (1992).
H. Suzuki, T. Ohno, J. Soc. Powder Technol, Jpn, 39, 877–884 (2002).
I. Matsui, J. Chem. Eng, Jpn, 38(8), 535–546 (2005).
Inzelt. G, Conducting Polymers A New Era in Electrochemistry, Springer, 1, 2008.
J. S. Bradley, in Clusters and Colloids, G. SCHMID (ed.) VCH, Weinheim, 1993, p. 459.
K. Ishikawa, J. Soc. Powder Technol, Jpn, 38, 731-740 (2001).
K. Ishikawa, K. Yoshikawa and N. Okada, Phys. Rev. B, 37, 5852-5855 (1988).

K. Kobayashi, J. Soc. Powder Technol, Jpn, 41, 473-478 (2004).
K. Megure, Y. Nakamura. Y. Hayashim, . Torizuka, K. Esumi, Bull. Chem. Soc.]pn. 1988. 61. 347.
K. Niihara, J. Ceram. Soc. Jpn, 99 (10), 974-982 (1991).
K. Uchino, E. Sadanaga and T. Hirose, J. Am. Ceram. Soc, 72(8), 1555–1558 (1989).
Keyse. R. J, et al. Microscopy Handbook, Vol. 39, Oxford, England: BIOS Scientific Publishers, 1998.
Kitaigorodski. A. L, Organic Chemical Christallography, New York: Counsultants Bureau, 1961.
Kricheldorf. H. R, Nuyken, O., Swift, G., Handbook of Polymer Synthesis, Marcel Dekker., Ch. 12, pp 1,3,4, USA, 2005.
Lee. E. S, Park. J. H., Wallace. G. G., Bae. Y. H, Polymer International, 53:400-405, 2004.
Li, S, et al., IEEE Trans. on Magnetics, Vol. 37, No. 4, 2001, pp. 2350–2352.
Liu. Y. C, Materials Chemistry and Physics 77, pp 791-795, 2002.
Lover, T, et al., Chem. Mater. Vol. 9, No. 4, 1997, pp. 967–975.
Lubin. G, Handbook of Composites, Van Nostrand Reinhold Company Inc., USA, pp1, 2, 1982.
Lvov, Y. M, M. R. Byre and D. Bloor, Crystall. Reports, Vol. 39, No. 4, 1994, pp. 696–716.
Lvov, Y. M., et al, Phil. Mag. Lett., Vol. 59, No. 6, 1989, pp. 317–323.
Lvov. Y, and H. Mohwald, (eds.), New York: Basel/Marcel Dekker, 2000, pp. 125–167.
Lvov. Y. M, and L. A. Feigin, Kristallografiya, Vol. 32, No. 3, 1987, pp. 800–815.
M. Arakawa, Funsai (The Micrometrics), No 27, 54–64 (1983).
M. Arakawa, J. Soc. Powder Technol, Jpn, 42, 582–585 (2005).
M. E. Labib, R. Williams, Colloid Interface Sci. 1984. 97, 356.
M. Haruta, Catalysts, 36(6) 310-318 (1994).
M. Komiyama, H. Hirai, Bull. Chem. Soc. Jpn. 1983, 56, 2833.
M. Takashige, T. Nakamura, Jpn. J. Appl. Phys, 20, 43-46 (1981).
Mann, S., et al., J. Chem. Soc.-Dalton Trans., No. 4, 1983, pp. 771–774.
Mann, S., J. P. Hannington, and R. J. P. Williams, Nature, Vol. 324, No. 6097, 1986, pp. 565–567.
Mravcakova. M, Boukerma. K, Omastova. M, Chehimi. M. M, Materials Science and Engineering C, 26, pp 306-313, 2006.
Mravcakova. M, Omastova. M, Potschke. P, Pozsgy. A, Pukanszky. B., Pionteck. J, Adv. Technol., 17: 715-726, 2006.
N. Wada, Chem. Eng., 9, 17–21 (1984).
Nabok. A. V, et al, IEEE Trans. on Nanotechnology, Vol. 2, No. 1, 2003, pp. 44-49.
Nabok.A. V, et al., Thin Solid Films, Vol. 327–329, 1998, pp. 510–514.
Nakanishi, T. B. Ohtani, and K. Uosaki, J. Phys. Chem. B, Vol. 102, No. 9, 1998, pp. 1571–1577.
Netzer, L., and J. Sagiv, J. Am. Chem. Soc., Vol. 105, No. 3, 1983, pp. 674–676.
Omastova. M, Chodak. I, Pionteck. J, Potschke. P, Journal of Macromolecular Science, Part A, 35:7, 1117-1126, 1998.
Omoto. M, Yamamoto. T, Kise. H, Journal of Applied Polymer Science, Vol. 55, 283-287, 1995.
P. H. Hess, P. H. Parker, Appl. Polymer. Sci 1966. 10, 1915.

Petty. M. C, in Languir- Blodgett Films, G. G. Roberts, (ed.), New York: Plenum Press, 1990, pp. 133–221.
Petty. M. C, M. R. Bryce, and D. Bloor, (eds.), New York: Oxford University Press, 1995.
Pionteck. J, Omastova. M, Potschke. P, Simon. F, Chodak. I, Journal of Macromolecular Science, Part B, 38:5, 737-748, 1999.
Puntes, V. F, and K. M Krishnan, IEEE Trans. on Magnetics, Vol. 37, No. 4, 2001, pp. 2210–2212.
R. R. Karimi, A. R. B. Shamili, Alireza Aslani and K. Kaviani. Physica B, Physics of Condensed matter, 405, (2010), 3096–3100.
Ranaweera. A. U, Bandara. H. M. N, Rajapakse. R. M. G, Electrochimica Acta, 52, pp 7203-7209, 2007.
Rizza, R, et al, Chem. Mater., Vol. 9. No. 12, 1997, pp. 2969–2982.
Roberts, G. G, Adv. Phys., Vol. 34. No. 4, 1985, pp. 475–512.
Roberts, G. G, in Langmuir-Blodgett Films, G. G. Roberts, (ed.), New York: Plenum Press, 1990.
Roberts, G. G., et al., J. Verwey, (ed.), North Holland: Amsterdam, 1983, p. 141.
Rogach, A. L, et al., J. Phys. Chem. B, Vol. 103, No. 16, 1999, pp. 3065–3069.
Ross, J, and G. G. Roberts, Proceedings of 2nd International Meeting on Chemical Sensors, Bordeaux, France, 1986, p. 704.
S. Sato, N. Asai and M. Yonese, Colloid Polym. Sci, 274, 889-893 (1996).
Sanjay. K. Mazumdar, CRC Press LLC, USA, pp 4-6, 2002.
Sarathy, K. V., et al, J. Phys. Chem. B., Vol. 103, No. 3, 1999, pp. 399–401.
Schultz, D. L., et al, IEEE, 25th PVSC, Washington, D.C., May 13–17, 1996, pp. 929–932.
Stefanis. A, and A. A. G. Tomlinson, Enfield, NH: Trans Tech. Publications, 2001.
T. Sekino, Mater. Integr, 13(11) 50-54 (2000).
T. Yokoyama, Sokeizai, 3, 6-11 (2005).
Tadros. T. H, Applied Surfactants, Wiley-VCH Verlag GmbH and Co. KGaA, pp. 1-5, 2005.
Talapin, D. V, et al., Physica E, Vol. 14, No. 1–2, 2002, pp. 237–241.
Tredgold. R. H, Order in Thin Organic Films, Cambridge, England: Cambridge University Press, 1994.
Tsukruk. V. V, Progr. Polym. Sci., Vol. 22, No. 2, 1997, pp. 247–311.
Ulman. A, (ed.), Boston, MA: Butterworth- Heinemann, 1995.
Ulman. A, From Langmuir-Blodgett to Self- Assembly, Boston, MA: Academic Press, 1991.
V. H. Thiele, J. Kowallik. J. Colloid Sci. 1965. 20, 679.
Vogel, W, et al, Vol. 16, No. 4, 2000, pp. 2032–2037.
Wallace. G. G, Spinks, G. M, Kane-Maguire. L. A. P, Teasdale. P. R, CRC Press LCC, USA, pp.51, 2003.
Wegner. G, Molecular Crystals and Liquid Crystals Science, Vol. 234, 1993, pp. 283–316.
Wu. T. M, Yen. S. J, Chen. E. C, Chiang. R. K, Journal of Polymer Science: Part B: Polymer Physics, Vol. 46, 727-733, 2008.
Y. Kurokawa, Y. Hosoya, Surface, 34(2) 100-106 (1996).
Yaacob, I. I, S. Bhandarkar, and A. Bose, J Mater. Research, Vol. 8, No. 3, 1993, pp. 573–577.
Yarwood. J, Analyt. Proc., Vol. 30, 1993, pp. 13–18.

14

Polypropylene Nanocomposites

Azza M. Mazrouaa
Petrochemical Department, Polymer Laboratory,
Egyptian Petroleum Research Institute, Nasr City, Cairo,
Egypt

1. Introduction

The possibility of manufacturing nano-composites materials with tailored properties at low cost has gained much interest. In fact, there is already more than two decades of research on those materials. Particular interest has been paid to clay nano-platelets and their composites with non-polar thermoplastic polyolefin matrixes, namely polypropylene (PP).

Imagine an industrialist and his design team relatively aware of the developments in the research with nano-fillers asking themselves: What can we do with nano-composites and make a net profit up to the 'promises' of the current state of the art? Research announced potential areas of interest for practical applications include mechanical performance, toughness improvement, surface hardening, fire retardancy, or, solvent and permeability reduction. However there remains the problem of how a company could set up the facility for compounding, and guarantee proper dispersion and minimization of health hazards. One should bear in mind that for industrial dissemination conventional equipments should be used and compounding achieved through in-line mixing of virgin resins and nanoclay master batches. Since the seventies polypropylene has been seen as the wonder engineering-commodity material with widespread application in numerous technical applications.

Current masterbatches are mainly based on thermoplastic polyolefin and anhydride functionalized PP as a compatibilizer. In principle, filling with a low incorporation level of nanoclay (typically less than 5%), makes PP adequate to applications with engineering requirements. Nevertheless, only well-dispersed and well-exfoliated nanoparticles can lead to the expected improvement of properties. The nanoparticle dispersion and exfoliation is usually assumed to be achieved during masterbatching, but the suppliers of master batches request a relatively high price. Underlining these evidences poor exfoliation was a common feature in moldings obtained using industry achievable processing conditions. There is an evident interest of bringing the benefits of nanocomposites at the laboratory scale to cost competitive industrial products. However the first available information leaves a number of treads that research could well follow, for example. Which level of exfoliation should be required to viable master batches? Is there any scope for hybrid compounding, i.e. combining particulate nanoclays with fibre reinforcements? Are there only a few niches of application for nanocomposites? Have nanofillers any chance of being full exfoliated within non polar matrixes? Do these nanocomposites will require alternative routes of processing? Should novel compatibilizers be developed in order to avoid unavoidable reagglomeration during injection molding? (Frontini & Pouzada, 2011).

2. Nanotechnology growth predicted

Nanocomposites, defined as polymers bonded with nanoparticles to produce materials with enhanced properties, have been in existence for years but are recently gaining momentum in mainstream commercial packaging use (Butschli 2004).The United States is leading in nanotechnology research with over 400 research centers and companies involved with over $3.4 billion in funding. Europe has over 175 companies and organizations involved in nanoscience research with $1.7 billion in funding. Japan is also very involved in research with over 100 companies working with nanotechnologies（Anyadike, 2005）. Globally, the market for nanocomposites is expected to grow to $250 million by 2008, with annual growth rates projected to be 18-25% per year (Principia, 2004). The global market for nanotechnology products was worth an estimated $11.7 billion in 2009. The market is projected to grow to more than $15.7 billion in 2010 and nearly $26.7 billion in 2015 at a compound annual growth rate (CAGR) of 11.1% from 2010 to 2015 (bccresearch, 2010).

3. What does nanocomposites really mean?

Perhaps it is necessary to make clear the terms "hybrids" and "nanocomposites" before the discussion of the nanocomposites, since it is somewhat ambiguous to identify whether materials fall into "nanocomposites" or not. The most wide-ranging definition of a hybrid is a material that includes two moieties blended on the molecular scale.

Commonly the term "hybrids" is more often used if the inorganic units are formed in situ by the sol-gel process (Kickelbick, 2007).Meanwhile, use of the word "nanocomposites" implies that materials consist of various phases with different compositions, and at least one constituent phase (for polymer/silica nanocomposites, that phase is generally silica) has one dimension less than 100 nm. A gradual transition is implied by the fact that there is no clear borderline between "hybrids" and "nanocomposites"(Kickelbick, 2007).

Expressions of "nanocomposites" seem to be very trendy, and although the size of the silica particles is above 100 nm, the composites are often called "nanocomposites" in some literature. Organic/inorganic composite materials have been extensively studied for a long time. When inorganic phases in organic/inorganic composites become nano sized, they are called nanocomposites. Organic/inorganic nanocomposites are generally organic polymer composites with inorganic nanoscale building blocks. They combine the advantages of the inorganic material (e.g., rigidity, thermal stability) and the organic polymer (e.g., flexibility, dielectric, ductility, and processibility). Moreover, they usually also contain special properties of nanofillers leading to materials with improved properties.

A defining feature of polymer nanocomposites is that the small size of the fillers leads to a dramatic increase in interfacial area as compared with traditional composites (Balazs et al., 2006; Caseri & Nalwa, 2004; Caseri,2006, 2007; Schadler, 2003; Schadler et al., 2007; Schaefer &Justice,2007; Winey &Vaia, 2007;, Krishnamoorti &Vaia, 2007).

The next time you look at a car, you could be looking at nanotechnology without even realizing it. For the past several years, car companies have been using nanocomposites instead of plastic to make certain car parts. In 2001, Toyota started using nanocomposites to make bumpers for their cars. In 2002, General Motors (GM) made nanocomposite "step-assists" – external running boards that help people get into and out of cars – an option on

the 2002 Chevrolet Astra and the GMC Safari (The Future of Automotive Plastics, 2003). Nanocomposites are lighter, stiffer, less brittle, and more dent- and scratch-resistant than conventional plastics. Some nanocomposites are also more recyclable, more flame retardant, less porous, better conductors of electricity, and can be painted more easily (Leaversuch & Buchholz, 2003).

4. How nanocomposites work?

Polymer nanocomposites are constructed by dispersing a filler material into nanoparticles that form flat platelets. These platelets are then distributed into a polymer matrix creating multiple parallel layers which force gases to flow through the polymer in a "torturous path", forming complex barriers to gases and water vapour, as seen in **Figure 1**. As more tortuosity is present in a polymer structure, higher barrier properties will result. The permeability coefficient of polymer films is determined using two factors: diffusion and solubility coefficients:

$$P = D \times S.$$

Effectively, more diffusion of nanoparticles throughout a polymer significantly reduces its permeability. According the Natick Soldier Center of the United States Army, "the degree of dispersion of the nanoparticles within the polymer relates to improvement in mechanical and barrier properties in the resulting nanocomposite films over those of pure polymer films". Nanoparticles allow for much lower loading levels than traditional fillers to achieve optimum performance. Usually addition levels of nanofillers are less than 5%, which significantly impact weight reduction of nanocomposite films. This dispersion process results in high aspect ratio and surface area causing higher performance plastics than with conventional fillers (Brody ,2003).

Fig. 1. Idealized Oriented Layered Nanoparticle

5. The most commonly used nanoparticles

Different types of fillers are utilized, the most common is a nanoclay material called montmorillonite—a layered smectite clay. Clays, in a natural state, are hydrophilic while polymers are hydrophobic. To make the two compatible, the clay's polarity must be modified to be more "organic" to interact successfully with polymers (Hay & Shaw, 2000; Ryan , 2003). One way to modify clay is by exchanging organic ammonium cations for

inorganic cations from the clay's surface (Sherman,1999). Additional nanofillers include carbon nanotubes, graphite platelets, carbon nanofibers, as well as other fillers being investigated such as synthetic clays, natural fibers (hemp or flax), and POSS (polyhedral oligomeric silsesquioxane). Carbon nanotubes, a more expensive material than nanoclay fillers which are more readily available, offer superb electrical and thermal conductivity properties. The major suppliers for nanoclays are Nanocor and Southern Clay. Inorganic nanoscale building nanoparticles of metals (e.g., Au, Ag), and metal oxides (e.g., TiO_2, Al_2O_3 which SiO_2 is viewed as being very important.

Carbon nanotube

Nano Silica

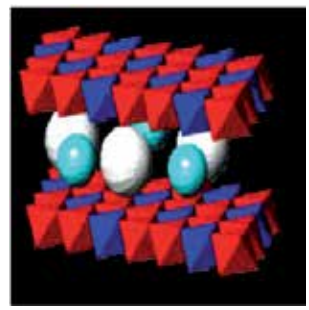

Layer Double Hydroxide

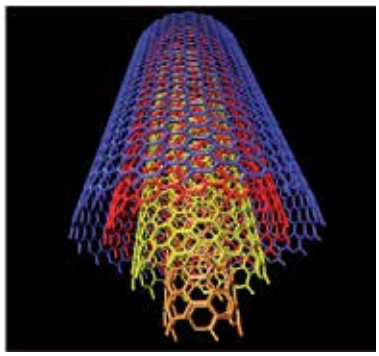

Carbon nanotubes [multiwall (MWNT)

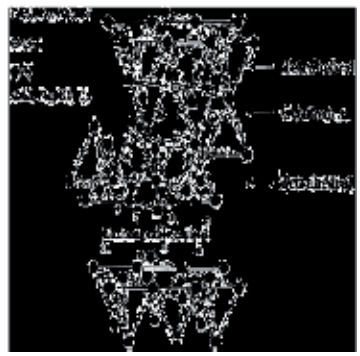

Engineered Nanoparticles**: Layered silica**

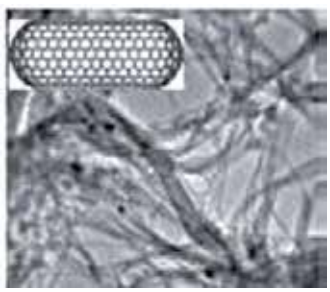

100 nm

Nanotubes

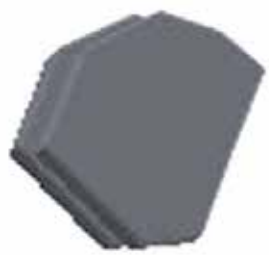

1 nm

Nanoplatelets

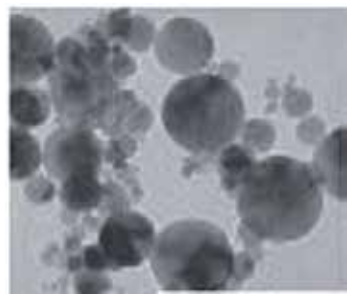

50 nm

Nanoparticles

Fig. 2. The most common used of nanoparticle

Using polypropylene, polyethylene, and other polymers reinforced with natural minerals such as calcium carbonate, zeolite, mica, and talc combined with efficient coupling agents has proven to be a successful technology to obtain tailored reinforcement and optimize the cost to property balance. One important material used as filler is the talc mineral since it has unique reinforcing features as softness, lubricity, excellent wetting and dispersion in plastics, and other organics. Talc is a hydrated magnesium silicate mineral widely used in polymers as reinforcing filler. Its plate-like structure provide the talc-filled materials with tailored properties to be used in some industrial and commercial applications such as in refrigerators jackets, packaged components, blocking of infrared in agricultural films, and in automotive and appliance markets. Talc-filled polypropylene composite has low specific gravity and combines excellent chemical resistance with low cost (Zihlif & Ragosta, 2003; Tripathi & Pillia, 1994; Hijleh et al.,2000; Mahanwar et al.,2006; Xie et al.,2001; Chen, 2004; Hajji et al. 1999; Kojima et al., 1993). **Figure 2**.

6. Polymer nanocomposite synthesis

The synthesis of polymer nanocomposites is an integral aspect of polymer nanotechnology. By inserting the nanometric inorganic compounds, the properties of polymers improve and hence this has a lot of applications depending upon the inorganic material present in the polymers. Solvent casting is one of the easiest and less time consuming methods for the synthesis of polymer nanocomposites.

There are three common methods used to enhance polymers with nanofillers to produce nanocomposites: melt compounding, in-situ polymerization and the solvent method.

1. **Melt compounding – or processing** – of the nanofillers into a polymer is done simultaneously when the polymer is being processed through an extruder, injection molder, or other processing machine. The polymer pellets and filler (clay) are pressed together using shear forces to help with exfoliation and dispersion (Brody, 2003; Zihlif & Ragosta, 2003).
2. **In-situ polymerization**, the filler is added directly to the liquid monomer during the polymerization stage.
3. **The solution method**, fillers are added to a polymer solution using solvents such as toluene, chloroform and acetonitrile to integrate the polymer and filler molecules [19]. Since the use of solvents is not environmentally-friendly, melt processing and in-situ polymerization are the most widely used methods of nanocomposite production.

As pointed out(Tripathi &Pillia,1994) nanocomposite systems can be prepared by various synthesis routes, thanks to the ability to combine different ways to introduce each phase. *The organic component can be introduced as:*

i. A precursor, which can be a monomer or an oligomer,
ii. A preformed linear polymer (in molten, solution, or emulsion states), or
iii. A polymer network, physically (e.g., semi crystalline linear polymer) or chemically (e.g., thermosets, elastomers) cross-linked.

The mineral part can be introduced as:

i. A precursor (e.g., TEOS) or
ii. Preformed nanoparticles.

Organic or inorganic polymerization generally becomes necessary if at least one of the starting moieties is a precursor.

7. Polypropylene nanocomposites

Polypropylene (PP) is a versatile material its use has significantly penetrated numerous sectors of the manufacturing, medical, and packaging industries. Polymer clay nanocomposites are multiphase organic/inorganic hybrid materials pioneered by researchers at Toyota, (Kojima et al., Usuki et al., 1993)which may exhibit significantly improved mechanical, flammability, and permeability properties relative to the base polymer matrix at very low clay loading. Although first demonstrated for nylon, polymer clay nanocomposites have since been prepared for a range of thermoplastic and thermoset polymers. However, the development of PP/clay nanocomposites poses special challenges because of polypropylene's hydrophobicity.

The reinforcement of polypropylene and other thermoplastics with inorganic particles such as talc and glass is a common method of material property enhancement. Polymer clay nanocomposites extend this strategy to the nanoscale. The anisometric shape and approximately 1 nm width of the clay platelets dramatically increase the amount of interfacial contact between the clay and the polymer matrix. Thus the clay surface can mediate changes in matrix polymer conformation, crystal structure, and crystal morphology through interfacial mechanisms that are absent in classical polymer composite materials. For these reasons, it is believed that nanocomposite materials with the clay platelets dispersed as isolated, exfoliated platelets are optimal for end-use properties.

Recent research has generated advances in polypropylene nanocomposites that are sufficient to motivate new technological applications. For example, PP-based nanocomposites have been developed for application as exterior automotive components (Sherman, 1999) Cone calorimetry measurements of peak heat release rate from maleated/ PP nanocomposites with 4% loading are reduced by 75% relative to the pure polymer (Gilman et al.,2000). These improvements are relevant to applications requiring reduced flammability. Yet, relative to other thermoplastic nanocomposites, such as nylon 6, the improvement in end-use properties for polypropylene nanocomposites has been modest. In addition, noting that many synthesized PP nanocomposites are likely to exist as nonequilibrium structures, research into the aging and rejuvenation of these mesoscale structures is warranted. Furthermore, better methods to characterize the full distribution and hierarchy of structural states present in PP nanocomposites are required because, for example, rare aggregates can seriously compromise nonlinear mechanical properties such as toughness, yield stress, and elongation at break. Finally, the interaction between clay platelets and polymer crystallization requires further attention because these interactions are likely a significant determinant of the end-use properties of polypropylene nanocomposites.

8. What is organoclay?

Organoclays are manufactured by modifying bentonite with quaternary amines, a type of surfactant that contains a nitrogen ion. The nitrogen end of the quaternary amine, the

hydrophilic end, is positively charged, and ion exchanges onto the clay platelet for sodium or calcium. The amines used are of the long chain type with 12-18 carbon atoms. After some 30 per cent of the clay surface is coated with these amines it becomes hydrophobic and, with certain amines, organophilic.

Fig. 3.

9. The nature of organoclays

The main component of organoclay is bentonite, a chemically altered volcanic ash that consists primarily of the clay mineral montmorillonite. The bentonite in its natural state can absorb up to seven times its weight in water, after treatment can absorb only 5 to 10 per cent of its weight in water, but 40 to 70 per cent in oil, grease, and other sparingly-soluble, hydrophobic chlorinated hydrocarbons. As the organoclay is introduced into water, the quaternary amine is activated and extends perpendicularly off the clay platelets into the water. A chlorine or bromine ion is loosely attached to the carbon chain. Since the sodium ions that were replaced by the nitrogen are positively charged, they bond with the chlorine ion, resulting in sodium salt that is washed away. The result is a neutral surfactant with a solid base, which is the organoclay. The hydrophilic end of the amine dissolves into the oil droplet because "like dissolves like," thus removing that droplet from water. Because the partition reaction takes place "outside" of the clay particle (in contrast to adsorption of oil by carbon, which takes place inside its pores), the organoclay does not foul quickly.

Organophilic clay can function is as a prepolisher to activated carbon, ion exchange resins, and membranes (to prevent fouling), and as a post polisher to oil/water separators, dissolved air flotation (DAF) units, evaporators, membranes, and skimmers. Organophilic clay powder can be a component or the main staple of a flocculent clay powder. They are excellent adsorbers for the removal of oil, surfactants, and solvents, including methyl ethyl ketone, t-butyl alcohol (TBA), and others.

10. Layered silicate / polypropylene nanocomposites

Layered silicate/polymer nanocomposites were first reported in 1950 as a patent literature (Carter et al.,1950) . However, it was not popular until Toyota researchers began a detailed

experimentation in the year of 1996 on the nylon 6/clay nanocomposites (Kojima et al., 1993). In recent years, nanocomposites received a great interest in academic, governmental and industrial studies (Kojima et al., 1993).The improvements in thermal, mechanical and flammability properties of clay/polymer nanocomposites are significantly higher than those achieved in traditional filled polymers. Up to now, these systems have experienced some success for several kinds of polar polymers. However, for polymers with low polarity, such as polyolefins, the improvements are not very significant due to the low compatibility between the clay and the polyolefins.

One of the most commonly used organophilic layered silicates is derived from montmorillonite (MMT). Its structure is made of several stacked layers, with a layer thickness between 1.2-1.5 nm and a lateral dimension of 100– 200 nm (Marchant & Krishnamurthy ,2002; Moore & Reynolds ,1997) . These layers organize themselves to form the stacks with a regular gap between them, called interlayer or gallery. The sum of the single layer thickness and the interlayer represents the repeat unit of the multilayer material, called d-spacing or basal spacing (d001), and is calculated from the (001) harmonics obtained from X-ray diffraction patterns. The clay is naturally a hydrophilic material, which makes it difficult to exfoliate in a polymer matrix. Therefore, the surface treatment of silicate layers is necessary to render its surface more hydrophobic, which facilitates exfoliation. Generally, this can be done by ion-exchange reactions with cationic surfactants, including primary, secondary, tertiary and quaternary alkylammonium cations (Fornes et al., 2002; Le Pluart et al.,2002).This modification also leads to expand the basal spacing between the silicate layers due to the presence of alkyl chain intercalated in the interlayer and to obtain organoclay (OMMT).

Polypropylene (PP) is one of the most widely used plastics in large volume. To overcome the disadvantages of PP, such as low toughness and low service temperature, researchers have tried to improve the properties with the addition of nanoparticles that contains polar functional groups. An alkylammonium surfactant has been adequate to modify the clay surfaces and promote the formation of nanocomposite structure. Until now, two major methods, i.e., in-situ polymerization(Ma et al., 2001; Pinnavaia, 2000) and melt intercalation (Manias et al.,2001) have been the techniques to prepare clay/PP nanocomposites. In the former method, the clay is used as a catalyst carrier, propylene monomer intercalates into the interlayer space of the clay and then polymerizes there. The macromolecule chains exfoliate the silicate layers and make them disperse in the polymer matrix evenly. In melt intercalation, PP and organoclay are compounded in the molten state to form nanocomposites.

As the hydrophilic clay is incompatible with polypropylene, compatibilization between the clay and PP is necessary to form stable PP nanocomposites. There are two ways to compatibilize the clay and PP. In the first approach, the enthalpy of the interaction between the surfactant and the clay is reduced. In the second approach, a compatibilizer, such as maleic anhydride grafted PP (PPgMA) can be used(Manias et al.,2001). The clay is melt compounded with the more polar compatibilizer to form an intercalated master batch. The master batch is then compounded with the neat PP to form the PP nanocomposite.

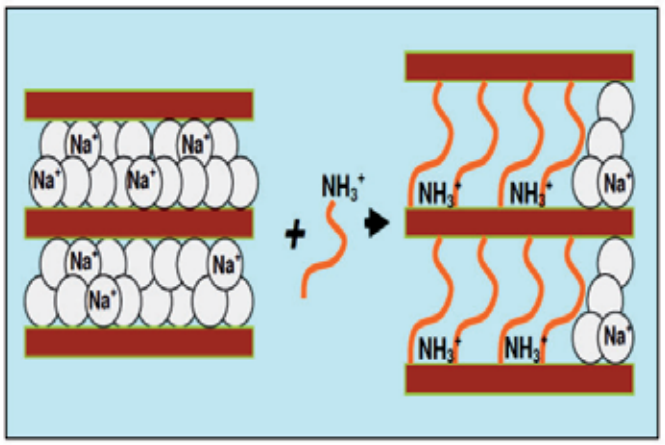

Fig. 4.a. Ion Exchange Reaction between Na-MMT and Alkyl Ammonium Molecules

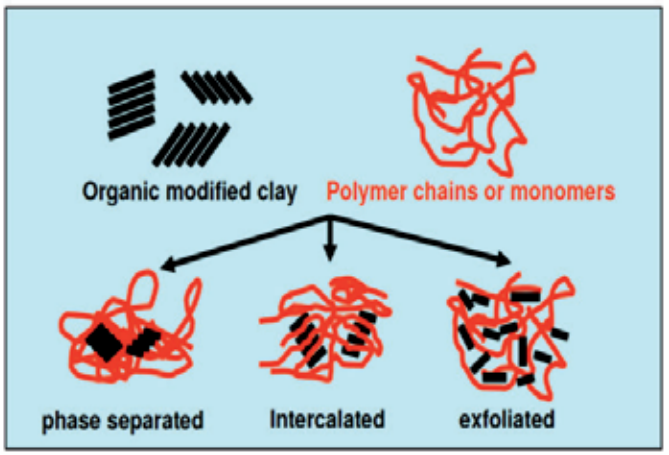

Fig. 4.b. Three main morphology achievable in nanocomposite structure

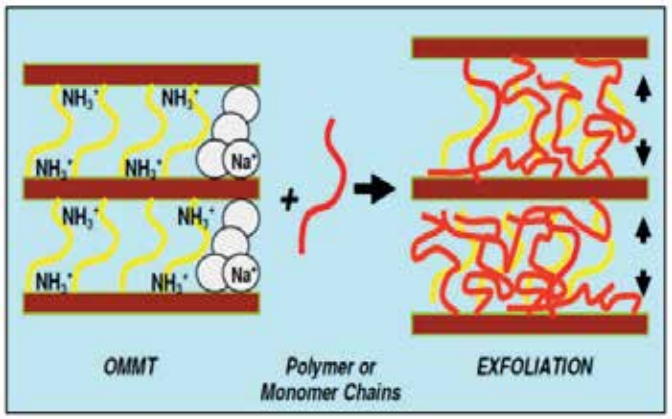

Fig. 4.c. Microstructural Development during Melt Intercalation Process

Mixtures of clay platelets and polymer chains compose a colloidal system. Thus in the melt state, the propensity for the clay to be stably dispersed at the level of individual disks (an exfoliated clay dispersion) is dictated by clay, polymer, stabilizer, and compatibilizer potential interactions and the entropic effects of orientational disorder and confinement. An isometric dimension of clay platelets also has implications for stability because liquid crystalline phases may form. In addition, the very high melt viscosity of polypropylene and the colloidal size of clay imply slow particulate dynamics, thus equilibrium structures may be attained only very gradually. Agglomerated and networked clay structures may also lead to nonequilibrium behavior such as trapped states, aging, and glassy dynamics.

Clay structure in polymer nanocomposites can be characterized as a combination of exfoliated platelets and intercalated tactoids. Clays themselves are layered silicate minerals with charged surfaces neutralized by interlayer counterions. Unless a liquid crystalline order disorder transition occurs, the exfoliated structure is spatially and orientationally disordered and the clay is dispersed at the level of individual disks. Intercalated clay retains interlayer ordering, at least within a particular tactoid; however, intergallery spacing is increased relative to natural clay because stabilizing surfactants, compatibilizers, and/ or matrix polymers are infiltrated within the clay galleries. In the extreme case of clay/polymer matrix immiscibility, intercalation spacing not much greater than the clay and its counterion indicates negligible penetration of polymeric or compatibilizing species between clay layers. Clay platelets or tactoids themselves comprise the mesoscale structure of nanocomposites. Possible structures include that of a dispersed suspension, a percolated network, or a liquid crystal with orientational order. The hierarchy of possible states is depicted in **Figure 5**.

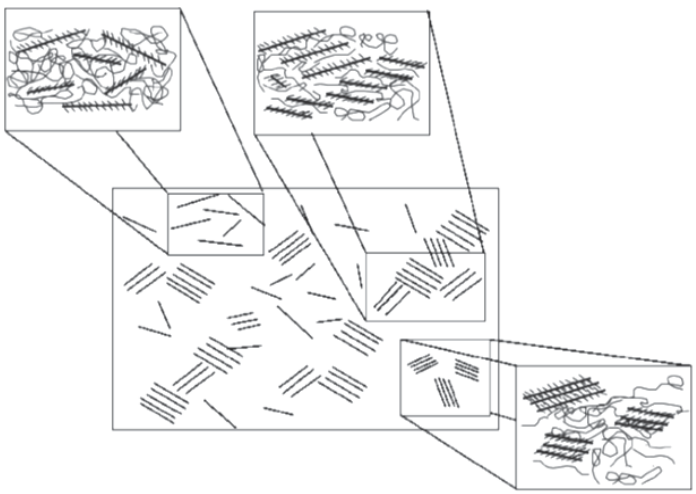

Fig. 5. Schematic of the hierarchy of clay structures in polypropylene nanocomposites of mixed morphology. Clay tactoids and exfoliated platelets comprise the mesoscale morphology. The internal intercalation structure of clay tactoids is determined by the compatibilizer and compounding conditions. (View this art in color at www.dekker.co

Polypropylene (PP) is widely used for many applications due to its low cost, low density, high thermal stability and resistance to corrosion. Blending polypropylene with clays to form nanocomposites is a way to increase its utility by improving its mechanical properties.

Layered silicates dispersed as a reinforcing phase in polymer matrix are one of the most important forms of hybrid organic-inorganic nanocomposites. MMT, hectorite, and saponite are the most commonly used layered silicates. Layered silicates have two types of structure: tetrahedral-substituted and octahedral substituted figure 6. In the case of tetrahedrally substituted layered silicates the negative charge is located on the surface of silicate layers, and hence, the polymer matrices can react interact more readily with these than with octahedrally-substituted material.

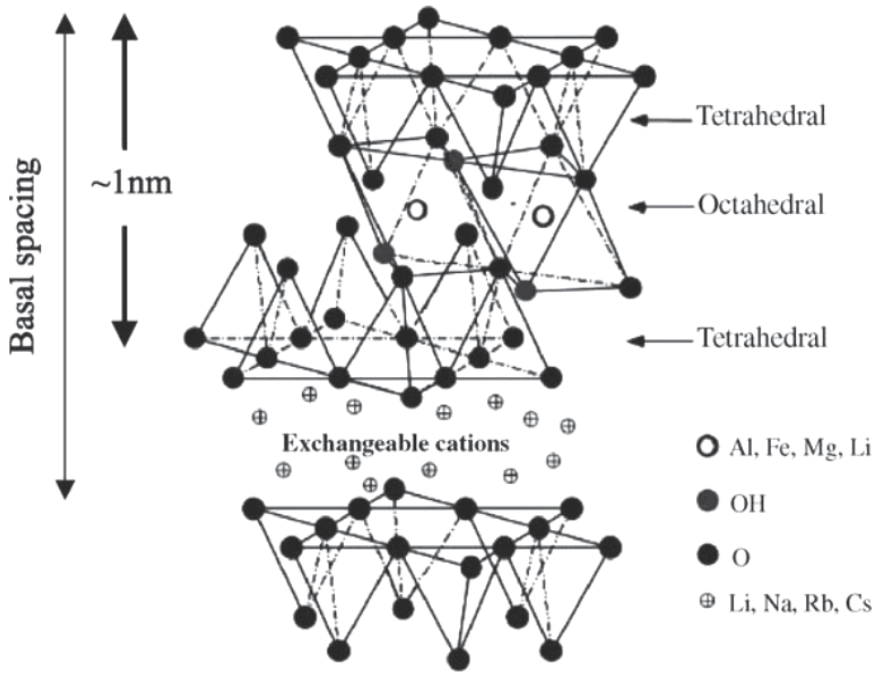

Fig. 6. Structure of Layered Silicates

Compared to conventional composites, polymer layered-silicate (PLS) nanocomposites have maximized polymer-clay interactions since the clay is dispersed on a nanometer scale.

There are three general methods for the preparation of polymer/ silica nanocomposites according to the starting materials and processing techniques: blending, sol-gel processes, and in situ polymerization.

Blending is generally just mixing of the silica nanoparticles into the polymer; *sol-gel process* can be done in situ in the presence of a preformed organic polymer or simultaneously during the polymerization of the monomer(s); and *in situ polymerization* involves the dispersion of nanosilica in the monomer(s) first and then polymerization is carried out.

Layered silicate/polypropylene nanocomposites were prepared by melt intercalation method. Homopolymers PP alone and maleic anhydride-grafted polypropylene (PPgMA) as a compatibilizer were used as the matrix. Clay (Na^+ montmorillonite, MMT) particles were used to obtain silicate nano-layers within the PP matrix. Structural modification of MMT

using hexadecyltrimethyl ammonium chloride (HTAC) was applied to obtain organophilic silicates (OMMT) (Kıvanç, 2006).The most recent methods to prepare polymer-layered-silicate nanocomposites have primarily been developed by several other groups. In general these methods (shown in **Figure 7**) achieve molecular level incorporation of the layered silicate (e.g. montmorillonite clay or synthetic layered silicate) in the polymer by addition of a modified silicate either to a polymerization reaction (in situ method), (Usuki et al.,1993,1997; Lan & Pinnavaia,1994) to a solvent-swollen polymer (solution blending), Jeon et al., 1998) or to a polymer melt (melt blending) (Giannelis,1996; Fisher et al.,1998). Additionally, a method has been developed to prepare the layered silicate by polymerizing silicate precursors in the presence of a polymer (Carrado & Langui, 1999)

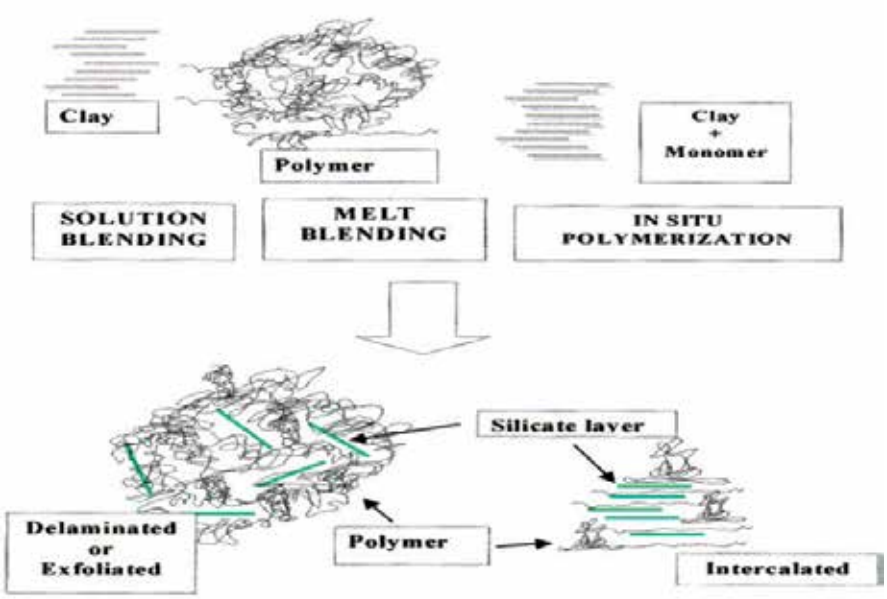

Fig. 7. Schematic representation of various methods (Solution blending, melt blending, and in situ polymerization). The delaminated (or exfoliated) and intercalated morphologies are shown.

Two terms (intercalated and delaminated) are used to describe the two general classes of nanomorphology that can be prepared. *Intercalated structures* are self assembled, well-ordered multilayered structures where the extended polymer chains are inserted into the gallery space between parallel individual silicate layers separated by 2-3 nm (see **Figure 8**). *The delaminated (or exfoliated)* structures result when the individual silicate layers are no longer close enough to interact with the adjacent layers' gallery cations (Lan & Pinnavaia, 1994). In the delaminated cases the interlayer spacing can be on the order of the radius of gyration of the polymer; therefore, the silicate layers may be considered to be well-dispersed in the organic polymer. The silicate layers in a delaminated structure may not be as well-ordered as in an intercalated structure. Both of these hybrid structures can also coexist in the polymer matrix; this mixed nanomorphology is very common for composites based on smectite silicates and clay minerals (Kroschurtz, 1993).

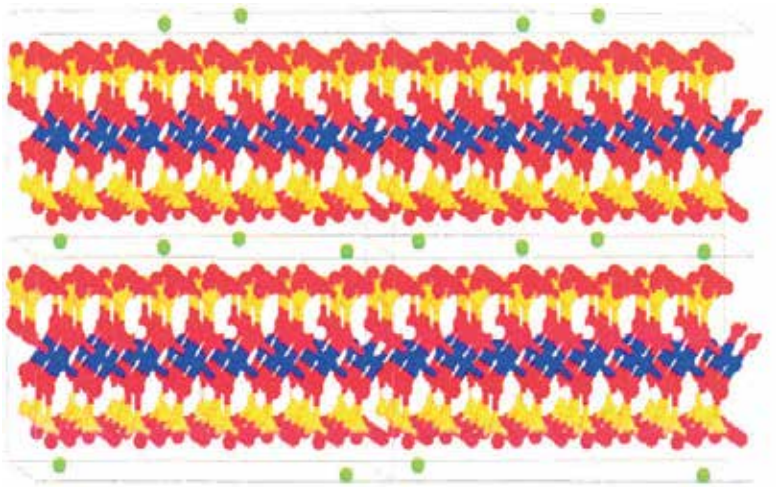

Fig. 8. Molecular representation of sodium montmorillonite, showing two aluminosilicate layers with the Na+ cations in the interlayer gap or gallery. The octahedral (O_h) alumina layer is shown as blue aluminum atoms surrounded by red oxygen atoms. The tetrahedral (Td) silicate layers are shown as yellow silicon atoms surrounded by red oxygen atoms. Hydrogen atoms are white and sodium (Na^+) cations are shown in green.

The very large commercial importance of polypropylene (PP) has also been driving an intense investigation of PP composites reinforced by particulates, fibers, and layered inorganic fillers (Karger, 1995;Karian,1999) .In particular, in the case of layered inorganic fillers, talc and mica had been traditionally attracting the most interest (Karian,1999). However, recent advances in polymer/clay and polymer/silicate nanocomposite material (Alexandre & Dubois, 2000; Giannelis et al., 1998) have inspired efforts to disperse montmorillonite-based fillers in PP. (Kato et al., 1997; Kawasumi et al., 1997; Hasegawa et al., 1998; Oya et al., 2000; Wolfet al., 1999; Reichert et al., 2000; Manias et al., 2000).

Although it has been long known that polymers can be mixed with appropriately modified clay minerals and synthetic clays, (Theng, 1979, 1974) the field of polymer/silicate nanocomposites has gained large momentum recently. Two were the major findings that pioneered the revival of these materials: First, the report of a nylon-6/montmorillonite material from Toyota research, (Kojima et al., 1993; Kojima et al.,1993) where very moderate inorganic loadings resulted in concurrent and remarkable enhancements of thermal and mechanical properties. Second, Giannelis et al. found that it is possible to melt-mix polymers with clays without the use of organic solvents (Vaia et al., 1993) .Since then, the high promise for industrial applications has motivated vigorous research, which revealed concurrent dramatic enhancements of many materials properties by the nanodispersion of inorganic silicate layers. Where the property enhancements originate from the nanocomposite structure, these improvements are generally applicable across a wide range of polymers (Alexandre & Dubois, 2000) .At the same time, there were also discovered

property improvements in these nanoscale materials that could not be realized by conventional fillers, as for example a general flame retardant characteristic (Gilman et al., 2000) and a dramatic improvement in barrier properties (Strawhecker & Manias ,2000; Xu et al.,2001).

Montmorillonite (mmt) is a naturally occurring 2:1 phyllosilicate, which has the same layered and crystalline structure as talc and mica but a different layer charge (Theng, 1979, 1974). The mmt crystal lattice consists of 1-nmthin layers, with a central octahedral sheet of alumina fused between two external silica tetrahedral sheets (in such a way that the oxygens from the octahedral sheet also belong to the silica tetrahedra). Isomorphic substitution within the layers (for example, Al^{3+} replaced by Mg^{2+} or Fe^{2+}) generates a negative charges defined through the charge exchange capacity (CEC)sand for mmt is typically 0.9-1.2 mequiv /g depending on the mineral origin. These layers organize themselves in a parallel fashion to form stacks with a regular van der Waals gap between them, called interlayer or gallery. In their pristine form their excess negative charge is balanced by cations (Na^{+}, Li^{+}, Ca^{2+}) which exist hydrated in the interlayer. Obviously, in this pristine state mmt is only miscible with hydrophilic polymers, such as poly (ethylene oxide) and poly(vinyl alcohol) (Strawhecker & Manias ,2000; Vaia et al.,1995). To render mmt miscible with other polymers, one must exchange the alkali counterions with cationic-organic surfactants, such as alkylammoniums (Alexandre & Dubois, 2000; Giannelis et al., 1998).

11. Production of layered silicate/polypropylene nanocomposites

The production of polypropylene nanocomposites is shown in Figure 9.The homopolymer PP was fed into Haake two-roll mixer at 190 o C. After melting of the PP in 1 min, clay particles in the amounts of 3, 5 and 10 wt. % were added into molten PP and the mixing was continued for 10 min in the mixer. The blended samples were collected and left for cooling. After cooling, the blends were pressed into 100 mm x 100 mm samples having a

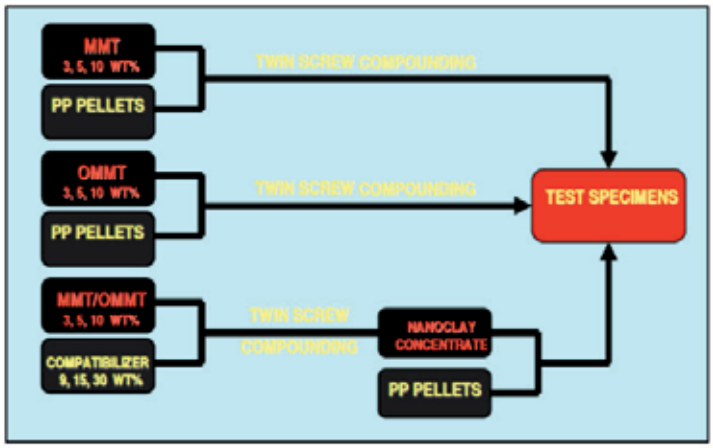

Fig. 9. Processing Stages for Clay/PP Nanocomposites

thickness of 1 mm using a hot press at 190°C. The tensile specimens were prepared by a pneumatic cutter and then the samples were left for two days to complete crystallization. **Kıvanç I_IK 2006**

12. Techniques used for the characterization of polypropylene/ nanocomposites

Generally, the structure of nanocomposites has typically been established using WAXD analysis and transmission electron micrographic (TEM) observation. Due to its easiness and availability WAXD is most commonly used to probe the nanocomposite structure (Giannelis, 1996; Giannelis et al., 1999; LeBaron et al.,1999; Vaia et al., 1999; Biswas & Sinha, 2001) and occasionally to study the kinetics of the polymer melt intercalation (Vaia et al.,1996) . By monitoring the position, shape, and intensity of the basal reflections from the distributed silicate layers, the nanocomposite structure (intercalated or exfoliated) may be identified. For example, in *an exfoliated nanocomposite*, the extensive layer separation associated with the delamination of the original silicate layers in the polymer matrix results in the eventual disappearance of any coherent X-ray diffraction from the distributed silicate layers. On the other hand, *for intercalated nanocomposites*, the finite layer expansion associated with the polymer intercalation results in the appearance of a new basal reflection corresponding to the larger gallery height. Although WAXD offers a convenient method to determine the interlayer spacing of the silicate layers in the original layered silicates and in the intercalated nanocomposites (within 1–4 nm), little can be said about the spatial distribution of the silicate layers or any structural non-homogeneities in nanocomposites.

Additionally, some layered silicates initially do not exhibit well-defined basal reflections. Thus, peak broadening and intensity decreases are very difficult to study systematically. Therefore, conclusions concerning the mechanism of nanocomposites formation and their structure based solely on WAXD patterns are only tentative. On the other hand, TEM allows a qualitative understanding of the internal structure, spatial distribution of the various phases, and views of the defect structure through direct visualization.

However, special care must be exercised to guarantee a representative cross-section of the sample. The WAXD patterns and corresponding TEM images of three different types of nanocomposites are presented in **Figure 10**. Both TEM and WAXD are essential tools (Morgan & Gilman, 2003) for evaluating nanocomposite structure. However, TEM is time-intensive, and only gives qualitative information on the sample as a whole, while low-angle peaks in WAXD allow quantification of changes in layer spacing. Typically, when layer spacing exceed 6–7 nm in intercalated nanocomposites or when the layers become relatively disordered in exfoliated nanocomposites, associated WAXD features weaken to the point of not being useful. However, recent simultaneous small angle X-ray scattering (SAXS) and WAXD studies yielded quantitative characterization of nanostructure and crystallite structure in N6 based nanocomposites (Mathias et al., 1999).

Very recently, (Bafna et al., 2003) developed a technique to determine the three-dimensional (3D) orientation of various hierarchical organic and inorganic structures in a PLS nanocomposite. They studied the effect of compatibilizer concentration on the orientation of various structures in PLS nanocomposites using 2D SAXS and 2D WAXD in three sample /camera orientations.

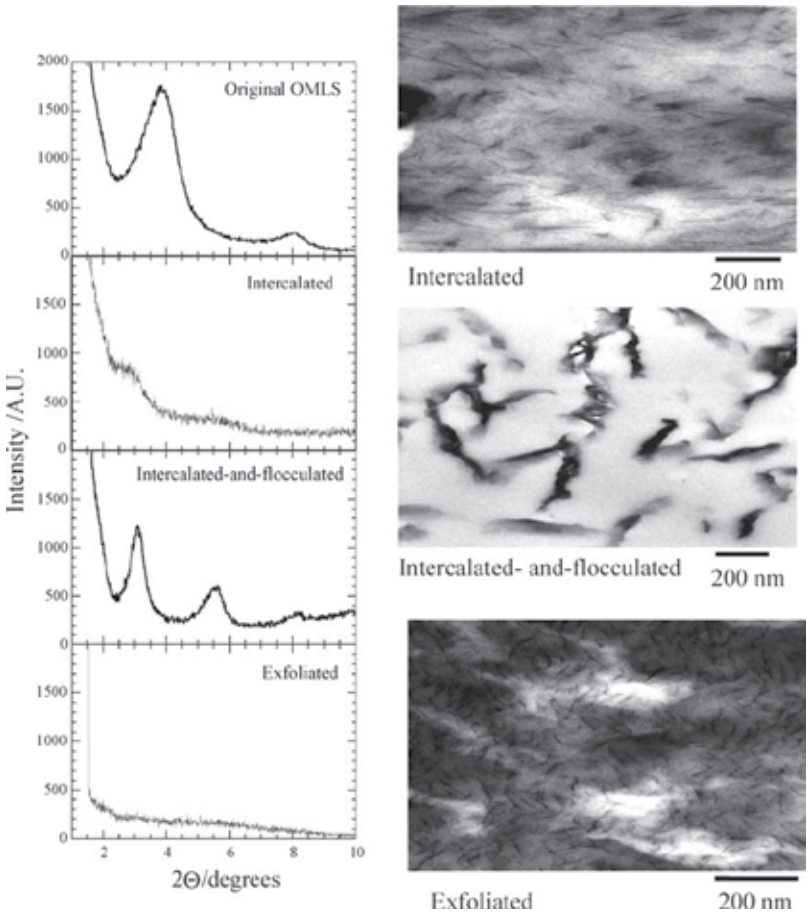

Fig. 10. (a) WAXD patterns and (b) TEM images of three different types of nanocomposites

13. The development and characterization of polypropylene-clay nanocomposites

The development and characterization of polymer-clay nanocomposites has been a subject of raising interest in the recent years (Vaia et al., 1996) . Polymer-layered silicate (PLS) nanocomposites exhibit outstanding properties that are synergistically derived from the organic and inorganic components. The enhanced properties are presumably due to the synergistic effects of nanoscale fillers within the polymer (Kojima et al., 1993). The delamination and dispersion of clays in the polymeric matrix is the key to design nanocomposites. In the ideal conditions, the delamination of the original clay structures, as well as the polymer intercalation in the clay can be achieved. Nanoparticles can significantly improve the stiffness, heat distortion temperature (HDT), dimensional stability, gas barrier properties, electrical conductivity and flame retardancy of polymer with only a 0.1–10 vol.% addition of dispersed nanophase (Wu et al., 2002; Tyan et al.,1999; Lan et al., 1996; Li et al., 2004; Ma et al.,2001; Li et al.,2001; Kawasumi et al.,1997; Usuki et al.,1997; Hasegawa et al., 2000). These performance improvements largely depend upon the spatial distribution,

arrangement of intercalating polymer chains and interfacial interaction between the silicate layers and the polymer (Giannelies, 1996; Giannelies et al., 1999; LeBaron et al., 1999; Ray & Okamoto, 2003). Nanoclays like purified Na^{+} or Ca^{+2} montmorillonites are inherently hydrophilic in nature, which leads to incompatibility with the hydrophobic polymer matrix with subsequent poor composite properties. Although, the modified clay is miscible with polar polymer like PS, Epoxy, Nylon etc., its dispersion within PE, PP, EVA, ABS etc is unsatisfactory (Komori & Kurada,2000; Cho & Paul, 2001). Grafting of polar functional groups onto polymer chains has been suggested to improve the properties in PE/clay nanocomposites (Fukushima & Inagaki, 1987).

Therefore, to obtain a nanocomposite with requisite properties, the inorganic clay must be modified with some organic surfactant, usually onium salt or an alkyl amine which, compatibilizes the surface chemistry of the clay and polymer matrix at the interface by replacing the inorganic cation and making the gallery space of the clay sufficiently organophilic to permit the entry of polymer matrix (Fukushima & Inagaki, 1987). PP nanocomposites have been the subject of research since several years (Boeing, 1997; Kurokawa et al., 1997; Kato et al., 1997; Reichert et al.,2000; Hasegawa et al.,1998; Zheng et al.,2001). Various organically modified nanoparticles have been prepared and incorporated within the PP matrix to enhance mechanical and thermal performance. However, the development of PP clay nanocomposites posses special challenges because of polypropylene's hydrophobicity. The dispersion of nanolayers strongly depends on the preparation techniques such as in-situ polymerization, solution blending or melt compounding (Okada et al., 1993; Akelah, 1995; Akelah et al., 1994; Giannelis, 1998; Zilg et al., 1998). Melt intercalation of inorganic clay mineral consisting of layered silicates with polymers is widely used, as it is environmental friendly and does not involve any solvent. Direct melt intercalation method offers convenient techniques for preparation of hybrids, which involve mixing the layered silicates with the polymer matrix above its softening point Rzaev et al., 2007). However, desired intercalation/ exfoliation of the clay galleries within PP based nanocomposites system posses host of technical issues which needs to explored and addressed.

14. Future of nanocomposites

By 2009, it is estimated that the flexible and rigid packaging industry will use five millionpounds of nanocomposites materials in the beverage and food industry. By 2011, consumption is estimated to be 100 million pounds. Beer is expected to be the biggest consumer by 2006 with 3 million pounds of nanocomposites until carbonated soft drinks bottles are projected to surpass that to use 50 million pounds of nanocomposites by 2011(Butschli,2004). Polymer nanocomposites are the future for the global packaging industry. Once production and materials cost are less, companies will be using this technology to increase their product's stability and survivability through the supply chain to deliver higher quality to their customers while saving money. The advantages that nanocomposites offer far outweigh the costs and concerns and with time the technology will be further refined and processes more developed. Research continues into other types of nanofillers (i.e., carbon nanotubes), allowing new nanocomposite structures with different improved properties that will further advance nanocomposite use in many diverse packaging applications.

15. Conclusion

The synthesis of polymer nanocomposites is an integral aspect of polymer nanotechnology. By inserting the nanometric inorganic compounds, the properties of polymers improve and hence this has a lot of applications depending upon the inorganic material present in the polymers. The improvements obtained in clay/PP nanocomposite structure can make this commercial thermoplastic polymer more suitable for automotive, construction and packaging applications. Different alkyl ammonium surfactants and compatibilizer was used to produce layered silicate/PP nanocomposites by the same melt intercalation technique.

Polypropylene nanocomposites are still challenging due to the lack of affinity of organophilic PP for hydrophilic clay. The reinforcement of polypropylene and other thermoplastics with inorganic particles such as talc and glass is a common method of material property enhancement. Polymer clay nanocomposites extend this strategy to the nanoscale. The anisometric shape and approximately 1 nm width of the clay platelets dramatically increase the amount of interfacial contact between the clay and the polymer matrix. Thus the clay surface can mediate changes in matrix polymer conformation, crystal structure, and crystal morphology through interfacial mechanisms that are absent in classical polymer composite materials. For these reasons, it is believed that nanocomposite materials with the clay platelets dispersed as isolated, exfoliated platelets are optimal for end-use properties. Yet, relative to other thermoplastic nanocomposites, such as nylon 6, the improvement in end-use properties for polypropylene nanocomposites has been modest. Thus research in the areas of synthesis and, especially, compounding, which are aimed at closing this performance gap, is necessary. Alternatively, improved fundamental understanding of the detailed interactions and chemistry between clays, amine surfactants, and maleic anhydride compatibilizers can help elucidate the complex thermodynamics of clay dispersion. In addition, noting that many synthesized PP nanocomposites are likely to exist as nonequilibrium structures, research into the aging and rejuvenation of these mesoscale structures is warranted. Furthermore, better methods to characterize the full distribution and hierarchy of structural states present in PP nanocomposites are required because, for example, rare aggregates can seriously compromise nonlinear mechanical properties such as toughness, yield stress, and elongation at break. Finally, the interaction between clay platelets and polymer crystallization requires further attention because these interactions are likely a significant determinant of the end-use properties of polypropylene nanocomposites.

16. References

Akelah, A. In: Prasad, P. E., Mark, N.J. and Fai, T.J. (1995). (eds), Polymers and Other Advanced Materials, pp. 625, *Plenum Press*, New York.

Akelah, A., Salahuddin, N., Hiltner, A., Baer, E. and Moet, A. (1994). Nanostruct. Mater., 4: 965.

Alexandre, M.; Dubois, P.(2000). *Mater. Sci., Eng. R: Reports* , 28, 1.

Anyadike.(2005). Nanotechnology in packaging. Retrieved on February 13, from Pira International at *http://pira.atalink.co.uk.packaging/130.html*

Bafna A, Beaucage G, Mirabella F, Mehta S.(2003). 3D hierarchical orientation in polymer–clay nanocomposite films. *Polymer* ;44:1103–15.

Balazs, A. C.; Emrick, T.; Russell, T. P.(2006). *Science,* 314, 1107.

Bccresearch.(2010).*wordpress.com/tag/nanotechnology* August 9.

Biswas M, Sinha Ray S. (2001).Recent progress in synthesis and evaluation of polymer–montmorillonite nanocomposites. *Adv Polym Sci .*;155:167–221.

Boeing, H.V.;(1997).Polyolefins, *Elsevier Reinhold*, New York.

Brody. (2003, December). "Nano, Nano" Food Packaging Technology. *Food Technology*, 52-54.

Buchholz, K. (2003).Nanocomposite debuts on GM vehicles. Automotive Engineering International Online. Accessed April 30. *URL: http://www.sae.org/automag/material/10-2001/index.htm*

Butschli. (2004, october). Nanotechnology in packaging. Retrieved on February 13, 2005 from Packaging World at *http://www.packworld.com/cds_print.html?rec_id=17883*

Carrado, K. A.; Langui, X.(1999). *Microporous Mesoporous Mater.,* 27, 87.

Carter L., Hendricks J.G., Bolley D.S., (1950).US 2,531,396; *[assigned to National Lead Co.].*

Caseri, W. Nalwa, H. S.,(2004) .(In Encyclopedia of Nanoscience and Nanotechnology; Ed.; *American Scientific Publishers: Stevenson Ranch*, CA ; Vol 6, pp 235-247. (b) Caseri, W. R. ,Kickelbick, G., (2006).*Mater. Sci. Technol*., 22, 807. (c) Caseri, W.(2007). In Hybrid Materials. Synthesis, Characterization, and Applications; Ed.; *Wiley-VCH: Weinheim*, Germany ; Chapter 2.

Chen, B. (2004). Polymer-Clay nanocomposites: an overview with emphasis on interaction mechanisms. *British Ceramic Transactions:* Vol. 103, No. 6, pg 241.

Cho, J.W. and Paul, D.R.;(2001). Nylon 6 Nanocomposites by Melt Compounding, *Polymer*, 42(3): 1083–1094.

Fisher, H.; Gielgens. L.; Koster, T. (1998).Nanocomposites from Polymers and Layered Minerals; *TNO-TPD Report* .

Fornes T.D., Yoon P.J., Hunter D.L., Keskkula H., Paul D.R.,(2002). *Polymer* , Vol.43, 5915–93.

Frontini , P. M. ; Pouzada, A. S. ; (2011). *eXPRESS Polymer Letters* Vol.5, No.8 , 661

Fukushima, Y. and Inagaki, S.; (1987). Synthesis of an Intercalated Compound of Montmorillonite and 6-polyamide, *J. Inclusion Phenom.,* 5(4): 473–482.

Giannelies, E.P. (1996). Polymer Layered Silicate Nanocomposites, *Adv. Mater*., 8(1): 29–35.

Giannelies, E.P., Krishnamoorti, R. and Manias, E. (1999). Polymer-Silicate Nanocomposites: Model Systems for Confined Polymers and Polymer Brushes, *Adv. Polym. Sci*., 138: 107–147.

Giannelis EP. (1996).Polymer layered silicate nanocomposites. *Adv Mater* ;8:29–35.

Giannelis, E. P. (1998). Krishnamoorti, R. K.; Manias, E. Adv. *Polym. Sci.,* 138, 107-148.

Giannelis, E.P. (1998). *Appl. Organomet. Chem*., 3(5): 490.

Gilman, J.W.; Jackson, C.L.; Morgan, A.B.; Harris, R.; Manias, E.; Giannelis, E.P.; Wuthenow, M.; Hilton, D.; Phillips, S.H.(2000). Flammability properties of polymer–Layered-silicate nanocomposites. Polypropylene and polystyrene nanocomposites. *Chem. Mater.,* 12 (7), 1866–1873.

Hajji, P.; David, L.; Gerard, J. F.; Pascault, J. P.; Vigier, G.(1999*). J. Polym. Sci., Part B: Polym. Phys*., 37, 3172.

Hasegawa, N., Kawasumi, M., Kato, M., Usuki, A. and Okada, A. (1998). Preparation and Mechanical Properties of Polypropylene-Clay Hybrids using a Maleic Anhydride-Modified Polypropylene Oligomer, *J. Appl. Polym. Sci*., 67(1): 87–92.

Hasegawa, N., Okamoto, H., Kato, A. and Uauki, M. (2000). Preparation and Mechanical Properties of Polypropylene-clay Hybrids Based on Modified Polypropylene and Organophilic Clay, *J. Appl. Polym. Sci.,* 78(11): 1918–1922.

Hay, J. N. & Shaw, S. J. (2000). Nanocomposites – Properties and Applications. Abstracted from "A Review of Nanocomposites 2000". Retrieved on February 13, 2005 from Azom.com at *http://www.azom.com/details.asp?ArticleID=921*

Hijleh, M., Ramadin, Y. and Zihlif, A. (2000). *Inter. J. Polym. Mater.,* 40: 377–394. *http://specialchem4polymers.com/resources/latest/displaynews.aspx?id=1965*

Jeon, H. G.; Jung, H. T.; Lee, S. D.; Hudson, S.(1998). *Polymer Bulletin* , 41, 107.

Karger-Kocsis, J., (1995).Ed. Polypropylene: Structure, Blends and Composites, vol. 3; *Chapman and Hall*: London.

Karian, H. G., (1999).Ed. Handbook of Polypropylene and Polypropylene Composites; *Marcel Dekker*: New York,.

Kato, M., Usuki, A. and Okada, A. (1997). Synthesis of Polypropylene Oligomer – Clay Intercalation Compounds, *J. Appl. Polym. Sci.,* 66(9): 1781–1785.

Kawasumi, M., Hasegawa, N., Kato, M., Usuki, A. and Okada, A. (1997). Preparation and Mechanical Properties of Polypropylene-Clay Hybrids, *Macromol.,* 30(20): 6333–6338.

Kickelbick, G. (2007).In Hybrid Materials. Synthesis, Characterization, and Applications; Ed.; *Wiley-VCH: Weinheim*, Germany ; Chapter 1.

Kıvanç IŞIK(2006).'' Layered Silicate / Polypropylene Nanocomposites'' July,*Izmir,* Turkey

Kojima Y., Usuki A., Kawasumi M., Okada A., Kurauchi T., Kamigaito O.,(1993). "Synthesis of nylon 6-clay hybrid by montmorillonite intercalated with 3- caprolactam", *Journal of Polymer Science.*: Part A, Vol.31, p. 983.

Kojima, Y.; Usuki, A.; Kawasumi, M.; Okada, A.; Fukushima, Y.; Kurauchi, T.; Kamigaito, O. (1993).Mechanical properties of nylon 6–clay hybrid. *J. Mater. Res.,* 8 (5), 1185–1189.

Kojima, Y.; Usuki, A.; Kawasumi, M.; Okada, A.; Fukushima, Y.; Kurauchi, T. T.; Kamigaito. O. (1993). *J. Mater. Res.*, 8, 1179- 1185.

Komori, Y. and Kurada, K.;(2000). Layered silicate – Polymer Intercalation Compounds, In: Pinnavaia, T.J. and Beal, G.W. (eds), Polymer Layered Silicate Nanocomposites, *Wiley,* New York.

Kroschurtz, J. S., (1993). Ed.; For definitions and background on layered silicate and clay minerals, see: Kirk-Othmer *Encyclopedia of Chemical Technology*, 4th ed.; John Wiley and Sons: New York ; Vol. 6.

Kurokawa, Y., Yusuda, H. and Oya, A. (1997). *J. Matter. Sci. Lett.*, 1670.

Lan, T., Kaviratna, P.D. and Pinnavaia, T.J. (1996). Epoxy Self-Polymerization in Smectite Clays, *J. Phys. Chem. Solids,* 57(6–8): 1005–1010.

Lan, T.; Pinnavaia, T.(1994). *J. Chem. Mater.,* 6, 2216.

Le Pluart L., Duchet J., Sauterau H., Ge´rard J.F.,(2002). *Journal of Adhesives* ,Vol.78, pp.645–662.

Leaversuch, R.(2003). Nanocomposites Broaden Roles in Automotive, Barrier Packaging. Plastics Technology Online. Accessed April 30. *URL: http://www.plasticstechnology.com/articles/200110fa3.html*

LeBaron, P.C., Wang, Z. and Pinnavaia, T.J. (1999). Polymer-Layered Silicate Nanocomposites: An Overview, *Appl. Clay Sci.,* 15(1–2): 11–29.

Li, J., Chixing, Z., Wang, G., Yu, W., Tao, Y. and Liu, Q. (2004). Preparation and Linern Rheological behaviour of Polypropylene/MMT Nanocomposites, *Polymer Composites*, 24(3): 323–331.

Li, X.C., Kang, T., Cho, W.J., Lee, J.K. and Ha, Z.C.S. (2001). Brill Transition in Nylon 10 12 Investigated by Variable Temperature XRD and Real Time FT-IR, *Macromol. Rapid Commun.,* 21(15): 1040–1043.

Ma J.S., Qi Z.N., Hu Y.L.,(2001). "Synthesis and characterization of polypropylene/clay nanocomposites", *Journal of Applied Polymer Science*, Vol. 82, p.3611.

Ma, J., Zhang, S. and Qi, Z.N. (2001). Synthesis and Characterization of Elastomeric Polyurethane/Clay Nanocomposites, *J. Appl. Polym. Sci.,* 82(6): 1444–1448.

Mahanwar, P., Bose, S. and Raghu, H. (2006). *J. Thermoplast. Comp. Mater*., 19: 491–506.

Manias E., Touny A., Wu L., Strawhecker K., Lu B., Chung T.C.,(2001). "Polypropylene/montmorillonite nanocomposites. Review of the synthetic routes and materials properties", *Chemical Materials*,Vol.10,p. 3516.

Manias, E.; Touny, A.; Wu, L.; Lu, B.; Strawhecker, K.; Gilman, J. W.; Chung, T. C. (2000).*Polym. Mater. Sci., Eng*., 82, 282.

Marchant D., Krishnamurthy J.(2002). *Industrial Engineering Chemical Resources*, Vol.41, pp. 6402–6408.

Mathias LJ, Davis RD, Jarrett WL.(1999). Observation of a- and g-crystal forms and amorphous regions of nylon 6-clay nanocomposites using solid-state 15N nuclear magnetic resonance. *Macromolecules*;32:7958–60.

Moore D.M., Reynolds R.C.,(1997). X-Ray diffraction and the identification and analysis of clay minerals. *Oxford: Oxford University Press.*

Morgan AB, Gilman JW.(2003). Characterization of poly-layered silicate (clay) nanocomposites by transmission electron microscopy and X-ray diffraction: a comparative study. *J Appl Polym Sci .*;87:1329–38.

Okada, A., Kojima, Y., Kawasumi, M., Fukushima, Y., Kurauchi, T. and Kamigaito, O.(1993). *J. Mater. Res.,* 8: 1179.

Oya, A.; Kurokawa, Y.; Yasuda, H. J. Mater. Sci. 2000, 35, 1045- 1050.

Pinnavaia T.J., (Ed.),2000. Polymer–Clay Nanocomposite, *Wiley, London*, p. 151.

Principia Partners. (2004, December). Polymer Nanocomposites Create Exciting Opportunities in the Plastics Industry: Updated Study from Principia. Retrieved on February 13, (2005) from Special Chem at *http://specialchem4polymers.com/resources/latest/displaynews.aspx?id=1965*

Ray, S.S. and Okamoto, M. (2003). Polymer/Layered Silicate Nanocomposites: A Review from Preparation to Processing, *Prog. Polym. Sci.,* 28(11): 1539–1641.

Reichert, P., Nitz, H., Klinke, S., Brandsch, R., Thomann, T. and Mulhaupt, R. (2000). Poly(propylene)/Organoclay Nanocomposite Formation: Influence of Compatibilizer Functionality and Organoclay Modification, *Macromol. Mater. Eng.,* 275(2): 8–17.

Ryan. (2003), January/February). Nanocomposites. *Polymer News*, Issue 8.

Rzaev, Z.M.O., Yilmazbayhan, A. and Alper, E. (2007). A one-step Preparation of Compatibilized Polypropylene-Nanocomposites by Reactive Extrusion Processing, *Adv. Polym. Tech.,* 26(1): 41–55.

Schadler, L. S.(2003). Nanocomposite Science and Technology; *Wiley- VCH: Weinheim*, Germany, Chapter 2. (b) Schadler, L. S.; Kumar, S. K.; Benicewicz, B. C.; Lewis, S. L.; Harton, S. E. (2007).*MRS Bull*., 32, 335. (c) Schadler, L. S.; Brinson, L. C.; Sawyer, W. G.(2007). *JOM* , 59, 53.

Schaefer, D. W.; Justice, R. S.(2007). *Macromolecules* , 40, 8501.
Sherman, L.M. Nanocomposites: (1999). A little goes a long way. *Plast. Technol*., 45 (6), 52–57.
Sherman, Lilli Manolis. (1999, June). Nanocomposites—A Little Goes a Long Way. Retrieved February 22, (2005) *from www.plasticstechnology.com/articles/articl_print1.cfm*
Strawhecker, K.; Manias, E.(2000). *Chem. Mater.*, 12, 2943-2949.
The Future of Automotive Plastics. (2003). *PR Newswire*. Accessed April 30.
Theng, B. K. G.(1974). Chemistry of clay-organic reactions; *Wiley: New York*.
Theng, B. K. G.(1979). Formation and properties of clay-polymer complexes; *Elsevier: Amsterdam*.
Tripathi, A. and Pillia, P. (1994). *J. Mater. Sci.: in Electronics*, 1: 143–147.
Tyan, H.L., Liu, Y.C. and Wei, K.H. (1999). Enhancement of Imidization of Poly(Amic Acid) through Forming Poly(Amic Acid)/Organoclay Nanocomposites, *Polymer*, 40(17): 4877–4876. URL: http://www.scprod.com/gm.html
Usuki, A., Kato, M., Okada, A. and Kurauchi, T. (1997). Synthesis of Polypropylene-Clay Hybrid, *J. Appl. Polym. Sci.,* 63(1): 137–138.
Usuki, A.; Kawasumi, M.; Kojima, Y.; Okada, A.; Kurauchi, T.; Kamigaito, O. (1993). Swelling behavior of montmorillonite cation exchanged for o-amino acids by e-caprolactam. *J. Mater. Sci.,* 8 (5), 1174– 1178.
Usuki, A.; Kojima, Y.; Kawasumi, M.; Okada, A.; Fukushima, Y.; Kurauchi, T.; Kamigaito, O.(1993). Synthesis of nylon 6–clay hybrid. *J. Mater. Res.* , 8 (5), 1179–1184.
Vaia RA, Jant KD, Kramer EJ, Giannelis EP.(1996). Microstructural evaluation of melt-intercalated polymer-organically modified layered silicate nanocomposites. *Chem Mater*.; 8: 2628–35.
Vaia RA, Price G, Ruth PN, Nguyen HT, Lichtenhan J.(1999). Polymer/layered silicate nanocomposites as high performance ablative materials. *Appl Clay Sci* .,15:67–92.
Vaia, R. A; Ishii, H.; Giannelis, E. P. (1993).*Chem. Mater.,* 5,1694-1696.
Vaia, R. A; Vasudevan, S.; Krawiec, W.; Scanlon, L. G.; Giannelis, E. P.(1995). *Adv. Mater.*, 7, 154.
Winey, K. I.; Vaia, R. A. (2007). *MRS Bull.* , 32, 314. (b) Krishnamoorti, R.; Vaia, R. A.(2007). *J. Polym. Sci.,* Part B: Polym. Phys., 45, 3252.
Wolf, D.; Fuchs, A.; Wagenknecht, U.; Kretzschmar, B.; Jehnichen, D.; Ha¨ ussler, L. (1999). *Proceedings of the Eurofiller 99*, Lyon- Villeurbanne; pp 6-9.
Wu, Z., Zhou, C. and Zhu, N. (2002). The Nucleating Effect of Montmorillonite on Crystallization of Nylon 1212/Montmorillonite Nanocomposite, Polym. Test., (4): 479–483.
Wu, Z.G., Zhou, C.X., Qi, R.R. and Zhang, H.B. (2002). Synthesis and Characterization of Nylon 1012/clay Nanocomposite, J. Appl. Polym. Sci., 83(11): 2403–2410.
Xie, X., Li, B. and Tjong, S. (2001). J. Appl. Polym. Sci., 80: 2105–2112.
Xu, R.; Manias, E.; Snyder, A. J.; Runt, (2001). J. Macromolecules,34, 337-339.
Zheng, L., Farris, R.J. and Coughlin, E.B. (2001). Novel Polyolefin Nanocomposites: Synthesis and Characterizations of Metallocene-Catalyzed Polyolefin Polyhedral Oligomeric Silsesquioxane Copolymers, Macromol., 34(23): 8034–8039.
Zihlif, A. and Ragosta, G. (2003). J. Thermoplast. Comp. Materials, 36: 273–283.
Zilg, C., Reichert, P., Dietsche, F., Engelhardt, T. and Mulhaupt, R. (1998). Kunststoffe, 88: 1812.

15

Rheological Properties of Surface Treated Glass Fiber Reinforced Polypropylenes in Molten State

Yosuke Nishitani[1], Chiharu Ishii[2] and Takeshi Kitano[3]
[1]*Kogakuin University,*
[2]*Hosei University,*
[3]*Tomas Bata University in Zlin*
[1,2]*Japan*
[3]*Czech Republic*

1. Introduction

Fiber reinforced thermoplastics (FRTP) are widely used to industrial applications such as automobiles and electric devices in recent years (Thomason & Vlug, 1996; Kitano et al., 2000; Nishitani et al., 1999, 2001; Hausnerova et al., 2006). Since the machine and the electric devices became small and lightweight, the good balance of the physical properties and processability of FRTP is desired strongly. Polyolefines represent a group of the most common used polymers as matrix for FRTP, because they are inexpensive, easily processed and recycled (Nishitani et al., 1998a, 1998b, 2007). On the other hand, glass fiber (GF) is the most used as reinforcement for FRTP so as to modify the mechanical properties such as stiffness, strength, toughness, heat resistance and so on, and the other properties. Hence, glass fiber reinforced polypropylene composites (GF/PP) are of particular interest in these fields. However, it is difficult to form a strong bond between filler (fiber) and polymer due to poor wettability of the filler (fiber) especially in nonpolar polymer (Shenoy, 1999). The interfacial bond can be enhanced and the mechanical properties of the composites will be improved by suitable surface treatment. Most of fillers (fibers) are pretreated before they are used as secondary phases in composite materials. As typical surface treatment for polymer matrix composites , we often use the coupling agent as follows: silanes, azidsilanes, titantes and organopolysiloxianes, and so on (Shenoy, 1999). In particular, the most effective methods for controlling of the interface and interphase adhesion between GF and PP in GF/PP composites in industrial fields are considered to use silane coupling agents (Mader, 1996; Nishitani et al. 1998b). Many authors have investigated the effect of surface treatment on the various physical and chemical properties of GF/PP composites (Yue & Quek, 1994; Thomason & Schoolenberg, 1994; Mader, 1996, 2001; Lee & Jang, 1997; Kikuchi et al., 1997; Van Den Oever & Peijs, 1998; Hamada et al., 2000). However, their properties will be able to still be improved more by the suitable control of the interphase adhesion between GF and PP.

In order to achieve higher performance in FRTP such as GF/PP, there is a key issue that the rheological properties in molten state is very critical for these materials to understand

proccesability, internal microstructures, their change and structure property relationship (Hausnerova, 2006, 2008a, 2008b; Nishitani, 2010a, 2010b, 2010c). In particular, although FRTPs undergo various flows during processing by flow molding such as injection, extrusion and compression, generally, the effect of surface treatment on processing properties has not been studied enough (Boaira & Chaffey, 1977; Han et al., 1981; Bigg 1982; Luo et al., 1983; Sani et al., 1985; Khan & Prud'Homme, 1987; Nishitani et al. 1998b, 2007; Shenoy 1999). Therefore, we need a proper rheological study on the effect of surface treatment taking into account the various factors such as type of fiber, its size and size distribution, and degree of agglomeration. However, since these factors are interrelated, the determination of the effect of surface treatment on the interphase adhesion is thought to be necessarily a complicated task. Han et al. showed that there were viscosity decrease and the first normal stress difference increase for $CaCO_3$/PP composites regardless of the type of coupling agent used (Han et al., 1981). In contrast, in the case of glass bead filled PP the effect of surface treatment was not so distinct, the viscosity increased after treatment by aminosilane coupling agent, and decreased when octylsilane and titanate coupling agents were used (Khan & Prud'Homme, 1987). Similar complex rheological behavior appeared as the results of surface treatment of $CaSiO_3$ filled PA6 (Luo et al., 1983) and ferrite filled PP (Saini et al., 1985).

Recently, we studied the effect of silane coupling agents on the rheological properties of short and long glass fiber reinforced polypropylene composites in molten state (Nishitani et al., 1998b, 2007). Surface treatment by silane coupling agents increased the storage modulus and reduced the peak in the loss tangent. Furthermore, decrease in the dynamic viscosity was affected by the concentration of coupling agents. Nevertheless, according to our survey of the previous results, the effect of surface treatment on the rheological properties is still not well known. It is therefore necessary to investigate systematically for further understanding of it. The objective of this chapter is to report the results on the effect of surface treatment by silane coupling agent on the rheological properties of short and long glass fiber reinforced polypropylene composites in the molten state which were obtained mainly in our previous studies.

2. Rheological properties of surface treated short glass fiber reinforced polypropylenes

Short fiber reinforced thermoplastic composites have been employed extensively in the plastic industry because of the excellent combination of their mechanical properties, chemical resistance, moderate cost, and recyclability performance. Short glass fiber reinforced polypropylene composites (GF/PP) are of particular interest (Nishitani et al., 2007). Despite great effort expended on research into GF/PP composites, their properties can still be improved by control of the interphase adhesion between GF and PP. One of the methods of improving the adhesion between polymer and fiber is the use of surface treatment agents (Shenoy, 1999). Treatment agents, when properly chosen, bring considerable improvement, particularly in mechanical and thermal properties. A typical surface treatment for GFs is a coupling agent. Another method involves the addition of PP modified by maleic anhydride (mPP) (Sasagi & Ide, 1980). Mechanical properties are improved by the increase in interfacial adhesion. The lower the degree of grafting of maleic anhydride to the modified PP and the higher its molecular weight is, the more effective the improvement is. Recently, a combination of these methods was investigated (Peltonen et al., 1995; Nishitani et al., 1998c, 2007), but the mechanism is still not fully understood. In particular, there have been few efforts to investigate the rheological properties of GF/PP

composites by these combinations. The aim of this section is to report the results of the effect of the fiber surface treatment with aminosilane coupling agent on the rheological properties of short glass fiber reinforced polypropylene composites (GF/PP) and of GF/PP composites supplemented by maleic anhydride modified PP (GF/mPP/PP). Rheological functions in the molten state were measured under steady state shear (viscous and elastic properties) and oscillatory flow (viscoelastic properties) regimes.

2.1 Materials and methods

The effect of surface treatment on the rheological properties of short glass fiber reinforced polypropylene (GF/PP) in molten state was investigated in this section. The materials used in this section were GF/PP and the same materials added with maleic anhydride modified PP (GF/mPP/PP). The polymers used were polypropylene (PP, Sumitomo Novelen, Sumitomo Chemical Co., Japan) and maleic anhydride modified PP (mPP, Sumitomo Chemical Co.) Glass fiber (GF, Micro Glass Fiber, Nippon Glass Fiber Co., Japan) was filled with PP. Surface treatment by aminosilane coupling agent (ASC, γ-aminopropyl-trietoxysilane, A1100, Nippon Unika Co., Japan) with different concentrations was performed on glass fibers. The GFs were pre-treated with ASC in the following way. ASC was mixed with 20 times its volume of water, then the hydrolyses ASC was further diluted in water to concentrations of 0.2, 0.5 and 1.0 wt.%, and the aqueous solutions were applied to GFs. The GF content was fixed with 20wt.% and 40wt.%. The compositions and average fiber lengths of the samples are shown in Table 1.

Composition (wt.%)	PP	20GF								40GF			
		GF/PP				GF/mPP/PP				GF/PP		GF/mPP/PP	
PP	100	80	80	80	80	75	75	75	75	60	60	55	55
mPP	-	-	-	-	-	5	5	5	5	-	-	5	5
GF	-	20	20	20	20	20	20	20	20	40	40	40	40
ASC	-	-	0.2	0.5	1	-	0.2	0.5	1	-	1	-	1
Fiber length (mm)	Original	1.038	-	-	1.177	1.020	-	-	1.134	-	-	-	-
	Remixed	0.648	-	-	0.731	0.620	-	-	0.674	-	-	-	-

Table 1. Composition and average fiber length of GF/PP and GF/mPP/PP composites.

The compounding of PP with GF was carried out at 200°C in a specially developed elastic extruder (Kataoka et al, 1976; Zang et al, 1995, Nishitani et al 1998c, 2007). The weighed amounts of the pellets used for making the 3mm thick compression molded samples were placed into the mold cavity. They were compressed for 3min under 5MPa at 200°C. Finally, the test specimens for the rheological measurements were cut from the molded sheets. And second time-mixed composites were also prepared in order to investigate the influence of this process on the effect of surface treatment.

The steady-state shear flow properties in the low shear rate region and the dynamic functions were measured using a rotational viscometer (cone-plate type, RGM 151-S, Nippon Rheology Kiki Co., Ltd., Japan). The cone radius R was 21.5mm, the gap between the central area of the cone and plate H was kept at 175μm, and the cone angle θ was 4°. The measurements were carried out at 200°C. Steady state shear properties (shear viscosity η, and the first normal stress difference N_1) as well as dynamic functions (storage and loss moduli G', G'', respectively,

dynamic viscosity η' and complex viscosity $|\eta^*|$) were determined as functions of the shear rate $\dot{\gamma}$ and angular frequency ω from 10^{-2} to 10 1/s (rad/s), respectively. The strain amplitude was chosen to be 25% (oscillatory angle ±1°) which is considered to be a large value in order to compare the results of the oscillatory and steady shear regimes.

2.2 Shear rate dependences

The shear viscosity η and the first normal stress difference N_1 are plotted against share rate $\dot{\gamma}$ for both the untreated and 1wt.% ASC treated GF/PP composites in Fig.1. In the lower shear region, between 0.05 and 0.5 1/s, the character of the viscosity curves of all the GF filled systems were similar to that of pure PP – i.e. they were nearly independent of the shear rate. It is thought that increase in shear viscosity was caused by enhanced resistance to shear flow arising from structure composed by reinforcing fibers in the system, and also from the increased fiber-polymer matrix interactions supported by surface treatment. In the shear rate region higher than 0.5 1/s, where the PP behaves in a pseudoplastic manner, the fibers tend to orient in the flow direction, and the effect of surface treatment by ASC diminishes diminishes(Fig.1(a)). The first normal stress difference N_1 data shown in Fig. 1(b) indicates an increase in elastic property as a result of the surface treatment by ASC. In general, the first normal stress difference N_1 increases with an increase in fiber length, with structure formation by the fibers, and with the elastic properties of fibers themselves. The degree of dispersion of fibers in a polymer matrix is also important factor influencing on the elastic properties of fiber reinforced composites in the molten state. When the fibers are surface treated, the structure formed can be changed easily. Furthermore, the apparent fiber modulus of a treated system will be higher than that of an untreated one because of the softened phase, which is able to change the structure in the region of the polymer- fiber interface. Although the first normal stress differences of untreated GF/PP composites in the high shear rate region reach the values close to those of the pure polymer matrix, those of the treated materials are higher.

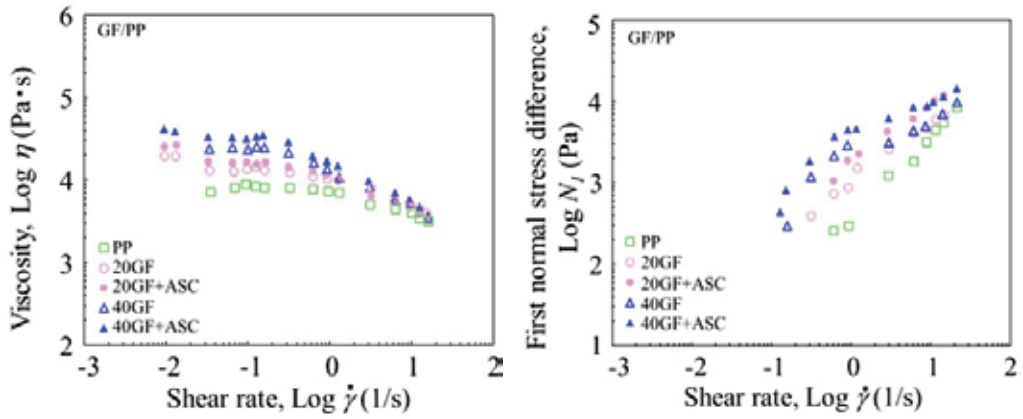

(a) Viscosity (b) The first normal stress difference

Fig. 1. Influence of silane coupling agent on steady shear flow properties of GF/PP composites: (a) viscosity as a function of shear rate, (b) the first normal stress difference as a function of shear rate

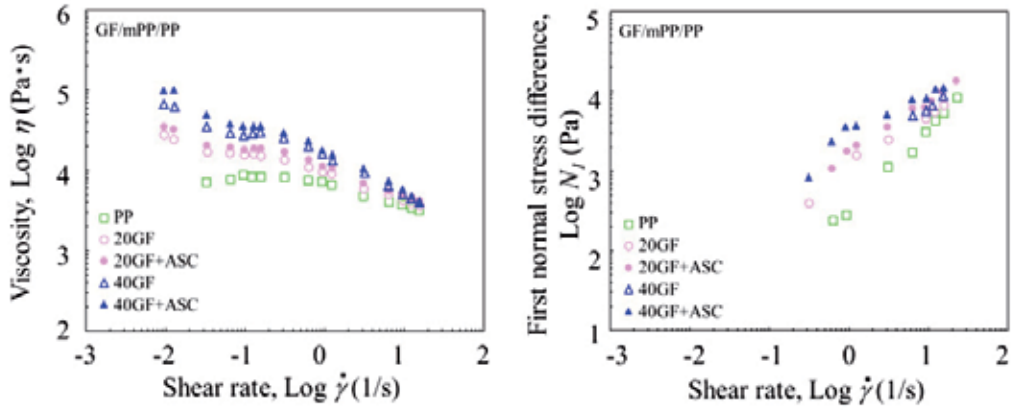

(a) Viscosity (b) The first normal stress difference

Fig. 2. Influence of silane coupling agent on steady shear flow properties of GF/mPP/PP composites: (a) viscosity as a function of shear rate, (b) the first normal stress difference as a function of shear rate

In the low shear rate region, the first normal stress difference increases with the fiber content, which may be due to the hydrodynamic effect associated with fiber orientation in the flow direction. The effect of surface treatment was identical to that in the high shear rate region. The shear viscosity and the first normal stress difference as a function of shear rate for maleic anhydride modified PP (5wt.%) added composites (GF/mPP/PP compositese) are plotted in Fig. 2. Although the overall level of the both functions η and N_1 was higher than that in GF/PP composites (Fig. 1), the effect of surface treatment by 1wt.% ASC on η and N_1 of GF/PP composites is similar to that of GF/mPP/PP.

The results demonstrated in Figs. 1 and 2 are somewhat different from those obtained in studies of particulate filled polymer systems, for example, mica filled PP (Boaira & Chaffey, 1977) or calcium carbonate filled PP (Han et al., 1981), where the increased values of shear viscosity and the first normal stress difference caused by the filler addition could be reduced to a greater or lesser extent – by surface treatment. Such discrepancies in the results can be explained by the different roles played by the coupling agent during processing as follows. First, it forms chemical bonds between the inorganic filler and polymer matrix, and assists physical adhesion by Van der Walls's forces. Second, it may behave as a lubricant, which decreases the friction between the filler and polymer matrix. Third, it changes the interfacial energy of the filler, and simultaneously supports better filler dispersion in the polymer matrix, and reduces agglomeration by wetting. Finally, a surface treatment agent can behave as an additive to make deformation of fiber assembly easier and to make the viscoelastic properties of a matrix polymer lower. It is thought that the mechanisms mentioned above do not occur separately, and therefore it is difficult to distinguish a particular type.

Regarding GF/PP and GF/mPP/PP composites investigated in this section, the adhesion between fiber and polymer matrix was improved. In addition, because of the improved protection against the breakage of fibers, the fiber length of treated materials can be kept

longer throughout the compounding and processing than that of untreated ones. Finally, the addition of maleic anhydride modified PP (mPP) increases the rheological properties (viscosity and the first normal difference), because mPP probably not only improves the surface treatment, but also forms chemical bonds between fiber and polymer matrix.

2.3 Angular frequency dependences

The storage and loss moduli G' and G'' as a function of angular frequency ω for GF/PP composites are shown in Fig. 3. The storage modulus G' of the GF/PP composites treated by 1 wt.% ASC was scarcely higher than that of the untreated ones, and it was almost independent of fiber content (20 or 40 wt.%), although generally G' should increase with fiber loading level (Fig.3(a)). Also, the loss modulus G'' of the treated GF/PP composites (Fig. 3(b)) was only slightly higher than that of the untreated composites. Unlike G', G'' increased with increasing the fiber content. Although G'' of the untreated composites (20 and 40 wt.% GF) increased over the whole angular frequency range covered by the experiments, this trend was valid only for angular frequencies higher than 0.1 rad/s in the case of the treated materials. In the frequency region lower than 0.1 rad/s, the surface treatment by ASC initiated the behaviour in which G'' was independent of ω, indicating a second rubbery plateau, i.e. the long-scale relaxation time. This behaviour implies the presence of an apparent yield stress, which will be attributed to the strong fiber structure formation imparted by the surface treatment. The properties of GF/mPP/PP composites, demonstrated in Fig. 4, showed the same trend of G' against frequency dependency as for GF/PP composites in Fig. 3(a). However, with 20wt.% GF and no ASC treatment, there was no evidence of plateau behaviour in the loss modulus.

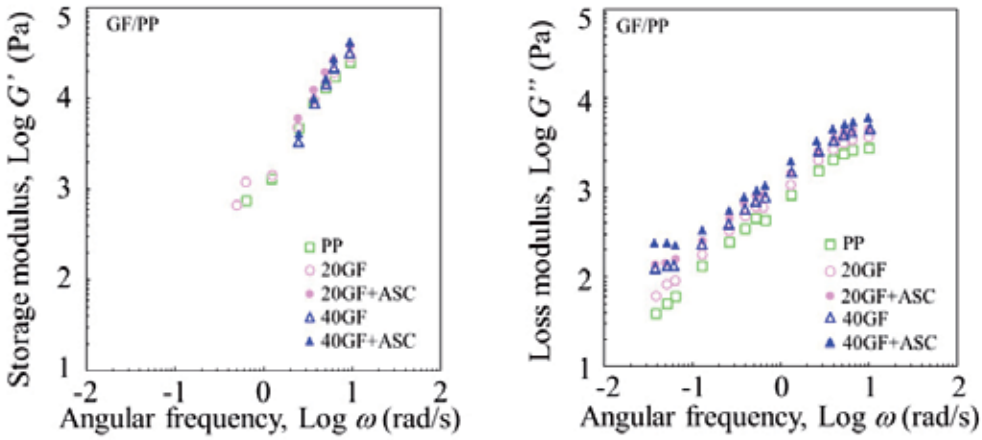

(a) Storage modulus (b) Loss modulus

Fig. 3. Influence of silane coupling agent on dynamic viscoelastic properties of GF/PP composites: (a) storage modulus as a function of angular frequency, (b) loss modulus as a function of angular frequency

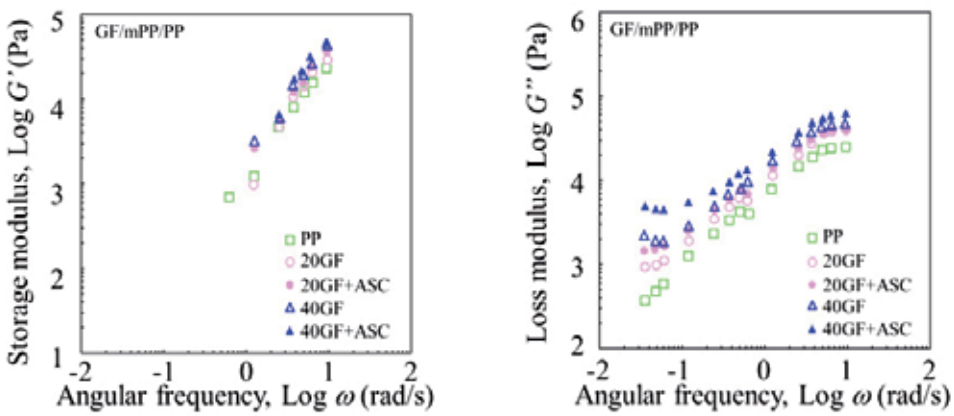

(a) Storage modulus (b) Loss modulus

Fig. 4. Influence of silane coupling agent on dynamic viscoelastic properties of GF/mPP/PP composites: (a) storage modulus as a function of angular frequency, (b) loss modulus as a function of angular frequency

2.4 Comparison of steady shear and dynamic flow data

Cox and Merz (Cox & Merz, 1958) observed a close similarity between the steady state shear and complex viscosities determined at corresponding values of the shear rate and angular frequency, respectively. This empirical rule can be written as follows:

$$\eta(\dot{\gamma}) = |\eta^*(\omega)| = \sqrt{\eta'^2(\omega) + \eta''^2(\omega)} \tag{1}$$

Where η, $|\eta^*|$ are the shear and complex viscosities, and η', η'' are the real and imaginary parts of the complex viscosity $|\eta^*|$, respectively. The validity of this relation for polymer melts and concentrated solutions has been amply verified. The steady state shear and complex viscosities both approached their limiting (zero viscosity) values as their arguments go to zero, and they decreased in a similar way with increasing $\dot{\gamma}$ or ω, although at high shear rates (angular frequency) $|\eta^*|$ may fall more rapidly than η. As proposed by Dealy (Dealy & Wissbrun, 1990), the Cox-Merz rule should be generally valid for flexible molecules; however, it is not suitable for almost any fiber filled polymer systems (Kitano et al., 1984a, 1984b; Li et al., 1997; Nishitani et al., 2007), since the viscosity increment caused by the fber addition would be different under the two types of flow.

In Fig. 5, double-logarithmic plots of η vs. $\dot{\gamma}$ and $|\eta^*|$ vs. ω are shown for both GF/PP and GF/mPP/PP composites. The η and $|\eta*|$ curves coincided relatively well in their plateau (Newtonian) regions at shear rates (angular frequencies) from 0.1 to 1 1/s (ras/s) for untreated samples. Nevertheless, the $|\eta*|$ values of the GF/PP treated by 1wt.% ASC, shown in Fig. 5(a), were clearly higher than the η level. In the case of the treated GF/mPP /PP, in Fig. 5 (b), η vs. $\dot{\gamma}$ and $|\eta*|$ vs. ω curves showed the same tendency as the untreated systems. Such behaviour supports the idea of the ASC surface treatment having different roles in GF/PP and GF/mPP/PP composites.

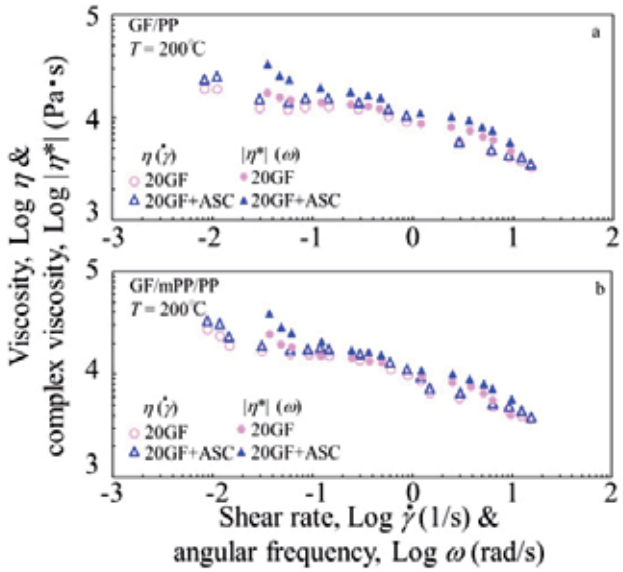

Fig. 5. Shear viscosity versus shear rate and complex viscosity versus angular frequency: (a) GF/PP composites, (b) GF/mPP/PP composites

2.5 Effect of coupling agent concentration

In order to clarify the influence of the concentration of the aminosilane coupling agent (ASC) on the rheological properties of GF/PP and GF/mPP/PP composites, both steady shear (η, N_1) and dynamic ($|\eta^*|$, G') functions are plotted against the ASC concentration C in Figs. 6 and 7. The content of fibers was fixed at 20wt.%., and the relative values representing the ratio of treated GF/PP and GF/mPP/PP to untreated GF/PP and GF/mPP/PP, respectively, are shown at two shear rates (angular frequencies) of 0.1 and 9.2 1/s (rad/s). The relationship between the relative viscosity η_r obtained from the steady shear flow measurements, and the ASC concentration C (wt.%) is demonstrated in Fig. 6(a). Generally, η_r increased slightly with increasing C, and for higher shear rate (9.2 1/s) it was almost independent of C for both systems. In order to discuss about the elastic response, the relation between the relative normal stress difference N_{1r}, and C is plotted in Fig. 6(b). It was found that whereas the N_{1r} of GF/mPP/PP composites showed a maximum at 0.5 wt.% ASC, that of GF/PP composites increased monotonously with increasing C. To conclude, the N_{1r} variation with amount of aminosilane coupling agent was much larger than that of η_r. Figs. 7(a) and 7(b) show the effect of the ASC concentration C on the viscoelastic properties. While the relative complex viscosity $|\eta^*|_r$ of the GF/PP system, in Fig. 7(a), increased with increasing C, it was almost independent of the amount of ASC for the GF/mPP/PP composite. The dependency of the relative storage modulus G'_r on the ASC concentration C of both composites shown in Fig. 7(b) was similar to that of $|\eta^*|_r$ vs. C curve for the GF/PP composites. However, the G'_r vs. C curve for GF/mPP/PP composites showed a peak at 0.2 wt.% ASC. In general, G'_r reached smaller values than N_{1r} shown in Fig. 6(b). As one explanation of this phenomenon, different deformation modes under the particular flow can be considered.

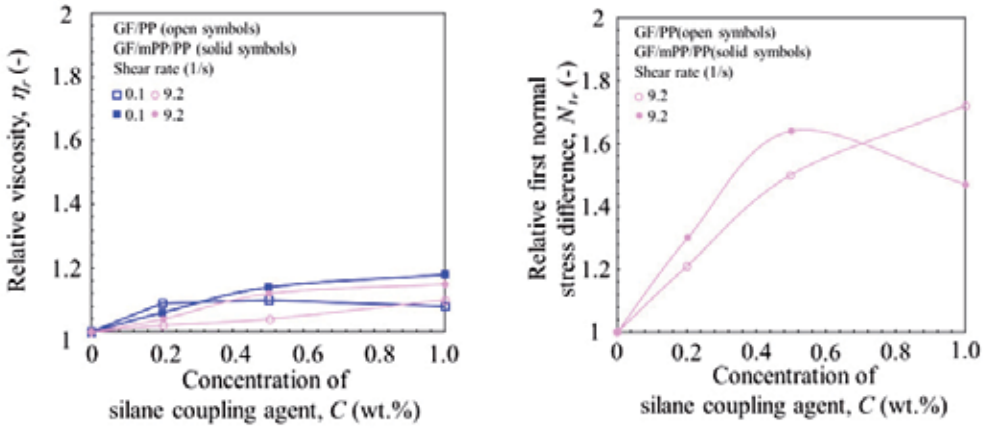

(a) Relative viscosity (b) Relative first normal stress difference

Fig. 6. Relationship between relative values of steady shear flow functions and concentration of silane coupling agnet for GF/PP and GF/mPP/PP composites: (a) relative viscosity, (b) relative first normal stress difference

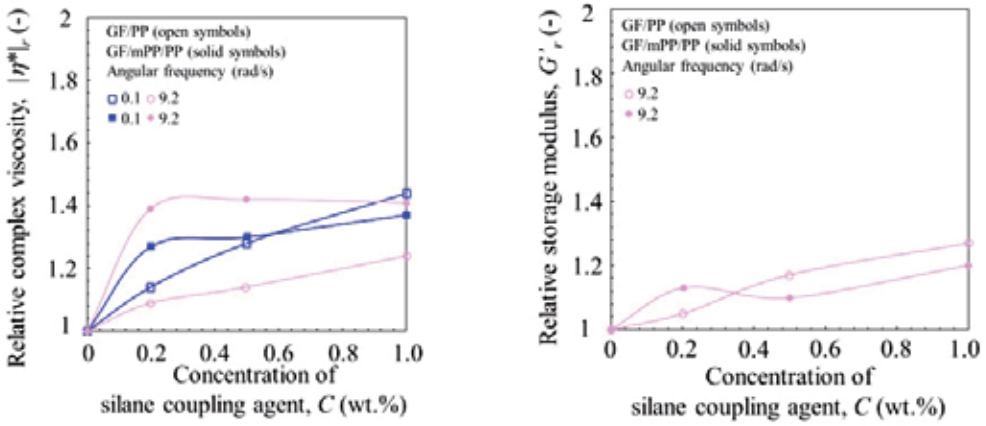

(a) Relative complex viscosity (b) Relative storage modulus

Fig. 7. Relationship between relative values of oscillatory flow functions and concentration of silane coupling agnet for GF/PP and GF/mPP/PP composites: (a) relative complex viscosity, (b) relative storage modulus

Finally, the effect of surface treatment with regard to the fiber content is described and summarized in Table 2. The increase in the ASC concentration seems to make the processing of composites more difficult due to the increase of viscous and elastic properties of the composites. However, mechanical properties such as tensile, bending and impact strength are highly enhanced by ASC treatment (Nishitani et al. 1998b, 1998d). Consequently, the optimum concentration of surface treatment agent has to be determined individually, according to the performance required for a particular product.

Relative values	$\dot{\gamma}$ (1/s) or ω (rad/s)	1 wt.% ASC			
		GF/PP		GF/mPP/PP	
		20 wt.% GF	40 wt.% GF	20 wt.% GF	40 wt.% GF
η/η_0	0.1	1.06	1.35	1.18	1.16
	9.2	1.10	1.16	1.17	1.02
$\lvert\eta^*\rvert/\lvert\eta^*\rvert_0$	0.1	1.45	1.46	1.38	1.91
	9.2	1.25	1.18	1.42	1.13
N_1/N_{10}	0.1	-	1.82	-	-
	9.2	1.72	1.68	1.47	1.42
G'/G'_0	0.1	-	-	-	-
	9.2	1.27	1.24	1.20	1.17

Table 2. Relative values of rheological properties for GF/PP and GF/mPP/PP composites

2.6 Yield stress

The presence or absence of a yield stress is of great importance in the molding of filler filled or fiber reinforced polymers, and also for the physical stability of many industrial products. Casson proposed an equation describing the steady state shear flow properties of the suspensions of solid particles in Newtonian liquids (Casson, 1959), so as to easily evaluate yield stresses:

$$\tau^{1/2} = \tau_0^{1/2} + k_1 \dot{\gamma}^{1/2} \tag{2}$$

Where τ is the shear stress, τ_0 represents its yield value, $\dot{\gamma}$ stands for shear rate, and k_1 is a constant. If the plots of $\tau^{1/2}$ against $\dot{\gamma}^{1/2}$ give straight lines, the yield stress can be obtained by extrapolation to $\dot{\gamma}$=0.

In this section, we discuss about the existence of the yield stresses of the GF/PP and GF/mPP/PP composites in the molten state and their relationship among the yield stress, content of dispersed fillers (fibers), and the structure of fiber assembly (Figs. 8 and 9). Fig.8 shows Casson's plots for GF/PP and the GF/mPP/PP composites. The line for pure PP is straight ones passing through the origin, suggesting the absence of a yield point. Concerning filled PP, the yield stresses, σ_y is determined only in the very low shear rate region ($\dot{\gamma}^{1/2}$ less than 0.4 $1/s^{1/2}$), where the flow data can be fitted by the straight lines. The σ_y of GF/PP composites, which is estimated from Fig. 8(a), seems to increase slightly with increasing GF content, and also by the ASC surface treatment of GF. The rate of σ_y increase for the GF/mPP/PP, Fig. 8(b), is larger than that for the GF/PP. This means that the addition of modified PP strongly influences on the yield stress appearance.

Such a trend can be seen clearly in Fig. 9, where the yield stresses of both composites are plotted as a function of the weight fraction of glass fiber ϕ_w in semi-logarithmic co-ordinates. The surface treatment of GF by silane coupling agent, and further the addition of modified PP increases the yield stress of the composites in the same manner as the increment of fiber

content. This behaviour is attributed to the strong structure formed by the fiber assembly, which are coupled by ASC, and strengthened by modified PP. Finally, it should be noted here that a yield stress is usually responsible for long scale relaxation times (the second rubbery plateau behaviour).

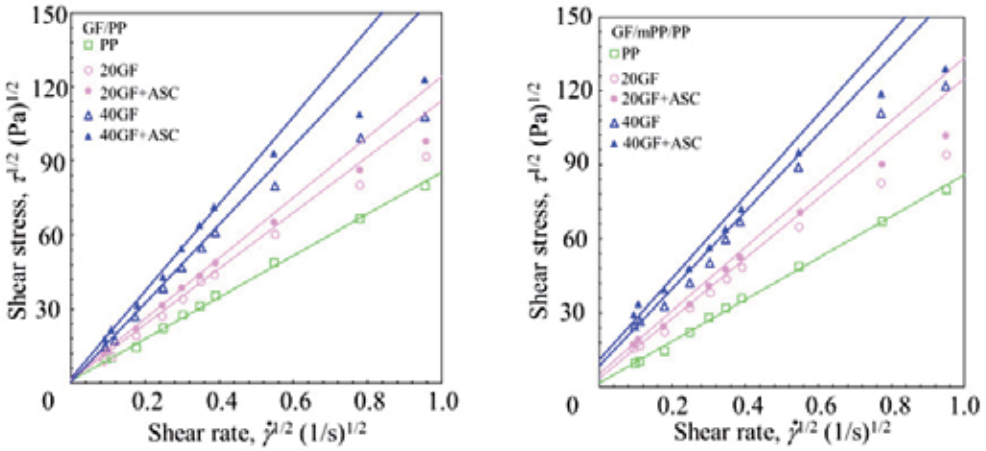

(a) GF/PP composites (b) GF/mPP/PP composites

Fig. 8. Casson's plots: (a) GF/PP composites, (b) GF/mPP/PP composites

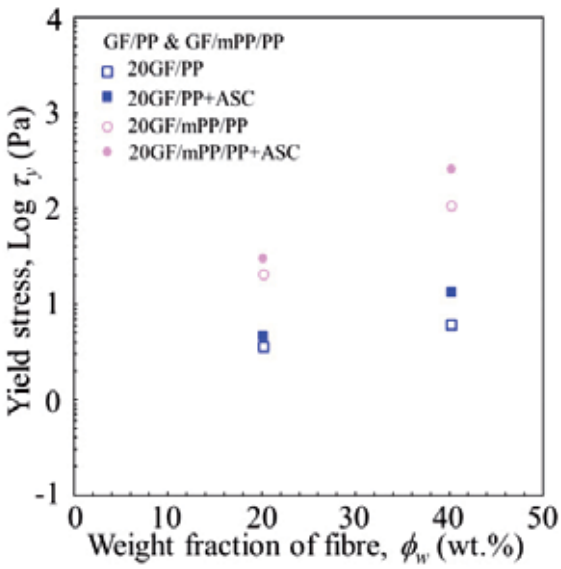

Fig. 9. Relationship between yield value of shear stress and weight fraction of fiber for GF/PP and GF/mPP/PP composites

2.7 Effet of re-mixing process on rheological properties

Re-mixing (second compounding) of short fiber reinforced polymers is generally carried out to avoid the non-uniform dispersion of fillers or fibers in a polymer matrix. Composites processed by injection molding undergo the second mixing in an extruder or injection molding machine. In this section, we investigated the influence of re-mixing on the ASC surface treatment. The plots of η vs. $\dot{\gamma}$ for the mixed GF/PP and GF/mPP/PP composites and remixed GF/PP-R and GF/mPP/PP-R ones are depicted in Fig. 10. The viscosities of the re-mixed composites were lower, and there was no clear difference between untreated and treated materials. The reason might be the decrease in the fiber length after re-mixing (see Table 1), and the simultaneous diminution of the influence of fiber length on the viscous properties.

In addition, the viscosity difference between GF/PP and GF/mPP/PP composites was reduced after second mixing. In contrast, the complex viscosity of re-mixed composites was different for treated and untreated materials, as shown in Fig. 11. The former showed the same tendency as the shear viscosity, but the latter values were not much affected by re-mixing.

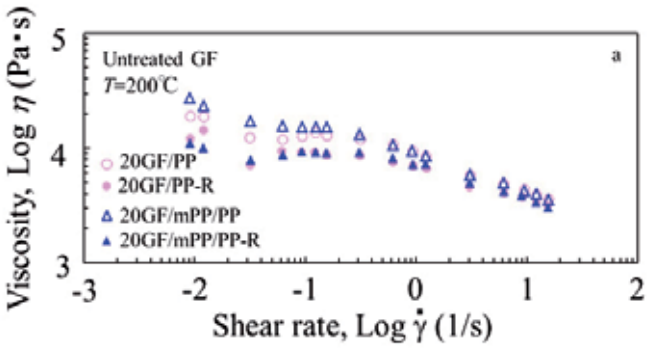

(a) Untreated composites

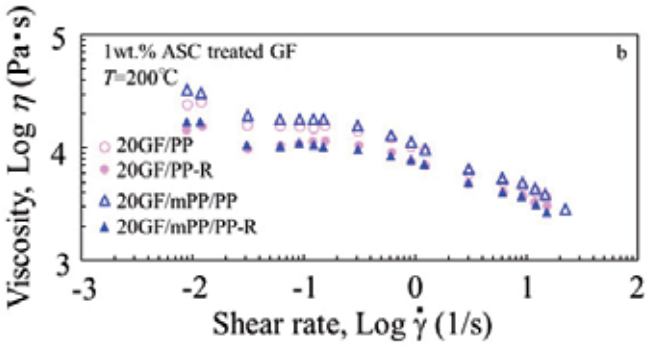

(b) ASC treated composites

Fig. 10. Effect of re-mixing on viscosity as a function of shear rate curves: (a) untreated composites, (b) ASC treated composites

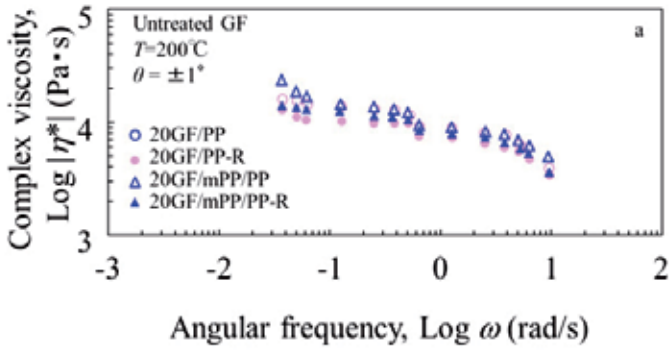

(a) Untreated composites

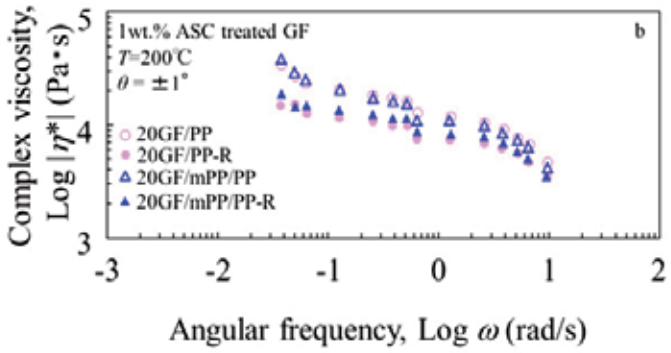

(b) ASC treated composites

Fig. 11. Effect of re-mixing on complex viscosity as a function of angular frequency curves: (a) untreated composites, (b) ASC treated composites

3. Rheological properties of surface treated long glass fiber reinforced polypropylenes

Fiber reinforced thermoplastic composites are usually fabricated by a flow molding process. For high performance fiber reinforced composites it is important to analyse the flow /deformation behaviour of fiber filled systems during the polymer processing, and to investigate the flow mechanisms and any changes in the internal structure of these systems. The flow properties of short fiber filled systems, whose reinforcement fiber length is up to several 100 micrometers, have been studied extensively (Czarnecki & White, 1980; Laun, 1984; Mutel & Kamal, 1986; Ausias et al, 1992; Basu et al, 1992; Greene & Wikes, 1995; Kim & Song, 1997). For these systems, non-uniformity of orientation or dispersion of fibers arises, depending on flow conditions, and it is well known that this anisotropic or heterogeneous structure will cause anisotropic physical properties (Kitano et al, 1981). On the other hand, researches into continuous or long fiber filled systems have not been widespread, because the measuring or analysing methods required are not established yet, and the flow behaviour becomes more complicated in this case (Davis & Mcalea, 1990; Groves & Stocks, 1991; Groves et al, 1992; Davis & Manson 1993; Greene & Wikes, 1995; Nishitani et al 1998a, 1998b, 2001).

The measuring methods for short fiber filled systems are seldom valid for long fiber filled ones. Steady shear flow measurements, usually used for short fiber filled systems, cannot be applied to long fiber filled ones, since the heterogeneity of the latter system is higher than that of the former, and the structure composed by the long fiber assembly changes gradually under large shear deformations. Then, the stable flow state cannot be obtained. Therefore, it is common for the flow properties of long fiber filled systems to be evaluated by dynamic viscoelastic properties, measured by means of oscillatory flow experiments under small strain/deformation amplitudes (Nishitani et al 1998b, 2001). When measuring the flow properties of fiber filled systems it is desirable to retain the initial state of fiber orientation or dispersion. The change in the initial state is easily occurred during the setting up of a sample when a cone-plate typed rheometer is used. Therefore, it is more appropriate to use a parallel-plate typed rheometer for the viscoelastic properties of long fiber filled systems. In addition, it is desirable to know the flow properties of continuous or long fiber filled composites in order to clarify unsolved problems such as the impregnation of matrix resin and the uniformity of the fiber distribution in composites.

Furthermore, various surface treatments are used in order to achieve the high performance. The methods of surface treatment for long fiber filled systems are the same ones as for short fiber filled systems, however the effect of the surface treatment on the rheological properties of long fiber filled composites is not understood enough yet.

In our previous works (Kitano et al, 1994, 2000; Nishitani et al, 1998a, 1998b, 1999, 2001) we investigated the fabrication methods and physical properties of long fiber reinforced polypropylenes, which were compression molded polypropylene fibers mixed homogeneously with long reinforcement fibers such as glass fiber, carbon fiber, aramid fiber, polyvinyl alchol fiber and polyamide 6 fiber by an apparatus called a "fiber separating and flying machine". The fabrication method employed here is a discontinuous and dry process similar to the stampable sheet molding method. This is superior to other manufacturing methods from the point of view of thermal efficiency, isotropic physical properties (because of the completely separated and homogeneously dispersed reinforcement fibers), and applicability to hybrid composites.

The objective of this section is to report the effect of surface treatment on the rheological properties, which is the dynamic viscoelastic properties in the molten state, investigated experimentally, for long glass fiber reinforced polypropylene composites (GFL/PP) prepared by the mentioned above. The present section discusses the dynamic viscoelastic properties in terms of various factors: angular frequency, concentration of silane coupling agent, various kinds of silane coupling agents, volume fraction of fiber, temperature and strain amplitude.

3.1 Materials and methods

The materials used in this section were surface treated long glass fiber reinforced polypropylene melts. Polypropylene fiber (PP, Showa aroma, Showa Denko K. K., Japan) was used as the matrix. Glass fiber (GF, Micro Glass Roving, Nihon Glass Fiber Co., Ltd., Japan, fiber diameter d=13μm) was used as reinforcement fibers. Surface treatment by different kinds of silane coupling agents with different concentrations was performed on glass fibers. Four types of silane coupling agents: aminosilane (ASC, A-1100, Nippon Unicar

Co. Ltd., Japan), diaminosilane (DAS, SH-6020P, Dow Corning Toray Co., Ltd., Japan), acrylsilane (ACS, A174, Nippn Unicar Co., Ltd.) and epoxysilane (ESC, A187, Nippon Unicar Co., Ltd.) were used as surface treatment agent. These details: code, component name and concentration are listed in Table 3.

Coupling agent	Code	Component Name	Concentration C (wt.%)	Volume fraction of fiber V_f (vol.%)
Aminosilane	ASC	γ-aminopropyltrietoxysilane	0.2, 0.5, 1.0	5, 10, 20, 30
Diaminosilane	DAS	γ-(2-minoethyl)aminopropyltrimetoxysilane	0.5	10, 20
Acrylsilane	ACS	γ-methacryloxypropyltrimetoxysilane	1.0	10, 20
Epoxysilane	ESC	γ-glycidxypropyltrimetoxysilane	1.0	10, 20

Table 3. Name of coupling agent, its component and code, its concentration and volume fraction of GF

All of the composite materials were compression molded from mixed mats prepared by the apparatus called a "fiber separating and flying machine" (Nishitani et al, 1999, 2001). This apparatus is schematically illustrated in Fig. 12. Continuous GF with volume fraction of 5, 10, 20 and 30 vol.% were fed into the "fiber separating and flying machine" apparatus simultaneously with PP fibers which are previously cut in 100 to 150mm. The collected mixed mats prepared by this apparatus were used as a base material for compression molding. Then the mixed mats were cut into 150 x 150 mm pieces, the weighed amounts of the mats for molded samples with 3mm thickness were piled into the mold cavity. These mats were kept in an air circulation oven at 120°C for 3 hours in order to remove the absorbed water in the fibers. Then the dried mats were compression-molded by a hot press in 3mm thick sheets for 3minutes under 5MPa at 200°C. Test specimens for viscoelastic properties measurements were cut from the sheets. The average length of glass fibers was 21.6mm, their orientation was generally three dimensional, and the degree of orientation gradually changed with the fiber content.

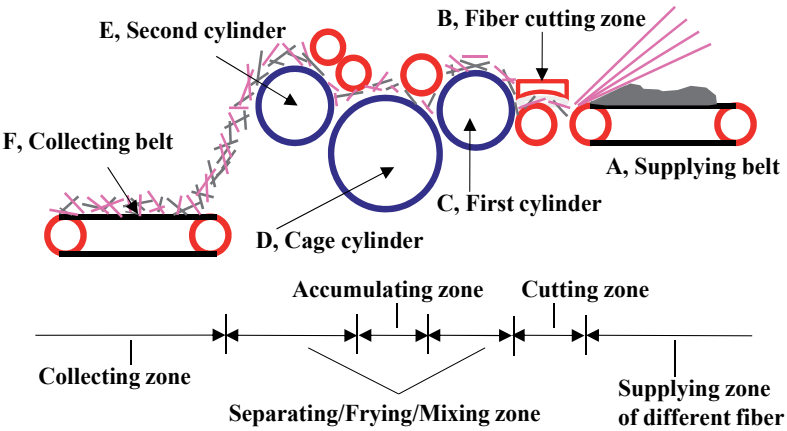

Fig. 12. Schematic diagram of the mixture mats production by the "Fiber separating and flying machine" apparatus

For long fiber reinforced composites it is difficult to estimate their rheological properties by using a cone-plate typed or capillary typed rheometer under steady shear flow. Therefore, specially designed rheometer is used for continuous fiber reinforced composites (Nishitani et al, 1998b, 1998c, 2001). In our experiments, a parallel-plate typed rheometer (151-S, Nippon Rheology Kiki Co., Ltd., Japan) was used to measure the dynamic viscoelastic properties of the samples. The specimens were compression-molded sheets cut into disks of 27 to 28 mm diameter. The gap between the two plates of 12.5mm radius was fixed at 3mm. Under such gap condition, a test specimen was slightly compressed in the molten state. The angular frequency varied from 10^{-2} to 10^{2} rad/s, and the forced oscillatory angle of lower plate was used at 0.5, 1.0 and 2.0 degree, corresponding to the strain amplitude of 4.4%, 8.7% and 17.5% in shear unit, respectively. The measurements were carried out for all the samples at 180, 200 and 220°C. Linear viscoelastic properties such as storage modulus G', loss modulus G'', dynamic viscosity η' and loss tangent tan δ were determined.

3.2 Angular frequency dependence

First, the effect of the surface treatment on the rheological properties of long glass fiber reinforced polypropylene composites (GFL/PP) is discussed. The rheological properties are evaluated by the dynamic viscoelastic properties in the molten state, which are strongly dependent on the internal micro structure formation of the polymer composites. We shall discuss the angular frequency dependence, which is the basic variable in dynamic viscoelastic properties. All the results discussed in this section were measured under an oscillatory angle of 0.5° (strain amplitude 4.4%) and the range of angular frequency was from 10^{-2} to 10^{2} rad/s. Fig. 13(a) shows the effect of the concentration of aminosilane coupling agent (ASC) on the relationship between the storage modulus G' and angular frequency ω of GFL/PP composites. G' of untreated GFL/PP increases with increasing ω. G' of ASC treated GFL/PP increases with increasing the concentration of ASC (from 0.1 to 1.0 wt.%) and shows the typical G' curve similar to highly filled systems although the content of GF in the composites is 10vol.%. The slopes of G' against ω become small in low ω region, indicating the "second rubbery plateau" i.e. the long-scale relaxation time (Ferry, 1980; Nishitani et al, 2001, 2007, 2010a, 2010b). This tendency is highly enhanced by the increase of the ASC concentration. This behaviour may be attributed to the fiber network formation, which is due to high aspect ratio, and the interfacial interaction between GF and PP. Fig. 13(b) shows the effect of the concentration of ASC on the relationship between the dynamic viscosity η' and ω of GFL/PP composites. η' decreases monotonously with increasing ω, and the slopes of η' against ω have a slope of an angle of approximately -45°. This behaviour shows the presence of an apparent yield stress in the low ω region. The effect of the concentration of ASC on η' or loss modulus G'' seems to show more complex behaviour. η' of the ASC treated GFL/PP composites having the concentration of ASC of less than 0.5 wt.% is less than that of untreated ones, although 1.0wt.% ASC treated GFL/PP composites shows higher η' than that of untreated ones, which means the treatment with low ASC concentration rather decreases η' or G'' (viscous properties) although increase G' (elastic property). These behaviour may be due to the action of the coupling agent as a wetting agent, lubricant or plasticizer.

In Fig. 14(a), the storage modulus G' is plotted against the angular frequency ω for various silane coupling agents treated GFL/PP composites. G' of all treated GFL/PP is higher than

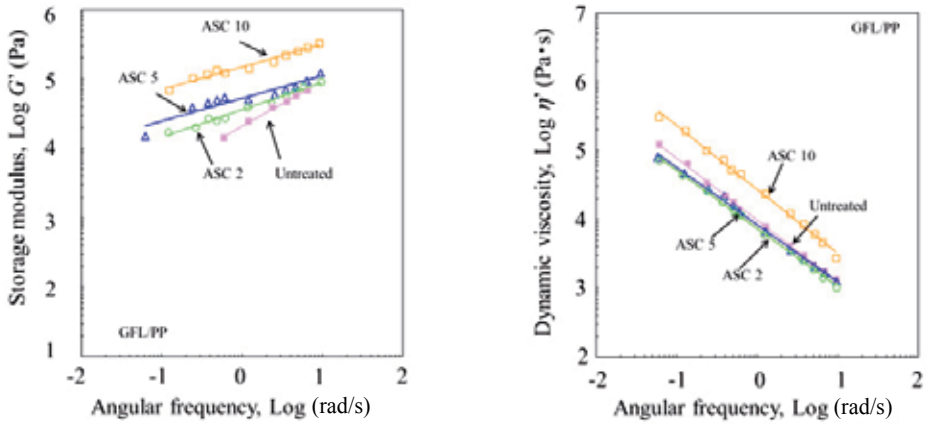

(a) Storage modulus (b) Dynamic viscosity

Fig. 13. Influence of concentration of aminosilane coupling agent on dynamic viscoelastic properties for GFL/PP composites: (a) storage modulus versus angular frequency, (b) dynamic viscosity versus angular frequency

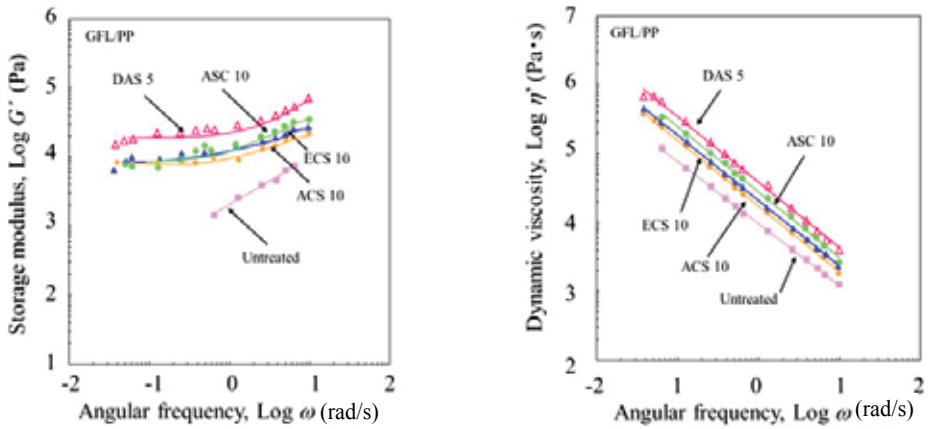

(a) Storage modulus (b) Dynamic viscosity

Fig. 14. Influence of different kinds of silane coupling agent on dynamic viscoelastic properties for GFL/PP composites: (a) storage modulus versus angular frequency, (b) dynamic viscosity versus angular frequency

that of untreated GFL/PP composites in a wide range ω region and shows the typical G' curve similar to that of highly filled systems, indicating the "second rubbery plateau", however the values of G' change with the types of silane coupling agents and increase in the following order: untreated < aclylsilane (ASC) < epoxysilane (ESC) < aminosilane (ASC) < diaminosilane (DAS). Fig. 14(b) shows the dynamic viscosity η' of various silane coupling agent treated GFL/PP composites as a function of ω. η' decreases monotonously with increasing ω, and the slopes of η' against ω have a slope of an angle -45°. As with G', η' of various silane coupling agent treated GFL/PP increases in comparison with η' of untreated

GFL/PP composites, and this increase of η' is in the same order as G'. In particular, both properties such as G' and η' appear conspicuously to be high for the GFL/PP composites with diaminosiane coupling agent (DAS). This trend showed the same tendency also by the mechanical properties such as impact strength and so on (Nishitani et al., 1998a)

Loss tangent tan δ, which is defined as the ratio of the loss modulus G'' and storage modulus G', can clarify the correlation between the elastic and viscous properties of the materials. Fig. 15 shows the relationship between tan δ and angular frequency ω for untreated and ASC 10 (1.0wt.%) treated GFL/PP composites with various volume fractions of fiber from 5 to 30 vol.%. Tan δ of untreated GFL/PP composites (Fig. 15 (a)) with volume fraction of fiber V_f less than 10vol.% (GFL10) increases with V_f and tan δ - ω curves have the peak. In high V_f region with V_f higher than 10vol.%, tan δ becomes smaller with increasing fiber content, and independent of ω in 30 vol.% (GFL30). It may be thought from these results that GF in the composites with higher fiber content contributes to a more dominant role for the elastic properties than the viscous ones. Tan δ of GFL30 is independent of ω, and these composites behave like solid materials because of the high rigidity of the structure composed with rigid fibers. On the other hand, tan δ of ASC 10 treated GFL/PP composites are shown in Fig. 15 (b) as a function of ω. Tan δ decreases gradually with increasing V_f. For composites with V_f higher than 20 vol.%, tan δ is independent of ω, behaving like solid materials. Although tan δ – ω curves of untreated GFL/PP composites have the peak values up to 20 vol.% (GFL20), those of ASC 10 treated GFL/PP composites have them up to 10 vol.% (GFL10). This fact indicates the decrease in viscous properties with high fiber content. By the surface treatment with ASC, this tendency is sifted to low fiber content region compared with untreated GFL/PP composites. These behaviour may be attributed to the strong interfacial interaction between GF and PP.

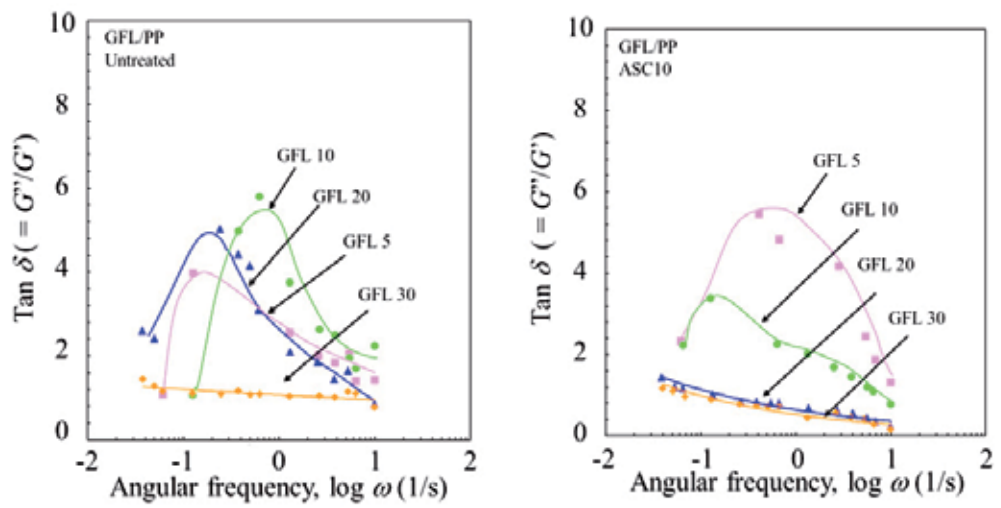

(a) Untreated GFL/PP composites (b) ASC 10 treated GFL/PP composites

Fig. 15. Influence of volume fraction of fiber on loss tangent for GFL/PP composites: (a) Untreated GFL/PP composites, (b) ASC 10 treated GFL/PP composites

In general, the influence of surface treatment by coupling agents on the dynamic viscoelastic properties of the polymer composites is complex. This is because the surface treatment by silane coupling agents play two of multiple roles simultaneously, as a coupling agent which improves the adhesion between fiber (filler) and polymer, a lubricant which reduce the friction, a plasticizer which helps to make the fiber and the polymer softer, a wetting agent which reduces agglomeration and a an additive to make deformation of fiber assembly easier and to lower the viscoelastic properties of a matrix polymer. It is thought that the mechanisms mentioned above do not occur separately, and therefore it is very difficult to distinguish a particular type. From the results in this section, it can be concluded that the surface treatment by the various silane coupling agents improves the viscoelastic properties. Although the viscous properties are dominant in low concentration of silane coupling agent, which remarkably shows the role acting by plasticizer and internal lubricant, the elastic properties increase with the concentration of silane coupling agent. Thus, it is found that the role of the coupling agent, which forms chemical bonds between GF and PP and physical adhesion, becomes lager gradually with the increase of the concentration. Moreover, with increasing fiber content, the effect of fiber itself on the viscoelastic properties of GFL/PP composites becomes higher than the effect of surface treatment on them, and then the elastic properties increase gradually.

3.3 Effect of coupling agent concentration

In general, rheological properties such as storage modulus G' and dynamic viscosity η' are considered to be sensitive indicators for the quantitative analysis of morphological change in the composite materials. To more clarify the influence of silane coupling agent on the rheological properties of GFL/PP composites, both the storage modulus G' and the dynamic viscosity η' are plotted against the aminosilane coupling agent (ASC) concentration C as a parameter of angular frequency (ω=0.127, 1.257 and 9.488 rad/s) in Figs. 16 and 17. In Fig. 16 (a), G' of GFL5 (GF content is 5vol.%) increases gradually with the increase of the ASC concentration C, except for data at 0.127 rad/s in low C region. G' of GFL10 (Fig. 16(b)) increases monotonously with increasing C as with G' of GFL5, and the increasing ratio of GFL10 is higher than that of GFL5. G' of GFL20 (Fig. 16(a)) increases rapidly with the surface treatment and has a constant value with C higher than 0.5 wt.%. However, in high fiber content region (GFL30, Fig. 16 (b)), G' shows the complex behaviour and has a minimum value. Moreover, the difference by the angular frequency becomes smaller with increasing the fiber content. On the other hand, η' against C curves, in Fig. 17, shows the different dependence on fiber content. η' of GFL5 and GFL20 shows the same tendency as G', and η' of GFL10 and GFL30 has a minimum value. It is found from these results that the storage modulus G', although showing the complex behaviour in high fiber content increases with the ASC concentration C according to fiber content. The dynamic viscosity η' shows the two kinds of tendencies, which increase with increasing C and have a minimum value. Therefore, the effect of ASC concentration on the viscoelastic properties shows the existence of an optimum concentration for systems at each volume fraction of fiber. In addition, these tendencies are similar in a wide range of angular frequency.

3.4 Effect of volume fraction of fiber

In order to clarify the effect of volume fraction of fiber on the viscoelastic properties of surface treated GFL/PP composites in this section, the relationship between the storage

modulus G' and the dynamic viscosity η' and volume fraction of fiber V_f at a typical angular frequency ω (ω =1.257 rad/s) are shown in Fig. 18 as a parameter of ASC concentration. The dependence of G' on V_f changes remarkably with the ASC concentration. G' of untreated GFL/PP composites increases with increasing V_f. On the other hand, G' of treated systems increases monotonously with V_f until it reaches the value of 2 to 5 x 10^6 Pa, and finally levels off at high V_f. This means that the elastic properties of treated GFL/PP composites are more dominant at relatively low contents than that of untreated systems. As with G', η' reaches the value of 2 to 5 x 10^6 Pa. In addition, the degrees of the increase of G' and η' become higher according to the ASC concentration order.

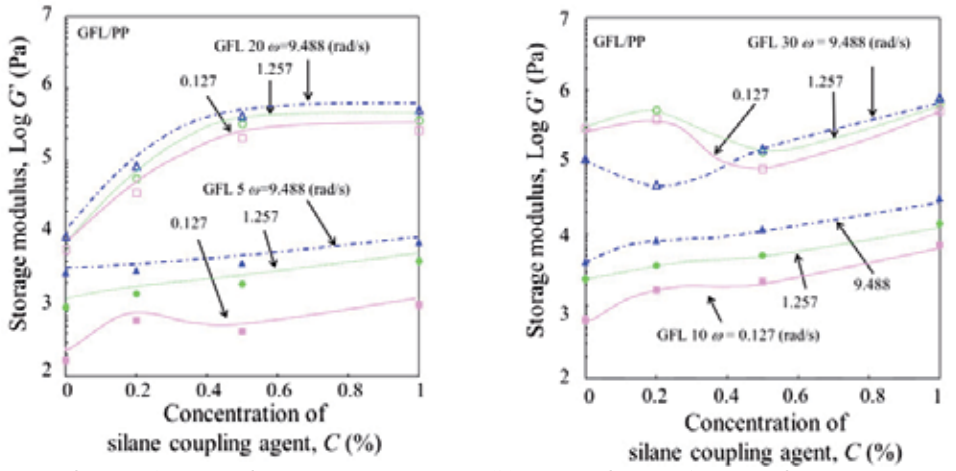

(a) GFL5/PP and GFL20/PP (b) GFL10/PP and GFL30/PP

Fig. 16. Relationship between storage modulus and concentration of aminosilane coupling agent for GFL/PP composites: (a) GFL5/PP and GFL20/PP, (b) GFL10/PP and GFL30/PP

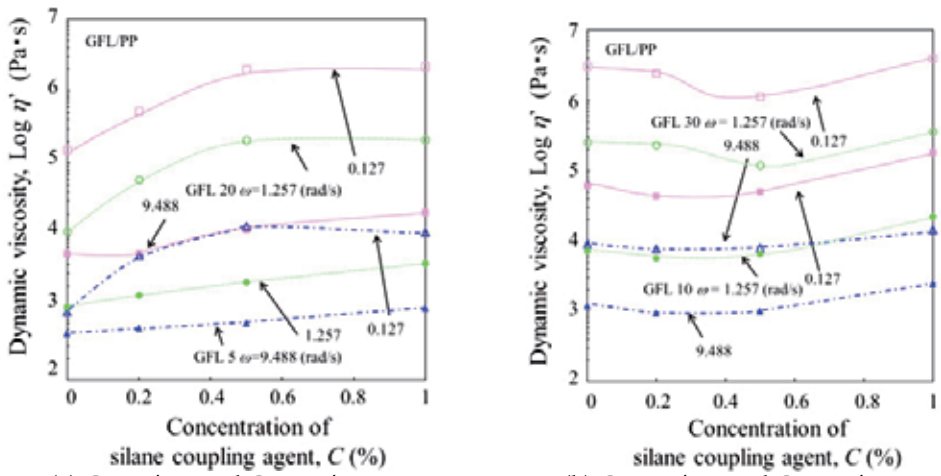

(a) GFL5/PP and GFL20/PP (b) GFL10/PP and GFL30/PP

Fig. 17. Relationship between dynamic viscosity and concentration of aminosilane coupling agent for GFL/PP composites: (a) GFL5/PP and GFL20/PP, (b) GFL10/PP and GFL30/PP

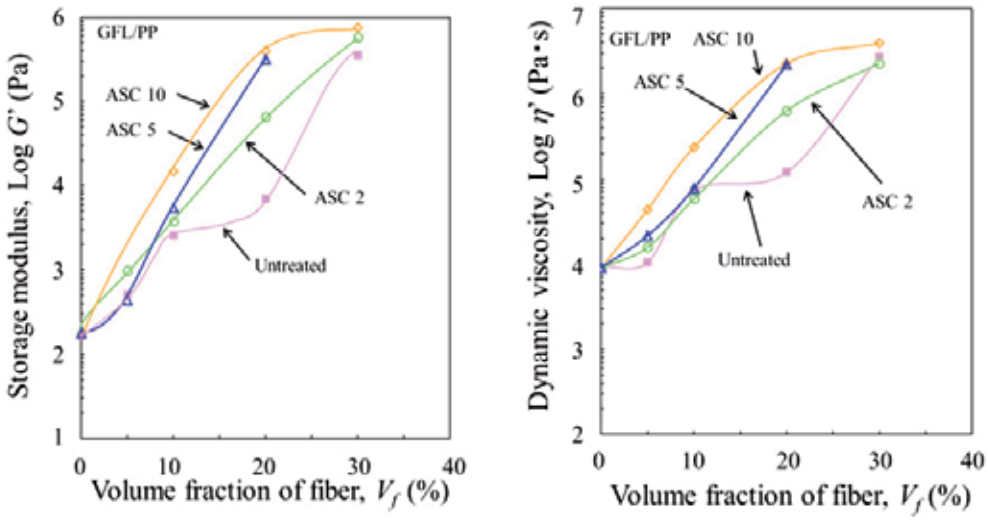

(a) Storage modulus (b) Dynamic viscosity

Fig. 18. Relationship between dynamic viscoelastic properties and volume fraction of fiber for GFL/PP composites at the angular frequency of 1.257 rad/s: (a) storage modulus, (b) dynamic viscosity

3.5 Temperature dependences

The influence of temperature on the viscoelastic properties of surface treated GFL/PP composites will be discussed here. Fig. 19 shows the storage modulus G' (Fig. 19(a)) and the dynamic viscosity η' (Fig. 19(b)) as a function of angular frequency ω as a parameter of temperature T for untreated and surface treated GFL10/PP composites. G' of untreated GFL/PP composites decreases with increasing T. However, G' of ASC10 treated GFL/PP composites corresponds approximately to the measurements at different temperatures. As with G', η' of treated systems at different temperatures are in accord with the one in a wide range of ω. It is found from the results of the measurements at different temperature that the surface treatment decreases the temperature dependence of viscoelastic behaviour, especially of elastic ones, although the untreated systems show the clear temperature dependences. Thus, the difference of processability with different temperatures is minimal by performing the surface treatment by silane coupling agent. These temperature dependences were almost same for the systems with different fiber content although not shown here. Accordingly, it is found from the results that the viscoelastic properties originating in the fiber network formation are dominant in the measuring ω region, the temperature dependences of them are relatively small and also these tendencies become stronger by the surface treatment of long GF.

3.6 Strain amplitude dependences

According to the report of Mutel and Kamal (Mutel & Kamal, 1986), the viscoelastic properties such as the storage modulus G' and the loss modulus G'' of polymer in the

molten state show the strain amplitude dependence if Lissajous figure (torque – shear rate loop) does not draw the perfect (harmonic) ellipse. A strain dependent but harmonic stress region was observed for filled melts in oscillatory shear as well as an non-harmonic stress region at low frequencies and large strain amplitudes. The strain dependent harmonic stress region is thought to be the result of the much longer time scales for the relaxation of fluid compared to the period of oscillations. In our experimental data in this section, the Lissajous figures almost draw the perfect ellipses.

To more clarify the effect of strain amplitude dependence on the viscoelastic properties of surface treated GFL/PP composites, the influence of the oscillatory angle Θ or strain amplitude on the storage modulus G' and the dynamic viscosity η' of untreated and treated GFL/PP composites at different angular frequencies ω is shown in Figs. 20, 21, 22 and 23. The strain amplitude was chosen to be 4.4, 8.7 and 17.5 % (which is corresponding to oscillatory angle of 0.5, 1.0 and 2.0°, respectively). Here, all the data were calculated by assuming the linearity was maintained. Although the effect of surface treatment on the strain amplitude dependences does not remarkably appear, G' decreases with increasing the strain amplitude and also with increasing V_f. And the degree of decrease of G' decreases with increasing the angular frequency. Thus, the smaller the angular frequency is, the higher the strain amplitude dependence for G' is in the same strain amplitude. The strain amplitude dependence of dynamic viscosity η' has the same tendency as that of G' although its dependence of η' is smaller than that of G'.

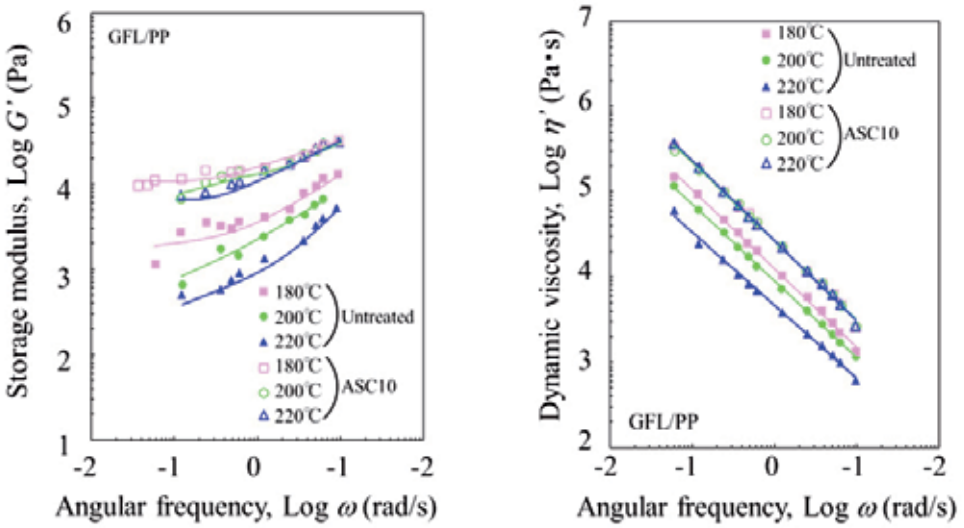

(a) Storage modulus (b) Dynamic viscosity

Fig. 19. Influence of temperature on dynamic viscoelastic properties for GFL/PP composites: (a) storage modulus, (b) dynamic viscosity

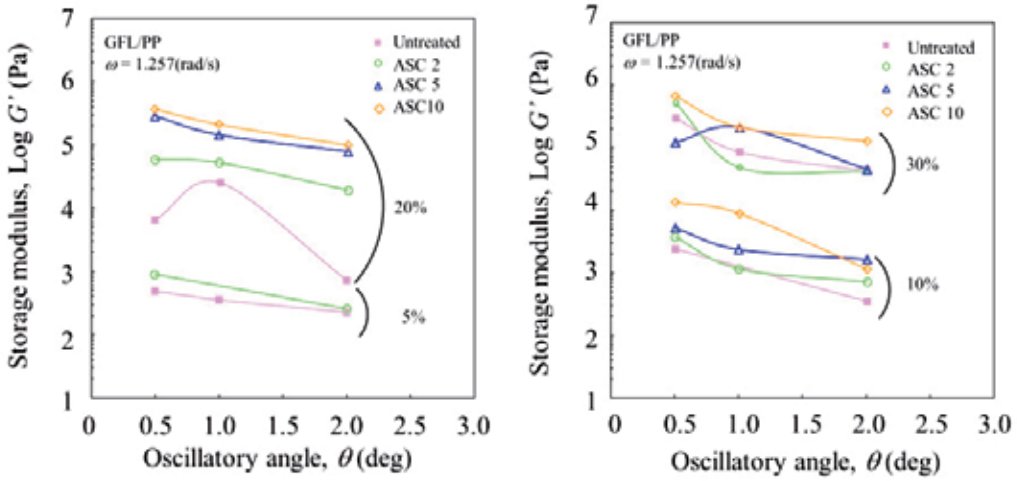

(a) GFL5/PP and GFL20/PP (b) GFL10/PP and GFL30/PP

Fig. 20. Influence of oscillatory angle (strain amplitude) on storage modulus for GFL/PP composites at the angular frequency of 1.257 rad/s; (a) GFL5/PP and GFL20, (b) GFL10/PP and GFL30/PP

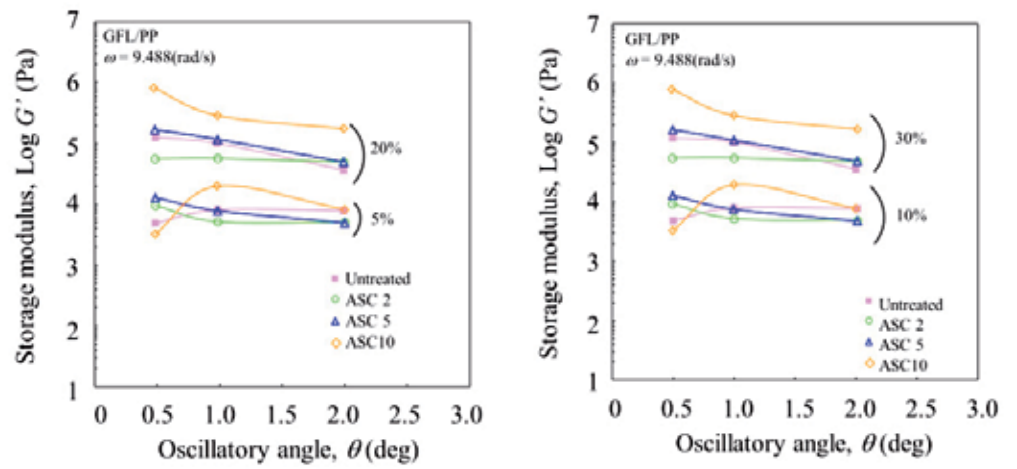

(a) GFL5/PP and GFL20/PP (b) GFL10/PP and GFL30/PP

Fig. 21. Influence of oscillatory angle (strain amplitude) on storage modulus for GFL/PP composites at the angular frequency of 9.488 rad/s; (a) GFL5/PP and GFL20, (b) GFL10/PP and GFL30/PP

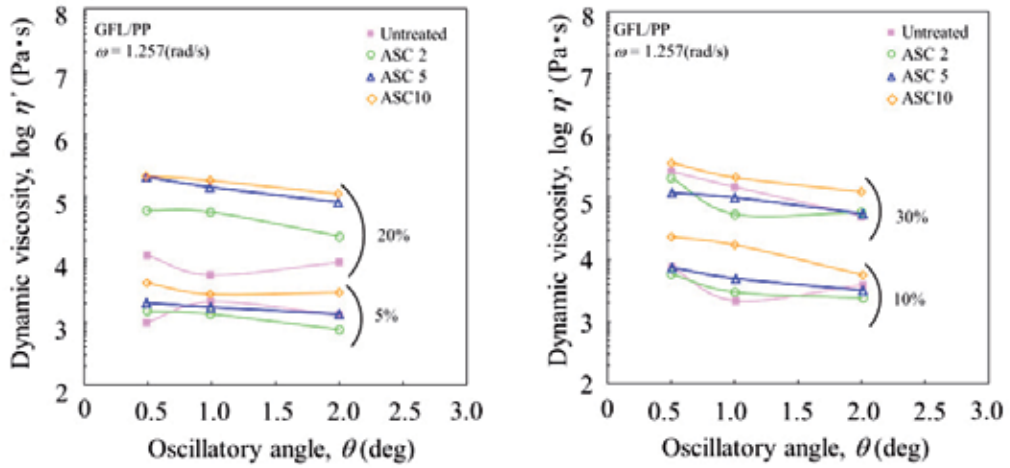

(a) GFL5/PP and GFL20/PP (b) GFL10/PP and GFL30/PP

Fig. 22. Influence of oscillatory angle (strain amplitude) on dynamic viscosity for GFL/PP composites at the angular frequency of 1.257 rad/s; (a) GFL5/PP and GFL20, (b) GFL10/PP and GFL30/PP

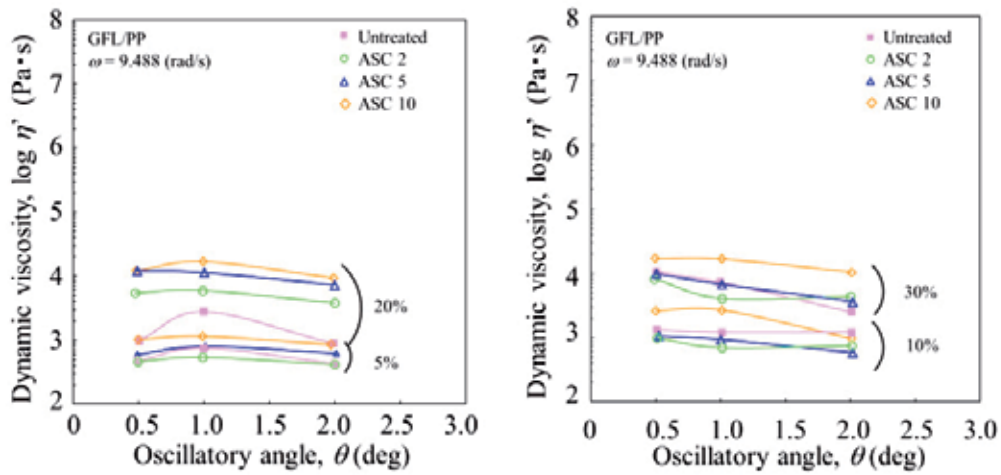

(a) GFL5/PP and GFL20/PP (b) GFL10/PP and GFL30/PP

Fig. 23. Influence of oscillatory angle (strain amplitude) on dynamic viscosity for GFL/PP composites at the angular frequency of 9.488 rad/s; (a) GFL5/PP and GFL20, (b) GFL10/PP and GFL30/PP

4. Conclusion

This chapter discusses the rheological properties of surface treated short and long glass fiber reinforced polypropylene composites in molten state. Glass fibers were surface-treated by silane coupling agent.

The first part deals with the effect of surface treatment on the rheological properties of 20 and 40 wt.% short glass fiber reinforced polypropylenes (GF/PP) and of the same composites containing maleic anhydride modified polypropylene (GF/mPP/PP). These GF/PP and GF/mPP/PP composites were extruded by an extruder specially designed for mixing. Steady state shear and dynamic viscoelastic properties in the molten state were measured using a cone plate typed rheometer. Surface treatment increased the rheological properties of the molten composites. This trend was more pronounced for composites containing modified PP (mPP). In the case of the GF/PP composites the increase was monotonous for all measured functions, while in the case of the GF/mPP/PP ones, the parameters representing elasticity showed peaks at 0.5wt.% aminosilane coupling agent(ASC, γ-aminopropyltrimethoxysilane). The Cox-Merz empirical law was found to be applicable to untreated GF/PP and GF/mPP/PP composites at low shear rates (or angular frequencies), where the materials showed the Newtonian plateau. As for ASC surface treated composites, GF/mPP/PP followed the same trend. On the other hand, GF/PP exhibited a higher complex viscosity than the steady state shear one over the whole range of angular frequencies (shear rates) covered by the experiments Surface treatment enhanced apparent yield stress, as did with increasing the glass fiber content. The effect of the latter was more pronounced in the case of the GF/mPP/PP series. The viscosities of the re-mixed composites became lower than those of the original ones, and the difference between untreated and ASC treated systems was detectable only in the case of the complex viscosity of the GF/mPP/PP composites.

The second part deals with the influence of surface treatment on the rheological behaviour of long glass fiber reinforced polypropylene melts (GFL/PP). Surface treatment by different kinds of silane coupling agents (aminosilane, diaminosilane, epoxysilane and acrylsilane) with different concentrations was performed on glass fibers. Glass fiber and polypropylene fiber mixed mats were prepared by a mixing machine which is called “Fiber separating/ flying machine” and then compression molded. Rheological properties on a rotational parallel plate rheometer were evaluated. Dynamic viscoelastic properties are discussed in terms of various factors: angular frequency, concentration of silane coupling agent, various kinds of silane coupling agents, volume fraction of fiber, temperature and strain amplitude. Surface treatment was shown to increase storage modulus and also reduce the peak of loss tangent, which means that the adhesion between the polymer matrix and the fibers is improved. Dynamic viscosity, however, was changed by the concentration of silane coupling agent. This is because the coupling agent acts to couple the fiber to the polymer matrix, as a wetting agent or as an internal lubricant. Diaminosilane coupling agent was the most effective of the various silane systems for enhancement of rheological behaviour. The dependence of the viscoelastic properties on the concentration of silane coupling agent showed the existence of an optimum concentration for systems at each volume fraction of fiber from the point of view of the processing of these composites. From the results of the measurement at different temperatures and strain amplitude, it was found that surface treatments decrease the temperature dependence of rheological behaviour, and that the dependence of viscoelastic properties on strain amplitude was minimal.

5. Acknowledgment

The authors would thank Nippon Glass Fiber Co. Ltd. for donating the glass fiber for this study. This research is a part of results of research in GF/PP composites research group of

workshop on interfacial scientific of composite material. We would like to thank the BERC and the Ogasawara Foundation for the Promotion of Science & Engineering for founding this study. A part of this study was financially supported by the grant from Kogakuin University. This article was also created with support of Operational Programme Research and Development for Innovations co-funded by the European Regional Development Fund (ERDF) and national budget of Czech Republic, within the framework of project Centre of Polymer Systems (reg. number: CZ.1.05/2.1.00/03.0111).

6. References

Ausias, G.; Agassant, J.F.; Vincent, M.; Lafleur, P.G.; Lavoie, P.A. & Carreau, P.J. (1992). Rheology of Short Glass Fiber Reinforced Polypropylene. *Journal of Rheology*, Vol.36, No.4, pp. 525-542 ISSN 0148-6055

Basu, D.; Banerjee, A.N. & Misra, A. (1992). Comparative Rheological Studies on Jute-Fibre- and Glass-Fibre-Filled Polypropylene Composite Melts. *Journal of Applied Polymer Science*, Vol.46, No.11, pp. 1999-2009 ISSN 0021-8995

Bigg, D.M. (1982). Rheological Analysis of Highly Loaded Polymeric Composites Filled with Non-Agglomerating Spherical Filler Particles. *Polymer Engineering and Science*, Vol.22, No.8, pp. 512-518 ISSN 0032-3888

Boaira, M. S. & Chaffey, C. E. (1997). Effect of Coupling Agents on the Mechanical and Rheological Properties of Mica Reinforced Polypropylene. *Polymer Engineering and Science*, Vol.17, No.10, pp. 715-718 ISSN 0032-3888

Cantwell, W.J.; Tato, W.; Kausch, H.H. & Jacquemet, R. (1992). Influence of a Fiber-matrix Coupling Agent on the Properties of a Glass Fiber/Polypropylene GMT. *Journal of Thermoplastic Composite Materials*, Vol.5, No.4, pp. 304-317 ISSN 0892-7057

Casson, N. (1959) *Rheology of Disperse Systems*, pp. 84-104. Pergamon Press, London

Cox, W.P. & Merz, E.H. (1958). Correlation of Dynamic and Steady Flow Viscosities. *Journal of Polymer Science*, Vol.28, pp.619-622 ISSN 0021-8995

Czarnecki, L. & White, J.L. (1980). Shear Flow Rheological Rroperties, Fiber Damage, and Mastication Characteristics of Aramid-, Glass-, and Cellulose-Fiber-Reinforced Polystyrene Melts. *Journal of Applied Polymer Science*, Vol.25, No.6, pp.1217-1244 ISSN 0021-8995

Davies, P. (1993). Rheological Properties of Stampable Tthermoelastic Composites. *Journal of Thermoplastic Composite Materials*, Vol.6, No.3, pp. 239-254 ISSN 0892-7057

Davis, S.M. & McAlea, K.P. (1990). Stamping Rheology of Glass Mat Reinforced Thermoplastic Composites. *Polymer Composites*, Vol.11, pp. 368-378 ISSN 0272-8397

Dealy, J.M. & Wissbrun, K.F. (1990). *Melt Rheology and Its Role in Plastics Processing*. Springer ISBN 978-0792358862

Fejes-Kozma, Zs. & Karger-Kocsis, J. (1994). Fracture Mechanical Characterization of a Glass Fiber Mat-reinforced Polypropylene by Instrumented Impact Bending. *Journal of Reinforced Plastics and Composites*, Vol.13, No.9, pp. 822-834 ISSN 0731-6844

Ferry, J. D. (1980). *Viscoelastic Properties of Polymers, 3rd Edition*, Wiley Press, ISBN 978-0471048947, New York

Greene, J.P.& Wilkes, J.O. (1995). Steady-State and Dynamic Properties of Concentrated Fiber-Filled Thermoplastics. *Polymer Engineering and Science*, Vol.35, No.21, pp. 1670-1681 ISSN 0032-3888

Groves, D.J. & Stocks, D.M. (1991). Rheology of Thermoplastic-Carbon Fibre Composite in the Elastic and Viscoelastic States. *Composites Manufacturing*, Vol.2, pp.179-184

Groves, D.J.; Bellamy, A.M. & Stocks, D.M. (1992). Anisotropic Rheology of Continuous Fibre Thermoplastic Composites. *Composites*, Vol.23, No.2, pp. 75-80 ISSN 0010-4361

Hamada, H. ; Fujihara, K. & Harada, A. (2000). Influence of Sizing Conditions on Bending Properties of Continuous Glass Fiber Reinforced Polypropylene Composites. *Composites Part A: Applied Science and Manufacturing*, Vol.31, No.9, pp. 979-990 ISSN 1359-835X

Han, C.D. ; Van den Weghe, T. ; Shete, P. & Haw, J.R. (1981). Effects of Coupling Agentes on the Rheological roperties, Processability, and Mechanical Properties of Filled Polypropylene. *Polymer Engineering and Science*, Vol.21, pp. 196-204 ISSN 0032-3888

Hausnerova, B. ; Honkova, N. ; Lengalova, A. ; Kitano, T. & Saha, P. (2006). Rheology and Fiber Degradation during Shear Flow of Carbon-Fiber-Reinforced Polypropylenes. Polymer Science, Ser.A., Vol.48, No.9, pp. 1628-1639 ISSN 0965-545X

Hausnerova, B. ; Honkova, N. ; Lengalova, A. ; Kitano, T. & Saha, P. (2008). Rheological Behavior of Fiber-Filled Polymer Melts at Low Shear Rate, Part 1 Modeling of Rheological Properties. *Polimery*, Vol.53, pp. 507-512 ISSN 0032-2725

Hausnerova, B. ; Honkova, N. ; Lengalova, A. ; Kitano, T. & Saha, P. (2008). Rheological Behavior of Fiber-Filled Polymer Melts at Low Shear Rate, Part 21 Experimental Investigation. *Polimery*, Vol.53, pp. 649-656 ISSN 0032-2725

Hong-Lie, L. ; Han, C. D. & Jovan, M. (1983). Effects of Coupling Agents on the Rheological Behavior and Physical/Mechanical Properties of Filled Nylon 6. *Journal of Applied Polymer Science*, Vol.28, No.11, pp. 3387-3398 ISSN 0021-8995

Kataoka, T. ; Kitano, T. Onishi, S. & Nakama K. (1976) Mixing Effect of Filler and Polymer by an Elastic Extruder. *Rheol. Acta*, Vol.15, pp. 268-270 ISSN 0035-4511

Khan, S.A. & Prud'Homme, R.K. (1987). Melt Rheology of Filled Thermoplastics. *Reviews in Chemical Engineering*, Vol.4, No.3-4, pp. 205-270 ISSN 0167-8299

Kikuchi, S. ; Fujita, Y. ; Sano, K. ; Inoguchi, H. ; Hiragushi, M.& Hamada, H. (1997). The Effect of GF/PP Matrix Interfacial Properties on the Weldline Strength in Short Glass Fiber Reinforced Polypropylene. *Composite Interfaces*, Vol.4, No.6, pp. 367-378 ISSN 0927-6440

Kim, J.K. & Song, J.H. (1997). Rheological Properties and Fiber Orientations of Short Fiber-Reinforced Plastics. *Journal of Rheology*, Vol.41, No.5, pp.1061-1085 ISSN 0148-6055

Kitano, T.; Kataoka, T. & Shirota, T. (1981). An Empirical Equation of the Relative Viscosity of Polymer Melts Filled with Various Inorganic Fillers. *Rheologica Acta*, Vol.20, No.2, pp.207-209 ISSN 0035-4511

Kitano, T. ; Kataoka, T. & Nagatsuka, Y. (1984). Dynamic Flow Properties of Vinylon Fibre and Glass Fiber Reinforced Polyethylene Melts. *Rheologica Acta*, Vol.23, No.4, pp.408-416 ISSN 0035-4511

Kitano, T.; Nagatsuka, Y.; Lee, M.; Kimijima, K & Oyanagi, Y. (1994). A Method for the Production of Randomly Oriented Fiber Reinforced Thermoplastic Composites and Their Mechanical Properties. *Seikei-Kakou (the Journal of Japanese Society of Polymer Processing, in Japanese)*, Vol.6, No.12, pp. 904-915 ISSN 0915-4027

Kitano, T. ; Haghani, E. ; Tanegashima, T. & Saha P. (2000). Mechanical Properties of Glass Fiber/Organic Fiber Mixed Mat Reinforced Thermoplastic Composites. *Polymer Composite*, Vol. 21, No.4, pp. 493-505 ISSN 0272-8397

Laun, H.M. (1984). Orientation Effects and Rheology of Short Glass Fiber-Reinforced Thermoplastics. *Colloid & Polymer Science*, Vol.262, No.4, pp.257-269 ISSN 0303-402X

Lee, N.-J. & Jang, J. (1997). The Use of a Mixed Coupling Agent System to Improve the Performance of Polypropylene-Based Composites Reinforced with Short-Glass-Fibre Mat. *Composites Science and Technology*, Vol.57, No.12, pp. 1559-1569 ISSN 0266-3538

Li, S. ; Järvelä, P.K. & Järvelä, P.A. (1997). A Comparison Between Apparent Viscosity and Dynamic Complex Viscosity for Polypropylene/Maleated Polypropylene Blends. *Polymer Engineering and Science*, Vol.37, No.1, pp. 18-23 ISSN 0032-3888

Mäder, E. ; Jacobasch, H.-J. ; Grundke, K. & Gietzelt, T. (1996). Influence of an Optimized Interphase on the Properties of Polypropylene/Glass Fibre Composites. *Composites Part A: Applied Science and Manufacturing*, Vol.27A No.9, pp. 907-912 ISSN 1359-835X

Mäder, E. ; Moos, E. & Karger-Kocsis, J. (2001). Role of Film Formers in Glass Fibre Reinforced Polypropylene - New Insights and Relation to Mechanical Properties. *Composites Part A: Applied Science and Manufacturing*, Vol.32, No.5, pp. 631-639 ISSN 1359-835X

Mutel, A.T. & Kamal, M.R. (1986). Characterization of the Rheological Behavior of Fiber-Filled Polypropylene Melts under Steady and Oscillatory Shear using Cone-and-Plate and Rotational Parallel Plate Rheometry. Polymer Composites, Vol.7, No.5, pp. 283-294 ISSN0272-8397

Nishitani, Y. ; Sekiguchi, I. ; Nakamura, K. ; Nagatsuka Y. & Kitano, T. (1998). Fabrication of Glass Fiber Reinforced Polypropylenes and their Physical Properties : 1. Influence of Surface Treatment of the Mechanical Properties. *Seikei-Kakou (the Journal of Japanese Society of Polymer Processing, in Japanese)*, Vol.10, No.2, pp. 129-138 ISSN 0915-4027

Nishitani, Y. ; Sekiguchi, I. ; Nakamura, K. ; Nagatsuka Y. & Kitano, T. (1998). Fabrication of Glass Fiber Reinforced Polypropylenes and their Physical Properties : 2. Influence of Surface Treatment of the Rheological Properties in Molten State. *Seikei-Kakou (the Journal of Japanese Society of Polymer Processing, in Japanese)*, Vol.10, No.2, pp. 139-148 ISSN 0915-4027

Nishitani, Y. ; Kitano, T. ; Nagatsuka, Y. ; Nakamura, K. & Sekiguchi, I. (1998). Influence of Surface Treatment on the Mechanical Properties of Short Glass Fiber Reinforced Polypropylenes and their Viscoelastic Properties in Molten State.. *Reserch Report of Kogakuin University (in Japanese)*, Vol.84, pp. 11-20 ISSN 0368-5098

Nishitani, Y. ; Sekiguchi, I. ; Nakamura, K. ; Tai, N. ; Nagatsuka Y. & Kitano, T. (1998). Influence of Fiber Length on the Mechanical Properties for Glass Fiber Reinforced Polypropylenes. *Kyouka Plastics (the Journal of Japan Reinforced Platics Society, in Japanese)*, Vol.44, No.5, pp. 197-203 ISSN 0452-9685

Nishitani, Y. ; Sekiguchi, I. ; Yoshimitsu, Y. ; Tahira, K. ; Saha, P. ; Nagatsuka Y. & Kitano, T. (1999). Long Glass Fibre Reinforced Polypropylenes : Fabrication and

Mechanical Properties. *Polymers & Polymer Composites*, Vol.7, No.3, pp. 205-215 ISSN 0967-3911

Nishitani, Y. ; Sekiguchi, I. ; Hausnerova, B. ; Nagatsuka Y. & Kitano, T. (2001). Dynamic Viscoelastic Properties of Long Organic Fibre Reinforced Polypropylene in Molten State. *Polymers & Polymer Composites*, Vol.9, No.3, pp. 199-211 ISSN 0967-3911

Nishitani, Y. ; Sekiguchi, I. ; Hausnerova, B. ; Zdrazilova, N. & Kitano, T. (2007). Rheological Properties of Aminosilane Surface Treated Short Glass Fibre Reinforced Polypropylenes. Part 1 : Steady Shear and Oscillatory Flow Properties in Molten State. *Polymers & Polymer Composites*, Vol.15, pp. 111-119 ISSN 0967-3911

Nishitani, Y. ; Ohashi, K. ; Sekiguchi, I. ; Ishii, C. & Kitano, T. (2010). Influence of Additon of Styrene-Ethylene/Butylene-Styrene Copolymer on Rheological, Mechanical and Tribological Properties of Polyamide Nanocomposites. *Polymer Composites*, Vol.31, No.1, pp. 68-76 ISSN 0272-8397

Nishitani, Y. ; Yamada, Y. ; Sekiguchi, I. ; Ishii, C. & Kitano, T. (2010). Effects of Addition of Functionalized SEBS on Rheological, Mechanical, and Tribological Properties of Polyamide 6 Nanocomposites. *Polymer Engineering and Science*, Vol.50, No.1, pp. 100-112 ISSN 0032-3888

Nishitani, Y. ; Sekiguchi, I. & Kitano, T. (2010). Rheological Properties of Various Carbon Fibers Filled PBT Composites. *Proceedings of the Polymer Processing Society 26th Annual Meeting –PPS-26-*, R01-134, Banff, Canada, July 4-8, 2010

Peltonen, P. ; Pääkkönen, E.J. ; Järvelä, P.K. & Törmälä, P. (1995). The Influence of Adhesion Promoters on the Properties of Injection Moulded Long-Glass-Fibre Polypropylene. *Plastics, Rubber and Composites Processing and Applications*, Vol.23, pp. 111-126 ISSN 0959-8111

Saini, D.R. ; Shenoy, A.V. & Nadkarni, V.M. (1985). Effect of Surface Treatments on Rheological, Mechanical and Magnetic Properties of Ferrite-Filled Polymeric Systems. *Polymer Engineering and Science*, Vol.25 , No.13, pp. 807-811 ISSN 0032-3888

Sasagi, I. & Ide, F. (1981). Effect of Grafting of Unsaturated Carboxylic Acid on Glassfiber-Reinforced Polypropylene. *Koubunshi Ronbunshu (the Journal of the society of Polymer Science, Japan, in Japanese)*, Vol.38, No.2, pp. 67-74 ISSN 0386-2186

Shenoy, A. V. (1999). *Rheology of Filled Polymer Systems*, Kluwer Academic Publishers, ISBN 0-412-83100-7, Dordrecht, The Netherlands

Thomason, J.L. & Schoolenberg, G.E. (1994). An Investigation of Glass Fibre/Polypropylene Interface Strength and its Effect on Composite Properties. *Composites*, Vol.25, No.3, pp. 197-203 ISSN 0010-4361

Thomason, J.L. & Vlug, M.A. (1996). Influence of Fibre Length and Concentration on the Properties of Glass Fibre-reinforced Polypropylene: 1. Tensile and Flexural Modulus. *Composites Part A: Applied Science and Manufacturing*, Vol.27, No.6, pp. 477-484 ISSN 1359-835X

Van Den Oever, M. & Peijs, T. (1998). Continuous-Glass-Fibre-Reinforced Polypropylene Composites II. Influence of Maleic-Anhydride Modified Polypropylene on Fatigue Behaviour. *Composites Part A: Applied Science and Manufacturing*, Vol.29, No.3, pp. 227-239 ISSN 1359-835X

Wu, H.F.; Dwight, D.W. & Huff, N.T., (1997) Effects of Silane Coupling Agents on the Interphase and Performance of Glass-fiber-reinforced Polymer Composites, *Composites Science and Technology*, Vol.57, No.8, pp. 975-983 ISSN 0266-3538

Yue, C.Y. & Quek, M.Y. (1994). The Interfacial Properties of Fibrous Composites - Part III Effect of the Thickness of the Silane Coupling Agent. *Journal of Materials Science*, Vol.29, No.9, pp. 2487-2490 ISSN 0022-2461

Zang, Z. ; Kitano, T. & Hatakeyama, T. (1995). Crystallization Behavior of Carbon Fiber Reinforced Polyamides: 1. Dynamic and Isothermal Crystallization. *International Polymer Processing*, Vol.10, No.2, pp. 165-171 ISSN 0930-777X

16

Composites Made of Polypropylene Nonwoven Fabric with Plasmas Layers

Maciej Jaroszewski, Janina Pospieszna, Jan Ziaja and Mariusz Ozimek
Wrocław University of Technology, Institute of Electrical Engineering Fundamentals
Poland

1. Introduction

Engineering of materials used for shielding from electromagnetic fields is currently one of the most extensively developing field of applications of composite materials (Bula et al., 2006; Jaroszewski & Ziaja, 2010; Koprowska et al., 2004, 2008; Sarto et al. 2003, 2005; Wei et al., 2006; Ziaja et al., 2008, 2009, 2010). The choice of suitable materials for the shields and their appropriate arrangement have an essential meaning. Development of lightweight and resistant to environmental exposure shielding materials is possible by using substrates of polypropylene and plasma technology (Ziaja&Jaroszewski, 2011).

The shields for suppression of electric field were made in the form of composites of polypropylene unwoven fabrics with deposited plasma layers. Additional advantage of the application of the method is the possibility of plasma cleaning of a fabric surface and modifying its surface properties. The unique properties of pulse plasma make possible to obtain metallic and dielectric coatings on polypropylene fabrics, which are not achievable by standard methods. The coatings are characterized by a good adhesion to the substrates.

The surface of the samples was examined in two ways: by metallurgical microscope Nikon MA200 and scanning microscope Quanta 200 in the low vacuum mode. To identify the structure of the obtained layers the X-Ray radiography was used. Additionally properties of the composites was studied using impedance spectroscopy. The method of impedance spectroscopy allows one to connect the measured frequency characteristics with the physical structure of tested material and the alternations in the structure. This method has been used by the authors to determine the properties of plasma layers deposited on a polypropylene nonwoven fabric (Jaroszewski et al., 2010a; Pospieszna et al., 2010; Pospieszna et al., 2010b).

2. Polypropylene nonwoven fabric with plasma layers in EM technique

Polypropylene materials (PP), because of their electric properties (such as surface resistivity ρ_s, volume resistivity ρ_v, dielectric loss factor tgδ, permittivity ε), mechanical properties and resistance to noxious agents (resistance to acids, bases, salts and organic solvents) are used in various industries. Polypropylene materials characterise, also, with the lowest specific density among widely used polymers. Those properties predispose polypropylene to be used as a substrate for composite protective screens shielding people and electric or electronic devices against noxious activity of electromagnetic (EM) fields. Composite shields

are fabricated through metallizing film surfaces or PP nonwoven fabric. Metallic layer thickness does not exceed several micrometres. One or several types of metal as well as conductive metal oxides can make up a metallic layer. Due to their lightness and mechanical strength, those composites are an alternative to classic EM field shielding materials.

Due to characteristic surface properties, PP is a very difficult material to metallize. Ideal for that purpose is the magnetron sputtering method described in papers (Ziaja&Jaroszewski, 2011; Ziaja et al., 2010; Ziaja et al., 2008). Obtained coefficients of shielding effectiveness (SE) of popular composites based on PP/Me matrixes exceed up to 60dB (Me=Zn SE exceeds 60 dB, Me=Cu SE approx. 35 dB, Ti approx. 30 dB).

SE does not depend solely on type of material and its surface and volume resistivity, but also on fabrication (crystal structure) of applied layers. Crucial for SE value is not only the number and resistivity of conductive bridges forming on nonwoven fabrics' surface, but also the specific surface area of applied layers. The more expanded the surface the higher the SE value. Therefore, in order to evaluate those composites' suitability for electromagnetic field shielding screens – apart from electric properties – surface morphology of applied layers has to be known.

3. Morphology of PP plasma composites

As means to determine crystal structure of layers, x-ray diffraction method was used. Surface morphologies and chemical composition was determined by a scanning microscope equipped with an x-ray microprobe.

Phase composition of samples was analysed by means of x-ray examination carried out on DRON-2 diffractometer producing Fe filtered Co radiation of λ= 1.7902 Å wavelength. Scanning was carried out according to the wide angle x-ray scattering method at $\Delta 2\Theta = 0.05^{o}$ spread with scattering angle $2\Theta = (40 \div 65^{o})$. Diffraction patterns were analysed by the Xrayan programme through comparison of interplanar d-spacing of reflection intensity I to PDF files data.

Morphology analysis of PP/Me composites' surface was carried out using the VEGA/SBH scanning electron microscope manufactured by TESCAN. The microscope is intended for scanning conductive samples in a high-vacuum chamber. At 30kV voltage the maximum resolution is 3.0 nm. Magnification ranges between 6-1000 000 times at specimen current from 1pA to 2uA. The electron optical column is composed of four lenses enabling smooth system configuration and scanning at an optimum resolution. The microscope is additionally equipped with an EDS system attachment [scattered electrons energy analysis] INCA PENTAFTx3 of 133 eV resolution. One of system parts is an analyser enabling point to line analysis of samples' chemical composition.

Structural and electric properties of PP/Me composites depend on magnetron sputtering process parameters (current density at sputtered electrode, pressure and composition of working gases, distance between nonwoven fabric and the target, deposition rate). By changing those parameters, chemical composition and structure of deposited layers can be manipulated, thus their electrical parameters can be modified. Usually, layer thickness is adjusted by changing gun power or deposition rate. X-ray radiography examination of layers deposited at the same rate, but at increasing power emitted on sputtered electrode are

characterised by increased intensity of characteristic lines. Examples of PP/Zn composites' x-ray spectra were presented in fig. 1. One can note, that at low gun power obtained Zn layers are half-amorphous, indicative of which is lack of Zn-characteristic reflections (fig. 1a). EM field shielding effectiveness is low and does not exceed 10 dB. By increasing the power, increased are not only the layers but their crystallisation as well, causing conductive bridges to form (fig. 1b, 1c, 1d). Surface conductivity decreases and coefficient of shielding effectiveness ranges between 10-30dB. Further power increase induces more conductive bridges of expanded specific surface area to form.

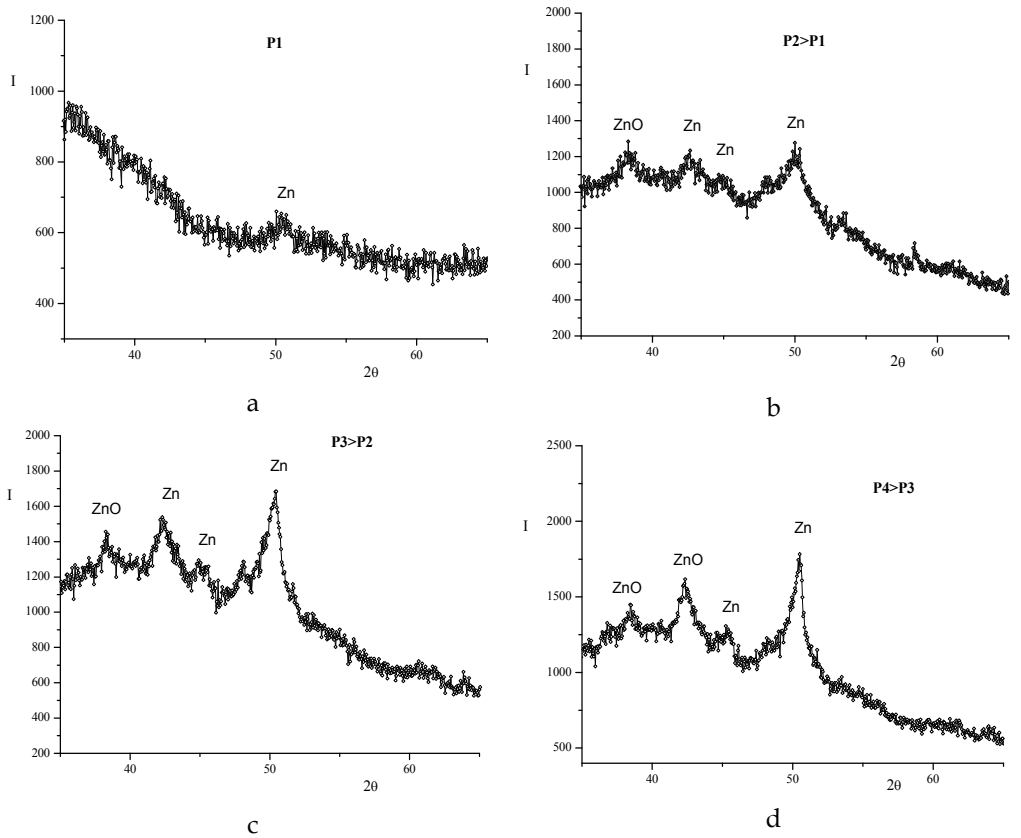

Fig. 1. X-ray radiography spectra of zinc layers deposited on polypropylene nonwoven fabric at different emitted power (P1, P2, P3, P4)

Not only surface fibres are coated with metal (fig 2a), but also the nonwoven fabrics' internal fibres (fig. 2b) and areas between fibres (fig. 2c). Similar crystallization are observable for zinc layers deposited on polypropylene film (fig. 3). A layer obtained in that manner characterises with large specific surface area, which disperses electromagnetic field and increases shielding coefficient SE at the same time. Cross-section of such composite is presented in Fig. 4. It comes to one's attention that metallic layers on fibre surface are solid and uniform. Best composites characterise with SE~ 60 dB, which not only stems from low surface resistivity, but also from expanded surface of metallic layers (fig. 5).

Similar results are observable for other metallic layers, e.g. Al, Ti. Higher layer crystallisation and tighter texture are also notable. Reference book (Ziaja&Jaroszewski, 2011) discusses the method of crystallising Ti layers.

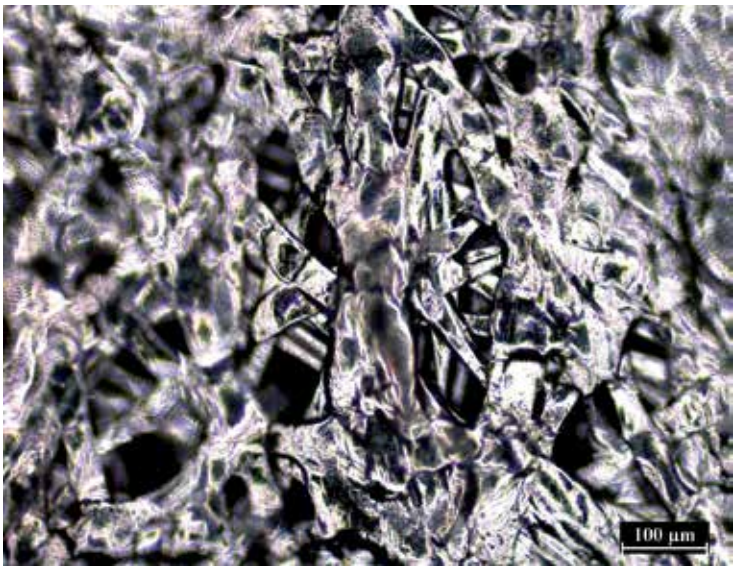

a

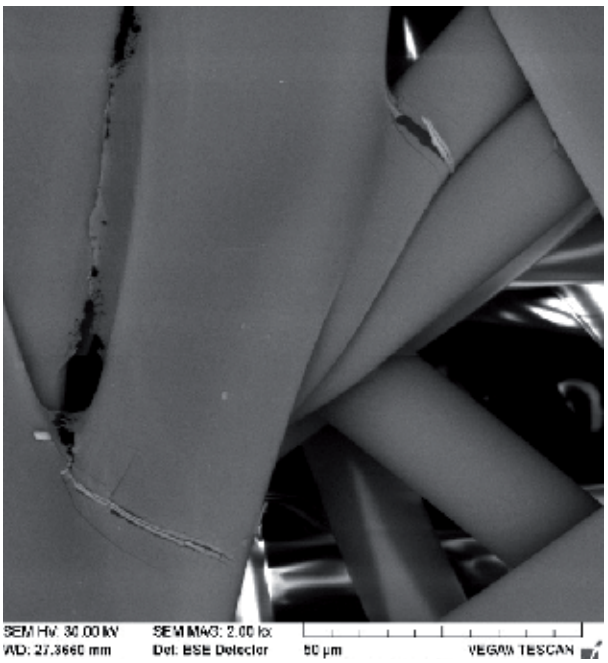

b

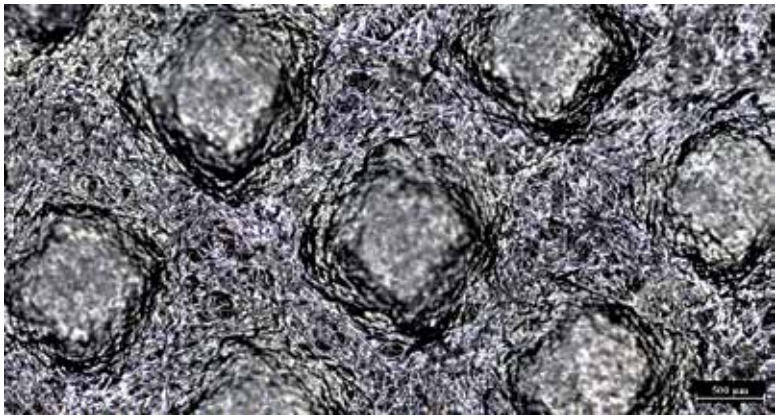

c

Fig. 2. Surface morphology of Zn layers deposited on polypropylene nonwoven fabric PP Film

Layers deposited on PP films display different behaviour. Layers obtained at highest gun powers remain amorphous. At identical layer deposition parameters the materials characterises with higher SE than the nonwoven fabric. It stems from continuous structure of layers deposited on film as opposed to conductive mesh formed on the surface of nonwoven fabrics. As in case of Ni, Fe or AI layers, SE of film is 10 dB higher.

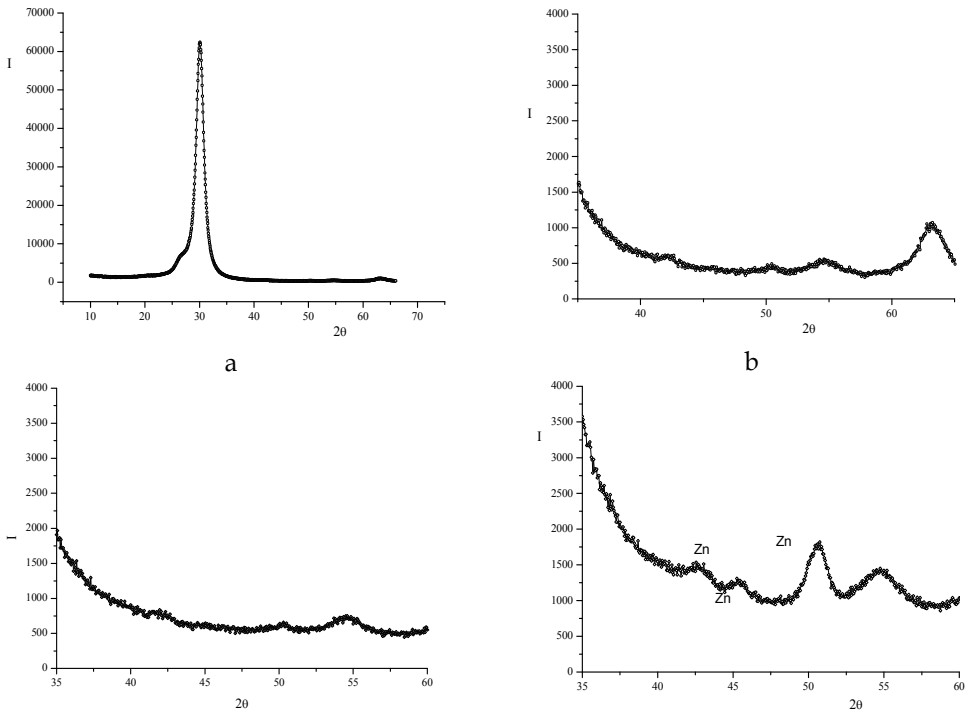

Fig. 3. X-ray radiography spectra of zinc layers deposited on polypropylene film at different emitted current densities

Similar relations in samples' morphology, were noticed by authors in composites with carbon plasma layers deposited on PP nonwoven fabric. They are still, however, characterised by lower SE compared to composites with metallic layers. Likewise promising results of using carbon layers were presented (Wang et al., 2011), where C layers were deposited by silk-screen printing. Presented layers were in form of short and long nanotubes, whose length was critical for SE.

Based on the above-mentioned, nonwoven fabrics with layers are an eligible alternative for classic shielding mats.

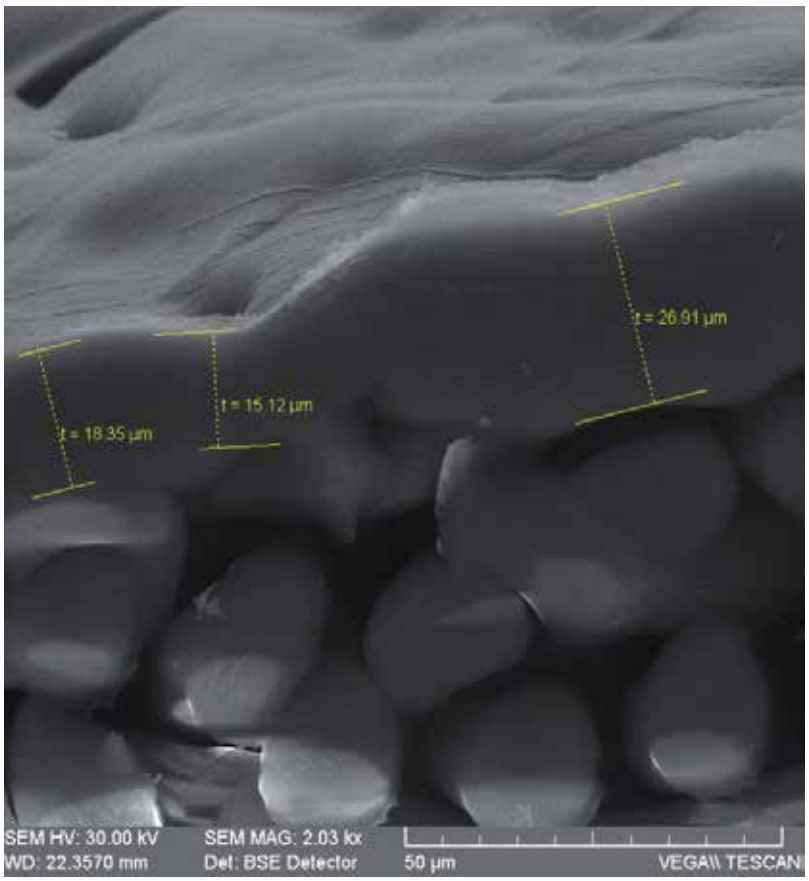

Fig. 4. Cross-section of zinc layers deposited on polypropylene nonwoven fabric

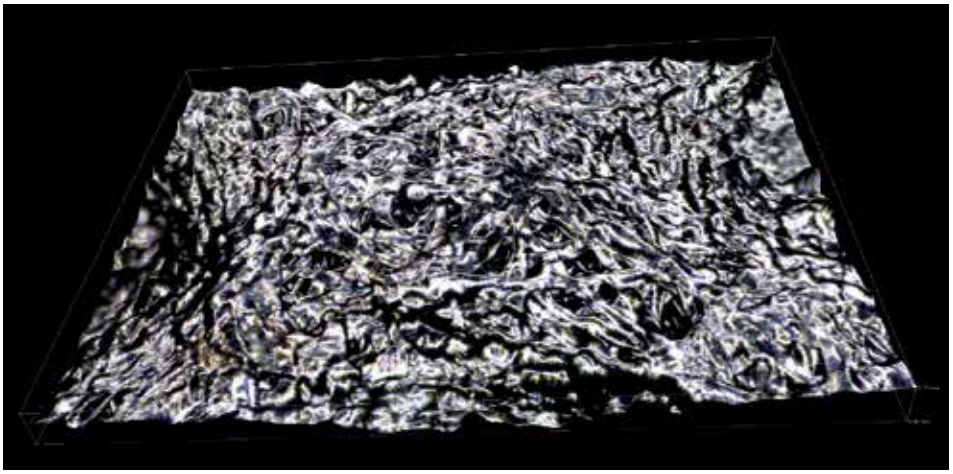

Fig. 5. Expanded surface of metallic layers deposited on polypropylene nonwoven fabric

4. Determination of composites dielectric properties by impedance spectroscopy

Impedance spectroscopy is a modern and exceptionally effective tool for analysing different materials, including complex composites systems. The method draws on measuring linear electric answer of examined material to excitation in form of low amplitude, sinusoidally alternating voltage $u(t) = Um \sin(\omega t + \psi_u)$. The voltage applied to the electrode system, between which examined specimen is placed, induces sinusoidal current $i(t) = Im \sin(\omega t + \psi_i)$ to flow through the sample with effective current I, at phase displacement by angle $\varphi = \psi_u - \psi_i$. Analysing that answer in wide spectrum of frequencies yields useful information on conductivity and polarisation phenomena taking place in the examined material.

In the field of frequencies, spectral transmittance $\underline{H}(\omega)$ is usually used for linear circuits to describe electrical answers. It is defined as a relation of complex responses $\underline{Y}$ and excitation $\underline{X}$ of investigated circuit:

$$H(\omega) = Y / X = Y\, ej\psi y / X\, ej\psi x = Y / X\, e\, j(\psi y - \psi x) = Y / X\, e\, j\, \varphi \tag{1}$$

where $\psi_y - \psi_x = \varphi$.
Its module

$$\left|\underline{H}(\omega)\right| = Y/X \tag{2}$$

and argument

$$\varphi = \varphi(\omega) = \arg \underline{H}(\omega) \tag{3}$$

are known as amplitude and phase characteristic of spectral transmittance.

In impedance spectroscopy, spectral transmittance $\underline{H}(\omega)$ usually has a form of either complex impedance $\underline{Z}(\omega)$ or complex admittance $\underline{Y}(\omega)$.

For a given two-terminal network, complex impedance is defined as relation of complex voltage $\underline{U}$ values and that voltage-induced current $\underline{I}$:

$$\underline{Z}(\omega) = \frac{\underline{U}(\omega)}{\underline{I}(\omega)} = \left|Z(\omega)\right| e^{j\varphi(\omega)} \tag{4}$$

$$\underline{Z}(\omega) = \mathrm{Re}\,\underline{Z} + \mathrm{Im}\,\underline{Z} = R + jX \tag{5}$$

where Re(Z) and Im (Z) are real and imaginary parts of complex impedance (resistance R and reactance X).

Expression describing complex admittance becomes:

$$\underline{Y}(\omega) = \frac{1}{\underline{Z}(\omega)} = \frac{\underline{I}(\omega)}{\underline{U}(\omega)} = \left|\underline{Y}(\omega)\right| e^{-j\varphi(\omega)} \tag{6}$$

$$\underline{Y}(\omega) = \mathrm{Re}\,\underline{Y} + \mathrm{Im}\,\underline{Y} = G + jB \tag{7}$$

where Re(Y) and Im(Y) are real and imaginary part of complex admittance (conductance G and susceptance B).

In practice, the examined sample can be assigned with an equivalent electrical model in form of either parallel or serial connection of resistor and capacitor (Fig. 6), which can be specified by relevant real and imaginary parts of investigated transmittance (admittance and impedance). Assumed model enables to separate active and passive current parts, in case of parallel equivalent of the sample (Fig. 6a) and voltage – in case of serial model (Fig. 6b).

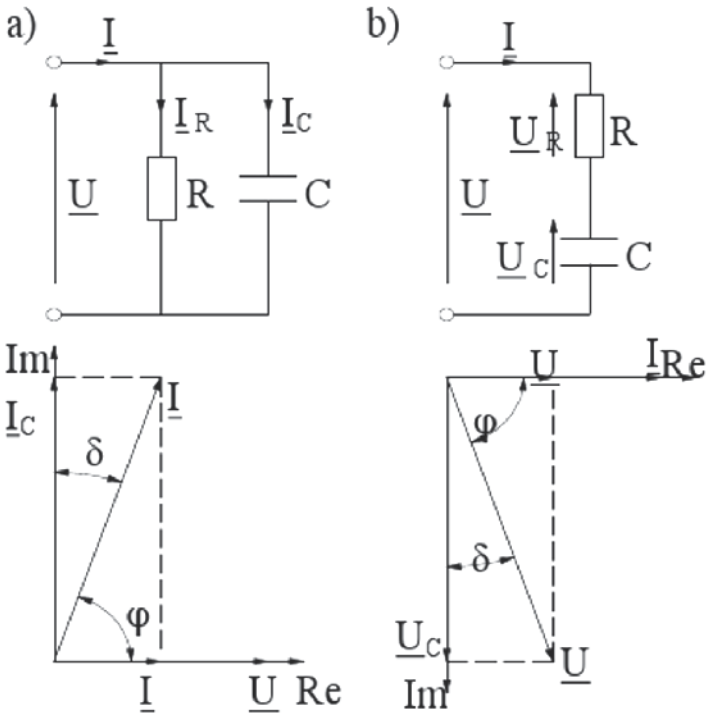

Fig. 6. Capacitor equivalent circuit with real dielectric phase vectors: a) parallel circuit, b) serial circuit.

In equivalent electrical model in form of parallel connection of resistance R resistor and ideal capacitor of C capacity, the active current part $I_R = U / R$ (U voltage phase) and passive $I_C = j\,\omega\,C\,U$ (voltage lags the current by $\pi/2$ phase) represent leakage current and capacitor charging current respectively. Complex admittance measured for that circuit can be represented by:

$$\underline{Y}(\omega) = \underline{I}(\omega) / \underline{U}(\omega) = (\underline{I_R} + \underline{I_C}) / \underline{U} = 1 / R_p + j\,\omega\,C_p = \\ = G_p + j\,\omega\,C_p = j\,\omega\,(C_p + G_p / j\,\omega) = j\,\omega\,(C' - j\,C'') = j\,\omega\,\underline{C} \tag{8}$$

where

$$\underline{C}(\omega) = (C' - j\,C'') = \underline{Y}(\omega) / j\,\omega \tag{9}$$

are defined as complex capacity and C′ and C″ are its real and imaginary parts respectively.

Complex material parameters can be determined using impedance measurement of simple test structures of given electrode geometry and dimensions of specimen (distance d and electrode surface S) and equivalent complex admittance circuit. Such material parameter is complex conductivity σ (ω), which is obtained by multiplying two-terminal network's complex admittance expression by the d/S parameter:

$$d / S\ (G_p + j\,\omega\,\underline{C_p}) = \sigma' + j\,\omega\,\varepsilon_o\,\varepsilon_r = \sigma'(\omega) + j\,\sigma''(\omega) = \underline{\sigma}(\omega) \tag{10}$$

where:

σ′ – material conductivity,
ε_0 – vacuum permittivity,
ε_r – relative permittivity of the material,
Its real and imaginary parts are σ′ and σ″ respectively.

Introduction of complex capacity C requires introduction of the notion of complex relative permittivity ε, to which it is proportionate by definition:

$$\underline{C}(\omega) = C_o\,\underline{\varepsilon} = C_o\,(\varepsilon' - j\,\varepsilon'') \tag{11}$$

where: C_o – geometric capacitance of the electrode system, real part ε′ and imaginary part ε″ of complex permittivity ε determine storage capacity and energy diffusive power respectively, however, energy losses are connected both to polarisation and insulation leakage current.

The measure of lag between dielectric polarisation and changes in electric field is the dielectric loss factor defined as:

$$tg\delta = \frac{I_R}{I_C} = \frac{1}{\omega RC} = \frac{\varepsilon''}{\varepsilon'} \tag{12}$$

where the angle δ is the cofactor of phase displacement φ to 90^O.

Obtained through measurements quantities: impedance Z(ω) and admittance Y(ω) can be adopted as basic values enabling further processing of results of measurements in order to give an adequate account of given material properties which are of interest to us.

When research results are subject to interpretation through impedance spectroscopy, one has to bear in mind, that measured quantities are a measure of analysed system's properties, which is composed of electrodes and located between them material. Hence, the measured quantities give a picture of the entire circuit in sinsuidally alternating electric field, including lead resistance and inductance, stray capacitance and phenomena related to electrode polarisation.

Dielectric response of the composite non-woven PP / plasma layer is a function of both the physical structure of substrate and applied layer. So far, studies carried out by impedance spectroscopy allowed us to:

- identify the degree of porosity of the substrate on which the plasma layer was applied(Jaroszewski et al., 2010),
- determine the effect of surface resistivity of the composite relaxation processes(Pospieszna et al., 2010, Pospieszna & Jaroszewski, 2010),
- identify the strong dependence of dielectric composite properties upon a number of formed metal/metal-oxide layers (Ziaja&Jaroszewski, 2011).

5. Conclusions

Polypropylene in form of nonwoven fabric is promising material for EM shield composites. However, the use of this material is dependent on the possibility to cover it with another material exhibit conductive properties. This is possible only by using magnetron techniques.

The processes of formation of conductive bridges at the nonwoven fabric surface and on the fibres inside are critical to the screening factor. These processes can be examined both by analysing the surface morphology and dielectric properties.

6. Acknowledgment

This publication was prepared with the key project – POIG no. 01.03.01-00-006/08 co-financed from the founds of European Regional Development Found within the framework of the Operational Programme Innovative Economy.

7. References

Bula K., Koprowska J., Janukiewicz J. (2006). Application of Cathode Sputtering for Obtaining Ultra-thin Metallic Coatings on Textile Products, Fibres & Textiles in EE, Vol. 14, No. 5 (59) (2006) pp.75 – 79

Jaroszewski M., Ziaja J. (2010). Zinck-unvowen fabric composite obtained by magnetron sputtering, Proceedings of Twelfth International Conference on Plasma Surface Engineering; September 13 - 17, 2010, PSE 2010, Garmisch-Partenkirchen, Germany, PSE 2010

Jaroszewski M., Pospieszna J., Ziaja J. (2010). Dielectric properties of polypropylene fabrics with carbon plasma coatings for applications in the technique of

electromagnetic field shielding, J. Non-Cryst. Solids, Volume 356, Issues 11-17, 2010, 625-628

Koprowska J., Ziaja J., Janukiewicz J. (2008). Plasma Metallization Textiles as Shields for Electromagnetic Fields, EMC Europe 2008, Hamburg, Germany, September 8-12, 2008, pp. 493-496

Koprowska J., Pietranik M., Stawski W. (2004). New Type of Textiles with Shielding Properties, Fibres &Textiles in Eastern Europe, vol. 12, (2004), n.3 (47), 39-42

Pospieszna J., Jaroszewski M., Bretuj W., Tchórzewski M. (2010a). Influence of surface and volume electrical resistivity on dielectric properties of carbon-polypropylene fabric composite obtained by plasma deposition, Electrotech. Rev. 2010, R. 86, nr 5, pp. 275-278

Pospieszna J., Jaroszewski M., Szafran G. (2010b). Influence of substratum on dielectric properties of plasma carbon films, Electrotech. Rev. 2010, R. 86, nr 11b/2010, pp. 308-310

Sarto F., Sarto M.S., Larciprete M.C., Sibilia C. (2003). Transparent films for electromagnetic shielding of plastics, Rev. Adv. Mater. Sci., (2003), n.5, 329-336

Sarto M. S., Li Voti R., Sarto F., Larciprete M. C. (2005). Nanolayered Lightweight Flexible Shields with Multidirectional Optical Transparency, IEEE Trans. on EMC, vol. 47, No 3, (2005) pp.602- 611

Wang L.B., See K.Y., Zhang J.W., Salam B., Lu A.C.W. (2011). Ultrathin and flexible screen-printed metasurfaces for EMI shielding applications, IEEE Transactions on Electromagnetic Compatibility, Vol. 53, No. 3, August 2011, pp. 700-704

Wei Q. F., Xu W. Z., Ye H., Huang F. L. (2006). Surface Functionalization of Polymer Fibres by Sputtering Coating, J. Industrial Textiles , Vol. 35 No. 4 (2006) pp. 287-294

Ziaja J., Jaroszewski M. (2011); EMI Shielding using Composite Materials with Plasma Layers, Electromagnetic Waves, Vitaliy Zhurbenko (Ed.), ISBN: 978-953-307-304-0, InTech, Available from: http://www.intechopen.com/articles/show/title/emi-shielding-using-composite-materials-with-plasma-layers

Ziaja J., Ozimek M., Janukiewicz J. (2010). Application of thin films prepared by impulse magnetron sputtering for shielding of electromagnetic fields, Electrotech. Rev. 2010, R. 86, nr 5, pp. 222-224

Ziaja J., Ozimek M., Koprowska J. (2009). Metallic and oxide Zn and Ti layers on textile as shields for electromagnetic fields, EMC Europe 2009 Workshop, Athens, Greece, 11-12 June 2009, pp. 30-33

Ziaja J., Koprowska J., Janukiewicz J. (2008). The use of plasma metallization in the manufacture of textile screens for protection against electromagnetic fields, Fibres & Textiles in Eastern Europe. 2008, vol. 16, nr 5, pp. 64-66

Ziaja J., Koprowska J., Janukiewicz J., (2008a). Using of plasma metallization for fabrication of fabric screens against electromagnetic field, FIBRES & TEXTILES in Eastern Europe 5, s. 70-72

Ziaja J., Koprowska J., Żyłka P. (2008b). Influence of nonwoven structures on surface resistivity of plasma titanium films. Proceedings of 6th International Conference ELMECO-6 : electromagnetic devices and processes in environment protection joint with 9th Seminar "Applications of Superconductors" AoS-9, Nałęczów, Poland, June 24-27, 2008. s. 95-96

17

Polypropylene Nanocomposite Reinforced with Rice Straw Fibril and Fibril Aggregates

Yan Wu[1], Dingguo Zhou[1], Siqun Wang[2],
Yang Zhang[1] and Zhihui Wu[1]
[1]*Nanjing Forestry University*
[2]*University of Tenneessee*
[1]*China*
[2]*USA*

1. Introduction

High thermoplastic content composites are those in which the thermoplastic component exists in a continuous matrix and the lignocellulosic component serves as reinforcing filler. The great majority of reinforced thermoplastic composites available commercially use inorganic materials as their reinforcing fillers, e.g., glass, clays, and minerals. These materials are heavy, abrasive to processing equipment, and non-renewable. In recent years, lignocellulosic fillers used to reinforce thermoplastics, especially polypropylene (PP), have expanded due to their strength, low density, relatively high aspect ratio and environmental benefits. Lignocellulosic materials such as wood fiber, wood flour, cellulose fiber, flax, and hemp have been given more attention by polymer manufactures (Bataille et al. 1989; Karnani et al. 1997). Futhermore, the micro/nanofibrils isolated from natural fibers have much higher mechanical properties as reported by Sakurada et al. (1962) that the cellulose crystal regions are a bundle of stretched cellulose chain molecules with Young`s modulus of 150 GPa and strength in the order of 10 GPa. Thus the micro/nanofibrils has the potential as the reinforcing materials to create innovative nanocomposites (Herrick et al. 1983; Stenstad et al. 2008; Turbak et al. 1983). Nevertheless, such fibers are used only to a limited extent in industrial practice, which may be explained by difficulties in achieving acceptable dispersion levels (Helbert 1996).

Two main methods, the chemical method, mainly by strong acid hydrolysis and mechanical method including a high intensity ultrasonication (Cheng, 2007a, 2007b; Wang & Cheng 2009), a high-pressure homogenizer treatment (Dufresne et al. 1997; Herrick et al. 1983; Nakagaito and Yano 2005; Stenstad et al. 2008; Turbak et al. 1983), a high pressure grinder treatment and a microfluidizer (Zimmermann et al. 2004), have been used to generate cellulose products. The product came from chemical method was described by cellulosic whisker or cellulose nanocrystal. However, the product isolated from mechanical method was defined by cellulose microfibril or microfibrillated cellulose.

Rice straw represents a potentially valuable source of fiber and has the potential to alleviate the shortage of wood fiber and petroleum resources. It is easy to obtain and its fiber is more

flexible than wood fiber, which can highly reduced wear of the processing machinery, together with its abundance and low price, giving it more utilization value. Therefore, it can be used as a direct substitute for wood composites, and also can be used to make plastics composites (Wu et al. 2009). The fibril and fibril aggregates were generated from rice straw pulp cellulose fiber by a high intensity ultrasonication (HIUS) treatment and were used to reinforce polypropylene (PP) by a novel compounding machine, a minilab extruder with a materials cycle system.

The objective of this work was to use rice straw pulp cellulose fiber to prepare environmental-friendly rice straw fibril and fibril aggregates (RSF) and evaluate the fibril and fibril aggregates as a novel reinforcing material to compound polypropylene (PP)/ RSF nanocomposite. The scanning electron microscopy (SEM), wide angle X-ray diffraction (WAXD), laser diameter instrument (LDI) were used to evaluate the characteristics of RSF. The RSF/PP nanocomposite was prepared by novel extrusion process. The interface compatibility and tensile properties of nanocomposite were investigated by FTIR and tensile test, respectively.

2. Materials and methods

The isotactic polypropylene (iPP) was supplied by FiberVisions, Georgia, in the form of homopolymer pellets with a melt flow index of 35g/10 min (230 ^{o}C, 160 g) and a density of 0.91 g cm^{-3}. The reinforcing filler was rice straw fibril and fibril aggregates (RSF) obtained from rice straw pulp fiber (Taonan paper and pulp company, Jilin province, North-east of China) that was cut to pass a screen (room temperature and relative humidity of 30%) with holes of 1 mm in diameter by a Willey mill before treatment. The maleated polypropylene (MAPP) was used as compatibilizing agent and Epolene G-3003 P has an acid number of 6 and a molecular mass of 125 722.

2.1 Fibril isolation

The milled rice straw pulp fiber was soaked in distilled water for more than 24 h, and then treated by high intensity ultrasonication (Sonics & Materials. INC, CT, 20kHz, Model 1500 W) for 30 min with 80% power level. After ultrasonication treatment, the obtained RSF aqua compound was kept in frozen.

2.2 Freeze drying

In order to avoid the aggregation of isolated RSF, the frozen RSF aqua compound was freeze-dry in Food Science, the University of Tennessee, Knoxville, TN, USA. The conditions of freeze drier (Virtis Genesis 12 EL) were -20 ^{o}C to + 20 ^{o}C over 4 days in 5 ^{o}C increments.

2.3 Compounding

The freeze-dry RSF was milled by a food processor and kept into a dessicator. The RSF/ PP nanocomposite was made by blending PP pellets with 1~6% MAPP (ratio of PP weight, wt%) and 2~11% RSF (ratio of total weight, wt%). All materials were then fed into a Haake Mini-Lab twin-screw extruder (Thermo Electron Corp., Hamburg, Germany). The blends were processed for 10 min, 20 min, 30 min at 50 rpm and 180 ^{o}C, 190 ^{o}C and 200 ^{o}C using a

counter-rotating screw configuration, respectively. The RSF/ PP nanocomposite was then extruded through a 2.5 mm cylindrical die. The extruder strands were granulated and hot pressing at a temperature of 175 °C and a pressure of 5 MPa for 10 min. The obtained sheets with nominal thickness of 270 μm were conditioned at 23 ± 2 °C and 50 ± 5% relative humidity for not less than 40 h prior to tensile test in accordance with Procedure A of Practice D 618.

Sample	PP	MAPP	RSF
PP	100	0	0
PP2M	98	2	0
PP2M2R	96	2	2
PP2M5R	93	2	5
PP2M8R	90	2	8
PP2M11R	87	2	11
PP1M	99	1	0
PP2M	98	2	0
PP3M	97	3	0
PP4M	96	4	0
PP5M	95	5	0
PP6M	94	6	0
PP1M5R	94	1	5
PP2M5R	93	2	5
PP3M5R	92	3	5
PP4M5R	91	4	5
PP5M5R	90	5	5
PP6M5R	89	6	5

Table 1. Proportion of RSF/PP nanocomposite (by weight, %)

2.4 Fibril diameter test

The laser diameter instrument (Winner 2005, Qingdao, China) was used to investigate the diameter distribution after HIUS treatment. The sample concentration for testing was 1.526% and three levels were tested for the sample.

2.5 Cellulose crystallinity

The wide angle X-ray diffraction (WAXD) was used to study the crystallinities of treated and untreated rice straw fiber and fibril aggregates. The Segal method was used to calculate the crystallinities of the samples (Cheng et al. 2007b; Thygesen et al. 2005). The equipment (Material Data. Inc. DX-2000) was a pinhole type camera that recorded the patterns on Fuji image plates. The operating voltage was 40 kV, current was 30 mA, and the exposed period was 3000s using CuKa radiation with a wavelength of 0.15418 nm. The crystallinity is

defined as the ratio of the amount of crystalline cellulose to the total amount of sample material including crystalline and amorphous parts. The Turley method was used to calculate the crystallinity (CrI) of the samples (Thygesen et al. 2005).

2.6 Mechanical characteristic

The tensile measurements were conducted on an Instron testing machine (Model 5567) with a length of 20 mm between the top and bottom clamps, a crosshead speed of 1 mm/min, and a load cell of 30 kN (Cheng et al. 2007a). The specimens were cut to drum shapes with width of 5 mm for the narrow portion and total length of 40 mm. Eight specimens were tested for each extruder condition according to the ASTM D 882 standard test method for tensile properties of thin plastic sheeting (ASTM D882-02). The overall significant differences of the influences on the tensile modulus and strength of polypropylene reinforced with RSF under different extruder conditions were conducted using a Statistic Analysis System (SAS) JMP version 6.0.2 software (SAS Institute, Cary, NC, USA).

2.7 FTIR testing

The functions of samples were tested by FTIR (Nicolet 380) accompanying with ATR. The sample scanning times was 64, the ratio of differentiate was 8.000, sampling plus was 2.0, the speed of moving lens was 0.6329, diaphragm was 100.00, wave range was 4000~400cm^{-1}.

2.8 Morphology characteristic

Polarized light microscopy (PLM, Olympus-BX51) and a digital image analysis software package (ImageJ) were used to observe the distributions of the RSF in the RSF/PP nanocomposite. The fractured surfaces of nanocomposite after tensile test were investigated by a scanning electron microscopy (SEM, LEO 1525). The freeze-dry samples were observed by SEM. The voltages were 5-10 kV and various magnification levels were used to obtain images.

3. Results and discussion

3.1 Morphology characteristic

Figure 1 was the distribution of RSF diameters treated by HIUS. As seen in the figure, the distribution of diameters of RSF ranged from 0.1 μm to 80 μm by HIUS treatment. The percentage was 6.3% of RSF which diameters were less than 500 nm; almost 90 percents of RSF distributed between 7.0 μm and 80 μm; the average diameter was 41 μm.

3.2 Crystallinity of fibers and fibrils

According to (Thygesen et al. 2005), the crystallinity of treated rice straw cellulose fiber was 72.9%, which was higher than untreated rice straw cellulose fiber of 71.3%. The reason may be that some of the amorphous cellulose were degraded and removed during the ultrasonication treatment. High crystalline fibers and fibril aggregates could be more effective in achieving higher reinforcement for composite materials (Eichhorn & Young 2001).

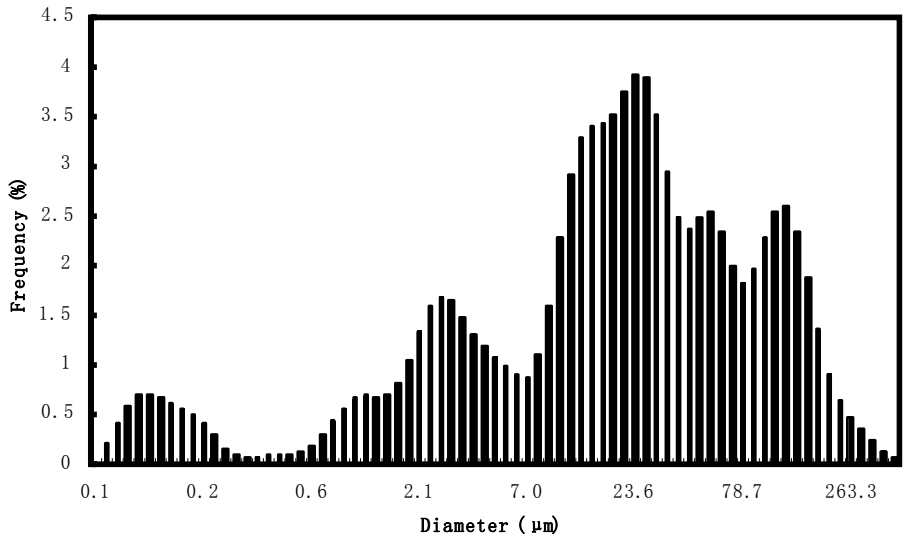

Fig. 1. Distribution of RSF diameters treated by HIUS

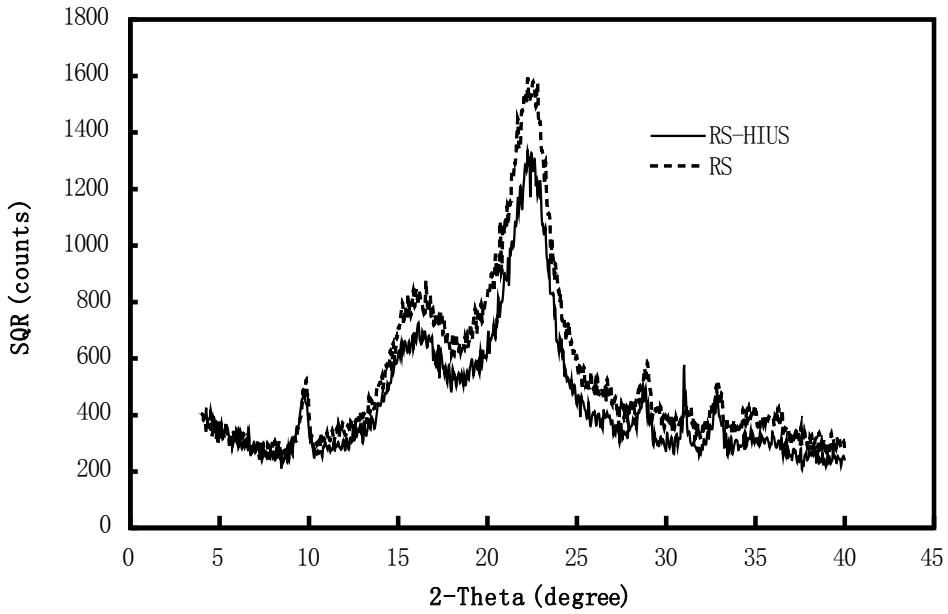

Fig. 2. CrI of untreated sample and sample treated by HPH

3.3 Effect of compounding conditions on RSF/PP nanocomposite tensile properties

The tensile strength of RSF/PP nanocomposite is shown in figure 3. The tensile strength of 5% rice straw fibril reinforcing PP nanocomposite was lower than PP/MAPP polymer. For the RSF/PP nanocomposite, the tensile strength increased with increasing cycle time from 10 min to 30 min at 180 °C. And the maximum value of tensile strength was 31.2 Mpa that appeared at the conditions of 190 °C, 20 min.

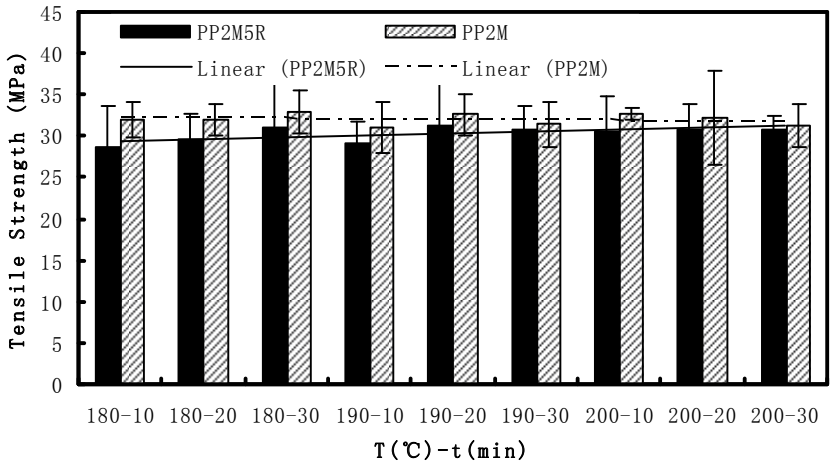

Fig. 3. Tensile strength of different extruder conditions

Figure 4 is the elastic modulus of PP/MAPP polymer and RSF/PP nanocomposite. The elastic modulus increased after added the 5% rice straw fibrils into the PP/MAPP polymer. For the PP/MAPP polymer, the elastic modulus increased significantly (R^2 = 0.53) with increasing compounding temperature and extruder cycle time. However, for the RSF/PP nanocomposite, the elastic modulus decreased with increasing compounding temperature and extruder cycle time, but this trend was not distinct.

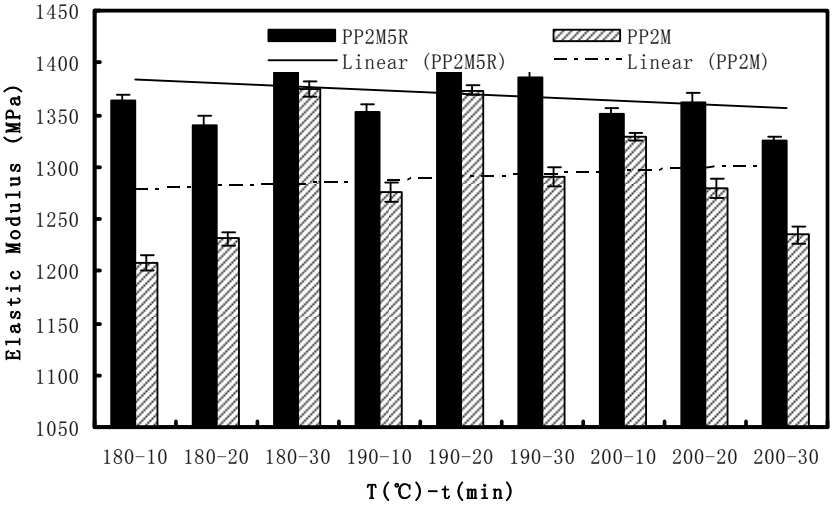

Fig. 4. Elastic modulus of different extruder conditions

The elongation at break was higher in PP/MAPP polymer than RSF/PP nanocomposite as shown in figure 5. With increasing compounding temperature and extruder cycle time the elongation at break decreased significantly (R^2=0.71) in PP/MAPP polymer, however, there had no big difference in RSF/PP nanocomposite.

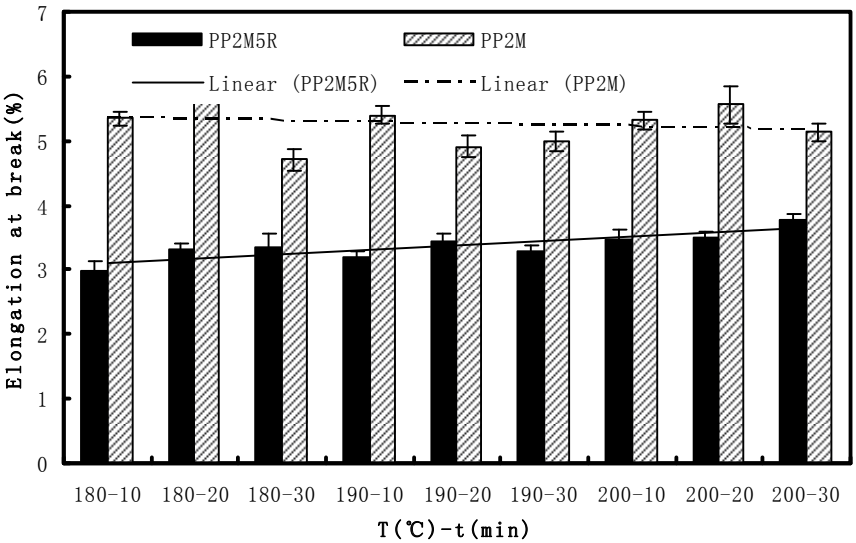

Fig. 5. Elongation of different extruder conditions

3.4 Effect of different RSF loadings on RSF/PP nanocomposite tensile properties

The tensile strength of RSF/PP nanocomposite with different fibril loadings is shown in figure 6. As the reference, the tensile strength of PP/MAPP polymer was also tested. The tensile strength at 5% RSF loading was up to the maximum value, 31.7 MPa, which was a little higher than the value of PP/MAPP polymer, 30.8 MPa. With increasing the fibril loadings the tensile strength decreased, but not distinct ($R^2 = 0.23$).

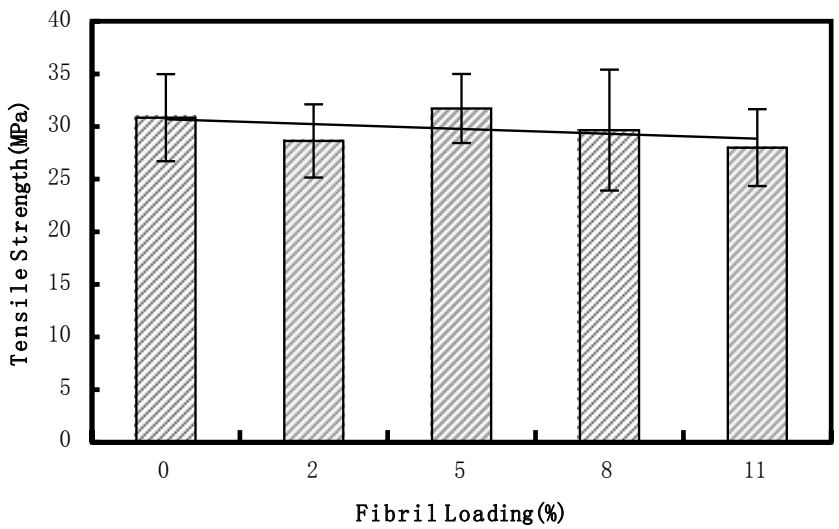

Fig. 6. Tensile strength of different fibril loadings

Figure 7 shows the elastic modulus of RSF/PP nanocomposite with different fibril loadings. The values were higher in RSF/PP nanocomposite than in PP/MAPP polymer. The fibril loadings from 2% to 8%, the elastic modulus increased significantly (R^2 = 0.70). The maximum was 1621 MPa at the 8% RSF, which was 17% higher than the value of PP/MAPP polymer. From 8% to 11% of RSF, the elastic modulus decreased.

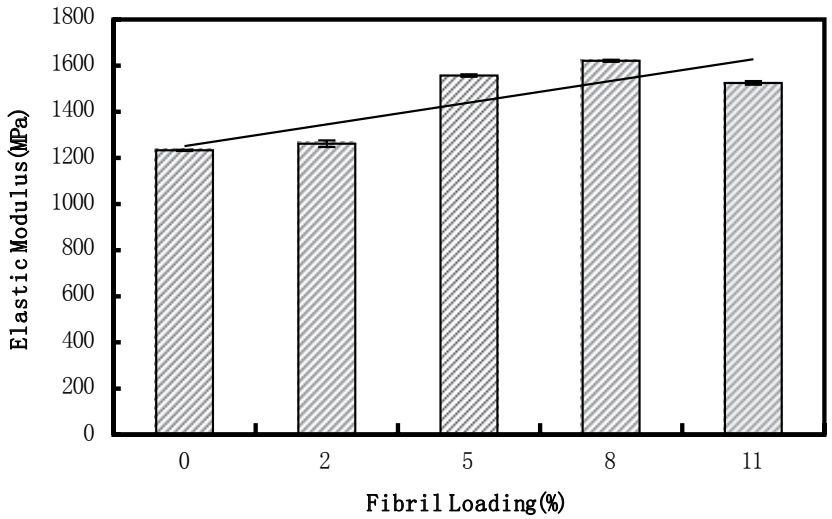

Fig. 7. Elastic modulus of different fibril loadings

The elongation at break showed a significant decreasing trend (R^2 = 0.89) with increasing the fibril loading (figure 8).

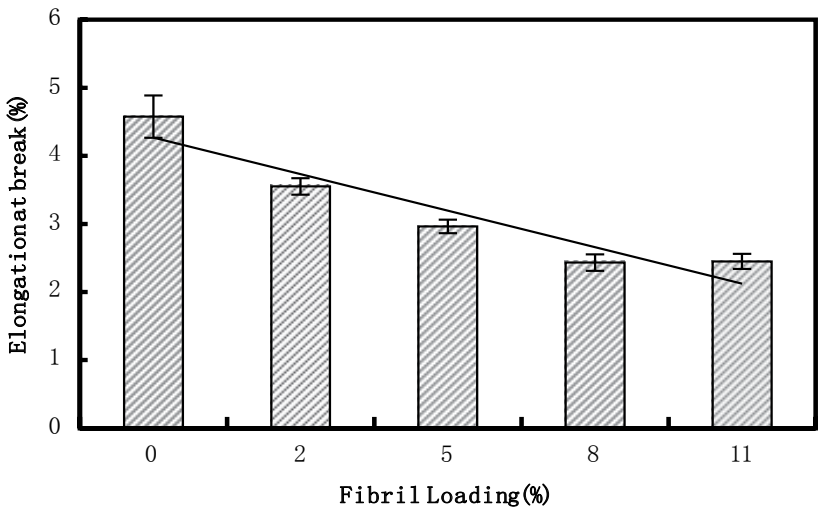

Fig. 8. Elongation of different fibril loadings

3.5 Effect of MAPP content on RSF/PP nanocomposite tensile properties

The tensile strength of PP/MAPP polymer decreased with increasing MAPP content from 1% to 6%, but not significant (figure 9). However, it showed a slightly increasing trend in RSF/PP nanocomposite as the MAPP content from 2% to 5%, then decreased when MAPP up to 6%.

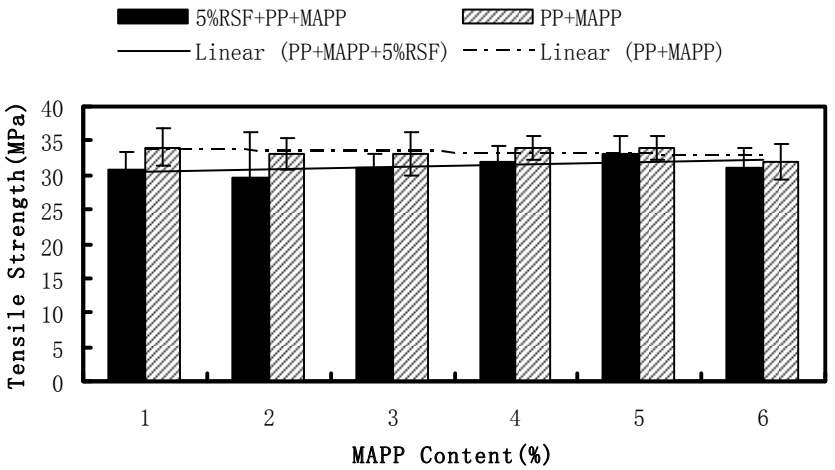

Fig. 9. Tensile strength of different MAPP contents

The elastic modulus and elongation at break appeared decreasing trend with increasing MAPP content both in PP/MAPP polymer and RSF/PP nanocomposite, as shown in figures 10 and 11. But the trends were not distinct according to the linear analysis.

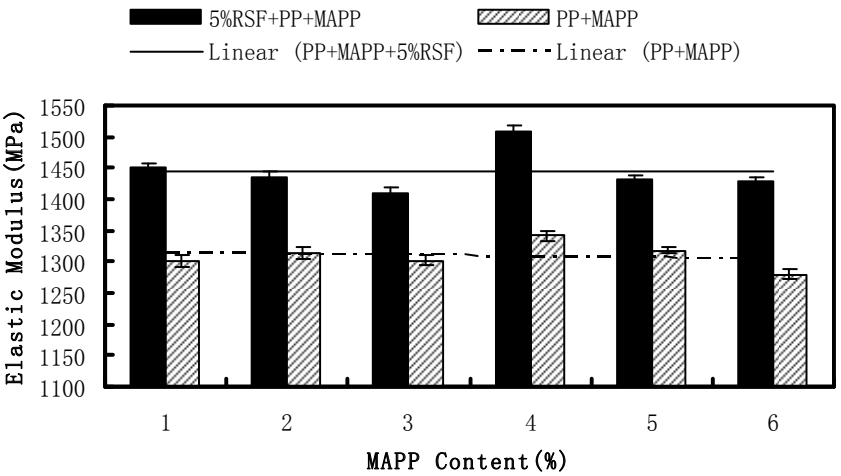

Fig. 10. Elastic modulus of different MAPP contents

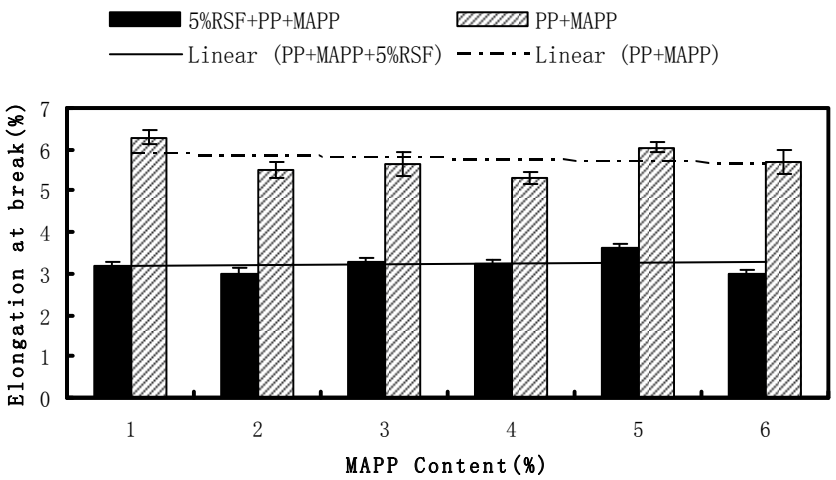

Fig. 11. Elongation at break of different MAPP contents

3.6 Effect of different ultrasonication treat condition on tensile properties

Figure 12 is the tensile strength of RSF/PP nanocomposite with different ultrasonication treat time RSF as the filler. For the ultrasonication treatment, the rice straw cellulose fiber content was 0.5% and 1%, respectively. As seen in this figure, the tensile strength increased distinctly (R^2=0.70 and R^2=0.96) with increasing ultrasonication treat time. The tensile strength of 0.5% rice straw cellulose fiber content was lower than 1% rice straw cellulose fiber content at different ultrasonication treat time.

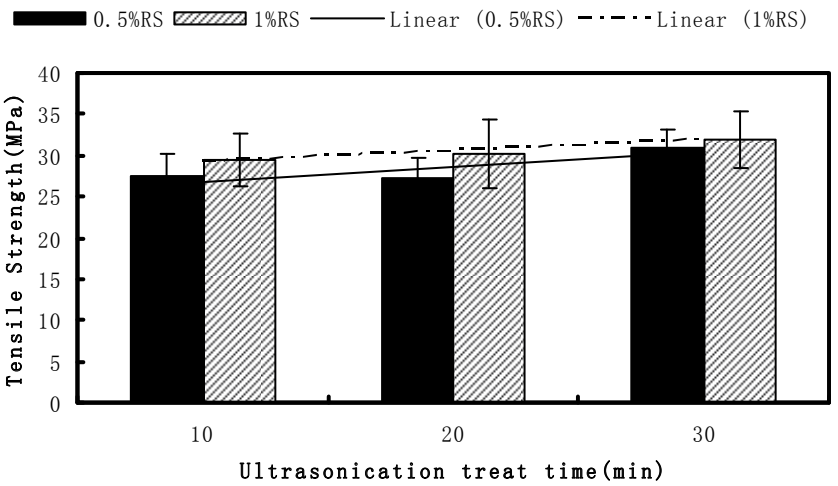

Fig. 12. Tensile strength of different ultrasonication treat time

The elastic modulus and elongation at break increased with increasing ultrasonication treat time as shown in figures 13 and 14. And also the elastic modulus and elongation at break were higher with 1% rice straw cellulose fiber content treated by ultrasonication as filler than 0.5%.

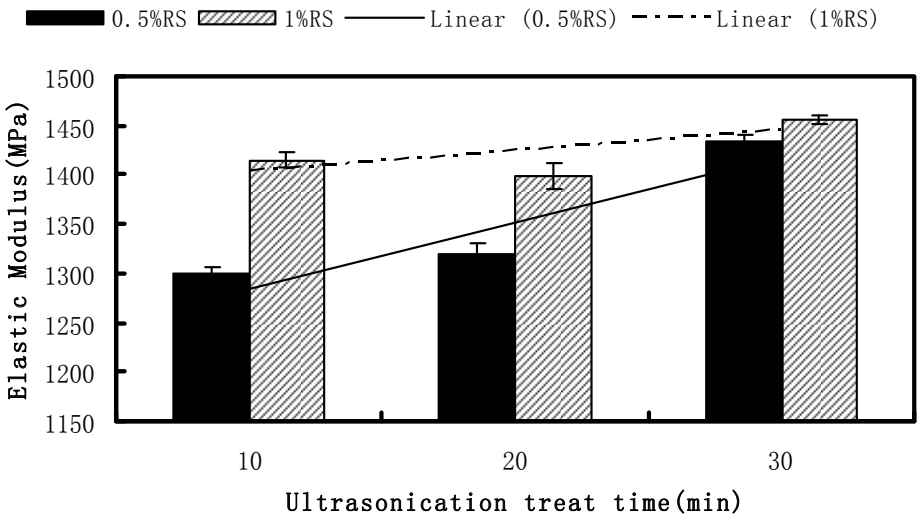

Fig. 13. Elastic modulus of different ultrasonication treat time

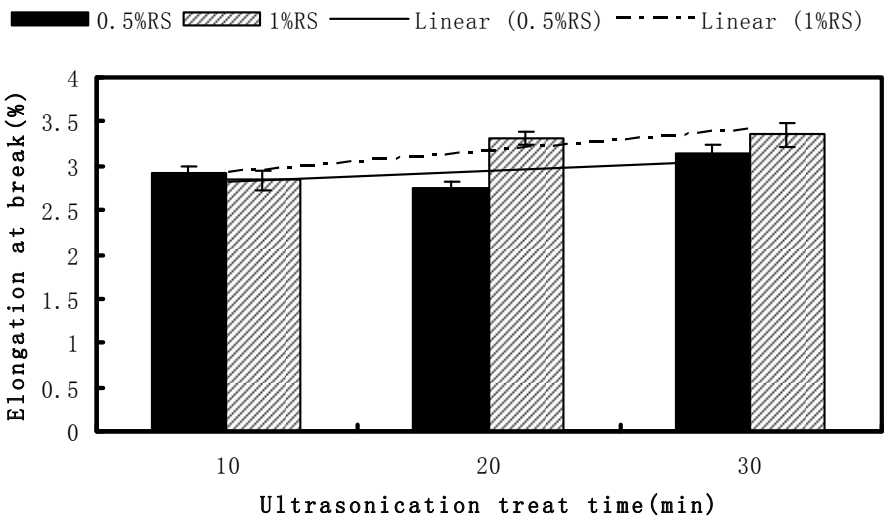

Fig. 14. Elongation at break of different ultrasonication treat time

3.7 FTIR analysis of RSF/PP nanocomposite

Figure 15 showed the FTIR spectra of PP, RSF/PP, RSF from up to down.

When adding MAPP and RSF into PP matrix, the FTIR spectra showed prodigious changes. CH_3 deformation of asymmetry stretching and CH_2 symmetry stretching moved to higher wavenumbers. Moreover, the frequency of CH_3 symmetry deformation decreased (1374CM^{-1} to 1372 CM^{-1}). The existence of C-O-C stretching at 1224 CM^{-1}, 1074 CM^{-1} and 1028 CM^{-1} indicated that PP and RSF were consistent by adding MAPP. Table 2 listed the vibration peaks and assignments of peaks of RSF/PP nanocomposite.

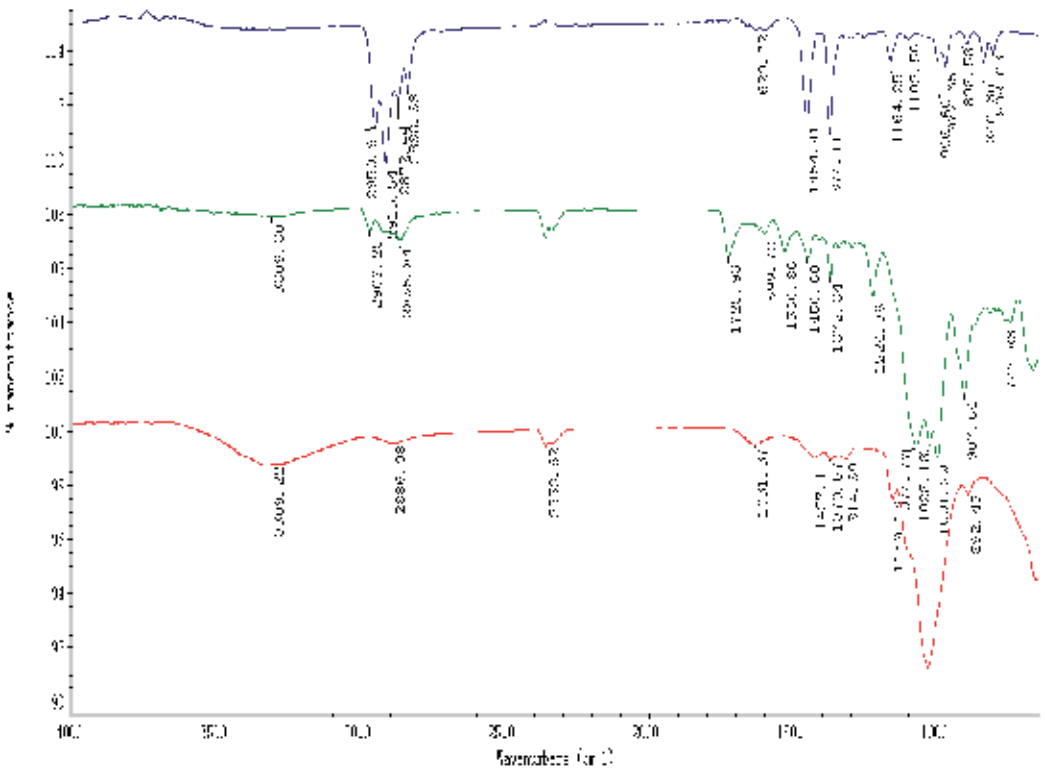

Fig. 15. FTIR curves of PP, RSF/PP nanocomposite and RSF

Wavenumber (cm-1)	Assignments
3309	-OH stretching
2969	CH3 deformation of asymmetry stretching
2865	CH2 symmetry stretching
1725	C=O stretching
1450	CH3 asymmetry deformation
1450	CH2 shearing
1372	CH3 symmetry deformation
1224, 1074, 1028	C-O-C stretching

Table 2. FTIR vibration peaks and assignments of peaks of RSF/PP nanocomposite

3.8 Morphology characteristics of fibers and fibrils

After ultrasonication treatment, the rice straw cellulose fiber changed into small size fibrils. The SEM pictures showed the appearance of untreated (figure 16a) and treated (figure 16b) rice straw cellulose fiber.

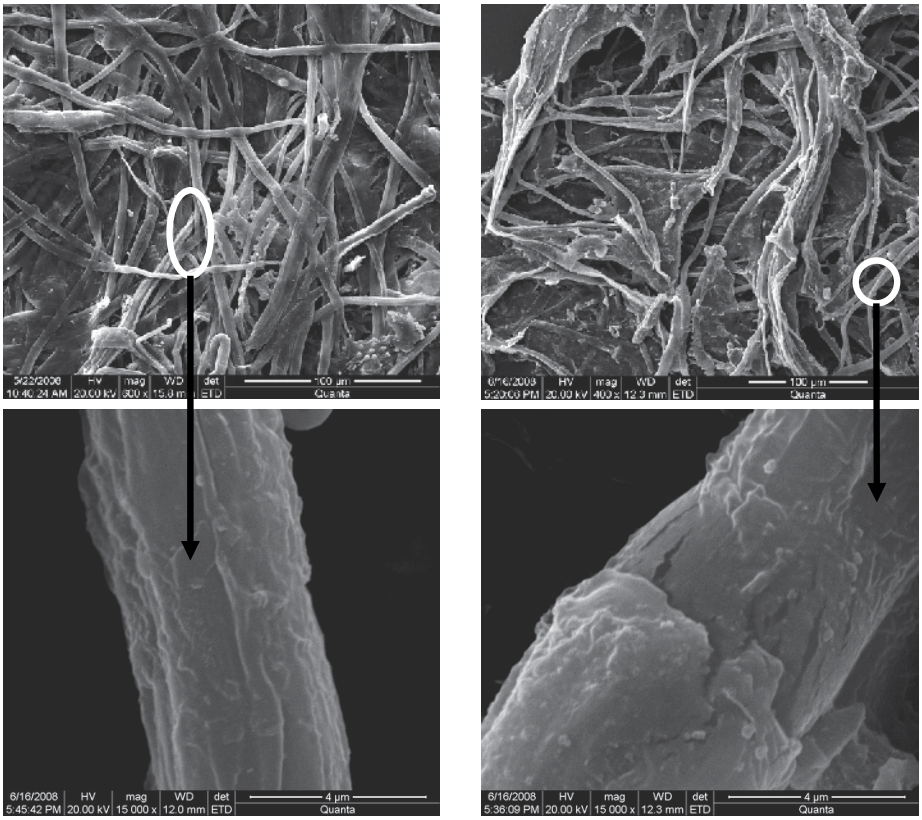

Fig. 16. SEM photos of untreated sample (a, left) and treated sample (b, right)

It can be seen from figure 13b inset figure that the fibrils peeled off from the fibers and the ultrasonication treatment made the surface of fibers producing fractures. The fibrils and microfibrils can form a kind of micro/nano-order-unit web-like network structure (Nakagaito & Yano, 2005), which can greatly expanded in the surface area that characteristic the RSF and increase the compounding abilities between fibrils/mircrofibrils and polymer. After the ultrasonication treatment, fibrils, fibrils aggregates and cellulose fibers together existed, and also the fibrils had a widely width (or diameter) ranges from tens of nanometer to micrometers as shown in figure 1. The fibrils with diameter less than 500 nm were peeled from the fibers, however, the fibril aggregates with diameter around 25 μm took the most place.

3.9 Fracture cross section morphology of RSF/PP nanocomposite

The fracture cross section morphology of RSF/PP nanocomposite after tensile test was observed by scanning electron microscopy (SEM). As shown in figure 17(a), the rice straw fibrils embedded into the polymer and exhibited better interaction with polymer. The fibrils were interconnected with the polymer and didn`t pull out from the polymer during the tensile test. However, the bigger size fiber still can be seen in the nanocomposite and it appeared the gas between the fiber and the polymer (figure 17b), which proved that the bigger size cellulose fiber and the polymer can not bond together easily or the compatibility was not as good as the fibril filler. And this may be the reason that the tensile strength in RSF/PP nanocomposite was

lower than PP/MAPP polymer. To improve the degree and homogenization of fibril will be a good way to increase the compatibility between RSF and polymer.

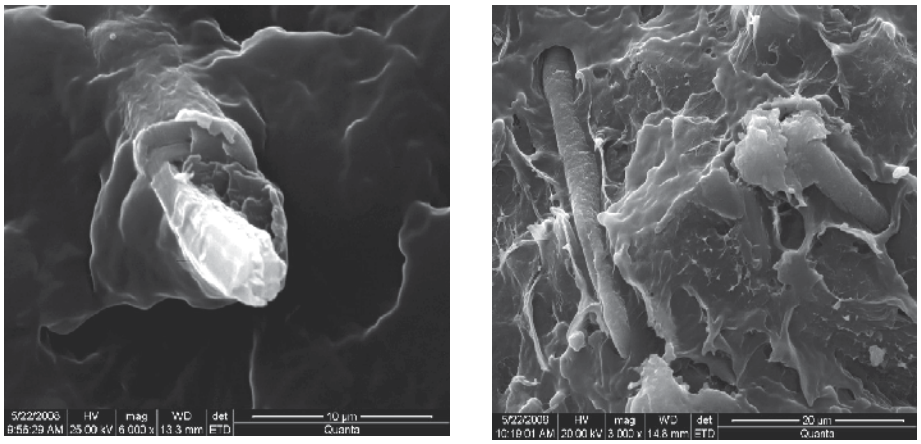

(a) (b)

Fig. 17. Fracture cross section SEM photos of RSF/PP nanocomposite after tensile test

It was seen in figure 18 of PLM picture, the distribution of RSF in the RSF/PP nanocomposite was good, which indicated the minilab extruder with a cycle system was a suitable machine to compound the polymer and cellulose fibrils.

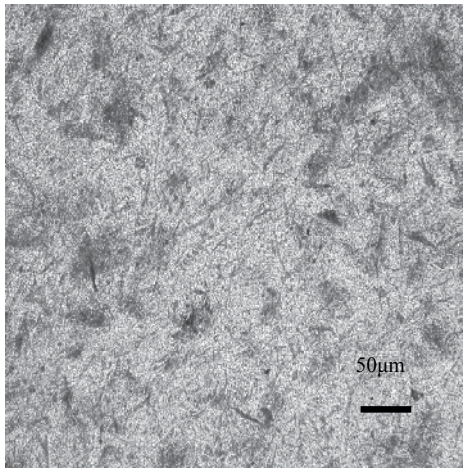

Fig. 18. PLM photo of RSF distribution in RSF/PP nanocomposite

4. Conclusions

The distribution of diameters of RSF ranged from 0.1 µm to 80 µm by HIUS treatment. The percentage was 6.3% of RSF which diameters were less than 500 nm; almost 90 percents of RSF distributed between 7.0 µm and 80 µm; the average diameter was 41 µm. The relative crystallinities of untreated rice straw cellulose fibers and rice straw cellulose fibers treated by HIUS were 71.3% and 72.9%, respectively.

The elastic modulus increased of RSF/PP nanocomposite comparing with PP/MAPP polymer. However, the tensile strength and elongation at break of 5% rice straw fibril reinforcing PP nanocomposite was lower than PP/MAPP polymer at different extruder compounding conditions. The tensile strength at 5% RSF loading was up to the maximum value, 31.7 MPa, which was a little higher than the value of PP/MAPP polymer, 30.8 MPa. The maximum was 1621 MPa at the 8% RSF, which was 17% higher than the value of PP/MAPP polymer. The elongation at break showed a significant decreasing trend with increasing the fibril loading. There was no distinct influence of tensile strength and elongation of nanocomposite and PP/MAPP polymer with increasing MAPP content. The maximum of elastic modulus was 1509 MPa at the 4% of MAPP. The tensile properties increased distinctly with increasing ultrasonication treat time. The tensile strength of 0.5% rice straw cellulose fiber content was lower than 1% rice straw cellulose fiber content at different ultrasonication treat time.

After adding MAPP and RSF into PP matrix, the FTIR spectra had big changes. The absorption peak of ester bonds (C-O-C) appeared at 1224 CM-1, 1074 CM-1 and 1028 CM-1, which proved that there had been a good compatibility between PP matrix and RSF. The SEM images showed: the fibrils were embedded into the PP/MAPP matrix, during the tensile test, which were not pulled out from the matrix.

5. Acknowledgment

The work is supported by Natural Science Foundation of China (31100417) and (31070492).

6. References

ASTM D (D 882 - 02) Standard test method for tensile properties of thin plastic sheeting.

Bataille, P.; Ricard, L. & Sapieha, S. (1989). Effects of cellulose fibers in polypropylene composites. *Polymer Composites*, Vol. 10, pp. 103, ISSN 1548-0569

Cheng, Q.; Wang, S.; Rials, T. & Lee, S. (2007a). Physical and mechanical properties of polyvinyl alcohol and polypropylene composite materials reinforced with fibril aggregates isolated from regenerated cellulose fibers. *Cellulose*, Vol. 14, pp. 593-602, ISSN 0969-0239

Cheng, Q.; Wang, S.; Zhou, D.; Zhang, Y. & Rials, T. (2007b). Lyocell-derived cellulose fibril and its biodegradable nanocomposite. *Journal of Nanjing Forestry University*, Vol. 31, No. 4, pp. 21-26, ISSN 1000-2006

Dufresne, A.; Cavaille, J.Y. & Vignon, M.R. (1997). Mechanical behavior of sheets prepared from sugar beet cellulose microfibrils. *Journal of Applied Polymer Science*, Vol. 64, No. 6, pp. 633-639, ISSN 1097-4628

Eichhorn, S.J. & Young, R.J. (2001). The Young`s modulus of a microcrystalline cellulose. *Cellulose,* Vol. 8, No. 3, pp. 197-207, ISSN 0969-0239

Herrick, F.W.; Casebier, R.L.; Hamilton, J.K. & Sandberg, K.R. (1983). Microfibrillated cellulose: morphology and accessibility. *Journal of Applied Polymer Science*, Vol. 37, pp. 797-813, ISSN 1097-4628

Helbert, W. J.; Cavaillé, Y.; Dufresne, A. (1996). Thermoplastic nanocomposites filled with wheat straw cellulose whiskers. Part I: processing and mechanical behavior. *Polymer Composites,* Vol. 17, pp. 604-611, ISSN 1548-0569

Karnani, R.; Mohan, K. & Ramini, N. (1997). Biofiber-reinforced polypropylene composites. *Polymer Engineering & Science*, Vol. 37, pp. 476, ISSN 1548-2634

Nakagaito, A.N. & Yano, H. (2005). Novel high-strength biocomposites based on micriofibrillated cellulose having nano-order-unit web-like network structure. Journal of Applied Physics, Vol. 80, pp. 155-159, ISSN 0021-8979

Sakurada, I.; Nukushina, Y. & Ito, T. (1962). Experimental determination of elastic modulus of crystalline regions in oriented polymer. *Journal of Polymer Science Part B: Polymer Physics*, Vol, 57, No. 165, pp. 651-660, ISSN 1099-0488

Stenstad, P.; Andresen, M. & Tanem, B. (2008). Chemical surface modifications of microfibrillated cellulose. *Cellulose*, Vol. 15, pp. 35-45, ISSN 0969-0239

Thygesen, A.; Oddershede, J.; Lilholt, H.; Thosmsen, A.B. & Stahl, K. (2005). On the determination of crystallinity and cellulose content in plant fibres. *Cellulose*, Vol. 12, No. 6, pp. 563-576, ISSN 0969-0239

Turbak, A.F.; Snyder, F.W. & Sandberg, K.R. (1983). Microfibrilated cellulose, a new cellulos product: properties, uses, and commercial potential. *Journal of Applied Polymer Science*, Vol. 37, pp. 815-827, ISSN 1097-4628

Wang, S. & Cheng, Q. (2009). A novel method to isolate fibrils from cellulose fibers by high intensity ultrasonication. Part I. Process optimization. *Journal of Applied Polymer Science*, Vol. 113, pp. 1270-1275, ISSN 1097-4628

Wu, Y.; Zhou, D.G.; Wang, S.Q.; Zhang, Y. (2009) Polypropylene composites reinforced with rice straw micro/nano fibrils isolated by high intensity ultrasonication. *BioResources*, Vol. 4, pp. 1487-1497, ISSN 1930-2126

Zimmermann, T.; Pohler, E. & Geiger, T. (2004). Cellulose fibrils for polymer reinforcement. *Advanced Engineering Materials,* Vol. 6, No. 9, pp. 754-761, ISSN 1527-2648

18

The Influence of Filler Component on Mechanical Properties and Thermal Analysis of PP-LDPE and PP-LDPE/DAP Ternary Composites

Kamil Şirin[1], Mehmet Balcan[2] and Fatih Doğan[3]
[1]*Celal Bayar University, Faculty of Science and Arts, Department of Chemistry, Manisa,*
[2]*Ege University, Faculty of Science, Department of Chemistry, İzmir,*
[3]*Çanakkale Onsekiz Mart University, Faculty of Education, Secondary Science and Mathematics Education, Çanakkale, Turkey*

1. Introduction

Composite material is a material system consisting of a mixture or combination of two or more micro-constituents mutually insoluble and differing in form and/or material composition. Particulate-filled thermoplastic composites have proved to be of significant commercial importance in recent years, as industrialists and technologists have sought to find new and cost-effective materials for specific applications (Shonaike & Advani, 2003; Ma et al., 2007). With addition of inorganic filler, various changes occur in the molecular and supermolecular structure of a thermoplastic resin. Composite properties depend on a variety of material-process variables (e.g., polymer matrix structure, filler content, chemical composition, surface activity, particle size and shape, compounding extruder design, mold design, and extruder-molding process conditions). Some changes may be latent or delayed (i.e., occurring later in the service life of the plastic part as a result of surrounding conditions). Reduction of molecular weight, crystal and spherulite size, and molecular mobility are among the most profound effects that solid filler has on the polymer matrix structure (Ayae & Takashi, 2004). The microstructure of the polymer–filler interphase is mirrored by the mechanical integrity of the molded part and long-term durability to extremes of surrounding temperatures and applied stresses. Calcium carbonate is very commonly used filler in the plastics industry. The incorporation of fillers such as calcium carbonate into thermoplastics is a common practice in the plastics industry, being used to reduce the production costs of molded products. Fillers are also used to modify the properties of plastics, such as the modulus and strength. High filler loadings, however, may adversely affect the processability, ductility, and strength of composites (Rai & Singh, 2003). Some polyolefins are prone to chain-scission reactions in the presence of free radicals. PP is degraded due to chain scission in β position to the macroradicals site, while PE is crosslinked, due to macroradical recombination (Braun et al., 1998). The use of organic

peroxides for controlled degradation of PP is the most important commercial application of the chain-scission or visbreaking of polyolefin chains and results in the so-called controlled rheology PP grades with enhanced melt flow behavior (Zweifel, 2001). Polypropylene (PP) filled with calcium carbonate is among the more recent development on the polyolefin market and in the last decade have shown impressive growth rates. In polyethylene sector, calcium carbonate fillers now play a role preferably in films and sheets. Low density polyethylene's (LDPE and LLDPE) are usually filled with very pure calcium carbonate grades.

Several studies dealing with the melt rheology, mechanical, deformation, impact behavior and thermal properties of various blend or composites were published during the last decade (Chen et al., 2004; El-Sabbagh et al., 2009; Kolarik & Jancar, 1992; Mishra et al., 1997; Sirin & Balcan, 2010, Zhang et al., 2002). Wang WY (Wang, 2007, 2008) was studied the preparation and characterization of calcium carbonate/Low-Density-Polyethylene and $CaCO_3$/acrylonitrile-butadiene-styrene composites. Tang *et al*. studied rheological properties of nano-$CaCO_3$/ABS composites such as shear viscosity, extension viscosity, and entry pressure dropped by capillary extrusion (Tang & Liang, 2003). Liang investigated the tensile, flow, and thermal properties of $CaCO_3$-filled LDPE/LLDPE composites (Liang, 2007). Effects of coupling agents on mechanical and morphological behavior of the PP/HDPE blend with two different $CaCO_3$ were studied by Gonzalez *et. al* (Gonzalez et al., 2002) . Also, several researches have reported different properties of ternary composites with calcium carbonate (Jancar & Dibenedetto, 1995; Kim et al, 1993; Premphet, 2000).

This study has focused on the investigation of the changes on thermal, mechanical and morphological properties of PP-LDPE/DAP (90/10 /0.06 wt. %) blend and PP-LDPE/DAP (90/10 /0.0 wt. %) blend when different ratios of 5-10-20 wt. % $CaCO_3$ are added. The blend (PP-LDPE/DAP (90/10/0.06 wt.%) used in this study was prepared in terms of heat sealing strength properties by the results based on our previous work (Sirin & Balcan, 2010) and is optimum as well (Şirin, 2008).

2. Experimental

2.1 Materials

Isotactic polypropylene (PP-MH418) and Low-density polyethylene (LDPE-I 22-19 T) were supplied as pellets by Petkim Petrochemical Company (Aliaga, Izmir, Turkey). The number-average molecular weight (*M*n), weight-average molecular weight (*M*w) and polydispersity index (PDI) values of PP and LDPE homopolymer were 20300, 213600 g.mol^{-1} and 10.5, and 29600, 157000 g.mol^{-1} and 5.3, respectively. The specific gravity of the PP-MH418 is 0.905 g.cm^{-3} and that of the LDPE-I 22-19 T is 0.919-0.923 g.cm^{-3}, with melt flow index of 4-6 g.10 min^{-1} (2.16 kg, 230 ± 0.5 ^{o}C) and 21– 25 g.10 min^{-1} (2.16 kg, 190 ± 0.5 ^{o}C), respectively. (2, 5-dimethyl-2, 5-di (tert-butyl peroxy)-hexane, (Sinochem, Tinajin/Chine) was used as dialkly peroxide (DAP). Calcium carbonate filler (AS 0884 PEW) was provided by Tosaf Company (Israel).

2.2 Preparation of blends

In the preparation of the composites, two different procedures were used. In the first procedure, PP-LDPE/$CaCO_3$ composites were prepared without addition of DAP. These composites are called as PC0, PC1, PC2 and PC3. In the second procedure, PP-LDPE/$CaCO_3$

composites were prepared with (0.06 % wt.) addition of DAP. These composites are called as PC4, PC5, PC6 and PC7.All compounds were prepared by using single screw extruder (Collin E 30P). The blends were prepared by melting the mixed components in extruder which was set at the extruder diameter: 30 mm, length to diameter ratio: 20, pressure: 9-10 bar, temperature scale composites from filing part to head were 190-250 ^{o}C and screw operation speed: 30 rev.min^{-1}. The composites were produced as 70 μm thick and 10 cm wide films. These ratios and their codes are given in Table 1. All of these composites were prepared as samples weighing 1000 grams, while keeping the PP-LDPE (90/10) ratio constant.

	Composition, wt %			
Sample Code	PP	LDPE	$CaCO_3$	DAP
PC0	90	10	-	-
PC1	90	10	5	-
PC2	90	10	10	-
PC3	90	10	20	-
PC4	90	10	-	0.06
PC5	90	10	5	0.06
PC6	90	10	10	0.06
PC7	90	10	20	0.06

Table 1. Nomenclature, components and composition of composites

2.3 Melt flow index (MFI) measurements

Melt flow index measurements of the composites were carried out on a MFI (MP-E) Microprocessor apparatus at 230 ^{o}C and under a 2.16 kg weight. The capillary die was 2.095 mm in diameter and 8 mm in length. About 5 g of composite was put into barrel and heated for 5 min to reach the predetermined temperature on the plunger to extrude the melt through the capillary die. After a steady flow state was reached, five samples were cut sequentially and their average weight value was obtained. Experiments were done according to ASTM D-1238.

2.4 Mechanical testing measurements

The tensile properties were determined using a Instron tensile tester (model 4411) following the ASTM D-638 procedure and using type 1 test specimen dimensions. The crosshead speed was set at 50 mm.min^{-1} and 5 samples were tested for each composition. Tensile stress at yield, tensile strength at break and elongation at break were determined from the recorded force versus elongation curve.

2.5 Hardness test measurements

Shore D scale was used to determine the hardness values of all samples. The tests were carried out Zwick/Roell apparatus of out at the room temperature and 76 cm Hg pressure hardness

test (Shore D) was performed according to ASTM D 2240. Hardness test measurements were carried out the dimensions of 60x60x4 mm at 50 N, at the room temperature.

2.6 Heat seal tester

Heat sealing testers of samples were carried out with a TP701 (trade name, Tester Sangyo K.K.) apparatus at 1 sec timer and 2 kg/cm^2 pressure.

2.7 Thermal measurements

Differential scanning calorimetric (DSC) analyses were performed in a Shimadzu DSC-50 thermal analyzer in nitrogen atmosphere. The samples were heated from 25 to 200 ^oC at 10 ^oC min^{-1}, cooled to 25 ^oC at the same rate, and re-heated and cooled under the same conditions. Melting (T_m) and crystallization (T_c) temperatures and enthalpies were determined from the second scan. T_m was considered to be the maximum of the endothermic melting peak from the heating scans and T_c that of the exothermic peak of the crystallization from the cooling scans. The heat of fusion (ΔH_f) and crystallization enthalpy (ΔH_c) were determined from the areas of melting peaks and crystallization peaks.

The crystallinty of composites were calculated with the total enthalpy method [see eq. (1)]; in all calculations, the heats of fusion at equilibrium melting temperature were 209 and 293 Jg^{-1}, for PP and LDPE crystals, respectively (Brandrup & Imergut, 2003)

$$(X_c) = \frac{\Delta H_f}{\Delta H_{crys}} x100 \quad (1)$$

ΔH_f = Heat of fusion (Jg^{-1})
ΔH_{crys} = 100% crystal polymer crystallization energy (Jg^{-1})
(X_c) = Crystallinty (%)

The various melting and crystallization parameters which were determined by means of heating and cooling scans for composites are given in Table 3. Thermogravimetric (TG-DTG-DTA) curves were performed on a Seteram Labsys TG-16 thermobalance, operating in dynamic mode, with the following conditions; sample weight ~5 mg, heating rate = 10 ^oC.min^{-1}, atmosphere of nitrogen (10 cm^3.min^{-1}), sealed platinum pan.

2.8 Scanning electron microscopy (SEM)

A Philips XL-305 FEG e SEM model scanning electron microscopy (SEM) was used to examine the morphologies of the composites

3. Conclusion

3.1 Mechanical analysis

$CaCO_3$ has a high chemical purity, which eliminates a negative catalytic effect on the aging of polymers. In addition, it has high whiteness and low refractive index that can help to reduce consumption of expensive abrasive pigments such as titanium dioxide. On the other

hand $CaCO_3$ is very well suited for the manufacture of colorful products. Low abrasiveness, which contributes to low wear of machine parts such as extruder screws and cylinders, is another advantage. These properties and its low cost make $CaCO_3$ a very strong alternative to be considered as filler.

Melt flow index (MFI) analysis of composites are shown in Table 2. MFI values of composites without peroxide showed small differences by increasing amount of $CaCO_3$. Contrariwise, MFI values of composites with peroxide are proportional to the increasing amount of $CaCO_3$. MFI values of composites without DAP are between 9 and 10 g/10 min, however addition of 0.06 %wt. DAP to the composites resulted MFI values to vary between 22 and 26 g/10 min. This increase in MFI values is a result of degradation of PP by the DAP.

Sample Code	MFI / g.10 min^{-1} ± 0.1	Tensile strength at break / $kg.cm^{-2}$ ±10	Tensile strength at yield/ $kg.cm^{-2}$±10	Elongation at break/ (%)±5	Hardness (ShoreD) ±1	Heat sealing strength/ $kg.cm^{-2}$ ± 0.1 at 145 °C	Heat sealing strength/ $kg.cm^{-2}$ ±0.1 at 150 °C
PC0	9.20	270	322	240	62.10	2.15	3.27
PC1	9.40	171	263	190	62.60	1.52	3.10
PC2	9.60	125	240	160	63.10	1.33	2.50
PC3	9.70	98	210	141	63.20	1.11	2.04
PC4	22.00	290	360	310	63.00	2.53	9.80
PC5	23.80	180	298	287	63.50	1.62	4.74
PC6	24.50	230	336	302	63.90	1.96	5.22
PC7	25.20	146	218	161	63.40	1.44	4.22

Table 2. MFI, heat sealing strength and mechanical analysis values of composites

Mechanical analysis of the composites such as tensile strength at break, tensile strength at yield and elongation at break are shown in Table 2. As shown in Table 2, samples with/without peroxides showed increase and decrease in their mechanical properties of composites in terms of increasing amount of $CaCO_3$. The highest values in mechanical properties were observed in PC6 . Even though PP, LDPE and $CaCO_3$ amounts were same in PC6 and PC2, there was only change in peroxide amounts. In other words, when PC6 and PC2 were compared it was observed that tensile strength at break, at yield, elongation at break values and heat sealing strength values of the composite PC6 showed high peaks. Table 2 summarizes tensile strength at break values for composites which do not contain peroxide displayed decreasing. However, by adding peroxide and increasing the amount of $CaCO_3$, these values showed increasing due to crosslinking of LDPE with the effect of peroxide. Furthermore, the tensile strength of the composites decreased with increasing amount of $CaCO_3$ due to the weak interfacial adhesion and dispersion of the $CaCO_3$ filler

to PP-LDPE surface. The decrease of yield stress is likely due to the depending between inorganic fillers and the PP matrix at large deformations. In particular, a higher drop in tensile strength at yield is observed for PP-LDPE/$CaCO_3$, possibly due to the splitting of aggregated particles as well as depending between $CaCO_3$ particles and the PP matrix. In Table 2, with/without peroxide it is clearly shown that elongation at break values of the composites decreases with increasing ratio of $CaCO_3$. On the other hand, while comparing samples with $CaCO_3$ to each other the highest mechanical properties were observed in PC6. The reason for this is that adding DAP effect LDPE by crosslinking and PP by degradation. Shore D values of the composites with/without DAP increase in some degree with increasing amount of $CaCO_3$. As mentioned above, the reasons for increase in shore d values of the composites are addition of DAP effect to LDPE by crosslinking, PP by degradation, and dispersion of $CaCO_3$ in PP and LDPE. Table 2 shows that, increasing amounts of $CaCO_3$ resulted a decrease on heat sealing strength values at 145 °C and 150 °C independent of DAP. Therefore, the decrease of heat sealing strength is owing to the depending between in organic filler and the blends matrix of deformations. PP-LDPE/$CaCO_3$ composites still gave better heat sealing strength results than homopolymer PP and LDPE. In previous studies, we have examined heat sealing strength of homopolymer PP and LDPE (Sirin & Balcan, 2010; Şirin, 2008) Same as in mechanical properties values, heat sealing strength values showed similar trend in composite PC6 for best results.

3.2 Morphology observation

Figure 1 (a-g) shows the scanning electron microscopy (SEM) micrographs of composites reinforced with different amounts of $CaCO_3$ (0, 5, 10, and 20 %wt.) and DAP (0, 0.06 %wt.). From these micrographs, it is clear that $CaCO_3$ fillers were dispersed well in PC4, PC6 and PC7 matrices with DAP of composites. In these matrices, a homogeneous dispersion of reinforcing particles can also be observed. Moreover, the fillers remained intact within the matrix. This indicates that good bonding existed between the $CaCO_3$ particles and matrix. In contrast, the agglomeration of fillers can be observed for the composites containing $CaCO_3$ particles and dialkylperoxide (DAP). In homogeneous dispersion of fillers can cause a loss in the mechanical strength of the composites considerably. At higher loading levels however, $CaCO_3$ will agglomerate and remain confined in the polymer matrix.

3.3 Thermal analysis of composites

The results of the thermal analysis that was carried out by means of differential scanning calorimetry (DSC) are presented in Table 3. Overall, there were increased effect of both the content of the $CaCO_3$ filler and its healing on the melting temperature (T_m) and the crystallization temperature (T_c). However, a decrease in the energy required for the fusion of the crystalline parts was noted when the content of the filler in the composite increased. The melting enthalpy and crystallinity % (X_c) of the $CaCO_3$ containing composites with DAP (0.06 %wt.) were a little higher than the composites without DAP. Yet, the values of heat of fusion remain lower than that of homopolymer PP or LDPE. It can therefore be noted that the filler alters the crystalline phase of the polymer.

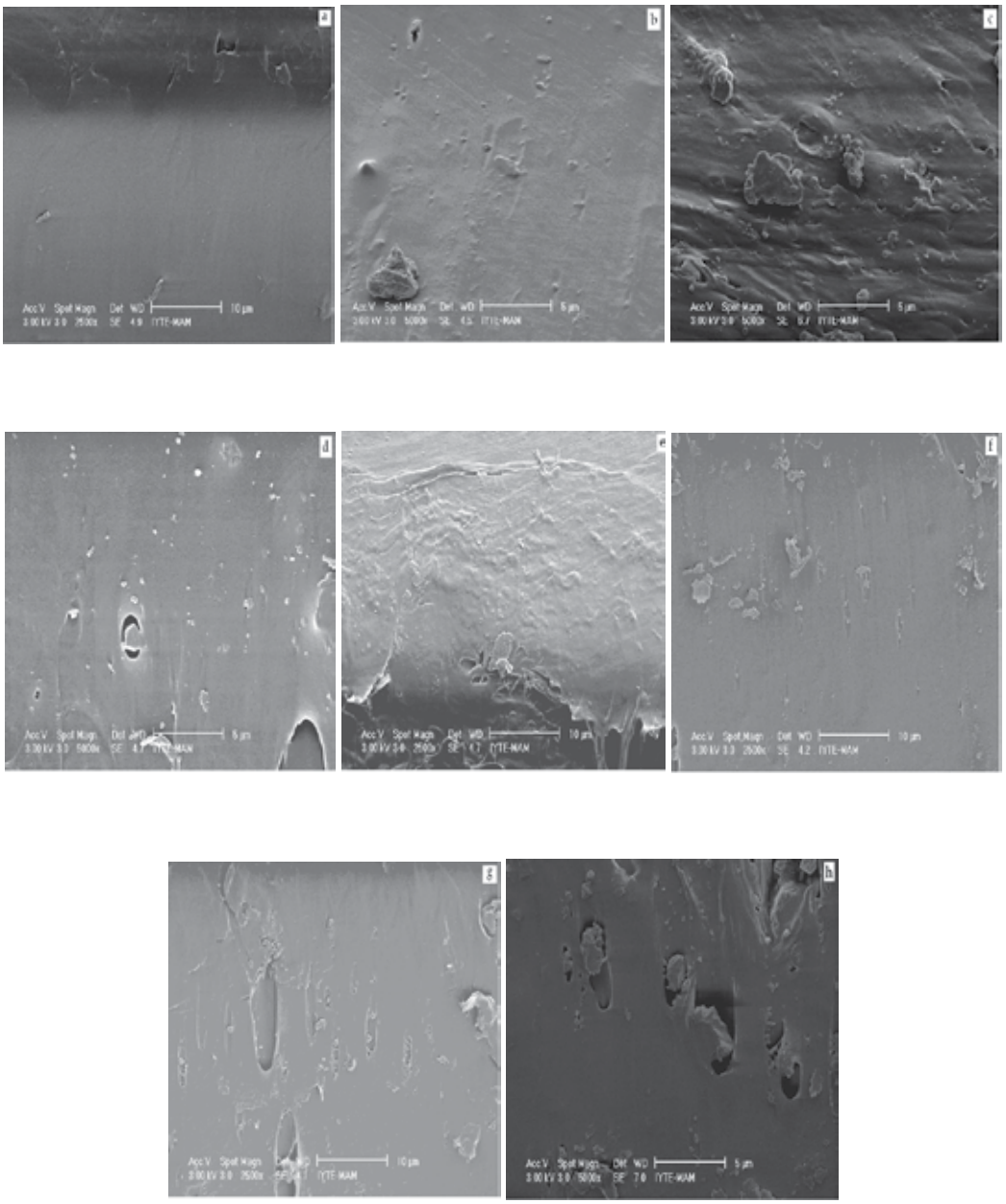

Fig. 1. SEM micrograph of blend and composites (**a**) PC0 (**b**) PC1 (**c**) PC2 (**d**) PC3 (**e**) PC4 (**f**) PC5 (**g**) PC6 (**h**) PC7

Melting (from second heating scans)					Crystallization (from second cooling scans)					
LDPE			PP		LDPE		PP		LDPE	PP
Sample Code	T_m/ °C	ΔH_f/ J.g^{-1}	T_m/ °C	ΔH_f/ J.g^{-1}	T_c/ °C	ΔH_c/ J.g^{-1}	T_c/ °C	ΔH_c/ J.g^{-1}	X_c/ %	X_c/ %
PC0	102.00	2.90	162.10	91.00	95.00	3.00	118.40	88.90	1.00	43.50
PC1	102.60	2.90	162.90	83.10	95.50	1.40	118.90	90.40	1.00	39.80
PC2	102.80	2.30	162.30	73.20	96.80	1.20	119.30	76.00	0.80	35.00
PC3	103.40	2.20	162.60	70.30	99.40	1.10	120.10	66.30	0.70	33.60
PC4	102.50	3.10	162.30	85.50	94.20	2.90	118.50	87.00	1.10	40.90
PC5	103.20	2.40	164.90	81.70	95.30	2.00	119.00	80.40	0.80	34.20
PC6	106.30	2.80	165.10	86.40	99.20	2.80	120.70	86.90	0.70	39.10
PC7	104.70	1.10	164.60	62.00	97.40	1.30	120.40	76.90	0.40	29.70

Table 3. Thermal properties of PP-LDPE/$CaCO_3$ composites

Thermal behavior of the composites was studied with a thermogravimetric analyzer under a protective nitrogen atmosphere. The temperature was scanned from 30 °C to 700 °C at a heating rate of 10 °C.min^{-1}. Figure 2 and 3 shows the typical thermogravimetric curves for composites with/without DAP and different filler contents are presented. 5 % and 20 % weight loss temperatures ($T_{-5\ \%}$ and $T_{-20\ \%}$) and maximum weight loss temperature ($^bW_{max.}T$), derived from the derivative weight loss and differential thermal analysis curves are tabulated in Table 4.

			TG			DTA
Compounds	$^aT_{on}$	$^bW_{max.}T$	weight loss/ (5 %)	weight loss/ (20 %)	residual	Endo
PC0	403	454	406	438	0.5	105.2, 162.2, 457
PC1	402	453	406	438	3	105.8, 162.6, 458
PC2	405	454	407	440	9	106.6, 163.2, 457
PC3	405	455	407	440	18	106.5, 163.5, 459
PC4	407	456	409	443	6	107.2, 164.4, 459
PC5	409	457	413	444	11	107.9, 165.7, 459
PC6	414	461	415	444	11	108.1, 167.3, 462
PC7	414	459	409	444	26	108.7, 164.5, 460

Table 4. Thermal decomposition values of all the compounds (^{a}The onset temperature, ^{b}Maximum Weight Temperature)

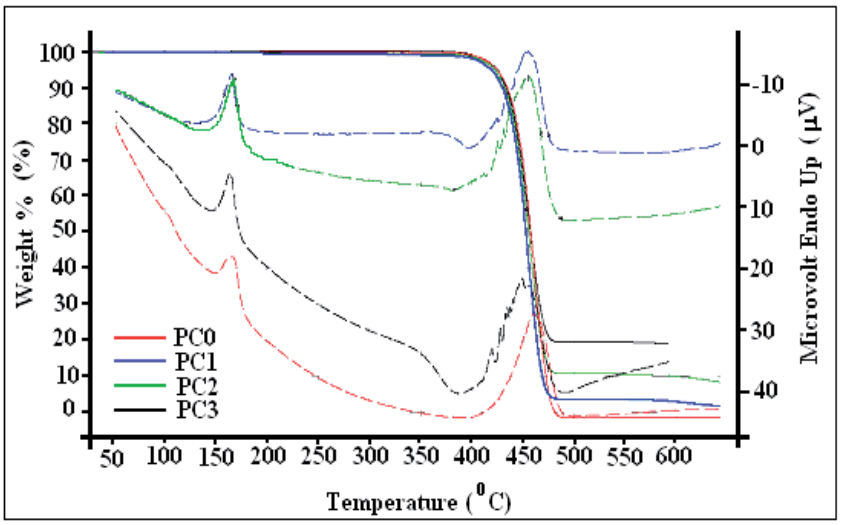

Fig. 2. TG and DTA curves of composites containing the different amounts of $CaCO_3$ (PC0, PC1, PC2, and PC3)

TG curves for all the compounds exhibits one stage decomposition and a similar characterizations. The thermal decomposition of composites occurs between 403 and 500 °C. The thermal stabilities of composites increased usually with increasing $CaCO_3$ content. PC6 has the highest thermal stability among the polymer blends. It is also shown that the rate curve related to compound shifts to a higher temperature. Also, three endothermic thermal effects at different temperature in DTA profiles correspond to the melting and the decomposition of composites. In DTA curves, the first two peaks are two melting peaks.

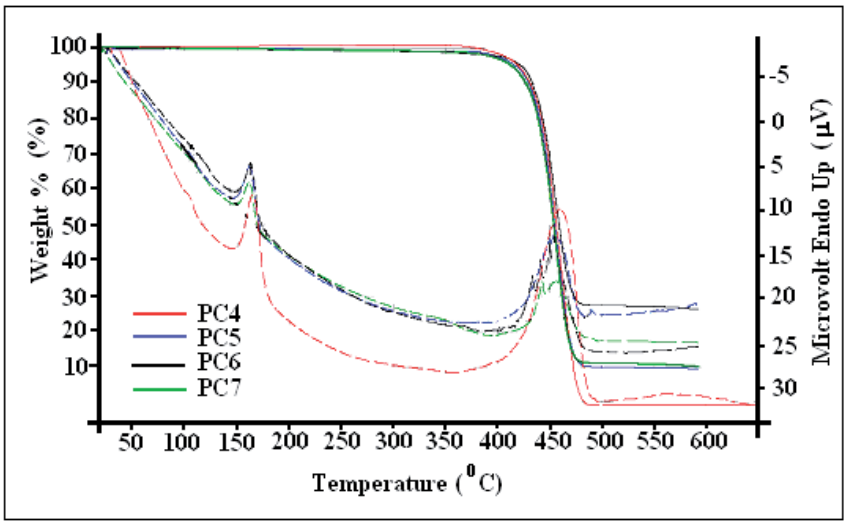

Fig. 3. TG and DTA curves of composites containing the different amounts of $CaCO_3$ (PC4, PC5, PC6 and PC7)

This is another proof showing that the components are incompatible. But $CaCO_3$ dispersed completely in the blends and it didn't result another peak. As observed, melting peaks were between 105-108 ^oC (LDPE) and 162-167 ^oC (PP), decomposition temperatures related to the maximum weight loss ($W_{max.}T$) were between 454-459 ^oC. In the case of composites, although PP and LDPE decomposition completely at 500 °C, according to the amount of $CaCO_3$ 5, 10, or 20 % amount of mass, remained due to the reason that $CaCO_3$'s decomposition temperature is between 850-900°C.

In conclusion, polypropylene-Low Density Polyethylene blends with/without DAP and containing different amount $CaCO_3$ filler component was prepared by melting-blend with a single-screw extruder. The effects of $CaCO_3$ filler component on mechanical and thermal properties of prepared composites were investigated. Addition of $CaCO_3$ particles to the polymer matrix with DAP significantly increased MFI values. It was observed that mechanical properties (tensile strength at break, at yield, elongation at break values and heat sealing strength values) of the composite PC6 showed high peaks. With addition of $CaCO_3$, while mechanical properties of the composites were decreasing shore D values showed increasing. Heat sealing strength at 150 ^oC increased by increasing amount of $CaCO_3$ particles in the polymer matrix with DAP. SEM images showed that $CaCO_3$ particles were well-dispersed in the polymer matrix with DAP. The observation of TG/DTG/DTA curves revealed that the thermal stabilities of composites increased usually by increasing amounts of $CaCO_3$ and the blends are incompatible.

4. Acknowledgements

This study was carried out in Petkim Petrochemical Holding A.Ş., Turkey. In addition, it was supported by the research funds of Celal Bayar University (Project No: FEF-2006/085).

5. References

Ayae, S. & Takashi K. (2004). Calcium carbonate/polymer composites: polymorph control for aragonite, *Composite Interfaces*, vol.11, No.4, pp.287-295(9), ISSN: 1568-5543

Brandrup, J. & Imergut, E.H.(2003). Polymer Handbook Second Edition, John Wiley and Sons, 4th Edition V-(13–27). ISBN: 978-0-471-47936-9

Braun, D.; Richter, S.; Hellmann, G.P. & Ratzsch, M. (1998). Peroxy-initiated chain degradation, crosslinking, and grafting in PP-PE blends, *Journal of Applied Polymer Science*, vol.68, No.12, pp.2019-2028. ISSN:1097-4628

Chen, N.; Wan, C.Y.; Zhang, Y. & Zhang, Y.X. (2004). Effect of nano-$CaCO_3$ on mechanical properties of PVC and PVC/Blendex blend. *Polymer Testing*, vol.23, No.2, pp.169-194, ISSN: 0142-9418

El-Sabbagh, A.; Steuernagel, L. & Ziegmann, G.(2009). Processing and modeling of the mechanical behavior of natural fiber thermoplastic composite: Flax/polypropylene. *Polymer Composites*, vol.30, pp.510-519, ISSN:1548-0569

Gonzalez, J.; Albano, C.; Ichazo, M. & Diaz, B.(2002), Effects of coupling agents on mechanical and morphological behavior of the PP/HDPE blend with two different $CaCO_3$. *European Polymer Journal*, 38(12), 2465-2475. ISSN: 0014-3057

Jancar, J. & Dibenedetto, A.T.(1995). Failure mechanics in ternary composites of polypropylene with inorganic fillers and elastomer inclusions: Part II Fracture toughness. *Journal of Materials Science*, 30(9), 2438-2445, ISSN:1573-4803.

Kim, B.K.; Kim, M.S. & Kim, K.J.(1993). Viscosity effect in polyolefin ternary blends and composites *Journal of Applied Polymer Science*, 48(7), 1271-1278

Kolarik, J. & Jancar, J. (1992). Ternary composites of polypropylene/elastomer/calcium carbonate: effect of functionalized components on phase structure and mechanical properties. *Polymer,* vol.33, pp.4961-4967. ISSN: 0032-3861

Liang, J.Z.(2007), Flow and mechanical properties of polypropylene-low density polyethylene blends. *Journal of Material Processing Technology,* 66, 158-164, ISSN:0924- 0136

Ma,C.G.; Mai, Y.L.; Rong, M.Z.; Ruan, W.H. & Zhang M.Q. (2007). Phase structure and mechanical properties of ternary polypropylene/elastomer/nano-$CaCO_3$ composites, *Composites Science and Technology*, vol.67, No.14, pp.2997-3005, ISSN: 0266-3538

Mishra, S.; Perumal, G.B. & Naik, J.B. (1997). Studies on Mechanical Properties of Polyvinyl Chloride Composites. *Polymer-Plastics Technology and Engineering*, vol.36, No.4, pp.489-500, ISSN: 1525-6111.

Premphet, K. & Horanont, P.(2000). Polymer, Phase structure of ternary polypropylene /elastomer /filler composites: effect of elastomer polarity, *Polymer*, 41, 9283–9290, ISSN: 0032-3861

Rai, U.S. & Singh, R.K. (2003). Synthesis and mechanical characterization of polymer-matrix composites containing calcium carbonate/white cement filler. *Materials Letters,* vol.58, pp.235– 240, ISSN:0167-577X

Shonaike, G.O. & Advani, S.G.(2003). Advanced Polymeric Materials Structure Property Relationships, CRC Pres, pp. 463-478, ISBN 1-58716-047-1, New York, USA

Sirin, K. & Balcan, M.(2010). Mechanical properties and thermal analysis of low-density polyethylene + polypropylene blends with dialkyl peroxide. *Polymer Advanced Technology*, vol.21, pp.250–255, ISSN: 1099-1581.

Şirin, K. (2008). Preparation of polymer blends and their composites, and determination of their properties, PhD.Thesis, Ege University, Izmir, Turkey.

Tang, C.Y. & Liang, J.Z.(2003), A study of the melt flow behaviour of ABS/$CaCO_3$ composites, *Journal of Materials Processing Technology*, vol.138, pp.408–410. ISSN: 0924-0136

Wang, W.Y.; Wang, G.Q.; Zeng, X.F.; Shao, L. & Chen, J.F. (2008). Preparation and properties of nano-$CaCO_3$/acrylonitrile-butadiene-styrene composites. *Journal of Applied Polymer Science*, vol.107, No.6, pp.3609-3614, ISSN:1097-4628

Wang, W.Y.; Zeng, X.F.; Wang, G.Q. & Chen J.F.(2007). Preparation and Characterization of Calcium Carbonate/ Low-Density-Polyethylene Nanocomposites. *Journal of Applied Polymer Science,* vol.106. No.3, pp.1932-1938. ISSN:1097-4628

Zhang, L.; Wang, Z.H.; Huang, R.; Li, L.B. & Zhang, XY. (2002). PP/elastomer/calcium carbonate composites: effect of elastomer and calcium carbonate contents on the deformation and impact behavior. *Journal of Materials Science,* vol.37, pp.2615-2621, ISSN:1573-4803

Zweifel, H. (2001).Plastic additives Handbook, Ch14, Crosslinking and Controlled Degradation of Polyolefin, ISBN: 3- pp.723, 446-19579-3, Switzerland

19

The Effects of Adding Nano-Calcium Carbonate Particles on the Mechanical and Shrinkage Characteristics and Molding Process Consistency of PP/nano-CaCO3 Nanocomposites

Karim Shelesh-Nezhad, Hamed Orang and Mahdi Motallebi
University of Tabriz
Iran

1. Introduction

The performance characteristics of plastic injection molded parts are depended upon the compositions of processing raw materials, parts and molds design specifications as well as the processing conditions. By appropriate incorporation of additives into a polymer matrix, it is possible to achieve the desired characteristics in the molded parts. Polypropylene (PP) is a semi-crystalline thermoplastic and is widely used for general applications. PP possesses the advantages of processing ease, very resistant to moisture absorption, and good chemical resistance to solvents. However, its applications as an engineering thermoplastic are limited due to its high shrinkage rate and relatively poor impact resistance at room or low temperatures (Lam et al., 2009).

Recent developments in fillers and reinforcements technology have made it possible to enhance the properties and applications of PP. In formulating different compositions of materials, it is essential to bring into account the cost effectiveness, adding value, ease of processing and wide range of applications. Types, shapes, concentrations and dimensional conditions of fillers and reinforcements may directly affect the processing ease, production consistency, molding cycle time, parts dimensional conditions, mechanical, thermal as well as tribological properties. Platelike and layered particles may lead to poor impact strength, and the impact resistance is in reverse proportion to particle size (DeBoest, 1988; Mohd Ishak et al., 2008). These fillers may act either as sites of stress concentration or micro cracks initiator. Micron-sized spherical fillers such as CaCO3 have marginal influence on the impact resistance (DeBoest, 1988). While nano-sized CaCO3 may act as a nucleating agent (Avella et al., 2006) and impact modifier (K. Yang & Q. Yang, 2006) in a polymer matrix. The presence of nano-CaCO3 may possibly facilitate the mobilization of macromolecular chains and improve the ability of matrix polymer to adapt to deformation and hence to increase the ductility and impact strength of composites. The nanoparticles may also initiate micro-void formations which locally deform the matrix surrounding the particles and initiate mass plastic deformation and, in consequence, increase the toughness and impact energy (Kemal

et al., 2009). Stiffness or Young's modulus can be readily improved by adding either micro- or nano-particles since rigid inorganic particles generally have a much higher stiffness than polymer matrices. However, strength strongly depends on the stress transfer between the particles and the matrix. For well-bonded particles, the applied stress can be effectively transferred to the particles from the matrix; this clearly improves the strength (Fu et al., 2008).

Due to its non-polar chemical structure, PP interacts poorly with the typically polar fillers such as CaCO3, and optimum dispersion is normally difficult to achieve. Compatibilisers are frequently used to improve the interfacial adhesion between CaCO3 and PP, in order to gain the envisaged enhancement in mechanical properties (Fuad et al., 2010). Bi-functional molecules such as maleic-anhydride grafted PP (PP-g-MAH) are commonly used as compatibilisers for PP and CaCO3 (Roberts & Constable, 2003).

The crystallographic morphology of PP matrix can be noticeably altered by the presence of nano-CaCO3 because of its nucleating effect (Lin et al., 2011; Zhang et al., 2004). The coated CaCO3 nanoparticles affect the crystallization of PP in two ways: by serving as heterogeneous nucleation sites and also by reducing the spherulitic growth rate due to block the diffusion of polymer chains. Heterogeneous nucleation is, however, the dominating step controlling the crystallization rate of the PP/CaCO3 nanocomposite blends (Lin et al., 2011).

Besides mechanical properties, thermal contraction and uniformity of molded samples may also be influenced by different concentrations of the nano-CaCO3 in PP matrix. The objective of this research is to determine mechanical performances, shrinkage behavior and at the mean time the injection molding consistency of PP filled with nano-CaCO3 particles. In this research, PP/nano-CaCO3 polymer nanocomposites of different compositions were prepared by using a twin-screw extruder. PP-g-MAH compatibiliser was applied to improve the interfacial interaction between nano-CaCO3 and PP, and to extend the dispersion of nanoparticles in polymer matrix. An injection molding machine was employed to produce the standard specimens. The melt pressure inside the mold cavity was measured during the injection molding process of PP-CaCO3 nanocomposites to assess the production consistency. Dimensional conditions of different samples were characterized in order to determine the effect of nano-CaCO3 inclusion on the shrinkage rates. Morphology was observed and tensile, flexural and impact properties were examined to ascertain the influence of nano-CaCO3 on the mechanical performances.

2. Experimental procedures

2.1 Material used, compounding and sample preparation

Polypropylene (PP500P, SABIC) has melt flow rate of 3.1 (2.16 kg at 230 °C) and density of 905 kg/m^3 was used as matrix resin. Nano-sized synthetic ultrafine surface treated precipitated calcium carbonate (Socal 312, Solvay, France) with mean particle diameter of 70 nm used as filler phase. PP-g-MAH compatibiliser (Priex 20097, Solvay, France) with a maleic anhydride content of 0.05 wt % and MFI of 15 (2.16 kg at 230 °C) was employed to promote the interfacial interaction between nano-CaCO3 and PP, and to extend the dispersion of nanoparticles in polymer matrix. Compounds used as processing materials are listed in the table 1.

Material	PP (wt%)	nano-CaCO3 (wt%)	PP-g-MAH (wt%)
PP	100	0	0
P5	94	5	1
P10	88	10	2
P15	82	15	3

Table 1. List of various compounds used in the experimentations

The neat PP and PP-g-MAH were dried in a vacuum oven at 80°C for 6 hours. Melt extrusion technique was applied to produce different compositions of PP/nano-CaCO3 by a ZSK-25 (Coperion Werner Pfliederer-Germany) co-rotating twin-screw extruder (D= 25 mm, L/D = 40) with a barrel temperature profile ranging from 160°C near the hopper to 200°C at the die and a screw speed of 400 rpm.

Molded samples utilized throughout the experimentations comprised standard tensile (ASTM D-638), flexural (ASTM D-790) and impact (ASTM D-256) specimens. An advanced microprocessor control injection molding machine (Poolad-110/380) with clamping force capacity of 110 tones and shot size capacity of 268 grams was employed to produce corresponding samples. The reciprocating screw diameter was equal to 45 millimeters and the ratio of screw length to diameter was 20. The values of molding parameters settings for standard tensile, flexural and impact specimens are given in table 2. The values of different settings were obtained on the basis of dimensional conditions of molds cavities and feed channels and in a manner to produce samples free of defects.

Molding Parameter	Unit	Value for tensile specimens	Value for Flexural and impact specimens
Nozzle Temperature	˚C	180	180
Mold Temperature	˚C	40	40
Injection Pressure	MPa	57	89
Injection Speed	cm^3/s	68	68
Holding Time	s	8	15
Holding Pressure	MPa	32	63
Screw feeding speed	rpm	108	108

Table 2. The values of molding parameters settings for standard tensile, flexural and impact specimens

2.2 Characterization

2.2.1 Molding process consistency

The uniformity of injection molding process of different compounds was characterized by melt pressure measurement inside the mold cavity. A piezo-electric sensor (9221 AA0.6, Kistler, Switzerland) incorporated inside the tensile mold cavity and located behind and in contact to the ejector pin to measure the force exerted to the pin by melt pressure during the cyclic molding process against the time. The influence of nano-CaCO3 inclusion in the PP

matrix resin on the sameness of pressure-time profiles and hence the variation of molding process was investigated. Two variables encompassing the maximum force and the force-time integral were chosen as the control parameters to assess the consistency of injection molding process during the molding cycles. For each compound, 10 samples were examined and the mean values of control parameters were considered.

2.2.2 Dimensional conditions

Standard tensile specimens (ASTM D-638) of PP with different contents of nano-CaCO3 were molded and employed to analyze the dimensional conditions and shrinkage rates. Figure 1, indicates the reference dimensions and their locations for shrinkage estimation of corresponding molded parts. The reference dimensions of matching cavity including cavity length, width and depth were equal to the 165.83, 19.10 and 3.20 millimeters respectively. The molded parts reference dimensions including parts length, width and thickness were measured with 0.01 mm accuracy after passing two weeks of molding. The differences of cavity dimensions and molded parts dimensions were considered as shrinkage values. For each compound, 5 samples were tested and the mean values were taken into account.

Fig. 1. Reference dimensions and their locations for shrinkage assessment of part length (L), part width (W) and part thickness (H)

2.2.3 Mechanical properties

Tensile, flexural and impact tests were performed based on the ASTM D-638, ASTM D-790 and ASTM D-256 standards respectively in order to analyze the effect of adding nano-CaCO3 particles on the mechanical performances of PP/CaCO3 nanocomposites. For each compound, 5 samples were tested and the mean values were considered. The specifications of testing equipment and conditions are presented in table 3.

Tensile test	
Manufacturer: Zwick/Roll	Model: TIFR010THA50
Load range: 0.5 g to 3000 kg	Adjusted load sensitivity: 0.5 g
Speed range: 1 to 200 mm/min	Adjusted crosshead speed: 50 mm/min
Impact resistance test	
Manufacturer: Gotech	Model: GT-7045-I
Capacity: 100 kg-cm	Test type: Izod-type
Flexural strength test	
Manufacturer: Gotech	Model: GT-7010A2
Load range: 3000 kg	Speed range: 10 to 200 mm/min
Extension range: 10.00 mm	Span: 30.00 mm
End point: 7.00 mm	Adjusted speed: 10 mm/min

Table 3. The specifications of mechanical properties testing equipment and conditions

2.2.4 SEM

A scanning electron microscope (Tescan VegaII) was employed to observe the dispersion of nano-CaCO3 particles in PP matrix in the fracture sections of impact specimens. Prior to SEM observations, the samples were made conductive by gold sputtering.

3. Results and discussions

3.1 Melt flow rate

Figure 2, indicates the melt flow rates of different compounds of PP/nano-CaCO3 with respect to the nano-CaCO3 contents.

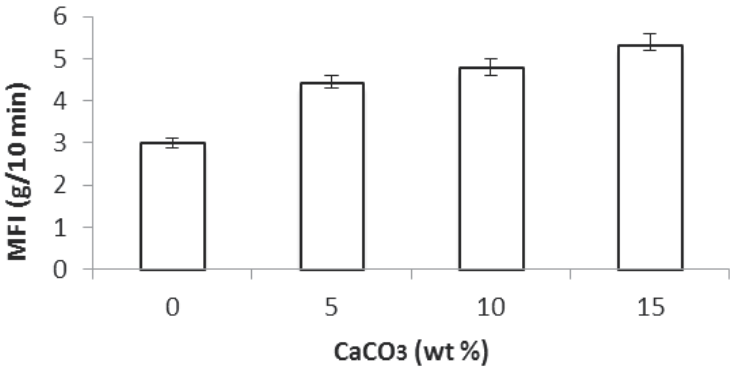

Fig. 2. Melt flow rate versus nano-CaCO3 contents

Inclusion of nano-CaCO3 considerably raised the melt flow rate. The presence of nano-CaCO3 in the molten PP has a rolling effect which facilitates sliding of melt on the cylinder wall of MFI tester (Jiang & Huang, 2008). According to Xie et al., spherical nanoparticles serve as ball bearings, reducing the interlayer interaction of melts (2004). The increment of MFI rate can facilitate the injection molding of thin-walled parts and can lead to the reduction of energy consumption of molding process.

3.2 Injection molding uniformity

The results of melt pressure measurement during the molding cycles for different compounds are indicated in table 4 and figure 3.

Material	Integral (N-s)		Max. Force (N)	
	Ave. Value	Std Dev.	Ave. Value	Std Dev.
PP	4953.29	133.30	843.28	8.75
P5	4923.87	138.26	820.49	11.20
P10	4894.25	50.45	826.49	7.49
P15	4468.54	52.53	800.05	4.46

Table 4. The magnitudes of control parameters and their deviations during the molding process

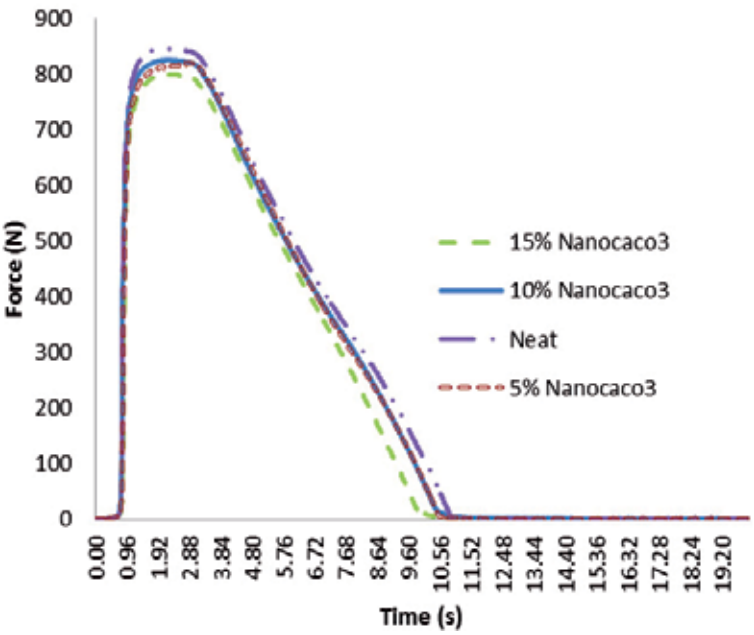

Fig. 3. Force-time traces of different compounds

As the nano-CaCO3 loading was increased, the maximum force and the force-time integral were decreased. This may be attributed to the influence of nano-CaCO3 on melt fluidity and crystallization behavior of PP matrix. By incorporating higher loading of nano-CaCO3 (10 and 15 wt%), the deviation of molding process was significantly declined. By adding 15 wt% of nano-CaCO3, the maximum force standard deviation dropped from 8.75 to 4.46 (N) and the force-time integral standard deviation declined from 133.30 to 52.53 (N-s). According to the figure 3, by increasing the nano-CaCO3 content in the PP matrix, a change in the slope on the right side of force-time profile is observed. This may possibly be related to the increase of PP crystallinity and, in consequence, higher thermal contraction of melt during the molding process, as a result of nano-CaCO3 presence.

3.3 Shrinkage behavior

Table 5, indicates the shrinkage rates along the flow, across the flow, and along the thickness of molded parts with respect to the amount of nano-CaCO3 content.

nano-CaCO3 (wt%)	Ave. Shrinkage along the flow (%)	Ave. Shrinkage across the flow (%)	Ave. Shrinkage along the flow thickness (%)
0	1.64	1.74	5.00
5	1.42	1.50	4.93
10	1.51	1.65	4.87
15	1.53	1.64	4.62

Table 5. Effect of nano-CaCO3 concentration on the shrinkage of PP/nano-CaCO3

The neat PP possessed the highest shrinkage rate. The inclusion of nano-CaCO3 reduced the thermal contraction because of its filling effect and its lower thermal contraction. The molded samples with concentration of 5 wt% nano-CaCO3 possessed the lowest shrinkage along the flow and across the flow directions. Addition of higher values of nano-CaCO3 (10, 15 wt%) to the PP, elevated the shrinkage rates along and across the flow directions. Nano-CaCO3 has nucleating effect and can lead to the increment of crystallization rate in the PP matrix (Chan et al., 2002; K. Yang & Q. Yang, 2006). Addition of higher values of nano-CaCO3 (10, 15 wt%) to the PP, slightly increased the tendency of non-isotropic thermal contraction along and across the flow directions. This can possibly be related to increment of PP crystallinity as a result of higher loadings of nano-CaCO3, and non-isotropic crystal growth of PP Matrix.

3.4 Morphology

Figure 4, indicates the presence and distribution of nano-CaCO3 (5 and 15 wt%) in the PP matrix in the cross sections of impact test samples. Higher concentration of nano-CaCO3 particles is observed in the PP matrix with higher content, i.e. 15wt%, of nano-CaCO3. Due to the surface modification of nano-CaCO3 and application of PP-g-MAH compatibiliser, relatively good dispersions of nanofillers were achieved. According to figure 4-b, more tendency to agglomerate is observed at 15 wt% loading of nano-CaCO3.

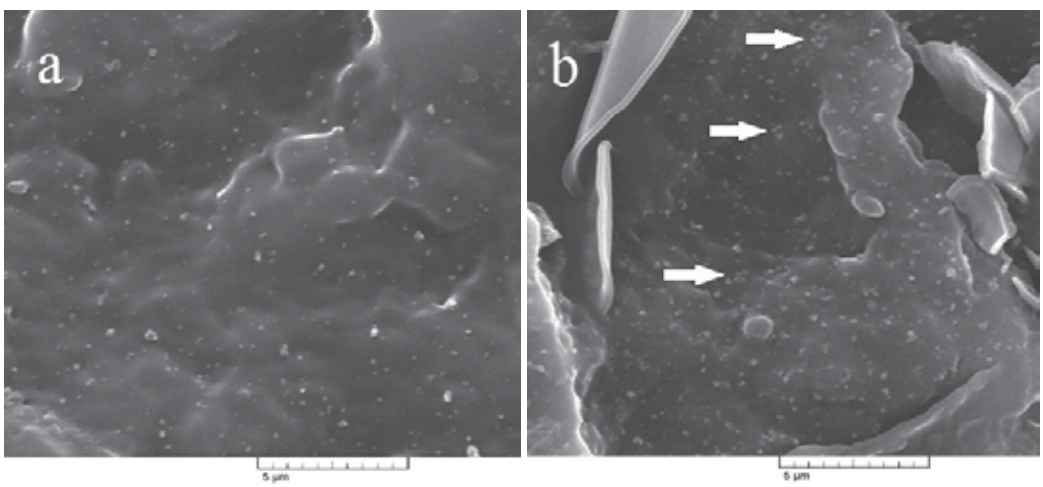

Fig. 4. Morphologies of PP/nano-CaCO3 at two loadings of (a) 5 and (b) 15 wt% of nano-CaCO3

3.5 Mechanical properties

The tensile tests results of various compounds of PP/nano-CaCO3 are indicated in Table 6 and Figures 5 and 6.

Material	Ave. Elastic modulus (Mpa)	Ave. Tensile Strength (Mpa)	Ave. Strength at break (Mpa)	Ave. Elongation at break (%)
PP	960.17	36.04	19.81	75.03
P5	971.65	35.67	11.62	122.88
P10	983.94	34.64	6.81	161.29
P15	990.41	33.80	7.58	118.87

Table 6. The results of tensile tests

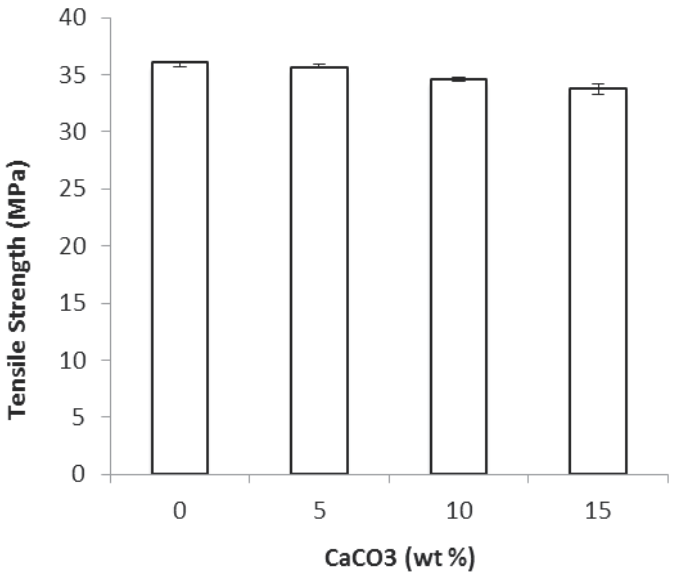

Fig. 5. Tensile strength of PP/nano-CaCO3 against nano-CaCO3 content

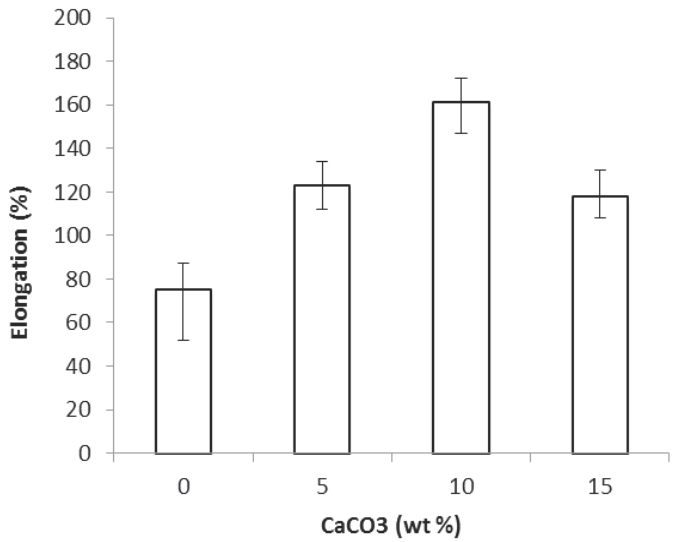

Fig. 6. Elongation of PP/nano-CaCO3 against nano-CaCO3 content

Figure 7, Compares the stress-strain characteristics of median specimens of different compounds.

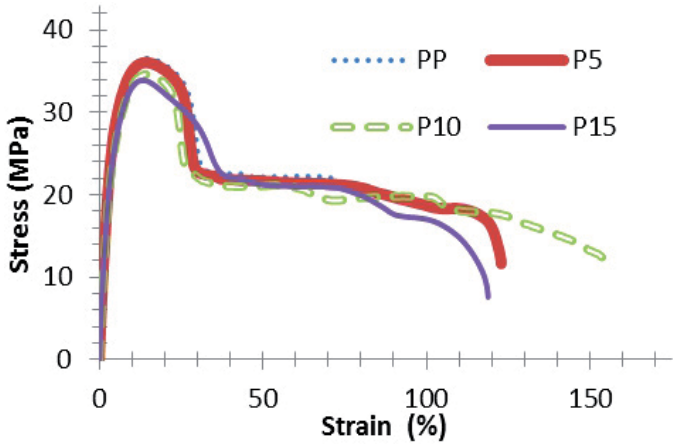

Fig. 7. The influence of adding nano-CaCO3 on the stress-strain behavior of PP/nano-CaCO3

The results of tensile tests revealed that the inclusion of nano-CaCO3 slightly increased modulus and decreased tensile strength and significantly increased the elongation at break. Addition of rigid particles to a polymer matrix can easily improve the modulus since the rigidity of inorganic fillers is generally much higher than that of organic polymers (Fu et al., 2008). The reduction of tensile strength may be attributed to the weakly bonded nanoparticles which promote matrix yielding (Kemal et al., 2009). According to Zhang et al., when CaCO3 particles were introduced, small and imperfect spherulites formed. The reduction of spherulite size and the disappearance of sharp interfaces among spherulites favored the increase of elongation at break for the PP/CaCO3 composites (2004). Xie et al. reported that the increases in elongation at break can be attributed to ellipsoidal voids formation in the matrix surrounding the particles, allowing ductile pull out (2004). At high fraction of nano-CaCO3 (i.e.15 wt%), the elongation at break was declined. This result is consistent with the morphology of corresponding compound which shows agglomeration sites of nano particles in the PP matrix as presented in figure 4-b.

Figure 8 depicts the results of flexural tests.

The incorporation of nano-CaCO3 led to the elevation of flexural strength in PP/nano-CaCO3 compounds. This may also be related to the nucleating effect of nano-CaCO3 in the PP matrix. Figure 9 shows the impact tests results.

Addition of nano-CaCO3 elevated the impact strength significantly. This may be explained by the fact that the presence of nano-CaCO3 in the PP matrix lead to a more uniform distribution of impact energy. Additionally, the presence of nano-CaCO3 may influence the crystallization behavior by reducing the spherulites size and subsequently alter the impact strength. Kemal et al. reported that the raise of toughness and impact energy may be attributed to enhanced micro-void formations initiated by nanoparticles, which locally deform the matrix surrounding the particles and initiate mass plastic deformation (2009).

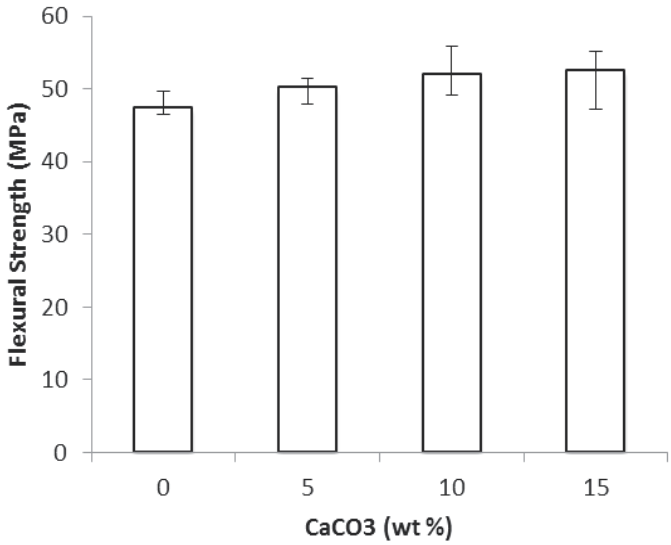

Fig. 8. Flexural strength of PP/nano-CaCO3 versus nano-CaCO3 content

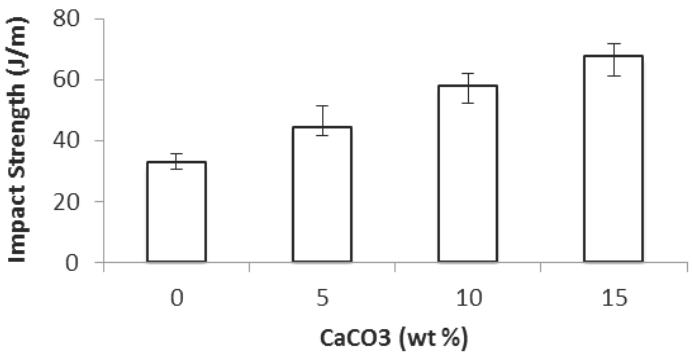

Fig. 9. Impact strength of PP/nano-CaCO3 versus nano-CaCO3 content

4. Conclusion

In this study the influences of nano-CaCO3 on the production consistency, shrinkage and melt flow rates, as well as mechanical properties of PP/nano-CaCO3 nanocomposites were experimentally investigated. PP-g-MAH compatibiliser with a maleic anhydride content of 0.05 wt% was employed to improve the interfacial adhesion between nano-CaCO3 and PP and to extend dispersion of nanoparticles in polymer matrix. Inclusion of nano-CaCO3 raised the melt flow rate as high as 77%. By incorporating higher loading of nano-CaCO3 (10 and 15 wt%), the deviation of molding process was significantly declined. The molded samples with concentration of 5 wt% nano-CaCO3 possessed the lowest shrinkage along the flow and across the flow. The results of tensile tests revealed that the inclusion of nano-CaCO3 slightly increased modulus and decreased tensile strength and significantly increased the elongation at break. At high fraction of nano-CaCO3 (i.e.15 wt%), the elongation at break was declined. Addition of nano-CaCO3 elevated the impact strength as

high as 107%. The nano-sized feature, shape and dispersion conditions of nano-CaCO3, played important roles in determining the performances of PP/nano-CaCO3.

5. References

Avella, M.; Cosco, S., Di Lorenzo, M.L., Di Pace, E. & Errico, M.E. Gentile G. (2006). Nucleation activity of nanosized CaCO3 on crystallization of isotactic polypropylene, in dependence on crystal modification, particle shape, and coating. *European Polymer Journal*, Vol. 42, pp. (1548–1557)

Chan, C.M.; Wu, J.S., Lee, J. X. & Chung, Y. K. (2002). Polypropylen/calcium carbonate nanocomposites. *Polymer*, Vol. 43, pp. (2981-2992)

DeBoest, J. F. (1988). Reinforced polypropylenes, In: *Engineering Plastics*, pp. (192-193)

Fu, S.Y.; Feng, X.Q., Lauke, B. & Mai, Y. W. (2008). Effects of particle size, particle/matrix interface adhesion and particle loading on mechanical properties of particulate–polymer composites. *Composites*: Part B, Vol. 39, pp. (933–961)

Fuad, M.Y.A.; Hanim, H., Zarina, R., Mohd Ishak, Z.A. & Hassan, A. (2010). Polypropylene/calcium carbonate nanocomposites – effects of processing techniques and maleated polypropylene compatibiliser. *eXPRESS Polymer Letters*, Vol. 4, pp. (611–620)

Jiang, G. & Huang, H.X. (2008). Online shear viscosity and microstructure of PP/nano-$CaCO_3$ composites produced by different mixing types. *Journal of Materials Sci*ence, Vol. 43, No. 15, pp. (5305–5312)

Kemal, I.; Whittle, A., Burford, R., Vodenitcharova, T. & Hoffman, M. (2009). Toughening of Unmodified Polyvinylchloride through the Addition of Nanoparticulate Calcium Carbonate. *Polymer*, Vol. 50, pp. (4066-4079)

Lam, T. D.; Hoang, T. V., Quang, D. T. & Kim, J. S. (2009). Effect of nanosized and surface-modified precipitated calcium carbonate on properties of CaCO3/polypropylene nanocomposites. *Materials Science and Engineering*: Part A, Vol. 501, pp. (87–93)

Lin, Y.; Chen, H., Chan, C.M. & Wu, J. (2011). Nucleating effect of calcium stearate coated CaCO3 nanoparticles on polypropylene. *Journal of Colloid and Interface Science*, Vol. 354, pp. (570–576)

Mohd Ishak, Z.A.; Kusmono, Chow, W.S., Takeichi, T. & Rochmadi (2008). Effect of Organoclay Modification on the Mechanical, Morphology, and Thermal Propertiese of Injection Molded Polyamide6/Polypropylene/ Montmorillonite Nanocomposites. *Proceedings of the Polymer Processing Society 24th Annual Meeting*, Salerno (Italy), June 2008

Roberts, D. & Constable, R.C. (2003). Chemical coupling agents for filled and grafted polypropylene composites, In: *Handbook of Polypropylene and Polypropylene Composites,* Karian, H. G., pp. (28–68), Marcel Decker, New York

Xie, X.L.; Liu, Q.X., Li, R.K.Y., Zhou, X.P., Zhang, Q.X., Yu, Z.Z. & Mai, Y.W. (2004). Rheological and Mechanical Properties of PVC/CaCO3 Nanocomposites Prepared by In Situ Polymerization. *Polymer*, Vol. 45, pp. (6665-6673)

Yang, K. & Yang Q. (2006). Morphology and mechanical properties of polypropylene/calcium carbonate nanocomposites. *Materials Letters*, Vol. 60, pp. (805-809)

Zhang, Q.X.; Yu, Z.Z., Xie, X.L. & Mai, Y.W. (2004). Crystallization and Impact Energy of Polypropylene/CaCO3 Nanocomposites with Nonionic Modifier. *Polymer*, Vol. 45, pp. (5985-5994)

20

Preparation of Polypropylene Nanocomposites Using Supercritical Technology

Jia Ma and Ton Peijs
Queen Mary University of London
UK

1. Introduction

In recent years polypropylene (PP) nanocomposites have attracted great interest in academia. The attractiveness of this new class of material lies in the large improvements in both mechanical and thermal properties, as well as in gas barrier and fire resistance (Grunes et al., 2003). Nanofillers, being additives of nanometre scale, are dispersed in PP matrix, offering multifunctional and high-performance polymer characteristics beyond those possessed by traditional filled materials.

Many methods have been employed for preparing PP nanocomposites (Wu & Lerner, 1993; Andrews et al., 2002; Zhao et al., 2003; Garcia-Leiner and Lesser, 2004). Among them, supercritical CO_2 technology has been intensively studied in recent years. The main advantages of this technology are that CO_2 is a 'green' non-combustible and non-toxic solvent and the addition of $scCO_2$ into the polymer can cause plasticization, which brings the opportunity to lower polymer viscosity, leading to improved dispersion, and to process the polymer at lower temperatures (Behles & Desimone, 2001; Cansell et al., 2003). Furthermore, CO_2 can act as a transport medium, which facilitates the diffusion of monomers, initiators and molecules into a polymer matrix (Kikic & Vecchione, 2003). The aim of this chapter is to provide a review of the use of supercritical CO_2 technology in the preparation of PP nanocomposites. In this chapter, the different nanofillers used, the processing methods based on using supercritical CO_2 technology and the resulting properties of the nanocomposites will be discussed in detail. The progress and challenges on various aspects of PP nanocomposites will also be discussed.

2. Nanofillers

The term 'nanofillers' is vague and no precise definition exists. Nanofillers are understood, in essence, to be additives in solid form, which differ from the polymer matrix in terms of their composition and structure. Nanofillers are of the order of 100 nm or less in at least one dimension.

Nanofillers are often added to enhance one or more of the properties of polymers. Inactive fillers or extenders raise the quantity and lower the cost price, while active fillers bring about targeted improvements in certain mechanical or physical properties. Common nanofillers include calcium carbonate, ceramic nanofillers, carbon black, carbon nanotubes (CNTs), carbon

nanofibres, cellulose nanowhiskers, nanoclays, gold particles, kaolin, mica, silica, silver nanoparticles, titanium dioxide, etc. Because of their impressive intrinsic mechanical properties, nanoscale dimensions and high aspect-ratio, nanofillers such as CNTs or nanoclays are among the most promising due to the fact that small amounts (less than 5 %) of them can provide the resulting nanocomposite material with significant property improvements.

2.1 Carbon Nanotubes (CNTs)

CNTs are considered to be ideal candidates for a wide range of applications in materials science because of their exceptional mechanical, thermal, and electronic properties (Baughman & Zakhidov, 2002). Carbon nanotubes exist as two types of structures: singlewall carbon nanotubes (SWNTs) and multiwall carbon nanotubes (MWNTs). Fig. 1 shows the schematic pictures of different types of carbon nanotubes. SWNT can be considered as graphene sheet rolled cylinders of covalently bonded carbon atoms with very high aspect ratios of 1000 or more. MWNTs consist of a number of graphene cylinders concentrically nested like rings in a tree trunk with an interlayer distance of ~0.34 nm.

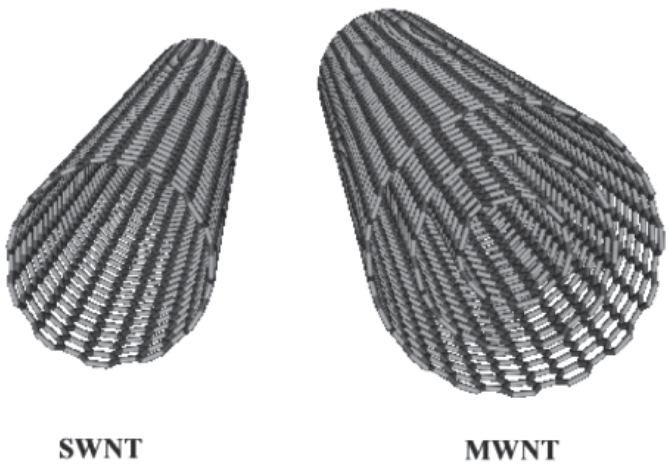

Fig. 1. A schematic illustration of a single-walled carbon nanotube and a multi-walled carbon nanotube (Dresselhaus et al., 2003).

The carbon-carbon covalent bonds in graphite and carbon nanotubes are considered to be one of the strongest atomic bonds in nature. The mechanical properties of CNTs have been extensively studied, both experimentally and theoretically (Yakobson et al., 1996; Lu, 1997). CNTs possess tensile moduli and strengths as high as 1 TPa and 150 GPa respectively. Especially in terms of strength CNTs are exceptional as this value is more than an order of magnitude higher than for high strength carbon fibres. Their density can be as low as 1.3 $g.cm^{-3}$, which is lower than commercial carbon fibres at 1.8-1.9 $g.cm^{-3}$. CNTs are thermally stable at up to 2800 ^{o}C in vacuum. Their thermal conductivity is about twice as high as that of diamond, while their electric-current-carrying capacity is 1000 times higher than that of copper wires (Thostenson et al., 2001).

Since the first CNTs and polymer composites were made in 1994 (Ajayan et al., 1994), large amounts of work have been done on polymer/CNT composites. Incorporating nanotubes

into plastics can potentially provide structural materials with a dramatic increase in both stiffness and strength. Extensive studies have been carried out producing strong polymer/CNT composites (Coleman et al., 2006; Moniruzzaman & Winey, 2006; Ahir, 2005, Wang et al., 2007). The effective use of CNTs as reinforcements still presents some major difficulties (Wang et al., 2007). The key challenge still remains in breaking down bundles of aggregated CNTs and reaching a fine dispersion in the selected polymer matrix. Much work needs to be done to optimise the conditions required for the potential dispersion of nanotubes, especially at higher CNT loadings, as well as a good interfacial interaction (Moniruzzaman & Winey, 2006).

CNTs have extremely low electrical resistance and their electric-current-carrying capacity is 1000 times higher than copper wires (Thostenson et al., 2001). Devices have been developed using CNTs such as field-emission displays (Fan et al., 1999). CNTs have also been widely used to produce conductive polymer composites (CPCs). It has been reported that the percolation threshold in CPC can be as low as 0.0025 wt% in the case of low viscosity thermosetting resins (Bryning et al., 2005). In thermoplastics the percolation threshold is typically around 1 wt%, but can be significantly lower using latex technology (Lu et al., 2008) and is highly dependent on processing history (Zhang et al., 2009; Deng et al., 2009a and 2009b).

2.2 Nanoclays

Clay is a natural, earthy, fine-grained material and is the main constituent of the sedimentary rocks in marine sediments and in soils. Clay minerals belong to the family of phyllosilicates (or layered silicate) and have particles less than 2 μm in size as stated in ISO 14688 (Moore & Reynolds, 1997). There are three main groups of clays: kaolinite, montmorillonite-smectite and halloysite, and most clay are a mixture of these different types. The shape of clay minerals is of a distinctive character. Montmorillonite, which has irregular flakes, is the most commonly used nanoclay in polymer/clay nanocomposites (Fig. 2a). Recently, sepiolite, a fibrous shaped mineral, has gained increasing attention as nanofiller reinforcement (Y.P. Zheng &Y. Zheng, 2006). Sepiolite is a needle-like shaped nanoclay composed with elemental particles of lengths of 0.2-4 μm, widths of 10-30 nm and thicknesses of 5-10 nm (Fig. 2b). Sepiolite can have a surface area as high as 200-300 $m^2 \cdot g^{-1}$ and normally it is found stuck together as bundles of fibres which can form micro-agglomerates. Sepiolite is a hydrous magnesium silicate with $[Si_{12}O_{30}Mg_8(OH)_4(H_2O)_4 \cdot 8H_2O]$ as the unit cell formula.

Compared with layered montmorillonite, the morphology of fibre-like sepiolite provides a lower specific surface area and smaller contact surface between the nanoclay particles. Therefore, polymer chains have a better chance not only of interacting with the external surface of the sepiolite, but also of penetrating into the structure, which facilitates a more even dispersion of the clays in the polymer matrix. Sepiolite provides a pseudoplastic and thixotropic behaviour which make it a valuable material in multiple applications to improve the processability, application or handling of the final product. Sepiolite has been successfully used to reinforce different polymers, such as poly (hydroxyethyl acrylate), epoxy, PP, etc (Bokobza et al., 2004; Y.P. Zheng &Y. Zheng, 2006; Bilotti et al., 2008).

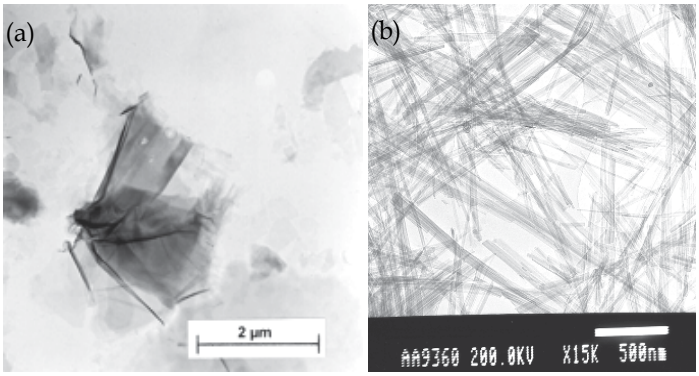

Fig. 2. The structure of (a) montmorillonite (Beermann & Brockamp, 2005) and (b) sepiolite (Bilotti et al., 2008)

3. Polypropylene nanocomposites

For decades we have been dealing with polymer microcomposites, where the length scale of the fillers is in micrometres. In the case of polymer nanocomposites, nanofillers, being additives of nanometre scale, are dispersed in a polymer matrix, offering multifunctional, high-performance polymer characteristics beyond those possessed by traditional filled polymeric materials. Improvements in physical and mechanical properties have been well documented in the literature (Dubois & Alexandre, 2006; Thostenson et al., 2001; Koo, 2006). Apart from mechanical enhancements, the value of polymer nanocomposites comes from providing value-added properties not present in the polymer matrix, without sacrificing the inherent processability and mechanical properties of the matrix. The multifunctional features consist of improved thermal, fire, and moisture resistance, decreased permeability, charge dissipation, and chemical resistance (Moniruzzaman & Winey, 2006; Bokobza et al., 2004; Koo, 2006). Because of PP's good balance between properties and cost and its wide usage in industry, PP nanocomposites have been extensively studied in recent years (Deng et al., 2009, 2010; Bilotti et al., 2008; Andrews et al., 2002; Liu & Wu, 2001).

The properties of nanocomposites can be greatly affected by the dispersion of the nanofillers in the polymer matrix (Ray & Okamoto, 2003). Generally, the better the dispersion, the better is the properties of the final nanocomposite. However, nanofillers are, in essence, agglomerates due to their high surface energy, and it is very difficult to disperse them in most polymers. Due to the lack of polar groups in PP, many efforts have been attempted to improve the dispersion of inorganic fillers such as clay and CNTs into a PP matrix for the preparation of effective PP nanocomposites and enhanced mechanical properties. The achievement of well-dispersed nanofillers is the most investigated research topic worldwide (Coleman et al., 2006; Koo, 2006; Ray & Okamoto, 2000; Lu et al., 2008).

4. Preparation methods

4.1 Traditional processing methods

Polymer nanocomposites are generally prepared by three methods: solution intercalation, in-situ polymerisation or melt compounding.

Solution intercalation has been known for over a century and has proved to be one of the most successful methods for incorporating nanofillers into polymers. Nanocomposites with water-soluble polymers such as poly (ethylene oxide) and poly (vinyl alcohol) and organic solvent-soluble polymers such as HDPE, have been successfully prepared via this method (Wu & Lerner, 1993; Ogata, et al., 1997; Joen et al., 1998; Wang et al., TP, 2007). In terms of PP nanocomposites, the poor solubility of PP in most organic solvents has severely limited the use of this method. Although PP nanocomposites have been reported being produced using xylene, tetrhydronaphthalene and decalin as solvents (Chang et al., 2005; Grady et al., 2002), elevated temperatures are necessary for the evaporation of these high-boiling solvents. Also, their application on an industrial scale is still hindered by the involvement of large quantities of organic solvent.

In-situ polymerisation has been intensively investigated in recent years. The advantage of this process is that the polymer chain can be grafted onto the nanofillers on a molecular scale. This gives excellent dispersion and the potential for good interfacial strength between the nanofillers and the polymer matrix. A relatively good dispersion can be maintained even with high nanotube loading in the matrix. Successful investigations have been reported in the literature from different groups on PP nanocomposites (Ma et al., 2001; Zhao et al., 2003; Koval'chuk et.al, 2008; Funk & Kaminsky, 2007). PP/ MMT nanocomposites were prepared by in-situ polymerization using a Ziegler-Natta catalyst (Zhao et al., 2003). PP/ MWNT nanocomposites have been fabricated by Funck and Kaminsky (2007) using a metallocene/ methylaluminoxane (MAO) catalyst. However, the molecular weight of the polymer is often significantly lower with a wide distribution by comparison with other methods.

Melt compounding is the most common method used to create thermoplastic polymer nanocomposites because it is a cost-effective technology for polyolefin-based systems and is compatible with current industrial practices, such as extrusion, injection moulding, etc (Andrews et al., 2002). However, melt compounding, especially in the case of PP matrices, is generally less effective at dispersing nanofillers such as CNTs and clays, and is limited to low nanofiller loadings due to the high viscosity of the composite systems caused by the addition of nanofillers (Andrews et al., 2002). Moreover, the high shear rates and high temperatures utilised can also cause thermal instability of the molten polymers (Potschke et al., 2003). One approach is using the masterbatch process, where a pre-mixed highly loaded nanofiller composite is diluted with a fresh polymer melt (Prashantha et al., 2009).

Much effort has been expended to facilitate the achievement of good dispersion of nanofillers and efficient stress transfer. The de-agglomeration of CNTs is necessary for dispersing individual nanotubes before mixing them with the polymer matrix. The ultrasonication process is the most common method, but severe sonication may make the tubes shorter (Saito et al., 2002, Inam et al., TP, J. Comp Materials, 2011). Milling and grinding is considered to be a cheap and fast method for industrial processes although it is the most destructive method for CNTs (Pierard et al., 2001). Non-covalent functionalizations, such as surfactants, are often utilised to overcome carbon nanotube entanglements resulting from Van der Waals forces (Bonduel et al., 2005). Covalent functionalization of CNTs helps to break up the CNT bundles and improves the polymer / CNT interfacial adhesion (Liu et al., 2005). Polymer wrapping has been proposed as an alternative method to achieve a good dispersion of the CNTs without destroying their electrical properties (Star et al., 2001). Dissociated CNTs were produced by grafting polymer chains directly onto the CNTs to achieve a homogeneous polymer coating on the CNT

surface (Peeterbroeck et al., 2007; Dubois & Alexandre, 2006). High-density polyethylene has been used to coat MWNTs when producing PP nanocomposites and composites in other polymer matrices such as ethylene-vinyl acetate, polycarbonate and polyamide (Deng et al., 2010; Star et al., 2001; Peeterbroeck et al., 2007; Dubois & Alexandre, 2006; Pötschke et al., 2008). Compared with the direct incorporation of CNTs in polymer melts, enhanced dispersion and improved properties have been reported.

There are two ways to modify the surface of hydrophilic clays in order to improve their dispersion in the polymer matrix. The first one is to modify the surface with cationic surfactants to make the silicate surface organophilic via ion exchange reactions (Lan & Pinnavaia, 1994; Shi et al., 1996). The second method is based on grafting polymeric molecules through covalent bonding to the hydroxyl groups existing on the particles. However, for polyolefin polymers such as PP and PE, they are non-polar and incompatible with silicate surfaces even after modifying them with non-polar long alkyl groups. Therefore, a compatibilizer is often needed to facilitate the interaction between the polymer and the clays (Hasegawa et al., 2000; Garcia-Lopez et al., 2003). Compatibilizers are usually polar functional oligomers providing both a hydrophobic part (which can be easily mixed with a polymer) and a hydrophilic part (which is compatible with clay). Maleic anhydride grafted polypropylene (PP-g-MA) is a commonly used compatibilizer to aid the dispersion of clay or CNTs in PP matrix (Bilotti et al, 2008 and 2010).

4.2 The supercritical fluid technique

In recent years, supercritical technology, especially supercritical carbon dioxide ($scCO_2$), has been widely applied in the processing of polymer nanocomposites. A supercritical fluid is defined as "any substance, the temperature and pressure of which are higher than their critical values, and which has a density close to, or higher than, its critical density" (Darr & Poliakoff, 1999). Fig. 3 shows a schematic representation of the density and organization of molecules of a pure fluid in solid state, gas state, liquid state and the supercritical domain. No phase separation occurs for any substance at pressures or temperatures above its critical values. In other words, the critical point represents the highest temperature and pressure at which gas and liquid can coexist in equilibrium.

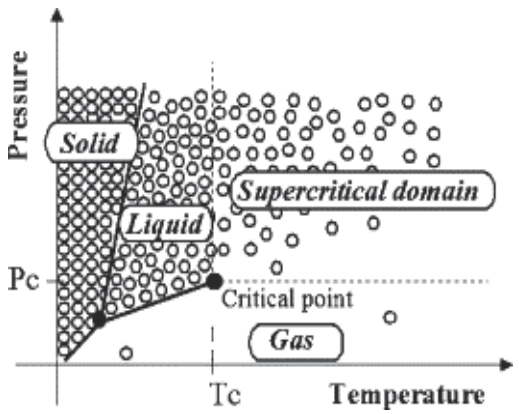

Fig. 3. A schematic representation of the microscopic behaviour of a pure fluid in the P-T plane phase diagram (Cansell et al., 2003)

Supercritical fluids are unique solvents with a wide range of interesting properties. Supercritical fluids have high diffusivities, similar to gas which allows them to effuse through solids, while also having liquid-like densities that allow them to act as effective solvents for many compounds. In addition, small changes in pressure and temperature greatly affect the density of a supercritical fluid and therefore many properties of SCF can be 'fine-tuned'. The unique properties of supercritical fluids allow them to be widely exploited in materials processing. The most promising developments are the processing of fine powders, core-shell particles, the processing and / or impregnation of aerogels, foams, surface modifications and the processing of polymers. (Cansell et al., 2003)

Among all the supercritical fluids, the use of $scCO_2$ is the most desirable for polymer processing because of its environmental compatibility as well as the following properties:

- CO_2 has relatively easily accessible critical points of 31.06 °C and 1070 psi (7.38 MPa) (Hyatt, 1984)
- The density of $scCO_2$ is easily tunable (Fig. 4). Therefore, the solvent strength and processes can be easily controlled
- CO_2 is non-combustible and non-toxic in contrast to most of the organic solvents suitable for supercritical applications
- It is also easily available because it occurs naturally as well as being the by-product of many industrial processes; therefore CO_2 is relatively inexpensive
- As CO_2 is a gas at ambient temperatures and pressures it can be easily removed, leaving no solvent residues in the processed material (Behles & Desimone, 2001)

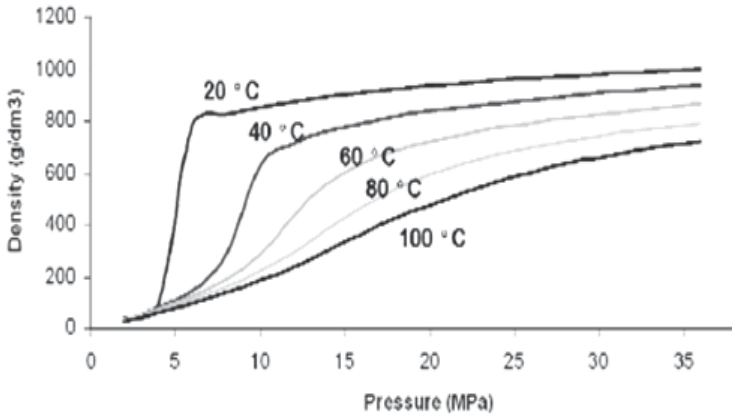

Fig. 4. The density of CO_2 as a function of pressure for a range of temperatures

$ScCO_2$ has found widespread application in industrial processes, including the extraction of metals or organic material, the decaffeination of green coffee beans, dry cleaning and degreasing, nano- and micro-particle formation, impregnation and dyeing, the processing and synthesis of polymers and composites, tissue engineering scaffolds, drug delivery, etc (Quirk et al., 2004; Hyde et al., 2001). The important fields most relevant to this Chapter are in the $scCO_2$ processing of polymers and composites which will be discussed in greater detail below.

$ScCO_2$ processing, as one of the new and cleaner processing methods for polymer nanocomposites, has recently received increasing attention. The solubility of polymers in $scCO_2$ is poor for many high molecular weight polymers. Table 1 gives a representative sample of the available literature data for the solubility of CO_2 in a variety of polymers. The low solubility is a result of the lower density of $scCO_2$ and the weak interaction between the CO_2 molecules and the non-polar groups of many polymers (Cansell et al., 2003). However, even for polymers which are not soluble in $scCO_2$, the CO_2 is still able to permeate resulting in substantial and sometimes dramatic changes in the properties of these polymers. The permeation of $scCO_2$ into a polymer causes it to swell. Aided by their zero surface tension, the addition of $scCO_2$ into the polymer phase gives the chains a greater mobility. The CO_2 molecules act as lubricants, which reduces the chain-chain interactions as it increases the inter-chain distance and free volume of the polymer. This is called plasticization. The physical properties of the polymer are changed dramatically, including the depression of the glass transition temperature (T_g), the lowering of interfacial tension and a reduction of the viscosity of the polymer melt. $ScCO_2$ may increase the crystallinity of the polymers because the polymer chains are given more freedom to align themselves into a more favourable order.

Polymer	Method[a]	Pressure [atm]	Temp. [°C]	Solubility
poly(methyl methacrylate)	GM-M	50	65	46 SCC/cm^3
	GM-D	204	70	10.5 wt.%
polystyrene	GM-M	13.2	25	14.5 SCC/cm^3
high-impact polystyrene	GM-D	204	70	0.5 wt.%
polycarbonate	GM-M	13.2	25	24 SCC/cm^3
	GM-D	68	25	13 g/100g
poly(ethylene terephthalate)	GM-D	136	40	1.5 wt.%
poly(vinyl chloride)	GM-D	68	25	8 g/100g
	GM-D	136	40	0.1 wt.%
poly(vinyl acetate)	GM-D	54.4	25	29 g/100g
low density polyethylene	GM-D	68	40	0.2 wt.%
high density polyethylene	GM-D	68	40	0.1 wt.%
polypropylene	GM-D	68	40	0.1 wt.%
	GM-D	204	25	0.1 wt.%
	BM	73	160	1.59 g/100g
	BM	61.2	200	1.09 g/100g
Nylon 66	GM-D	68	40	1.8 wt.%
polyurethane	BM	136	40	2.2 wt.%
Teflon	GM-D	68	40	0.0 wt.%

[a]Method: GM-M, gravimetric method (microbalance); GM-D, gravimetric method (desorption); BM, barometric method. Units: SCC/cm^3, cm^3(STP)/cm^3 of polymer; g/100g, g of CO_2/100g of polymer.

Table 1. The solubility of CO_2 in polymers (Tomasko et al., 2003)

Garcia-Leiner and Lesser (2004) have studied the use of $scCO_2$ in the processing of a variety of polymers (s-PS, FEP, and PTFE) using a modified single-screw extruder with a CO_2 injection (Fig. 5). The present of CO_2 significantly enhanced the processability of the polymer–CO_2 system by plasticization effect and the hydrostatic contribution. This presented an effective alternative to process intractable or high melt viscosity polymers.

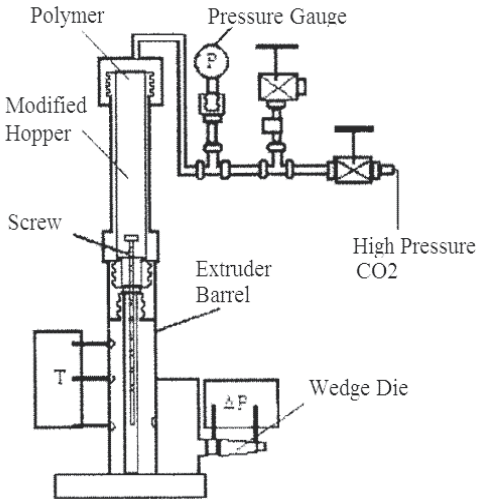

Fig. 5. Modified extrusion system for CO2-assisted polymer processing (Garcia-Leiner & Lesser, 2004)

A wide range of opportunities have opened up for $scCO_2$ that have an impact on the plastics industry (Tomasko et al., 2003). These include usages for extraction, foaming and impregnation. Extraction occurs merely by removing the soluble extractant material, such as any unreacted monomer, while leaving the insoluble substrate. Foaming occurs when rapid decompression forms gaseous CO_2 inside the polymer, leaving the polymer in the form of a porous (micro) material. This is very important in supporting the growth of blood vessels and collagen fibres in the matrix of biodegradable polymers or when the final product is intended to be used as a catalyst. As for impregnation, CO_2 can act as a transport medium facilitating the diffusion of monomers, initiators and molecules to impregnate a polymer, while the CO_2 can be cleanly removed afterwards. A better dispersion of the molecules has been provided within the polymer matrix. Substances impregnated into polymers have included dyes, fragrances, drugs for controlled release, anti-microbial and anti-fungal agents, and nanoparticles (Kikic & Vecchione, 2003).

The effective dispersion of the fillers in the polymer matrix and the improvement of polymer-filler interactions are two key challenges in the field of polymer nanocomposites. The development of polymer processing technologies in $scCO_2$ has enabled the synthesis of very complex polymer nanocomposites. Zerda et al. (2003) developed poly (methyl methacrylate) / montmorillonite composites via in-situ polymerization. $ScCO_2$ was used as the reaction medium to distribute homogeneously the monomer and the initiator and allowing polymerization under lower viscosity conditions. The modulus of the nanocomposites increased 50% with 40 wt % of clay content. A significant improvement in physical properties has also been reported by Green et al. (2000) for $scCO_2$ processed poly

(methyl methacrylate) / silicate nanocomposites, in which $scCO_2$ acted as both a plasticizer for the polymer matrix and a carrier for the monomer. Polystyrene / clay has also been produced via in-situ polymerization by Li et al. (2006), where styrene monomer and initiator were directly intercalated into organomontmorillonite (OMMT) with the aid of $sCCO_2$.

For PP nanocomposites, PP will become plasticized when treated with CO_2. Varma-Nair et al. (2003) have suggested that 1% CO_2 could be dissolved in PP at 50 °C at 180 psi. Both decreases in T_m and T_c of PP in presence of CO_2 have been reported in the literature (Varma-Nair et al., 2003; Garcia-Leiner & Lesser, 2003). Studies in PP have indicated improvements in the dispersion of nanofillers in the matrix via melt compounding in $scCO_2$ (Garcia-Leiner & Lesser, 2003, Ma et al, 2007, Zhao & Huang, 2008). Zhao & Huang (2008) improved a twin-screw extruder with the aid of $scCO_2$ for the preparation of PP / clay nanocomposites (see Fig. 6). A CO_2 injection system was connected to the extruder and several kneading and reverse conveying elements were added to prevent CO_2 from leaking. This continuous extrusion process of PP nanocomposites using $scCO_2$ has set good examples for $scCO_2$ usage in an industrial environment.

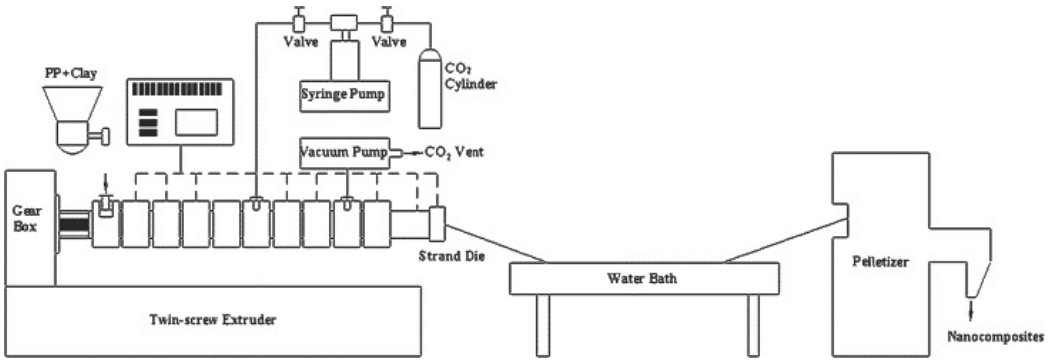

Fig. 6. $ScCO_2$ used in the extrusion process for the preparation of PP/ clay composites (Zhao & Huang, 2008)

5. Morphology and properties of PP nanocomposites

The preparation methods have crucial impact on the dispersion of the nanofillers and the final properties of the nanocomposites. In this section, the morphology of the PP nanocomposites and various nanocomposite properties will be discussed.

5.1 Morphology

Polymer-grafted CNTs were used in the study of Yang et al. (2008). They reported that PP-g-MWNTs were dispersed individually in the PP matrix at 1.5 wt%, but difficulty was found at higher CNT contents (Yang et al., 2008). Deng et al. (2010) reported that large bundles of MWNTs were present in their PP/MWNT samples using traditional melt compounding methods and better dispersions of MWNTs were observed for the HDPE coated MWNTs samples. The scanning electron microscopy (SEM) images of fracture surfaces of the nanocomposites are presented in Fig. 7. The HDPE coats the MWNTs and reduces the tendency of the nanotubes to aggregate and is partly miscible with the PP matrix. Ma et al.

(2010) studied the use of $scCO_2$ to assist melt compounding of PP nanocomposites. The nanocomposites are prepared in an autoclave. The autoclave was filled with liquid CO_2 and held at 2175 psi and 200 °C under stirring for 30 min. In their work, pristine MWNTs without HDPE coating were observed to exhibit good dispersion in the PP matrix under $scCO_2$ assisted mixing (Fig. 7c). This indicates the great efficiency of $scCO_2$ being a processing lubricant between the polymer chains enhancing the polymer diffusion.

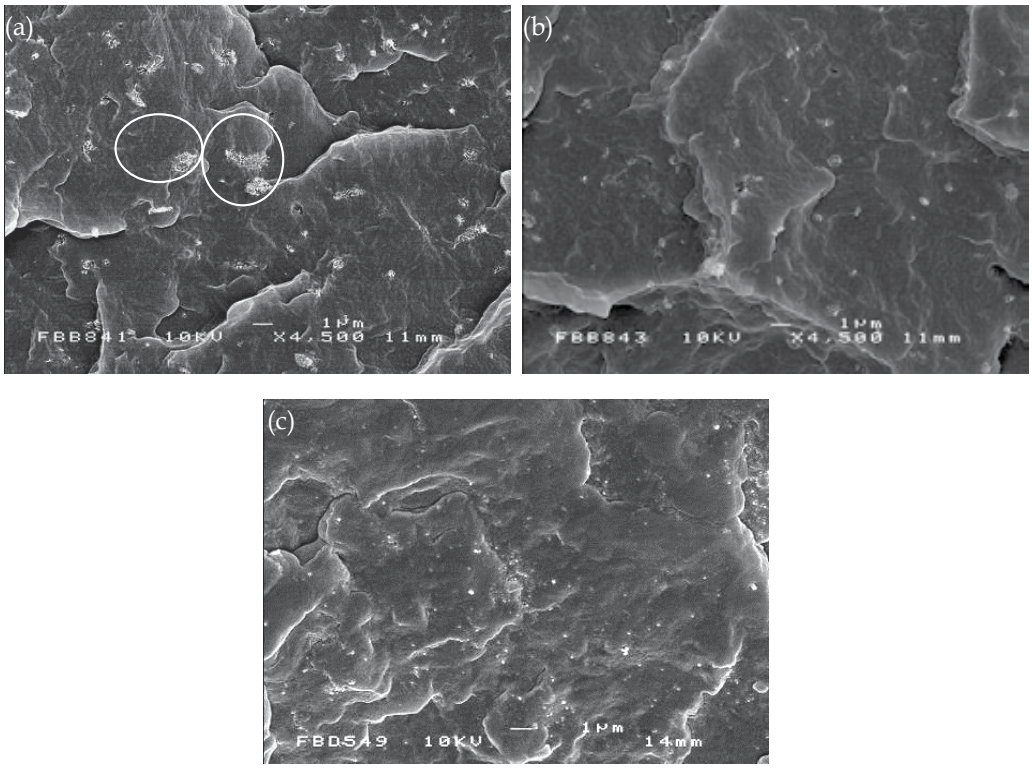

Fig. 7. SEM images of freeze-fractured samples of PP nanocomposites with 0.5 wt.% MWNT loading (a) melt-compounded MWNT (b) melt-compounded PP/coated MWNT (Deng et al., 2010) (c) $scCO_2$ PP/MWNT (Ma et al., 2010)

In Zhao & Huang' (2008) work, a better dispersion of clays in PP matrix was also confirmed with $scCO_2$ assisted mixing. Fig. 8 shows that the sample prepared with 2.5% CO_2 has more uniform distributed clay and aggregations of clay are much thinner.

Ma et al. (2007) also reported a good dispersion of sepiolite clays in PP matrix with $scCO_2$ assisted mixing. Without the use of any compatibilizer, the dispersion of sepiolite in the PP matrix improved significantly in the $scCO_2$ assisted mixing compared to melt mixing. This indicates that compatibilizers such as PP-g-MA are not needed to achieve good dispersions in the case of $scCO_2$ assisted processing of polyolefins. This is of particular relevance because the role of compatibilizers, such as PP-g-MA, is generally regarded as essential for the creation of well dispersed nanoclays composites based on polyolefins using traditional melt compounding methods.

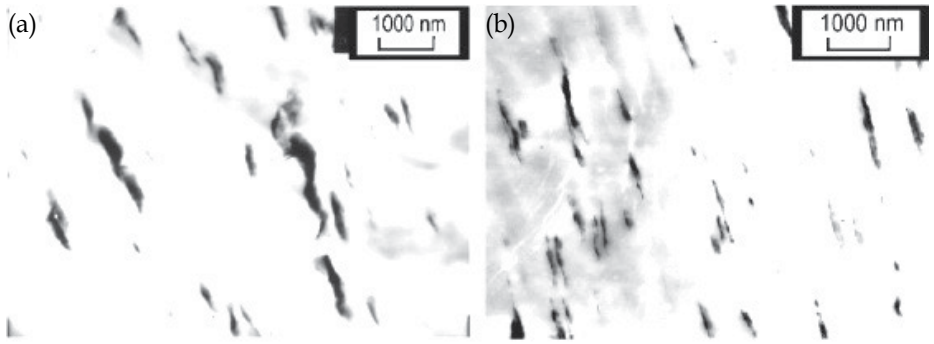

Fig. 8. TEM images of PP/clay nanocomposites prepared (a) without and (b) with 2.5% CO_2 (Zhao & Huang, 2008)

5.2 Mechanical properties

The mechanical properties including the tensile strength and Young's modulus of the PP nanocomposites can be significantly enhanced by the incorporation of nanofillers. Andrews et al. (2002) fabricated PP / MWNT composites by a shear mixer and found a modulus increase from 1.0 GPa to 2.4 GPa with a relatively high nanotube content of 12.5 wt%. However, this was at the expense of a reduction in yield stress from 30 MPa to 18 MPa. Similarly, Wang and Sheng (2005) found that the modulus of the PP nanocomposites increased from 788 MPa to 908 MPa by the addition of 7 wt% Attapulgite clay, but at the expense of a reduction in strength from 32 MPa to 26 MPa. Deng et al. (2010) investigated the effects of a HDPE coating onto MWNTs on the mechanical properties of PP / MWNT composites produced by melt compounding. A property increase from 1.42 GPa to 1.79 GPa for Young's modulus and from 34.5 MPa to 37.9 MPa for tensile strength, was achieved at relatively low loadings (0.5 wt%) of coated MWNTs.

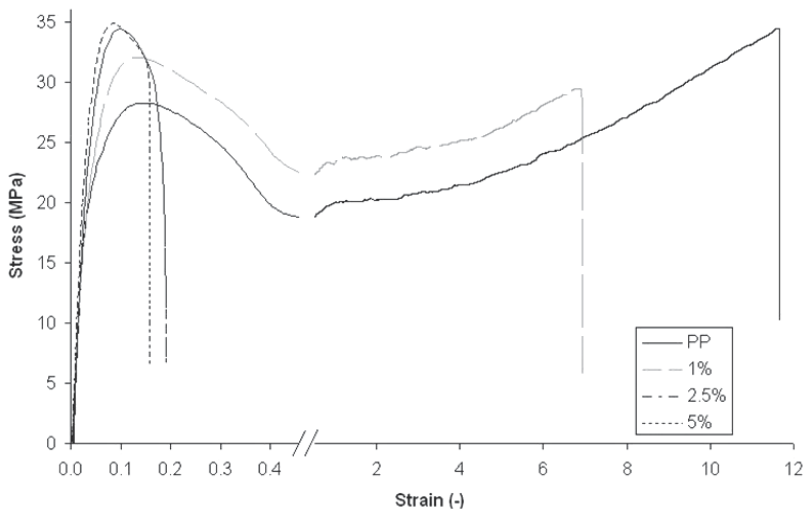

Fig. 9. Stress-strain curves of $scCO_2$ PP / sepiolite nanocomposites with different clay contents (Ma et al., 2007)

The elongation at break of the nanocomposites is often decreased. The increase of nanofiller content compromises the ductile nature of the PP matrix. Yielding followed by drawing still occurred in the 1 wt% sepiolite samples; while 2.5 wt% and 5 wt% sepiolite samples show brittle fractures at low strains (Fig. 9).

The effect on the modulus and yield stress of the $scCO_2$ processed PP nanocomposites was studied for the addition of MWNTs and sepiolite clays (Ma et al., 2007 and 2010). The results were compared with traditional melt compounded nanocomposites.

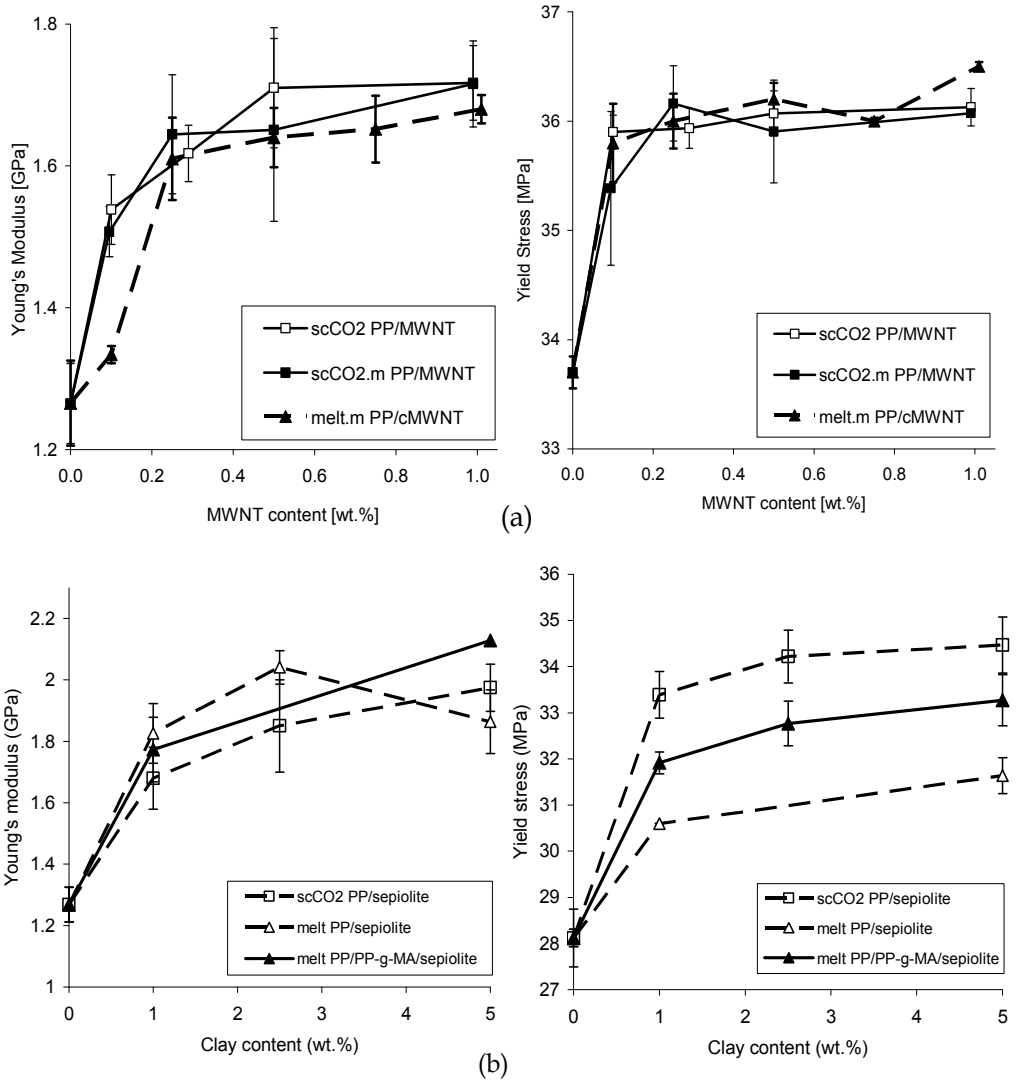

Fig. 10. The Young's modulus and yield stress of $scCO_2$ processed and melt-compounded PP nanocomposites (a) PP / MWNT nanocomposites (b) PP / sepiolite nanocomposites. The label, melt.mPP/cMWNT, in the figure represents melt-compounded and masterbatch based HDPE-coated MWNT PP nanocomposites (Ma et al., 2007; Ma et al., 2010)

Increases of both properties were observed in all systems with the nanofiller content as expected. The melt-compounded and masterbatch based PP/coated MWNT composites show a continuous modulus increase up to 1.7 GPa by the addition of 1.0 wt% CNT loading (Fig. 10a). This is as a result of the de-aggregation of the MWNT bundles by the HDPE coating (Ma et al., 2010). $ScCO_2$ processed nanocomposites with pristine MWNTs also showed a competitive increase in Young's modulus. Furthermore, the use of masterbatch in the $scCO_2$ assisted mixing method did not show much improvement in terms of Young's modulus. Similarly, increases in yield stress were observed for $scCO_2$ PP / MWNT samples, with a significant 6 % increase at 0.1 wt% CNT loading followed by roughly constant values across the rest of the CNT loading range up to 1 wt% (Fig. 10a). The degree of reinforcement of pristine MWNTs is as good as for melt-compounded PP/coated MWNT composites. This indicates that $scCO_2$ assisted mixing achieves a better dispersion of CNTs without the need for a HDPE coating. The enhanced mechanical properties are also benefited from the relatively low shear forces involved in $scCO_2$ assisted mixing, which causes less nanotube breakage and damage.

In Ma et al.' (2007) work about PP/sepiolite nanocomposites, the Young's modulus of melt compounded PP nanocomposites (no PP-g-MA used as compatibilizer) shows a reduction at 5 wt% sepiolite loading (Fig. 10b). This corresponds to the aggregation of clay at higher loadings with the absence of PP-g-MA. This is in contrast to the analogous material with PP-g-MA, which shows a 68 % increase in modulus from 1 to 5 wt% clay content. The modulus for $scCO_2$ processed PP nanocomposites without PP-g-MA shows a steady increase in modulus (by up to 56 % for 5 wt% sepiolite). In terms of yield stress, $scCO_2$ processed PP nanocomposite without PP-g-MA shown the highest increase in yield stress of up to 23 % for 5 wt% sepiolite, which was benefited from the good dispersion of the sepiolite and also the benefit of preserving the clay fibre length when using $scCO_2$ assisted mixing.

5.3 Characterization of PP

5.3.1 Thermal behaviour

Nanofillers increase the crystallization temperature (T_c) of PP. It has been observed for both CNT and clay nanocomposites (Ma et al., 2007; Bilotti et al., 2008; Lee et al., 2008). The nanofillers act as nucleating agents enabling PP to crystallize at a higher temperature during the cooling process. This increase in T_c is dependent on the nanofiller content, which suggests that higher loadings of nanofiller can provide higher nucleating efficiency. It has been reported that SWNTs are more effective nucleating agents than MWNTs, which provided larger increase in T_c (Miltner et al., 2008). Furthermore, pristine MWNTs also give a stronger nucleation effect than HDPE coated MWNTs, which suggests that the surface of the nucleating agents plays an important role in the crystallization process (Ma et al., 2010). It was also found that a more pronounced nucleating effect was observed for very low CNT loadings. Although nucleating agents significantly increase the number of nucleation sites, above certain loadings the introduction of more CNTs may hinder chain mobility and retard crystal growth.

Apart from the T_c, the crystallinity of PP has also been increased by the addition of nanofillers (Bilotti et al., 2008). The Young's modulus of the composites has been reported to increase with polymer matrix crystallinity in the work of Coleman et al. (Coleman et al., 2004). Similar results were also shown in other studies that changes in the crystallinity and the

crystalline morphology of the polymer matrix can have pronounced effects on the mechanical properties of nanocomposites (Bhattacharyya et al., 2003; Wang et al., 2007). Hence, the mechanical reinforcing effects observed are a combination of the modification of the PP matrix through increased crystallinity as well as true reinforcing effects from CNT fillers.

The effect of nanofillers on the melting temperature (T_m) of PP is not clear. Yang et al. (2008) and Bikiaris et al. (2008) have observed an increase in T_m. Lee et al. (2008) has reported a decrease in T_m of PP. Other authors reported that T_m remains unchanged (Seo et al., 2005; Jin et al., 2009).

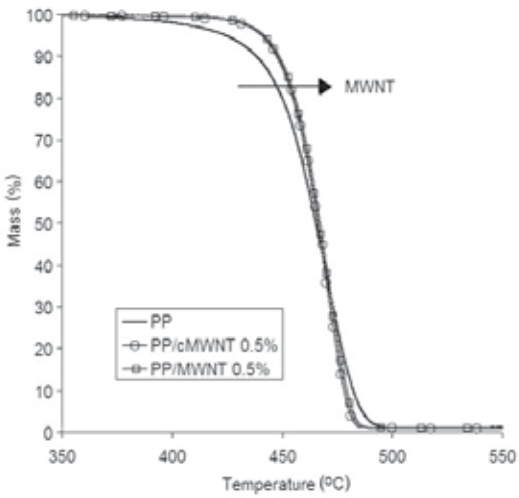

Fig. 11. The TGA of PP / MWNT nanocomposites processed using $scCO_2$ assisted mixing, showing a slightly retarded thermal degradation of nanocomposites by the presence of MWNTs (Ma et al., 2010)

The thermal stability of PP is also slightly improved by the addition of the nanofillers. TGA shows that the thermal degradation of PP is retarded by the presence of CNTs (Fig. 11). PP / MWNT nanocomposites showed a higher onset decomposition temperature (T_{onset}). The Reason is that the CNTs hinder the flux of degradation products and improves the heat dissipation within the composites (Huxtable et al., 2003). Seo & Park (2004) have observed a T_{onset} increase from 278 ˚C to 352 ˚C at the addition of 5 wt% of MWNTs. The effect of the clay surface modification on the thermal stability of PP has been studied by Tartaglione et al. on the melt-compounded PP / sepiolite composites (Tartaglione et al., 2008).

5.3.2 Microstructure of PP

PP can crystallize in three crystalline modifications: monoclinic (a), hexagonal (β), and orthorhombic (γ) (Bruckner et al., 1991). These phases can be examined by XRD. The XRD patterns for all the PP nanocomposites shows peaks corresponding to PP α-phase at 2θ = 14, 17, 18.5, 21.5, 21.9 and 25.4 ° for six major reflections: (110), (040), (130), (111), (041) and (060) plane, respectively. Most studies showed that only a phase of PP was present in the PP nanocomposites and no other forms of PP crystallites were detected. This indicates that the addition of sepiolite does not affect the crystal modification of the final PP molecules

However, Wang & Sheng (2005) did report that the relative intensities of 040 peaks and 110 peaks can change (Fig. 12) and an increase in the I_{040} / I_{110} ratio was found. This preferential orientation of PP crystal growth has also been found with the addition of MWNTs and sepiolite clays (Ma et al., 2007 and 2010). Data of relative intensities are listed in Table 2. This increase indicates that the addition of sepiolite promotes a preferential orientation of PP crystals growing with (040) planes parallel to the sepiolite surface and the b-axis perpendicular to it (Ferrage et al., 2002; Wang & Sheng, 2005).

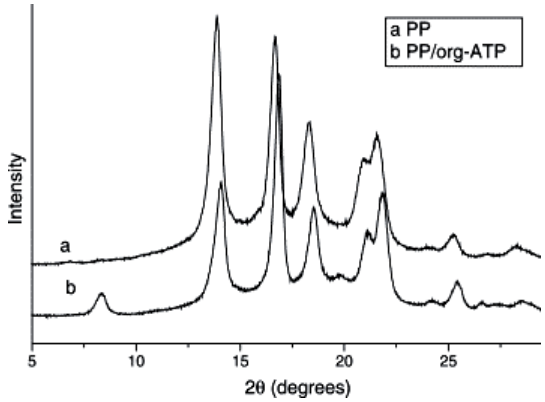

Fig. 12. XRD patterns of (a) PP and PP/org-ATP nanocomposites (Wang & Sheng, 2005)

Sepiolite [wt.%]	0	1	2.5	5
PP/sepiolite	0.80	2.41	2.40	2.24
PP/PP-g-MA/sepiolite	0.80	1.40	3.00	2.71

Table 2. Ratio of intensity between diffraction peaks of (040)*a* and (110)*a* in XRD patterns (Ma et al., 2007)

6. Conclusion

Researches on nanofillers such as CNTs and nanoclays reinforced PP nanocomposites have attracted wide attention. The properties of the nanocomposites can be significantly improved by the addition of nanofillers. The challenge in producing high performance PP nanocomposites is to achieve homogeneous dispersion of nanofillers thus obtaining efficient stress transfer. Among the nanocomposite preparation methods, $scCO_2$ assisted mixing is an interesting alternative to produce PP nanocomposites as it overcomes some of the issues in the traditional melt compounding process, such as high viscosities, high temperatures and high shear stresses involved, which can all lead to polymer degradation. The plasticization of $scCO_2$ could reduce the PP viscosity, decrease the T_m of the PP, and hence increase the processablity of nanocomposites and improve the dispersion of nanofillers. $ScCO_2$ assisted mixing also benefits from a better preservation of nanotube or nanofibre lengths. Good nanofiller dispersion and mechanical properties were achieved without using the aid of compatibilizers such as PP-g-MA or polymer coated nanofillers, which are commonly used aiding the dispersion of nanofillers in the melt compounding process. This is all very encouraging from an economical point of view.

7. References

Ahir, S. (2005) Polymer Containing Carbon Nanotubes: Active Composite Materials. In: *Polymeric Nanostructures and Their Applications*. Nalwa, S., American Scientific Publishers, ISBN: 1-58883-068-3 California

Ajayan, P.; Stephan, O.; Colliex, C. & Trauth, D. (1994) Aligned Carbon Nanotube Arrays Formed by Cutting a Polymer Resin-Nanotube Composite. *Science*. Vol.265, No.5176, pp.1212-1214, ISSN 0036-8075

Andrews, R.; Jacques, D.; Minot, M. & Rantell, T. (2002) Fabrication of Carbon Multiwall Nanotube/Polymer Composites by Shear Mixing. *Mater. Eng*. Vol.287, No.6, pp.395-403, ISSN 1438-7492

Baughman, A. & Zakhidov, W. (2002) Carbon Nanotubes - The Route Toward Applications. *Science*. Vol.297, No.5582, pp.787-792, ISSN 0036-8075

Beermann, T. & Brockamp, O. (2005) Structure analysis of montmorillonite crystallites by convergent-beam electron diffraction. *Clay Miner*. Vol.40, No.1, pp.1-13, ISSN 0009-8558

Behles, J. & DeSimone, J. (2001) Developments in CO_2 Research. *Pure Appl. Chem*. Vol.73, No.8, pp.1281-1285

Bhattacharyya, A.; Sreekumar, T.; Liu, T.; Kumar, S.; Ericson, L.; Hauge, H. & Smalley, R. (2003) Crystallization and Orientation Studies in Polypropylene/Single Wall Carbon Nanotube Composite. *Polym*. Vol.44, No.8, pp.2373-2377, ISSN 0032-3861

Bilotti, E.; Fischer, H. & Peijs, T. (2008) Polymer nanocomposites based on needle-like sepiolite clays: Rffect of functionalized polymers on the dispersion of nanofiller, crystallinity, and mechanical properties. *J. Appl. Polym. Sci*. Vol.107, No.2 pp.1116-1123, ISSN 0021-8995

Bilotti, E.; Ma, J. & Peijs, T. (2010) Preparation and Properties of Polyolefin/Needle-Like Clay Nanocomposites. In: *Advances in Polyolefin Nanocomposites*. Mittal V., Taylor & Francis (CRC Press), USA.

Bokobza, L.; Burr, A.; Garnaud, G.; Perrin, M. & Pagnotta, S. (2004) Fibre Reinforcement of Elastomers: Nanocomposites Based on Sepiolite and Poly(hydroxyethyl acrylate). *Polym. Int*. Vol.53, No.8, pp.1060-1065, ISSN 0959-810

Bonduel, D.; Mainil, M.; Alexandre, M.; Monteverde, F. & Dubois, P. (2005) Supported Coordination Polymerisation: A Unique Way to Potent Polyolefin Carbon Nanotube Nanocomposites. *Chem. Commun*. Vol.14, No.6, pp.781-783

Bruckner, S.; Meille, S.; Petraccone, V. & Pirozzi, B. (1991) Polymorphism in Isotactic Polypropylene. *Prog. Polym. Sci*. 16, No.2-3, pp.361-404

Bryning, M.; Islam, M.; Kikkawa, J. & Yodh, A. (2005) Very Low Conductivity Threshold in Bulk Isotropic Single-Walled Carbon Nanotube–Epoxy Composites. *Adv. Mater*. Vol.17, No.9, pp.1186-1191

Cansell, F.; Aymonier, C. & Loppinet-Serani, A. (2003) Review on Materials Science and Supercritical Fluids. *Curr. Opin. Solid State Mater. Sci*. Vol.7, No.4-5, pp.331-340

Chang, t.; Jensen, L.; Kisliuk, A.; Pipes, R.; Pyrz, R. & Sokolov, A. (2005) Microscopic mechanism of reinforcement in single-wall carbon nanotube / polypropylene nanocomposites. *Polym*. Vol.46, No.2,pp.439-444

Coleman, J.; Cadek, M.; Blake, R.; Nicolosi, V.; Ryan, K.; Belton, C.; Fonseca, A.; Nagy, J.; Gun'ko, Y. & Blau, W. (2004) High Performance Nanotube-Reinforced Plastics:

Understanding the Mechanism of Strength Increase. *Adv. Funct. Mater*. Vol.14, No.8, pp.791-798

Coleman, J.; Khan, U. & Gun'ko, Y. (2006) Mechanical Reinforcement of Polymers Using Carbon Nanotubes. *Adv. Mater*. Vol.18, No.6, pp.689-706

Darr, J. & Poliakoff, M. (1999) New Directions in Inorganic and Metal-Organic Coordination Chemistry in Supercritical Fluids. *Chem. Rev*. Vol.99, No.2, pp.495-542

Deng, H.; Skipa, T.; Zhang, R.; Lillinger, D.; Bilotti, E.; Alig, I. & Peijs T. (2009a) Effect of melting and crystallization on the conductive network in conductive polymer composites. *Polym*. Vol.50, No.15, pp.3747-3754

Deng, H.; Zhang, R.; Reynolds, C.; Bilotti, E. & Peijs, T. (2009b) A Novel Concept for Highly Oriented Carbon Nanotube Composite Tapes or Fibres with High Strength and Electrical Conductivity. *Macromol. Mater. Eng*. Vol.294, No.11,pp.749-755

Deng, H.; Bilotti, E.; Zhang, R. & Peijs, T. (2010) Effective Reinforcement of Carbon Nanotubes in Polypropylene Matrices. *J. Appl. Poly. Sci.* Vol.118, No.1, pp.30-41

Dresselhaus, M.; Lin, Y.; Rabin, O.; Jorio, A.; Souza Filho, A.; Pimenta, M.; Saito, R.; Samsonidze Ge, G. & Dresselhaus, G. (2003) Nanowires and nanotubes. *Mater. Sci. Eng*. Vol.23, No.1, pp.129-140

Dubois, P. & Alexandre, M. (2006) Performant Clay/Carbon Nanotube Polymer Nanocomposites. *Adv. Eng. Mater*. Vol.8, No.3, pp.147-154

Fan, S.; Chapline, M.; Franklin, N.; Tombler, T.; Cassell, A. & Dai, H. (1999) Self-oriented regular arrays of carbon nanotubes and their field emission properties. *Science*. Vol.283, No.5401, pp.512-514

Ferrage, E.; Martin, F.; Boudet, A.; Petit, S.; Fourty, G.; Jouffret, F.; Micoud, P.; De Parseval, P.; Salvi, S.; Bourgerette, C.; Ferret, J.; Saint-Gerard, Y.; Buratto, S. & Fortune, J. (2002) Talc as Nucleating Agent of Polypropylene: Morphology Induced by Lamellar Particles Addition and Interface Mineral-matrix Modelization. *J. Mater. Sci*. Vol.37, No.8, pp.1561-1573

Fleming, G. & Koros, W. (1986) Dilation of Polymers by Sorption of Carbon Dioxide at Elevated Pressures. 1. Silicone Rubber and Unconditioned Polycarbonate. *Macromol*. Vol.19, No.8, pp.2285-2291

Funck, A. & Kaminsky, W. (2007) Polypropylene carbon nanotube composites by in situ polymerization. *Compos. Sci. Technol*. Vol.67, No.5, pp.906-915

Garcia-Leiner, M. & Lesser, A. (2003) Melt Intercalation in Polymer-Clay Nanocomposites Promoted by Supercritical Carbon Dioxide. *Polym. Mater. Sci. Eng*. Vol.89, pp.649-650

Garcia-Leiner, M. & Lesser, A. (2004) CO_2-assisted polymer processing: A new alternative for intractable polymers. *J. Appl. Polym. Sci.* Vol.93, No.4, pp.1501-1511

Garcia-Lopez, D.; Picazo, O.; Merino, J. & Pastor, J. (2003) Polypropylene Clay Nanocomposites: Effect of Compatibilizing Agents on Clay Dispersion. *Eur. Polym. J*. Vol.39, No.5, pp.945-950

Grady, B.; Pompeo, F.; Shambaugh, R. & Resasco, D. (2002) Nucleation of polypropylene crystallization by single-walled carbon nanotubes. *J. Phys. Chem. B*. Vol.106, No.23, pp.5852-5858

Green, J.; Rubal, M.; Osman, B.; Welsch, R.; Cassidy, P.; Fitch, J. & Blanda, M. (2000) Silicon-Organic Hybrid Polymers and Composites Prepared in Supercritical Carbon Dioxide. *Polym. Adv. Technol*. Vol.11, No.8-11, pp.820-825

Grunes, J.; Zhu, J. & Somorjai, G. (2003). Catalysis and Nanoscience. *Chem. Commun*. Vol.7, No.18, pp.2257-2260

Hasegawa, N.; Okamoto, H.; Kato, M. & Usuki, A. (2000) Preparation and Mechanical Properties of Polypropylene-Clay Hybrids based on Modified Polypropylene and Organophilic Clay. *J. Appl. Polym. Sci*. Vol.78, No.11, pp.1918-1922

Huxtable, S.; Cahill, D.; Shenogin, S.; Xue, L.; Ozisik, R.; Barone, P.; Usrey, M.; Strano, M.; Siddons, G.; Shim, M. & Keblinski, P. (2003) Interfacial Heat Flow in Carbon Nanotube Suspensions. *Nat. Mater*. Vol.2, No.11, pp.731-734

Hyatt, J. (1984) Liquid and Supercritical Carbon Dioxide as Organic Solvents. *J. Org. Chem.* Vol.49, No.26, pp.5097-5101

Hyde, J.; Licence, P.; Carter, D. & Poliakoff, M. (2001) Continuous Catalytic Reactions in Supercritical Fluids. *Appl. Catal., A*. Vol.222, No.1-2, pp.119-131

Jin, S.; Kang, C.; Yoon, K.; Bang, D. & Park, Y. (2009) Efect of compatibilizer on morphology, thermal, and rheological properties of polypropylene/functionalized multi-walled carbon nanotubes composite. *J. Appl. Polym. Sci*. Vol.111, No.2, pp.1028-1033

Joen, H.; Jung, H.; Lee, S. & Hudson, S. (1998) Morphology of polymer/Silicate Nanocomposites High Density Polyethylene and a Nitrile Copolymer. *Polym. Bull.* Vol.41, No.1, pp.107-111

Kikic, I. & Vecchione, F. (2003) Supercritical Impregnation of Polymers. *Curr. Opin. Solid State Mater. Sci*. Vol.7, No.4-5, pp.399-405

Koo, J. (2006) *Polymer Nanocomposites: Processing, Characterization, and Applications*. McGraw-Hill, ISBN 0071458212, 9780071458214, New York

Koval'chuk, A.; Shevchenko, V.; Shchegolikhin, A.; Nedorezoca, P.; Klyamkina, A. & Aladyshev, A. (2008) Effect of carbon nanotube functionalization on the structural and mechanical properties of polypropylene/MWCNT composites. *Macromol*. Vol.41, No.20, pp.7536-7542

Lan, T. & Pinnavaia, T. (1994) Clay-Reinforced Epoxy nanocomposites. *Chem. Mater*. Vol.6, No.12, pp.2216-2219

Lee, G.; Janannathan, S,; Chea, H.; Minus, M. & Kumar, S. (2008) Carbon nanotube dispersion and exfoliation in polyperopylene and structure and properties of the resulting composites. *Polym*. Vol.49, No.7, pp.1831-1840

Li, J.; Xu, Q.; Peng, Q.; Pang, M.; He, S. & Zhu, C. (2006) Supercritical CO_2-Assisted Synthesis of Polystyrene/clay Nanocomposites via in situ Intercalative Polymerisation. *J. App. Polym. Sci.* Vol.100, No.1, pp.671-676

Liu, L.; Barber, A.; Nuriel, S. & Wagner, H. (2005) Mechanical Properties of Functionalized Single-Walled Carbon-Nanotube/Poly(vinyl alcohol) Nanocomposites. *Adv. Funct. Mater*. Vol.15, No.6, pp.975-980

Liu, X. & Wu, Q. (2001) PP/Clay Nanocomposites Prepared by Grafting-Melt Intercalation. *Polym*. Vol.42, No.25, pp.10013-10019

Lu, J. (1997) Elastic Properties of Carbon Nanotubes and Nanoropes. *Phys. Rev. Lett.* Vol.79, No.7, pp.1297-1300

Lu, K; Grossiord, N; Koning, C.; Miltner, H.; Mele, B. & Loos, J. (2008) Carbon Nanotube/Isotactic Polypropylene Composites Prepared by Latex Technology: Morphology Analysis of CNT-Induced Nucleation. Macromol. 41, pp. 8081

Ma, J.; Bilotti, E.; Peijs, T. & Darr, J. (2007) Preparation of Polypropylene/Sepiolite Nanocomposites Using Supercritical CO2 Assisted Mixing. *Eur. Polym. J.* Vol.43, No.12, pp.4931-4939

Ma, J.; Deng, H. & Peijs, T. (2010) Processing of Polypropylene/Carbon Nanotube Composites Using ScCO2-Assisted Mixing. *Macromol. Mater. Eng*. Vol.295, No.6, pp.566-574

Ma, J.; Qi, Z. & Hu, Y. (2001) Synthesis and characterization of polypropylene/clay nanocomposites. *J. Appl. Polym. Sci*. Vol.82, No.14, pp.3611-3617

Moniruzzaman, M. & Winey, K. (2006) Polymer Nanocomposites Containing Carbon Nanotubes. *Macromol*. Vol.39, No.16, pp. 5194-5205

Moore, D. & Reynolds, R. (1997) *X-Ray Diffraction and the Identification and Analysis of Clay Minerals* (2nd edition). University Press, ISBN 0195087135, New York

Ogata, N.; Kaawakage, S. & Ogihara, T. (1997) Poly(vinyl alcohol)-Clay and Poly(ethylene oxide)-Clay Blends Prepared Using Water as Solvent. *J. Appl. Polym. Sci*. Vol.66, No.3, pp.573-581

Peeterbroeck, S.; Laoutid, F.; Taulemesse, J.; Monteverde, F.; Lopez-Cuesta, J.; Nagy, J.; Alexandre, M. & Dubois, P. (2007) Mechanical Properties and Flame-Retardant Behavior of Ethylene Vinyl Acetate/High-Density Polyethylene Coated Carbon Nanotube Nanocomposites. *Adv. Funct. Mater*. Vol.17, No.15, pp.2787-2791

Pierard, N.; Fonseca, A.; Konya, Z.; Willems, I.; Van-Tendeloo, G. & Nagy, J. (2001) Production of short carbon nanotubes with open tips by ball milling. *Chem. Phys. Lett.* Vol.335, No.1-2, pp.1-8

Potschke, P.; Bhattacharyya, A.; Janke, A. & Goering, H. (2003) Melt Mixing of Polycarbonate/Multi-wall Carbon Nanotube Composites. *Compos. Interfaces*. Vol.10, No.4-5, pp.389-404

Pötschke, P.; Pegel, S.; Claes, M & Bonduel, D. (2008) A Novel Strategy to Incorporate Carbon Nanotubes into Thermoplastic Matrices. *Macromol. Rapid Commun*. Vol.29, No.3, pp.244-251

Prashantha, K.; Soulestin, J.; Lacrampe, M.; Krawczak, P.; Dupin, G. & Claes, M. (2009) Masterbatch-Based Multi-Walled Carbon Nanotube Filled Polypropylene Nanocomposites: Assessment of Rheological and Mechanical Properties. *Compos. Sci. Technol*. Vol.69, No.11-12, pp.1756-1763

Quirk, R.; France, R.; Shakesheff, K. & Howdle, S. (2004) Supercritical Fluid Technologies and Tissue Engineering Scaffolds. *Curr. Opin. Solid State Mater. Sci.* Vol.8, No.3-4, pp.313-321

Ray, S. & Okamoto, M. (2003) Polymer/Layered Silicate Nanocomposites: A review from Preparation to Processing. *Prog. Polym. Sci.* Vol.28, No.11, pp.1539-1641

Saito, T.; Matsushige, K. & Tanaka, K. (2002) Chemical Treatment and Modification of Multi-Walled Carbon Nanotubes. *Physica B*. Vol.323, No.1-4, pp.280-283

Seo, M. & Park, S. (2004) A kinetic study on the termal degradation of multi-walled carbon nanotubes-reinforced poly(propylene) composites. *Macromol. Mater. Eng*. Vol.289, No.4, pp.368-374

Seo, M.; Lee, J. & Park, S.(2005) Crystallizaiton kinetics and interfacial behaviors of polypropylene composites reinforced with multi-walled carbon nanotubes. *Mater. Sci. Eng.* Vol.404, No.1-2, pp.79-84

Shi, H.; Lan, T. & Pinnavaia, T. (1996) Interfacial Effects on the Reinforcement Properties of Polymer-Organoclay Nanocomposites. *Chem. Mater.* Vol.8, No.8, pp.1584-1587

Star, A.; Stoddart, J.; Steuerman, D.; Diehl, M.; Boukai, A.; Wong, E.; Yang, X.; Chung, S.; Choi, H. & Heath, J. (2001) Preparation and Properties of Polymer-Wrapped Single-Walled Carbon Nanotubes. *Angew. Chem. Int. Ed.* Vol.40, No.9, pp.1721-1725

Tartaglione, G.; Tabuani, D,; Camino, G. & Moisio, M. (2008) PP and PBT composites filled with sepiolite: Morphology and thermal behavior. *Compos. Sci. Technol.* Vol.68, No.2, pp.451-460

Thostenson, E.; Ren, Z. & Chou, T. (2001) Advances in the science and technology of carbon nanotubes and their composites: a review. *Compos. Sci. Technol.* Vol.61, No.13,pp.1899-1912

Tomasko, D.; Li, H.; Liu, D; Han, X.; Wingert, M.; Lee, L. & Koelling, K. (2003) A Review of CO2 Applications in the Processing of Polymers. *Ind. Eng. Chem. Res.* Vol.42, No.25, pp.6431-6456

Varma-Nair, M.; Handa, P.; Mehta, A. & Agarwal, P. (2003) Effect of Compressed CO2 on Crystallization and Melting Behavior of Isotactic Polypropylene. *Thermochim. Acta.* Vol.396, No.1-2, pp.57-65

Wang, L. & Sheng, J. (2005) Preparation and properties of polypropylene / org-attapulgite nanocomposites. *Polm.* Vol.46, No.16, pp.6243-6249

Wang, Z.; Ciselli, P. & Peijs, T. (2007) The Extraordinary Reinforcing Efficiency of Single-Walled Carbon Nanotubes in Oriented Poly(vinyl alcohol) Tapes. *Nanotechnol.* Vol.18, No.45, 455709

Wu, J. & Lerner, M. (1993) Structural, Thermal, and Electrical Characterization of Layered Nanocomposites Derived from Sodium-Montmorillonite and Polyethers. *Chem. Mater.* Vol.5, No.6, pp.835-838

Yakobson, B.; Brabec, C. & Bernholc, J. (1996) Nanomechanics of Carbon Tubes: Instabilities beyond Linear Response. *Phys. Rev. Lett.* No.76, No.14, pp.2511-2514

Yang, B.; Shi, J.; Pramoda, K. & Goh, S. (2008) Enhancement of the mechanical properties of polypropylene using polypropylene-grafted multiwalled carbon nanotubes. *Compos. Sci. Technol.* Vol.68, No.12, pp.2490-2497

Zerda, A.; Caskey, T. & Lesser, A. (2003) Highly Concentrated, Intercalated Silicate Nanocomposites: Synthesis and Characterisation. *Macromol.* Vol.36, No.5, pp.1603-1608

Zhao, H.; Zhang, X.; Yang, F.; Chen, B.; Jin, Y.; Li, G.; Feng, Z. & Huang, B. (2003) Synthesis and characteriztion of polypropylene/montmorillonite nanocomposites via an in-situ polymerization approach. *Chin. J. Polym. Sci.* Vol.21, No.4, pp.413-418

Zhao, Y. & Huang, H. (2008) Dynamic rheology and microstructure of polypropylene/clay nanocomposites prepared under Sc-CO_2 by melt compounding. *Polym. Test.* Vol.27, No.1, pp.129-134

Zheng, Y. & Zheng, Y. (2006) Study on Sepiolite-Reinforced Polymeric Nanocomposites. *J. App Polym Sci.* Vol.99, No.5, pp.2163-2166

Zhang, R.; Dowden, A.; Deng, H.; Baxendale M. & Peijs T. (2009) Conductive network formation in the melt of carbon nanotube/thermoplastic polyurethane composite. *Compos. Sci. Technol*. Vol.69, No.10, pp.1499-1504

21

Charging Property and Charge Trap Parameters in Porous Polypropylene Film Using Thermally Stimulated Current

Fukuzo Yoshida and Masahiko Yoshiura
Osaka Institute of Technology Osaka, Japan

1. Introduction

The polymeric materials are utilized in industry and an ordinary household with the characteristic that a natural organic material does not have. Research and development are performed actively now because the polymers are materials with a variety of functionality (Imai et al., 2002; Ishii et al., 2009; Ishimoto et al., 2009; Varlow & Li, 2002). By such a background, we aimed at the polymer system piezoelectric material which let it give piezoelectricity as the sensor function. For typical piezoelectric material(Koga & Ohigashi,1985;Lindner etal.,2002), PZT and $BaTiO_3$ are well known until now. In contract, the PVDF of the polymer system piezoelectric material immobilized CF_2 dipolar orientation. Piezoelectric modulus d_{33} of the porous polymer electrets is higher than PVDF, and in a polymer system, polaristation reversal happens.

However, the electrical conduction mechanism of the porous polymer electrets(Cao et al.,1998;Xia et al.,1999) is complicated, and a study is gone ahead with as an important theme for the development. It has been considered that charge carrier traps in a substance play an important role in the charging phenomenon. For this theme, the thermally stimulated current (TSC)(Braünlich,1979;Chen & Kirsh,1981;Ikezaki & Hori,1998;Baba & Ikezaki,1992;Ikezaki & Murata,2006;Oka & Ikezaki,1992;Perlman & Creswell,1971;Yoshida et al.,1998) is one effective measurement. The TSC measurement activates a sample by corona discharge or light and gives a sample heat stimulation by constant heating rate and takes out electric charge in inside of sample to produce a current of the external circuit. This measurement is not a change of state other than a sample, and is extremely high sensitive measurement.

On the other hand, the surface boundary and charging phenomenon are complicated because the inner structure of the sample is not uniform. As a result, it is thought that the signal of the TSC spectrum which measured is a compounds of TSC spectra caused by several charge traps. We developed the evaluation method using the characteristic of the TSC measurement. This evaluation method separates plural TSC spectra precisely and evaluates the information of the trap precisely. As for this separation method (named AEM separation system), it is done computation process on Windows. Above all, an escape

frequency factor proposed a directly ratable method (named AEM-v(Yoshida & Maeta,1991)) for the first time even if a waveform condition of the TSC spectrum was bad.

Polymer system piezoelectric material to use for this study is porous polypropylene. The temperature characteristic of the surface charge electric potential was examined directly by the thermally stimulated charge decay (TSCD) other than TSC measurement.

In this study, it applied the AEM separation system which we proposed to the separation of the TSC spectrum and analyzed the property of the trap which imperforate polypropylene and porous polypropylene formed.

2. Materials and methods

An experiment sample is the polypropylene which is one of the four major general- purpose resin. It shows the different polypropylene (PP) of three kinds of properties in Table 1. A polypropylene film as prepared (PP1) and the polypropylene drawn film (PP2) to two axes (Futamura Chemicals) were used as base polymers. The porous film containing pores of several micro meters in radius prepared (PP3) was drawn to the thickness of 75μm.

sample name	type	Thickness (μm)
PP1	solid	50
PP2	solid(drawn to two axis)	50
PP3	porous(drawn to two axis)	75

Table 1. Three PP films used in this experiment.

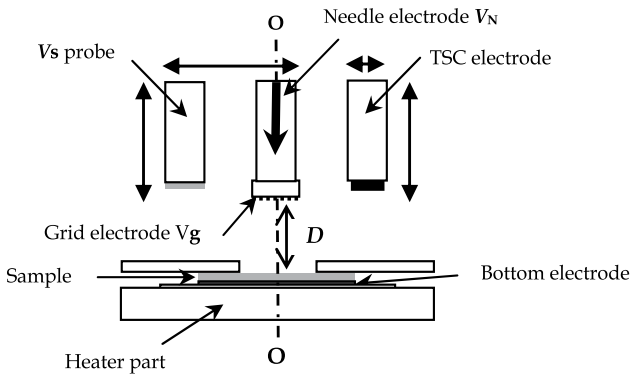

Fig. 1. Electrode arrangement for various measurements in the cryostat.

Figure 1 shows the electrode arrangement that various measurements are possible. The corona electrical charging of the sample removing was performed by a needle electrode to central axis O-O. The corona charge was carried out with voltage V_N of tungsten needle electrode fixed at ±3 kV and the grid voltage V_g at less than ±2 kV for 60 s at 1 atm. The corona discharge was measured under constant humidity after pouring the dry gas of the fixed quantity. Surface potential V_s was measured with surface potential electrometer (Model 344, Trec Japan). The TSC measurement was performed by removing the TSC electrode to the central axis shown in Fig. 1 with a separation of D=1mm from the sample.

The open TSC signal was measured under a vacuum using electrometer (Keithley 610C). As a result of having made shielding on an external circuit, it enabled very sensitive TSC measurement. The TSC observation temperature region reached in the range of 430 K from 250 K using LN_2 cryostat.

Figure 2 shows diagram of the TSC measurement. This figure is an example applying bias electric field (E_b) for present temperature (T_b) and setting time (t_b). This experiment performed charge injection by corona electrical charging not bias electric field. The corona charging processed a sample in the polarity of each positive and negative. After one corona charging process, the TSC spectra were measured two times in succession. It calls the TSC spectrum "1st run TSC" and "2nd run TSC" sequentially. The TSCD measurement is the basically same as TSC. The upper part electrode which showed in Fig. 1 becomes the surface potential prove.

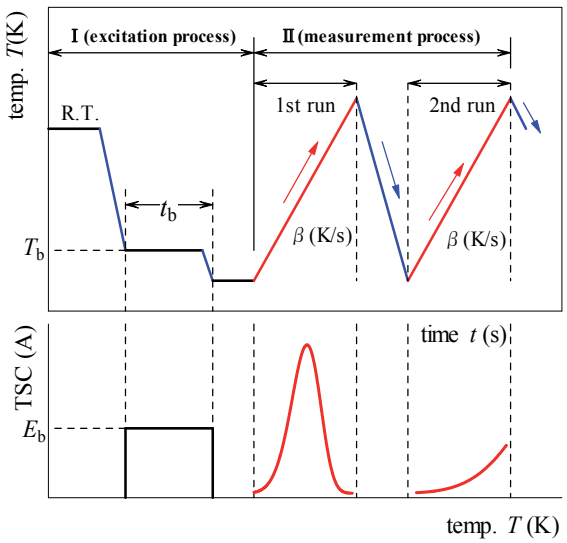

Fig. 2. Diagram of the TSC measurement

3. TSC spectrum analysis

AEM-v is necessary for the construction on the AEM separation system which we are proposed.

3.1 AEM theory

AEM-v is able to evaluate the escape frequency factor v utilizing all the data of an object TSC spectrum. The advantageous property of this method is that both the v and E_t value could be determined. The equation used in AEM-v was derived from an equation of the TSC with constant heating rate β under the condition of first-order slow retrapping is expressed as:

$$I(T) = I_o \exp\left\{\frac{-E_t}{kT} - \frac{\nu}{\beta}\int_{T_o}^{T} \exp\left(\frac{-E_t}{kT}\right) dT\right\} \tag{1}$$

The following symbols are used : $I_o = n_o e \mu v \tau A E$ (A), n_o: the carrier density of the filled traps at t =0 (m^{-3}), e: the electric charge (C), μ: the carrier mobility ($m^2/V \cdot s$), v: an escape frequency factor (s^{-1}), τ: the life time of a free carrier (s), A: the area of the electrode (m^2), E: the applied electric field (V/m), E_t: energy depth of carrier trap(eV), k: the Boltzmann's constant 8.617×10^{-5} (eV/K), β: the heating rate (K/s), T : the absolute temperature (K), T_o : the absolute temperature from which the heating begins after filling of the traps with carrier at the time t.

The theoretical TSC spectrum shown in Fig.3 was calculated by eq.(1) with a TSC maximum m (T_{mo} , I_{mo}) and trap depth E_{to} . The basic formula of AEM-v becomes the eq.(2). The escape frequency factor v is thus expressed by a ratio of I_a to I_b:

$$\nu = \frac{\frac{\beta k}{E_t}\left\{\ln\frac{I_a}{I_b} + \frac{E_t}{k}\left(\frac{1}{T_a} - \frac{1}{T_b}\right)\right\}}{\sum_{n=0}(-1)^n \frac{(n+1)!}{\left(\frac{E_t}{kT_b}\right)^{n+2}} \exp\left(\frac{-E_t}{kT_b}\right)\left[1 - \left(\frac{T_a}{T_b}\right)^{n+2} \exp\left\{\frac{-E_t}{k}\left(\frac{T_a - T_b}{T_a T_b}\right)\right\}\right]} \tag{2}$$

The integral terms in eq. (1) were integrated by the asymptotic expansion series. As shown in the equation, eq. (2) contains no TSC peak coordinates. Three coordinate points on the TSC spectrum, noted as a (T_a, I_a), b (T_b, I_b) and c (T_c, I_c) as shown in Fig. 3 are used for an application of AEM-v.This equation, therefore, made possible not only the evaluation of v value from a TSC spectrum without a maximum peak, but also the continuous determination of v values from any point on a TSC spectrum.

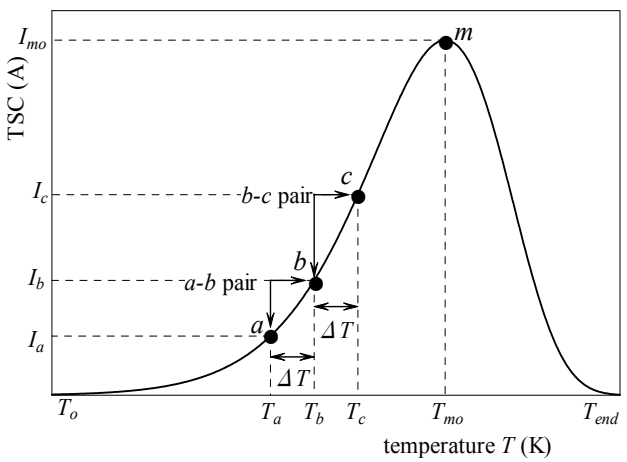

Fig. 3. Coordinate on the TSC spectrum of the AEM-v.

Although two pairs of data points from a TSC spectrum are required for AEM-v, at least three points satisfy the requirement by using one point in common for both pairs. The convenient method to select data by its temperature coordinate, is shown in Fig. 3. In the method, named "moving coordinates method", two pair (a-b and b-c) of points at a same temperature separation (ΔT), as shown in Fig.3, is selected, holding a point at temperature (T_b) in common and inputting their coordinates into the calculation. The E_t and v values at

the intermediate temperature (T_b) are evaluated. In other words, for a calculation of v value, E_t value which assumed and *a*-*b*pair are given in eq.(2). The same calculation is carried out to the other b-c pair at the same time. As a result, it is converged by a computer until v value which calculated in both pairs becomes the same value. Numbers of the E_t and v values were calculated for the coordinates of two pairs of points with ΔT =0.2 K interval, shifting by 0.2 (K) for higher values and plotted continuously on T_b. As the results, this smaller temperature interval of data provides more sensitivity to detect a composite TSC objective.

Three characteristics of AEM-v are shown in Fig. 4. These characteristics applied to a single relaxation TSC theory spectrum of Fig.3. Then, it can calculate the peak temperature T_m of TSC spectrum of to be shown in Fig.4(c) from an E_t and v values at the same temperature T. The part of flat shape means that a target TSC spectrum is caused by single relaxation. The values of three parameters were estimated from the means of the vertical axis of the temperature range indicating the flat shape. It can be understood that the flat shapes of the characteristics in the temperature region of the whole TSC spectrum indicate the signal to be caused by a single trap. Naturally, this peak temperature T_m is temperature indicating the maximum current I_{mo} of the TSC spectrum of Fig. 3.

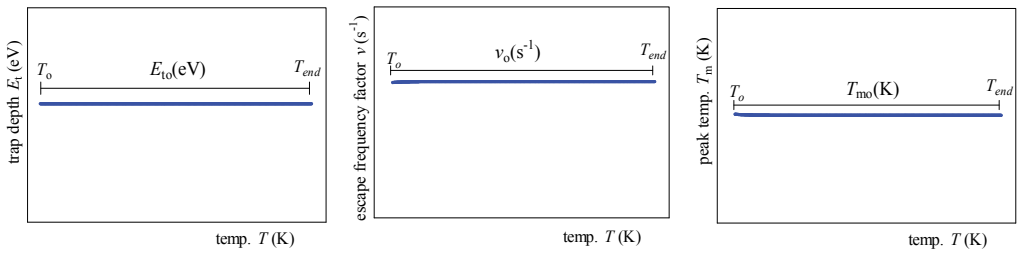

(a) E_t-T characteristic (b) v-T characteristic (c) T_m-T characteristic

Fig. 4. Three characteristics of AEM-v which applied to the TSC spectrum of the single trap.

The thermal cleaning method and partial heating are known as experimental separation methods of composite TSC spectrum and only initial rising part of TSC spectrum was used for estimation of E_t value. The initial rise method(Garlick & Gibson,1948) is the only one procedure to apply to data without a peak until now. However, in AEM-v, an application is possible to an omniformity-shaped TSC spectrum.

The initial rising (signal from T_o to T_S) part of a TSC spectrum calculated with arbitrary coefficients (E_{to}, T_{mo} and I_{mo}) was shown in Fig. 5. The attached map of Fig. 5 is an application result of AEM-v. E_t and v values were evaluated by the AEM-v from a part of a TSC spectrum or that without a maximum using three coordinates for the first time. Furthermore, it can be understood that the detection of the peak temperature T_m is possible from the initial part of a TSC spectrum.

The maximum coordinate of TSC spectrum and E_t value is necessary to calculate a theoretical TSC spectrum. In other word, among the maximum coordinate m of TSC spectrum, maximum current I_m is required. AEM-I(Yoshida et al.,1991) which we proposed can calculate maximum current I_m of the TSC spectrum as well as an evaluation of E_t values. It need a maximum temperature T_m in addition to two points, a point and b on the TSC spectrum which were shown in Fig.3 The basic formula of AEM-I is given in the next expression.

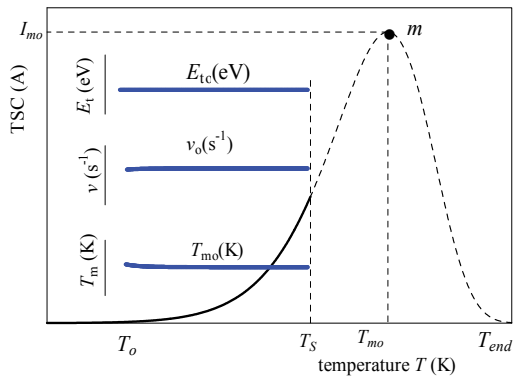

Fig. 5. Three characteristics of AEM-*v* which applied to the initial rising part of TSC spectrum.

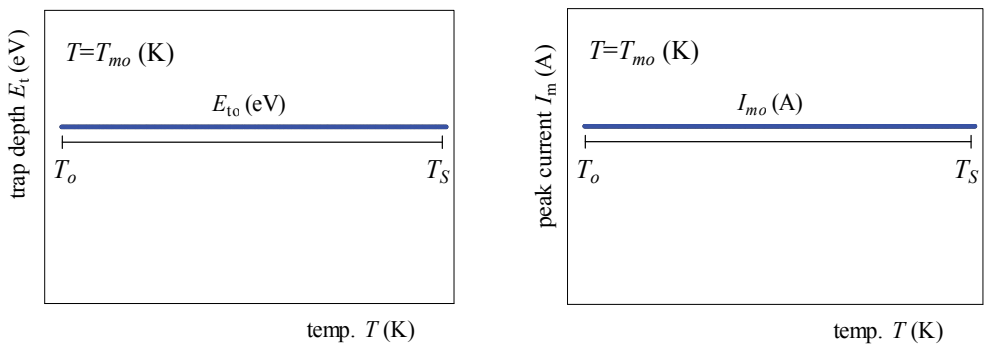

(a) I_m-T characteristic (b) E_t-T characteristic

Fig. 6. A result of having applied AEM-*I* to TSC spectrum of Fig.5.

I_m was calculated with two coordinate of a TSC spectrum and T_m obtained from AEM-*v*. Two characteristics of AEM-*I* were presented in Fig. 6. Like Fig. 5, the flat shape means the signal was detected from a single trap. It was able to evaluate maximum coordinate and trap depth E_t of the TSC spectrum by AEM-*v* and AEM-*I*. As a result, the calculation of the TSC theoretical spectrum is enabled and is shown with a dashed line in Fig. 5. In AEMs, the reconstruction of the whole TSC spectrum is possible from the part of the TSC observed in this way.

$$A_I = -\ln\frac{I_a}{I_b} + \left(\frac{T_b}{T_m}\right)^2 \left[\sum_{n=0}(-1)^n \frac{(n+1)!}{\left(\frac{A_I T_a}{T_b - T_a}\right)^n} \exp\left\{\frac{A_I T_a (T_b - T_m)}{T_m (T_b - T_a)}\right\}\left\{1 - \left(\frac{T_a}{T_b}\right)^{n+2} \exp(-A_I)\right\}\right] \quad (3)$$

$$E_t = A_I \frac{k T_b T_a}{T_b - T_a} \quad (4)$$

3.2 AEM separation system

AEM-*v* can do a judgment whether or not the contribution of the trap is single. The merit of AEM-*v* is enabled the separation of a compound TSC spectrum without thermal cleaning

measurements. We name "AEM separation system" as this separation method and carry it out by computerization.

Then, we explain the procedure of this separation method using the calculated TSC spectrums. A separation object is a compound TSC spectrum formed of two traps.

At first the TSC spectrum is screened by AEM-*v*. Then, the observed TSC spectrum can visualize by the information from a trap. Because both peaks (P_1 and P_2) are exposed, Fig.7 shows that it is the signal from two traps (C_1 peak to show in Fig.10 and C_2 peak) easily.

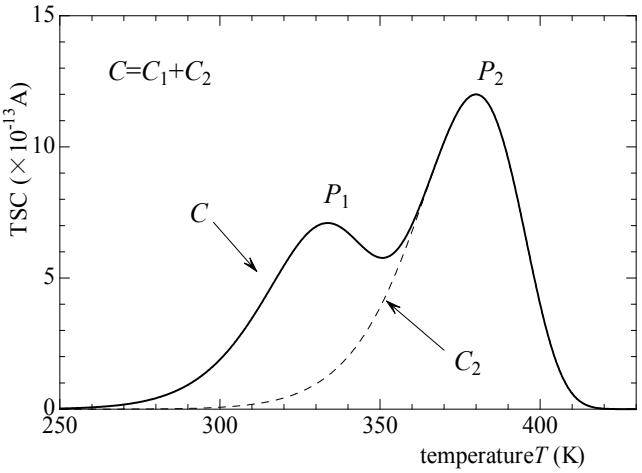

C_1 curve:$E_{to,1}$=0.570(eV),$T_{mo.1}$=330.00(K),$I_{mo,1}$=6.000(×10^{-13}A)
C_2 curve:$E_{to,2}$=0.740(eV),$T_{mo.2}$=380.00(K), $I_{mo,2}$=12.00(×10^{-13}A)

Fig. 7. Compound TSC spectrum consisting of two traps.

Figure 8 is the result that is applied AEM-*v* to a compound TSC spectrum of Fig. 7. An abscissa of Fig.8 is the temperature region that used in calculation. Figure 8(a) and (b) are trap depth E_t and escape frequency factor v respectively. A flat part is the temperature region that is strong in the contribution of the single trap. This E_t-T characteristic can evaluate E_t values of 0.570eV and 0.740eV. In particular, the large flat part of T_m-T characteristic (Fig.8(c)) leads to a T_m value. The big divergence of the neighborhood of 350 K expresses the place that is strong in contribution of the combined signal. Then, using provided T_m=380.00(K), AEM-*I* is applied.

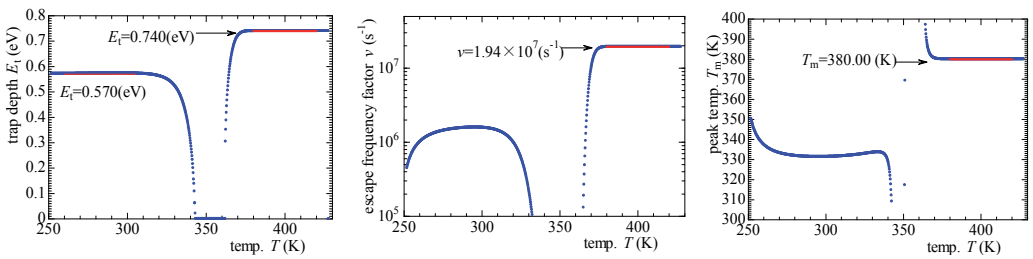

(a) E_t-T characteristic (b) v-T characteristic (c) T_m-T characteristic

Fig. 8. Three characteristics that applied AEM-*v* to Fig.7.

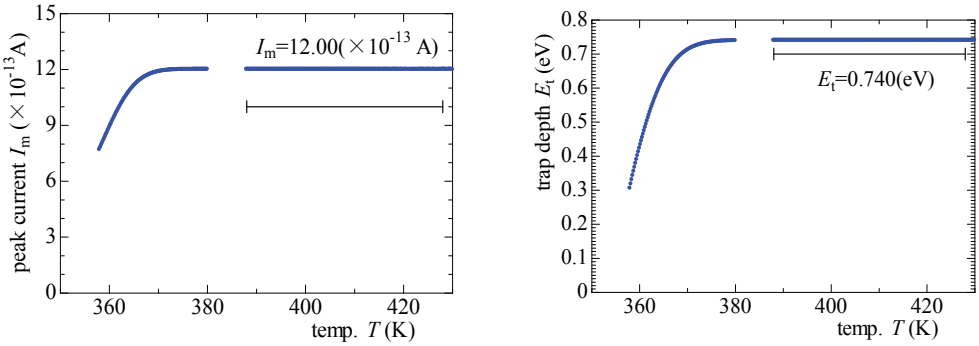

(a) I_m-T characteristic (b) E_t-T characteristic

Fig. 9. As a result of having applied AEM-*I* to the P_2 peak of Fig.7.

Figure 9 is two characteristics of AEM-*I* which applied to P_2 peak of Fig.7 to target separation. I_m value is found from a flat part of Fig. 9(a). In this case, an E_t value is found by a flat part of Fig.9(b) or Fig. 8(a). When the maximum coordinate of the TSC spectrum is exposed, AEM-*LH* (Maeta & Sakaguchi,1980;Maeta & Yoshida,1989)is applicable. And AEM-*LH* enables an evaluation of trap depth E_t again, too. At this stage, the AEM separation system fine-tunes the maximum coordinate of the TSC spectrum to raise the flat shape of E_t-T characteristic more fine. The C_2 curve of Fig.7 calculated using maximum coordinate (380.00, 12.00) and E_t (0.740eV) which were detected.

It is the newly exposed TSC spectrum (C_1 curve) which deduct C_2 curve from C curve targeted for separation in Fig. 10. Figure 11 shows the result that applied AEM-*I* to C_1 curve. Here, AEM-*I* was applied after determination of the peak temperature T_m (330.00K) by AEM-*v*. Because two characteristics show flat in all temperature region, this C_1 curve understands that it is the signal caused by a single trap.

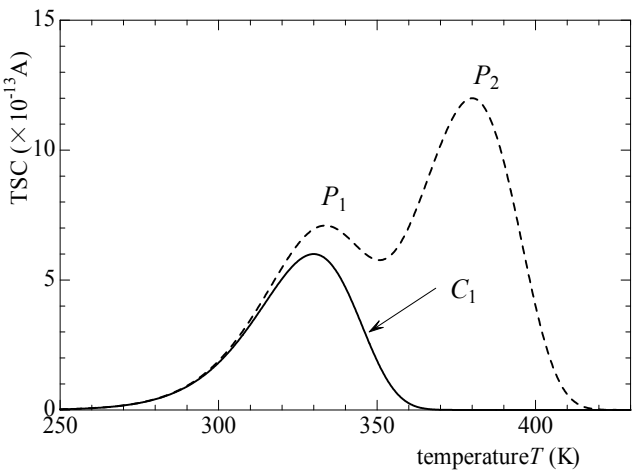

Fig. 10. The C_1 curve exposed from a compound TSC spectrum.

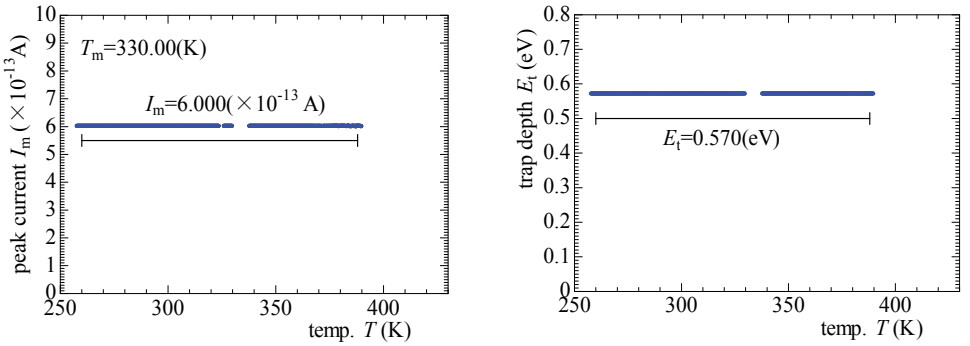

(a) I_m-T characteristic (b) E_t-T characteristic

Fig. 11. The result that applied AEM-I to C_1 curve in Fig.10.

Figure 12 is an example looking like a single TSC spectrum in an appearance.

Contribution of trap signal (C' curve) is closer than a compound TSC spectrum of Fig. 7. Figure 13 shows the result that applied AEM separation system to Fig. 12.

Three characteristics detect a C' curve is compound contribution in high sensitivity.

This result can evaluate E_t of the outline as 0.740eV directly even if do not separate a TSC spectrum. If a flat part can be detected on a TSC spectrum, the separation is possible.

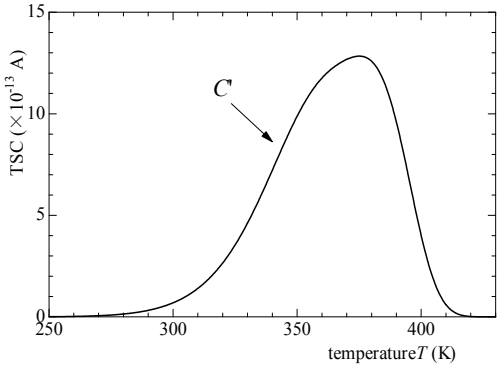

Fig. 12. An example of the TSC spectrum of strong multiplicity.

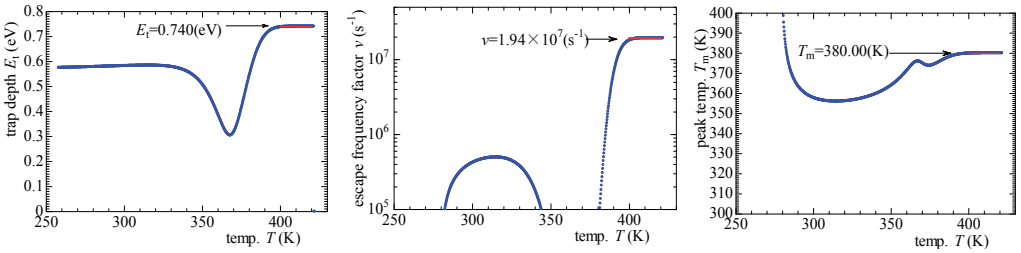

(a) E_t-T characteristic (b) v-T characteristic (c) T_m-T characteristic

Fig. 13. Three characteristics that applied AEM-v to Fig.12.

4. Experimental results

4.1 Grid voltage dependence of the surface potential

Figure 14 is surface potential V_s properties of three kinds of PP when changed the grid voltage V_g. The needle voltage V_N is fixed at each ±3kV.The corona discharge condition is charging time t_d 60s at room temperature under 1 atm. In positive corona charge, the maximum charged potential became ca. 1.1kV and ca.1.25kV each in PP1 and PP2. And PP3 of the porous PP film became ca.1.47kV. On the other hand, as for the negative corona charge, PP1 and PP2 became ca.-300V and ca.-690V each, and PP3 became ca.-820V. This result shows that charged surface potential of the positive corona charge is high in all film. This accords with a report that PP of the contact charging is easy to be charged with electricity in a plus.

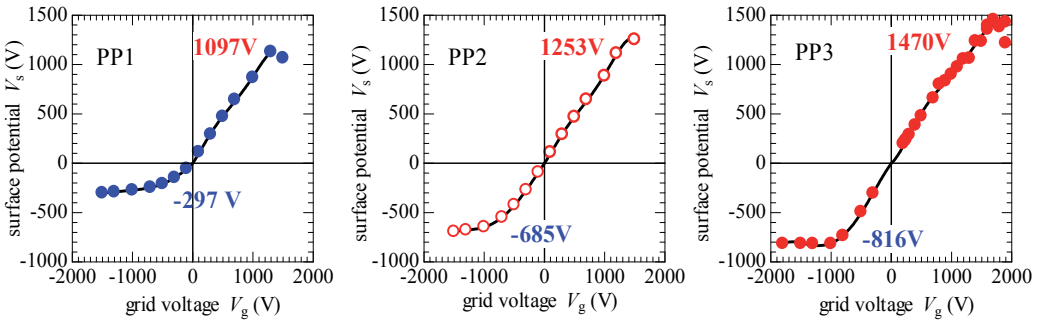

(a) PP1 film (b) PP2 film (c)PP3 film

Fig. 14. Grid voltage dependence of the surface potential.

Figure 15 showed Fig.14 in a mass. It is revealed that clear saturation happens in surface potential by the negative corona charge. On the other hand, for positive corona charge, the surface potential shows linear charging characteristics to ca.1kV of the grid voltage.

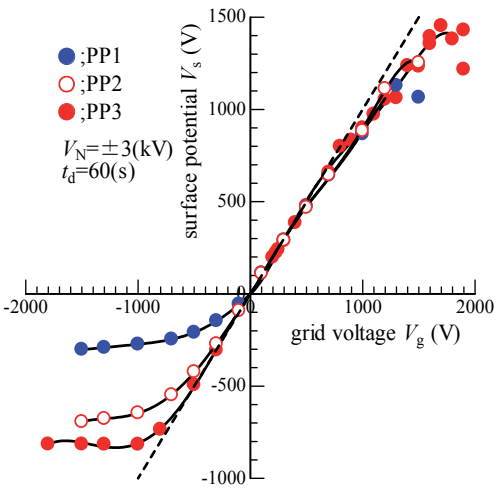

Fig. 15. Comparison of three kinds of PP films.

4.2 Isothermal potential decay

Isothermal decay of the surface potentials were measured during 10^4s as shown in Fig.16. Each characteristic standardized it in surface potential V_{so} at the time of the start of measurement. In positive corona charge, PP1 and PP2 of the solid film are quick in decay, and the decay of ca.4% of initial values is seen in progress for 3h. However, decay is not seen for the negative corona charge. In contrast, even if PP3 passes for 3h, it holds initial potential. In positive corona charge, Time constant of the decay for PP1,PP2 and PP3 were revealed to be 121h, 161h and 806h, respectively.

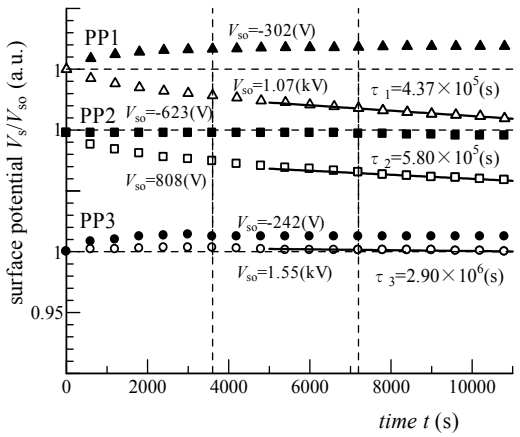

Fig. 16. Isothermal surface potential decay curves for porous and solid PP films at room temperature (▲,■,●:negative charged, △,□,○:positive charged).

4.3 Thermally stimulated charge decay

In generally, temperature condition is important factor in examining the electric-electronic industry material. Therefore, the next performed thermally stimulated charge decay (TSCD) experiment of the PP films. In Fig.17, TSCD characteristics from positively charged PP films were presented. Charge decay of PP1 and PP2 occurred around 390K and 280K, respectively, although PP3 released the charge above 410K. At 430K, PP1, PP2, and PP3 lost 20%, 78%, and 7% of initial surface potential V_{so}, respectively.

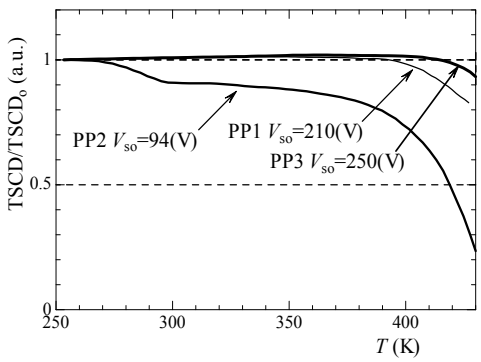

Fig. 17. TSCD characteristics from positively corona charged PP films.

4.4 Thermally stimulated current

The sample which used by TSCD experiment has a TSC experiment successively without exposing a sample to air from a good point of the measuring apparatus. As a result, because it is identical test items, both experimental results compare it directly and can analyze it precisely. TSC spectra measured for PP1, PP2, and PP3 are shown in Fig. 18(a),(b), and (c), respectively.

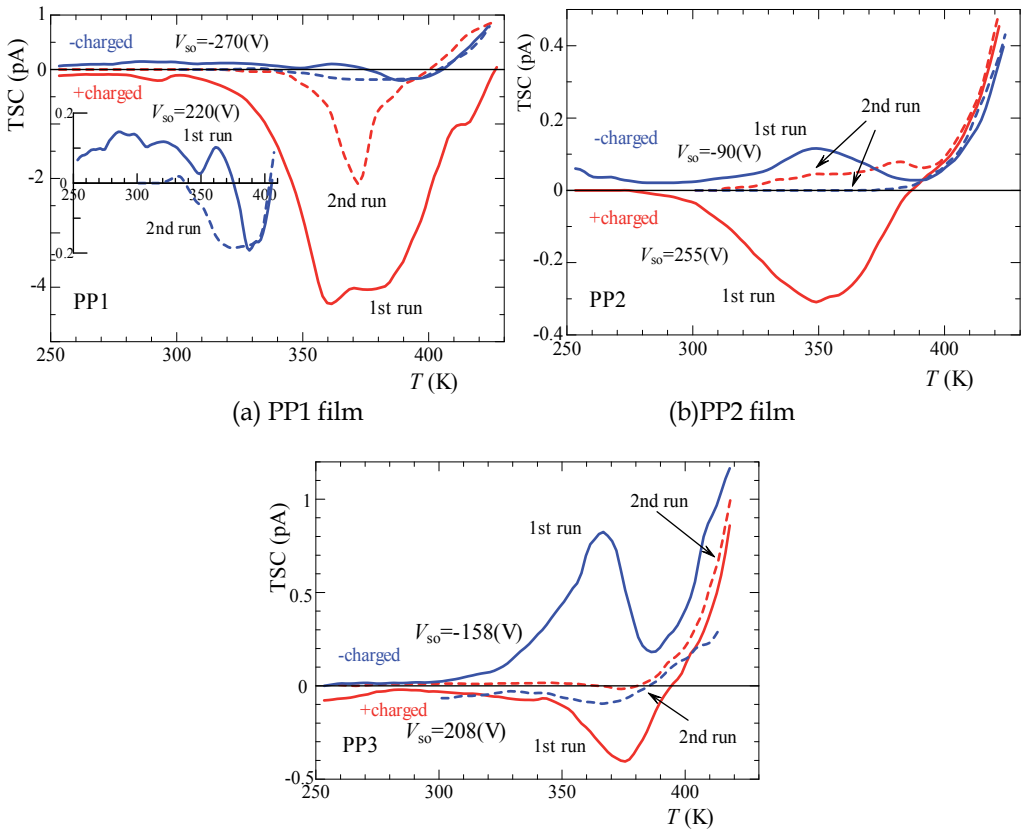

(a) PP1 film (b)PP2 film

(c)PP3 film

Fig. 18. TSC characteristics for porous PP and solid PP.

In the figures, TSC spectrum recorded after positively charged was presented by red line, beside that after negatively charge was shown by blue line. Solid line represented TSC recorded during initial heating after being charged, though the second heating that performed without charging after the film was rapidly frozen caused TSC spectrum shown by dashed line. The attached map in Fig. 18(a) shows an enlarged picture of negative charged TSC spectrum. A plurality of TSC peaks are observed in a temperature region 375 K from 250 K. It was shown that the magnitude of TSC signals in the base polymer, PP1, charged positively were larger than that charged negatively. The TSC spectrum of PP3 is observed with each charge polarity in ca.370K and ca.375K. In each sample, signal detected in the second run clearly decreased. In every case, however, the increasing current was

observed about 400K. As a result of Blank experiment, we regard the increase current at high temperature as a thing by the thermolysis ion.

5. Separation of the actual survey TSC spectrum

Generally, as for the observed TSC, the single trap contribution is rare, and a plurality of signal overlaps in most actual survey TSC spectra thermally. Many insulating materials are easy to catch the temperature distortion from the badness of conduction of heat. In other word, this cannot ignore the influence that a heat cycle history gives a sample. This has been regarded as a cause to disturb an accurate evaluation. The solution must separate the signal contribution of the trap from one TSC measurement. This can be settled by the AEM separation system which it described in Chapter 3. In addition, the AEM separation system can separate thermal noise and the residual current by other causes in a separation process. This chapter uses the actual survey TSC spectrum of Fig.18(b) for an example and explains a separation process.

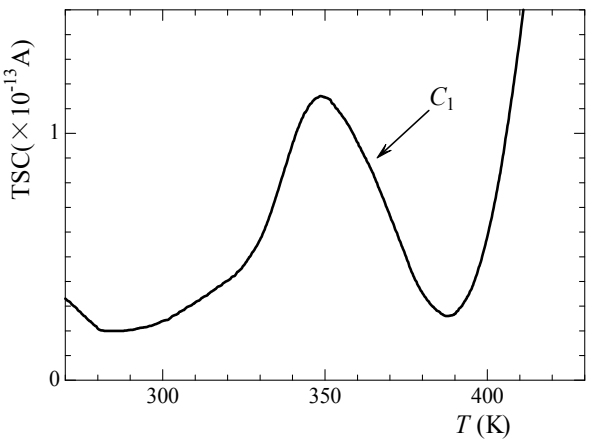

Fig. 19. An example of a TSC spectrum targeted for separation.

Figure 19 is a TSC spectrum targeted for separation and shows the each characteristic in Fig. 20. The maximum coordinate of the TSC spectrum is provided by pushing forward AEM-*I* and a process from AEM-*v*. And trap depth E_t evaluates it in AEM-*LH*. In each characteristic of Fig.20, temperature region that seems to be contributed from a single trap was estimated. Using TSC maximum coordinate (349.00K, 1.150×10^{-13}A) and trap depth E_t (0.764eV) decided by the screening of the TSC spectrum, P_m peak of Fig. 21(a) was calculated by eq. (1). Figure 21 shows the temporary separation of the TSC spectrum. The C_2 curve of Fig.21(a) is the resultant curve of removal of a P_m peak from actual survey TSC spectrum C_1. Figure 21(b) is the result of application of AEM-*LH* to C_2 curve. At the stage, the maximum of the TSC spectrum is revealed. And the TSC spectrum which was calculated using this TSC maximum coordinate and trap depth E_t results the P_h peak of Fig. 21(c). The C_3 curve is obtained by removal of P_h peak from C_2 curve. The minus current of the neighborhood of 350K of the C_3 curve shows that P_h peak and agreement of the C_2 curve are incomplete. Therefore it is necessary to revise a P_m peak.

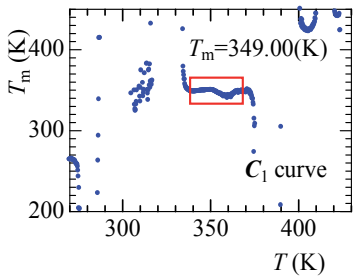

(a)T_m-T characteristic from AEM-v

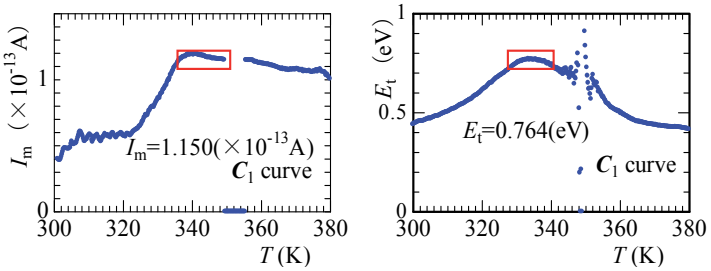

(b) I_m-T characteristic from AEM-I (c) E_t-T characteristic from AEM-LH

Each evaluation is averaged in a part surrounded with the square of each part.

Fig. 20. Characteristic from each AEM of Fig.19.

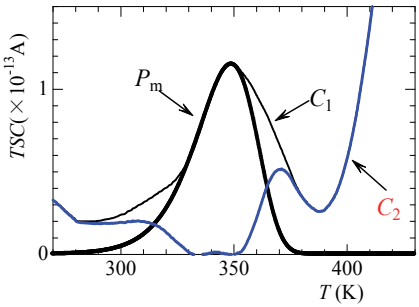

(a) Calculation of the P_m peak

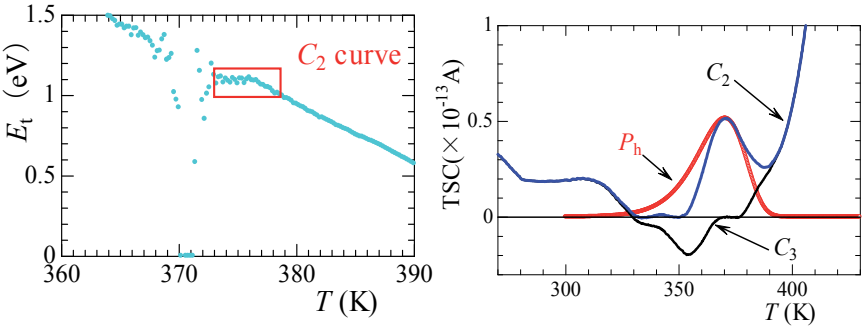

(b) E_t-T characteristic of the C_2 curve (c) Calculation of the P_h peak

Fig. 21. Temporary separation process of the TSC spectrum.

Figure 22 is a revision process of the P_m peak. The C_4 curve of Fig. 22(a) is obtained by removal of P_h peak from C_1 curve. The E_t-T characteristic of the C_4 curve become Fig.22(b). The P_{mo} peak of Fig.22(c) is the result that P_m peak was revised using an E_t value of Fig.22(b) and the maximum of the TSC spectrum. The P_{mo} peak is the TSC signal which decided. Furthermore, Fig.23 shows the revision process of the P_h peak. The C_5 curve of Fig. 23(a) is obtained by removal of P_{mo} peak from actual survey TSC spectrum C_1. The E_t-T characteristic of the C_5 curve become Fig.23(b). The P_{ho} peak of Fig.23(c) becomes the correction curve of the P_h peak. P_{ho} peak accord with actual survey TSC spectrum C_2 well in comparison with P_h peak of Fig.21(c).The AEM separation system repeats such a calculation process in all temperature region of the measured TSC spectrum. Figure 24 is TSC signal and the residual current C_r that were finally decided.

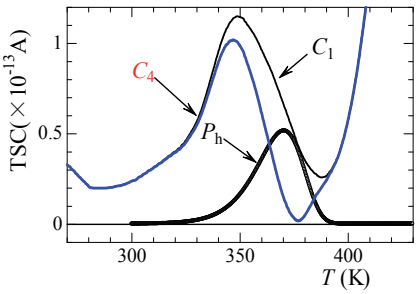

(a) C_4 curve of an exposed low temperature side TSC spectrum

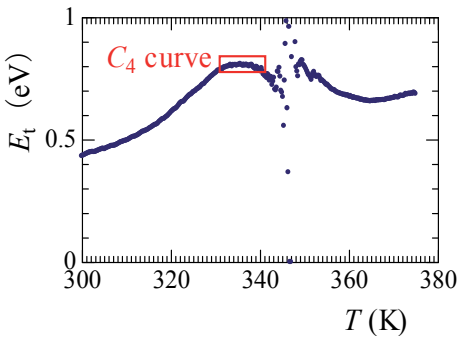

(b) E_t-T characteristic of the C_4 curve

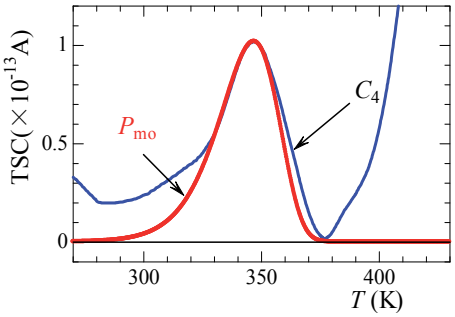

(c)The actual survey TSC spectrum which corrected at P_h peak

Fig. 22. Revision separation process of the TSC spectrum.

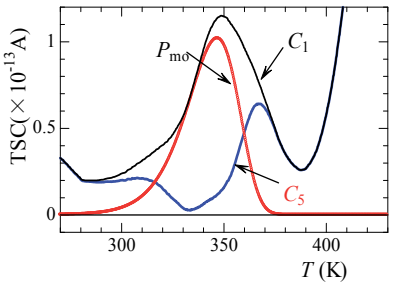

(a) The high temperature side TSC spectrum which was corrected

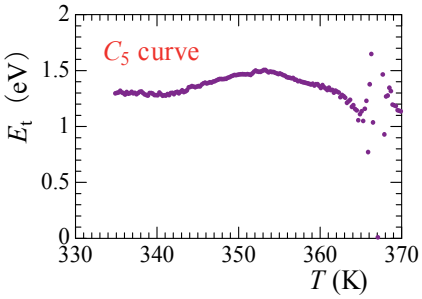

(b) E_t-T characteristic of the C_5 curve

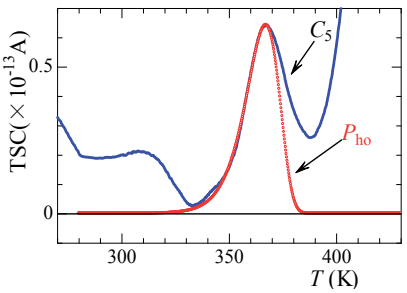

(c) The actual survey TSC spectrum which corrected at P_{mo} peak

Fig. 23. Revision separation process of the TSC spectrum.

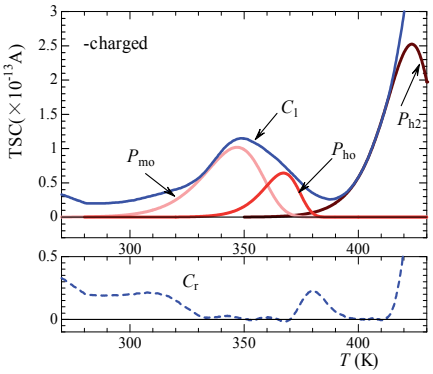

Fig. 24. TSC spectrum separation result of the negative corona charge of the PP2 film.

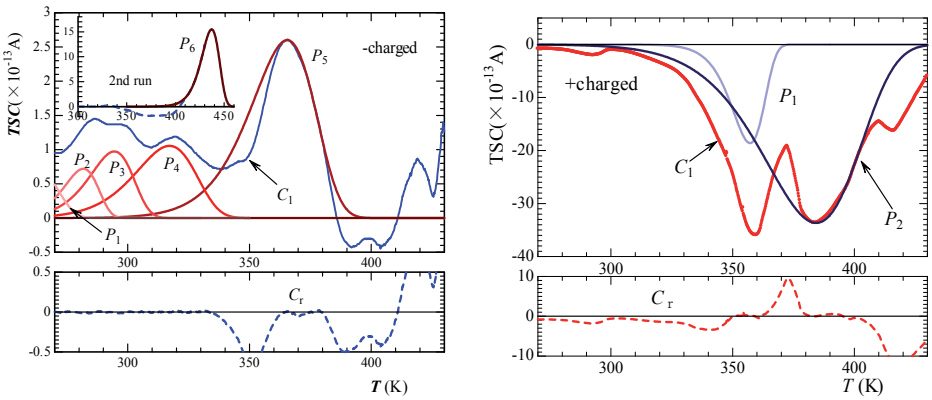

a) negative corona charge (b) positive corona charge

Fig. 25. Separation result of PP1 film.

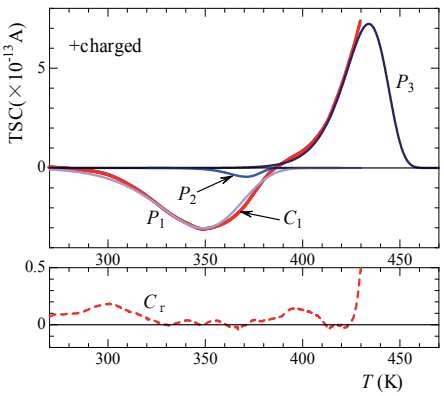

Fig. 26. Separation result of PP2 film due to the positive corona charge.

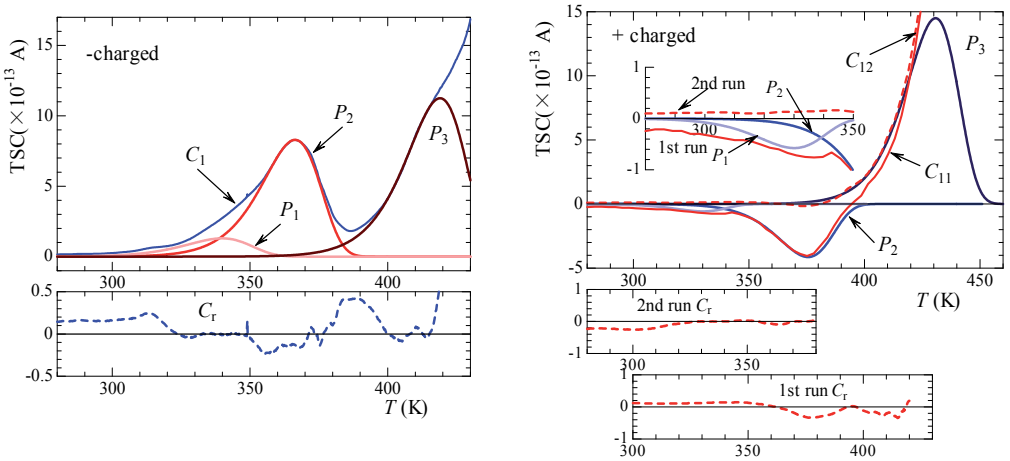

(a) negative corona charge (b) positive corona charge

Fig. 27. Separation result of PP3 film.

Figure 25-27 are the result that separated a TSC spectrum of three kinds of PP film. In Fig. 25(a) are negative corona charge, Fig. 25(b) are positive corona charge. The residual current C_r after the separation spreads and displays it.

The negative corona charge TSC spectrum was separated at the peaks from P_1 to P_6. Actual survey TSC spectrum C_1 deducts 2nd run TSC and removes the increase current of high temperature region. P_5 peak accords with the high temperature side of the maximum peak of the C_1 curve well, but understand that C_1 curve is distorted in the low temperature side. Because the low temperature side of the C_1 curve accords with a temperature region of inversion current observed in 2nd run TSC, it is considered as influence. The P_6 peak to show in attached map is a separation result of the 2nd run TSC.

On the other hand, in the case of positive corona charge, actual survey TSC spectrum C_1 was separated by two TSC spectra (a P_1 peak and P_2 peak). A P_2 peak and the disagreement in the neighborhood of 370 K of C_1 curve are regarded as the influence of a peak observed in the neighborhood of 370 K of the 2nd run TSC to show in Fig. 18(a).

Then, a result of the PP2 film is shown in the Fig. 26. In the case of negative corona charge, we already showed it at a point of the explanation of the separation process of Chaper 5. For the positive corona charge, the C_1 curve was separated at three peaks from P_1 to P_3.The P_3 peak is the reconstruction of the TSC spectrum from the actual survey C_1 spectrum only for the initial rising part that it explained by AEM-v theory.

Finally Fig. 27 is a separation result of PP3 film. In the 2nd run TSC, the main peaks less than 400 K are cleaned. In negative and positive corona charge, it was divided into the TSC spectrum from three traps. The P_3 peak of the positive corona charge is inversion TSC separated by 2nd run TSC (C_{12} curve). In attached map of Fig.27(b), the enlarged figure of separation result less than 350K is shown. The Cr curve is a result expect the TSC signal.

6. Discussions

A signal for the contribution of the single trap must be separated to evaluate the information of the trap from the measured TSC spectrum. The information of trap to be discussed in this chapter is the result that applied all AEM separation system. Furthermore, we discuss the escape frequency factor v of the trap here and mention the origin of the trap.

6.1 Trap depth E_t and observation temperature T_m

The trap depth E_t values of the TSC signals separated are plotted to the peak temperatures T_m as are shown in Fig. 28.

Generally the trap depth is deepened so that an observed tempearature region of the TSC signal becomes the high temperature. However, the separation result does not necessarily behave like that. The origin of various traps is thought about. In PP1 film to show in Fig. 28(a), there are four traps (from P_1 to P_4 peak) from about 0.59eV to about 0.95eV in less than 350K for negative corona charge. And there is a trap of 0.841eV (P_5 peak) by 400K from 350K. In the case of positive corona charge, two traps (1.61eV of P_1 peak and 0.617eV of P_2 peak) exist in the same temperature region. Only P_6 peak (1.77eV) of the negative corona charge exists when it becomes than 400K.

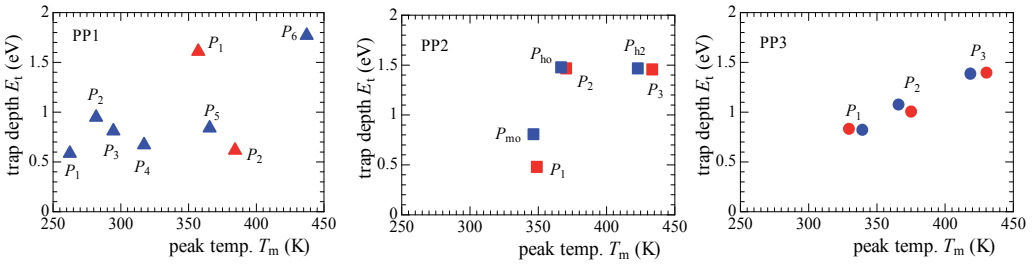

(a)PP1 film (▲:+charged,▲:-charged)

(b)PP2 film (■:+charged,■:-charged)

(c)PP3 film (●:+charged,●:-charged)

Fig. 28. Correlation of trap depth E_t of three PP film.

In the case of PP2 film to show in Fig. 28(b), three traps exist in the almost same temperature region more than 350 K regardless of polarity of the charge. The depth trap of P_1 peak (0.473eV) is different from P_{mo} peak (0.801eV) greatly. However, as for four trap (P_{ho}, P_2, P_{h2} and P_3 peak), about 1.5eV is evaluated regardless of polarity of the corona charge. When PP2 film compare with PP1 film in the negative corona charge, it understands that the number of charge trapping decreases solid film two axis orients it. Furthermore, the TSC intensity of the P_2 peak of PP1 film for the positive charge is very big. As for the polymeric film which drawn, electrical specification is known to be improved. In the case the solid film has much number of the traps for negative corona charge and it is thought that space charge accumulation that a trap forms is bigger than drawn film for positive corona charge. This does not contradict it about the high insulation that drawing operation of the film gives.

Then, Fig.28(c) is a separation result of the porous film. It is understand that three discrete peaks do not depend on the corona charging polarity. In both P_1 peak, temperature regions less than 350K and both P_2 peak are observed each in the temperature region of 400K from 350K. And there is both P_3 peak in the temperature regions more than 400K. Trap depth E_t of each peak was evaluated as about 0.82eV-0.83eV, about 1.0eV-1.1eV and about 1.4eV from the temperature region sequentially. Each peak regardless of polarity of corona charge understands that it is the same trap depth.

6.2 Escape frequency factor *v* and observation temperature T_m

Figure 29 are the result that evaluated escape frequency factor v for the observation temperature T_m. The v value of P_1 -P_5 peaks for negative corona charge of solid film (PP1) to show in Fig. 29(a) is about 10^8 s^{-1}-10^{14} s^{-1}. In particular, the v value of P_1 peak for positive corona charge is high with about 10^{20} s^{-1}. With the two axis drawing solid film (PP2) to show in Fig.29(b), P_{ho} and a v values of the P_2 peak are about 10^{17} s^{-1} and P_{h2} and P_3 peak are about 10^{14}-10^{15} s^{-1}. As for this, order of the v value accords well about the observation region of each peak. In contrast, there are approximately 5 orders of differences even if P_{mo} and P_1 peak are the same observation regions.

On the other hand, the v values of the porous film (PP3) accord regardless of corona charge polarity well at both peaks. The v value of each peak is about 10^9-10^{10} $s^{-1}$of the P_1 peak, about 10^{11}-10^{12} $s^{-1}$of the P_2 peak and about 10^{13}-10^{14} $s^{-1}$of the P_3 peak.

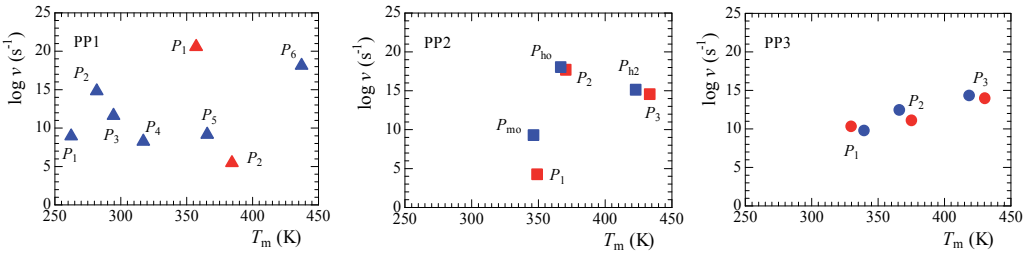

(a)PP1 film (▲:+charged,▲:-charged)

(b)PP2 film (■:+charged,■:-charged)

(c)PP3 film (●:+charged,●:-charged)

Fig. 29. Correlation of escape frequency factor v of three PP film.

6.3 Magnitude of attenuation of the charged potential

In TSC measurement, the charged potential measured twice of potential (V_{so}) before the start of measurement and residual potential (V_{se}) in the room temperature after the measurement.

sample	polarity	TSC			
		V_{so}(V)	V_{se}(V)	$\Delta V_{s,TSC}$(%)	ave.$\Delta V_{s,TSC}$(%)
PP1	-	-269	-189	-29.7	-33.4
	+	219	138	-37.0	
PP2	-	-89	-2	-97.8	-96.6
	+	272	12.6	-95.4	
PP3	-	-158	-132	-16.5	-12.1
	+	208	192	-7.69	

Table 2. Magnitude of attenuation of the charged potential.

Table 2 shows a result of the magnitude of attenuation of the charged potential. $\Delta V_{s,TSC}$ is a decrement ratio of V_{se} value for the V_{so} value. The ave. $\Delta V_{s,TSC}$ is the mean of $\Delta V_{s,TSC}$ value. A ave. $\Delta V_{s,TSC}$ value of PP1 and PP2 is about 33% and about 97% each. A value of ave.$\Delta V_{s,TSC}$ of the porous film is about 12%. A ave.$\Delta V_{s,TSC}$ value of both solid film understands that two axis drawing film comes to have a bigger degree of the decrement. In the case of positive charge, the TSC experiment shows in particular a decrease in TSC strength of the two axis drawing film. As for this, the decrease in trap charges such as an electronic charge to contribute to charged potential or ionic carrier is thought about. In addition, as for the decrease in ave.$\Delta V_{s,TSC}$, it is thought about the property of the trap such as trap depth and the escape frequency factor having changed. The porous film has less magnitude of attenuation of ave.$\Delta V_{s,TSC}$ than both solid films. Seeing from a point of view of the charged retentivity of charge, the trap which a porous film forms means that it is an important factor in the retention capacity at the high temperature.

6.4 The origin of the trap

We discuss the correlation between trap depth E_t and the escape frequency factor v. In Fig.30, the data (v-E_t correlation) of all provided traps by AEM separation system were plotted. Three domains A, B and C were assumed to three peaks P_1, P_2 and P_3, respectively.

Three domains are shown in the circle of dashed line in Fig.30. There is the trap formed of PP2 film in domain A and C. In the PP1 film, the trap is distributed widely other than P_5 peak in domain A.

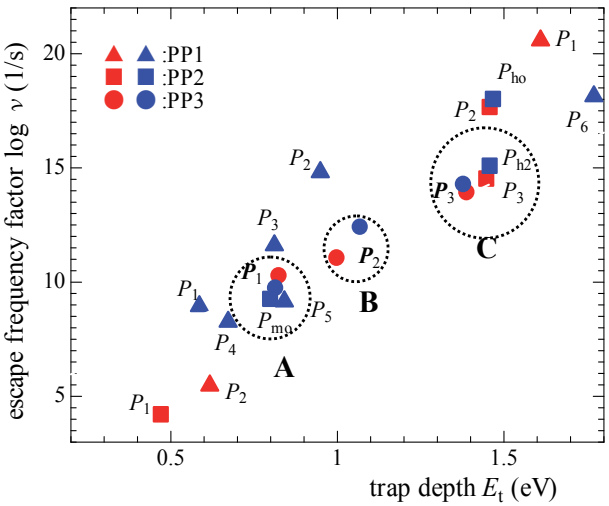

Fig. 30. Correlation of escape frequency factor v and trap depth E_t of three PP film.

The difference in trap distribution of both solid films is regarded as thing by the crystallinity. Table 3 shows correlation of v by E_t of three domains of the porous film. At first, the trap indicating the same correlation as in domain A of the porous film seems to be P_5 of PP1 film and the P_{mo} of PP2 film. Then, the trap of domain C corresponds to P_{h2} and P_3 peak of PP2 film. In order word, in the origin of the trap of the P_1 peak of the porous film, even solid film is formed. And it is thought that a trap of the P_3 peak of the porous film is a trap formed two axis drawing solid film. The dramn structure of the polymer material is complicated, but traps of domain A and domain C is formed in an amorphous part and a crystal part, respectiviely. And it is thought that the trap of the porous film which there is in domain B was formed making polypropylene porous structure. It seems to be possible that this trap is formed in a pores and a boundary of the resin.

Domain	E_t (eV)	v (s^{-1})
A	0.80-0.84	10^9-10^{10}
B	1.0-1.1	10^{11}-10^{12}
C	1.4-1.5	10^{14}-10^{15}

Table 3. Three domain of the PP3 film.

There are P_{ho} peak and P_2 peak formed of PP2 film in the upper part of domain C. The E_t value of both peaks is similar to domain C, but approximately three figures of v value are high. In addition, the trap of the P_1 peak of the PP2 film is located under. The trap (about 0.47eV) of this P_1 peak is considerably lower than trap depth of domain A located near. As a result, it is thought that the property of the trap which PP2 film has with the same two drawing film

reduces charging retention capacity in comparison with porous film. When this fact compares the result of the ave. $\Delta V_{s,TSC}$ of Table 2 and TSCD characteristics of Fig.17, it is clear.

The solid film (PP1) which lowest charged quantity, however, is higher than two axis drawn solid film (PP2) from the viewpoint of charging retention capacity in the high temperature. As for the one cause, the action of trap of the P_6 peak of the high-temperature range of the negative corona charge is thought about.

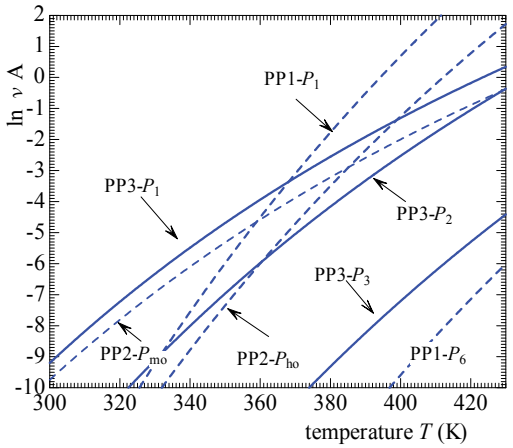

Fig. 31. A detrapping rate of the trapped carrier of the traps in the three domains.

The detrapping rates of the trapped carrier calculated in consideration of Bolzmann factor A(=exp(-E_t/kT)) were presented in Fig. 31. The vA value was calculated in negative corona charging in the observation temperature region of the TSC spectrum using evaluated E_t and v. In the figure, only a P_1 peak (PP1- P_1) of the PP1 film is positive corona charging. The porous film (PP3) and the solid films (PP1 and PP2) are shown with a solid line and a dashed line, respectively. From the viewpoint of charge retention at the high temperature, the vA value for the temperature should be low. At first, it compares the vA value of three peaks of the porous film. The vA value of the P_1 peak (PP3- P_1) is the highest of all, and those of P_2 peak (PP3- P_2) and the P_3 peak (PP3- P_3) followed in order of magnetude of vA value. The detrapping characteristic of P_{mo} peak(PP2- P_{mo}) of the PP2 film resembles that of PP3-P_1. The vA value of P_{ho} peak(PP2- P_{ho}) of the PP2 film increased more rapidly for the temperature than those of the other peaks, and it seems that this trap does not contribute to the charge retention at the high temperature. And it may be said that the P_1 peak (PP1- P_1) of the PP1 film of the positive corona charge is the trap which does not contribute to the charge retention at the high temperature from a reason some as the P_{ho} peak. It is thought that P_{h2} peak and P_3 peak of PP2 film in domain C do not contribute to charge retention from a difference of the film structure with the porous film. As described above, it will be thought that the P_6 peak (PP1- P_6)of PP1 film contributes to charge retention from the result of the vA value.

On the other hand, for the positive corona charge, the trap of P_1 and the P_2 separated, could explain the result. Then trap phenomena more than 430K of both corona charging are suggested when TSCD characteristics and a result of ave. $\Delta V_{s,TSC}$ are added.

As a result of these, it is thought that the formation of the trap of the porous film forms it on an amorphous part and a crystal part as well as a pores and the boundary of the resin. The action of each domain is thought about as follows. It is thought that the trap of all domains takes the increase of the charged quantity. As for the piezoelectricity that a porous film has, it is thought that a trap of domain B participates. And, about the charging retention capacity of the high-temperature range, it is thought that a trap of domain C participates.

7. Conclusions

Using the polypropylene films of the solid state and the porous state, TSC measurements were performed. The next results became clear.

1. The surface potential isothermal decay for the positive corona charge maintained initial potential in the porous film in the progress for 3h, but was the decrement of approximately 4% with both solid films.
2. Both of solid film and porous film, as for the polypropylene, positive corona charge was higher in charged potential maximum than negative corona charge. Porous film showed the highest in the maximum charged potential.
3. From TSCD characteristics, an axis drawn solid film showed the earliest decrement of the charge potential at 430K. The decrement decreased sharply from temperature of about 385K and, for positive corona charge, was approximately 22% of initial value. The porous film had decrement from temperature more than about 410K regardless of corona charging polarity. In the porous film of the positive corona charge, decrement was caused from temperature more than about 410K and, in temperature of 430K, maintained the potential of approximately 93%.
4. As a result of having evaluated a trap by AEM separation method in a TSC spectrum, the trap of the porous film understood that it was distributed over three domains from the property.

   Domain A: E_t: 0.80-0.84eV, v: 10^9-10^{10} s^{-1}
   Domain B: E_t: 1.0-1.1eV, v: 10^{11}-10^{12} s^{-1}
   Domain C: E_t: 1.4-1.5eV, v: 10^{14}-10^{15} s^{-1}

   Because trap which was formed in an amorphous part because domain A existed in all film and domain B were only porous film, it was thought that it was formed in the surface boundary of a pores, and, in domain C, it was thought with the trap of a crystal part formed by extension of the film.
5. It was thought that all traps participated in charging as an action of trap which porous film formed and a trap of domain C participated in the heat resistance of the charging maintenance mainly in particular. In addition, it was thought a trap of domain B acted on piezoelectricity.

8. References

Baba, A. & Ikezaki, K.: "Drawing and annealing effects on thermally stimulated currents in polypropylene films",J. Appl. Phys.Vol. 72, No.5, pp.2057-2059, (1992)

Braünlich, P.: "Thermally Stimulated Relaxation in Solids", Springer-Verlag (1979), ISBN 3-540-09595-0 Springer-Verlag Berlin Heidelberg New York.

Cao, Y., Xia, Z., Li, Q., Shen, L. & Zhou, B.: "Study of Porous Dielectrics as Electret Materials",IEEE Trans. on Dielectrics and Electrical Insulation, Vol.5, No.1,pp.58-62, (1998)

Chen, R. & Kirsh, Y.: "Analysis of Thermally Stimulated Processes", Pergamon Press, Oxford (1981), ISBN 0 08 022930 1.

Garlick, G. F. J. & Gibson, A. F.: "The electron trap mechanism of luminescence in sulphide and silicate phosphors", Proc. Phys. Soc.,, Vol.60, p.574, (1948)

Ikezaki, K. & Hori, T. : "Fundamental Electric Properties of Powder-Formed Materials—Thermally Stimulated Current Spectra of Polymetic Powders—"J. Inst. Electrostatics Jpn., Vol.22, No.2, pp.79-82, (1998) [in Japanese]

Ikezaki, K. & Murata. Y. : "Derivation of Intrinsic Thermally Stimulated Current Spectra of Polymeric Powder Samples"J. Inst. Electrostatics Jpn., Vol.30, No.1, pp.14-19, (2006) [in Japanese]

Imai, T., Hirano, Y., Kojima, S. & Shimizu, T.: "Preparation and Properties of Epoxy-Organically Modified Layered Silicate Nanocomposites", Conf. Rec. 2002 IEEE ISEI, pp.379-383, Boston, USA (2002-4)

Ishii, K., Nagata, K., Osawa, H. & Nanba, N.: "Piezoelectric Properties in Porous Fluoropolymer Having Isolated Voids",Trans. Inst. Electr. Eng. Jpn., Vol.129-A, No.5, pp.373-378, (2009) [in Japanese]

Ishimoto, K., Tanaka, T., Ohki, Y., Sekiguchi. Y. & Murata, Y.: "Thermally Stimulated Current in Low-density Polyethylene/MgO Nanocomposite —On the Mechanism of its Superior Dielectric Properties—",Trans. Inst. Electr. Eng. Jpn., Vol.129-A, No.2, pp.97-102, (2009) [in Japanese]

Koga, K. & Ohigashi, H.: "Piezoelectrisity and related properties of vinylidene fluoride and trifluoroethylene copolymers", J. Appl. Phys., Vol.59, No.6, pp.2142-2150, (1985)

Lindner, M., Bauer-Gogonea, S., Bauer, S., Paajanen, M. & Raukola, J.: "Dielectric barrier microdischarges:Mechanism for the charging of cellular piezoelectric polymers", J. Appl. Phys., Vol.91, No.8, pp.5283-5287, (2002)

Maeta, S. & Sakaguchi, K.: "On the Determination of Trap Depth from Thermally Stimulated Currents", Jpn. J. Appl. Phys., Vol.19, No.3, pp.519-526, (1980)

Maeta, S. & Yoshida, F.: "On the Determination of Trap Depth from Thermally Stimulated Currents II", Jpn. J. Appl. Phys., Vol.28, No.9, pp.1712-1717, (1989)

Oka, K. & Ikezaki, K.: "Effect of Etching Treatment on Thermally Stimulated Current in Spherulitic Polypropylene", Jpn. J. Appl. Phys., Vol.31, No.4, pp.1097-1101, (1992)

Perlman, M. M & Creswell, R.: "Thermal Current Study of the Effect of Humidity on Charge Storage in Mylar", J. Appl. Phys., Vol.42, No.2, pp.531-533, (1971)

Varlow, B. R. & Li, K.: "Non-linear Characteristics of Filled Resins under Alternating Field", 2002 Annu. Rep. CEIDP, pp.52-55, Cancun, Mexico (2002-10)

Xia, Z., Gerhard-Multhaupt, R., Nunstler, W. K., Wedel, A. & Danz, R.: "High surface-charge stability of porous polytetrafluoroethylene electret films at room and elevated temperatures", J. Phys. D: Appl. Phys., Vol.32, pp.L83-85, (1999)

Yoshida, F., Kamitani, Y., Maeta, S., Yoshiura, M. & Ohta, T.: "Thermally Stimulated Currents in Polyaniline Film and their Analyses",Trans. Inst. Electr. Eng. Jpn., Vol.118-A, No.9, pp.1035-1042, (1998) [in Japanese]

Yoshida, F. & Maeta, S.: "Proposal of Asymptotic Estimation v Method Evaluating Escape Frequency Factor from a Partial Thermally Stimulated Current Curve Directly", Trans. Inst. Electr. Eng. Jpn., Vol.111-A, No.4, pp.323-331, (1991) [in Japanese]

Yoshida, F., Tanaka, M. & Maeta, S.: "Proposal of Asymptotic Estimation I Method with High Sensitivity to Thermally Stimulated Current Curve and its Application to New Analysis",Trans. Inst. Electr. Eng. Jpn., Vol.111-A, No.2, pp.104-110, (1991) [in Japanese]

22

Morphology and Thermo Mechanical Properties of Wood/Polypropylene Composites

Diene Ndiaye[1,*], Bouya Diop[1], Coumba Thiandoume[2], Papa Alioune Fall[1], Abdou Karim Farota[1] and Adams Tidjani[2]
[1]*Universite Gaston Berger de Saint-Louis,*
[2]*Universite Cheikh Anta Diop de Dakar,*
Senegal

1. Introduction

Because of the future scarcity of fossil raw material and taking into account current environmental concerns, the development of eco-materials occupies a large number of research centers. Wood polymer composites (WPC) made from wood flour and polymer matrices, are part of this logic. In today's world, the growing needs of the population and the growing technological innovation are pushing industrial and researchers to move towards so-called new generation products such as wood polymer composites whose production increases considerably from year to year. In recent years, wood–fibers have gained significant interest as reinforcing material for commercial thermoplastics. They are now fast evolving as a potential alternative to inorganic fillers for various applications. These composites made from blends of thermoplastics and natural fibers have gained popularity in a variety of applications because they combine the desirable durability of plastics with the cost effectiveness of natural fibers as fillers or reinforcing agents and several advantages like low density, high specific properties, non-abrasive to processing equipment, low cost and most importantly biodegradability (Timmons et al., 1971). In tropical countries, fibrous plants are available in abundance; these fibers with high specific strength improve the mechanical properties of the polymer matrix. Wood is renewable, recyclable and biodegradable, characteristics well appreciated by environmentalists. For these reasons, combining the plastic timber produces a more accepted material. However, consumers want more and more natural materials. But in practice there are a lot of waste that can be exploited in combination with polymers to form composites that are resistant thermoplastic timber, recyclable and can be burned for energy recovery. The addition of wood wood flour, into the polymer matrix leads to an improvement in the stiffness of the composite and decreases in the abrasiveness on processing equipment and density of the product compared to mineral fillers. Because of these attributes, Wood/polypropylene composites (WPCs) are used in a variety of innovative applications. A composite material is a blend of at least two different elements. The new material thus formed, has properties that the elements alone do not possess. Wood polymer composite consists of a wooden frame

* Corresponding Author

called reinforcement (load) that provides the mechanical strength and protection called matrix that is the plastic (thermosetting or thermoplastic resin), which ensures the cohesion of the structure and transmission efforts towards the reinforcement while ensuring the cohesion of the material, gives it its final form and provides the interface with the mechanical environment and additives (accounting, anti-UV, antioxidants, fire retardants) which give the composite properties particular requirements for durability and performance of these materials for outdoor use. However the primary drawback of using wood–fibers for reinforcement is the poor interfacial adhesion between polar-hydrophilic wood–fibers and non polar-hydrophobic plastics (Dième et al., 2008). The WPC are used in four areas: Building materials account for 75% of production. The products concerned are mainly patios, fences, doors, windows and moldings decorative. The consumer and industrial products account for 10% of this market. In this domain, WPC are used in making furniture, cabinets, floor, pallet handling, brackets, boxes and containers. Motor vehicles occupy 8% of this sector. WPC are like interior components of vehicles such as door panels, components of trunk, empty-pockets, cargo cover and so on. Other applications include mainly municipal infrastructure, marine applications, etc... They account for 7% of the production. Among the products manufactured facilities parks, picnic tables, modules, games, etc... Interfacial interactions are very weak in wood/polymer composites , because the surface free energy of both the filler and the polymer is very small (Maldas & Kokta, 1993). As a consequence adhesion must be improved practically always to achieve acceptable properties. Various techniques are used or at least tried for the improvement of interfacial adhesion including the treatment of the wood with sodium hydroxide (Ichazo et al. 2001; Cantero et al. 2003), coupling with functional silanes (Ichazo et al. 2001), or the coating of wood flour with stearic acid (Stark N.M., 1999; Raj R.G. & Kokta B.V., 1991). However, polymers functionalized with maleic anhydride (Kazayawoko et al., 1999; Bledzki A. K. & Faruk O., 2002). The functional groups of these polymers were shown to interact strongly or even react chemically with the surface of wood (Lu et al., 2005; Kazayawoko et al. 1997), while the long alkyl chains diffuse into the matrix making stress transfer possible. The aim of this work is to develop composite materials from polyolefin (polypropylene) and wood flour with coupling agent. One of most popular methods to improve the durability of wood is chemical modification by some small chemical reagents. Among these reagents, acid anhydrides, inorganic acid esters, acid chlorides, aldehydes, lactones, reactive vinyl compounds, epoxides and isocyanates are most useful compounds. In this research, maleic anhydride was selected for its active ring-anhydride group, which is capable of easily reacting with hydroxyl groups on wood without reversed effect on environment and resultantly reducing amounts of hydroxyl groups. Consequently, it's a promising way to improve the wood durability. A first series of specimen was obtained by blending wood flour and polymeric material. In a second series, polypropylene grafted- maleic anhydride was added to the previous ingredients. The first key point for the production of acceptable WPC is the compatibility between wood and polymer host matrix. Wood is hydrophilic in nature (high surface tension), which lowers the compatibility with hydrophobic polymeric material (low surface tension) during composite preparation; this leads to WPCs with poor dispersions of wood fibers [Kazayawoko et al., 1999, 1997; Woodhams et al., 1984; Li Q. & Matuana LM., 2003). Scanning the literature, one can find different surface treatments that have been experienced to improve wood/polymer

adhesion in composites. Remind that the level of adhesion and/or the dispersion state of wood are the key points for the improvement of mechanical properties of the composites. Indeed, the wood particles which have high strength and modulus – with good adhesion and uniform dispersion – can impart better mechanical properties to the host polymer in order to obtain a composite with better properties than those of the unfilled polymer. Substantial research has been carried out on the surface modification of wood fibers with coupling agents to improve the strength properties of WPCs (Woodhams et al., 1984; Li Q. & Matuana L. M., 2003), among these, the addition of maleated polypropylene (MAPP) in polypropylene (PP)-based WPCs has been shown to appreciably improve the dispersion of fibers in the matrix and the mechanical properties of WPCs because of the formation of linkages between the OH groups of wood and maleic anhydride. Many authors (Kazayawoko et al., 1999; Woodhams et al., 1984) in-depth studies have elucidated the mechanisms of adhesion between MAPP treated wood fibers and the PP matrix that cause the improvement. In our study the effects of the incorporation of wood particles with and without a compatibilizing agent on the processing and properties of WPC and the effects of wood flour concentrations on the mechanical properties of the composites were investigated and the results are discussed.

2. Experimental

2.1 Materials

The wood flour particles of 425 microns (40-mesh) in size were kindly donated by American Wood fibers (Schofield, WI) and are constituted predominantly with ponderosa pine, maple, oak, spruce, southern yellow pine, cedar. The wood was oven dried at 100°C for 24 h before processing to remove moisture. The isotactic polypropylene matrix (PP) has a density of 0.9 g/cm^3 and a melt flow index of 2.5 g/10 min, it was provided by Solvay Co. Polypropylene grafted with maleic anhydride (MAPP) with an approximate maleic anhydride (MA) content of 3 wt. % was purchased from Aldrich Chemical Company, Inc. (Milwaukee, WI). All ingredients were used as received.

2.2 Compounding and processing

Before compounding, the wood flour was dried in an oven for at least 48 h at 105°C to a moisture content of less than 1%. The dried wood flours were stored in a sealed plastic container to prevent the absorption of water vapor. The PP matrix, dried wood flour, MAPP, were added to a high-intensity mixer (Papenmeier, TGAHK20, Germany) and dry-blended at room temperature for 10 min. After blending, the compounded materials were stored in a sealed plastic container. Several formulations were produced with various contents of wood flour, PP and MAPP (table 1). For the mechanical property experiments, test specimens were molded in a 33-Cincinnati Milacron reciprocating screw-injection molder (Batavia, OH). The nozzle temperature was set to 204°C. The extrudate, in the form of strands, was cooled in the air and pelletized. The resulting pellets were dried at 105°C for 24 h before they were injection-molded into the ASTM test specimens for flexural, tensile (Type I, ASTM D 638), and Izod impact strength testing. The dimensions of the specimens for the flexural tests were 120x 3x 12 mm^3 (Length x Thickness x Width). The different samples and their code are listed in table 1.

2.3 Electron and optical microscopy

The state of dispersion of the wood inside the polymeric matrix was analyzed using optical microscopy on samples of 100–200 lm thick. Scanning electron microscopy (SEM) was used to obtain microphotographs of the fracture surfaces of the wood composites. These fractures have been performed in liquid nitrogen to avoid any deformation. SEM has been performed using a FEI Quanta 400 microscope working at 30 kV. The polymer surface was examined with LEICA optical microscope working in a transmission mode. Samples were thin enough that no special preparation of the samples was needed for their observations with the optical microscope.

2.4 Differential scanning calorymeter (DSC)

Wood, natural and synthetic polymers are subject to a degradation of the mechanical properties under the influence of increased temperatures (Munker M., 1998). It is very important to have knowledge about the effect of the processing temperatures in relation to the processing duration because there is always thermal stress during the manufacturing of WPC. Important properties concerning the thermal stability of the WPC are obtained from the differential scanning calorimetric (DSC). DSC is widely used to characterize the thermal properties of WPCs. DSC can measure important thermoplastic properties, including the melting temperature (Tm), heat of melting, degree of crystallinity [$x(\%)$] crystallization, and presence of recyclates/ regrinds, nucleating agents, plasticizers, and polymer blends (the presence, composition, and compatibility). Thermal analysis of the WPC samples was carried out on a differential scanning calorimeter (PerkinElmer Instruments, Pyris Diamond DSC, Shelton, Connecticut) with the temperature calibrated with indium. All DSC measurements were performed with powdered samples of about (8–10)±0.5mg under a nitrogen atmosphere with a flow rate of 20 ml/min. Three replicates were run for each specimen. All samples were subjected to the same thermal history with the following thermal protocol, which was slightly modified from the one reported by (Valentini L. et al., 2003):

First, the samples were heated from 40 to 180°C at a heating rate of 20°C/min to erase the thermal history.

Second, the samples were cooled from 180 to 40.00°C at a cooling rate of 10°C/min to detect the crystallization temperature (Tc).

Finally, the samples were heated from 40 to 180°C at a heating rate of 10°C/min to determine Tm. Tm and the heat of fusion (ΔH_m) were calculated from the thermograms obtained during the second heating. The values of (ΔH_m) were used to estimate $x(\%)$, which was adjusted for each sample.

2.5 Mechanical tests

Tensile tests (tensile strength and tensile strain) and three-point flexural tests (flexural strength) were carried out on an Instron 5585H testing machine (Norwood, MA) with crosshead rates of 12.5 and 1.35 mm/min according to the procedures outlined in ASTM standards D 638 and D 790, respectively eight replicates were conducted to obtain an average value for each formulation. Before each test, the films were conditioned in a 50% relative humidity chamber at 23°C for 48 h. The Izod impact strength was measured with an

Instron impact pendulum tester (model PW5) according to ASTM D 256 with acutely notched specimens (notch depth = 2 mm) at room temperature. Each mean value represented an average of eight tests. The impact strength is defined as the ability of a material to resist the fracture under stress applied at a high speed. The impact properties of composite materials are directly related to their overall toughness. In the Izod standard test, the only measured variable is the total energy required to break a notched sample. Specimens for the test had the following dimensions 50 x 12.7 x 3.2 mm^3. Eight replicates for each composition were tested for impact strength.

Sample	PP (%)	Wood (%)
WPPC0	100	0
WPPC1	95	5
WPPC3	75	25
WPPC4	50	50

(a)

Sample	PP (%)	Wood (%)	MAPP (%)
WPPC0*	95	0	5
WPPC1*	90	5	5
WPPC3*	70	25	5
WPPC4*	45	50	5

(b)

Table 1. Composition and code of the wood/polymer composites (percentage is in weight). The star (*) denotes a composite with Wood/PP and 5% wt MAPP.

3. Results and discussions

The results are discussed in several sub-sections in accordance with the goals of the study.

3.1 Structure and morphology (SEM)

Figure 1 and figure 2 show the micrographs of WPCs. It is well known that the properties of wood polymer composites are highly dependent on the wood dispersion and adhesion with the polymer matrix. Figure 1a shows the SEM image of the pure PP fracture surface which was smooth and featureless. As for the WPC, the wood's particles are detected as white dots in figure 1b, 2a and 2b. These figures reveal more separate wood chips and polymer areas for the non compatibilized system. The micrograph in Fig.1c and fig.2c, show that with MAPP there is better dispersion and less voids than without MAPP in fig.1b, fig.2a and fig.2b. On the other hand, between the fig.2a and 2b, it is visible that the dispersion is better in figure 2b; where there's less wood, these two figures show that dispersion decrease with wood loading. When the wood content was enough higher, the particles were uniformly distributed in the PP matrix. They exhibited many single disperse particles and aggregates integrated with particles. The matrix is not enough to encapsulate the solid micro particles of wood. However, large aggregates were found, and the aggregate size increased substantially in these micrographs with higher with higher wood loading wood. The copolymers in the blends can act as a compatibilizer decreasing the interfacial tension between the blend components of the mixture while enhancing the dispersion of dispersed phase in the matrix (Moon H.S., 1994). MAPP improves interfacial adhesion and prevents the debonding of even very large particles. Interfacial interactions and the strength of adhesion determine micromechanical deformation processes and the failure mode of the composites (Renner et al., 2009). The SEM micrographs taken from the surface of broken specimens provide indirect information about the failure mode and interfacial adhesion. Fig.1c

and fig.2c present the fracture surface of specimens prepared with MAPP. The coverage of the wood with the polymer and the relatively small number of holes related to debonding or fiber pull out indicate good adhesion. On the other hand, the opposite is observed in composites prepared without MAPP. The number of debonded particles is quite large, the contours of particles remaining on the surface are sharp, and adhesion seems to be poor, at least compared to MAPP modification.

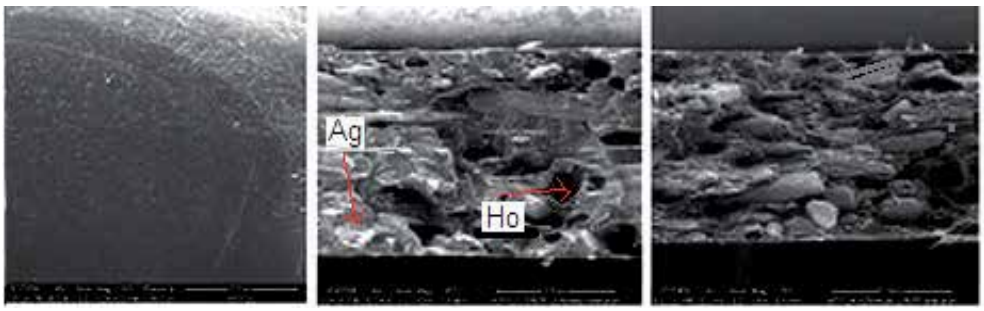

(a) (b) (c)

Fig. 1. SEM micrographs of (a) pure PP and composites containing (b) wood/PP (25/75) and (c) wood/PP/MAPP (25/70/5). Ho seems holes and Ag seems aggregate.

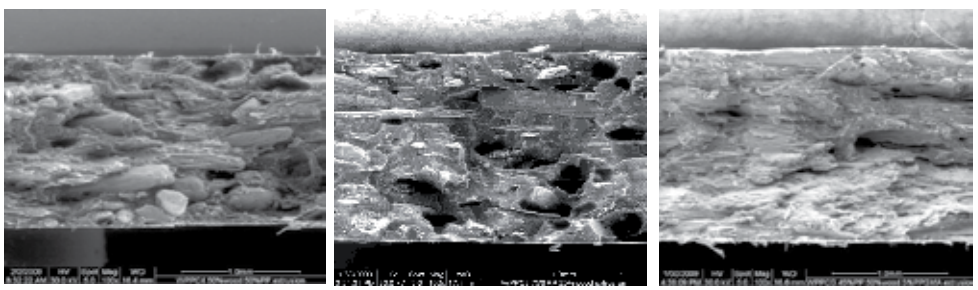

(a) (b) (c)

Fig. 2. SEM micrographs (a) Wood/PP (50/50), (b) Wood/PP (25/75) and (c) Wood/PP /MAPP (25/70/5).

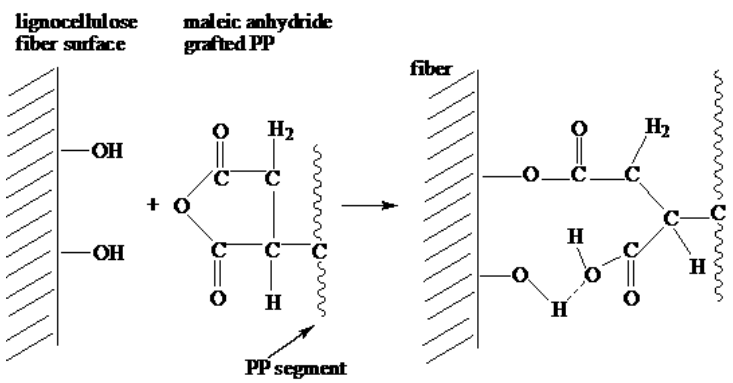

Fig. 3. Schematic description of the grafting of maleic anhydride with wood (Gauthier et al., 1999).

Figure 3 shows the summary of the grafting reaction of MAPP with wood.

3.2 Thermal and crystallization behavior

In this work, the thermal stability, the process of crystallization and melting of PP in its composites with wood (red pine) are studied by SEM analysis and differential scanning calorimetry, respectively, as a function of the wood content and coupling agent.

The physical properties of the WPC could be significantly affected by the crystallization characteristics of PP. Table 2 summarizes the results obtained from this heating run for all of the samples. The measurements were performed immediately after the melt-quenching thermal and crystallization behavior. The physical properties of the WPC could be significantly affected by the crystallization characteristics of PP. The measurements were performed immediately after the melt-quenching scans, so the samples had the same thermal history without an aging cycle. The curves revealed the following thermal events with increasing temperature: the cold crystallization process characterized by T_c and the cold crystallization enthalpy ΔH_c, and the melting process with following characteristics melting temperature (T_m) and melting enthalpy (ΔH_m). Comparing the thermograms and calorimetric parameters collected in table 2, one can see that with a filling of wood, as shown in this table, neat PP represented a tiny broad exothermic peak at 120°C, which indicated a rather low cold crystallization capability. However, in the case of WPC, this peak was sharper and appeared at much higher temperature, and the crystallization enthalpies increased correspondingly.

Sample code	Tc(°C)	$-\Delta H_c$(J/g)	Tm(°C)	ΔH_m(J/g)	χ(%)	χ_{corr} (%)
WPPC0	120.8	87.9	160.1	89.2	37.9	37.9
WPPC1	123.4	94.9	160.8	95.7	34.3	38.2
WPPC3	124.7	92.7	162.5	93.0	30.1	40.1
WPPC4	125.1	89.0	162.7	90.7	20.6	41.2

Table 2. Thermal and Crystalline Properties of the neat PP and WPCs

The double endothermic melting peaks are visible on the thermograms, as shown in fig.4. Due to the reorganization during heating; the composite appears to slide to a more stable phase that melts at a higher temperature. We know that for pure PP one endothermic peak of melting occurs at 160°C corresponding to melting of its crystalline phase. On the thermograms of samples with a rate of wood more than 25%, we notice a slight peak at 110°C after the main crystallization peak around 120°C (cooled from the melt) and another small peak at 145°C (heating) before the main melting peak of the composite which arrived at 160°C. This corroborates the heterogeneity of the material. Scanning the literature, some authors have noticed these very specific peaks. Maillard and co-author (Maillard et al., 2008) observed these peaks at the same temperatures. Some authors (Quilin et al., 1993) believe that this is not a real effect, but simply a result in heat capacities between the samples of pure PP and those impregnated wood, causing an apparent shift in temperature

measurement. According to the data listed in table 2, the Tc values of all the WPC were greatly increased compared to that of neat PP.

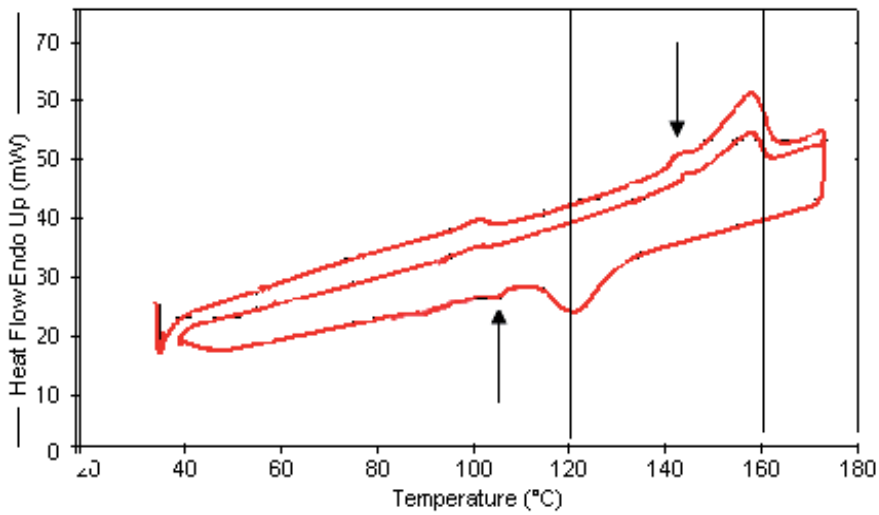

Fig. 4. DSC curve of heating and cooling of WPPC3

In the meantime, ΔH_C were decreased gradually with increasing the rate the rate of wood incorporated. This phenomenon between reinforcing material and polymer matrix has been reported in many other articles (Nam et al., 2001; Sinha et al., 2002). Generally, with the addition of lower content of wood, the polymer in the WPC, formed crystals much more easily because of the nucleation effect of the wood particles. However, when it reached certain content, the appearance of some aggregates restricted the crystallization behavior of PP. These results suggested that the incorporation of wood enhanced the cold crystalline ability of PP. The crystallization arrives sooner in WPC than in pure PP; this phenomenon was ascribed to a nucleating effect of the wood, which accelerated the crystallization speed of PP. The addition of wood flour had the effect of shifting Tm to higher temperatures. This increase was accompanied by an increased of crystallinity $x(\%)$. We corrected the degree of crystallinity of the composites $x_{cor}(\%)$ in the equation (1) by taking into account the wood-flour concentration:

$$x_{cor}(\%) = \frac{\Delta H_m}{(1\text{-}MF).\Delta H_o} \tag{1}$$

where ΔH_m and ΔH_o are respectively the melting enthalpies of the composite and polymer with 100% crystallinity and MF is the mass fraction of the wood in the composite.

This result can be explained by the agglomeration of the wood's particles. More wood's particles were added, and more aggregates were formed. In general, larger aggregates contributed to the crystallization of PP. This significantly conformed by the gradually decrease of ΔH_C that corresponded to the increase in wood content. With wood loading, the T_m increases for all WPC; this was ascribed to the poor thermal conductivity of wood. In

the composite, wood flour acted as an insulating material, hindering the heat conductivity. As a result, the WPC compounds needed more heat to melt. Similar findings were previously reported by Matuana and co-author (Matuana L. M. & Kim J.W., 2007) for PVC based wood–plastic composites. They found that the addition of wood flour to the PVC resin caused significant significant increase in the temperature and energy at which fusion between the particles started. The delayed fusion time observed in rigid PVC/wood flour composites was attributed to the poor thermal conductivity of the wood flour; this decreased the transfer of heat and shear throughout the PVC grains. These phenomena were consistent with the results of this study.

3.3 Mechanical properties

Tensile strength, flexural strength, module of elasticity (MOE) and elongation at break provide an excellent measure of the degree of reinforcement provided by the fiber to the composite (Mueller D.H. & Krobjilowski A., 2003). It can be seen from fig.5a and fig.5b respectively that the tensile strength and the tensile modulus increase with wood content.

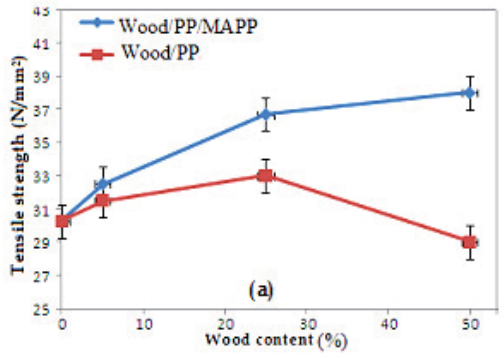

(a)

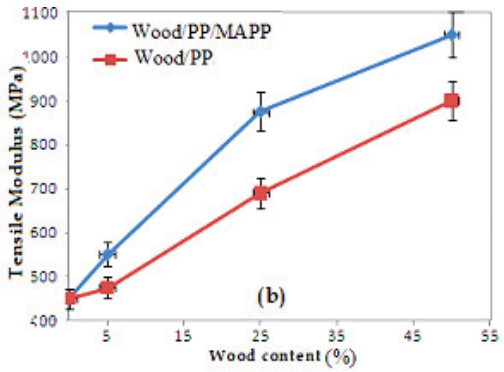

(b)

Fig. 5. Tensile strength and tensile modulus respectively in (a) and (b) versus wood content.

Tensile strength increases over WPC. Whereas, without compatibilizer, the tensiles strength of the composites are in the range of 33.5–28.5 N/mm^2 at wood loading from 5% to 50%, suggesting that, there is little stress transfer from the matrix to the fibers irrespective of the amount of wood present. When MAPP was incorporated into the WPC, the wood was relatively well dispersed and the interaction has occurred between the wood and matrix that was corresponding to the improved tensile strength. The use of MAPP improves interaction and adhesion between the fibers and matrix leading to better matrix to stress transfer. Similar observations were reported by Felix and Gatenholm (Felix J. M. & Gatenholm P., 1991) where tensile strength of the composites increased linearly with fiber content when MAPP treated fibers were used instead of untreated fibers. Myers et al. (Myers et al., 1993) reported 21% increase in tensile strength for a 50:50 wood flour polypropylene composites when MAPP was used as a compatibilizer. Stark and Rowlands (Stark N. M. & Rowlands R. E., 2003) also reported a 27% increase in tensile strength of composite prepared with 40% wood–fiber and 3% MAPP. At lower filler content the tensile modulus does not seem to be affected by improved adhesion (Felix J. M. & Gatenholm P., 1991). However at higher filler loading the tensile modulus of the composites with compatibilizer was much superior to that of the composites without compatibilizer. Compatibilizers can change the molecular morphology of the polymer chains near the fiber–polymer interphase. Yin et al. (Yin et al., 1999) reported that the addition of coupling agent (MAPP) even at low levels (1–2%) increases the nucleation capacity of wood– fibers for polypropylene, and dramatically alters the crystal morphology of polypropylene around the fiber. When MAPP is added, surface crystallization dominates over bulk crystallization and a transcrystalline layer can be formed around the wood–fibers. Crystallites have much higher moduli as compared to the amorphous regions and can increase the modulus contribution of the polymer matrix to the composite modulus (Sinha et al., 2002). The elongation at break (Fig.6) decreases steadily with the wood–fiber content. There is no significant difference in elongation at break for composites with and without compatibilizer so we have only represented the stress versus strain for only WPC without coupling agent. The steep decline in elongation immediately on filler addition is obvious, because wood–fibers have low elongation at break and restrict the polymer molecules flowing past one another. This behavior is typical of reinforced thermoplastics in general and has been reported by many researchers (Felix J.M. & Gatenholm P., 1991). Adding a suitable interface modifier will promote the stability of the morphology in wood plastic composite (Snijder M.H.B. & Bos H.L., 2000). The crystallinity results can help to explain the results from the mechanical testing. The strength and modulus are increasing with wood content in WPC at the same time, in the DSC curves (not represented here), the degree of crystallinity of these samples increases. Introducing wood filler modifies the mechanical behavior by making the material stiffer, which is characterized by the significantly decreased failure strain. The addition of wood decreases the compatibility between the hydrophilic wood material and hydrophobic matrices (binders) and entanglement between the PP and its molecules. This results in poor interphase properties and a lower strain to failure of the composite. The percentage elongation of all the composites with wood decreased with wood loading until 50% as compared to neat polymer. From the stress–strain curve of the composites with different wood loading (fig.6a), it is found that the stress–strain curve of pure polypropylene is similar to that of brittle materials. The behavior is perfectly elastic, the stress increases linearly with strain. However, addition of wood makes the matrix more ductile. This is evident from the elongation at break values of the composites. The flexural strength (fig.6b) increase with wood loading and the coupling agent make this phenomenon more pronounced.

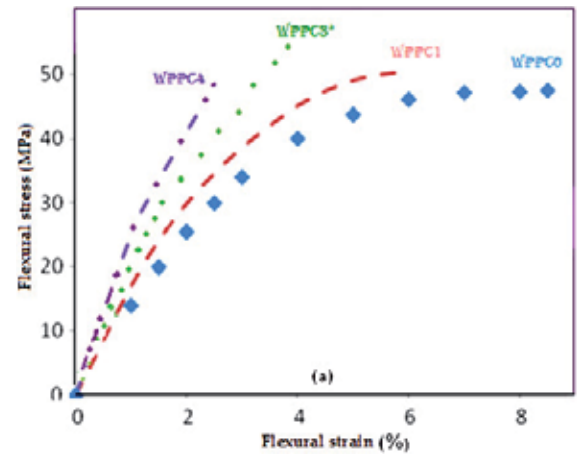

(a)

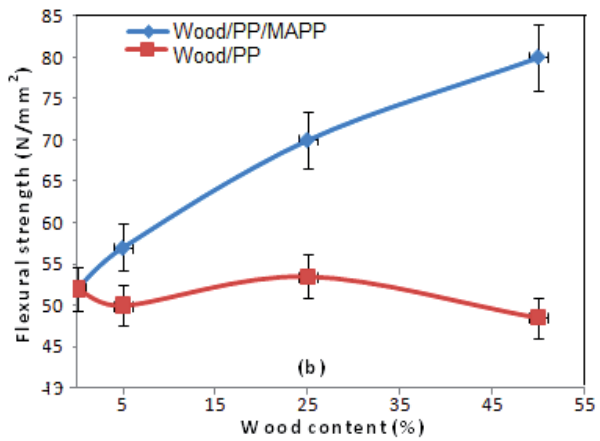

(b)

Fig. 6. Curves of: (a) Flexural stress/strain and (b) flexural strength function of wood content.

Figure 7 exhibits the curves of Izod impact strength function of wood incorporated. It is important to note that the impact test machine used in this study did not provide enough energy to break the neat PP because of the high flexibility of the PP matrix. By contrast, all of the composites with and without MAPP broke completely. For the impact property testing, composites with high wood fiber content possess low impact strength and notched impact strength decreases with the increasing of wood flour content. The positive effect of the coupling agent reduces this phenomenon. The main factors influencing impact strength is the size of the disperse phase. Impact strength of WPC blends decreases as a function of dispersed phase (Albano et al., 2002). SEM micrographs (Figures 1b, 1c and 2) show some fracture surfaces of WPC where the fibers are still covered by the polymer matrix; this result indicates that matrix cohesive failure was the dominant failure mode. Wood flour is kind of stiff organic filler, comparing to PP, so adding wood flour could decrease the impact strength of composite. The scanning electron microscope illustrated that the polymer intimately associated in the wood structure altered the mode of fracture. Composite treated with MAPP like interface modifier exhibited better impact strength than the untreated ones

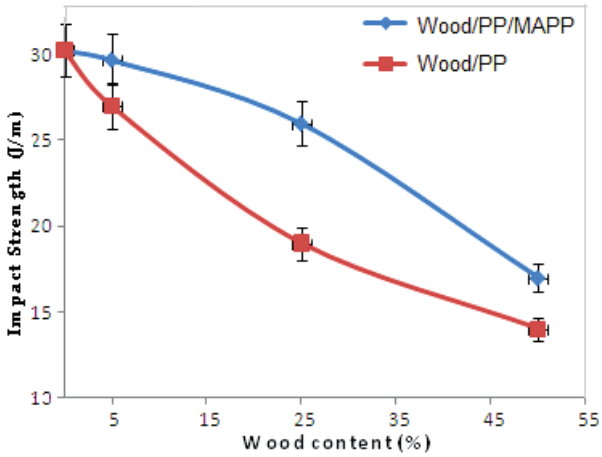

Fig. 7. Izod impact strength of WPC as function of wood content

since the debonding behavior between the interface of wood flour and PP matrix absorb larger impact energy in modified composites than the unmodified ones. Decreased impact strength of wood/ PP/MAPP composites was explained with the stronger interfacial adhesion and rigidity created by the larger functionality of MAPP used (Hristov et al., 2004). It was clear that the addition of wood particles impaired the impact strength of the wood polymer composites. The wood's particles were rigid with high strength and high modulus, which cannot generate deformation when impact is exerted on them. So, they cannot absorb impact energy by terminating the cracks or producing craze. Therefore, the brittleness of the composites increased and the impact strength decreased. A larger number of bonds may form on a unit surface of the wood in the case of larger functionality and this could lead to better stress transfer, but this was contradicted by our results. However, the filler/coupling agent interaction is only one side of the interphase forming in these composites and we must consider also the coupling agent/polymer interface. Large functionality leads to more reactions with the wood and shorter free chains, which cannot entangle with the polymer as efficiently as longer molecules. This leads to smaller deformability of the interphase, and of the entire composite.

4. Conclusion

The effects of the incorporation of wood particles both with and without a compatibilizing agent on the processing and properties of WPC composites were investigated. The morphology (SEM) indicates that the composites treated with MAPP modifiers exhibit much better bonding between flour and matrix. Heat deflection temperature increases with the increasing of wood flour content. When exposed to a source of chemical degradation, the morphology of WPC may be change, and in some cases disruption of the crystalline order occurs as detected by reduction in the fractional crystallinity of PP. Tensile strength, tensile modulus and flexural strength are significantly increased with increasing wood flour content. Mechanical properties, measured in tensile and flexural tests, demonstrated that the wood flour used in this work act as effective reinforcing agents for PP. Addition of wood flour, at all levels, resulted in more rigid and tenacious composite, but had lower impact energy and lower percentage of elongation as compared to the polymer matrix. The increase in mechanical properties demonstrated that MAPP is an effective compatibilizer for wood polypropylene composites. The presence of wood in the composite generated imperfect adhesion between the

components of the composite; this increased the concentration of stress and decreased the impact strength. Increasing the wood content in the composites led to an increased stress concentration because of the poor bonding between the wood flour and the polymer. Although crack propagation became difficult in the polymeric matrix reinforced with filler. The results show that the presence of wood flour in the composite was accompanied by an evolution of the crystallization. This study demonstrated that wood flour could be successfully used as a reinforcing material in a polypropylene matrix. MAPP coupling agent improves the compatibility between wood flour and PP resin. Taking these advantages into account, wood flour reinforced composites can be manufactured successfully using injection moulding. They represent a suitable material which is an alternative to glass fibers reinforcements for lots of applications in the range of lower mechanical loads. The manufacture of wood polymer composites allows not only to recover the waste wood from the forest industry, but also to reduce the use of fossil resources.

5. References

Albano C.; Reyes J.; Ichazo M.; Gonzalez J.; Brito M. & Moronta D. Analysis of the mechanical, thermal and morphological behavior of polypropylene compounds with sisal fibre and wood flour, irradiated with gamma rays. *Polymer Degradation and Stability,* vol.76, (2002), pp. 191–203.

Amash A. & Zugenmaier P. Morphology and properties of isotropic and oriented samples of cellulose fibre-polypropylene composites. *Polymer, vol*. 41, No.4, (2000), pp. 1589–1596.

Bledzki A. K.; Faruk O. & Huque M. Physico-mechanical studies of wood fiber reinforced composites. *Plastics Technology and Engineering*, vol.41, No.3, (2002), pp. 435–451.

Cantero G.; Arbelaiz A.; Mugika F.; Valea A. & Mondragon I. Mechanical behavior of wood/polypropylene composites: Effects of fiber treatments and ageing processes. *Journal* of *Reinforced Plastics* and *Composites*, vol. 22, (2003), pp. 37–50.

Dièn e N.; Fanton E.; Morlat-Therias S.; Vidal L.; Tidjani A. & Gardette J.L. Durability of wood polymer composites: Part 1. Influence of wood on the photochemical properties. *Composites Science and Technology*, vol. 68, (2008), pp. 2779–2784.

Felix J. M. & Gatenholm P. The nature of adhesion in composites of modified cellulose fibers and polypropylene. *Journal of Applied Polymer Science*, vol.42, (1991), pp. 609–620.

Gauthier R.; Gauthier H. and Joly C. Compatibilization between lignocellulosic fibers and a polyolefin matrix *Proceedings of the Fifth International Conference on Woodfiber-Plastic Composites, Forest Products Society, Madison, WI, May 1999, p. 153*

Hristov V. N.; Krumova M.; Vasileva St. & Michler G.H. Modified polypropylene wood flour composites. Fracture deformation and mechanical properties. *Journal of Applied Polymer Science,* vol.92, No.2, (2004), pp. 1286–1292.

Ichazo MN, Albano C, Gonzalez J, Perera R, Candal MV. Polypropylene/wood flour composites: treatments and properties. Compos Struct 2001; 54:207–14

Kazayawoko M.; Balatinecz J.J. & Woodhams R.T. Diffuse reflectance Fourier transform infrared spectra of wood fibers treated with maleated polypropylenes. *Journal of Applied Polymer Science*, vol.66, No.6, (1997), pp. 1163–1173.

Kazayawoko M.; Balatinecz J.J. & Matuana L.M. Surface modification and adhesion mechanism in wood fiber-polypropylene composites. *Journal of Mater Science*, vol. 34, No.24, (1999), pp. 6189–992.

Li Q. & Matuana L. M. Surface of Cellulosic Materials Modified with Functionalized Polyethylene Coupling Agents. *Journal of Applied Polymer Science,* vol.88, No.2, (2003), pp. 278-286

Lu J. Z.; Negulescu I. I. & Wu Q. Maleated wood-fiber/high densitypolyethylene composites: coupling mechanisms and interfacial characterization. *Composite Interfaces*, vol. 12, No. 1-2, (2005), pp. 125–140.

Maillard D. & Prud'homme R. E. The crystallization of ultrathin films of polylactides Morphologies and transitions. *Canadian Journal of Chemistry,* vol.86, No.6, (2008), pp. 556-563.

Maldas D. & Kokta B.V. Interfacial adhesion of lignocellulosic materials in polymer composites: an overview. *Composites Interfaces*, vol.1, No.1, (1993), pp. 87–108.

Matuana L.M. & Kim J.W. Fusion Characteristics of Wood-Flour Filled Rigid PVC by Torque Rheometry, *Journal of Vinyl & Additive Technology*, vol;13, No.1, (2007), pp. 7-13.

Meyrs E.G.; Chahyadi I.S.; Gonzalez C. & Coberly C.A. Wood flour and polypropylene or high-density polyethylene composites: influence of maleated polypropylene concentration and extrusion temperature on properties. *In: Walcott MP, editor. Wood fibres/polymer composites: fundamental concepts, processes, and material options. Madison,USA: Forest Product Society,* (1993), pp. 49 –56.

Moon H. -S.; Ryoo B. -K. & Park J. -K., J. *Polymer Science, Part B: Polymer Physic, vol.32* (1994), pp. 1427-1435.

Mueller D.H. & Krobjilowski A. New Discovery in the Properties of Composites Reinforced with Natural Fibers. *Journal of Industrial Textiles*, vol.33, No.2, (2003), pp. 111–130.

Munker M. Werkstoffe in der Fertigung, 3, (1998), 15.

Nam P. H.; Okamoto M.; Kotaka T.; Hasegawa N. & Usuki, A. A hierarchical structure and properties of intercalated polypropylene/clay nanocomposites, *Polymer*, vol.42, (2001), 9633-9640

Quilin D. T.; Caulfield D. F. & Koutski J. A. Crystallinity in the polypropylene/cellulose system and crystalline morphology, *Journal of Applied Polymer Science*, vol.50. (1993), pp. 1187-1194

Raj R.G. & Kokta B.V. Reinforcing high density polyethylene with cellulosic fibers I: The effect of additives on fiber dispersion and mechanical properties. *Polymer Engineering Science*, vol. 31, No. 18, (1991), pp. 1358–1362.

Renner K.; Móczó J. & Pukánszky B. Deformation and failure of wood flour reinforced composites: effect of inherent strength of wood particles. *Composites Science and Technology*, vol.69, No.10 (2009), pp. 1653–1659.

Sinha R. S.; Maiti P.; Okamoto M.; Yamada K.. & Ueda K. New Polylactide/Layered Silicate Nanocomposites. 1. Preparation, Characterization, and Properties, Macromolecules, vol.35, (2002), pp. 3104-3110.

Snijder M.H.B. & Bos H.L. Reinforcement of polypropylene by annual plant fibres: optimization of the coupling agent efficiency. *Composites Interfaces*, vol.7, No.2, (2000), pp. 69-79.

Stark N. M. Wood fiber derived from scrap pallets used in polypropylene composites. *Forest Products Journal*, vol.49, No 6, (1999), pp. 39 – 46.

Stark N. M., Rowlands RE. Effects of wood fiber characteristics on mechanical properties of wood/polypropylene composites. *Wood Fiber Science,* vol.35, No.2, (2003), pp. 167–174.

Timmons T. K; Meyer J. A. & Cote W. A. Polymer location in the wood polymer composite. *Wood Science,* vol. 41, No. 1, (1971), pp. 13–24.

Woodhams, R. T.; Thomas G. &. Rodgers D. K. Wood fibers as reinforcing fillers for polyolefins. *Polymer Engineering Science,* vol.24, No.15, (1984), pp. 1166-1171.

Yin S.; Rials T.G. & Wolcott M.P. Crystallization behavior of polypropylene and its effect on woodfiber composite properties. *In: Fifth international conference on wood fiber–plastic composites, Madison, WI, Forest Products Society, (1999 May 26–2), pp.* 139–146.

23

Solidification of Polypropylene Under Processing Conditions – Relevance of Cooling Rate, Pressure and Molecular Parameters

Valerio Brucato and Vincenzo La Carrubba
Dipartimento di Ingegneria Chimica, Gestionale, Informatica, Meccanica Università di Palermo, Palermo
Italy

1. Introduction

Polymer transformation processes are based on a detailed knowledge of material behaviour under extreme conditions that are very far from the usual conditions normally available in the scientific literature. In industrial processing, for instance, materials are subjected to high pressure, high shear (and/or elongational) rates and high thermal gradients. These conditions lead often to non-equilibrium conformational states, which turn out to be very hard to describe using classical approaches. Moreover, it is easy to understand that the analysis of the relationships between the processing conditions and the morphology developed is a crucial point for the characterisation of plastic materials. If the material under investigation is a semicrystalline polymer, the analysis becomes still more complex by crystallisation phenomena, that need to be properly described and quantified. Furthermore, the lack of significant information regarding the influence of processing conditions on crystallization kinetics restricts the possibilities of modelling and simulating the industrial material transformation processes, indicating that the development of a model, capable of describing polymer behaviour under drastic solidification conditions is a very complex task.

However, new innovative approaches can lead to a relevant answer to these scientific and technological tasks, as shown by some recent developments in polymer solidification analysis (Ding & Spruiell, 1996, Eder and Janeschitz-Kriegl, 1997, Brucato et al., 2002) under realistic processing conditions. These approaches are based on model experiments, emulating some processing condition and trying to identify and isolate the state variable(s) governing the process.

So far, due to the experimental difficulties, the study of polymer structure development under processing conditions has been mainly performed using conventional techniques such as dilatometry (Leute et al., 1976, Zoller, 1979, He & Zoller, 1994) and differential scanning calorimetry (Duoillard et al., 1993, Fann et al., 1998, Liangbin et al., 2000). Investigations made using these techniques normally involve experiments under isothermal conditions. However experiments under non isothermal conditions have been limited to cooling rates several orders of magnitude lower than those experienced in industrial processes, which often lead to quite different structures and properties. Finally, in the last

years, experiments revealing the crystallinity evolution by measures of crossing light scattering, have been conducted at intermediate cooling rate (Strobl, 1997, Piccarolo, 1992).

For the sake of completeness, it should be conceded that the complexity of the investigation concerning polymer solidification under processing conditions is even greater if the wide latitude of morphologies achievable is considered, especially when dealing with semicrystalline polymers. This would have to take into account also the complexity introduced by the presence of the crystallization process (Eder & Janeschitz-Kriegl, 1997).

Generally speaking, polymer crystallization under processing conditions cannot be considered an "equilibrium" phenomenon, since it is not possible to separate the thermodynamics effects on the processes from the kinetic ones. Furthermore, crystallization of polymeric materials is always limited by molecular mobility, and very often leads to metastable phases, as recently shown by Strobl (Strobl, 1997). Further evidences of the formation of metastable phases under drastic conditions (high cooling rates and/or high deformation rates) have been widely reported for iPP (Piccarolo, 1992, Piccarolo et al., 1992a). Choi and White (Choi & White, 2000) described structure development of melt spun iPP thin filaments, obtaining conditions under which different crystalline forms of iPP were obtained as a function of cooling rate and spinline stresses. On the basis of their experimental results together with many others available in literature, the authors have constructed a diagram, which indicates the crystalline states formed at different cooling rates in isotropic quiescent conditions. Continuous Cooling Transformation curves (CCT) have been reported on that diagram. According to the authors, at low cooling rates and high stresses, the monoclinic a-structure was formed, whereas at high cooling rates and low stresses a large pseudo-hexagonal/smectic ("mesophase") region was evident.

The formation of metastable phases normally takes place in a cooling rate range not achievable using the conventional techniques mentioned above; nevertheless it is worth reminding that the behaviour of a given semi-crystalline polymer is greatly influenced by the relative amount of the constitutive phases. From this general background the lack of literature data in this particular field of investigation should not be surprising, due to the complexity of the subject involved. The major task to tackle is, probably, to identify the rationale behind the multiform behaviour observed in polymer solidification, with the aim of finding the basic functional relationships governing the whole phenomenon. Therefore a possible approach, along this general framework, consists of designing and setting-up model experiments that could help to isolate and study the influence of some experimental variables on the final properties of the polymer, including its morphology. Thus a systematic investigation on polymer solidification under processing conditions should start on the separate study of the influence of flow, pressure and temperature on crystallization.

Due to experimental difficulties, there are only a few reports on the role of pressure in polymer crystallization, especially concerning its influence on the mechanical and physical properties. Moreover, the majority of studies made at high pressure have concentrated only on one polymer, polyethylene, dealing with the formation of extended chain crystals, as shown by Wunderlich and coworkers (Wunderlich & Arakaw, 1964, Geil et al., 1964, Tchizmakov, 1976, Wunderlich, 1973, 1976, 1980, Wunderlich & Davison, 1969, Kovarskii, 1994). The pressure associated with such investigations tends to be extremely high (typically 500 MPa) with respect to the pressures normally used in industrial processes. Furthermore, the experimental conditions normally investigated were quasi-isothermal. This implies that

the obtained results may not be applied to conventional polymer processing, involving very high thermal gradients.

The purpose of this chapter is to provide a general experimental route for studying the crystallization behaviour of isotactic polypropylene under high cooling rates and pressure.

In this respect, two complementary devices were used. The first involves a special equipment that has been developed, and widely tested, to quench polymeric samples at atmospheric pressure in a wide range of cooling rates (from 0.1 up to ca 2000 °C/s) under quiescent conditions and with the use of which it has been possible to collect much information about the influence of cooling rate on the final properties. The second was an innovative equipment specifically designed to evaluate the combined effect of typical injection moulding pressures (up to 40 MPa) and temperature gradients (up to a maximum of ca 100 °C/s), with the aid of a modified injection moulding machine. The results show that the influence of pressure on polymer crystallization is not as obvious as one may expect. An increase of cooling rate generally determines a transition from crystalline to non-crystalline (or pseudo-crystalline) structures. As for the influence of pressure, in iPP an increase in pressure results into a decrease of crystallinity, owing to kinetic factors, such decreased mobility related to the increased Tg.

In the last part of the chapter, a discussion on the influence of molecular parameters on the crystallization kinetics of iPP under processing conditions is presented. As a matter of fact, the crystalline structure of iPP quenched from the melt is affected not only by cooling rate, or generally by processing conditions, but also by molecular parameters like molecular mass (Mw) and molecular mass distribution (Mwd). Different configurations (isotacticity and head-to-tail sequences) or addition of small monomeric units and nucleating agents can also influence the final structure (De Rosa et al., 2005, Foresta et al., 2001, Sakurai et al., 2005, Nagasawa et al., 2005, Raab et al., 2004, Marigo et al., 2004, Elmoumni, 2005, Chen et al., 2005).

Influence of molecular weight on polymer crystallization is controversial. Stem length indeed interferes with entanglement density, thus determining a rate controlled segregation regime of topological constraints in non crystalline regions. Very low molecular weight tails of the distribution are shown to positively affect crystallization kinetics although their thermodynamic action should not favour perfection of crystallites (Strobl, 1997).

It is known from the literature that crystallization kinetics of semicrystalline polymers is influenced by the presence of contaminants. The main effect of the addition of a nucleating agent is an increase of the final crystallinity level together with a higher final density and a finer and homogeneous crystal size distribution. This typical effect of enhancement of the overall crystallization kinetics allows one to infer that crystallization kinetics are nucleation-controlled, being the nucleation step the rate determining one whilst the growth rate remains almost unaffected (Nagasawa, 2005, Raab, 2004).

On the other hand, the incorporation of a small content of ethylene units in the polypropylene chains has an influence on the regularity of the molecular structure. In fact, a change in tacticity induced by the shortening of isotactic sequences was observed (Zimmermann, 1993). Although this has a negative influence on crystallisation kinetics, an opposite effect should come from the enhanced mobility due to the presence of the ethylene sequences. As a result of these counteracting effects, a relatively narrow window of cooling rates exists in which an enhancement of crystallization kinetics sets in (Foresta et al., 2001).

A better understanding of the relation between processing and properties can be achieved if the absolute crystallinity during transformation can be predicted as a function of processing conditions. This prediction has to be supported by a crystallization kinetics model; here a modified two-phase non-isothermal form of the Kolmogoroff-Avrami-Evans model was used to describe the crystallization kinetics (Avrami, 1939, 1940, 1941, Evans, 1945, La Carrubba et al., 2002a, Brucato et al., 1993). The main purpose of this analysis is to underline the relevance of thermal history resulting from various cooling conditions on the crystallization kinetics of different grades of iPP containing various additives such as nucleating agents and small content of ethylene.

More specifically, the discussion attempts to identify relevant material parameters determining quiescent non isothermal crystallization kinetics simulating polymer solidification under processing conditions. One has obviously to cope with commercially relevant grades, which implies constraints in the span they cover. Therefore limitations arise not only due to the intrinsic poor significance of material parameters to crystallization kinetics but also owing to the limitation on the grades one can recover on the market. Finally, one of the main issues of this part of the chapter is the appropriate comparison among the investigated iPP samples in order to outline, when possible, the influence on the crystallization kinetics of average molecular mass, molecular-mass distribution, isotacticity, copolymerization with small amount of ethylene units and the addition of nucleants.

2. Description of the experimental procedure

2.1 Rapid cooling experiment at atmospheric pressure

A schematic drawing of the experimental set-up is shown in **fig. 1 a**. The sample, properly enveloped in a thin aluminium foil, so as to avoid leakage of material while in the molten state, (see **fig. 1 b**), and sandwiched between two identical flat metallic slabs, is heated to a suitable high temperature in a nitrogen fluxed environment.

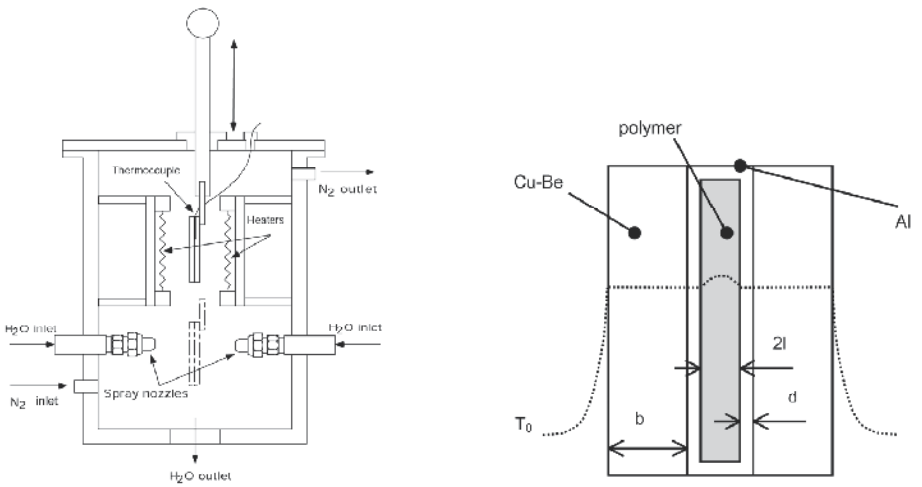

Fig. 1. a. Scheme of the experimental set-up for quench experiments; b. Sample assembly and temperature profiles. b=1-2 mm; l=50-100 μm; d=10 μm

A fast response, 12.5 μm thick (Omega type CO2), thermocouple buried inside one of the slabs allows to record the whole thermal history by a data acquisition system.

A Cu-Be alloy was chosen for the production of the metallic slabs, owing to its high Young's Modulus coupled with a high thermal conductivity (see Goodfellow Catalogue, 1996).

After keeping the sample system at a temperature above the equilibrium melting temperature for a time sufficient to erase memory effects (Alfonso & Ziabicki, 1995, Ziabicki & Alfonso, 1994), the sample assembly was moved to the lower zone of the container where it was quenched by spraying a cooling fluid on both faces through two identical nozzles positioned symmetrically opposite to each face of the sample assembly (**fig. 1a**).

The cooling rate was varied by changing the cooling fluid, its flow rate and temperature, or by changing the thickness of the sample assembly. However, the coolant temperature may not be crucial if it is sufficiently lower than the polymer solidification temperature.

Once the sample reached the final temperature it was immediately removed from the sample assembly and kept at low temperature (-30°C) before further characterization.

Three typical thermal histories (i.e. variation of temperature with time) obtained using this device are shown in **fig. 2**. Results of an extended set of experiments are reported in **fig. 3** as recorded variation of cooling rate with sample temperature. The data in **fig. 3** represent the range of variation of cooling rate covering five orders of magnitude (0.01-1000°C/s). This result is particularly significant when compared to standard DTA or DSC runs which cover only the lowest two decades of this cooling rate range (0.01-1°C/s). It is worth noting that for crystallization kinetics the high cooling rates are very informative, especially for fast crystallizing polymers, such as polyolefins. However, the high cooling rates severely restrict the possibility to detect the structural modifications taking place during solidification. The latter is the main constraint with respect to the real-time information provided by DTA and DSC measurements.

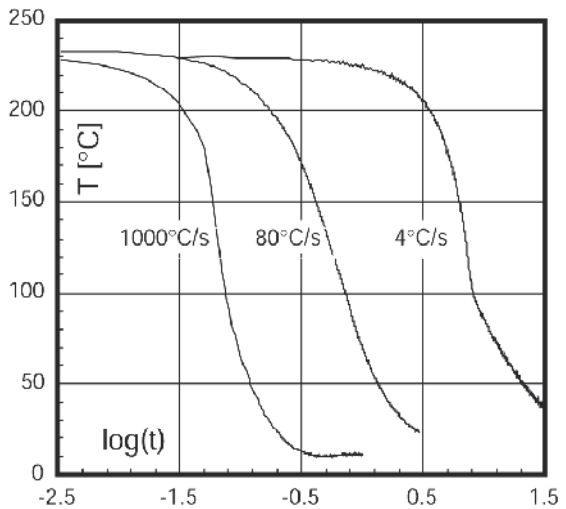

Fig. 2. Typical thermal histories for spray cooled samples

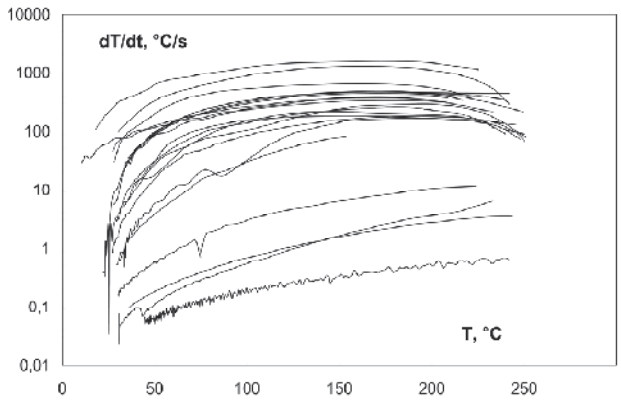

Fig. 3. Typical experimental cooling rates variation with sample temperature

With respect to the thermal histories in **fig. 2**, one will note that there is no temperature plateau associated with crystallization, the process occurring during cooling. This is due to the fact that temperature was measured on the metal slabs and not in the bulk of the polymer sample, albeit the latter has a negligible mass and volume relative to the size of the metal slabs. Furthermore, the very high heat flux to which the polymer was subjected masks the effect of the latent heat of crystallization. So, only the temperature-time history is recorded and, therefore, at the end of the cooling process one gets a thin polymeric film with a known thermal history. Sample structure depends on its thermal history and this relationship can be experimentally assessed if the "length scale" of structural features developed is small compared to the sample thickness and if the final structural features are uniform throughout the whole sample (Titomanlio et al., 1997, Titomanlio et al., 1988a, Titomanlio et al., 1988b). The sample homogeneity is thus crucial to the method envisaged since the recorded thermal history is the only available information for the determination of the final structure of the sample. The proposed model experiment is addressed to design a method for the characterization of the non-isothermal solidification behaviour encompassing typical cooling conditions of polymer processing. Only temperature history determines the structure formed as the melt solidification takes place in quiescent conditions. A discussion on the temperature distribution in a mono-dimensional heat exchange regime and the evaluation of structure distribution obtained along the thickness follows.

2.1.1 Cooling mechanism

We will consider now the effect of the applied heat flux on the temperature distribution of the metal in the sample assembly. Later in the next section the temperature distribution across the sample in contact with the metal will be examined.

The shape of the temperature profile in a flat slab having the following characteristics, thickness $2b$ and thermal conductivity k, and conditions, initial temperature T_i, suddenly exposed to a cooling medium at temperature T_0 and draining heat from the slab with a heat exchange coefficient h it is determined by the dimentionless Biot number:

$$Biot = h \times b / k \tag{1a}$$

For our experimental conditions the highest value of *Biot* number is estimated to be 0.3. Although this value does not fulfil the classical requirements for a flat temperature profile distribution within the slab (which requires *Biot* < *0.1*), the slab "cooling time" is practically unaffected by slab conductivity, therefore the so-called "regular regime" conditions still apply (Isachenko et al., 1987). In other words, the maximum Biot number for achieving a flat temperature profile is:

$$\mathrm{Biot}_{max}=0.1 \tag{1b}$$

On the other hand, an estimate of the response time of the slabs assembly can be easily taken as the time needed for the mid plane to undergo 99% of a sudden drop of the wall temperature. The solution of such transient heat conduction problem gives the characteristic time τ_R as (Carslaw et al., 1986, Bird et al., 1960):

$$\tau_R = 2b^2 / \alpha \tag{2}$$

Where α and b are thermal diffusivity and half thickness of the slab respectively. Using the values of $\alpha = 2.6\ 10^{-5}\ m^2/s$ (copper-beryllium 2% alloy – Goodfellow Catalogue, 1996) and b=0.001m in **equation (2)** gives τ_R=0.07 s. Note that the fastest cooling rate in our experiments has a characteristic time τ_A =0.33 s, which is about five times τ_R. Furthermore, since the real wall boundary thermal condition on the slab is not as sharp as the assumed stepwise drop of the wall temperature, the heat conduction inside the assembly does not affect the cooling history to any appreciable extent. Applying a more realistic boundary condition, i.e. a wall temperature depending on the heat flux, does not lead to a sudden wall temperature drop, and the ratio τ_A / τ_R becomes larger.

In the experiments water sprays were used to drain heat from the slab, therefore the associated heat transfer coefficient depends very much on the flow rate of the cooling medium, as shown in **figs. 4 a-b**. Here the heat flux was evaluated according to the lumped temperature energy balance on a slab of volume *V=Sx2b*, having a heat capacity c_p and density ρ:

$$\rho c_p V\, dT / dt \;=\; h\, 2S\,(T_0 - T) = -h2S\big(T - T_0\big)$$

$$dT / dt = (T_0 - T) / \tau_l = -\big(T - T_0\big) / \tau_l \qquad \tau_l = \rho c_p b / h \tag{3}$$

Where *S* is the slab surface, *h* heat transfer coefficient, T_0 the coolant temperature and *T* the lumped sample temperature. By assuming that the heat exchange coefficient *h* is constant, then slope of the cooling rate versus temperature curve is also constant, while the slab temperature decays exponentially with time.

Fig. 4a shows that below the maximum and using smaller nozzles, giving lower mass flow rates, there are two heat transfer regimes separated by the Leidenfrost temperature, i.e. by the onset of temperature for the production of a boiling layer nucleated by the surface of the slab. In **fig. 4b** the increase of coolant mass flow rate results in the disappearance of the Leidenfrost temperature and brings about an extension of the linear dependence of heat flux to a higher temperature range up to the maximum (Ciofalo et al., 1998).

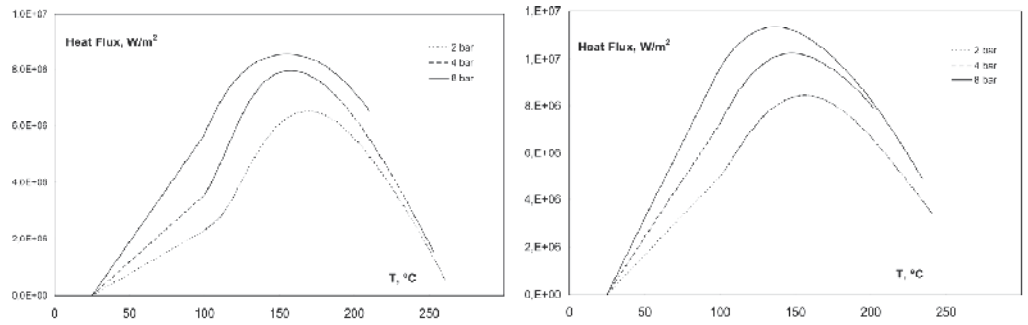

a b

Fig. 4. Heat Flux variation with sample assembly temperature for two different (a, small nozzles and b, large nozzles) spray nozzles

As long as the heat flux depends on temperature linearly, a constant heat transfer coefficient can be successfully used. This condition is well identified in the low driving force (low temperature difference) region. This result can be understood considering that the heat transfer of convection induced by the liquid drops impacting onto the solid surface is similar to that of nucleated boiling, since it promotes the renewal of the liquid layer close to the solid surface. Indeed the two mechanisms take place in parallel and the spray cooling effectiveness can be varied by changing the mass flow rate of the coolant and, at high values of the mass flow rate, the same value of the heat exchange coefficient is attained in a temperature range spanning from ambient temperature to about 150°C. This last point is particularly relevant for fast crystallizing polymers since high heat transfer coefficients are required at low temperatures to quench them effectively, as in the case of iPP.

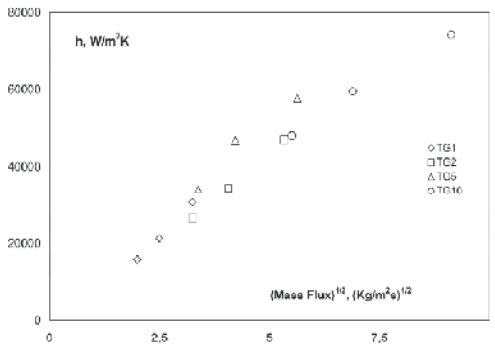

Fig. 5. Heat exchange coefficient vs. coolant mass flux for four different spray nozzles

The relationship between the liquid convection heat transfer coefficient, *h*, and the mass flow rate is summarized in **fig. 5** for all the nozzles used in this work**.** Within an error of ±10% there is a square root dependence of *h* on mass flow rate (Ciofalo et al., 1998).

The time constant, τ_l , obtained from **equation (3),** attains a minimum value of about 0.05 s. A comparison of the values of $5 \times \tau_l$ and τ_R (98.5% of the overall temperature drop) shows

that the driving force (i.e. the temperature drop) is larger in the fluid than in the Cu-Be slab, i.e. the heat transfer is mainly controlled by the fluid heat transfer. At the same time and the definition of τ_l suggests that another way to change linearly the slope of the cooling curves of **figs. 4 a-b** is by modifying the slab thickness. Moreover **equations (2)** and **(3)** show that the ratio τ_l / τ_R is proportional to the inverse of the thickness, suggesting that one should use the thinnest possible slab to achieve a more uniform temperature distribution through the thickness.

In principle the time constant, τ_l, drawn from **figs. 4 a-b** could be used as a parameter to rigorously identify the overall cooling process (Ding & Spruiell, 1996). When the solidification temperature of the polymer falls in a range in which there is a change of the heat transfer regime, the heat transfer coefficient will also change with temperature while the use of τ_l becomes meaningless, as it is no longer constant. On the other hand, the value of τ_l changes slightly when the temperature range where solidification takes place is quite narrow (of the order of 10°C). Although an average value of τ_l could be used, it is preferred to use an equivalent parameter to identify the cooling process, which is the average cooling rate in the range of temperatures within which the polymer solidifies (Brucato et al., 2002, Piccarolo, 1992, Piccarolo et al., 1992a, Piccarolo et al., 1992b, Brucato et al., 1991a, Brucato et al., 1991b, Piccarolo et al. 1992, Piccarolo et al., 1996, Brucato et al., 2009). This parameter, indeed, imposes not only the experimental time to be constant, but also the characteristic range of temperatures in which a given polymer solidifies. For iPP, the average cooling rates at around 70°C (Piccarolo et al., 1992a, Brucato et al., 2002, Brucato et al., 2009) has been chosen, as the parameters characterizing the cooling effectiveness for that polymer. Although this is a semi-quantitative measure of cooling effectiveness, the whole thermal history is available to compare experimental results with predictions from non isothermal kinetic models (Piccarolo et al., 1992a, Brucato et al., 1991a). Furthermore, if the kinetic constant vs. temperature relationship is mapped to the temperature vs. time profile, it is clear that an underestimate of the effective cooling rate is obtained only at low cooling rates. With an exponential temperature decay most of the solidification takes place around the maximum of the kinetic constant, i.e. in the chosen temperature interval.

2.1.2 Temperature distribution in the polymer sample

The solution of **equation (3)**, introducing the dimensionless temperature of the Cu-Be slab Θ_{Cu} with boundary conditions $T=T_i$ for $t=0$ and constant heat exchange coefficient h, is:

$$\Theta_{Cu} = \exp\left(-t / \tau_l\right) \tag{4}$$

where T_i and T_0 are the initial and final temperatures respectively.

If sample thickness is very small compared to that of the slab, **equation (4),** representing the time dependence of the slab temperature (i.e. the temperature at the sample surface), becomes an exponential decay equation with a time constant defined by **equation (3)**. Furthermore, in the case of very high cooling rates, this dependence of temperature on time extends to high temperatures. The smallest characteristic times are then obtained in the largest temperature range.

An estimate of the temperature profile in the polymer sample under these cooling conditions is, therefore, conservative and may well provide a case for achieving the maximum cooling rates with this technique, aiming to achieve a homogeneous thermal history throughout the entire sample thickness. As it has been previously pointed out, this condition must be satisfied in order to devise a direct relationship between structure obtained and the associated thermal history.

The temperature distribution in the solid polymer sample can well be approximated by the Fourier equation for transient heat conduction within a medium of constant thermal diffusivity, i.e.

$$dT_{pol} / dt = \alpha \times \partial^2 T_{pol} / \partial x^2 \tag{5a}$$

Or, in dimensionless form, i.e.

$$d\Theta_{pol} / dFo = \partial^2 \Theta_{pol} / \partial \xi^2 \tag{5b}$$

Where: $\xi = x / l$, dimensionless half depth; l =slab half depth; $Fo = \alpha t / l^2$ =Fuorier number;

With boundary conditions:

1. When $Fo = 0$ then $\Theta_{pol} = 0 \ \ \forall \xi$ (flat temperature profile before cooling);
2. For $\xi = 0$, $\partial \Theta_{pol} / \partial \xi = 0 \ \forall Fo \geq 0$ (symmetry.)

The cooled wall boundary condition is an exponential decay of temperature according to experimental observation:

3. For $\xi = 1$, $\Theta_{pol} = \phi(Fo) = \exp(-t / \tau) \ \forall Fo \geq 0$ (τ = exponential time constant, s) (6)

However, **Equation (5.b)** neglects the heat generated by the latent heat of crystallization. An analytic solution of **equation (5.b)** with the boundary conditions given by **equations (6)** is provided in some texts (Luikov, 1980), i.e.

$$\Theta_{pol}(\xi, Fo) = \frac{\cos\left(\xi \cdot \sqrt{Pd}\right)}{\cos\sqrt{Pd}} \cdot \exp(-Pd \cdot Fo) + \sum_{n=0}^{\infty} \frac{2\cos\left[(2n+1)\pi/2 \cdot \xi\right]}{(\pi/2 + n\pi)\sin\left[(2n+1)\pi/2\right]} \exp\left(-\mu_n^2 \cdot Fo\right) \tag{7}$$

With $\mathrm{Pd} = \mathrm{l}^2 / \alpha \cdot \tau$, *Predvotitelev* number (dimensionless time constant) and $\mu_n = \pi / 2 + n\pi$ **.**

A similar analytic solution is also provided in other texts (Carslaw & Jaeger, 1986), but (probably due to a misprint) any attempt to use the reported solution has failed.

Prediction of temperature profiles for an iPP slab (Brangrup & Immergut, 1989, van Krevelen, 1972) cooled with an exponential decay from T_i=230°C to T_0=5°C, are summarized for the case of two sample thicknesses (0.2 and 0.1 mm) in **figs. 6** and **7** respectively. The smallest time constant, $\tau_l = 0.05s$, corresponding to the fastest experiment performed, is considered. While diagrams **a)** of **figs. 6** and **7** show the calculated temperature distribution across the thickness (only half sample is considered), diagrams **b)** shows the calculated dependence of cooling rate on temperature at different sample depth along the thickness

direction. One can observe that for a sample thickness of 0.1 mm (**fig. 7**) the temperature distribution is almost flat across thickness. Significant deviations on the cooling rate versus temperature dependence are observed only at temperatures significantly higher than the range of solidification for most polymers.

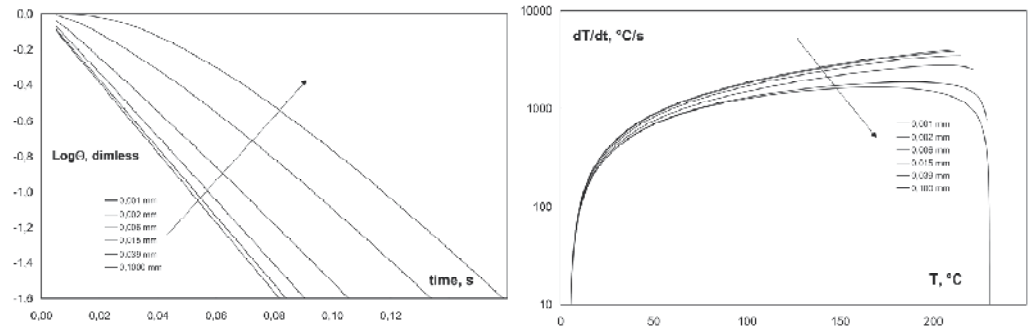

a b

Fig. 6. iPP film (half thickness=100μm) cooled from 230 to 5°C with an exponential decay with time for characteristic time τ=0.05s. a) calculated temperature distribution across the thickness; b) calculated cooling rate vs. temperature at different sample depth

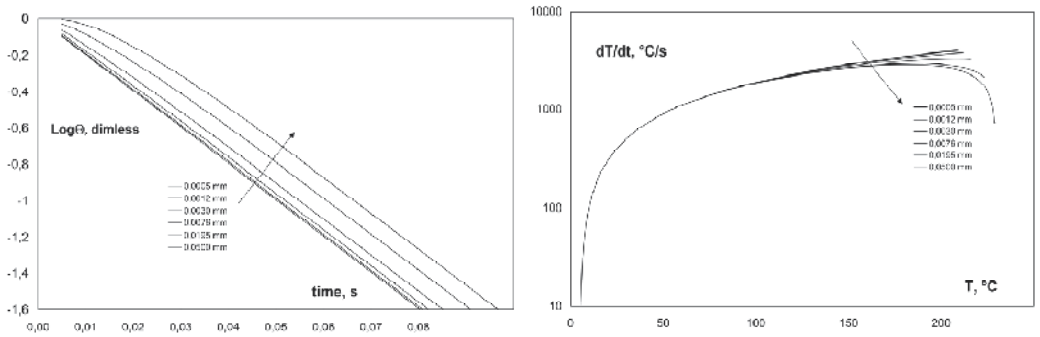

a b

Fig. 7. iPP film (half thickness=50μm) cooled from 230 to 5°C with an exponential decay with time for characteristic time τ=0.05s. a) calculated temperature distribution across the thickness; b) calculated cooling rate vs. temperature at different sample depth

Although this result may appear to be in contradiction with the constraint expressed by **equation (1b),** the analysis of the regimes involved in transient heat conduction, reported in advanced textbooks (Isachenko et al., 1987), provides a consistent explanation. When a solid is suddenly exposed to a coolant kept at a constant temperature T_0, the temperature profile could experience two regimes: an initial one corresponding to dissimilar temperature profiles, and a second one, called "regular", whereby the temperature profiles are almost parallel to each other and self similar at different times. Depending on the *Biot* number the second regime may also not take place and the condition *Biot<10* determines the onset of the second regime controlling the transient heat conduction for most of the cooling time. The condition expressed by **equation (1b)** may thus be seen to be more restrictive than it is

necessary, determining that the flat temperature is the controlling factor for most of the time during cooling of the solid from T_i to T_0.

In the regular regime of transient heat conduction, the onset of almost parallel temperature profiles determines a condition by which at different times the slope of the profile is the same in different sample positions, leading to the same cooling rate at the same temperature and to a correct interpretation of the calculated results reported in **figs. 6** and **7**. The temperature profile may thus be seen as a perturbation propagating from the external surface to the interior as the calculation of **figs. 6** and **7** shows. For larger sample thickness, as in **fig. 6**, although the temperature profile is not flat, the temperature distribution regime is regular and the cooling rate at lower temperatures is still almost constant throughout the sample. This is not so for cooling rates evaluated at temperatures higher than ca 80°C. On the other hand, for small sample thickness, as is shown in **figs. 7**, the heat transfer regime in the sample is always regular even at temperatures as high as 180°C.

As for the influence of the latent heat on the temperature distribution, which is neglected in **equation (5.b)**, one can observe that, although the heat of crystallization affects the temperature profile of the sample, and/or the thermal history to which it is subjected, the overall effect is only moderate. Indeed an estimate of the increase in sample temperature due to latent heat of crystallization, with the assumption that heat release takes place adiabatically, only produces maximum values of about 40°C, if the polymer sample crystallizes to the maximum allowable extent. Although this value may seem large when compared to the effect of temperature on the crystallization kinetics, it must be remembered that at low cooling rates, crystallization takes place over longer time intervals, and consequently does not affect appreciably the temperature of the sample since the heat is being released slowly. With respect to adiabatic conditions, a smaller temperature increase will, indeed, take place during cooling. Furthermore, the "heat sink" effect played by the metal slabs on the polymer film makes the temperature increase negligible. At high cooling rates, on the other hand, the heat is released in a shorter time interval, however in this case the temperature of the sample is controlled by very high heat fluxes and, consequently, the temperature is not affected very much either (Brucato et al., 2002, Brucato et al., 2000, La Carrubba, 2001). Moreover, if very drastic cooling conditions are applied, the sample only experiences a low degree of crystallization and, therefore, releases smaller amount of heat, which affects the temperature even less.

2.2 Rapid cooling under pressure

In order to evaluate the combined effect of typical injection molding pressures and temperatures, a new equipment was designed as a natural extension of the previously described apparatus. A standard Negri Bossi NB25 injection moulding machine was used as a source of molten polymer supplied at a pre determinable and maintainable pressure at which the polymer can be injected into a preheated mould cavity.

A special injection mould has been designed such that samples could be cooled at a known cooling rate and under a known pressure (Brucato et al., 2002, Brucato et al., 2000, La Carrubba, 2001). This heated mould consists of a conical cavity (the sprue), which is located in the fixed platen of the injection molding machine, coupled to a "diaphragm". The front of the cavity is sealed with a high tensile, high thermal conductivity copper-beryllium

"diaphragm", which is spray cooled on the opposite side when the quench starts. A schematic representation of the apparatus is shown in **fig. 8**. The cavity is located within a brass block where eight cartridge heaters with a total power of 2 kW are inserted. The diaphragm is located in the moving platen of the machine. The whole apparatus (cavity and Cu-Be diaphragm) has been designed in such a way that it can be placed in and removed from an injection moulding machine as a normal injection mould tool. A cooling channel, which allows the diaphragm to be spray cooled by pressurized water (at 8 bars) on one side, is also located in the mobile part. A thermocouple (type E, diam.=0.05 mm) inserted inside the diaphragm close to the wall facing the polymer sample records the thermal history during cooling, whilst a pressure sensor (type Dynisco PT46) mounted in the cavity allows measurement of pressure during the experiment. The pressure sensor and the thermocouple are connected to a data acquisition system, constituted by a National Instrument card LAB-LC coupled with an Apple–Macintosh LC computer.

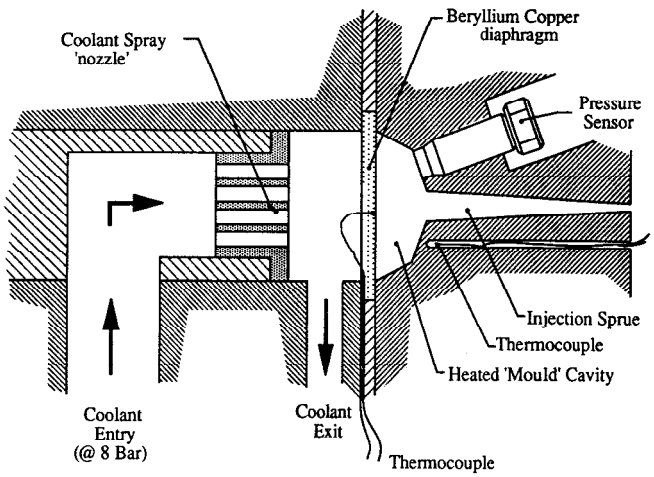

Fig. 8. Apparatus for solidification under pressure fitted to the modified injection molding machine

The experimental methodology of recording the thermal history experienced by the surface of rapidly cooled samples and then analyzing the resulting sample morphology has been adopted. Using the above described configuration, a thin layer in contact with the diaphragm solidifies under a known recorded thermal history and under a constant recorded pressure history. Internal layers of the polymer are cooled with different cooling rates, which can be calculated by solving the transient heat transfer equation **(7)**. In order to relate thermal history to the structure formed, the relationship between cooling rate evaluated at 70°C (characteristic temperatures of iPP) and depth in the sample can be calculated based on the conduction heat transfer problem **(eq. 7)**, as shown in **fig. 9**. This is a sort of "transformation function" or "mapping function", which converts the depth in the sample in an equivalent value of cooling rate, thus enabling the physical data to be mapped as a function of cooling rate rather than of the sample depth. This transformation functions allow the effect of pressure superimposed to that of cooling rate to be properly identified and quantified. Thin slices (50 to mm) microtomed across a direction parallel to the cooled

surface are then used for post-solidification characterization methods (Brucato et al., 2000, La Carrubba, 2001), being each slice characterized by a well defined cooling rate (averaged across slice thickness).

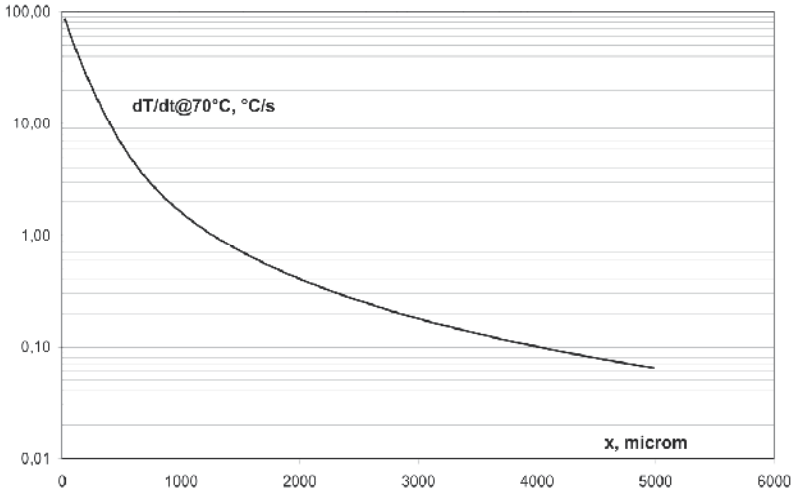

Fig. 9. Depth-Cooling Rate "mapping function"

3. Materials and characterization

Several iPP grades were analysed, with the aim of encompassing a wide latitude of crystallization behaviour and to highlight the influence of molecular parameters on iPP crystallization. The main features of the different grades of iPP tested are listed in **Table 1**.

Material name	Mw	Mwd	Xs(*)	notes
HPB	430000	6.6	2.9	
M2	208000	3.5	4.5	
M6	391000	5.6	4.6	
M7N	379000	5.3	3.4	+ Talc 1000 ppm
M9	380000	3.8	5.0	Copolymer 0.5% ethylene
M12	252000	5.4	13.9	
M14	293000	7.3	5.2	Copolymer 3.1% ethylene+DBS
M16	293000	7.3	5.2	Copolymer 3.1% ethylene
iPP1	476000	6		
iPP2	405000	26		bimodal MWD
iPP3	489000	9.7		
iPP4	481000	6.4		

Table 1. Main Characteristics of the iPPs examined. (*)Xylene soluble weight percentage

Since cooling rate in the present devices is too fast for recording any macroscopic change during the solidification process, only the final structure of the solidified sample was evaluated. The final features of the samples, analyzed by suitable macroscopic probes, such as powder Wide Angle X-Ray Diffraction (WAXD) patterns and density measurements were related to thermal history.The X-ray diffraction measurements have been performed by a Philips vertical diffractometer equipped with a Philips PW1150 generator. The Cu-Ka Nickel filtered radiation was detected in the interval 6-45°, applying steps of 0.05° in the interval 10-35° and of smaller steps of 0.2° elsewhere with a counting time of 60 s per step throughout. The gradient column technique was used for density measurements.

4. Results

4.1 Crystallization of iPP at atmospheric pressure

The results of the correlation for iPP3 between the structural features of quenched samples, assessed through the macroscopic probes cited above (WAXD and density), and thermal history, identified by the relevant cooling rate in the range of temperatures where the polymer solidifies (70°C for iPP), are shown in **figs. 10a** and **b** for density and WAXD patterns dependence on cooling rate, respectively. Such results point out the features of the proposed method of characterization already reported by the authors (Piccarolo, 1992, Brucato et al., 1993), with respect to change of structure and density with cooling rate. A broad range of density were identified as well as extreme structural features in the WAXD patterns. The WAXD patterns reported in **fig. 10b** show that at low cooling rates only the stable a monoclinic phase is observed with small amounts of the β phase, as identified by the reflection at 2θ=16.1°. The crystalline order, determined by the width of the peaks, continuously decreases on increasing cooling rate up to a point where only two broad diffraction peaks are observed, showing the presence of the so called mesomorphic phase of iPP (Corradini et al., 1986, Guerra et al., 1990). At intermediate cooling rates, the coexistence of the two phases is revealed, over a narrow range of cooling rates, by the superposition of the two broad peaks of the mesomorphic phase and the faint residues of the peaks related to the a monoclinic phase.

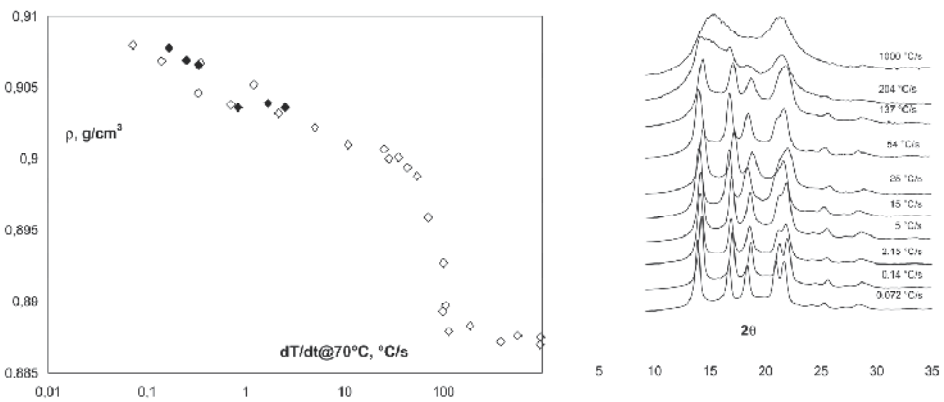

Fig. 10. a. Density dependence on cooling rate (measured at 70°C) of iPP3. Open symbols: rapid cooling experiments; filled symbols: standard constant cooling rate experiments (DSC) b. Dependence of WAXD powder patterns of iPP3 on cooling rate (measured at 70 °C)

Furthermore, changes of the WAXD patterns agree with the density measurements, making the two methods consistent and comparable. Although a qualitative cross check can be made for the data in **fig. 10b**, a quantitative comparison can only be obtained by WAXD deconvolution (Martorana et al., 1997). This last has been extensively used to determine the phase content and its dependence on cooling rate. This dependence of phase content on cooling rate, in turn, has been used for the determination of non-isothermal crystallization kinetics. The model adopted was based on the crystallization kinetics of two phases competing for the transformation from melt to solid (Brucato et al., 1998, Piccarolo et al., 1992a, Brucato et al., 1993). The reason for two parallel crystallization mechanisms stems from the WAXD patterns dependence on the cooling rate. In the case of iPP, for example, the patterns show that the stable phase disappears while the mesomorphic phase content increases with increasing cooling rate.

The density versus cooling rate curve of **fig. 10.a** shows three zones characterized by different features related to the WAXD based phase content dependence on cooling rate reported in **fig. 11**:

i. At low cooling rates where only stable phases are formed, the density decreases to a small extent with the log of the cooling rate. Below ca 5°C/s a slight decrease of density is observed, related to the formation of small amount of β phase formed (Piccarolo, 1991).
ii. At the highest cooling rates, a low-density plateau is observed related to the mesomorphic phase set-in, since a limiting packing condition has been approached. The nature of the mesomorphic phase is not well known, the most acknowledged hypothesis being a packing very similar to the α-monoclinic phase but with a low range order (Corradini et al., 1986). The most significant feature of this phase, indeed, is that it transforms to the stable α-monoclinic phase upon ageing, which is relevant for the post processing behaviour of iPP. Previous studies point out that the kinetics of this transformation to be measurable only above 80°C (Struik, 1978). More recent annealing experiments, discussed elsewhere (Gerardi et al., 1997) show that such transformation can take place at much lower temperatures and can cause significant density changes.
iii. In an intermediate cooling rate range the material density shows a very high sensitivity to changes in cooling rate. In this zone the stable phase content decreases while that of the mesomorphic phase increases as the cooling rate is increased. This transition is strongly dependent on the material characteristics, e.g. nucleating agents and molecular weight (Sondegaard et al., 1997). Solidification under these intermediate cooling rates shows the effect of the competition between the a monoclinic and the mesomorphic phases in the transformation from melt to solid. The slope of the density curve in this region is a measure of the sensitivity of the crystallization kinetics towards the cooling rate for a given polymer.

To sum up, although the mapping of the structural features provides a general understanding of the relationship between the thermal history and the associated structure formed during a quenching experiment, the density dependence on cooling rate provides an immediate, quantitative information on the non isothermal crystallization behaviour of the polymer. In this respect the identification of the narrow range of cooling rates at which the transition from a monoclinic to mesomorphic phase takes place provides quantitative information on the material non-isothermal crystallization kinetics.

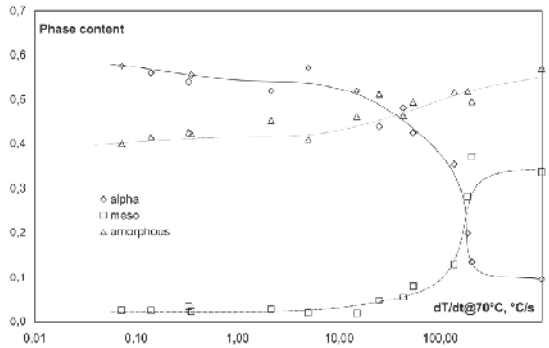

Fig. 11. WAXD deconvolution of iPP3. Phase content vs. cooling rate (measured at 70 °C)

A model-based interpretation of such transitional cooling rates performed on the crystallization kinetics parameters has been published recently (La Carrubba et al., 2002a).

4.2 Crystallization of iPP under pressure

The results of the density measurements made on iPP4 samples solidified under pressure are reported in **figs. 12.a** and **b**. Four different pressure conditions have been explored: 0.1 MPa, 8 MPa, 24 MPa, 40 MPa using two different diaphragm size 3.5 mm and 8 mm thick, (see **fig. 8**). In **fig. 12.a** is shown the density depth profile for the 3.5 mm thick diaphragm, and in **fig. 12.b** the density depth profile for the 8 mm thick diaphragm. Samples obtained with the 3.5 mm thick diaphragm were subjected to an experimental surface cooling rate (measured at 70°C -Brucato et al., 2002) of about 100°C/s. Samples solidified using the 8 mm thick diaphragm experienced a surface cooling rate of about 20°C/s. It is worth noting that the surface cooling rate depends on the coolant heat transfer and on the diaphragm thermal inertia. Changing the diaphragm thickness is, indeed, a simple and reliable way to tune the surface cooling rate (La Carrubba, 2001).

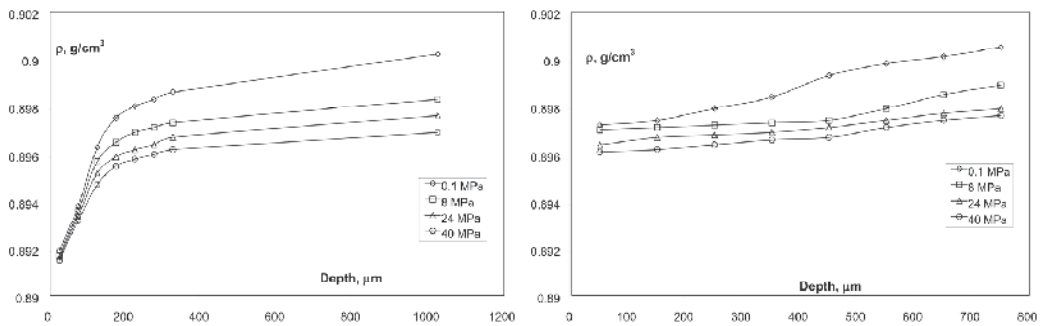

a b

Fig. 12. iPP4 Density depth profile for different solidification pressures from 0.1 to 40 MPa: a. diaphragm 3.5 mm thick; b. diaphragm 8 mm thick

The curves in **fig. 12a** and **b** show that for both experiments and at all pressures, density increases from the surface to the bulk of the sample. This behavior can be related to the

expected increase in crystallinity since the internal layers are cooled at progressively lower rates. In **fig. 12a** and **b** it is shown that the highest level of the density increase takes place in the vicinity of the surface, and that this is independent of the applied pressure.

Both **figs. 12a** and **b** show also somewhat unexpected results, in so far as a density decrease with pressure occurs at all depths in the sample. The reduction of density due to pressure is minimum at the sample surface and grows with depth. Furthermore, the majority of the density change is observed by varying the pressure from 0.1 to 8 MPa, which is quite low especially if compared with the typical pressure values used in injection moulding. This experimental result may be relevant for modeling the shrinkage and the internal stress distribution in injection molded products. Particularly important is the fact that this effect is more pronounced in the bulk of the sample.

Fig. 13 is obtained by plotting the density data in **figs. 12a** and **b** against the cooling rate calculated at 70°C by using a transient heat conduction model (equation (7). The value of the calculated cooling rate was averaged across every slice (50μm thick). The use of the transient model was also validated by overlapping the data referred to a surface cooling rate of 100 and 20 °C/s. In **fig. 13** it is also shown that at constant cooling rate the final density decreases with pressure. The same trend is obtained with respect to cooling rate, indicating that the density drop above 10-20 °C/s is independent of the solidification pressure. Finally, **fig. 13** shows that the decrease of density with pressure vanishes with increasing cooling rate, implying that the influence of pressure is more pronounced in the bulk of the sample. This is a very important information in process simulation.

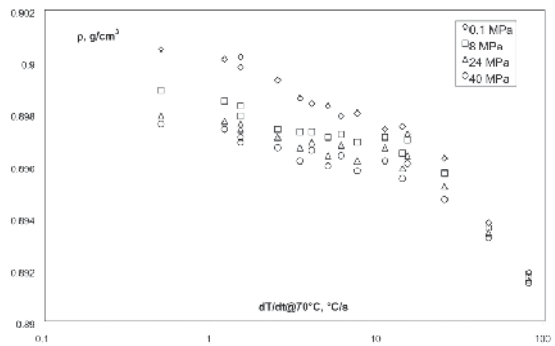

Fig. 13. iPP4 Density versus cooling rate evaluated at 70°C for different solidification pressures from 0.1 to 40 MPa

A similar pressure dependence of the density has also been observed by He and Zoller (He and Zoller, 1994) using a standard dilatometer and measuring the specific volume of this sample during crystallization from the melt. A constant slow cooling rate (2.5 °C/min) under constant pressure was used, bringing the sample back to a fixed pressure at the end of the test. It is worth noting that the majority of experiments have provided information on specific volume under pressure, whereas in our work we have measured the density at ambient pressure after solidification under pressure. He and Zoller observed an increase of specific volume with increasing crystallization pressure in the case of iPP, i.e. the specific volume in the solid phase at the end of the solidification curve is slightly higher than the one measured at the beginning of the melting curve. This behavior demonstrates that during

solidification under pressure some structural transformations take place giving final lower density values. Although He and Zoller have attempted to explain the reduction in density with the formation of the γ phase, which is less dense than the α phase, the samples in our study did not show any evidence of the presence of the γ phase (La Carrubba et al., 2000). The experiments performed by He and Zoller are in agreement with our results, which show that the final density (measured at atmospheric pressure) of samples solidified under pressure is, in fact, lower than that of the samples solidified at atmospheric pressure. We have repeated the PVT measurements on iPP and have published the results in a recent paper (La Carrubba et al., 2002b), where a comparison between specific volumes of samples crystallized at different pressures and/or cooling rates has revealed a decrease in density with increasing cooling rate and pressure. Thereafter, WAXD experiments were performed on slices cut in the transverse direction with respect to the direction of the heat flux. All experiments were performed by the synchrotron radiation source of the DESY center in Hamburg. A very long accumulation time (5 frames of 1 minute) was applied in order to achieve statistically significant results and a good reproducibility.

A qualitative analysis of the diffraction patterns has lead to the conclusion that the alpha phase content decreases on increasing cooling rate, for all the adopted pressures used (Brucato et al., 2000, La Carrubba et al., 2002a, La Carrubba et al., 2000). The data have shown that increase in pressure decreases the alpha phase content. This is better shown by WAXD data after a deconvolution procedure that has already been discussed elsewhere (Martorana et al., 1997). The program employed (implemented on MATLAB) uses a best-fitting procedure to calculate the positions and the intensity and of the alpha phase including mesomorphic phase peaks and that of the amorphous halo.

In **fig. 14** are shown plots of the phase content of the samples against pressure at four different values of cooling rates, ranging from 1.5 to 80 °C/s. A decrease of alpha phase is noticed, which is in agreement with the data from density and micro hardness measurements, showing that the change in the alpha phase content with pressure is highest within the first 10 MPa. By examining the data in **fig. 14** one notes that the decrease of the alpha phase with pressure tends to vanish when the cooling rate increases, particularly for cooling rates above 20°C/s. Additionally, the reduction of the alpha phase is mostly balanced by an increase of the mesomorphic phase content while the amorphous phase seems to be only slightly affected by pressure.

This last point is also very relevant, in so far it shows that as the main effect of pressure is to replace the alpha phase by the mesomorphic phase, leaving almost unaffected the amorphous content. It has been already shown, in fact, that the main effect of increasing the cooling rate at ambient pressure is the substitution of the alpha phase with the mesomorphic one (Piccarolo, 1992, La Carrubba et al., 2002a). In other words, the qualitative effect of pressure (at a constant cooling rate) on the final structure appears to be the same as an increase of cooling rate alone at a constant pressure (La Carrubba et al., 2000). This results is also illustrated in **fig. 15**, reporting the phase fraction, as calculated from the WAXD deconvolution of the samples, crystallized at atmospheric pressure using the rapid quenching apparatus. One can easily see how the decrease of the alpha phase with increasing cooling rate is accompanied by an increase of the mesomorphic phase (**fig. 14**). This observation is a further confirmation of the possibility to adopt a master curve approach to describe the bahaviour of iPP under pressure and high cooling rates.

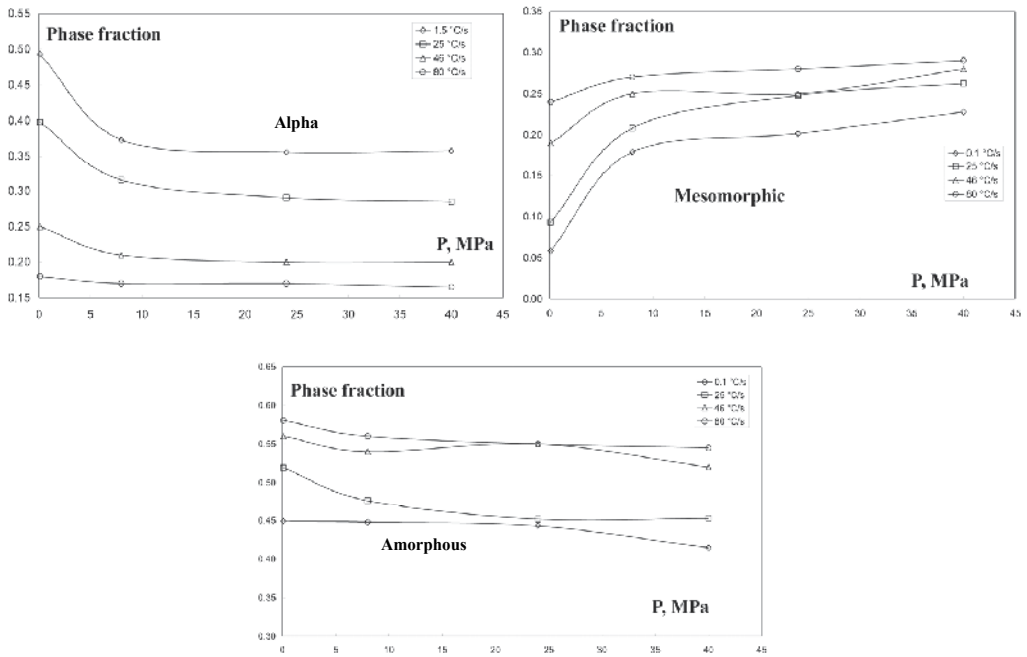

Fig. 14. Phase content of iPP4 from WAXD deconvolution as a function of pressure

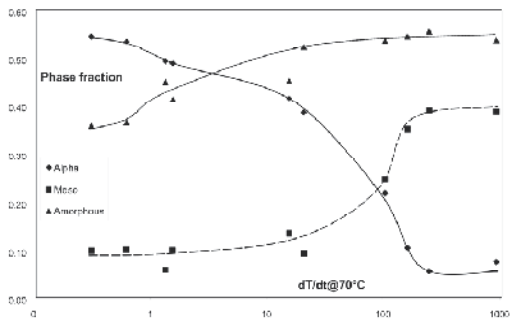

Fig. 15. WAXD deconvolution of iPP4 at 0.1 MPa, showing the phase relative content

4.3 Crystallization kinetics model

When dealing with crystallization of iPP, the numerous crystalline modifications of this material must be accounted for, since α, β or γ crystals may form upon solidification from the melt. The resulting complex frame can be simplified based on some experimental evidences, supported by several references (Foresta et al., 2001, Nagasawa et al., 2005, Raab et al., 2004, Marigo et al., 2004). As for the β phase, it basically shows up only if specific β nucleants are added, therefore for commercial non-*b*-nucleated iPP's it does not form; traces of γ form crystals are often present, but always in minor amount and in a narrow window of operating conditions (i.e. cooling rates), hence its presence is neglected without affecting the reliability of the results.

Under the aforementioned hypotheses, as two different crystalline phases are formed (α and mesomorphic), at least two kinetic processes take place simultaneously. The simplest model is a parallel of two kinetic processes non-interacting and competing for the available molten material. The kinetic equation adopted here for both processes is the non-isothermal formulation by Nakamura et al. (Nakamura et al., 1973, Nakamura et al., 1972) of the Kolmogoroff Avrami and Evans model (Avrami, 1939, 1940, 1941, Evans, 1945).

The model is based on the following equation:

$$X(t) / X_\infty = 1 - \exp\left[-E(t)\right] \tag{8}$$

Where $X(t)$ and X_∞ are the crystallized volume fraction at time t and in equilibrium conditions, respectively. For simplicity and for the sake of generalization X_∞ is here assumed to be a material constant, although it has been reported its dependence upon the crystallization history (crystal size distribution and degree of perfection, Ziabicki, 1976).

$E(t)$ is the expectancy of crystallized volume fraction if no impingement would occur. A different formulation of the model can be easily obtained by differentiation of equation (8):

$$d\xi / dt = (1 - \xi)\dot{E}(t) \tag{9}$$

Where:

$$\xi = X(t) / X_\infty \tag{10}$$

Since in the case of interest two crystalline phases develop, the simplest extension of the present model is to assume that those phases grow independently in parallel, competing each other for the residual fraction of available melt. Under this hypothesis the rate equation, for the general case of m crystalline phases developing simultaneously, becomes:

$$d\xi_i / dt = (1 - \sum_i \xi_i)\dot{E}_i(t) \qquad \text{for i= 1…m} \tag{11}$$

The following function, suggested by several authors (Ziabicki, 1976, La Carrubba et al., 2002a), can be adopted for the expression of the time derivative of the expectancy, leading to a rate equation proportional to the fraction of untransformed material times the current value of the kinetic constant, in which nucleation and growth rates have been lumped together (nucleation and growth are therefore isokinetic):

$$d\xi_i / dt = (1 - \sum_i \xi_i) n_i \ln 2 \left[\int_0^t K_i(T) ds\right]^{n_i - 1} K_i(T) \qquad \text{i= 1…m} \tag{12}$$

The form adopted in equation (12) for the time derivative of the expectancy reduces to the classical *Avrami* form, with a dimensionality index n_i for the i^{th} phase, if an isothermal experiment is considered. As for the dependence of the rate constant K_i on temperature, the simplest expression that one can consider is a Gaussian shaped curve:

$$K_i(T) = K_{0,i} \exp\left[-4\ln 2\left(T - T_{\max,i}\right)^2 \cdot D_i^{-2}\right] \qquad \text{i= 1…m} \tag{13}$$

where D_i, $T_{\max,i}$ and $K_{0,i}$ are the half width, the temperature where the maximum of K_i is attained and the maximum value of K_i itself, respectively (Ziabicki, 1976).

The governing equations with reference to two phases (alpha and mesomorphic phase) are:

$$d\xi_\alpha / dt = \left(1 - \xi_\alpha - \xi_m\right) n_\alpha \ln 2 \left[\int_0^t K_\alpha(T)\, ds\right]^{n_\alpha - 1} K_\alpha(T) \tag{14}$$

$$d\xi_m / dt = \left(1 - \xi_\alpha - \xi_m\right) n_m \ln 2 \left[\int_0^t K_m(T)\, ds\right]^{n_m - 1} K_m(T) \tag{15}$$

Where α and m indices stand for the alpha monoclinic and the mesomorphic phases respectively. This system of two coupled ordinary differential equations can be integrated with the appropriate initial conditions ($\xi_a=\xi_m=0$ for $t=0$). The integration leads to crystallinity development with time under any temperature history.

Fig. 16a shows a typical *K(T)* curve for the two different phases, and **fig. 16b** outlines the influence of two main parameters, the product of K_0*D (nearly the area under the *K(T)* curve sometimes called crystallizability, Ziabicki, 1976) and the Avrami index *n*. This latter is representative of the sensitivity of the crystallization kinetics to the cooling rate, a larger *n* leads in fact to a faster dependence of final crystallinity on cooling rate, the curves crossover is however always the same, i.e. about one half of the maximum attainable crystallization at an abscissa of K_0*D. The crystallizability is a cooling rate scaling factor of crystallization kinetics; as a matter of fact, a larger value of K_0*D leads to a shift along the abscissa of the curve, i.e. along the cooling rate, such that the larger the crystallizability the more pronounced the material tendency to crystallize.

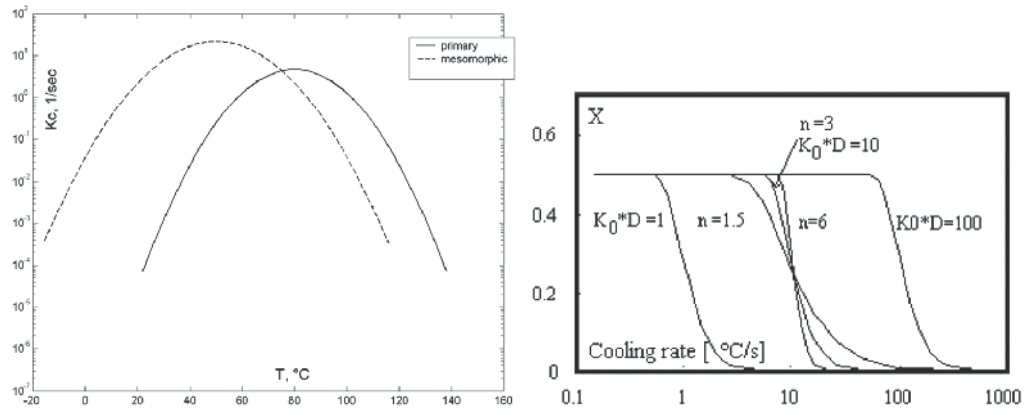

a b

Fig. 16. a. Kinetics constant versus temperature for a and mesomorphic phase; b. Crystallinity volume fraction as a function of cooling rate for various values of n (Avrami index) and K0*D (crystallizability).

Before discussing the results obtained concerning the sensitivity of the cited parameters on polymer composition, it is worth to point out the intrinsic limitations of the approach adopted related to its empirical nature. They depend on the origin of the KAE equation describing the nucleation and growth without diffusivity constraints and without accounting for the possible non isokinetic contribution of each mechanism, with a simple mathematical extension to the non isothermal conditions and finally without accounting for the complexity of crystallization in polymer melts, clearly a multistage process (Strobl, 1997). A slightly different modelling is represented by the so-called "Schneider rate equations" (Schneider et al., 1988); Schneider et al underline that their approach consists in an application of Avrami's (and Tobin's) impingement model leading to a different mathematical and more easy-to-handle formulation, based on a set of differential equations instead of dealing with integral equations. In other words, although their formulation enhances the applicability to process modelling, the physics behind it is completely described by the Avrami model. Therefore the use of Schneider's approach is more advisable when dealing with "non-lumped" problem, to be solved by coupling of transport equations.

All things considered, an analysis of the literature studies on polymer crystallization kinetics shows that the isokinetics approach is the most widely adopted (see the recent review by Pantani et al – Pantani et al., 2005); moreover, the limitations imposed by the isokinetic hypothesis do not weaken the self consistency and the abundance of information here provided. In any case, the limits of the aforementioned approach can be overcome by recalling the original Kolmogoroff's model (which accounts for the number of nuclei per unit volume on spherulitic growth rate) and determining the average radius of spherulites based on geometrical considerations (i.e. counting the number of nuclei), as shown by Zuidema et al. (Zuidema et al., 2001) and Pantani et al. (Pantani et al., 2002). This approach has however some limitations since it can be applied only to conditions where a recognizable spherulitic morphology is formed thus either low cooling rates or conditions where the spherulites are dispersed in a non crystalline matrix as in the case of mesomorphic iPP phase (Piccarolo, 1991). This possible refinement of the analysis is however far beyond the scope of the present work both due to its limitations and to the macroscopic approach adopted aiming to describe crystallization kinetics parameters in the broadest possible range of quiescent solidification conditions, i.e. under conditions emulating, but for the role of orientation and pressure, polymer processing.

4.4 Density data and crystallization kinetics model parameters for various iPPs

Figs. **17.a** and **b** and 18.a and b show a comparison of the density dependence upon cooling rate for the iPP grades studied, whereas **Table 2** reports the crystallization kinetics model parameters calculated by a best fitting procedure not only on the basis of the final monoclinic and mesomorphic content of the quenched samples, taken from the deconvolution of the WAXD patterns, but also accounting for results which provide the time and the temperature at the maxima of the crystallization rate (isothermal tests and DSC measurements) respectively. For this purpose a multiobjective optimization code was adopted.

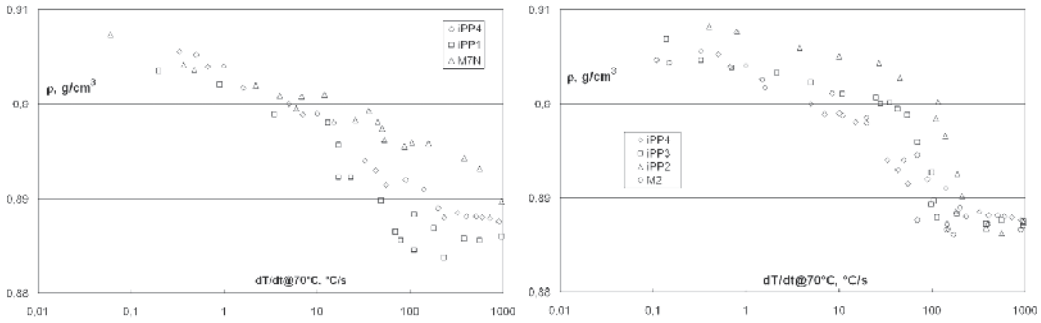

a b

Fig. 17. a.Effect of nucleating agents b.Effect of molecular weight distribution onto the density versus cooling rate behavior.

It should be noticed that **Table 2** reports for the mesomorphic phase a range of values both for the Avrami index n and for X_∞. The uncertainty in those parameters is however not critical for the purpose of the present work. As a matter of fact, a variability of n between 0.4 and 0.5 reflects into very slight changes in the temperature field in which crystallization takes place; consequently, the influence of this parameter is of minor entity. As for X_∞ of the mesomorphic phase, although its variability could turn into larger changes in the crystallization temperature window, its influence is confined to a cooling rate region in which the crystallization of the alpha phase is very little (very high cooling rates), thus not affecting the alpha phase kinetic parameters.

Material	*monoclinic*						*meso*					
	K_0, sec^{-1}	T_{max}, °C	D, °C	n	X_∞	K_0*D, °Csec^{-1}	K_0, sec^{-1}	T_{max}, °C	D, °C	n	X_∞	K_0*D, °Csec^{-1}
HPB	1.6	82	28	2	0.55	44.8	1.6	57	19	0.4 - 0.5	0.45 - 0.55	30.4
M2	1.4	77.3	33	3.0	0.60	46.2	0.6	40	30			18
M12	2.5	79	30	2.0	0.51	75	3.3	42	31			94
M7N	8.0	82	30	2	0.48	240	n.a.	n.a.	n.a.			n.a
M9	2.0	70	36	3.0	0.53	102	2.0	40	36			72
M6	2.4	66	40	3.0	0.54	96	2.0	40	40			80
M14	40	72	29	3.0	0.40	1160	1.0	40	34			34
M16	1.8	71	33	3.0	0.50	99.4	1.0	40	34			34
iPP1	1.6	82	28	2	0.55	44.8	1.6	57	19			30.4
iPP2	3.5	73	34	2	0.50	255.5	1.5	40	31			60
iPP3	2.7	70	35	2	0.57	189	0.22	40	40			8.8
iPP4	4.5	85	27	2	0.45	121	0.27	53.5	33.8			9.12

Table 2. Crystallization Kinetics Parameters

As for the Avrami index of the crystalline alpha phase, **Table 2** reports values equal to 2.0 or 3.0, due to a slight round-off with respect to the results obtained via simulation. The Avrami index is here intended as a mere fitting parameter, in line with most of the literature concerning polymer crystallization kinetics (see for instance the review of Pantani et al. – Pantani et al., 2002 and the review of Di Lorenzo et al. - Di Lorenzo & Silvestre, 1999), although its exact physical meaning should indicate the dimensionality of growth (namely 3 or 4 for volume filling depending whether nucleation is predetermined of sporadic). In other words, the Avrami index points out only the sensitivity of the crystallization kinetics to the cooling rate, a larger n leads in fact to a faster dependence of final crystallinity on cooling rate, the curves crossover being always the same, i.e. about one half of the maximum attainable crystallization at an abscissa of K_0*D.

Table 2 shows that differences in materials do not appear to be related in a simple way to kinetic parameters. This may be due to the fact that the set of materials investigated in this work, since representative of iPP's of industrial use, does not cover a wide range of fundamental molecular parameters Mw and Mwd. As a matter of fact, the limited range of the molecular parameters here explored probably does not comply with a complete enlightenment of the role played by each single factor onto the crystallization behaviour.

Nevertheless, some information can be drawn from the table summarizing material kinetics behaviour. For example, the so called "crystallizability", i.e. the product K_0*D instead of the two separate kinetic parameters, allows one to discuss the differences in the non isothermal crystallization behaviour in relationship to the materials investigated in this work. The crystallizability, roughly corresponding to area under the kinetic constant curve versus temperature, has the dimension of a cooling rate, and indicates somehow the ability of the polymer to crystallize (Ziabicki, 1976). A comparison of crystallizability values gives a good insight into the influence of molecular parameters on the crystallization kinetics behaviour. For instance, referring to the monoclinic phase only, it can be observed that the smallest value of K_0*D was obtained for the sample without additives having the highest Mw and narrowest Mwd. The highest values of crystallizability are however observed for nucleated iPP's (M7N and M14). All things considered, it should be however underlined that differences in crystallizability below a factor 2-3 cannot be considered reliably assessed by the crystallization kinetics method, due to the intrinsic errors in the evaluation of both K and D throughout the best fitting procedure. If one looks at **fig. 17a**, reporting density as a function of cooling rate for three polymers having similar features (molecular mass and distribution) except for the presence of nucleating agents, one comes to the conclusion that the presence of nucleants shifts the density cut-off towards larger values of cooling rate; as a matter of fact, the calculated crystallizability of the iPP denominated M7N (strongly nucleated) results larger than the one of iPP1 and iPP4.

Higher values of crystallizability are observed when the molecular weight distribution is broader (see for instance materials iPP2 and iPP3). This behaviour is clearly shown in **fig. 17b**, where four polymers with Mwd ranging from 3.5 (M2) to 26 (iPP2) are reported. The observable shift of density cut-off towards larger cooling rate upon increasing Mwd is correctly accompanied by a parallel increase of crystallizability (see **Table 2**).

On the other hand, no direct and obvious correlation may be found to relate crystallizability to Mw. This apparent inconsistency can be reasonably explained by recalling the already mentioned low variability of molecular weights of the iPP grades investigated in this work, related to their "commercial" nature. Consequently, in the light of crystallization behaviour, all the iPP molecular weights listed in **Table 2** have to be considered rather similar, being their difference in molecular weight not sufficient to develop dissimilar crystallization kinetics. Addition of small amounts of ethylene units in the copolymer does not influence significantly any of the kinetic parameters mentioned above, the small changes of the product K_0*D mainly depending on the differences in Mwd and not upon the ethylene content. No significant differences in the product K_0*D may be argued between materials M6, M9 and M16, although the second couple is copolymerized with ethylene. Also the amount of ethylene used in the copolymerization process does not appear to be relevant. These results are confirmed by density data shown in **fig. 18a**.

On the contrary, the couple of nucleated materials (M7N e M14) that basically differ from the others for the addition of ethylene in the latter, show a large difference in the crystallizability, suggesting a synergetic effect of copolymerization with the addition of a nucleating agent on crystallization kinetics. Although the enhancement of chain mobility, which increases with ethylene content, and nucleation are both factors promoting the crystallization kinetics, the source of the synergy is not simple to interpret. The tacticity index does not seam to have a significant influence on the kinetics of monoclinic alpha phase. **Fig. 18b** shows that the density cut-off of M12, with a lower tacticity, is slightly anticipated with respect to the one of MP6; on the other hand, crystallizability of M12 is somehow lower than the one of M6 (see **Table 2**).

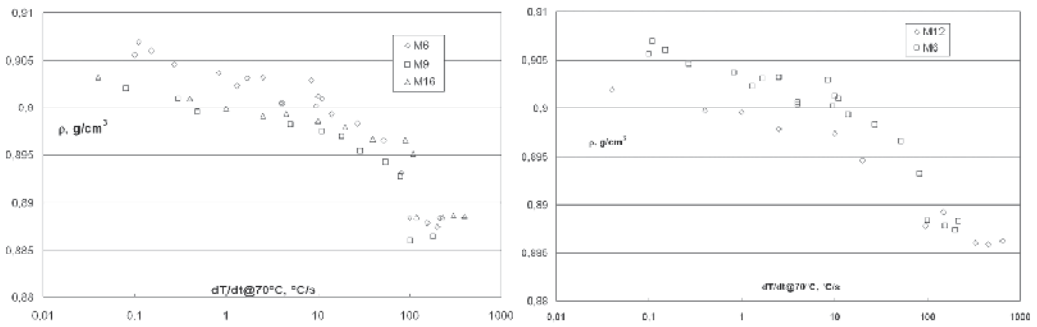

a b

Fig. 18. a.Effect of tacticity b. Effect of ethylene content onto the density cooling rate behavior

Other kinetics parameters of the monoclinic phase are more difficult to be related to molecular parameters. Additionally, their physical meaning is not straightforward with the exception of Avrami index *n*. This last, in principle, represents the dimensionality of the growth and the kind of nucleation. Experiments, however, rarely well correlate with a value of *n* in line with the dimensionality of the crystallization process under observation.

Furthermore, the correlation of mesomorphic phase kinetics parameters appears difficult, probably this can be related to the fact that mesomorphic phase determinations are affected by a larger uncertainty due to the broader WAXD peaks characterizing this phase.

With this respect, some recent cooling experiments performed on a nanocalorimeter (De Santis et al., 2007) have shown two distinct crystallization peaks (alpha and mesomorphic

phase) appearing in a quite large range of cooling rates, the crystallization of the alpha taking place up to ca 1000 °C/s. The apparent contradiction with the results here presented (alpha phase disappearing above 200-300 °C/s) may be consistently solved if one considers that the amount of alpha phase formed at high cooling rates is of the order of a few percent, hence below the measure limits of WAXD (around 5%). Secondly, being the sample mass undergoing the DSC cooling run in the nanocalorimeter of the order of a few ng, the enhancement of crystallization due to the "surface effect" (high constraints due to the low sample size with respect to the average radius of giration) must be taken into account. Thirdly, the presence of a mesomorphic phase crystallization peak at room temperature justifies the difficulties encountered in iPP amorphization, as confirmed by the present results where a consistent value of the crystallization kinetic constant of the mesomorphic phase at room temperature is shown (see **Table 2**).

Finally, if one considers that, with a few exceptions, the study was executed on a set of materials of industrial interest, a conclusion can be drawn about the fact that crystallization kinetics are mainly influenced only by the presence of nucleating agents. The influence of copolymerization on crystallization kinetics being relevant only if coupled with nucleation.

5. Conclusion

An experimental route for investigating polymer crystallization over a wide range of cooling rates (from 0.01 up to 1000 °C/s) and pressures (from 0.1 to 40 MPa) is illustrated, using a method that recalls the approach adopted in metallurgy for studying structure development in metals. Two typologies of experimental set-up were used; respectively an apparatus for fast cooling of thin films (100 to 200 mm thick) at various cooling rates under atmospheric pressure and a device (based on a on-purpose modified injection moulding machine) for quenching massive samples (about 1-2 cm^3) under hydrostatic pressure fields.

In both cases ex-situ characterization experiments were carried out to probe the resulting structure, using techniques like density measurements and Wide Angle X-ray Diffraction (WAXD) patterns. The cooling mechanism and the temperature distribution across the sample thickness were analysed. Results show that the final structure is determined only by the imposed thermal history and pressure.

Experimental results of quiescent crystallization at ambient pressure for various grades of isotactic polypropylene (iPP) are reported, showing the reliability of this experimental approach to assess not only quantitative information but also a qualitative description of the crystallization behaviour. In order to thoroughly describe the crystallization kinetics as a function of molecular and operating parameters, the methodological path followed was the preparation of quenched samples of known cooling histories, calorimetric crystallization isotherms tests, Differential Scanning calorimetry (DSC) cooling ramps, Wide Angle X-ray Diffraction (WAXD) measurements and density determination. The WAXD analysis performed on the quenched iPP samples confirmed that during the fast cooling at least a crystalline structure and a mesomorphic one form. The diffractograms were analysed by a deconvolution procedure, in order to identify the relationship between the cooling history and the distribution of the crystalline phases. The whole body of results (including calorimetric ones) provides a wide basis for the identification of a crystallization model suitable to describe solidification in polymer-processing operations, based on the Kolmogoroff-Avrami-Evans non-isothermal approach.

A systematic investigation about the crystallization kinetics under cooling rates typical of polymer processing for several commercial isotactic polypropylene grades was carried out, aiming to highlight the relevance of a number of molecular parameters, including molecular weight and distribution, tacticity, ethylene units content and nucleating agents.

The approach adopted, although the equations used are clearly empirical, is rather general and it surely represents a development with respect to phenomenological procedures describing relationships between structure and processing conditions. In the intention of the work, the kinetic parameters are the connections among such macroscopic observations.

Furthermore, the chapter provides a large amount of consistent experimental data under non-isothermal conditions (cooling rate range from below 0.1 to above 1000°C/s) for a broad set of commercial iPP's so far not extensively reported in literature.

It should be however underlined that he model provides values of K(T) comparable for the different grades, K(T) being the reciprocal of half-crystallization isothermal time regardless the value of the Avrami index. The most influential factor turned out to be the presence of nucleating agents, which shifts toward larger value the material intrinsic "crystallizability" (represented by area under the "bell-shaped" crystallization kinetics constant vs. temperature curve). In particular, the effect of molecular weight does not appear to be very relevant, due to the limited range of molecular weights available in material grades of a "commercial" nature. On the other hand, an increase in the polydispersity index significantly reflects into a parallel increase in crystallizability. Finally, addition of small amounts of ethylene units in the copolymer does not influence the kinetic parameters.

6. References

Alfonso, G. C. & Ziabicki A. (1995). *Coll Polym Sci*, Vol.273, p. 317, ISSN: 0303-402X.

Avrami M. (1939). *J Chem Phys*, Vol.7, p.1103, ISSN: 0021-9606.

Avrami M. (1940). *J Chem Phys*, Vol.8, p.212, ISSN: 0021-9606.

Avrami M. (1941). *J Chem Phys*, Vol.9, p.177, ISSN: 0021-9606.

Bird, R.B.; Stewart, W.E.; & Lightfoot, E.N. (1960). *Transport Phenomena*, Wiley, New York, ISBN-13: 978-0470115398

Brandgrup, J. & Immergut, E. H (1989). *Polymer Handbook*, John Wiley and Sons, ISBN: 0-471-81244-7

Brucato, V.; Crippa, G.; Piccarolo, S. & Titomanlio, G. (1991a). *Polym Eng Sci*, Vol.31, p.1411, ISSN: 1548-2634.

Brucato, V.; Piccarolo, S. & Titomanlio G. (1991b). *Proceedings of European Regional Meeting of the Polymer Processing Society*, Palermo, p.299.

Brucato, V.; Piccarolo, S. & Titomanlio, G. (1993). *Makromol Chem Macrom Symp*, Vol.68, p.245, ISSN: 1022-1360.

Brucato, V.; Piccarolo, S. & Titomanlio, G. (1998). *Int J Form Proc*, Vol.1, No.1, p.35, ISSN: 1292-7775.

Brucato, V.; Piccarolo, S. & La Carrubba, V. (2000). *Int Pol Proc*, Vol.15, No.1, p.103, ISSN: 0930-777X.

Brucato, V.; Piccarolo, S. & La Carrubba, V. (2002). *Chem Eng Sci*, Vol.57, p.4129, ISSN: 0009-2509.

Brucato V.; Kiflie Z., La Carrubba V., Piccarolo S. (2009). *Adv Pol Techn,* Vol.28, No.2, p.86, ISSN: 1098-2329.

Carslaw, H. S. & Jaeger, J. C. (1986). *Conduction of Heat in Solids*, Oxford Science, London, ISBN-13: 978-0198533689.

Chen J.H., Tsai F.C., Nien Y.H. & Yeh P.H. (2005). *Polymer*, Vol.46, p.5680, ISSN: 0032-3861.
Choi, C. & White, J. L. (2000). *Polym Eng Sci*, Vol.40, No.3, p.645, ISSN: 1548-2634.
Ciofalo, M.; Di Piazza, I. & Brucato, V. (198). *Int J Heat Mass Transfer*, Vol.42, p.1157, ISSN: 0017-9310.
Corradini, P.; Petraccone, V.; De Rosa, C. & Guerra, G (1986). *Macromolecules*, Vol.19, p.2699, ISSN: 0024-9297.
De Rosa C.; Auriemma F. & Resconi L. (2005). *Macromolecules*, Vol.38, p.10080, ISSN: 0024-9297.
De Santis F.; Adamovsky S.; Titomanlio G. & Schick C. (2007). *Macromolecules*, Vol. 40, No.25, p.9026, ISSN: 0024-9297.
Di Lorenzo M.L. & Silvestre C. (1999). *Prog Polym Sci*, Vol.24, p.917, ISSN: 0340-255X.
Ding, Z. & Spruiell J. (1996). *J Polym Sci Part B: Polym Phys*, Vol.34, p.2783, ISSN: 1099-0488.
Douillard, A.; Dumazet, Ph.; Chabert, B. & Guillet, J. (1993). *Polymer*, Vol.34, No.8, p.1702, ISSN: 0032-3861
Eder, G. & Janeschitz-Kriegl, H (1997). *Structure development during processing 5: Crystallization. Material Science and Technology, vol. 18*; Weinheim: H.E.N. Meijer ed.
Elmoumni, A.; Gonzalez-Ruiz, R.A.; Coughlin, E.B. & Winter H.H. (2005). *Macrom. Chem. Phys.*, Vol.206, p.125, ISSN: 1521-3935.
Evans U.R. (1945). *Trans. Faraday Soc.*, Vol.41, p.365, ISSN: 0956-5000.
Fann, D.M.; Huang, S.K. & Lee, J.Y. (1998). *Pol Eng Sci*, Vol.38, No.2, p.265, ISSN: 1548-2634.
Foresta T., Piccarolo S. & Goldbeck-Wood G. (2001). *Polymer*, Vol.42, p.1167, ISSN: 0032-3861.
Geil, P.H.; Anderson, F.R.; Wunderlich, B. & Arakawa, T. (1964). *J Polym Sci A:Polym Chem,* Vol.2, p.3707, ISSN: 1099-0518.
Gerardi, F.; Piccarolo, S.; Martorana, A. & Sapoundjieva, D. (1997). *Macromol. Chem Phys*, Vol.198, p.3979, ISSN: 1521-3935.
Gobbe, G.; Bazin, M.; Gounot, J. & Dehay, G. (1988). *J Polym Sci B: Polym Phys*, Vol.26, p.857, ISSN: 1099-0488.
Goodfellow Catalogue (1996). *Goodfellow,* Cambridge Limited, p.318.
Guerra, G.; Vitagliano, V.; De Rosa, C.; Petraccone, V. & Corradini, P. (1990). *Macromolecules*, Vol.23, p.1539, ISSN: 0024-9297.
He, J. & Zoller, P. (1994). *J Polym Sci B: Polym Phys*, Vol.32, No.6, p.1049, ISSN: 1099-0488.
Isachenko, V. P.; Ossipova, V. A. & Sukomel A. S., (1987). *Heat Transfer,* MIR, Moscow, ISBN: 089875027X.
Kovarskii, A. (1994). *High-Pressure Chemistry and Physics of Polymers*, CRC Press, ISBN: 9780849342394.
La Carrubba, V.; Brucato, V. & Piccarolo, S. (2000). *Polym Eng Sci*, Vol.40, No.11, p.2430, ISSN: 1548-2634.
La Carrubba, V. (2001). *Polymer Solidification under pressure and high cooling rate, Ph.D. Thesis*, CUES, Salerno, ISBN: ISBN: 88-87030-27-8.
La Carrubba, V.; Brucato, V. & Piccarolo, S. (2002a). *J Polym Sci B: Polym Phys* Vol.40, p.153, ISSN: 0024-9297.
La Carrubba, V.; Briatico, F.; Brucato, V. & Piccarolo, S. (2002b). *Polym Bull*, Vol.49, p.159, ISSN: 0170-0839.
La Carrubba, V.; Piccarolo, S. &Brucato, V. (2007). *J Appl Polym Sci*, Vol.104, p.1358, ISSN: 1097-4628.
Leute, U.; Dollhopf, W. &Liska, E. (1976). *Colloid Polym Sci*, Vol.254, No.3, p.237, ISSN: 0303-402X.
Liangbin, L.; Huang, R.; Ai, L.; Fude, N.; Shiming, H.; Chunmei, W.; Yuemao, Z. & Dong W. (2000). *Polymer*, Vol.41, p.6943, ISSN: 0032-3861.
Luikov, A.V. (1980). *Heat and Mass Transfer*, MIR, Moscow, ISBN 13: 9780080166322.

Marigo, A.; Marega, C.; Causin, V. & Ferrari P. (2004). *J Appl Pol Sci*, Vol.91, p.1008, ISSN: 1097-4628.
Martorana, A.; Piccarolo, S. & Scichilone, F. (1997). *Macromol Chem Phys*, Vol.198, p.597, ISSN: 1521-3935.
Nagasawa, S.; Fujimori, A.; Masuko, T. & Iguchi, M. (2005). *Polymer*, Vol.46, p.5241, ISSN: 0032-3861.
Nakamura, K.; Katayama, K. & Amano T. (1973). *J Appl Pol Sci*, Vol.17, p.1031, ISSN: 1097-4628.
Nakamura, K.; Watanabe, T.; Katayama, K. & Amano T. (1972). *J Appl Pol Sci*, Vol.16, p.1077, ISSN: 1097-4628.
Pantani, R.; Speranza, V.; Coccorullo, I. & Titomanlio, G. (2002). *Macrom Symp*, vol.185, p.309, ISSN: 1521-3900.
Pantani, R.; Coccorullo, I.; Speranza, V. & Titomanlio, G. (2005). *Prog Polym Sci*, Vol.30, p.1185, ISSN: 0079-6700.
Piccarolo, S. (1992). *J Macromol Sci B*, Vol.31, No.4, p.501, ISSN: 0022-2348.
Piccarolo, S.; Saiu, M.; Brucato, V. & Titomanlio, G. (1992a). *J Appl Polym Sci*, Vol.46, p.625, ISSN: 1097-4628.
Piccarolo, S.; Alessi, S.; Brucato, V. & Titomanlio, G. (1992b). *Proceedings of Crystallization of Polymers, a NATO Advanced Research Workshop*, Mons, p.475.
Piccarolo, S. & Brucato, V. (1996). *Proceedings of the PPS12-Annual Meeting*, Sorrento, p.663.
Raab, M.; Scudla, J.; & Kolarik, J. (2004). *European Polymer J*, Vol.40, p.1317, ISSN: 0014-3057.
Sakurai, T.; Nozue, V.; Kasahara, T.; Mizunuma, K.; Yamaguchi, N.; Tashiro, K.; Amemiya, Y. (2005). *Polymer*, Vol.46, p.8846, ISSN: 0032-3861.
Schneider, W.; Koppl, A. & Berger, J. (1988). *Int Pol Proc*, Vol.2, p.151, ISSN: 0930-777X.
Strobl, G. (1997). *The Physics of polymers, Concepts for Understanding Their Structures and Behavior*, Springer, New York, ISBN: 978-3-540-25278-8.
Struik, L.C.E. (1978). *Physical ageing in amorphous polymers and other materials*, Elsevier, Amsterdam, ISBN-13: 978-0444416551.
Tchizmakov, M.B.; Kostantinopolskaja, M.B.; Zubov, Yu.A.; Bakeev, N.Ph.; Kotov, N.M. & Belov, G.P. (1976). *Visokomol Soed*, Vol.A18, p.1121.
Titomanlio, G.; Speranza, V. & Brucato, V. (1997). *Int Polym Proc*, Vol.12, No.1, p.45, ISSN: 0930-777X.
Titomanlio, G.; Piccarolo, S. & Levati, G. (1988a). *J Appl Polym Sci*, Vol.35, p.1483, ISSN: 1097-4628.
Titomanlio, G.; Rallis, A. & Piccarolo, S. (1988b). *Polym Eng Sci*, Vol.29, p.209, ISSN: 1548-2634.
Van Krevelen, W. (1972). *Properties of Polymers*, Elsevier, Amsterdam, ISBN: 978-0-08-054819-7.
Wunderlich, B. & Arakaw, T. (1964). *J Polym Sci Part A: Polym Chem*, Vol.2, p.3697, ISSN: 1099-0518.
Wunderlich, B. (1973). *Macromolecular Physics, Vol. 1*, Academic Press, New York, ISBN-13: 978-0127656014.
Wunderlich, B. (1976). *Macromolecular Physics, Vol. 2,* Academic Press: New York, ISBN-13: 978-0127656021.
Wunderlich, B. (1980). *Macromolecular Physics, Vol. 3*, Academic Press: New York, ISBN-13: 978-0127656038.
Wunderlich, B. & Davison T. (1969). *J Polym Sci Part A:Polym Chem*, Vol.7, p.2043, ISSN: 1099-0518.
Ziabicki, A. & Alfonso, G.C. (1994). *Coll Polym Sci*, Vol.272, p.1027, ISSN: 0303-402X.
Zimmermann, H.J. (1993). *J Macromol Sci-Phys*, Vol.B32, p.141, ISSN: 0022-2348.
Ziabicki, A. (1976). *Fundamentals of Fibre Formation*, Wiley, London, ISBN: 0-471-98220-2.
Zuidema, H.; Peters, W.M.P. & Meijer H.E.H. (2001). *Macrom Theory Simul*, Vol.10, p.447, ISSN: 1521-3919.
Zoller, P. (1979). *J Appl Polym Sci*, Vol.23, No.4, p.1051, ISSN: 1097-4628.

24

Tailoring of Morphology and Mechanical Properties of Isotactic Polypropylene by Processing

K. Schneider[1], L. Häussler[1] and S.V. Roth[2]
[1]*Leibniz-Institut für Polymerforschung Dresden,*
[2]*DESY, Hamburg,*
Germany

1. Introduction

The deformation behaviour of semi-crystalline materials is mainly determined by the behaviour of the two components – the crystalline and the amorphous phase with their characteristic temperature-dependent mechanical behaviour and sometimes their anisotropy. So the crystalline phase is elastically with a rather high modulus. Above a certain stress the crystallites break down into smaller fragments. Aligned chains enable recrystallisation. The mobility in the amorphous phase depends on the difference between the ambient temperature and the temperature characteristic of the glass transition, which is the dominant relaxation process in the temperature range under investigation. On the other side the amorphous phase is constrained within the crystalline one. So it shows to some extent stress relaxation or frozen stress. Both phases are connected via anchor molecules, bridging the phase boundaries. Those molecules are mainly responsible for stress transfer between the phases.

The actual morphology and so the subsequent interaction of the different phases within a samples are mainly determined by processing and the thermal history of the material. For instance, in an injection moulded plate the properties can be extremely dependent on the position and direction of a specimen, changing from relatively brittle to highly stretchable (Schneider, 2010).

The whole stress-strain curves of semi-crystalline materials generally show three characteristic regions. Although the initial region prior to the yield point apparently behaves elastically, stress relaxation due to rearrangements in the amorphous phase can be observed also here. The mobility in the amorphous phase depends on the difference between the ambient temperature and the temperature characteristic of the glass transition, which is the dominant relaxation process in the temperature range under investigation. In the case of confined stretched amorphous regions between crystalline phases the glass transition temperature can be changed significantly. After the yield point typically local necking occurs with high local strain while the overall strain remains moderate. In the case of dog-bone specimens then the neck propagates over the whole specimen during constant load. In the true stress-strain diagram necking is a fast local deformation from the yield strain to the

strain of the fully yielded specimen. In the third step during further elongation strain hardening occurs, until finally the specimen fails. Here the strain hardening modulus can be a relevant parameter for the long term stability against creep (Kurelec, 2005).

Already in his first model of structural changes during deformation Peterlin (Peterlin, 1971) discussed spherulites consisting of lamellae separated by amorphous regions. Due to tie molecules stress is transferred between the lamellae inducing deformation and finally disintegration and rearrangement in the form of fibrillae. Later numerous authors modified and enhanced Peterlin's approach to describe their experiments. The discussion gained new impetus after the first online structure investigation during deformation by Zuo et al. (Zuo, 2005).

Breese and Beaucage (Breese, 2004, 2008) gave an overview of older models. Finally, they describe mechanical behaviour with a model refining the models of Weeks and Porter (Weeks, 1974) and Gibson, Davies and Ward (Gibson, 1978) in the sense that the effects of the orientation process on the modulus of the non-fibrous gel component are incorporated into the model by allowing a transition to fibres.

To describe the deformation behaviour of semi-crystalline polymers Strobl et al. (Hong, 2004, 2006) separated different mechanisms of stress transfer with respect to amorphous and crystalline units. They distinguished between four phases: onset of local block sliding (1), collective motion slightly below the yield point (2), disassociation of crystalline blocks and transformation into fibrils (3) and the start of disentangling (4).

In most models the common process of cavitation in polymers during deformation is not yet incorporated. Many systems show a characteristic whitening during plastic deformation due to the formation of voids or cavities with a typical length scale growing up to the wavelength of visible light, i.e. some hundreds of nanometres (Pawlak, 2010; Men, 2004). It is obvious that these large-scale structures are not accessible with a conventional small angle X-ray scattering setup. But at least the beginning of this process should be well detectable by X-ray scattering due to the strong difference in electron density between the polymer and the voids in the relevant angular range accessible by USAXS (Ultra-SAXS (Lode, 1998; Gehrke, 1995; Roth, 2006)).

In previous studies Davies et al. (Davies, 2004) demonstrated a continuous generation of the voids in the plastic phase starting at the yield point, which led to a conspicuous increase in the scattering power. Furthermore, a change in the diffuse scattering profile indicates a monotone change in the size and in the shape of the voids.

Stribeck et al. (Stribeck, 2008) described nanostructure evolution in Polypropylene during online mechanical testing with simultaneous SAXS and refined details of the interaction between the different phases including cavitation.

As an example the properties of isotactic Polypropylene (iPP) samples, produced by compression and injection moulding as well as after hot stretching, respectively, were investigated under stepwise loading. Simultaneously the structural changes were characterised by Synchrotron-SAXS and –WAXS and discussed together with the mechanical properties. It was found that there is a highly preoriented structure within the injection moulded specimen, which strongly influences the further temperature-dependent deformation behaviour. The influence of temperature and pre-orientation on the deformation behaviour is

described extending the present models of plastic deformation. The detailed knowledge of the structure and the microscopical behaviour of the material enables the tailoring of the processing conditions for material with certain mechanical behaviour.

Recently we published an overview about our first investigations about the structural changes in iPP during deformation using SAXS, WAXS, DSC and SEM-micrographs (Schneider, 2010, 2011). The present work will complement and round up the investigations described in those papers.

2. Experimental

2.1 General procedure

In order to investigate structural modifications during deformation X-ray scattering experiments were performed on samples mounted in a miniaturised tensile rig placed in the synchrotron X-ray beam. The synchrotron radiation is necessary to have sufficient intensity to get high time resolution. A general description of the equipment was given by Davies et al. (Davies, 2004).

The actually used experimental arrangement and the specimen geometry are illustrated in figure 1.

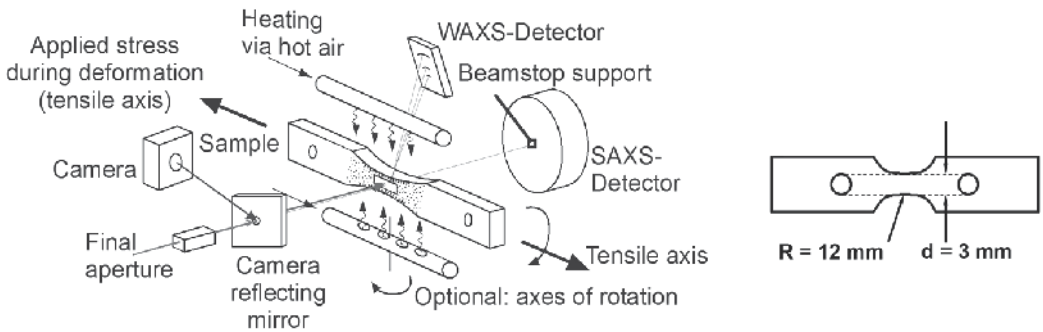

Fig. 1. Sketch of the experimental arrangement for SAXS and WAXS during deformation (left) and waisted specimen (mini-dumbbell) mainly used for simultaneous structure and mechanical investigation (right), the dimensions of the specimen can be scaled.

To investigate local strain-dependent properties, small waisted specimens were used in order to concentrate the stress in the centre of the specimen. By using a relatively large radius of curvature (12 mm) compared to the specimen width (3 mm) the stress state in the middle of the specimen is in good approximation maintained constant. The strain was determined optically by observing the deformation of a grid pattern applied on the specimen surface. The grid pattern was applied using a self-made flexible ink and a mesh size of 0.35 mm. Alternatively, also a classical image correlation analysis for strain estimation can be used. A comparison of stress-strain curves of the waisted specimens with standardised dog-bone specimens shows a good consistency: The curve progression from the beginning to the yield point as well as during strain hardening (that is where the yielded parallel region of the dog-bone specimen is deformed in a uniform way) are identical. For the range of neck formation and propagation in the dog-bone specimen an estimation of true

stress and strain via global strain measurement are not possible. Only a local strain measurement solves this problem. In the present context the specimens are approximated as incompressible. This allows us to calculate the true stress σ_t from the measured force F, initial cross section A and tensile strain ε_t as $\sigma_t = F * (1 + \varepsilon_t) / A$.

In order to keep the beam in a fixed position relative to the gauge length of the waisted sample throughout the measurement, both grips were moved simultaneously in opposite direction.

To get simultaneous SAXS and WAXS patterns, the WAXS could be monitored only in a limited range using a tilted detector. By using a horizontal tensile direction the vertically arranged WAXS detector monitors mainly the equatorial scattering of the sample. To follow also quick changes exclusively in the crystalline phase WAXS measurements were performed alternatively with the WAXS detector directly in the beam behind the sample and a sampling rate of 1 s.

For temperature-dependent tensile and scattering experiments a small heating device blows locally preheated air at the sample.

Besides the global scanning of samples the experimental setup generally also permits spatially resolved pattern recording, e. g. around a crack tip, if it is employed in a microfocus beamline. The described arrangement was successfully used investigating semi-crystalline polymers during deformation (Schneider, 2006, 2010, 2011) and fracture (Schneider, 2008, 2009).

2.2 Measurements at synchrotron beamlines

WAXS and SAXS measurements during deformation were performed at the synchrotron beamlines BW4 and P03 at HASYLAB in Hamburg, Germany (Roth, 2006). At BW4 the wavelength of the X-ray beam was 0.13808 nm, the beam diameter was about 400 µm. The SAXS images were collected by a two-dimensional MarCCD-detector (2048 x 2048 pixels of 79.1 x 79.1 µm²). The sample-to-detector distance was set to 4080 mm. The WAXS images were collected by a two-dimensional PILATUS 100K-detector (487 x 195 pixels of 172 x 172 µm²). The position of the WAXS detector was estimated using certain reference reflexes of iPP. By a special procedure the position of the tilted WAXS-detector was determined to have a tilt angle of 22.7°. The distance between the sample and the point of normal incidence was 247 mm. Exposure times were chosen in the range of 5 to 60 s per pattern. The frame rate, determined by exposure and data storage, was 15 to 70 s per pattern.

Additionally, WAXS measurements were performed at the synchrotron beamline P03 at HASYLAB (for a beamline overview see Roth et al., 2011) with a wavelength of 0.0941 nm and a beam size of about 15 µm diameter, using a PILATUS 300K-detektor (487 x 619 pixels of 172 x 172 µm²). The detector was placed vertically in the beam in a distance of 144.9 mm, the sampling rate was 1 s. To prevent sample damage due to the high intensity of the used X-ray beams at P03 during the measurements normally slow scans along or across the sample were performed.

For the discussion all SAXS- and WAXS-2D-patterns are shown with vertical tensile direction. For specimens with fibre symmetry this means that the fibre axis and so the scattering vector s_3 is also vertical, the scattering vector s_{12} is always horizontal.

2.3 Supplementary investigations of the material properties

For the investigation of the general temperature-dependent stress-strain-behaviour and the preparation of specimens for dynamic mechanical analysis (DMA) of highly stretched specimens short dogbone-specimen (parallel length 25 mm, specimen width 10 mm, thickness 4 mm, strain rate 80 mm/min) were measured with a testing machine Zwick 1456 from Zwick, Germany with heating chamber and optical strain measuring system.

DMA was performed by a rheometer ARES G2 from TA-instruments in torsion mode with a heating rate of 5 K/min and a frequency of 1 rad/s (6.28 Hz) as well with a dynamic mechanical spectrometer EPLEXOR 150N from GABO QUALIMETER Testanlagen GmbH, Germany in tensile mode with a heating rate of 3 K/min and a frequency of 1 Hz.

For qualitative comparison of crystallinity and the melting behaviour of samples stretched under certain conditions some differential scanning calorimeter (DSC) measurements were performed on drawn samples using a DSC Q 1000 from TA-instruments. The specimens were measured between -80 and 230 °C with a heating rate of 20 K/min. Before each scan the sample was equilibrated at constant temperature for 300 s. In the case of heating into the melting region a heating rate of 10 K/min and a subsequent cooling rate of 80 K/min were used.

As qualitative check of the discussed structures some SEM images of the drawn samples were taken on a Zeiss Gemini Ultra plus SEM.

2.4 Material and sample preparation

The investigations were done on isotactic polypropylene (iPP), grade HD 120 MO from Borealis. Both injection and compression moulded plates were used. The melt temperature in injection moulding was 245 °C, the mould temperature was 40 °C. The mould has a film gate with a width of the half of plates thickness.

Compression moulded plates were used, produced by heating injection moulded plates to 210 °C for 5 minutes in a vacuum press. Then the plates were cooled down to room temperature at 15 K/min. The specimen used for scattering have always a thickness of about 1 mm. Mini-dumbbell specimens were produced by CNC milling. For the investigation of the general temperature-dependent stretching behaviour from the plates with 4 mm thickness short dumbbell specimen (parallel length 25 mm, specimen width 10 mm, thickness 4 mm) were produced also by CNC milling.

3. Evaluation of scattering data

3.1 SAXS data evaluation

The evaluation of SAXS images is strongly related to the approach for materials with fibre symmetry developed by Stribeck (Stribeck, 2007). Data processing was realised with the software package pv-wave from Visual Numerics.

The images were normalised with respect to the incident flux and blind areas were masked. Considering the sample absorption the instrument background was subtracted. By translation and rotation the images were aligned in that way that the tensile direction is

vertical and the beam position in the middle of the patterns. Finally, the patterns were averaged with respect to the four quadrants of the detector. The blind area of the beam stop is interpolated assuming a Guinier-type behaviour of intensity in this range.

Generally, SAXS realises a projection of the specimen structure into the reciprocal space, where it produces a slice of the Fouriertransform (FT) of the structure whose amplitude is measured. A single back-transformation would deliver a projection of the autocorrelation function of the structure.

Complete information about the specimen would be available only by tomographic methods with a stepwise rotation of the sample (see e.g. Schroer, 2006) or using inherent symmetry properties of the sample. Under the assumption of fibre symmetry of the stretched specimen around the tensile axis, from the slices through the squared FT-structure the three-dimensional squared FT-structure in reciprocal space can be reconstructed and hence also the projection of the squared FT-structure in reciprocal space. The Fourier back-transformation of the latter delivers slices through the autocorrelation function of the initial structure. Stribeck pointed out that the chord distribution function (CDF) as Laplace transform of the autocorrelation function can be computed from the scattering intensity I(s) simply by multiplying I(s) by the factor $L(s) = -4\pi^2(s_{12}^2 + s_3^2)$ prior to the Fourier back-transformation. Here s is the scattering vector with the component s_{12} in transversal direction and s_3 in fibre direction.

The interpretation of the CDF is straightforward (Stribeck, 2001), since it has been defined by the Laplacian of Vonk's multidimensional correlation function (Vonk, 1979). It presents autocorrelations of surfaces from the scattering entities in that way that positive values characterise distances between surfaces of opposite direction, negative values distances between surfaces of the same direction, see figure 2.

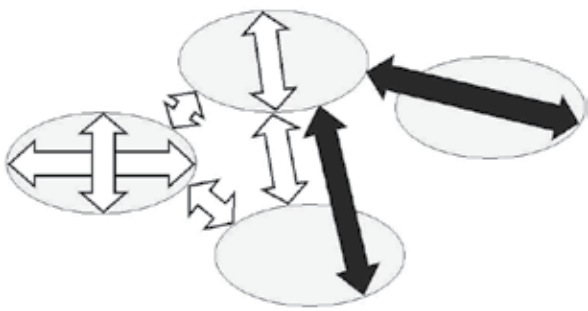

Fig. 2. Information of CDF's: In any particular structure positive values of the CDF represent correlations of interfaces with opposite direction (light arrows); negative values represent correlation of interfaces with the same direction (dark arrows).

Hence positive peaks in the vicinity of the origin characterise size distributions of the primary domains. In the case of semi-crystalline materials this can be crystallites as well as amorphous regions in-between. If cavitation occurs it will be superimposed by the size of the cavities. Also a relatively small amount of cavities will be visible because the difference in electron density is here much higher than between crystalline and amorphous phase within the polymer.

Following negative peaks characterise distances between adjacent repetition units ("long periods").

Positive peaks at greater distances describe size and orientation of domains (from the beginning of the first domain to the end of the second one). In well oriented systems also peaks of higher order can be observed.

For detailed discussion the CDF's can be presented as contour plots or as density plots in the plane.

3.2 WAXS data handling

Unfortunately, the PILATUS detector has some dark regions. After masking the beam stop those regions were reconstructed using the symmetry properties of the pattern.

For the qualitative discussion in the present case the individual images were not normalised with respect to the incident flux and not corrected with respect to background scattering.

4. Results

4.1 Mechanical behaviour of injection moulded iPP

The temperature-dependent stress-strain-behaviour of iPP is shown in figure 3.

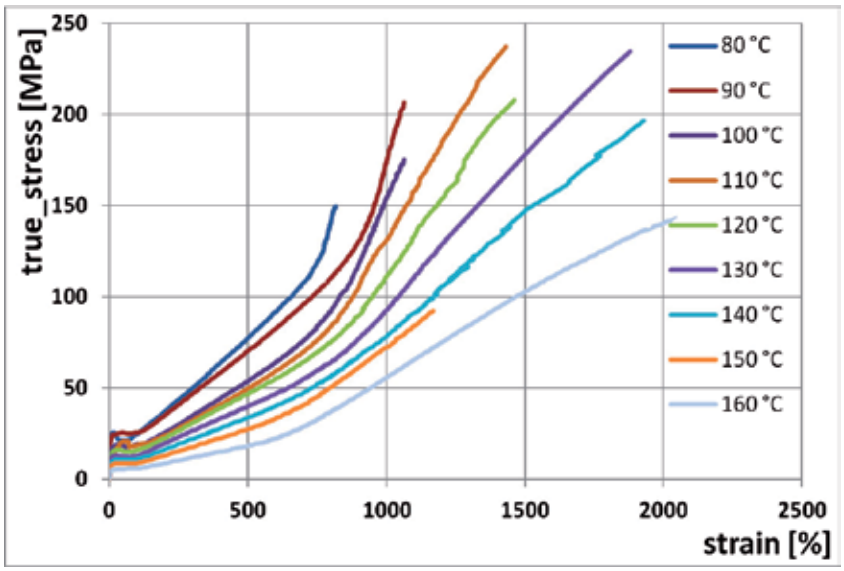

Fig. 3. Temperature-dependent stress-strain-behaviour

The general behaviour is characterized by a decrease of the initial modulus as well as the yield stress with temperature. Yielding of the material is finished at a strain of about 600 … 900 %, afterwards there is a strain hardening. The strain hardening modulus (slope of the true stress vs. strain curve in the region of strain hardening) decreases with the temperature.

The stress at failure initially increases with the temperature. At temperatures above 130 °C the stress at failure again decreases. The strain at failure increases steadily to finally more than 2000 %.

There is some whitening of the specimens, mainly due to cavitation. It starts at lower temperatures above the yielding point. With increasing temperatures the initiation of whitening shifts to higher strains. At temperatures above 110 °C it happens in the strain hardening region, with increasing temperature nearer to failure.

The small decay in the curves above the yielding point is due to the fact, that these experiments were performed with tensile bars with parallel gauge length and a distance of the optical marks of about 10 mm. Using samples with waisted geometry and strongly localized optical strain measurement this decay can be prevented to the greatest extent (Schneider, 2010).

4.2 Crystallite identification

According to Bragg's law the positions of WAXS reflexes refer to the distance between crystalline planes within the crystallites. In the compression moulded as well as in the injection moulded plates a couple of crystalline reflexes could be identified. The reflexes with the highest intensity within the relevant angular region are summarised in table 1.

Reflex	Intensity (qualitatively)	d / nm	Scattering angle 2 Θ / deg	
			P03	BW4
1 1 0	strong	0.6269	8.608	12.64
0 4 0	strong	0.5240	10.303	15.13
1 3 0	strong	0.4783	11.291	16.59
1 1 1	strong	0.4170	12.957	19.05
0 4 1	strong	0.4058	13.316	19.58

Table 1. Crystalline reflexes of iPP, which were used for the calibration of the detector distance as well as for the further discussion of crystallite orientation and changes during deformation.

4.3 Elastic crystallite deformation

Loading of the samples below the yield point causes a certain deformation of Debye-Scherrer patterns of the crystallites. According to Bragg's law a scattering signal refers to the spacing between lattice planes. The shift inversely reflects the strain vertical to the corresponding plane. In the present context the longitudinal tension as well as the transversal compression could be followed. Due to the stiffness of the crystallites deformations only in the range of about 1 % could be found, which are difficult to be resolved with the pixel size of the used detector. By unloading the samples the crystallite reflexes shift again to the initial positions. Similarly, also the thermal expansion of the crystals could be found only qualitatively.

This behaviour we reported yet in the past (Schneider, 2010), where we compared the mismatch between crystalline and global strain by a factor in the order of 10 indicating the different stiffness of the crystallites compared to that of the whole specimen due to the relatively soft amorphous regions.

In the present context the shift of the observed (h k 0)-reflexes in equatorial direction (perpendicular to tensile direction) display the transversal crystalline strain of the crystallites aligned in tensile direction.

Cyclic loading and unloading gives an estimation of the elastic crystalline strain also during plastic deformation. Figure 4 shows transversal crystalline strain of the (1 1 0)-reflex vs. the overall tensile strain for 3 consecutive loading cycles. The first strain amplitude was 0.12, the remaining strain after unloading 0.04. The following cycles were conducted within the overall elastic region. The shift of other (h k 0)-reflexes yield the same result.

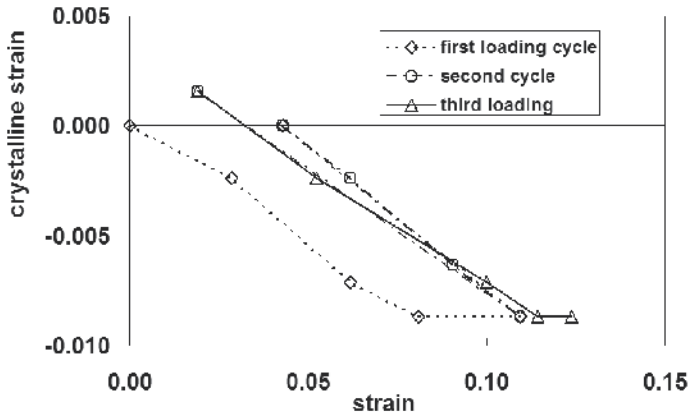

Fig. 4. Transversal crystalline strain vs. optically measured tensile strain of semi-crystalline iPP specimen estimated via the shift of the (1 1 0)-reflex at room temperature.

In a range of up to about 8 % strain the crystallites deform transversally by about -0.8 %. The mismatch between crystalline and global strain indicates the different stiffness of the crystallites compared to the whole specimen due to the relatively soft amorphous regions. During further loading the strain of the crystallites remains constant. This means that further deformation is realised on the micro-scale only by the amorphous phase and by additional shear dislocation of the crystallites.

4.4 Crystallite orientation of the samples and reorientation during drawing

In a preliminary investigation at BW4 stepwise loading at different temperature was performed. The stress-strain-diagrams captured during these measurements are presented in detail recently (Schneider, 2010, 2011), they are comparable to the mechanical behaviour of the preliminary tests. The stress-strain-level is slightly lower due to the generally lower strain rate. For the flat samples under investigation the transmission was 0.83 in the unstretched state. During stretching and simultaneous thinning the transmission generally increased to 0.96.

The images were always transformed to reference coordinate systems with respect to the scattering angles (scattering angle 2Θ and azimuthal angle φ or scattering vectors s_{12} and s_3). For further discussion the scattering intensity was projected over a selected range of φ on the 2Θ-axis. Figure 5 shows some characteristic equatorial cuts together with the transformed pattern.

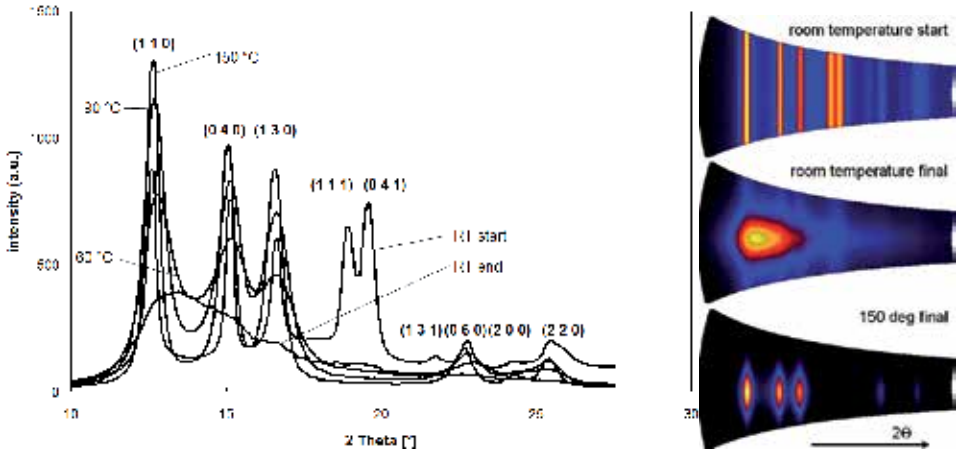

Fig. 5. Equatorial scattering intensity of undeformed iPP at room temperature and during strain hardening at elevated temperatures. The curves always show a projection of the angular range of ±2 ° around the equatorial direction. Right: WAXS-patterns, azimuthal angle vs. scattering angle 2Θ at three characteristic points: undeformed as well as immediately before failure at room temperature and 150 °C.

During deformation the WAXS patterns change in a quite characteristic way, see figure 6. Initially the intensity of the crystalline peaks is relatively constant over the azimuthal angle pointing to a homogeneous distribution of crystallite directions. At deformations below the yield point slight changes in the intensity of the peaks are reversible.

Above the yield point the deformation behaviour is strongly temperature-dependent. Generally in the investigated equatorial direction only the (h k 0)-peaks remain and the scattering intensity concentrates azimuthally in equatorial direction. This is generally an indication of orientation of crystallites with the c-axis (chain direction) in tensile direction. But while the peaks sharpen with increasing temperature, which is an indication of growing crystallites, they decrease strongly and broaden at temperatures in the range immediately above room temperature. This indicates a gradual disruption of crystallites into smaller fragments. Finally, at room temperature the distinct peaks disappear but give a broad halo in the angular range of the previous peaks. This indicates a rough orientation of the chains or very small crystallite fragments in tensile direction, probably in the form of fibrils. However, the thermal mobility of the chains seems to be all in all insufficient to establish new crystallites.

After these recent investigations with simultaneous SAXS and WAXS measurements with limited range of the WAXS-detector (Schneider, 2010) some representative WAXS measurements were repeated at elevated temperatures with whole WAXS-range and certain temperature-strain-program. The samples were heated to 110 °C in the tensile rig. At this temperature the samples were stretched to about 300 %. Afterwards they were heated

stepwise to temperatures below the melting temperature and cooled again up to 80 °C, both with and without load. The individual behaviour is described in detail.

The investigated injection moulded samples showed initially mostly homogeneous WAXS pattern with Debye-Scherrer patterns related to the reflexes mentioned in table 1. The samples are to a large extent crystallised. Heating the samples to about 110 °C didn't change the WAXS pattern.

During stretching the samples to about 300 % the pattern changed drastically, see figure 6. The intensity of the rings concentrates to certain positions, characteristic for well aligned crystallites in stretching direction.

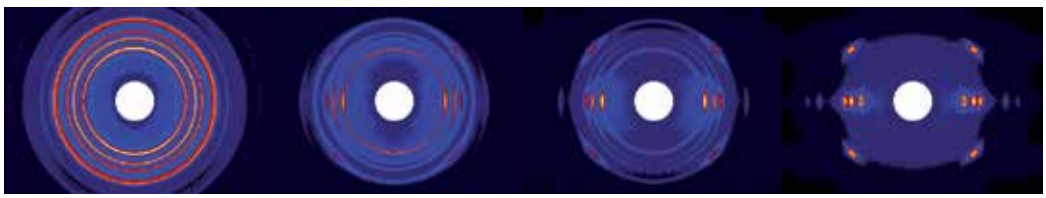

Fig. 6. Changing of the WAXS pattern during deformation at 110 °C (strain from left to right: 0 %, 70 %, 85 %, 300 %) of a waisted specimen (mini-dumbbell). The stretching direction is vertical.

Under the condition of fibre symmetry signals in the pattern vertical to the tensile direction report highly oriented lamellae or lamellar fragments in tensile direction. This final pattern remains mainly constant also during further heating to about 160 °C (below the melting point) under load as well as unloaded.

Further heating of the samples very close to the melting point creates a sharpening and broadening of the crystalline reflexes in azimuthal direction: Apparently the thermal stress is released, the mobility of the unloaded crystallites becomes higher and the orientation of it becomes a little bit less, see figure 7.

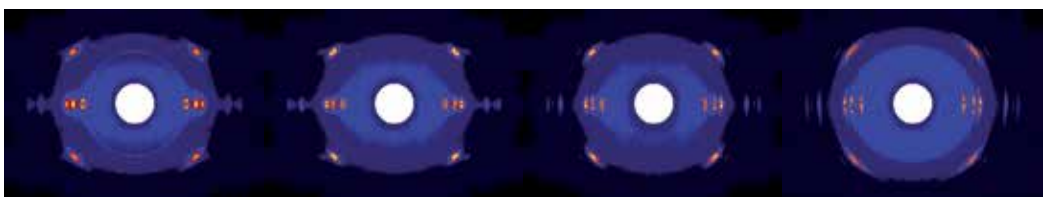

Fig. 7. Sharpening of the WAXS reflexes during deformation approaching the melting point (temperature from left to right: 110, 160, 165, 170 °C) of a waisted specimen (mini-dumbbell). The stretching direction is vertical.

Immediately above the last position in figure 7 the sample melts and all WAXS-reflexes disappear.

4.5 Crystallisation behaviour during subsequent cooling

The azimuthal width of the standard reflexes of the stretched iPP – if present - remains mainly constant also during following crystallisation processes by cooling. Cooling to about

140 °C doesn't change the pattern. During further cooling different routes of crystallisation can be observed, see figure 8.

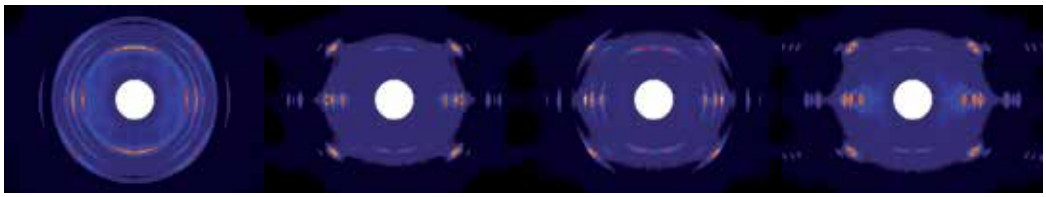

Fig. 8. Pattern during recrystallisation of a stretched iPP sample at temperatures below 140 °C: Isotropic pattern after crystallisation from the melt, a slight preferential orientation may be observed (creation of crystallites with a wide range of orientation); crystallisation of the common stretched lamellar fragments; generation of a meridional double-reflex (daughter lamellae); creation of a new series of (h k 1)-crystallites (from left to right). The stretching direction is vertical.

While the generally present reflexes of the lamellar fragments remain nearly unchanged, notable is the formation of a new meridional double-reflex with different strength. This reflex is discussed in the literature often as the formation of epitactic daughter lamellae (Kumaraswamy, 2000). Otherwise in some cases a whole system of reflexes in the plane of the (h k 1)-reflexes is found, which is described in the literature as nano-oriented crystals (Okada, 2010). The appearance of the latter depends strongly on a small temperature window below the melting point, to which the stretched sample must be heated.

4.6 Structural changes across a sample – influence of a temperature gradient

In the present investigations there had been a certain temperature gradient across the samples. So the initial temperature of the sample before cooling was different across the sample. As a consequence finally all the different structures discussed above could be found side by side in the same sample.

4.7 SAXS during stretching

From the set of successive scattering patterns during the deformation for the following discussion only patterns and the corresponding CDF's were chosen where characteristic changes could be seen.

The respective results of SAXS from stretching at room temperature are shown in figure 9. The regular circular form of the CDF from the beginning is nearly unchanged to about 6 % strain also during unloading. It represents the randomly distributed crystallites, which were deformed elastically, as discussed in the section about WAXS above. The diameter of the inner ring in the CDF indicates a lamellar thickness of 9.8 nm. The isotropic ring in the negative direction represents the long period of 17.7 nm. The following second positive and negative reflexes indicate a certain correlation with the third neighbours. Missing higher-order reflexes indicate that there are surprisingly no remarkable correlations above the third neighbours. During deformation below the yield point (loading, unloading, relaxation and repeated loading) this general situation is unchanged.

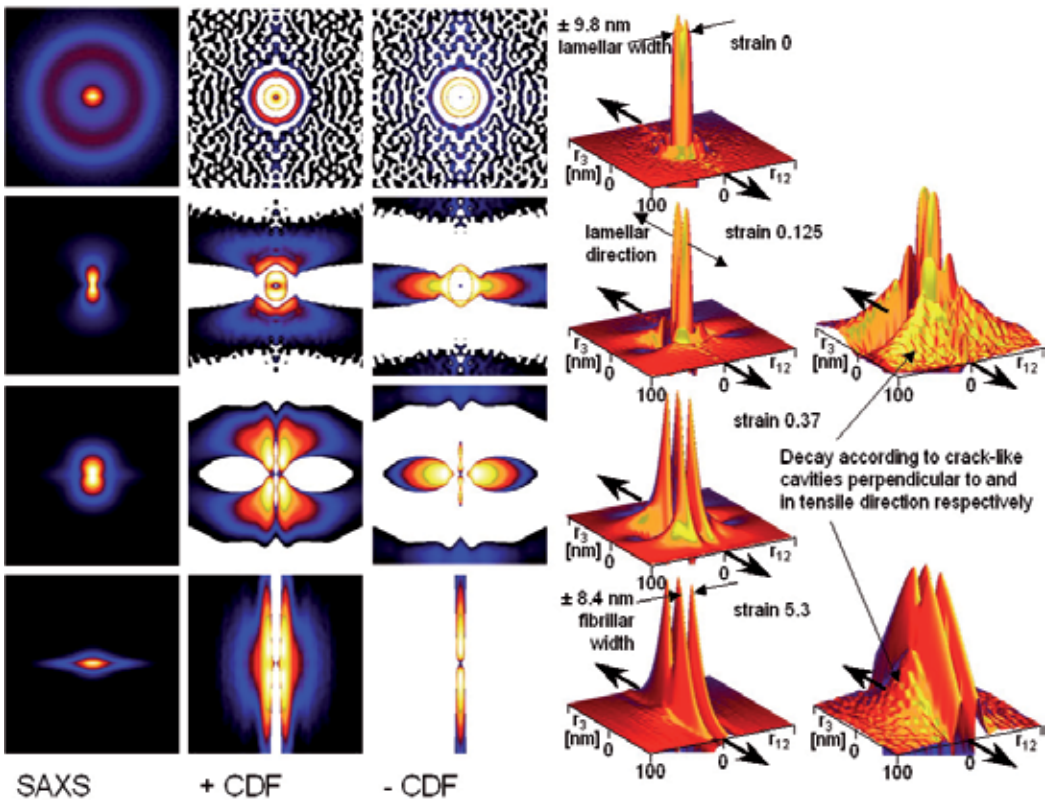

Fig. 9. Deformation of iPP at room temperature, from left to right: SAXS patterns, positive and negative CDF's (always log scale, pseudo-colour) as well as a surface plot of the CDF's (linear scale and for two strains also log scale) at different strains ε = 0.0, 0.125, 0.37 and 5.3 (from top). Each square of the pattern covers a range – 0.12 nm^{-1} < s_1, s_3 < 0.12 nm^{-1}, each square of the 2D-CDF covers a range of – 100 nm < r_{12}, r_3 < 100 nm, fibre direction always vertical. The stretching (fibre) direction is indicated in the surface plots by arrows.

Beyond the yield point the situation changes drastically. First of all it is noticeable that the total scattering intensity as well as the extrapolated intensity I_0 increase dramatically suggesting the activity of new strong scatterers – presumably cavities, which exhibit a strong scattering contrast to iPP due to their extremely low electron density. They start as small cracks transversal to the tensile direction and finally deform to long drawn cavities between fibrils. According to their successive growth and hence their broadly distributed dimensions they hardly show distinct scattering signals, but overlap with the signals arising from the lamellae or their fragments. The growing cavities are also responsible for the whitening of the cold drawn samples (see also Pawlak, 2010). In contrast to the scanning experiments with a microbeam reported by Roth (Roth, 2003), which allows to resolve certain individual voids, here over a large ensemble of cavities is averaged. Within the CDF's these cavities are reflected by the broad initial decay in fibre direction, at higher strains perpendicular to fibre direction, see figure 9, CDF's in log scale on the right.

Yet at a strain of 12.5 %, the beginning of the yielding region, the structure becomes anisotropic. While thickness of the lamellae remains constant, they align perpendicular to

the tensile direction. The correlation to the next neighbours in transversal direction is lost and concentrated within a 4-point-pattern. This indicates occasionally an internal shear deformation. Under the external stress the lamellae are sheared and finally break down into certain blocks as described by Strobl (Hong, 2004).

A new transversal correlation length is established at about 37 % strain. By shearing the lamellar blocks break down to a size which later represents the dimensions of the fibrils. According to the relatively low internal mobility the aligned chains are not able to form new crystallites. Their mean dimension in transversal direction is with 8.4 nm clearly below the lamellar thickness. This correlates with the WAXS results, which also indicate the final disappearance of the lamellar transversal order during cold drawing. Ultimately, at high strains, this transversal correlation dominates the whole CDF.

The general changes within the oriented chains – within crystallites as well as non-crystallized stretched chains – are shown in the sketch in figure 10, deformation at room temperature is shown in steps a), b), c), f) and g).

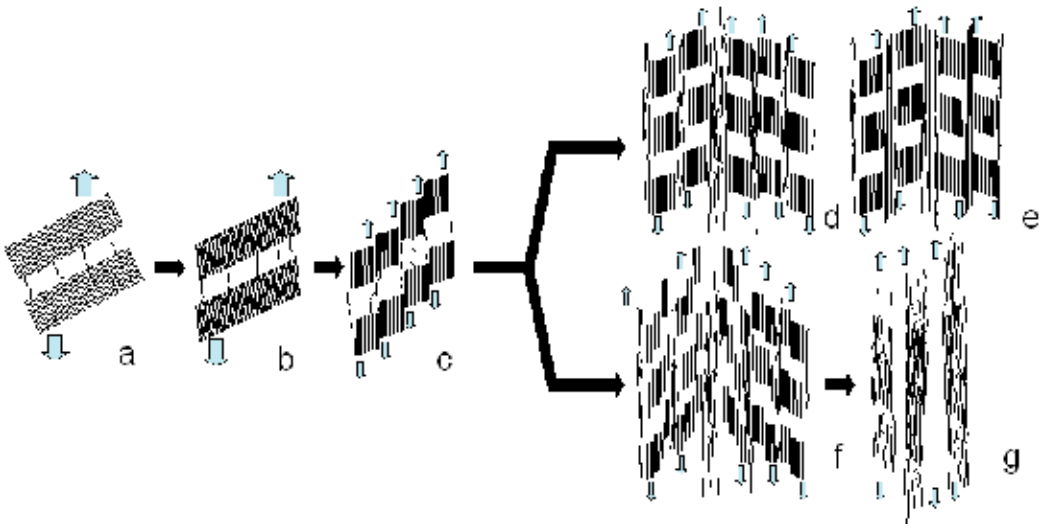

Fig. 10. Sketch of the transformations of the oriented chains during deformation, in-between are additional amorphous chains: a) lamellae with some tie-molecules, b) elastic shear-deformation of lamellae under small load and reorientation with respect to the load, c) fracture of lamellae into smaller blocks due to local stress concentration caused by tie molecules, d) stretched aligned, but not re-crystallised chains between the blocks during stretching at higher temperatures, e) some of the fibrillar arranged molecules crystallise, final stage in the case of hot stretched iPP, f) further dissolution of the blocks creating more extended chains at room temperature, g) finally, there are several strands of extended chains, not crystallised, with some amorphous regions in between, final stage in the case of cold stretched iPP.

With increasing temperature the deformation behaviour totally changes. The patterns and the CDF's of the stretching of iPP at 130 °C are shown in figure 11. Here the averaged as well as the extrapolated maximum intensity I_0 does not change dramatically above the yield

point. Instead soon the lamellae align in tensile direction increasing their correlation in this direction, indicated by higher order of reflexes in the CDF's. The transversal displacement of the reflexes suggests that the aligned lamellae are shifted against each other. The situation does not change generally also at high strains. This interpretation is also supported by the WAXS results described above. The deformation is shown schematically in figure 10 a) – e).

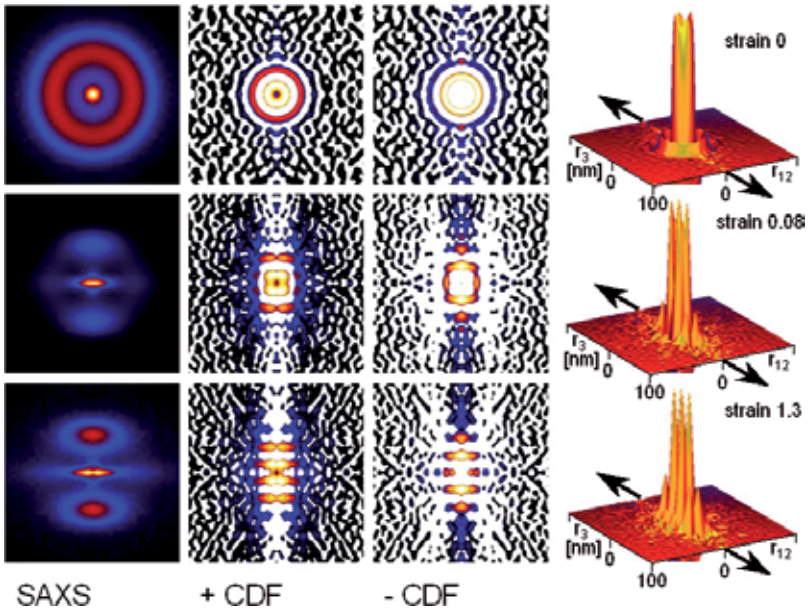

Fig. 11. Deformation of iPP at at 130 °C, from left to right: SAXS patterns, positive and negative CDF's (always log scale, pseudo-colour) as well as a surface plot of the CDF's (linear scale) at different strains ε = 0.0, 0.08 and 1.3 (from top). Each square of the pattern covers a range – 0.12 nm^{-1} < s_1, s_3 < 0.12 nm^{-1}, each square of the 2D-CDF covers a range of -100 nm < r_{12}, r_3 < 100 nm, fibre direction always vertical. The stretching (fibre) direction is indicated in the surface plot by arrows.

With increasing temperature also the whitening is remarkably reduced indicating that due to the higher mobility of the amorphous phase nearly cavitation is negligible as compared to the extent observed at room temperature.

Over the whole deformation range stress relaxation is observed as soon as the tensile rig was stopped. However since this can be ascribed to the amorphous phase, SAXS results remain mostly unaffected.

4.8 Influence of processing on the samples morphology

The influence of injection moulding on a preliminary orientation of the crystallites and their deformation we described recently (Schneider, 2010). It was shown, that injection moulded specimens in injection direction as well as the compression moulded and quickly cooled specimens are highly stretchable. By contrast the specimens transversal to the injection direction fail very soon. Here in some cases even crazing could be observed before failure.

This points out that there will be a strong structural anisotropy due to the processing history (shear stress as well as cooling rate).

4.9 DSC investigation of unstretched and stretched specimens

To check the thermal behaviour respectively melting of different stretched samples some DSC measurements were performed. In a first test samples were pre-stretched at different temperatures to about 500 %. The heating peaks of the first heating curves of the stretched samples are shown in fig. 12.

It seems to be possible to split each curve into 2 individual melting peaks whose positions shift with the stretching temperature to higher values. Furthermore, while the high-temperature peak is nearly constant the low-temperature peak increases with stretching temperature.

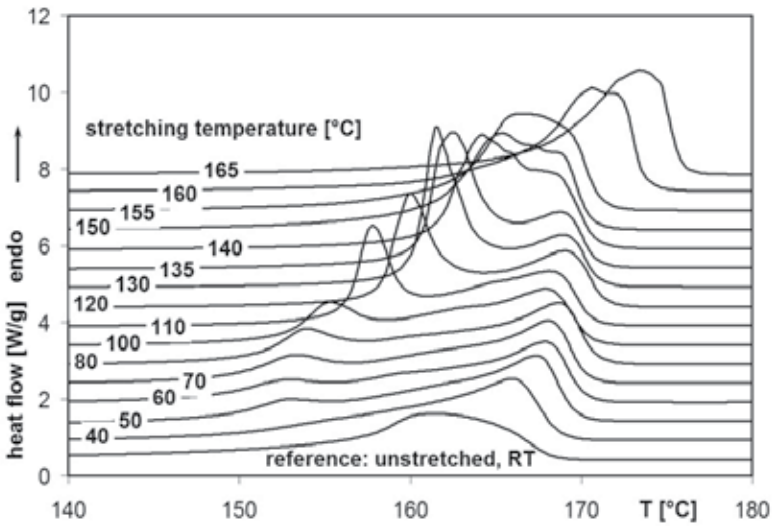

Fig. 12. DSC-measurements: first heating curves of compression moulded iPP-specimens stretched at different temperatures. For clarification the curves are vertically shifted.

To check, whether there are two individually melting crystalline species in a second series samples, stretched to about 500 % at 110 °C, were heated to different temperatures behind the first peak in the heating curve. Afterwards they were cooled to room temperature before they were heated over the melting point in a second run, see figure 13.

The position of the first peak flutters a little bit due to the different specimen taken from a stretched sample. Heating in the first run well above the melting temperature – 175 or 200 C – the second heating curve is similar to the first one with a slight double peak. If the first heating is stopped at 160 °C, the second heating curve has the narrower double peak, shifted to higher temperatures. Surprisingly in the case of the interrupted first heating at 165 °C the second heating peak is shifted to remarkable higher values and only a unique peak is observed.

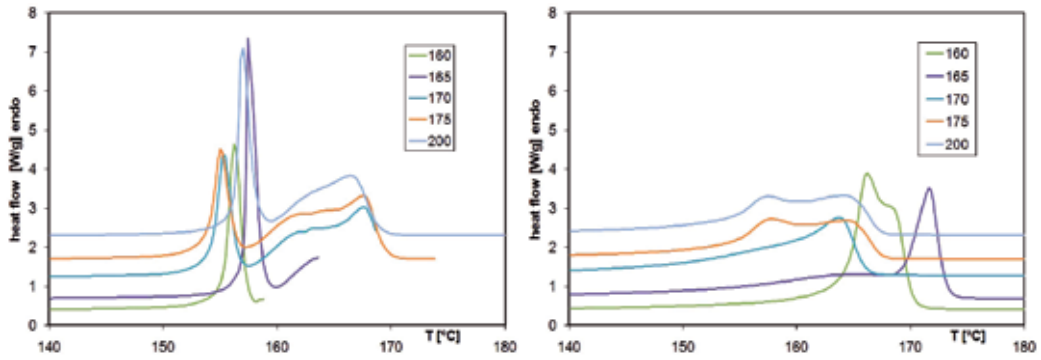

Fig. 13. DSC-measurements: first and second heating curves of compression moulded iPP-specimens stretched at 110 °C to about 500 %. The first heating was stopped at different temperatures after the first peak in the heating curve, see the label within the diagram. For clarification the curves are vertically shifted.

4.10 DMA investigation of unstretched and stretched specimens

The general different interaction of amorphous and crystalline regions in the initial (spherulitic) as well the highly stretched (fibrillar) state was investigated with DMA. The stretched material was produced by hot-stretching of small tensile samples from plates with a thickness of 4 mm and 10 mm width at different temperatures.

With shear and tensile load two independent measurements were performed, see figure 14. Under shear load the crystallites (fibrils) and the amorphous regions are more or less in series, under tensile load they are parallel. Accordingly the combination of the moduli is quite different.

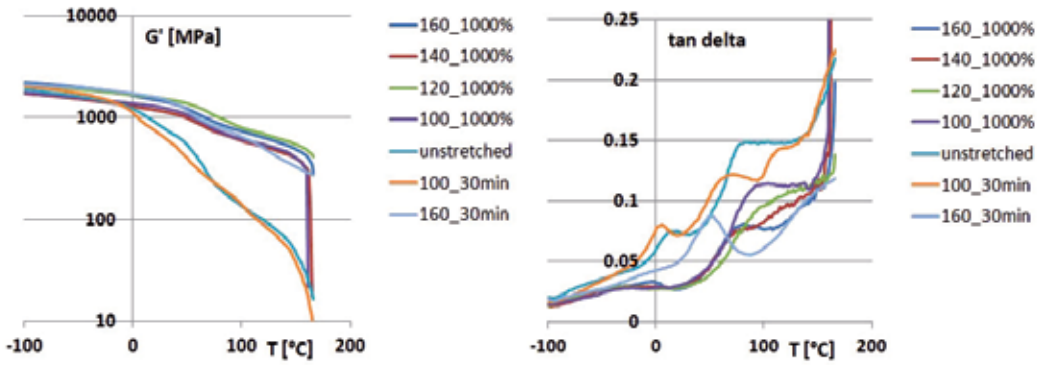

Fig. 14. Measurement under torsion: G' (storage modulus) and loss tangent of differently treated iPP: injection moulded, annealed and hot-stretched samples. Parameters of the sample preparation are shown in the legend

At low temperatures the storage modulus is almost the same: Crystalline as well as amorphous regions behave stiff. At the common glass transition temperature at about 0 °C there is a small peak in the loss tangent and a decrease in the storage modulus due to the

onset of the mobility of the amorphous regions of the unstretched (annealed or not annealed) sample. This content is nearly missing in the case of the stretched samples.

In the range between room temperature and melting temperature there is a continuous drop in the storage modulus of the unstretched samples due to the increasing mobility of the amorphous phase with temperature. The amorphous phase is constrained between the crystalline one. Therefore, here is such a high temperature dependence of the mobility. Annealing at 100 °C enables some post- or re-crystallisation causing an increase in modulus and a decrease in the loss-tan. Annealing at 160 °C, i.e. shortly below the melting point, supports the further crystallization. The relatively strong drop down of G' remains.

The situation is totally different after high stretching. The signal of the undisturbed amorphous phase nearly totally disappears; the constrained amorphous phase enables only very slight molecular motion between the aligned crystallites. Annealing at increasing temperatures reduces this remaining mobility.

The behaviour under tensile load is somewhat different, see figure 15.

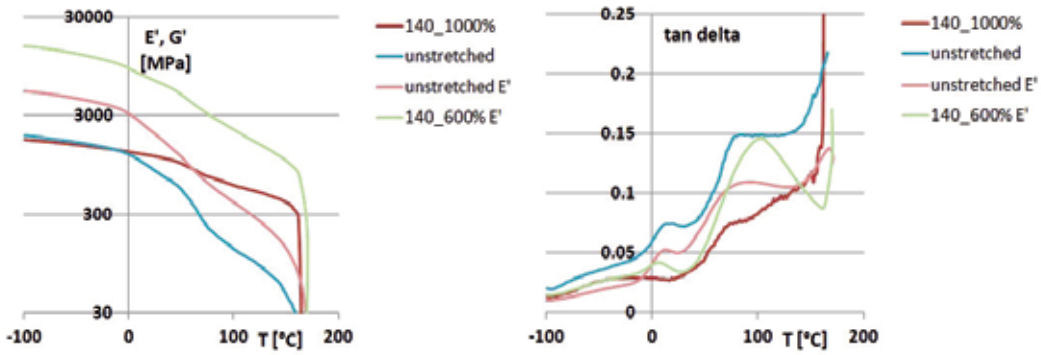

Fig. 15. Measurement under tension: E' (storage modulus) and loss tangent of differently treated iPP in comparison to the torsion measurement G': injection moulded and hot-stretched

Besides the generally higher values of the tensile modulus with respect to the shear modulus according to $E = 2 (1 + \mu) * G$, the crystalline and the amorphous phase after the stretching are more or less parallel. By this a noticeable increase in E', small contribution of the glass transition near 0 °C and a further softening around 100 °C appears.

4.11 Micrographs and SEM of stretched specimens

Micrographs under polarized light of iPP crystallised within a rheometer as well a stretched sample are shown in figure 16. Here the change from spherulitic to fibrillar structure is clearly visible. SEM images were taken to verify the described general deformation behaviour. Figures 17 to 20 show the compression moulded unstretched reference specimens and specimens stretched at room temperature, 90 °C and 150 °C. The specimens were cut in tensile direction, and vapour deposited with platinum. Stretching direction and thus s_3-axis are always vertical in the figures 17 to 20, the s_1-axis horizontal.

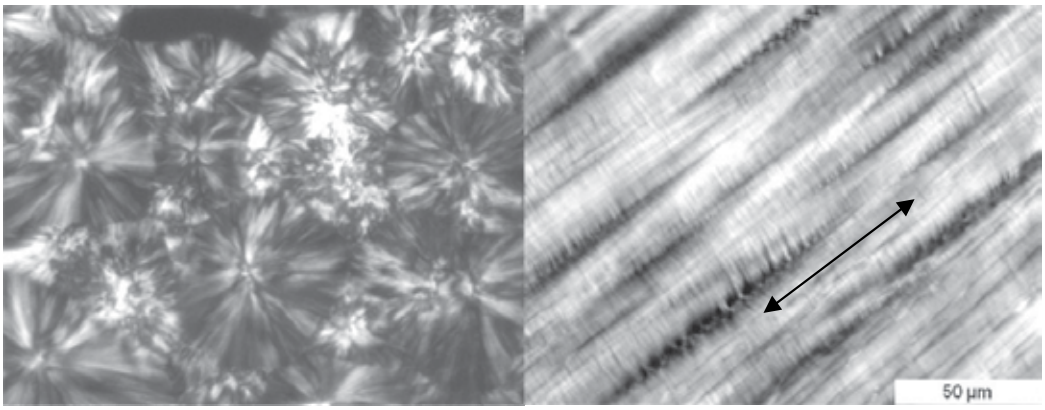

Fig. 16. iPP crystallised within a rheometer without shear and cold stretched sample with fibrillar strands (stretching direction diagonal, see arrow)

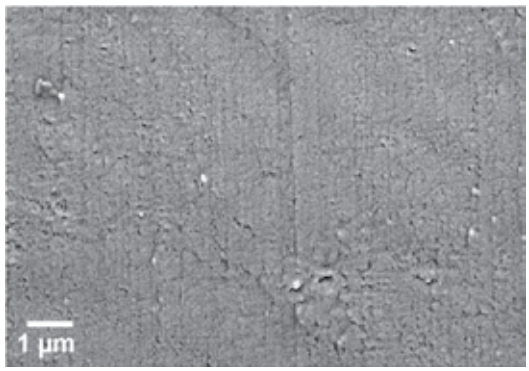

Fig. 17. Scanning electron micrograph of the unstretched reference iPP sample.

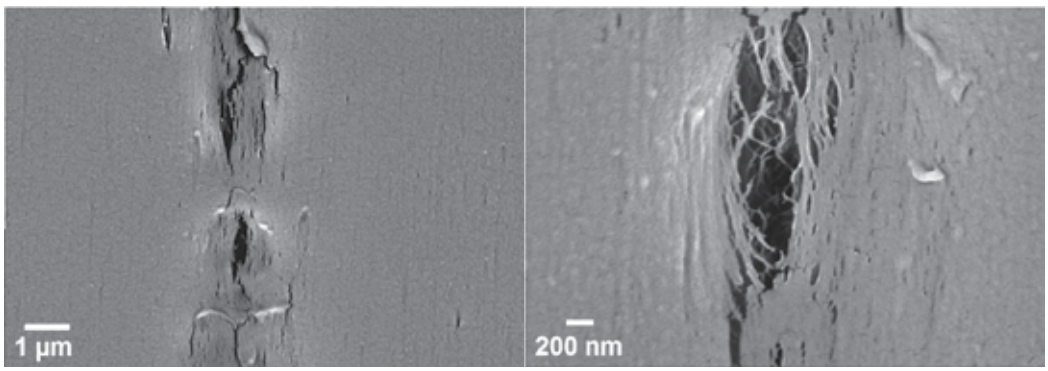

Fig. 18. Scanning electron micrograph of the iPP sample stretched at room temperature. Stretching direction vertical.

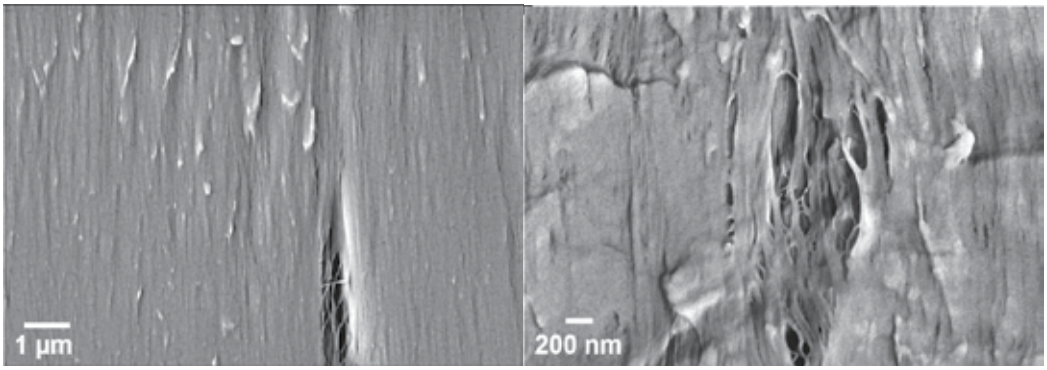

Fig. 19. Scanning electron micrograph of the iPP sample stretched at 90 °C. Stretching direction vertical

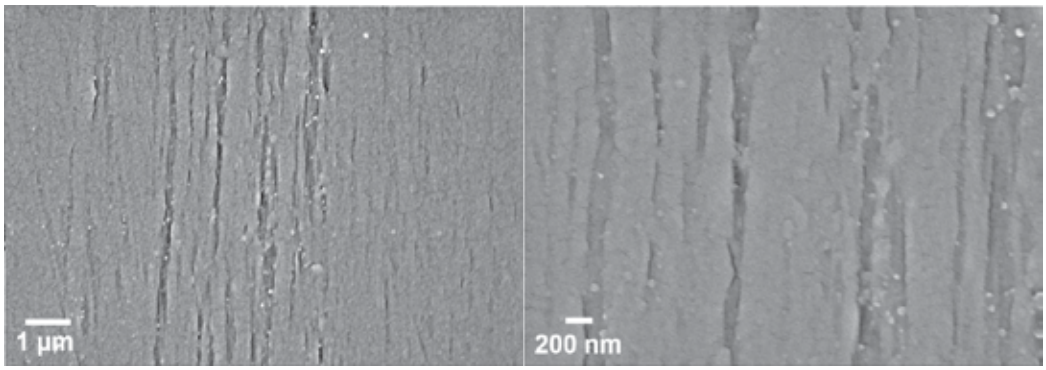

Fig. 20. Scanning electron micrograph of the iPP sample stretched at 150 °C. Stretching direction vertical.

Figure 17 to 20 show the voids in the stretched samples the formation of which was discussed above. Their size decreases with increasing stretching temperature. In the sample stretched at 150 °C they are not found. The lamellae and fibrillae are not visible at the present magnification, only a slight texture in stretching direction can be seen. A similar trend was reported recently by Pawlak (Pawlak, 2010), who found voids only at stretching temperatures below 60 °C, at higher temperatures only deformed spherulites and fibrils.

5. Discussion

Stretching semi-crystalline iPP at temperatures changes the morphology totally. Below about 80 °C the crystallites become destroyed, the stretched fragments oriented in stretching direction. This causes the wide peak in the WAXS pattern without a fine structure referring to the individual crystalline parameters. A strong cavitation appears because the transversal strength of the lamellae is less than that of the stretched amorphous phase, which one transfers stress to the lamellae. The relatively stiff but irregularized structure fails at comparable low stresses.

Stretching above about 80 °C causes a destruction of the initial morphology without cavitation. The crystalline/lamellar fragments were oriented via the stress transferred by the

tie molecules in stretching direction. Due to the high degree of crystallinity and mainly the transferred stress the amorphous regions between the oriented crystallites are in confined geometry and stretched. The stress of the amorphous phase is in balance to a load of the crystallites, which are slightly deformed on this way. The total degree of crystallinity changes only marginal. The frozen stresses can relax only approaching the melting temperature. There also the load of the crystallites goes down and the orientation in stretching direction becomes worse.

By aligning of crystallites or lamellar fragments by stretching as nuclei for subsequent crystallisation the whole morphology of a later fully crystallised material can become highly oriented. By this way the mechanical properties can become strongly improved. The accessible orientation by shearing a melt during processing is much lower than this route. This procedure to improve mechanical properties is normally used in hot drawing of melt spun fibres. But the present investigations show, that it should also be possible for macroscopic respectively 3-dimensional structures. It is much easier than the compression procedures of undercooled melt to get highly oriented material (Okada, 2010). The process is strongly dependent on the temperature regime. In the case of too strong heating all crystallites can melt and the sample will crystallise later on in a spherulitic or in the presence of nucleating agents and with sufficient quick cooling in an unoriented manner.

The splitting of the melting peak of stretched iPP seems to be initially due to the frozen internal stresses. The first peak appears if the stresses are finally released. This is, dependent on the stretching temperature, between 150 and 165 °C. The second heating shows again a double melting peak between 165 and 173 °C. The first part is due to the remaining lamellar fragments, the second due to the new established fibrils. If the first heating was to 165 °C, only a unique melting peak of the fibrils above 170 °C is found. It seems that this is also the region where the multitude of new crystalline reflexes is observed. This discussion of the material behaviour corrects our first conclusions about the melting behaviour of the different phases in stretched iPP, which we published recently (Schneider, 2010).

To describe the temperature-dependent stress-strain behaviour of semi-crystalline materials we established a model on the basis of the described structural elements. It describes the interaction of the temperature-dependent mobility of the amorphous phase, the initially relative stable crystalline phase, the step-wise re-arrangement of the crystalline phase with respect to orientation and transformation via crystallite fragments and extended chains into fibrils. It will be soon published separately.

6. Conclusion

The experiments revealed the continuously changing interplay of elastic and plastic deformation and energy dissipation (the transformations of amorphous and crystalline phases) during deformation of semi-crystalline polymers using the example of iPP. Due to the high number of parallel processes, here the use of structure characterisation by X-ray scattering techniques was used in small and wide angle range and complemented by mechanical tests, DMA, DSC and SEM. The combination of these methods is likely to provide a well-founded basis for understanding material structure. DSC is an essential extension to characterise crystallisation behaviour.

It was found that there is a strong temperature-dependent interaction of deformations within the amorphous phase and reorientations as well as transformations of crystalline units. They are strongly determined by the molecular structure as well as the processing-dependent initial morphology of the samples. According to the temperature-dependent mobility within the amorphous phase the stress transfer to the crystalline phase and so the changes within this phase are also strongly temperature-dependent.

On the other side by re-melting, stretching and re-crystallizing semi-crystalline material it is possible to get materials with highly improved mechanical behaviour due to well-defined and strongly oriented re-crystallisation. Of cause for using this general technique the parameters of treatment must be optimized.

The mechanisms found and discussed here in the case of iPP seem to be very universal. It might also apply to other polymers. This will be checked in the future by additional investigations.

The detailed understanding of the multiple deformation and structure-establishing processes is an essential base for the development of semi-crystalline materials with well-defined properties.

7. Acknowledgement

The authors are grateful to HASYLAB for beamtime within the projects II-20060086 and I-20100280 and A. Timmann, J. Perlich and M. A. Kashem for local support, and N. Stribeck (University of Hamburg) for the support in the course of data evaluation. They thank their colleagues from the IPF for support, in particular V. Körber for the construction of the tensile rig, W. Jenschke for the software support for the tensile rig, R. Boldt for SEM micrographs, R. Vogel and R. Jurk for DMA-measurements, and D. Krause for sample preparation.

8. References

Breese, D.R. & Beaucage, G. (2004). A review of modeling approaches for oriented semi-crystalline polymers, *Current Opinion in Solid State and Materials Science*, Vol. 8 (2004), pp. 439-448

Breese, D.R. & Beaucage, G. (2008). Modeling the mechanical properties of highly oriented polymer films: A fiber/gel composite theory approach, *Journal of Polymer Science: Part B: Polymer Physics*, Vol. 46, No. 6 (2008), pp. 607-618

Davies, R. J. et al. (2004). The use of Synchrotron X-ray Scattering coupled with in situ Mechanical Testing for studying Deformation and Structural change in Isotactic Polypropylene, *Colloid. Polym. Sci.,* Vol. 282 (2004), pp.854-866

Gehrke, R. et al. (1995). An ultrasmall angle scattering instrument for the DORIS-III bypass, *Rev. Sci. Instrum.* Vol. 66 (1995), pp. 1354-1356

Gibson, A.G. at al. (1978). Dynamic mechanical behaviour and longitudinal crystal thickness measurements on ultra-high modulus linear polyethylene: a quantitative model for the elastic modulus, *Polymer,* Vol. 19 (1978), pp. 683-693

Hong, K. et al. (2004). A model treating tensile deformation of semi-crystalline polymers: Quasi-static stress-strain relationship and viscous stress determined for a sample of

polyethylene. *Macromolecules,* Vol. 37, 2004, pp.10165-73 and Model treatment of tensile deformation of semicrystalline polymers: Static elastic moduli and creep parameters derived for a sample of polyethylene, *Macromolecules,* Vol. 37 (2004), pp.19174-79

Hong, K. & Strobl, G. (2006). Network stretching during tensile drawing of polyethylene: A study using X-ray scattering and microscopy, *Macromolecules* Vol.39 (2006), pp.268-273

Kumaraswamy, G. et al. (2000). Shear-Enhanced Crystallization in Isotactic Polypropylene: 2. Analysis of the formation of the Oriented 'Skin', *Polymer* Vol.41 (2000), pp.8931-8940

Kurelec, L. et al. (2005). Strain hardening modulus as a measure of environmental stress crack resistance of high density polyethylene, *Polymer,* Vol. 46 (2005), pp. 6369-6379

Lode, U. et al. (1998). Development of crazes in polycarbonate, investigated by ultra small angle X-ray scattering of synchrotron radiation, *Macromol. Rapid Commun.* Vol. 19 (1998), pp.35-39

Men, Y.M. et al. (2004). Synchrotron Ultrasmall-Angle X-ray Scattering Studies on Tensile Deformation of Poly(1-butene), *Macromolecules* Vol. 37 (2004), pp. 9481-9488

Okada, K.N. et al. (2010). Elongational crystallization of isotactic polypropylene forms nano-oriented crystals with ultra-high performance, *Polymer Journal* Vol. 42 (2010), pp.464-473

Pawlak, A. & Galeski, A. (2010). Cavitation and morphological changes in polypropylene deformed at elevated temperatures, *Journal of Polymer Science: Part B: Polymer Physics* Vol.48 (2010), pp.1271-1280

Peterlin, A. (1971). Molecular model of drawing polyethylene and polypropylene, *J. Mat. Sci.* Vol.6 (1971), pp.490-508

Roth, S.V. et al. (2003). Fatigue behaviour of industrial polymers - a microbeam small-angle X-ray scattering investigation, *J. Appl. Cryst.* Vol.36 (2003), pp.684-688

Roth, S.V. et al. (2006). Small-angle options of the upgraded ultrasmall-angle x-ray scattering beamline BW4 at HASYLAB, *Rev. Sci. Instrum.* Vol.77 (2006), 085106

Roth, S.V. et al. (2011). In situ observation of cluster formation during nanoparticle solution casting on a colloidal film, *J. Phys. Condens. Matter* Vol. 23 (2011), 254208

Schneider, K. et al. (2006). The Study of Cavitation in HDPE Using Time Resolved Synchrotron X-ray Scattering During Tensile Deformation, *Macromolecular Symposia* Vol.236 (2006), 241-248

Schneider, K. & Schöne, A. (2008). Online-structure characterisation of polymers during deformation and relaxation by Synchrotron-SAXS and WAXS, In: *Reinforced Elastomers: Fracture Mechanics, Statistical Physics and Numerical Simulations*; Kaliske, M.; Heinrich, G. & Verron, E. (Eds.); EUROMECH Colloquium 502, Dresden, 2008 pp.79-81

Schneider, K. et al. (2009). Investigation of changes in crystalline and amorphous structure during deformation of nano-reinforced semi-crystalline polymers by space-resolved synchrotron SAXS and WAXS, *Procedia Engineering* Vol.1 (2009), pp.159-162

Schneider, K. (2010). Investigation of Structural Changes in Semi-Crystalline Polymers During Deformation by Synchrotron X-Ray Scattering, *Journal of Polymer Science: Part B: Polymer Physics,* Vol.48 (2010), pp.1574-1586

Schneider, K. et al. (2011). Online structure investigation during deformation and fracture using synchrotron radiation, *Proceedings of 13. Problemseminar "Deformation und Bruchverhalten von Kunststoffen"*, CD-ROM, ISBN 978-3-86829-400-2, Halle-Merseburg, 29.6.-1.7.2011, pp. 122-130

Schroer, C.G. et al. (2006). Mapping the local nanostructure inside a specimen by tomographic small-angle x-ray scattering, *Appl. Phys. Lett.* Vol.88 (2006), 164102

Stribeck, N. (2001). Extraction of domain structure information from small-angle X-ray patterns of bulk materials, *J. Appl. Cryst.* Vol.34 (2001), pp.496-503

Stribeck, N. (2007). *X-Ray Scattering of Soft Matter*, ISBN 978-3-540-69855-5, Springer. Heidelberg, 2007

Stribeck, N. et al. (2008). Nanostructure Evolution in Polypropylene During Mechanical Testing, *Macromol. Chem. Phys.* Vol. 209 (2008), pp.1992-2002

Vonk, C.G. (1979). A small angle X-ray scattering study of polyethylene fibres, using the two-dimensional correlation function, *Colloid Polym. Sci.* Vol. 257 (1979), pp.1021-1032

Weeks, N.E. & Porter, R.S. (1974). Mechanical properties of ultra-oriented polyethylene, *Journal of Polymer Science: Part B: Polymer Physics* Vol.12 (1974), pp.635-643

Zuo, F. et al. (2005). An in Situ X-ray Structural Study of Olefin Block and Random Copolymers under Uniaxial Deformation. *Macromolecules*, Vol. 38 (2005), 3883

25

Structure of Polypropylene Fibres Coloured with Organic Pigments

Jan Broda
University of Bielsko-Biala
Poland

1. Introduction

Polypropylene is known as a versatile and valuable fibre-forming polymer material, which is widely used for the production of medical and hygienic products, carpets and floor coverings, apparel and household textiles, filtering media, agro and geotextiles, automotive interior and many other technical textiles. The wide range of goods comprises a variety of products including mono- and multifilaments, staple fibres, tapes and fibrillated fibres as well as spun-bonded and melt-blown nonwovens.

For the formation of polypropylene textiles different techniques were developed. The common method used for the formation of mono- and multifilaments is classical melt spinning.

In melt spinning, polypropylene in powder or pellet form is heated above the melting point and then is extruded through fine orifices of a spinneret into the air. Below spinneret in the air thin streams are intensively cooled and subjected to an intense stretching. During cooling the liquid streams solidify. Finally, solidified filaments are taken by final take-up device.

Formation of fibres with good properties requires proper selection of formation parameters. Changes of the particular parameters have a great impact on the fibres' structure.

The significant changes of the fibres' structure were observed right from the beginning of their production (Natta, 1961; Ross, 1965; Sheehan & Cole, 1964). It was stated that inside the fibres both, less ordered mesophase and well ordered crystalline phase can be formed.

Mesophase reveals intermediate order between amorphous and crystalline phases. In the first studies it was labelled as smectic (Natta & Corradini, 1960) or paracrystalline (Miller, 1960). Further studies revealed that mesophase is made up of bundles of parallel chains, which maintain typical for all polymorphic forms of polypropylene three-fold helical conformation. Bundles are terminated in the direction of the chain axis by helix reversals or other conformational defects (Androsch et al., 2010). In the bundles long range ordering maintains only along the chain axes, whereas in lateral packing a large amount of disorder is present (Natta & Corradini, 1960). The mesophase is formed by quenching of the molten polypropylene (Miller, 1960; Wyckoff, 1962) or by deformation of the crystalline structure (Saraf & Porter, 1988; Qiu, 2007). As for the fibres, the mesophase was observed in fibres taken at low take-up velocity (Spruiell & White, 1975; Jinan et al., 1989, Bond & Spruiell, 2001) in fibres intensively cooled in water with addition of ice or in the mixture of dry ice

and acetone (Sheehan & Cole, 1964; Choi & White, 1998; Yu & White, 1999; Choi & White, 2000), in fibres extruded at the high extrusion temperature (Dees & Spruiell, 1974) and fibres extruded from polypropylene with low molecular weight (Lu & Spruiell, 1987).

The content of the mesophase significantly decreases in fibres taken at other parameters. At certain conditions the mesophase completely disappears and inside fibres only two-phase structure, crystalline and amorphous, is formed. The high crystalline content was obtained in fibres extruded at low extrusion temperature and taken at high take-up velocities (Spruiell & White, 1975; Bond & Spruiell, 2001).

Investigations of the crystalline structure revealed that inside the fibres the crystalline phase is usually built from α crystals. The α form is one of the three known polymorphic forms of polypropylene (Brückner et al.,1991; Lotz et al., 1996). It can be easily obtained by crystallization of polymer melts or solutions. It is the most stable and the most often encountered form in different polypropylene products.

The structure of the α form was early established. Natta and Corradini (Natta & Corradini, 1960) proposed a model based on the monoclinic unit cell. According to this model, polypropylene helices of the same hand are arranged in layers parallel to the *ac* plane. Layers of isochiral helices alternate with layers formed from helices of the opposite hand. The model was commonly accepted and confirmed by subsequent studies of Mencik (Mencik, 1972), Hikosaka (Hikosaka & Seto, 1973) and Corradini (Corradini et al., 1980).

During investigations of the fibres' structure in few cases, except commonly encountered α form, crystals of β form were observed. The β form occurs rarely in the polypropylene products and its formation requires special crystallization conditions. It was revealed that the β form arises during crystallization of a sheared melt (Leugering & Kirsch, 1973), crystallization in a temperature gradient (Lovinger et al., 1977) or during crystallization in the presence of special additives (Tjong et al., 1996; Varga, J. et al. 1999; Li & Cheung, 1999; Varga, 2002). The β form was obtained in the case of fibres containing efficient β nucleating agents and extruded at appropriately selected spinning parameters (Yu & White, 2001; Takahashi, 2002).

The β form exhibits complex structure and during the years different models characterizing this structure were proposed. Finally, the arrangement of the β form was discovered only several decades after its initial observation. It was shown that the β form consists of the characteristic left-handed or right-handed helices arranged in the original packing schemes. Lotz (Lotz at al, 1994) and Meille (Meille at al., 1994) proposed a model of the frustrated structure based on a trigonal cell containing three isochiral helices.

The structure of fibres is formed during the crystallisation, which occurs below spinneret orifices, in the cooling zone, by solidification of the extruded stream. The crystallization rate is comparable to the cooling rate of the polypropylene in the spinning line. Therefore, the formation of crystalline structure in the melt-spinning process depends strongly on the spinning conditions and polymer characteristics.

During the formation of fibres the crystallization takes place in non-isothermal conditions in the field of high tensile stress. Cooling rate and tensile stress strongly affect polypropylene crystallization.

During formation at low take-up velocities the cooling rate plays the dominant role. At low take-up velocity the cooling rate and the applied tensile stress are low. The crystallization proceeds at relatively high temperatures and in the as-spun fibres monoclinic α crystals are formed. When take-up velocity is increased the cooling rate is enhanced. Simultaneously, the crystallization temperature decreases. By crystallization in such conditions the structure with high mesophase content is formed. Further increase of take-up velocity leads to an increase of the tensile stress. Consequently, the molecular orientation of polypropylene chains increases significantly. At higher molecular orientation the crystallisation temperature increases. The crystallisation rate rapidly increases and the crystal structure with highly oriented monoclinic crystals is formed.

2. Dyeing of polypropylene fibres

Polypropylene fibres are highly crystalline and show extremely low wettability. Due to the aliphatic structure of the polypropylene chain fibres have no polar groups and no dye sites capable of reacting permanently with dye molecules. Therefore, polypropylene fibres cannot be coloured by bath methods commonly used for the coloration of other natural and synthetic fibres. Over the years many efforts were undertaken for improving the fibres' dyeability. Various methods include copolymerizing with other monomers, grafting of dye sites, adding dyeable polymers before fibres spinning, adding dyeable filaments before fibre processing, dissolving or dispersing additives of low molecular weight in the polymer melt, treating to modify the surface of fibres after extrusion or adding halogen compounds (Zhu & Yang, 2007). All mentioned techniques have not found broader commercial application. The mainstream technique for the coloration polypropylene fibres consists of using pigments. Despite of its disadvantages, low flexibility and suitability only for a large-scale manufacturing coloration with pigments has a great importance. The most coloured polypropylene textiles are made from fibres coloured this way.

Pigments used for the fibres coloration must be finely dispersed and stable to the thermal conditions and environment applied in fibres formation. Most of the pigments reveal tendency to agglomerate and form large aggregates, which clog the spinneret orifices and spoil the fibres properties. To avoid spinning problems, fine dispersed pigment concentrates, so called masterbatches, are commonly used. Pigment concentrates are made from previously dispersed pigments mixed with polypropylene resin at high pigment concentration. The concentrates are usually mixed in a proper ratio with polymer granulate or powder. Some concentrates are injected directly into the polypropylene melt during fibre formation.

For the coloration of polypropylene fibres inorganic and organic pigments are used. Most inorganic pigments reveal low to moderate colour strength combined with good to excellent thermal stability, lightfastness and weather resistance. Inorganic pigments are easily dispersible. For polypropylene coloration inorganic pigments for black and white colours are mostly applied. For this purpose carbon black and titanium dioxide white pigment based on the rutile modification are used.

Coloration effects are usually achieved with organic pigments. Organic pigments provide high colour strength and high light stability. Some pigments heave negative influence on the efficiency of light stabilizers and limited heat resistance. By reason of above mentioned negative influence only selected groups of pigments can be used. In the literature the

following groups of pigments are usually mentioned: azo pigments, isoidolinones, perylene, anthraquinone, quinacridone and phthalocyanine.

During mass coloration pigments are mixed physically with the polypropylene melt in the barrel of the extruder.

It is well known that impurities and foreign substances present in crystallizing polymer strongly affect its crystallisation. Impurities provide a foreign surface, what reduces free energy of the formation of primary nuclei and significantly reduces their critical dimensions. As a result of the formation of heterogeneous nuclei the nucleation density in the crystallizing melt significantly increases. Consequently, the crystallisation temperature is higher and the crystallisation rate rapidly increases.

On the basis of investigations of nucleating ability of many compounds Binsbergen revealed that good nucleating agents are insoluble in the polypropylene melt or crystallize earlier at higher temperature prior polypropylene crystallisation (Binsbergen, 1970). Pigments have such desired properties and fulfil requirements for good nucleating agents of polypropylene. The most pigments form stable crystals, which are insoluble in the polypropylene melt. The rough surface of pigments crystals enables the epitaxial growth of polypropylene crystals. The various geometries of the contact surface can lead to the formation of the different polypropylene modifications.

3. Nucleating ability of phthalocyanine and quinacridone pigments

The nucleating ability toward polypropylene crystallisation for some pigments was investigated and the efficient ability of quinacridone and phthlacyanine was revealed (Broda, 2003a). The investigation were performed in non-isothermal conditions by polarizing microscopy and differential scanning calorimetry (DSC).

Phthalocyanine and quinacridone belong to organic pigments, which are commonly used for the coloration of polypropylene fibres. The chemical formulae of pigments are presented in Figure 1.

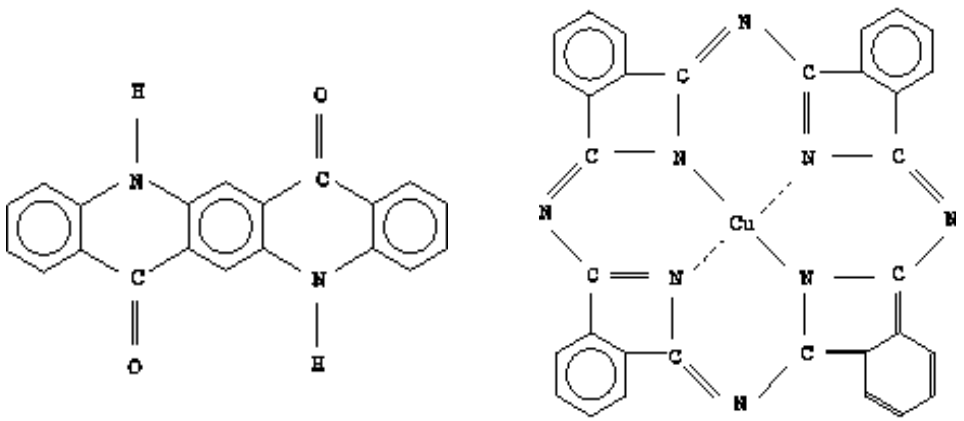

a) b)

Fig. 1. Chemical formulae of: a) quinacridone, b)phthalocyanine blue

The blue phthalocyanine pigment (Pigment Blue 15, C.I.74160) is built of a tetrabenzoporphyrazine nucleus with a central copper atom. The molecule assumes a planar conformation and possesses a square shape with a side length of 1.3 nm. The red quinacridone pigment (Pigment Violet 19, C.I.73900) belongs to deeply colored pigments characterized by a relatively small molecular size. The molecule of dimensions 1.406 x 0.52 nm is formed from five heterocyclic rings. The molecule is planar with no significant departure of the carbonyl groups from a molecular plane defined by all nonhydrogen atoms.

Both pigments added to quiescent melt accelerate polypropylene crystallization. In the presence of pigments the crystallization temperature moves toward higher temperature. The increase of the crystallization temperature for phthalocyanine and quinacridone pigment is 13 K and 14.5 K, respectively (Broda et al., 2007). Such increase of the crystallization temperature is very high and comparable with the increase observed for effective nucleating agents. In the presence of pigments the nucleation density significantly increases. Consequently, the overall crystallization rate is enhanced and, as a result, fine spherulitic structure is formed.

The nucleating ability of both pigments results from their crystalline structure. Both pigments form fine dispersed crystals, which have very high thermal stability. The degradation temperature of phthalocyanine and quinacridone pigments is higher then 400 and 500 °C, respectively, what considerably exceeds the melting temperature of polypropylene.

The surface structure of pigments crystals enables the epitaxial growth of the polypropylene.

In crystals of the quinacridone pigment planar molecules are arranged in parallel stacks, with the molecule tilted to the stacking direction. The neighboring stacks adopt a herringbone arrangement. In crystals each molecule is bonded through hydrogen bonds to four adjacent molecules. Very strong intermolecular hydrogen bonds combined with strong van der Waals' forces ensure quinacridone pigments the high heat and chemical resistance.

Seven different crystalline forms of quinacridone are known (Filho & Oliveira 1992; Potts et al. 1994, Lincke, 2000). Most synthetic methods lead to the formation of an unstable α form. Subsequent treatments lead to the more stable β and γ forms, most commonly used as commercial pigments.

In the investigations the γ form of the quinacridone pigment was used. For years this modification has been known as a very efficient nucleating agent for the β form of polypropylene (Leugering, 1967; Moos & Tilger, 1981). Stocker and co-workers showed that the *β* form of polypropylene grows epitaxially on the surface of the γ crystals of the quinacridone pigment (Stocker et al., 1998). The epitaxy involves the (110) plane of the trigonal unit cell of the polypropylene, which contacts the *bc* surface of the γ crystals of the quinacridone.

Hydrogen atoms of stacked benzene rings form on the surface *bc* of the γ quinacridone crystals a parallel array of bulges and grooves. The spacing between grooves 0.65 nm is close to the axis repeat distance of the polypropylene helix. The arrangement of polypropylene chains on the pigment surface perpendicularly to the parallel grooves ensures nearly perfect matching of the above-mentioned dimensions and in this way enables the epitaxial growth of β crystals.

The formation of the β form is confirmed by WAXS measurements. In the WAXS pattern of polypropylene crystallized by addition of the quinacridone pigment characteristic β peaks are observed (Fig.2).

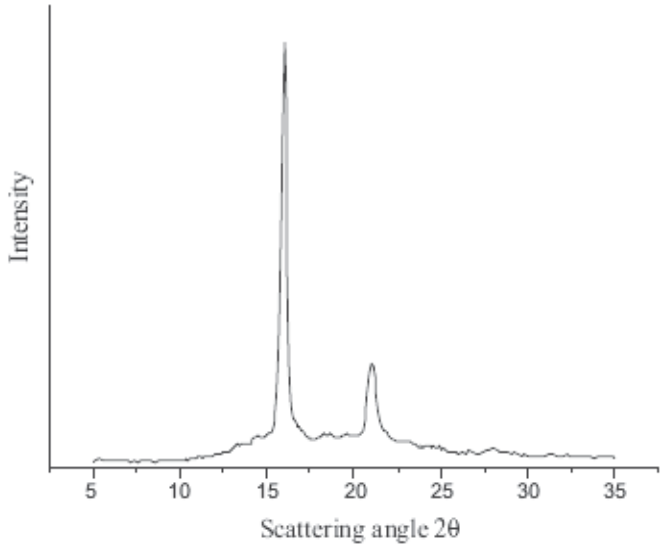

Fig. 2. WAXS pattern of polypropylene crystallized in the presence quinacridone pigment.

In crystals of the copper phthalocyanine fairly rigid molecules can be packed in different arrangements giving rise to different polymorphs. In literature ten different polymorphic forms of copper phthalocyanine are described (Erk & Hengelsberg, 2003). From all polymorphic forms commercial interest exhibits the first recognized α form and the most thermodynamically stable β form.

Each polymorphic form of phthalocyanine is built from molecules arranged in uniform stacks with rings tilted with respect to the stacking direction. For the α and β forms the molecules are tilted in stacks with respect to the stacking direction by 25° and 46°, respectively.

The interactions between molecules within stacks are mainly defined by π-π interactions. The interplanar distance between adjacent molecules is consistent with a van der Waals bond and equals 0.34 nm. In the β modification neighboring stacks are arranged in a herringbone style. In the α form the herringbone interactions are not present.

Crystals of phthalocyanine tend to form needles or rods parallel to the stacking direction. The side faces of crystals are mainly covered by aromatic hydrogen atoms, while the basal faces expose the π system and the copper atom. The lateral surfaces exhibit nonpolar character, while the basal surfaces have relatively polar character.

The aromatic hydrogen atoms occurring on the lateral surfaces of the pigments crystals are arranged in parallel rows. The shallow nonpolar grooves formed between such rows force polypropylene molecules to assume a stretched conformation over some distance, making the nucleation much easier (Binsbergen, 1970).

The investigated α form of phthalocyanine promotes mostly formation of the α form of polypropylene. On the wide-angle X-ray scattering (WAXS) pattern for polypropylene crystallized in the presence of phthalcoyanine pigment, crystalline peaks characteristic for the α form are observed (Fig.3).

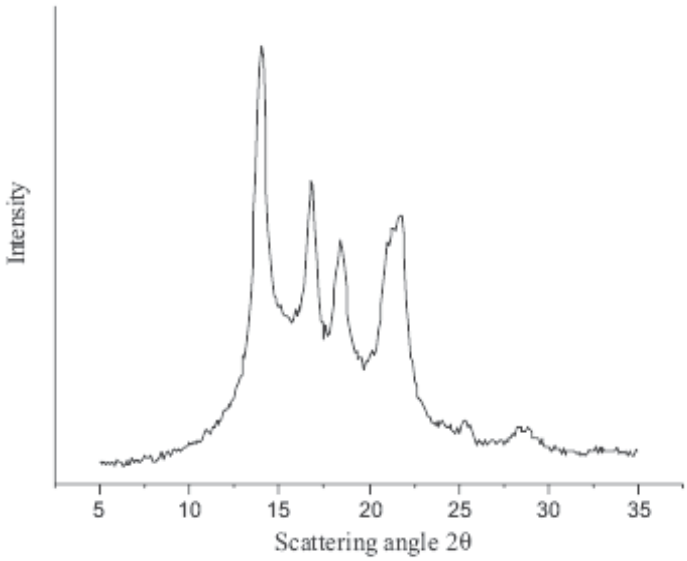

Fig. 3. WAXS pattern of polypropylene crystallized in the presence phthalocyanine pigment.

4. Structure of coloured fibres

The investigations of morphology and structure of coloured fibres were carried out. The morphology of fibres was investigated for samples sputtered with gold by scanning electron microscopy (SEM). The fibres structure was studied by the wide angle X-ray scattering (WAXS) and small angle X-ray scattering (SAXS) methods.

During formation of fibres coloured with pigments the structure containing crystalline, mesophase and amorphous phases is formed. Content of particular phases changes across a broad range depending on formation parameters.

4.1 Structure of fibres coloured with quinacridone pigment

Table 1 presents structural parameters determined on the basis of WAXS patterns for fibres coloured with quinacridone pigment.

For fibres taken at very low velocity 100 m/min the high crystalline structure without mesophase is formed. The structure consists mainly from β crystals with admixture of a small amount of α crystals.

The content of β form is usually characterised by the K value, which is determined as a ratio of the intensity of the $(300)_\beta$ peak to the sum of intensities of the $(110)_\alpha$, $(040)_\alpha$, $(130)_\alpha$ and $(300)_\beta$ peaks on the WAXS patterns (Turner Jones, 1964).

Extrusion temperature [°C]	Take-up velocity [m/min]	Crystallinity index	K value
210	100	0.54	0.95
	200	0.52	0.47
	300	0.51	0.09
	400	0.51	0.03
	880	0.51	0.03
	1050	0.52	0.03
	1350	0.52	-
250	100	0.51	0.93
	200	0.51	0.33
	300	0.50	0.08
	400	0.51	-
	880	0.52	-
	1050	0.52	-
	1350	0.52	-

Table 1. Structural parameters of fibres coloured with quinacridone pigment

In fibres the relatively high amount of β crystals is formed already at low pigment concentration. For fibres containing 0.1% of pigment the K value achieves relatively high value of 0.76. With the increase of the pigment concentration until 0.5% the β form content successively increases. For the pigment concentration of 0.3% and 0.5% the *K* value grows to 0.89 and 0.95, respectively. Similar high K value is observed for different extrusion temperature, 210, 225 and 250 °C (Broda, 2004c).

The K value observed in fibres coloured with quinacridone pigment is comparable to the value obtained during crystallization of polypropylene melt in quiescent conditions in the presence of very effective β nucleating agents.

The appearance of β crystals in the coloured fibres taken at low velocity is a result of the ability of quinacridone pigment to nucleate β modification of polypropylene and appropriate crystallisation conditions. During formation of fibres at low take-up velocity the crystallisation occurs at low cooling rate and low molecular orientation. In these conditions, during solidification of fibres, pigment takes part in the nucleation process. The crystallisation proceeds on heterogeneous nuclei produced with the participation of pigments. As a result of the crystallisation fine spherulitic structure is formed (Fig.4) (Broda, 2003c).

The low cooling rate favours the formation of the β form of polypropylene (Huang et al., 1995). The crystallization process starts at the relatively high temperature, above the lower critical temperature for the formation of the β modification (Lovinger et al., 1977). As a result of the epitaxial growth on the surface of quinacridone crystals, the crystals of β modification are formed. At this temperature, the growth rate of β crystals exceeds the growth rate of α crystals (Varga, 1989). The β nuclei formed on the surface of pigment crystals quickly grow forming the high amount of β crystals.

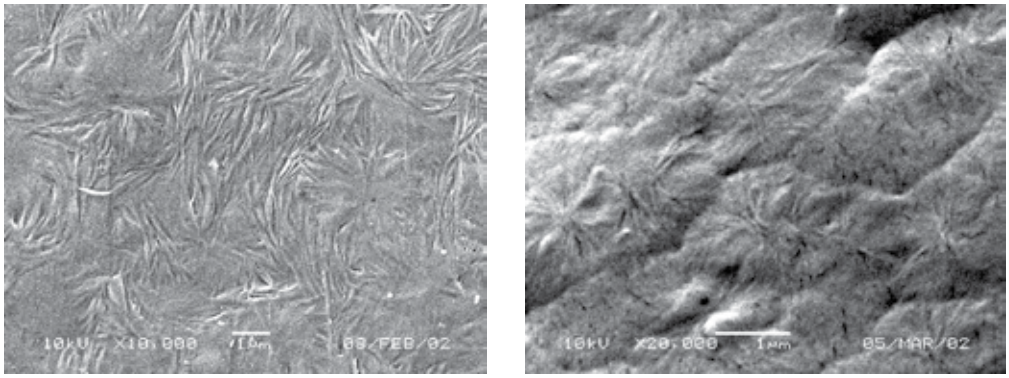

a) b)

Fig. 4. Spherulitic structure of fibres coloured with quinacridone taken at very low velocity: a) gravity spun ; b)100 m/min.

In the fibres taken at higher velocities the crystalline structure changes. With the increase of the take-up velocity the content of the β form rapidly decreases. For fibres extruded at 210°C taken at 200 m/min and 300 m/min the K value decreases to 0.47 and 0.09, respectively. For the fibres extruded at higher melt temperature 250 °C the decrease of the β form content is even higher. For fibres taken at 200 m/min and 300 m/min the K value drops to 0.33 and 0.08. In the same time the content of the α form increases and the crystallinity index does not change significantly.

The increase in take-up velocity and the extrusion temperature results in the increase of the cooling rate. Consequently, the crystallization temperature moves toward lower values. The crystallization starts at lower temperature and then quickly, by further cooling, moves below the critical temperature for the formation of β crystals. Then, the smaller part of the material crystallizes at conditions favourable for the formation of the β form. At the beginning of the crystallization process β crystals are formed. During crystallization temperature decreases into the range below the critical temperature and remaining crystallisable material crystallizes at a lower temperature, forming α crystals.

In temperature below the low critical temperature the growth rate of α crystals is higher than the growth rate of *β* crystals (Fillon et al., 1993). Then α nuclei grow quickly, while the growth of the *β* nuclei is strongly constrained.

With the increase in take-up velocity, the temperature is lower and lower, and less and less material can crystallize at a temperature above the critical temperature for the formation of β crystals. With the increasing take-up velocity more and more material crystallize at lower temperatures and β form content decreases.

For the fibres taken at medium velocities, from 400 to 1050 m/min only the minimal content of β crystals is formed. The crystalline structure is built almost exclusively from the α crystals. In the fibres produced without pigments at the same conditions the high mesophase content was observed (Broda, 2004a). This fact suggests that at medium take-up velocities the quinacridone pigment induces the formation of α crystals. The investigations of Rybnikar (Rybnikar, 1991) and Mathieu (Mathieu et al., 2002) showed that *γ* quinacridone reveals a versatile nucleating ability and may induce either α or *β* modification of

polypropylene. The versatile nucleating ability of the quinacridone pigment results from the fact that the spacing between the grooves on the *bc* surface of γ crystal is similar as well to the interchain distance of the isochiral helices in the (010) plane of the α form of polypropylene. By the arrangement of polypropylene helices parallel to the grooves the nearly perfect match between above-mentioned dimensions may be achieved and the epitaxial growth of α crystals may be initiated.

By further increase of the take-up velocity the structure with the high content of well oriented α crystals is formed. It is know that during formation of fibres at high velocities the molecular orientation has a great influence on the polymer crystallization. Under high molecular orientation certain chain segments become aligned. Bundles of aligned segments form so called row nuclei, which initiate lamellae growth in the perpendicular direction. At high velocities a big number of row nuclei is formed. In this condition the heterogeneous nucleation on pigments loses its importance. The nucleation proceeds without the participation of pigments. Crystals of pigment do not participate in the formation of row nuclei and do not disturb their formation. Relatively small amount of pigment does not affect the mobility of polypropylene chains and does not influence the growth of polypropylene crystals. The growing polypropylene crystals push out pigment outside crystals to the amorphous regions.

The crystallisation in coloured fibres occurs at the same rate and at the same temperature as in non-coloured fibres. The lamellar crystals formed on the row nuclei alternate with the amorphous areas forming fibrillar structure (Broda, 2004b). The long period for coloured fibres determined on Small Angle X-Ray Scattering (SAXS) measurements equals 10.6 nm and has the similar value as in the case of non-coloured fibres (Broda, 2003b).

4.2 Structure of fibres coloured with phthalocyanine pigment

The values of the crystallinity index and K value for fibres coloured with phthalocyanine pigment calculated on the basis of WAXS measurements are presented in Table 2.

Extrusion temperature [°C]	Take-up velocity [m/min]	Crystallinity index	K value
210	100	0.57	0.31
	200	0.56	0.14
	300	0.53	-
	400	0.51	-
	880	0.42	-
	1050	0.43	-
	1350	0.52	-
250	100	0.54	0.29
	200	0.52	0.09
	300	0.44	-
	400	0.40	-
	880	0.36	-
	1050	0.31	-
	1350	0.36	-

Table 2. Structural parameters of fibres coloured with phthalocyanine pigment

For fibres taken at low take-up velocity 100 m/min the high crystalline structure is formed. The cristallinity index reaches high value of 0.57. The crystalline structure is built mainly from α crystals with an addition of β crystals. The content of the β crystals characterised by the K value equals 0.31.

Similarly as for fibres coloured with quinacridone at low take-up velocity, phthalocyanine participates in the nucleation process. The crystallisation starts on heterogenous nuclei formed on the crystals surface. The numerous nuclei grow forming fine spherulitic structure.

Phthalocynine is known as efficient nucleating agent of the α form of polypropylene. The high crystalline structure of the fibres results from its high nucleation ability. Appearance of the small number of β crystals is surprising.

The ability to nucleate β crystals can be explained by the surface geometry of phthalocyanine crystals. For α modification of the phthalocyanine the distance between grooves on the lateral surfaces equals 1.19 nm (Honigmann et al. 1965). This dimension is comparable with the spacing of 1.1 nm between helices of the same hand in the trigonal cell of the β form of polypropylene.

The compatibility of these dimensions is responsible for a good nucleating ability toward the β form of several calcium dicarboxylates (Li et al., 2002) and may also explain the formation of a certain amount of β crystals in fibres coloured with phthalocyanine.

With the increase of the take-up the content of β crystals rapidly decreases. For fibres taken at take-up velocity 200 m/min and extruded at 210 °C and 250 °C the *K* value drops to 0.14 and 0,09, respectively. At higher velocities β crystals are not observed.

At higher cooling rates the crystallization conditions for formation of the *β* form are less favorable. On the surface of the phthalocyanine pigment only α nuclei are formed. The growth of nuclei leads to formation of the high crystalline structure built only from α crystals.

Similarly to fibres coloured with quinacridone at high take-up velocity above 1000 m/min, pigment does not participate in the nucleation process. In these conditions, under high molecular orientation numerous row nuclei are formed. Row nuclei quickly grow forming well oriented lamellar α crystals. In fibres the fibrillar structure is formed (Fig.5)

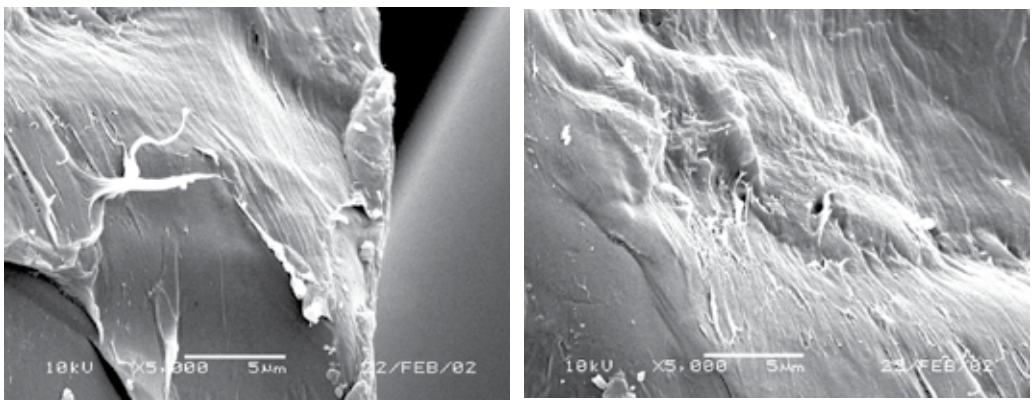

Fig. 5. Fibrillar structure in fibres coloured with phthalocyanine taken at 1350 m/min.

4.3 Structure of fibres coloured with the mixture of quinaridone and phthalocyanine pigments

Mixing of pigments is the common procedure for achieving different colour effects. By mixing of qunacridone and pthtalocyanine two pigments with different efficient nucleating ability toward polypropylene crystallisation are introduced. One can expect that by mixing of both pigments a competition between formation of α and β nuclei will be observed. Such competition, together with a different growth rate of both forms, should lead to formation of a structure with different constitution.

Table 3 presents structural parameters determined on the WAXS measurements for fibres coloured with the 1:1 mixture of quinacridone and phthalocyanine.

Take-up velocity [m/min]	Crystallinity index -	K value -
100	0.53	0.75
200	0.53	0.52
300	0.53	0.14
400	0.51	0.05
880	0.52	0.04
1050	0.51	-
1350	0.52	-

Table 3. Structural parameters of fibres coloured with the mixture of quinaridone and phthalocyanine pigments

At the lowest velocity 100 m/min inside fibres the crystalline structure consisting of both polymorphic modifications is formed. The K value equals 0.75. The content of β crystals is much higher than the content of α crystals. Nevertheless, the content of the β form is much lower in comparison to fibres coloured with quinacridone alone, but significantly greater in comparison to fibres coloured with phthalocyanine (Broda, 2003d).

In fibres taken at very low velocities pigments participate in the formation of the crystallization nuclei. By coloration with the mixture of pigments, both pigments reveal their nucleating activity. On the surface of the quinacridone the β nuclei, while on the surface of phthalocyanine crystals the α nuclei, are formed.

Different content of both modifications in the fibres may be caused by a different number of produced nuclei and/or different rate of crystals growth.

By even proportion of both pigments and their similar dispersion one can assume that the number of the quinacridone crystals equals the number of the phthalocyanine crystals. Both pigments reveal their nucleating activity at similar temperature and formation of α and β nuclei occurs at similar conditions. Taken into account the above mentioned statements, there is no indication of significantly greater number of the β nuclei. The higher content of the β crystals in the fibres coloured with the mixture of pigments have to result from the higher rate of crystals growth.

During formation of fibres at low velocity the crystallization occurs at high temperature. The crystallization temperature exceeds the critical temperature for the formation of the β form. In temperature above critical, the growth rate of the β form crystals exceeds the growth rate of the α crystals (Lovinger et al., 1977). Due to higher growth rate, the β crystals grow quicker and even by equal number of both nuclei form the structure with the high content of the β form crystals.

For fibres formed at higher velocities the crystallization conditions prefer the formation of the α form crystals. Similarly as for fibres coloured with quinacridone, the content of the β form rapidly decreases.

Similarly as for fibres coloured with particular pigments at high velocities, the mechanism of the nucleation changes. The crystallization proceeds without pigments on row nuclei formed under high molecular orientation. As a result, in all fibres the structure consisting of the α modification characterized by the same crystallinity index and the same lamellar thickness is produced.

5. Influence of processing on the structure of polypropylene fibres coloured with quinacridone pigment

To achieve final properties, as-spun fibres obtained by the spinning line are usually submitted to further processing. During processing the fibres structure formed by spinning undergoes further transformation. Heat stabilisation and drawing are of a great importance. Both treatments strongly affect the structure of the fibres and their final properties.

During heat stabilisation of as-spun fibres coloured with quinacridone pigment the less thermodynamically stable β crystals transform into α crystals.

In the case of fibres extruded at the lowest velocity exhibiting the highest amount of β crystals the first changes of the content of β form are observed at heating at 140°C. The amount of β crystals decreases already after 3 minutes of stabilization. For longer time decrease of the β form content is more pronounced. The K value decreases from 0.95 for not stabilized fibres to 0.63 for fibres stabilized for 5 minutes. After a very long time the high amount of β crystals remains unchanged. For the fibres stabilized at higher temperatures, in the range 140–148°C, the β form content gradually decreases with the increment of the stabilization temperature. The content of the β form decreases quickly during the first minutes of heating. For longer times of heating (up to 10 min) further changes of the β form content are less meaningful. After certain time the β→α transition stops. Despite the long time of stabilization the content of β crystals does not change. During stabilization at 150°C a rapid drop of the β form content is observed already after 3 minutes of heating. In this time the K value drops to 0.1. Then, after 10 minutes the β crystals disappear (Broda, 2004d).

The transition of the polymorphic forms of polypropylene was observed many times. It was stated that the β→α transition is not reversible and occurs in the temperature range of 130 to 150°C (Forgacs et al., 1981; Varga, 1995). For years several mechanisms of the transition have been proposed. Garbarczyk suggested that the β→α transition proceeds in a solid state in three intermediate stages based on rotations and translations of polypropylene chains (Garbarczyk, 1985, 1989). Due to considerable differences in unit cells of both modifications, Samuels stated that the β→α transition must take via the liquid phase (Samuels & Yee,

1972). The investigations of Vleeshouwers confirmed that the transition is connected to the melting of β crystals (Vleeshouwers, 1997). Zhou proved that the melting of β crystals occurs partially, starting from the less perfect crystals possessing the lowest melting temperature (Zhou et al., 1986). Rybnikar suggested that new α crystals are formed on the lateral faces of the remaining thickened β lamellae by regular, probably epitaxial, overgrowth (Rybnikar, 1991). Varga and Fillon stated that the transition can be attributed to the formation of α nuclei within the β crystals during secondary crystallization at temperatures below 100°C (Varga, 1986; Fillon et al., 1993).

Taking into consideration the above mentioned statements, one can conclude that the changes of the β form content in fibres with quinacridone results from the melting of β crystals and their recrystallisation into α crystals. At temperatures near 140°C only a small fraction of the less perfect β crystals is melted. After the melting of such crystallites the transition stops in spite of the long time of stabilization. At higher temperatures, closer to the melting point of β crystals the greater part of the β lamellae is melted and the transition proceeds further. At 150°C, the temperature above the melting temperature of β crystals, all β lamellae melt and recrystallize, forming α crystals. At this temperature the β→α transition is completed within few minutes.

The changes, which occur in the fibres' structure during drawing depend on drawing temperature. During drawing at room temperature the crystalline structure with the high content of β crystals transforms into mesophase. The significant changes are observed already at draw ratio of 2. At this draw ratio the β form content drops to half of the value for undrawn fibres. With the increase of the draw ratio the transition from crystalline structure to mesophase proceeds further and the content of the β form gradually decreases. At draw ratio of 7 all crystalline structure transforms into mesophase and β crystals disappear.

During drawing at 120°C the gradual transition from β form to α form is observed. As a consequence the β form content in fibres gradually decreases. At draw ratio of 2 the *K*-value drops to 0.45. At higher draw ratios of 3 and 5 it drops to 0.07.

The transition of β crystals into mesophase generated by drawing at room temperature results from pulling polypropylene chains from the lamellar crystals (Ran et al. 2001). As a result, partial destruction of the crystals is observed. Due to limited molecular mobility at room temperature, chains pulled from the crystals aggregate into bundles with no specific arrangement of helical hands. Such bundles, representing a collection of helical segments with a random assembly of helical hands, form the mesophase. At low draw ratios only a few chains are pulled out from the crystals. At higher draw ratios the number of pulled chains increases. Consequently, the β form content in drawn fibres gradually decreases, while the mesophase content increases. At higher draw ratios, the regular lamellar structure of β crystals is completely destroyed and the β form disappears.

During drawing at 120°C chains pulled out from polypropylene crystals posses much higher mobility and may form assemblies ready to crystallize into well ordered α form crystals.

6. Conclusions

Organic pigments commonly used for the coloration of polypropylene fibres exhibit nucleating ability toward polypropylene crystallisation. The rough surface of pigments'

crystals enables epitaxial growth of polypropylene. The various geometry of the surface of pigments' crystals ensures matching of polypropylene chains in different way, what leads to the formation of different polymorphic forms of polypropylene. The red quinacridone pigment promotes mainly formation of the β form crystals. On the contrary the blue phthalocynine pigment enables growth of α crystals.

During fibres coloration pigments are added to the polypropylene granulate and mixed with the polypropylene melt. Presence of insoluble pigments' crystals effect the polypropylene crystallisation. The influence of pigments on the structure of fibres reveals at the lowest take-up velocity. Then, pigments participate in the nucleation process. For fibres coloured with quinacridone almost only β crystals are formed. For fibres coloured with phathalocynine the formation of the high crystalline structure containing α crystals with the addition of the small amount of β crystals is observed. For fibres coloured with the mixture of both pigments the structure with α and β crystals is produced.

For higher velocities the cooling rate increases and the crystallisation conditions favour formation of the α form crystals. As a result in fibres coloured with pigments the β form content rapidly decreases.

By further increment of the take-up velocity the nucleation ability of pigments does not influence the polypropylene crystallisation. Inside fibres under high molecular orientation numerous row nuclei are formed. The crystallisation proceeds on row nuclei without pigments.

By processing of fibres with high content of β form crystals transitions: β→α and β→mesophase are observed. The direction and range of transition depends on the processing parameters.

7. References

Androsch. R. et al. (2010). Mesophases in polyethylene, polypropylene, and poly(1-butene). *Polymer,* Vol.51, Issue 21, pp. 4639-4662.

Binsbergen, F. L. (1970). Heterogeneous nucleation in crystallization of polyolefins. I. Chemical and physical nature of nucleating agents. *Polymer* , Vol.11, Issue 5, pp. 253-267.

Bond, E.B. & Spruiell, J.E. (2001). Melt spinning of metallocene catalyzed polypropylenes. I. On-line measurements and their interpretation. *J.Appl.Polym.Sci.,*Vol. 82, Issue 13, pp. 3223-3236.

Broda, J. (2003a). Nucleating activity of the quinacridone and phthalocyanine pigments in polypropylene crystallization. *J.Appl.Polym.Sci.,* Vol.90, Issue 14, pp. 3957-3964.

Broda, J. (2003b). Polymorphism in Polypropylene Fibres. *J.Appl.Polym.Sci.,* Vol. 89 , Issue 12, pp. 3364-3370.

Broda, J. (2003c). Morphology of the noncoloured and coloured polypropylene fibers. *Polymer,* Vol.44, Issue 5, pp. 1619-1629.

Broda, J. (2003d). Structure of polypropylene fibres coloured with a mixture of pigments with different nucleating ability. *Polymer* Vol.44 , Issue 22, pp 6943-6949.

Broda, J. (2004a). WAXS Investigations of The Mass Coloured Polypropylene Fibers. *Fibres and Textiles in Eastern Europe,* Vol.11, pp. 95

Broda, J. (2004b). SEM Studies of Polypropylene Fibres Coloured with Quinacridone Pigment, *Microscopy and Analysis,* Vol. 91, Issue 5, pp. 5-6.

Broda, J. (2004c). Polymorphic composition of colored polypropylene fibers. *Crystal Growth & Design*, Vol.4, Issue 6, pp. 1277- 1282.

Broda, J. (2004d). Influence of Processing on Structure of β-Nucleated Poly(propylene) Fibers. *J. Appl. Polym. Sci.,* Vol.91, Issue 3, pp. 1413-1418.

Broda, J. (2007). The influence of additives on the structure of polypropylene fibres. *Dyes & Pigment,* Vol.74, Issue 3, pp. 508-511.

Brückner, S. et al. (1991). Polymorphism in isotactic polypropylene. *Prog Polym. Sci.* Vol.16, Issue 2-3, pp. 361-404.

Choi, C.H. & White, J.L. (1998). Comparative study of structure development in melt spinning polyolefin fibers. *Intern.Polym.Proc.,* Vol.13, Issue 1, pp. 78-87.

Choi, D. & White, J.L. (2000). Structure development in melt spinning syndiotactic polypropylene and comparison to isotactic polypropylene. *Intern.Polym.Proc.*, Vol.15, Issue 4, pp. 398-405.

Corradini, P. et al. (1980). Structural variations in crystalline isotactic polypropylene (alpha-form) as a function of thermal treatments. *Gazz.Chim.Ital.,* Vol.110, Issue 7-8, pp.413-418.

Dees, J.R. & Spruiell, J.E. (1974). Structure development during melt spinning of linear polyethylene fibers. *J.Appl.Polym.Sci.,* Vol. 18, Issue , Issue 4, pp.1053-1078.

Erk, P. & Hengelsberg, H. (2003). Phthalocyanine Dyes and Pigment, In *The Porphyrin Handbook*; Kadish, K. M., Smith, K. M., Gulard, R., pp 106-149, Academic Press, ISBN 10: 0-12-393201-7, Amsterdam.

Filho, D. S. & Oliveira, C. M. F. (1992). Crystalline modifications of linear trans-quinacridone pigments. *J. Mater. Sci.,* Vol. 27, pp. 5101-5107.

Fillon, B. et al. (1993). Self-nucleation and recrystallization of polymers. Isotactic polypropylene, β phase: β-α conversion and β-α growth transitions. *J. Polym.Sci. Part B. Polym. Phys.*, Vol. 31, Issue 10, 1407-1424.

Forgacs, P. et al. (1981). Study of the beta-alpha solid-solid transition of isotactic polypopylene by synchrotron radiation. *Polymer Bulletin*, Vol. 6, Issue 1-2, pp. 127-133.

Garbarczyk, J. (1985). A study on the mechanism of polymorphic transition beta-alpha in isotactic polypropylene. *Makromol Chem.* , Vol. 186, Issue 10, pp.2145-2151.

Garbarczyk, J. et al (1989). Influence of additives on the structure and properties of polymers .4. study of phase-transition in isotactic polypropylene by synchrotron. *Polym. Commun.*, Vol. 30, Issue 5, pp.153-157.

Hikosaka, M. & Seto, T. (1973). Order of molecular chains in isotactic polypropylene crystals. *Polym.J.,* Vol.5, Issue 2, pp.111-127.

Honigmann, B. Et al.(1965). Beziehungen zwischen den strukturen der modifikationen des platin- und kupferphthalocyanins und einiger chlorderivate . *Z. Kristallogr.* Vol.122, Issue 3-4, pp. 185-205.

Huang, M. R. et al. (1995). β nucleators and β crystalline form of isotactic polypropylene. *J. Appl. Polym. Sci.,* Vol 56, Issue 10, pp. 1323-1337.

Jinan, C.; et al. (1989). Nonisothermal orientation-induced crystallization in melt spinning of polypropylene. *J. Appl.Polym. Sci.*, Vol. 37, Issue 9, pp. 2683-2697.

Leugering, H. J. (1967). Einfluß der kristallstruktur und der überstruktur auf einige eigenschaften von polypropylen. *Makromol. Chem.* Vol. *109*, Issue 1, pp.204-216.

Leugering, H. J.& Kirsch, G.(1973). Effect of crystallization from oriented melts on crystal-structure of isotactic polypropylene . *Angew. Makromol. Chem.*, Vol.*33*, Issue OCT, pp. 17-23.

Li, J. X. & Cheung, W. L. (1999). Conversion of growth and recrystallisation of *β*-phase in doped iPP. *Polymer*, Vol.40, Issue 8, pp. 2085-2088.

Li, X. et al. (2002). Calcium dicarboxylates nucleation of β-polypropylene. *J.Appl.Polym.Sci.* , Vol. 86, Issue 3, pp. 633-638.

Lincke, G. (2000). A review of thirty years of research on quinacridones. X-ray crystallography and crystal engineering. *Dyes Pigm.,* Vol.44, Issue 2, pp.101-122.

Lotz, B. et al. (1996). Structure and morphology of poly(propylenes): A molecular analysis *Polymer,* Vol. 37, Issue 22, pp. 4979-4992.

Lotz, B. et al. (1994). An original crystal-structure of polymers with ternary helices *Comptes rendus de l academie des sciences serie II,* Vol.319. Issue 2, pp.187-192.

Lovinger, A. J. et al. (1977). Studies on the α and β forms of isotactic olypropylene by crystallization in a temperature gradient. *J. Polym. Sci.Polym. Phys. Ed.,* Vol. 15, Issue 4, pp. 641-656.

Lu, F.M. & Spruiell, J.E. (1987). The influence of resin characteristics on the high speed melt spinning of isotactic polypropylene. I. Effect of molecular weight and its distribution on structure and mechanical properties of as-spun filaments *J.Appl.Polym.Sci.* , Vol.34, Issue 4, pp.1521-1539.

Mathieu, C. et al. (2002). Specificity and versatility of nucleating agents toward isotactic polypropylene crystal phases *J. Polym.Sci. Part B. Polym. Phys.* , Vol.40, Issue 22, pp.2504-2515.

Meille, S.V. et al.(1994). Structure of beta-isotactic polypropylene - a long-standing structural puzzle. *Macromolecules*, Vol.27, Issue 9, pp.2615-2622.

Mencik, Z. (1972). Crystal-structure of isotactic polypropylene. *J.Macromol.Sci., Part B.*, Vol. 6, Issue 1, pp.101-115.

Moos, K. H. & Tilger, B. (1981). Nukleierung und Polymorphie in isotaktischem Polypropylen. *Angew. Makromol.Chem.,* Vol.94, Issue 1, pp. 213-225.

Natta, G. & Corradini, P. (1960). Structure and properties of isotactic polypropylene. *Nuovo Cimento Suppl.,* Vol. 15, No. 10, pp. 40- 51.

Miller, R.L. (1960). On the existence of near-range order in isotactic polypropylenes *Polymer*, Vol.1, Issue 2, pp. 135-143.

Potts, G. D.; et al. (1994). The crystal structure of quinacridone: An archetypal pigment. *J. Chem. Soc., Chem. Commun.*, Vol.40, Issue Pt01, pp. 2565-2566.

Qiu, J. et al. (2007). Deformation-induced highly oriented and stable mesomorphic phase in quenched isotactic. *Polymer,* Vol. 48, Issue 23, pp.6934-6947.

Ran, S. et al. (2001). Structural and morphological studies of isotactic polypropylene fibers during heat/draw deformation by in-situ synchrotron SAXS/WAXD. *Macromolecules*, Vol.34, Issue 8, pp. 2569-2578.

Ross, S.E. (1965). Some observations concerning behavior of polypropylene polymers and fibers. *J.Appl.Polym.Sci.,* Vol.9, Issue 8, pp. 2729-2748.

Rybnikar, F. (1991). Transition of β to α phase in isotactic polypropylene. *J. Macromol. Sci.-Phys.,* Vol.30, Issue 3, pp. 201-223.

Samuels, R. J. & Yee, R.Y. (1972). Characterization of structure and organization of beta-form crystals in type-iii and type-iv beta-isotactic polypropylene spherulites *J. Polym. Sci. Part A-2 Polymer Phys.,* Vol.10, Issue 3, pp. 385-432.

Saraf, R.F. & Porter, R.S. (1988). A deformation induced order-disorder transition in isotactic polypropylene. *J.Polym.Eng.Sci.,* Vol. 28, Issue 13, pp. 842-851.

Sheehan, W.C. & Cole, T.B. (1964). Production of super-tenacity polypropylene filaments. *J.Appl.Polym.Sci.,* Vol. 8, Issue 5, 2359-2388.

Spruiell, J.E.& White, J.L. (1975). Structure development during polymer processing - studies of melt spinning of polyethylene and polypropylene fibers. *Polym.Eng.Sci.,* Vol. 15, Issue 9, pp.660-667.

Stocker, W. et al. (1998). Epitaxial Crystallization and AFM Investigation of a Frustrated Polymer Structure: Isotactic Poly(propylene), β Phase. *Macromolecules.* Vol.31, Issue 3, pp. 807-814.

Takahashi, T. (2002). Crystal modification in polypropylene fibers containing β-form nucleating agent. *Sen Gakkaishi,* Vol.58, No. 10, pp.357-364.

Tjong, S. C. et al. (1996). Morphological behaviour and instrumented dart impact properties of beta-crystalline-phase *Polymer*, Vol.37, Issue 12, pp. 2309-2316.

Turner Jones, A.; et al. (1964). Crystalline forms of polypropylene *Makromol.Chem.* , Vol. *75*, Issue 1, pp.134-154.

Varga, J. (1986). Melting memory effect of the beta-modification of polypropylene. *J. Therm. Anal.* Vol.31, Issue 1, pp.165-172.

Varga, J. (1989). β-Modification of polypropylene and its two-component systems. *J.Therm. Anal.*, Vol.*35*, Number 6, pp.1891-1912.

Varga J. (1995). Crystallization, melting and supermolecular structure of isotactic polypropylene, In: *Polypropylene: Structure, Blends and Composities*; *Structure and Morphology Copolymers and Blends Composites,* Karger-Kocsis, J., pp. 56-115 , Chapman & Hall, ISBN 9780412614309, London.

Varga, J. et al. (1999). Highly active thermally stable beta-nucleating agents for isotactic polypropylene. *J. Appl. Polym. Sci.* , Vol.74, Issue 10, pp. 2357-2368.

Varga, J. (2002). Beta-modification of isotactic polypropylene: Preparation, structure, processing, properties, and application. *J. Macromol. Sci., Phys. B.*, Vol. B41, Issue 4-6, pp.1121-1171.

Vleeshouwers, S. (1997). Simultaneous in-situ WAXS/SAXS and DSC study of the recrystallization and melting behaviour of the alpha and beta form of iPP. *Polymer*, Vol.38, Issue 13, 3213- 3221.

Yu, Y.; White, J.L. (1999). Structure development in melt spinning polypropylene-EPM blends and dynamically vulcanized polyolefin TPEs. *Intern.Polym.Proc.,* Vol.14, Issue 2, pp. 159-167.

Yu, Y.; White, J.L. (2001). Comparison of structure development in quiescent crystallization, die extrusion and melt spinning of isotactic polypropylene and its compounds containing fillers and nucleating agents. *Polym.Eng.Sci.,* Vol. 41, Issue 7, pp.1292-1298.

Wyckoff, H.W. (1962). X-ray and related studies of quenched, drawn, and annealed polypropylene. *J.Polym.Sci.*, Vol.52, Issue 173, pp.83-114.

Zhou, G. et al. (1986). Studies on the beta-form of isotactic polypropylene .1. characterization of the beta-form and study of the beta-alpha-transition during heating by wide angle X-ray-diffraction. *Makromol. Chem.,* Vol. 187, Issue 3, pp. 633-642.

Zhu, M.F. & Yang, H.H. (2007) Polypropylene fibers, In: *Handbook of fiber chemistry,* Lewin M., pp.139-260, CRC Press, ISBN 10 08247-2565-4, Boca Raton.

Edited by Fatih Doğan

This book aims to bring together researchers and their papers on polypropylene, and to describe and illustrate the developmental stages polypropylene has gone through over the last 70 years. Besides, one can find papers not only on every application and practice of polypropylene but also on the latest polypropylene technologies. It is also intended in this compilation to present information on polypropylene in a medium readily accessible for any reader.

ISBN 978-953-51-6214-8

Photo by XXLPhoto / iStock

IntechOpen